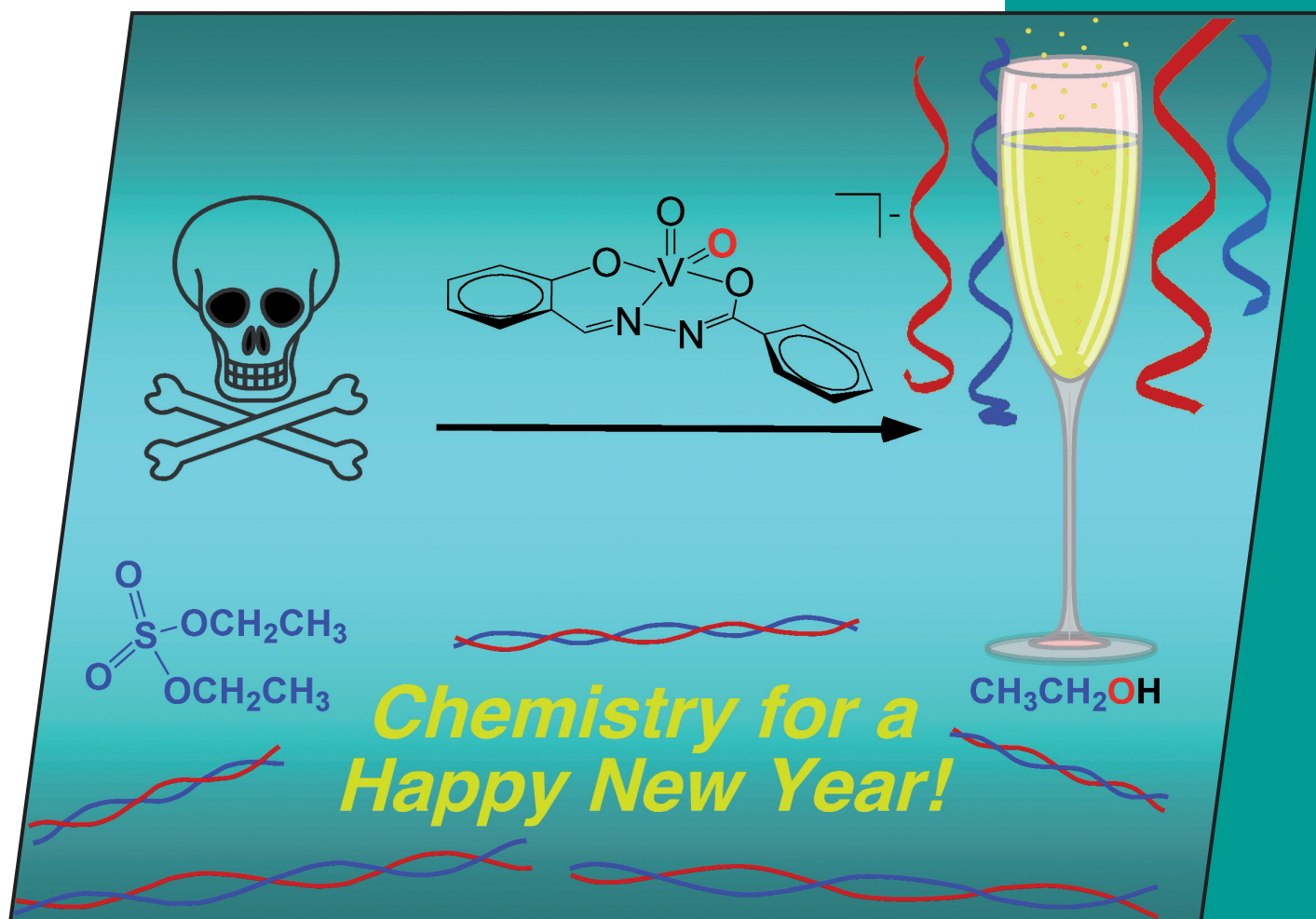


1/2009
1st January Issue

EurJIC
European Journal of
Inorganic Chemistry



Cover Picture

Jonathan J. Wilker et al.

Oxidovanadium Complexes for Consumption of Alkylating Toxins

Microreview

Roger Alberto

Chemistry of Technetium–Water Complexes

WILEY-VCH

www.eurjic.org

A Journal of

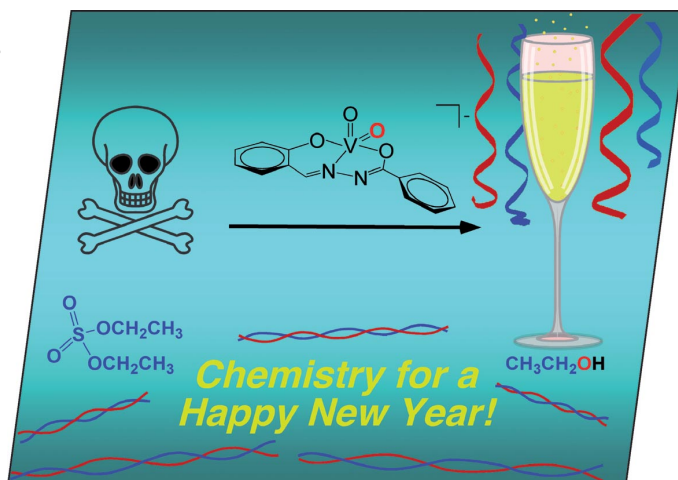




A union formed by chemical societies in Europe (ChemPubSoc Europe) has taken the significant step into the future by merging their traditional journals, to form two leading chemistry journals, the *European Journal of Inorganic Chemistry* and the *European Journal of Organic Chemistry*. Three further members of ChemPubSoc Europe (Austria, Czech Republic and Sweden) are Associates of the two journals.

COVER PICTURE

The cover picture shows oxidovanadium complexes transforming alkylating toxins into alcohols. Variation of the electron-donating ability of the ligand was found to permit a degree of control over the reactivity with alkylating agents. Kinetic studies revealed a small range of k_{obsd} values for this series of $\text{K}[\text{VO}_2(\text{sallyph}(\text{R})_2)]$ complexes ($\text{R} = -\text{NO}_2$, $-\text{H}$, $-\text{CH}_3$, $-\text{OCH}_3$) examined. These experiments were carried out with an ultimate goal of developing compounds to consume toxins and prevent DNA alkylation damage. Details are discussed in the Short Communication by J. J. Wilker et al on p. 33ff.



Trust pervades all



Karen Hindson,
Editor EurJIC

At the time of writing, the dust had not yet settled after the financial crises in banking and probably will still hang over us when this is published. My thoughts turned to the essential trust in banks, or more specifically the violation of it, and the wide repercussions that have shaken world economies and will continue to do so for a long time to come. Certainly, chemical companies and – in the academic world – research grants will not escape the effects. This train of thought brought me to the trust that is existential for scientific publishing.

When you submit a manuscript to a journal a meshing series of trust relationships are kicked off. The journal trusts that its authors submit only their own unpublished work to only one journal, that all authors agree to be included, and that none has been included that were not involved in the research. You trust that the journal will initiate appropriate peer review, process the manuscript if accepted and publish it without delay. I am pleased to report that the publication times of EurJIC have again dropped (Figure 1). The median publication time for all

Shorter publication times

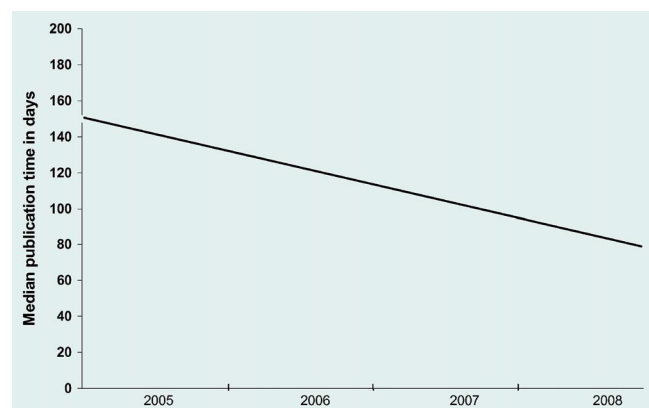


Figure 1. Median times from submission to online publication from January 2005 to October 2008. As the times vary widely per issue depending largely on vacation periods, the regression line through the data for each issue is shown.

manuscripts is below 90 days from submission to online publication. Short Communications appear online now as fast as 62 days after they arrive in the editorial office.

The peer review process takes time and involves risk of misuse of intellectual property – why does the scientific community put its faith in this system, which certainly is not perfect? Not only do reviewers provide important input to a manuscript and even the research itself, similar to the discussions and questions at conference lectures, the process also prevents fragmentation and duplication of research results, because an expert reviewer in the field will be aware of the recent – and not so recent – literature. This professional service on the part of editors and peer reviewers reduces rampant proliferation of repetitive research in the quality journals and therefore, the time a scientist requires to find and to read the pertinent literature. Together author and reviewers are more likely to ensure that all the relevant previous work is covered and spurious publications are avoided. An editor will undertake time-consuming investigations if an author has reason to suspect unethical use of confidential papers for review. Checks and balances in the form of Ethical Guidelines and, if necessary, appropriate punishment are in place to maintain confidence in a single-blind system. Editors from different publishers work closely together when premeditated deviation from the accepted norm is suspected. At present the community believes that the peer review system is the best available, and worldwide chemical societies ensure that their journals and editors are accountable. For EurJIC the societies are the ChemPubSoc Europe group (see Figure 2 and the following guest editorial by Wolfram Koch of the German Chemical Society).

Editors cooperate to ensure authors' rights

I wish at this point to thank the many peer reviewers of EurJIC for the thorough and valuable reports that they have provided. Throughout

Authors value peer review comments



Figure 2. Logos of ChemPubSoc Europe and the individual societies who own EurJIC.

this year several authors have mentioned the excellent comments with appreciation.

In general, people want to know the person they have to trust. Per definition, you cannot know the peer reviewers whom you have to trust for a particular paper in a single-blind system where the reviewers remain anonymous. Here, however, I wish to introduce you to the new members in our International Advisory Board and to the Editorial Office teams at EurJIC.

This year we say goodbye to several long-standing Advisory Board members that have helped to shape the journal from the start and even before, since they were also responsible for a predecessor journal. Not only as editor, but also on behalf of the societies, I wish to thank Professors G. Erker, T. M. Klapötke, G. Natile and M. Pfeffer for their belief in the new journal and their ready advice in any matter that I put to them. Also Professors G. Bertrand and S. Brooker of the initial International Advisory Board have earned their retirement, and we wish them every success in the future. New to the Board are Professors Remi Chauvin from France, Karsten Meyer and Franc Meyer from Germany, Alberto Credi from Italy, and Bryan W. Eichhorn from the USA.

The teams of EurJIC and EurJOC work very closely together, and all work for both journals, though with different

Meet the EurJIC team

responsibilities depending on their chemistry specialties. As a result, at no time are you left without a competent contact for any aspect of the publication procedure. Two of the editorial team (see Figure 3) provide over forty years of experience in these journals and adding my background



Figure 3. From left to right: Jennifer O'Donnell, Udo Eberhardt, Arlette Itken-Fuder, Robert Temme, Preeti Vashi.

that began in *Angewandte Chemie* we provide jointly over 60 years in publishing! Dr Robert Temme and Dr Udo Eberhardt are Organic Chemists, and as such they take over the responsibility for the Inorganic Chemistry papers after they have been copyedited. Both started in the German predecessor journals, *Chemische Berichte* and *Liebigs Annalen*. Publication, online and in print, is directed by their competent hands. The third Organic Chemist, Dr Jennifer O'Donnell from Canada, joined the team in the middle of 2006 and extends our editing in-house team, in particular for the Organometallic Chemistry papers. Besides me, the competence in Inorganic Chemistry is provided by Deputy Editor Dr Preeti Vashi, who hails from Zimbabwe and has been with the journal since March 2004, and Associate Editor, Dr Arlette Itken-Fuder from Turkey, who joined us in June of that year. They assist me in the selection of the referees and the final decisions based on the comments, but are chiefly responsible for editing the papers, including the organization of the freelance copyeditors. Our editorial assistants and secretaries (see Figure 4) have been keeping the system running smoothly for many years, the



Figure 4. From left to right: Carmen Leitner, Denis Ott, Silke Lautenschläger, Carola Goldenstein, Ursula Lerch, Audrey Bauer, Steffi Schieweck, Dietmar Syndikus.

“newest” member having joined us in 2004. Assistants Dietmar Syndikus and Ursula Lerch prepare the uploaded data, checking that all the necessary material has been supplied in a form suitable for publication and pre-coding the papers prior to editing. In our secretarial office both Audrey Bauer, who is mainly responsible for EurJIC, and Carola Goldenstein provide friendly help with submission or information on the status of your manuscript and can direct you to the person concerned if the query falls outside their competence. They are ably assisted by Steffi Schieweck, whom we share with ChemBioChem. Finally, Silke Lautenschläger, Denis Ott and Carmen Leitner complete the production team, and Monika Silz is responsible for our marketing activities.

**Highly professional,
yet personal**

As indicated above, every member of the EurJIC team has years of experience that ensures a high degree of professionalism, yet all strive to provide a per-

sonal service. That they succeed is shown by the letters we receive from satisfied authors. If you have not yet published a paper in EurJIC, I invite you to try us – you’ll like us!

To make our office even more efficient, the e-mail address of the inorganic and organic journals will be separated as from January 1, 2009. In future the address of EurJIC will be self-explanatory: eurjic@wiley-vch.de. Nevertheless, the success of EurJIC lies not in these details, but in the excellent papers that the authors entrust to us. I would like to take this opportunity to thank our authors and wish them all the best for 2009.



Karen Hindson
Editor

New e-mail address for EurJIC in 2009

Our e-mail address will change from ejic-ejoc@wiley-vch.de to eurjic@wiley-vch.de as of the beginning of 2009. Our sister journal, EurJOC, will have eurjoc@wiley-vch.de as its new contact address. Messages sent to the old e-mail address will be redirected for a short while after the change; however, we recommend that you use the new e-mail address to contact the specific journal for the fastest response.

From *Chem. Eur. J.* to *ChemSusChem*: All from ChemPubSoc Europe

Wolfram Koch*^[a]



Photo: Nachrichten aus der Chemie

Only two decades ago, the European publishing landscape for chemistry was characterized by fragmentation and a large number of chemistry journals owned and published by European chemical societies. Most of these journals had little impact, and their economic performance was less than satisfactory. While discussions about this unfortunate situation and a possible consolidation of efforts had come up every now and then, it was only in the early and mid-nineties of the last century that such developments actually occurred and bore fruit. From the start it was recognized that the prerequisite for success was quality and that it would be necessary to expand into disciplines other than inorganic and organic chemistry probably sooner rather than later. However, the amalgamation of the existing journals into new journals jointly owned by chemical societies was difficult, as the national pride of society members in their national journal, and in some cases the need to change the language of publication to English, had to be overcome. But finally, upon the encouragement of Jean-Marie Lehn, the Gesellschaft Deutscher Chemiker and Wiley-VCH took the initiative. The first member of what would become a large family of European chemistry journals, *Chemistry—A European Journal*, covering all areas of chemistry, saw the light of day in 1995. Only three years later the journal was officially owned by the national chemical societies of Belgium, France, Germany, Greece, Italy, Netherlands, Portugal, and Spain. Eight months later Hungary, the Czech Republic and Poland joined the owners, and a month later Sweden. The contract with Austria was signed in 2000, and today 14 European chemical societies are the joint owners of this journal, which has in the meantime developed into a highly successful journal publishing full papers, communications and a variety of review-type articles with a current Impact Factor of 5.330.

This group of 14 societies adopted the name Editorial Union of Chemical Societies (EUCHEM Soc) for its further publishing activities, all of which are being pursued together with Wiley-VCH, the group's long-time partner in society publishing; and there has been a lot of activity. In 1998, the *European Journal of Organic Chemistry* and its counterpart, the *European Journal of Inorganic Chemistry*, were founded. These journals replaced a large number of society journals and have now developed into leading journals in their fields. Only two years later,



ChemPhysChem and *ChemBioChem* joined the journals family, followed by *ChemMedChem* in 2006 and *ChemSusChem* in 2008.

Also here, existing society journals, such as the *Journal de Chimie Physique et de Physico-Chimie Biologique* of the former Société Française de Chimie or the journals *Il Farmaco* and *Annali di Chimica* of the Società Chimica Italiana were transformed and used as a basis for the new products. In all cases, the flagship journal of the Gesellschaft Deutscher Chemiker, *Angewandte Chemie*, was used as a carrier journal in the start-up phases. And, watch out, a new project is already in the pipeline and will be announced soon!

The success of this approach of combining the competence of various chemical societies to create new platforms for publishing chemical research results was soon picked up in other parts of the world. The Asian Chemical Editorial Society (ACES) was created, and its first product, *Chemistry—An Asian Journal*, was launched in 2006. Today, eleven Asian societies are co-owners of the journal. The Asian and European initiatives work closely together and mutually support each other's top journal.

However, the name EUCHEM Soc for the group of the European owner societies quickly turned out to be less adequate than originally anticipated, in particular after the former Federation of European Chemical Societies (FECS) changed its name into European Association for Chemical and Molecular Sciences, abbreviated as EuCHEMS. As a consequence of this similarity in names and also to make the purpose of this partnership, namely to publish top-notch chemistry journals, more visible, the partner societies decided to change the name of their alliance to the Chemical Publishing Society Europe.

ChemPubSoc Europe is the new name for the well-established and successful group of 14 European chemical societies that are the owners and co-owners of and responsible for the continuously growing portfolio of highly successful and relevant chemistry journals. Whenever you see the name ChemPubSoc Europe on the cover of a journal, you can be sure that you hold a premier source of chemical information in your hands—made in Europe for the world!

Wolfram Koch

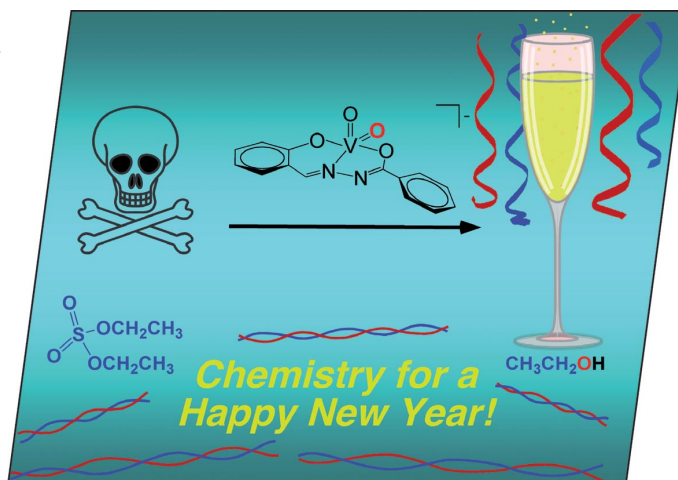
[a] Prof. Dr. W. Koch
Gesellschaft Deutscher Chemiker/German Chemical Society
Varrentrappstrasse 40–42, 60486 Frankfurt am Main (Germany)
Fax: (+49) 69-7917-307
E-mail: w.koch@gdch.de



A union formed by chemical societies in Europe (ChemPubSoc Europe) has taken the significant step into the future by merging their traditional journals, to form two leading chemistry journals, the *European Journal of Inorganic Chemistry* and the *European Journal of Organic Chemistry*. Three further members of ChemPubSoc Europe (Austria, Czech Republic and Sweden) are Associates of the two journals.

COVER PICTURE

The cover picture shows oxidovanadium complexes transforming alkylating toxins into alcohols. Variation of the electron-donating ability of the ligand was found to permit a degree of control over the reactivity with alkylating agents. Kinetic studies revealed a small range of k_{obsd} values for this series of $\text{K}[\text{VO}_2(\text{sallyph}(\text{R})_2)]$ complexes ($\text{R} = -\text{NO}_2$, $-\text{H}$, $-\text{CH}_3$, $-\text{OCH}_3$) examined. These experiments were carried out with an ultimate goal of developing compounds to consume toxins and prevent DNA alkylation damage. Details are discussed in the Short Communication by J. J. Wilker et al on p. 33ff.



CONTENTS

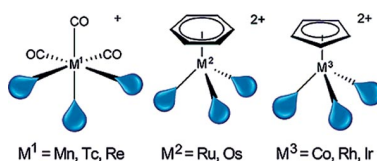
MICROREVIEW

Manganese Triad Aqua Ions

R. Alberto* 21–31

The Chemistry of Technetium–Water Complexes within the Manganese Triad: Challenges and Perspectives

Keywords: Technetium / Aqua ions / Labeling / Bioorganometallics / Radiopharmaceuticals / Water chemistry



Pure aqua complexes are frequent for the 3d but scarce for the 4d and 5d transition-element series. Since water can conveniently be substituted, aqua complexes facilitate biomedical applications. This microreview discusses complexes of the manganese triad containing water ligands. A particular focus is placed on technetium and its organometallic aqua ion $[\text{}^{99}\text{Tc}(\text{OH}_2)_3(\text{CO})_3]^+$.

SHORT COMMUNICATIONS

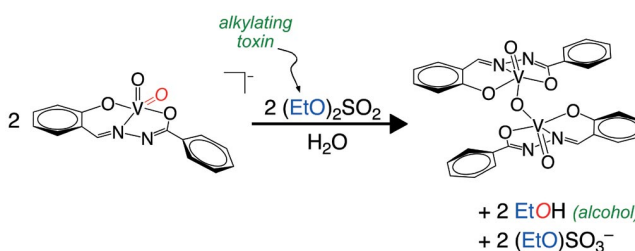
Carcinogen Detoxification

J. M. Fautsch, P. E. Fanwick,
J. J. Wilker* 33–37



Oxidovanadium Complexes for the Consumption of Alkylating Toxins

Keywords: Bioinorganic chemistry / Vanadates / Alkylation / Hydrolysis / Substituent effects



Oxidovanadium complexes are known to consume alkylating toxins and yield alcohols. These reactions may help in the

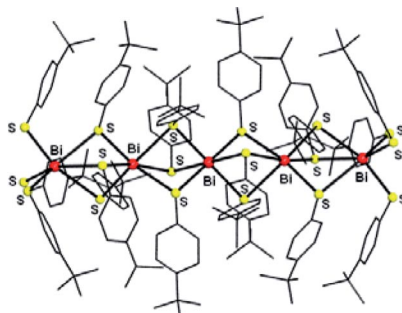
development of second-generation cancer prevention compounds.

Bismuth Thiolates

J.-X. Chen, X.-Y. Tang, Z.-G. Ren,
Y. Zhang, J.-P. Lang* 38–41

Synthesis and Structure of an Unprecedented Linear Pentanuclear Bismuth(III) Zwitterionic Thiolate Complex

Keywords: Bismuth / Zwitterions / S ligands / Structure elucidation

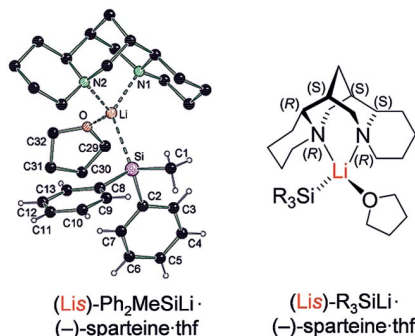


A rare pentanuclear bismuth(III) zwitterionic thiolate complex, $[\text{Bi}_5(\text{Tab})_{18}](\text{PF}_6)_7(\text{NO}_3)_8 \cdot 6\text{MeCN}$ [1; Tab = 4-(trimethylammonio)benzenethiolato], was obtained from the reaction of $\text{Bi}(\text{NO}_3)_3$ with TabHPF₆ in a 1:4 molar ratio in MeCN/MeOH in the presence of Et₃N.

FULL PAPERS

Lithiosilanes

On the basis of X-ray crystal structures of monomeric, (–)-sparteine-coordinated lithiosilanes, the influence of the steric demand of the substituents at silicon on their molecular structures was studied. NMR spectroscopic studies indicated equivalent structures in solution and in the solid state. DFT calculations provided very small energy differences between the diastereomers.

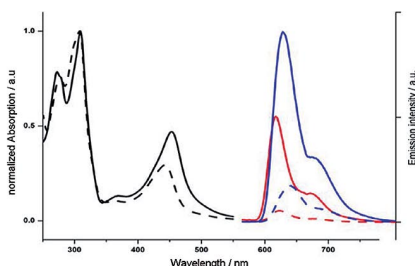
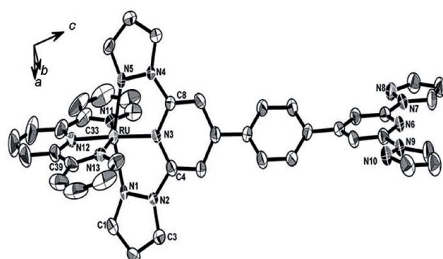


C. Däschlein, C. Strohmann* 43–52

Structural Studies on (–)-Sparteine-Coordinated Lithiosilanes

Keywords: Lithium / Silanes / X-ray diffraction / Arene ligands / NMR spectroscopy

Polypyridylruthenium Complexes



F. Schramm, R. Chandrasekar,
T. A. Zevaco, M. Rudolph, H. Görls,
W. Poppitz, M. Ruben* 53–61

(Polypyridyl)ruthenium(II) Complexes
Based on a *Back-to-Back* Bis(pyrazolylpyridine) Bridging Ligand

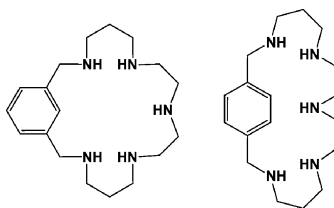
Keywords: Ruthenium / Back-to-back ligands / N ligands / Bridging ligands

Two ruthenium(II) complexes were synthesised by using a linear *back-to-back* bridging ligand based on a dipyrazolylpyridine coordination unit. The structural, electrochemical and spectroscopic proper-

ties show that this new bridging ligand can be considered as structural and electronic alternative to the widely used terpyridine-based bridging ligand systems.

Azacyclophane Ligands

Two new cyclophanes differing only in the aromatic ring substitution have been prepared. Potentiometric measurements suggest the *m*-substituted ligand is tetradentate in the CuL²⁺ complex whereas the *p*-cyclophane is tridentate. DFT calculations suggest this change in the coordination mode is not principally related to first coordination sphere effects but to changes in the hydrogen bond network.

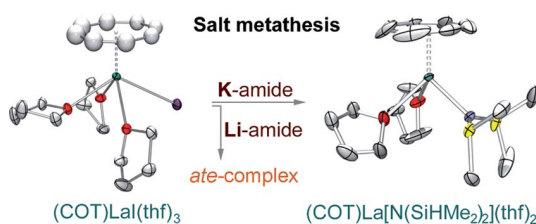


A. G. Algarra, M. G. Basallote,* R. Belda,
S. Blasco, C. E. Castillo, J. M. Llinares,
E. García-España,* L. Gil, M. Á. Máñez,
C. Soriano, B. Verdejo 62–75

Synthesis, Protonation and Cu^{II} Complexes of Two Novel Isomeric Pentaazacyclophane Ligands: Potentiometric, DFT, Kinetic and AMP Recognition Studies

Keywords: Cyclophanes / Macrocyclic ligands / Copper / Kinetics / Density functional calculations

(Amido)(COT)lanthanide Complexes



Reaction of (COT)LnI(thf)₃ with Li[N(SiHMe₂)₂] yields (COT)dilanthanide sandwich complexes featuring distinct hetero-bridged core moieties Ln(μ-I)_nμN-

(SiHMe₂)₂Ln (Ln = La: *n* = 1, *m* = 2; Ln = Nd, Sm: *n* = 2, *m* = 1). Utilization of K[N(SiHMe₂)₂] affords a (COT)monolanthanide silylamide complex.

C. Meermann, K. Ohno, K. W. Törnroos,
K. Mashima,* R. Anwander* 76–85

Rare-Earth Metal Bis(dimethylsilyl)amide Complexes Supported by Cyclooctatetraenyl Ligands

Keywords: Cyclooctatetraenyl ligands / Silylamido ligands / Lanthanides / Iodido ligands / Agostic interactions

CONTENTS

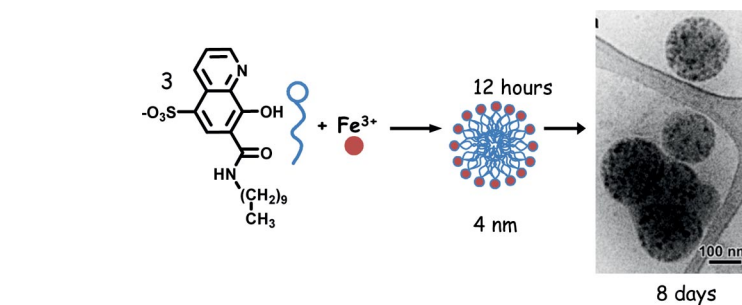
Iron Nanospheres

J. Brandel, S. Torelli,* G. Gellon,
G. Serratrice, J.-L. Putaux,
J.-L. Pierre..... 86–92



From Molecular to Nanostructured Iron Complexes of Amphiphilic Chelators Based on 8-Hydroxyquinoline Subunits – Evidence of Self-Assembled Edifices Mimicking Siderophores from Marine Bacteria

Keywords: Iron / Amphiphiles / Chelates / Nanostructures / Self-assembly



Iron-containing nanospheres were obtained from self-assembly of an amphiphilic siderophore derived from 8-hydroxyquinoline. Cryogenic transmission electron

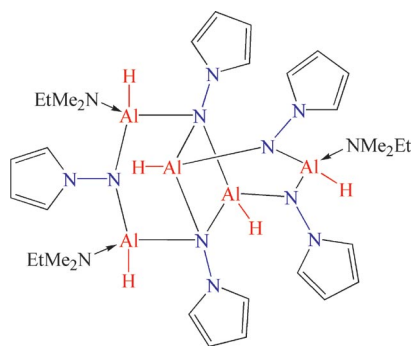
microscopy images revealed evolution from micelles to flecked spherical structures with time.

Aluminum Hydrazides

W. Uhl,* A. Vogelpohl 93–97

Reactions of Hydrazines with $\text{AlH}_3 \cdot \text{NMe}_2\text{Et}$ – Formation of Aluminum-Nitrogen Heterocycles

Keywords: Aluminum / Hydrazides / Heterocycles / Cage compounds



Heterocyclic or cage-like compounds are formed by the double deprotonation of the hydrazine derivatives $\text{H}_3\text{C}_6-(\text{H})\text{N}-\text{N}(\text{H})-\text{C}_6\text{H}_5$ and $\text{H}_2\text{N}-\text{NC}_4\text{H}_4$ with $\text{AlH}_3 \cdot \text{NMe}_2\text{Et}$. 1-Aminopyrrole gave a novel structural motif, in which five Al-H fragments are bridged by five dianionic hydrazinediido ligands.

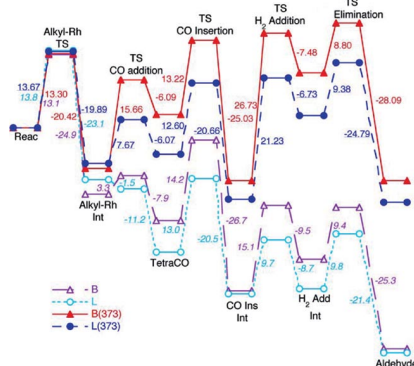
Hindered CO Addition

C. Ghio, R. Lazzaroni,
G. Alagona* 98–103



Computational Results Provide a Synthetically Unprecedented Explanation for the β -Regioselectivity in the Rh-Catalyzed Hydroformylation of Vinylidene Substrates

Keywords: Regioselectivity / Homogeneous catalysis / Density functional calculations / Hydroformylation



In the hydroformylation of 1,1-diphenylethene, a high activation barrier was found for the branched alkyl-Rh(CO)₃ intermediate, but not for the linear intermediate. The path leading to the branched aldehyde is thus abandoned early. CO addition, instead of CO migratory insertion or H₂ oxidative addition and aldehyde reductive elimination, was found to be the critical step.

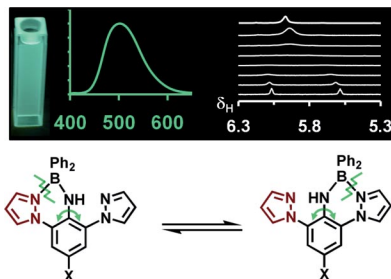
Boron Dyes

T. J. Morin, S. V. Lindeman,
J. R. Gardinier* 104–110

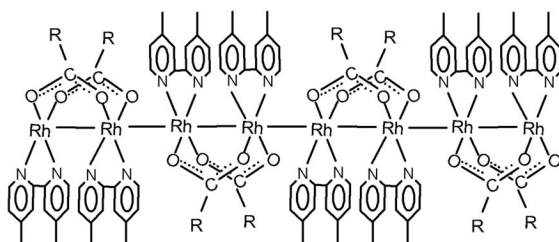


Molecular Motion and Performance Enhancement of BORAZAN Fluorescent Dyes

Keywords: Chelates / Boron / Electrochemistry / UV/Vis spectroscopy / Fluorescence / Dyes/pigments / Density functional calculations



Diphenylboryl complexes of 2,6-bis(pyrazolyl)anilines are more robust and more highly-emissive colour-tuneable fluorophores than derivatives with only one pyrazolyl bound to the aniline ring. Evident from VT-NMR studies, the origin of these favourable characteristics is likely kinetic via promotion of chelate ring formation should dissociation occur.



The rhodium(II) complexes $[\text{Rh}_2(\mu\text{-OOCCH}_3)_2(\text{Me}_2\text{bpy})_2(\text{H}_2\text{O})_2]^{2+}$ were chemically and electrochemically reduced to the $\text{Rh}^{1.5+}$ wire $\{[\text{Rh}_2(\mu\text{-OOCCH}_3)_2(\text{Me}_2\text{bpy})_2]^{+}\}_n(\text{BF}_4)_n$ with infinite Rh–Rh

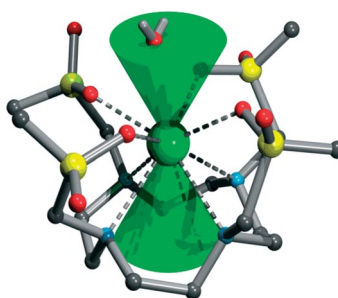
bonds. The molecular wire shows strong antiferromagnetic properties. Redox properties of the wires prepared chemically and electrochemically are similar.

**M. Rak, F. P. Pruchnik,* L. Z. Ciunik,
F. Lafolet, S. Chardon-Noblat,
A. Deronzier** 111–118

Synthesis and Structural and Physicochemical Characterization of $\{[\text{Rh}_2(\mu\text{-OOCCH}_3)_2(\text{dmbpy})_2][\text{BF}_4]\}_n$ Molecular Wire

Keywords: Rhodium / Mixed-valent compounds / Nanostructures / Electrochemistry / Magnetic properties

The set of DOTA-like complexes lacking a directly coordinated water molecule is studied to explore the relationship between the second hydration sphere and MRI-relevant parameters, and the influence of the ligand pendant arms (size, hydrophilicity) on the complex properties is discussed.

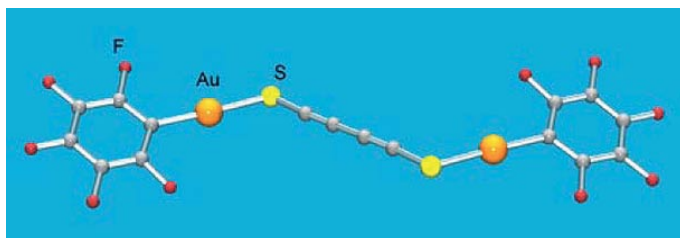


Relativity of Ln^{III} -DOTP^R Complexes

**Z. Kotková, G. A. Pereira, K. Djanashvili,
J. Kotek, J. Rudovský, P. Hermann,
L. Vander Elst, R. N. Muller,
C. F. G. C. Geraldés, I. Lukeš,*
J. A. Peters*** 119–136

Lanthanide(III) Complexes of Phosphorus Acid Analogues of H_4DOTA as Model Compounds for the Evaluation of the Second-Sphere Hydration

Keywords: Contrast agents / Lanthanides / NMR spectroscopy / Phosphinate complexes / Phosphonate complexes



The cleavage of bis(1,2,3-thiadiazole)s provides a new family of bis(alkynethiolate)-gold(I) derivatives $[\text{Au}_2(\text{S}-\text{C}\equiv\text{C}-\text{spacer}-\text{C}\equiv\text{C}-\text{S})\text{L}_2]$ ($\text{L} = \text{PR}_3$ or C_6F_5). X-ray stud-

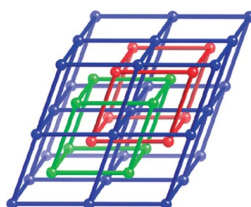
ies confirm the dinuclear structure for $(\text{PPN})_2[\text{Au}_2(\text{S}-\text{C}\equiv\text{C}-\text{C}\equiv\text{C}-\text{S})(\text{C}_6\text{F}_5)_2]$ and $[\text{Au}_2\{3,5-(\text{S}-\text{C}\equiv\text{C})_2-\text{C}_7\text{H}_7\text{N}\}(\text{PPh}_3)_2]$ {PPN = bis(triphenylphosphane)iminium}.

**E. Cerrada, M. Laguna,*
N. Lardies** 137–146

Bis(1,2,3-thiadiazole)s as Precursors in the Synthesis of Bis(alkynethiolate)gold(I) Derivatives

Keywords: S ligands / Gold / Phosphanes / Structure elucidation

A series of interesting coordination polymers with V-shaped 4,4'-oxybis(benzoic acid) have been prepared. The crystal structures and topological analysis of these compounds, along with a systematic investigation of the effect of metal ions and neutral ligands on their ultimate frameworks, will be discussed.



Metal–Organic Frameworks

**J.-Q. Liu, Y.-Y. Wang,* Y.-N. Zhang,
P. Liu, Q.-Z. Shi,
S. R. Batten*** 147–154

Topological Diversification in Metal–Organic Frameworks: Secondary Ligand and Metal Effects

Keywords: Coordination polymers / Coordination modes / Ligand effects / Crystal engineering

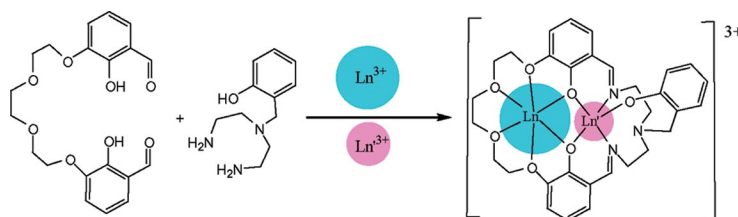
CONTENTS

Lanthanide(III) Complexes

S. Tamburini,* S. Sitran, V. Peruzzo,
P. A. Vigato 155–167

The Role of Functionalisation, Asymmetry and Shape of a New Macrocyclic Compartmental Ligand in the Formation of Mononuclear, Homo- and Heterodinuclear Lanthanide(III) Complexes

Keywords: Compartmental macrocycles / Heterodinuclear complexes / Lanthanide(III) Schiff base / NMR of paramagnetic systems / Lanthanide oxides



A [1+1] asymmetric compartmental macrocycle, bearing a $-\text{CH}_2\text{C}_6\text{H}_4\text{OH}$ pendant arm, and related mononuclear, Ln_2 homodinuclear and LnLn' heterodinuclear complexes are reported. Their properties in the

solid-state and in different coordinating solvents have been investigated. The final decomposition at 1200°C of the heterodinuclear complexes gives pure $\text{LnLn}'\text{O}_3$ oxides.

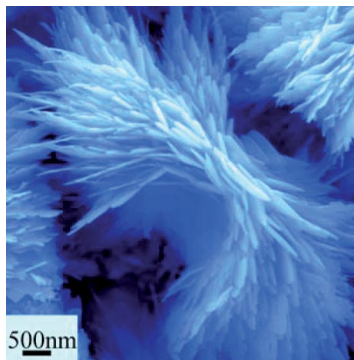
Hierarchical Architectures

Y. J. Zhang, S. W. Or,* X. L. Wang,
T. Y. Cui, W. B. Cui, Y. Zhang,
Z. D. Zhang 168–173



Hydrothermal Synthesis of Three-Dimensional Hierarchical CuO Butterfly-Like Architectures

Keywords: Hydrothermal synthesis / Copper oxide / Nanostructures / Self-assembly



Hierarchical butterfly-like CuO architectures composed of oriented attached rhombic nanoplatelets were synthesized by a simple hydrothermal method. The mechanism for the formation of the CuO hierarchical architectures is proposed.

* Author to whom correspondence should be addressed.



Supporting information on the WWW (see article for access details).

If not otherwise indicated in the article, papers in issue 36 were published online on December 9, 2008

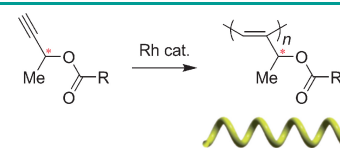


Helical Polymers

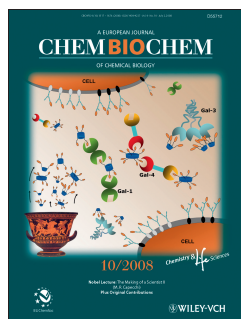
Y. Suzuki, M. Shiotsuki, F. Sanda,* T. Masuda*

Synthesis and Helical Structure of Poly(1-methylpropargyl ester)s with Various Side Chains

Something's screwy: Optically active poly(1-methylpropargyl ester)s with various substituents can be obtained by polymerization with a rhodium catalyst. The polymers have a *cis*-stereoregular main chain and form a predominantly one-handed helical structure. As a result, they exhibit high rigidity and chiral amplification.



Chem. Asian J.
DOI: 10.1002/asia.200800131

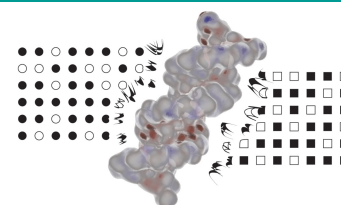


DNA Structures

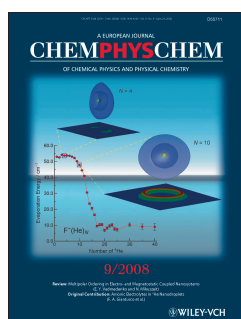
B. D. Heuberger, C. Switzer*

An Alternative Nucleobase Code: Characterization of Purine–Purine DNA Double Helices Bearing Guanine–Isoguanine and Diaminopurine 7-Deaza-Xanthine Base Pairs

DNA's alter ego: Synthetic purine–purine DNA double helices are shown to have stability comparable to canonical DNA.



ChemBioChem
DOI: 10.1002/cbic.200800450

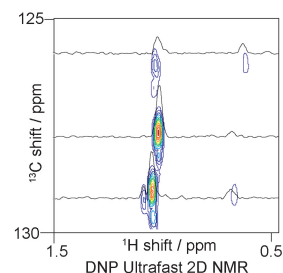
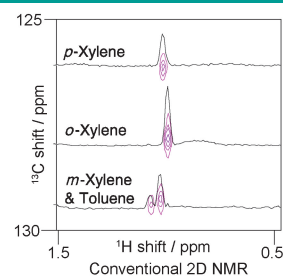


NMR Spectroscopy

M. Mishkovsky, L. Frydman*

Progress in Hyperpolarized Ultrafast 2D NMR Spectroscopy

Sensitive multidimensional NMR: The combination of *ex situ* dynamic nuclear polarization (DNP) and single-scan 2D NMR methodologies opens new vistas in the collection of multidimensional data with high sensitivity. Experimental results show the benefits expected for optimized spectroscopic acquisitions implemented on small- and medium-sized organic molecules (see figure).



ChemPhysChem
DOI: 10.1002/cphc.200800461

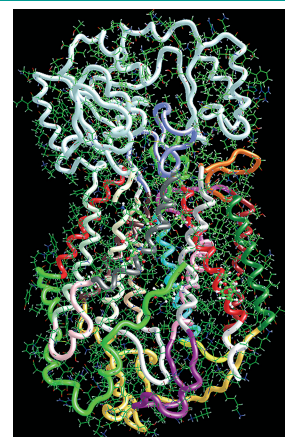


Pharmacophore Mapping

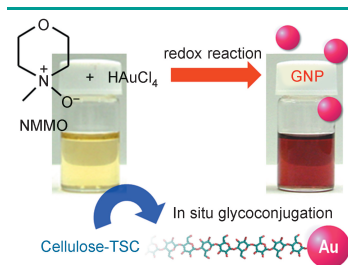
A. Pedretti, L. De Luca, C. Marconi, G. Negrisoni, G. Aldini, G. Vistoli*

Modeling of the Intestinal Peptide Transporter hPepT1 and Analysis of Its Transport Capacities by Docking and Pharmacophore Mapping

The intestinal hPepT1 transporter is involved in the active absorption of dietary peptides and peptidomimetic drugs. The aim of this study was to generate a model for hPepT1 by fragments. The model was validated by docking analyses and pharmacophore mapping using a set of 50 known ligands. The results suggest that the model can be used to predict the transport of peptide-like molecules.



ChemMedChem
DOI: 10.1002/cmdc.200800184



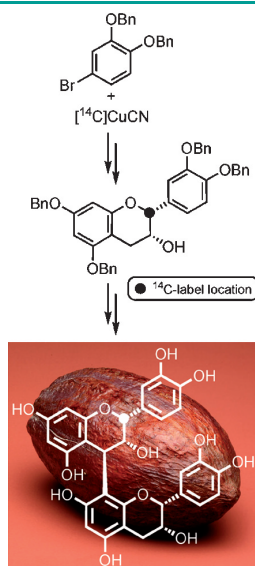
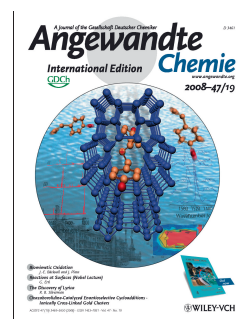
Angew. Chem. Int. Ed.
DOI: 10.1002/anie.200803922

Nanoparticle Synthesis

S. Yokota, T. Kitaoka,* M. Opietnik, T. Rosenau, H. Wariishi

Synthesis of Gold Nanoparticles for In Situ Conjugation with Structural Carbohydrates

Sugaring the pill: Gold nanoparticles (GNPs) were successfully synthesized from tetrachloroauric acid through a novel redox reaction in an aqueous *N*-methylmorpholine-*N*-oxide (NMMO) solution, which is a well-known solvent for structural carbohydrates such as cellulose (see picture, TSC = thiosemicarbazone). This unique approach allowed facile, simultaneous GNP synthesis and in situ glycosurface modification in one pot.



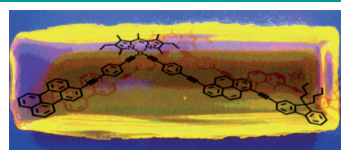
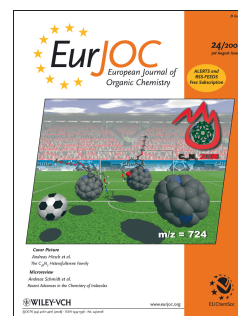
Eur. J. Org. Chem.
DOI: 10.1002/ejoc.200800886

Radiolabeled Polyphenols

F. Viton, C. Landreau, D. Rustidge, F. Robert, G. Williamson, D. Barron*

First Total Synthesis of ¹⁴C-Labeled Procyanidin B2 – A Milestone Toward Understanding Cocoa Polyphenol Metabolism

Health benefits of foods consumed for pure pleasure received much recognition in the recent years. Cocoa and dark chocolate are particularly rich in procyanidins. We developed the first asymmetric total synthesis of [jy]ntprocyanidin B2 and applied it to the preparation of a regioselectively radiolabeled ¹⁴C-analogue, which will be used to strengthen our knowledge on the metabolism of procyanidins.



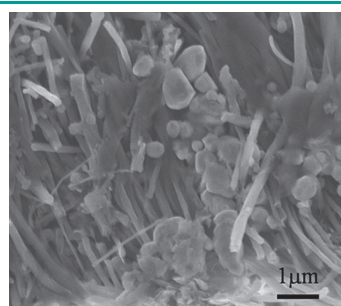
Chem. Eur. J.
DOI: 10.1002/chem.200801384

Energy Transfer

A. Harriman,* L. Mallon, R. Ziessel*

Energy Flow in a Purpose-Built Cascade Molecule Bearing Three Distinct Chromophores Attached to the Terminal Acceptor

Piecing together a multicomponent molecular array (see graphic) that absorbs incident photons over a wide spectral range and concentrates the emission into a narrow band, thereby producing a highly efficacious solar concentrator.



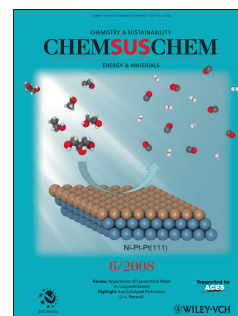
ChemSusChem
DOI: 10.1002/cssc.200800170

Lithium-Ion Batteries

C. Sotowa, G. Origi, M. Takeuchi, Y. Nishimura, K. Takeuchi, I. Y. Jang, Y. J. Kim, T. Hayashi, Y. A. Kim,* M. Endo, M. S. Dresselhaus

The Reinforcing Effect of Combined Carbon Nanotubes and Acetylene Blacks on the Positive Electrode of Lithium-Ion Batteries

Carbon—the new black: The advantages of using carbon nanotubes together with acetylene blacks as cathode fillers include not only enhancement of the electrical and the thermal properties of the electrode but also enhancement of the density of the electrode and a decrease in the electrolyte absorption time. The use of carbon nanotubes as multifunctional fillers in both cathode and anode materials for lithium-ion secondary batteries may increase.





1. General Information

The *European Journal of Inorganic Chemistry* (EurJIC) is a fully peer-reviewed journal publishing 36 issues per year.

EurJIC publishes articles on inorganic, organometallic, bioinorganic, physical inorganic and solid-state chemistry. Three types of contributions are accepted for publication:

- **Full Papers** are articles with an Experimental Section that describe a major contribution to the development of an area of research of importance.
- **Short Communications** are brief reports on results of high significance and urgency. Generally, they are no longer than about 8 pages or 3–4 typeset pages. A justification for urgent publication should accompany submission.
- **A Microreview** is a highly focused overview of a selected topic. In general it includes a concise overview of the author's own research; reference to all appropriate work by others is essential.

Manuscripts should be submitted online. The URL is:
<http://www.manuscriptXpress.org>

A single file containing all tables, graphics, Supporting Information (where appropriate) etc. is required. Acceptable file formats are Microsoft Word, Rich Text Format, Postscript and PDF.

Authors can follow the progress of their manuscript on their **personal homepage**, which is created automatically upon initial registration.

All submissions must be in accordance with the *Ethical Guidelines for Publication in Journals and Reviews* issued by the European Association for Chemical and Molecular Sciences (EuCheMS). **The author must inform the editor of manuscripts submitted, soon to be submitted, or in press at other journals that have a bearing on the manuscript being submitted.** Any manuscript already available on personal/group web pages will be considered by the editors as already published and will not be accepted. If a manuscript is a revised/extended version of a manuscript previously rejected by EurJIC, the author must inform the editor about the previous submission in the cover letter and explain in detail which changes have been made. Authors should reveal all sources of funding for the work presented in the manuscript and should declare any conflict of interest.

We encourage authors to submit pictures for the cover page. A template, [eurjiccover.pdf](#), is available under the link "For Authors" on our journal homepage (<http://www.eurjic.org>).

On behalf of our authors who are also US National Institutes of Health (NIH) grantees, Wiley-VCH will deposit the peer-reviewed version of the manuscript in PubMed Central (PMC). PMC may display the material 12 months after Wiley-VCH has published the article. By assuming this responsibility, we will ensure that our authors are in compliance with the NIH request and make certain that the appropriate version of the manuscript is deposited. We reserve the right to change or rescind this policy.

2. Manuscript Preparation

2.1 Manuscript Structure

Templates (MS Word for Win/Mac) should be used for all types of contributions and can be found under the **For Authors** link on our journal homepage (<http://www.eurjic.org>). A manuscript should comprise: ♦ Title ♦ Keywords ♦ Abstract ♦ Main Text including Introduction, Results and Discussion etc. ♦ Experimental Section ♦ Acknowledgments (optional) ♦ Captions ♦ Tables ♦ References ♦ Schemes and Figures ♦ Table of Contents entry including a Key Topic (two or three words highlighting the most important aspect of your paper), a short text (max. 350 characters) and a graphical element (use of free colour is strongly recommended). ♦ For Microreviews only: Biographical sketches and a portrait-quality photograph of all authors (when several authors from one institution are involved, group photographs are preferred).

2.2 Text

The text should be left-justified only to avoid end-of-line word divisions.

Abbreviations and acronyms should be used sparingly and consistently. Where they first appear in the text, the complete term – apart from the most common ones such as NMR, IR, thf, *t*Bu etc. – should also be given.

In the Experimental Section, quantities of reactants, solvents etc. should be included in parentheses [e.g. A solution of triphenylphosphane (500 mg, 1.91 mmol) in dichloromethane (15 mL) was added to...].

NMR spectroscopic data should be quoted as in the following example: ^1H NMR (300 MHz, C_6D_6 , 25 °C): δ = 1.3 (s, 18 H, SiMe_3), 0.9 (d, $^3J_{\text{H,H}}$ = 5.7 Hz, 2 H, 2-H) ppm.

GUIDELINES FOR AUTHORS

Symbols of physical quantities, but not their units (e.g. *T* for temperature, *J*, λ), stereochemical information (*cis*, *trans*, *Z*, *R*), locants (*N*-methyl), symmetry and space groups (*P*₂₁/*c*), and prefixes in formulas (*t*Bu) or compound names (*tert*-butyl) **must be in italics**. Latin phrases, such as “in situ”, should not.

Stereochemical descriptors, such as D- and L-, and molar (M) or normal (N) should be in **small capitals**.

Use only characters from the Symbol and Normal Text character sets, especially when inserting Greek letters and characters with umlauts, accents, tildes, etc.: α , \ddot{a} , \grave{a} , \tilde{a} , \AA .

EurJIC follows the latest IUPAC recommendations for nomenclature. However, avoid complicated, multi-line names if a simpler version (e.g. alcohol **4**, ketone **5**, compound **6** accompanied by a structural formula) could be used instead.

2.3 Compound Characterization

All new compounds must be fully characterized and their purity verified by analytical methods appropriate to the discipline (e.g. high-resolution NMR spectroscopy, X-ray structure analysis, elemental analysis, etc.). Any deviations from the expected norm need to be explained.

2.4 Tables

Tables should be introduced as such from the appropriate menu. This creates a cell format, which ensures that the rows and columns are reproduced correctly.

2.5 References

We strongly recommend the use of the Endnotes feature of Word. If you prefer not to use this function, references should be indicated by numbers in square brackets as superscripts and, if applicable, after punctuation (example: text.^[1]).

Journal titles should be abbreviated according to the Chemical Abstracts Service Source Index (CASSI).

Examples:

[1] a) A. Einstein, A. N. Other, *Eur. J. Inorg. Chem.* **2003**, 1–15; b) R. Schoenfeld, *The Chemist's English*, 3rd ed., VCH, Weinheim, **1990**, p. 111.

If a paper has been published online but has not appeared in print yet, it is cited by listing the author names and then the abbreviated title of the journal followed by the DOI number, e.g.:

[1] J. J. Schneider, J. Engstler, *Eur. J. Inorg. Chem.*, DOI: 10.1002/ejic.200501145.

2.6 Graphics

Graphics (including structural formulas, schemes, figures, equations and small graphical items that appear in tables) must be submitted camera-ready.

Schemes should be self-explanatory: reaction conditions should therefore be given above the arrows rather than in the caption.

Use abbreviations consistently: R¹, R² (not R₂), R', R'', Ph, Me, Et, *i*Pr, *t*Bu, Ph, Bn (benzyl), Bz (benzoyl), Hal, L, M (metal), X (heteroatom).

Consult the following table for the appropriate size of lettering. Lettering smaller than 3.0 mm will reproduce poorly. Please use only one size of lettering per graphic and the same letter font for all graphics.

Table 1. Guide for preparing graphics.

| Letter Size | Font | Maximum Graphic Width ^[a] | |
|---------------|-----------|--------------------------------------|-----------------|
| | | 1-Column Format | 2-Column Format |
| | Arial | | |
| 3.0 mm | 12 | 13 cm | 26 cm |
| 3.5 mm | 14 | 15 cm^[b] | – |
| 4.0 mm | 16 | 17 cm^[b] | – |
| 4.5 mm | 18 | 19 cm | – |

[a] Most graphics are in 1-column format. [b] We prefer lettering of 3.5 or 4.0 mm with maximum graphic widths of 15 or 17 cm, respectively.

The settings for one-column graphics constructed with Chem Draw are shown in Figure 1. These settings help ensure the correct letter-size-to-graphic-width ratio for best reproduction.

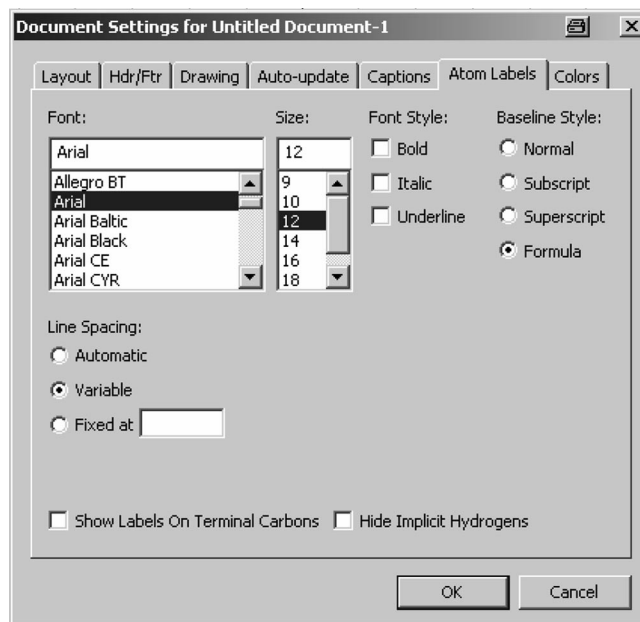


Figure 1. Chem Draw settings for one-column graphics.

In the revised version please submit **each graphic in its own file** within a graphic folder. For good reproduction, the following formats are preferred: *.cdr, *.cdx, *.tif, *.pdf, *.psd, *.ai, *.fh, *.qxd, *.pct, *.eps. The resolution should be a minimum of 300 dpi in general and 600 dpi for bitmap graphics.

3. Crystallographic Data

Authors must deposit the data of X-ray structure analyses in a crystallographic database before submitting their manuscript, so that referees can access the information electronically. The two databases, the Cambridge Crystallographic Data Centre (CCDC) and the Fachinformationszentrum Karlsruhe (FIZ) have the same procedure for the deposition of data and both will be pleased to pro-

vide help. In general, you will receive a depository number from the database two working days after electronic deposition. Send your data to the appropriate address below and quote the standard text, including the depository number, in your manuscript.

- **For all compounds without C–H bonds**

Fachinformationszentrum Karlsruhe (FIZ)
76344 Eggenstein-Leopoldshafen, Germany

Phone: +49-(0)7247/808-205

Fax: +49-(0)7247/808-666

E-mail: crysdata@fiz-karlsruhe.de

FTP: <ftp.fiz-karlsruhe.de> (under path /pub/csd)

WWW: <http://www.fiz-karlsruhe.de> (under “Products and Services”)

Further details of the crystal-structure investigation(s) may be obtained from the Fachinformationszentrum Karlsruhe, 76344 Eggenstein-Leopoldshafen, Germany, on quoting the depository number(s) CSD-....

- **For all compounds with at least one C–H bond:**

Cambridge Crystallographic Data Centre (CCDC)

12 Union Road, Cambridge CB2 1EZ, UK

Phone: +44-(0)1223/336-408

Fax: +44-(0)1223/336-033

E-mail: deposit@ccdc.cam.ac.uk

WWW: <http://www.ccdc.cam.ac.uk>

CCDC-***** contains the supplementary crystallographic data for this paper. These data can be obtained free of charge from The Cambridge Crystallographic Data Centre via www.ccdc.cam.ac.uk/data_request/cif.

NOTE: Please use the free online **Checkcif** service provided by the International Union of Crystallography and submit the Checkcif

report along with your manuscript: <http://journals.iucr.org/services/cif/checkcif.html>.

Finally, before you return your revised manuscript, please update your database entry if necessary.

4. Supporting Information

A manuscript may include electronic Supporting Information which will be accessible only on the WWW. Authors must keep a copy to make available to readers who do not have access to the Internet.

In general, supporting information should be designated as such and pasted into the manuscript template for peer review. Videos and other formats that cannot be included in this way may be sent to the editorial office as e-mail attachments (eurjic@wiley-vch.de). Supporting information does NOT include CIF files, which must be submitted to either the FIZ or the CCDC.

5. Keyword Catalogue

To increase the visibility of articles in the Internet, we have compiled a keyword catalogue common to our chemistry journals that is available online (<http://www.eurjic.org>). Please use at least three keywords from this list.

6. Detailed Guidelines

Detailed information on manuscript preparation can be found in the complete Notice to Authors on the homepage of the journal.

The Chemistry of Technetium–Water Complexes within the Manganese Triad: Challenges and Perspectives

Roger Alberto*^[a]

Keywords: Technetium / Aqua ions / Labelling / Bioorganometallics / Radiopharmaceuticals / Water chemistry

The chemistry of technetium is essentially driven by radio-pharmaceutical applications. These comprise the syntheses of novel complexes but, moreover, the combination of targeting biomolecules with metal complexes. Aqua ions are especially convenient for facilitating the introduction of metal cations into biomolecules, but are nonexistent for Tc and Re in the Mn triad. This microreview will discuss the chemistry of those Tc complexes that contain H₂O as ligands. Special attention will be paid to organometallic aqua ions, i.e. complexes that are typically organometallic with water as ligand.

Of particular interest is the coordination chemistry of [M(OH₂)₃(CO)₃]⁺ (M = Mn, Tc, Re) complexes in water since it is the origin of the widely applied radiopharmaceutical research with ^{99m}Tc and ¹⁸⁸Re. The chemistry of organometallic aqua ions is not confined to Werner-type ligands, hence, a further emphasis will be placed on pure organometallic chemistry in water.

(© Wiley-VCH Verlag GmbH & Co. KGaA, 69451 Weinheim, Germany, 2009)

Introduction

Among the elements of the manganese triad, the chemistry of technetium is probably the least developed. A major reason might be its artificial origin from nuclear fission, and another the related radioactivity. Besides gathering fundamental knowledge, the development of an element's chemistry is essentially driven by application. This statement is supported for technetium by the very well developed +V oxidation-state chemistry, structurally represented by the [Tc=O]³⁺ moiety and stabilized by additional tetradentate ligands. The accessibility of corresponding complexes in one step from [TcO₄]⁻, the exclusive starting material for any technetium chemistry, may be a further reason. The ultimate goal of synthetic technetium chemistry, with radiopharmaceutical applications in mind, is the preparation of complexes in one step directly from water. This con-

straint has confined exploration of the other oxidation states, less in the past but certainly at present. Model chemistry with the weak, long-lived (212000 years) β-emitter ⁹⁹Tc is performed on a milligram to gram scale. Standard chemical analytical methods are applicable for characterization. Application with the short-lived (6 h) metastable isotope ^{99m}Tc is done on the nanogram level with the exclusive option of radio-chromatographic analyses (very rarely mass spectrometry).

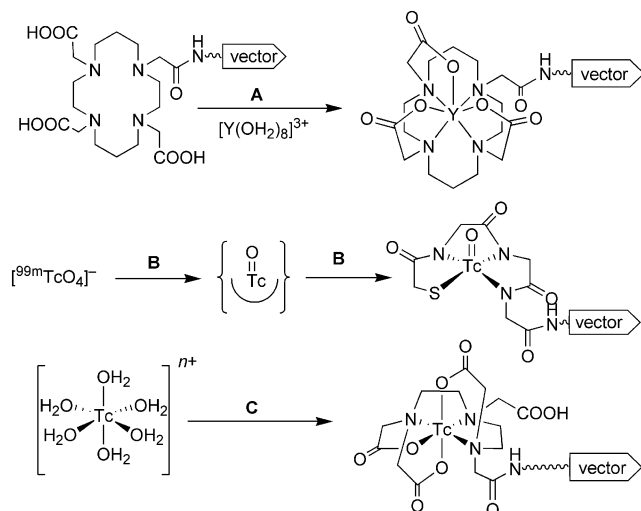
The compulsion of synthesizing in water led to new innovative routes and interesting approaches to receive certain target compounds with the potential for nuclear medicine. Syntheses from water resulted in the preparation of products or intermediates comprising coordinated H₂O, a ligand that is relatively rare throughout the 2nd and 3rd transition-element series. Such complexes, particularly those of technetium, will be the focus of this microreview. Fundamental coordination or organometallic chemistry with any of the Mn-triad elements can be performed under any conditions. However, to be potentially useful, water is

[a] Institute of Inorganic Chemistry, University of Zürich, Winterthurerstrasse 190, 8057 Zürich, Switzerland
E-mail: ariel@aci.uzh.ch



Roger Alberto studied chemistry at the ETH Zürich, Switzerland. He received his Diploma (1982) and his Dr. sc. nat. (1988, Prof. G. Anderegg) for research on technetium(IV) complexes from aqueous and organic solvents at the Laboratory of Inorganic Chemistry, ETH-Zurich. As an Alexander von Humboldt fellow, he performed studies on high-valent organometallic technetium complexes at the Technical University of Munich, TUM (Prof. W. A. Herrmann and Prof. F. Baumgärtner) and at the Los Alamos National Laboratory (Prof. A. P. Sattelberger). From 1991 he became a senior research scientist at the Paul Scherrer Institute (PSI), where his research on organometallic aqua ions of technetium started. Another focus was on novel Ag, Tc and Re complexes for application in radioimmunotherapy and -diagnostics of cancer. After further scientific visits to the TUM, and two visits to Tohoku University, Sendai Japan (Prof. K. Yoshihara, 1993/94) he earned his habilitation degree (1998, Prof. H. Berke). He received an associate Professorship in Inorganic Chemistry (1999) and was promoted to full Professor in 2006 at the University of Zürich. His research interests focus on inorganic medicinal chemistry, on basic technetium and rhenium chemistry in water as well as on photocatalytic H₂ production.

the only solvent of relevance and to which synthetic conditions have to be “reduced” (Scheme 1). The basic chemistry and radiopharmacy of technetium has been the subject of several recent reviews and books.^[1–3] This microreview will focus on those reactions in which coordinated water is involved as a coligand, as a ligand and on uncommon syntheses that have been performed in water with aqua ions of technetium.



Scheme 1. Current labelling procedure for M^{3+} aqua ions (A) [note, Y^{3+} is usually only partially hydrated in the presence of coordinating anions in solution], labelling procedures without aqua ions (B) and ideal situation for ^{99m}Tc (C).

Aqua Ions of Technetium

The importance of aqua ions for radiolabelling purposes is probably best demonstrated by the impact typical trivalent ions of radionuclides such as ^{177}Lu , ^{90}Y or ^{153}Sm have in nuclear medicine.^[4,5] These and other metal ions exist in one oxidation state and are fully or partially hydrated. A labelling process, thus, requires only “normal” ligand substitution with a bifunctional chelator (BFC) for the labelling process (path A in Scheme 1). Typical ligands are of the DOTA type; very strong multidentate chelators that stably bind metal ions by substituting the hydrated ligand shell. Correspondingly, labelling can be performed at a very low ligand (and therefore biomolecule) concentration with the concomitant formation of one and only one product. Numerous examples exist in the literature that were the basis for the strong interest and the success of these radionuclides. Since $[^{99m}\text{TcO}_4]^-$ is the exclusive starting material for technetium, redox chemistry (path B in Scheme 1) is always involved in the labelling process giving rise to side products or incomplete coordination (radiochemical purity <98%). Although some of the standard labelling procedures have managed to achieve a quantitative (>98%) yield, it would be much more convenient to start from a well-defined metal compound (an aqua ion for instance, path C in Scheme 1) for which labelling would only consist of ligand substitution, comparable to what has been de-

scribed above for the $M^{3+}(\text{aq})$ family. However, binary aqua ions $[\text{Tc}(\text{OH}_2)_6]^{n+}$ do not exist and it is, at least, questionable if they would exist under “normal” conditions. A recently published Pourbaix diagram based on theoretical calculations and experimental data evidenced the three major species in water to be $[\text{TcO}_4]^-$, TcO_2 and Tc^0 , with $\text{Tc}^{2+}(\text{aq})$ or $\text{Tc}^{3+}(\text{aq})$ likely to exist only in a small section of the acidic branch of the Pourbaix diagram (Figure 1).^[6]

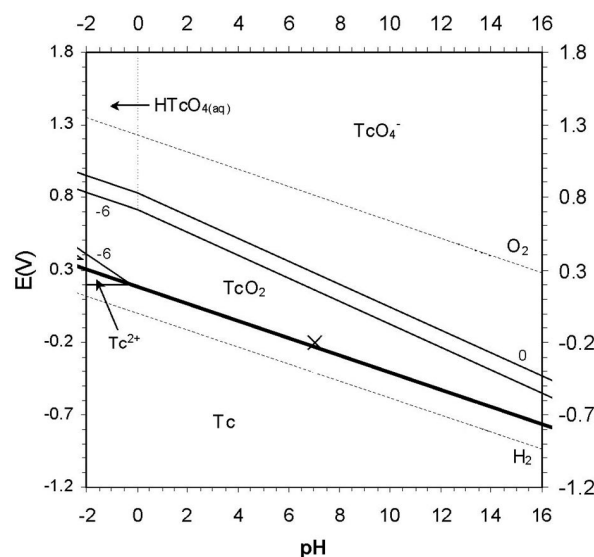


Figure 1. Pourbaix diagram for the Tc-H₂O system (reprinted with permission).^[6]

This nonexistence or, more positively, undiscovery of the binary aqua ions of technetium does not come as a surprise. It is a common fact that transition-metal elements of the 2nd and 3rd series exert increased stabilities in the higher oxidation states. Hence, lower oxidation states are prone to oxidation with concomitant formation of bridged oxo or hydroxo, di- or oligomeric species or the formation of metallic bonds.^[7] The only divalent aqua ion of the 2nd or 3rd transition-metal series is $[\text{Ru}(\text{OH}_2)_6]^{2+}$ whereas for the trivalent cations Mo^{3+} (as a dimetallic aqua ion), Ru^{3+} , Rh^{3+} and Ir^{3+} have been characterized.^[8–10] No aqua ions of technetium are synthetically accessible so far. However, polarographic studies in solution at low concentrations indicate that $\text{Tc}^{3+}(\text{aq})$ should exist.^[11–13] The situation for Tc^{2+} is somewhat similar. Although no fully hydrated species have been characterized, the binary acetonitrile complex $[\text{Tc}(\text{NCCH}_3)_6]^{2+}$ has recently been prepared from the dinuclear precursor $[\text{Tc}_2(\text{NCCH}_3)_{10}]^{4+}$. Acetonitrile and water are very different ligands, still, the existence of these acetonitrile complexes give at least some hope that hydrated species might also exist but have not yet been discovered due to inappropriate synthetic approaches.^[14–16] To clarify the question about the existence or nonexistence of fully hydrated cations certainly remains one of the basic challenges in technetium (and rhenium) chemistry. Important hints for a possible existence are available from electrochemical studies; however, a focus on synthetic efforts is lacking so far.

Partially Hydrated Species

As outlined in the introduction the motivation behind the search for fully hydrated species is driven by the likely ease of the preparation of labelled compounds, besides fundamental aspects of course. Multidentate ligands are crucial in shielding the metal centre in biological media against transmetallation to other potentially coordinating sites. Such chelators have some drawbacks in the aqua-ion concept because of their relative bulky nature and little structural flexibility for tuning the chemical or biological properties of the bioconjugated complex.

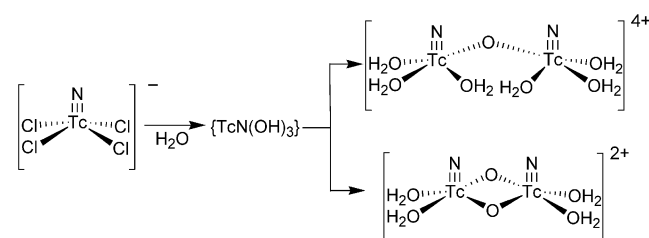
Hydrated Coordination Compounds

A basic concept in organometallic catalysis is the design of active complexes comprising an exchangeable ligand (a weakly bound solvent molecule for instance) together with nonreactive spectator ligands. The latter ones tune the properties of the metal centre while the former allow substrates to bind. Translating this approach to labelling chemistry: one or more water molecules would ideally be the exchangeable ligand(s) while the ligand sphere would be completed through further stably bound and innocent ligands. This aspect is very well mirrored in nature by the “heme” moiety, for instance, which is often referred to as a “different form of iron”.^[17] For labelling purposes (in contrast to catalysis), coordinated water has to exchange irreversibly for a ligand group that is attached via a spacer to a biomolecule. Probably one of the first structurally characterized^[18] technetium complexes comprising a water ligand was the so-called pink Tc^I complex *trans*-[Tc(NO)(NH₃)₄(OH₂)]Cl₂ with one coordinated water molecule *trans* to the [NO]⁺ ligand.^[19] This complex, for which the ruthenium as well as the osmium analogues exist, was reversibly oxidized at +0.8 V vs. NHE to the Tc^{II} complex [Tc(NO)(NH₃)₄(OH₂)]Cl₃.^[20] Although prepared a long time ago and belonging to the classical technetium complexes, no subsequent investigations into the (labelling) chemistry of this interesting complex have been performed. In particular, a very remarkable feature of [Tc(NO)(NH₃)₄(OH₂)]²⁺ is its pK_a value of 7.4 for the coordinated water, which is exceptionally low for a Tc^I centre.

As will become evident later, the reactivity of [⁹⁹Tc(NO)(NH₃)₄(OH₂)]²⁺ is related to [Tc(OH₂)₃(CO)₃]⁺. It also has similar structural principles as well as a pK_a value in the same range. Complex [Tc(NO)(NH₃)₄(OH₂)]²⁺ is stable in water and the single H₂O ligand is labilized by the *trans*-standing nitrosyl ligand. Therefore, it could potentially be exchanged for an anchoring group conjugated to a biomolecule. The synthesis of the ^{99m}Tc analogue for radiopharmaceutical purposes has not been attempted, and since [Tc(NO)(NH₃)₄(OH₂)]²⁺ could be a versatile building block for biomolecule labelling it merits more efforts in this direction.

One of the most unique examples of partially hydrated technetium complexes with the potential for labelling chemistry are hydrated Tc–nitrido complexes. Within the chemis-

try of the {Tc≡N}^{3+/2+} core, the Tc^{VI} complexes [TcNCl₄][−] and [TcNBr₄(OH₂)][−] have originally been prepared by the direct reaction of HCl with [TcO₄][−] in the presence of azide.^[21,22] The complex [TcNCl₄][−] is an important starting material for fundamental nitrido chemistry of technetium. The higher homologue [ReNCl₄][−] and the isovalent complexes [RuNCl₄][−] and [OsNCl₄][−] have also been described and are of basic importance as starting materials for nitrido chemistry of the corresponding elements.^[23] In aqueous solution, [TcNCl₄][−] hydrolyzes to what was originally called “nitridotechnetic acid”, [TcN(OH)₃]. Under acidic conditions partially hydrated complexes of the composition [(OH₂)₃NTc(μ-O)TcN(OH₂)₃]⁴⁺ and [(OH₂)₂NTc(μ-O)₂TcN(OH₂)₃]²⁺ formed, a behaviour that is unprecedented and did (and still does) not have parallels among the nitrido complexes of the neighbouring transition elements (Scheme 2).^[24]

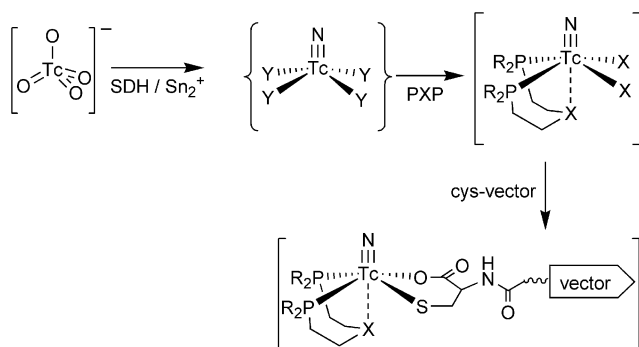


Scheme 2. The unique aqua ions of the Tc–nitrido core.^[24]

The actual importance of the {Tc≡N}^{3+/2+} core for labelling chemistry (see later) should encourage the study of the syntheses and nature of the ^{99m}Tc analogues. Although [Tc≡N]^{3+/2+} complexes are nowadays directly formed in situ, it would be an advantage to have {Tc≡N} aqua ions as starting materials. According to the concept of developing labelling procedures, different kinds of ligands could be evaluated with the same precursor and with regard to kinetic and thermodynamic behaviour. It has been said that the [Tc≡N]²⁺ core is extremely stable towards hydrolysis, thus, once formed, it should be present in solution as a partially or fully hydrated complex.^[25] Because of the high dilution of ^{99m}Tc complexes no bi- or oligometallic species would form, simply because a corresponding bimolecular reaction would be too slow.^[26] The appropriateness of these two dinuclear aqua ions of the [Tc≡N]³⁺ core has been shown with different ligands. One of the better known examples was the reaction with diethyl dithiocarbamates and related ligands in aqueous solution to give complexes [{⁹⁹TcN(S₂CNEt₂)₂(μ-O)₂}]²⁺.^[27]

In contrast to the isoelectronic [Tc=O]³⁺ core, which is the best studied structural motif in radiopharmaceutical chemistry, the [⁹⁹Tc≡N]^{3+/2+} core is more stable with regard to decomposition reactions. If not stabilized by strong chelators, complexes with the [⁹⁹Tc=O]³⁺ core tend to hydrolyze with subsequent disproportionation to ⁹⁹TcO₂ and [⁹⁹TcO₄][−], a behaviour that is not found for the [⁹⁹Tc≡N]^{3+/2+} core. A recent and innovative labelling method in which complexes of the type [^{99m}Tc≡N(PXP)Cl₂] (Scheme 3) were formed from water in a first step was based

on this stability. Succinic dihydrazide was the nitrido source and SnCl_2 the reducing agent.^[28–30] It should be noted at this point that the synthesis of nitrido complexes in the presence of b-type ligands always lead to Tc^{V} and not to Tc^{VI} compounds.^[31] In a subsequent step the two chloride ligands were substituted by a biomolecule pendent ligand (a cysteine for instance), which led to the irreversible labelling of the targeting molecule. Although the precursor complex did not explicitly contain a water ligand, it was speculated that H_2O mediates the exchange process.



Scheme 3. Preparation of $\{\text{Tc}\equiv\text{N}\}$ -based complexes in an aqueous environment. Y stands for H_2O or halide ligands, X = N or S.^[36]

Besides the complexes discussed above, technetium compounds containing H_2O as ligands are very rare and have not been explored systematically. Some compounds such as the dihydrated Tc^{I} complex $\text{trans}[\text{Tc}(\text{OH})_2(\text{dppe})_2]^+$ have been found as byproducts. Some water ligands were simply loosely bound in Tc complexes of the type $[\text{TcO}(\text{L}^4)(\text{OH}_2)]^+$ *trans* to the terminal oxido ligand but are of no relevance for substitution reactions.^[32] The oxido ligand exerts a strong *trans* influence and so substitution of water did not induce a labelling opportunity since any ligand in this position is too weakly bound. The structural motif $[\text{N}\equiv\text{Tc}-\text{OH}_2]^{2+}$ was also found in many complexes but, again, the position *trans* to the nitrido group is too unstable to be useful for irreversible labelling.^[33–35] It is interesting to note that the aforementioned “aqua ions” of technetium are rather found in low than in middle oxidation states. Even the nitrido “aqua ions” are only formally in the +VI oxidation state. The strong π -donor capacity of the nitrido ligand transfers electron density onto the Tc centre, thereby rendering it more b-type or soft. This explains the distinct tendency of the $[\text{Tc}\equiv\text{N}]^{2+}$ core to strongly bind to soft ligand atoms such as phosphorus or sulfur. The complex $\text{trans}[\text{Tc}(\text{OH})_2(\text{dppe})_2]^+$ is of particular interest since the oxidation state is Tc^{I} , a region in which typical organometallic ligands are expected but not usually water. This behaviour already sheds light on what will be discussed below about the existence of low-valent aqua ions of carbonyl-technetium complexes.

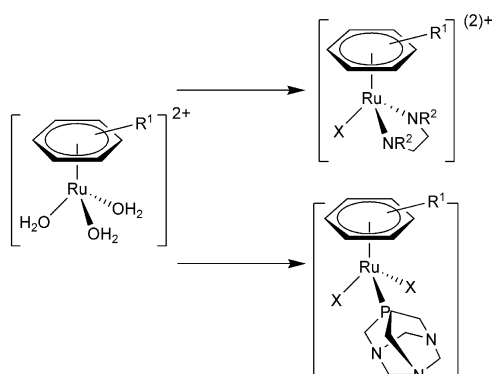
Hydrated Organometallic Compounds

The combination of H_2O and organometallic ligands on the same metal centre seems to be a conflicting idea. Tradi-

tionally, organometallic chemists fight against moisture (and oxygen). Typical soft ligands with π -acceptor capacities such as CO or carbocyclic ligands together with pure σ donors such as water or ammonia should not match the electronic properties of a given electronic configuration. Whereas the soft ligands would prefer electron-rich metals, the hard ligands prefer middle to high oxidation states and electron-deficient metal cations. What could happen (and does indeed) is the disproportionation into a soft and hard metal as found, e.g., for $[\text{Co}_2(\text{CO})_8]$ in the presence of amines.^[37] Still, organometallic aqua ions do exist. The last, comprehensive and excellent review on organometallic aqua ions appeared some 14 years ago!^[38] Since then only a small number of new organometallic aqua ions have been added to the list, filling the gap between classical soft organometallic complexes and (middle) hard coordination compounds. The scarcity of research towards mixed organometallic–water complexes is somewhat surprising since the advent of organometallic complexes in biology or medicine (bioorganometallic chemistry) is based in part on uncommon organometallic complexes or complex fragments.^[39] The first organometallic aqua ion (as we call it), $[(\eta^6\text{-C}_6\text{H}_6)\text{-M}(\text{OH}_2)_3]^{2+}$ (M = Ru, Os), was published as early as 1981. It can be considered as prototypical for the structure as well as for the reactivity of organometallic aqua ions.^[40] The reactivity pattern obeys what has been outlined in the introduction for the combination of metal complexes with e.g. targeting vectors. The three water molecules can be replaced by ligands attached to biomolecules leading to labelling, whereas the carbocyclic ligand acts “only” (but decisively) as a spectator ligand influencing the electronic properties and reactivities of the metal centre. Furthermore, taking the nonexistence of $[\text{Os}(\text{OH}_2)_6]^{2+}$ (in contrast to $[\text{Ru}(\text{OH}_2)_6]^{2+}$) into account, the existence of $[(\eta^6\text{-C}_6\text{H}_6)\text{Os}(\text{OH}_2)_3]^{2+}$ made the positive influence of the arene ligand on the electronic properties of the metal centre immediately obvious. Comparable to “heme” (a new form of iron), one can characterize the $[(\eta^6\text{-C}_6\text{H}_6)\text{Os}]^{2+}$ core as a new form of osmium in water. The stabilization of the d orbitals, going along with the coordination of the arene ring, is probably best mirrored by the $\text{p}K_{\text{a}}$ (3.5) of $[(\text{C}_6\text{H}_6)\text{Os}(\text{OH}_2)_3]^{2+}$ which is much closer to $\text{Ru}^{3+}(\text{aq})$ ($\text{p}K_{\text{a}} = 2.4$) than to the one estimated for $[\text{Ru}(\text{OH}_2)_6]^{2+}$ ($\text{p}K_{\text{a}} = 6\text{--}8$).^[41] The coordination of a π acceptor thus renders the metal centre substantially harder and opens it to coordination chemistry with σ donors, a relevant feature for application in biological or medicinal studies. It should not be forgotten that the aqua ligands also influence the metal centres along similar trends. The soft (oxidation sensitive) $[\text{Ru}(\text{OH}_2)_6]^{2+}$ for instance reacted with cyclooctadiene (COD) to form the unusual compound $[(\text{COD})\text{Ru}(\text{OH}_2)_4]^{2+}$, which was found to be of exceptionally high redox stability in contrast to $[\text{Ru}(\text{OH}_2)_6]^{2+}$ itself.^[42]

Complexes of the general type $[(\eta^6\text{-arene})\text{Ru}(\text{OH}_2)_3]^{2+}$, the lower homologues of the archetype $[(\eta^6\text{-C}_6\text{H}_6)\text{Os}(\text{OH}_2)_3]^{2+}$, have proven their versatility and suitability for application in the biomedical field in general and in the treatment of cancer in particular.^[43–46] These complexes

show a very high degree of flexibility with regard to ligand variability. Substituents on the arene ring have been altered in order to influence lipophilicity and pharmacokinetics, coligands that replaced one or more of the three aqua ions on the metal centre also changed the biochemical properties and probably the mode of action and, last but not least, targeting molecules have been conjugated for site specific drug delivery. Essentially, the availability of solvated ions in general and aqua ions in particular made this possible (Scheme 4).^[47–50]



Scheme 4. The prototypical behaviour of $[(\eta^6\text{-C}_6\text{H}_5\text{-R})\text{Ru}(\text{OH}_2)_3]^{2+}$ -based complexes: R^1 can be varied to modulate target affinity and specificity, ligands X influence reactivity and the additional ligands PTA (bottom) or en (top) determine the overall charge and physico-chemical behaviour.^[47–50]

It should be emphasized that a similar situation was also encountered for the group 9 elements. Down the cobalt-triad all three organometallic aqua ions $[(\text{Cp}^*)\text{M}(\text{OH}_2)_3]^{2+}$ exist and are important in bioorganometallic chemistry.^[39,51] We note that most of the mixed organometallic aqua complexes are formal d^6 or d^8 centres and other electronic configurations, if ever, are very rare. We also note that when going to the right in the transition-element series the organometallic coligands have increasing donating properties. The CO ligand is essentially not present, probably with the exception of $[\text{Ru}(\text{OH}_2)_5(\text{CO})]^{2+}$.^[52]

As discussed in the beginning, the situation for the manganese triad is similar. Where $[\text{Mn}(\text{OH}_2)_6]^{2+}$ and $[\text{Mn}(\text{OH}_2)_6]^{3+}$ exist, no pure aqua ion is known for technetium and rhenium so far. Conceptually and in parallel to the iron triad one would have to apply π -acceptor ligands in order to counterbalance the relatively high electron density on the metal cation for stabilizing an organometallic group 7 aqua ion of d^6 configuration. Hence, CO ligands come into play. We synthesized the Tc^{I} complex $[\text{TcCl}_3(\text{CO})_3]^{2-}$ directly from $[\text{TcO}_4]^-$. When dissolved in water, $[\text{TcCl}_3(\text{CO})_3]^{2-}$ quantitatively exchanged the three chlorides for water with the formation of a novel member in the series of organometallic aqua ions, namely $[\text{Tc}(\text{OH}_2)_3(\text{CO})_3]^+$.^[53–55] The corresponding rhenium complex $[\text{ReBr}_3(\text{CO})_3]^{2-}$ was directly prepared from $[\text{ReBr}(\text{CO})_5]$ and, upon dissolution in water, gave the analogous complex $[\text{Re}(\text{OH}_2)_3(\text{CO})_3]^+$. Since its original preparation a more direct route to $[\text{Re}(\text{OH}_2)_3(\text{CO})_3]^+$ has been developed, bypassing the preparation of $[\text{ReBr}_3(\text{CO})_3]^{2-}$ as a direct precursor.^[56] Upon refluxing

commercially available $[\text{ReBr}(\text{CO})_5]$ in water, the aqua ion was also formed in high yield. To complete the series, $[\text{Mn}(\text{OH}_2)_3(\text{CO})_3]^+$ was recently prepared from its acetone precursor $[\text{Mn}(\text{acetone})_3(\text{CO})_3]^+$.^[57,58] The crystal structures of $[\text{TcCl}_3(\text{CO})_3]^{2-}$ and, more importantly, of $[\text{Re}(\text{OH}_2)_3(\text{CO})_3]^+$ have been elucidated and are shown in Figure 2.^[59]

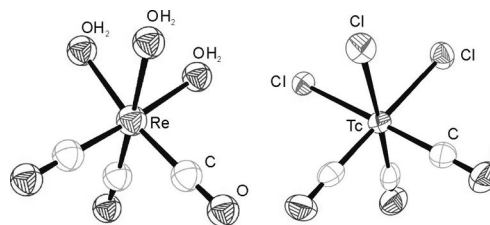


Figure 2. ORTEP representations of $[\text{Re}(\text{OH}_2)_3(\text{CO})_3]^+$ (left) and of the precursor complex $[\text{TcCl}_3(\text{CO})_3]^{2-}$ (right).^[59]

Basic Properties of $[\text{M}(\text{OH}_2)_3(\text{CO})_3]^+$ ($\text{M} = \text{Mn}, \text{Tc}, \text{Re}$)

The hydrolytic behaviour and the redox stability of these three organometallic aqua ions are of relevance with regard to application in bioorganometallic chemistry. We emphasize that complexes $[\text{M}(\text{OH}_2)_3(\text{CO})_3]^+$ offer an opportunity to directly compare the behaviour of homologous 3d, 4d and 5d elements, a situation that is not encountered among binary aqua complexes. As expected, a singly deprotonated complex $[\text{M}(\text{OH})(\text{OH}_2)_2(\text{CO})_3]$ is elusive since rapid condensation reactions lead to di- tri- and tetranuclear $\mu\text{-OH}$ -bridged species, some of which have been structurally characterized.^[60] However, the conjugated base $[\text{Re}(\text{OH})(\text{OH}_2)_2(\text{CO})_3]$ formally appeared in a recent crystal structure.^[59] Relevant numbers for mutual comparison are the $\text{p}K_a$ values. Because of the rapid (but reversible) formation of polynuclear species the $\text{p}K_a$ values were not directly accessible. They have been estimated to be 7–8 for rhenium^[61] and 9–10 for manganese.^[57] For technetium, a value in between the two extremes could be expected. These $\text{p}K_a$ values are surprisingly low for formal “ M^{+} ” aqua ions and mirror the electron-withdrawing effect of the CO ligands. The metal centre is rendered harder or more electron-deficient than what would be expected from a formal d^6 centre. With the biological or medicinal application of $[\text{M}(\text{OH}_2)_3(\text{CO})_3]^+$ in mind the water self-exchange rate is an important magnitude since it confines e.g. the rate of labelling of biomolecules or the direct interaction with natural ligands such as guanine. The self-exchange rate constants k_{ex} have been determined for all three elements and were found to be 23 s^{-1} for Mn, 0.49 s^{-1} for Tc^[62] and 0.0054 s^{-1} for Re^[63] at 298°C . This series impressively demonstrates the decrease of reaction rates down a triad. It follows the rate trends given in many inorganic text books. Manganese is about 5000 times faster than rhenium and about 100 times faster than technetium. The water self-exchange rates are relatively small for rhenium and technetium and rationalize the observed slow biomolecule labelling rates found with the radionuclides $^{99\text{m}}\text{Tc}$ or ^{188}Re . Indeed, heating is fre-

quently required to achieve a reasonable labelling rate especially if ligand (biomolecule) concentrations are relatively dilute.

Before discussing coordination chemistry the reactivity of $[\text{}^{99}\text{Tc}(\text{OH}_2)_3(\text{CO})_3]^+$ with CO in water shall briefly be touched on since it represents one of the few examples in literature in which H_2O was exchanged for CO under moderate conditions. In addition, it demonstrates that ^{99}Tc NMR spectroscopy is a very useful tool for characterizing different Tc complexes directly in solution.^[64] Under 44 bar of ^{13}CO , the CO ligands on the Tc centre exchanged with a rate of $0.82 \times 10^{-4} \text{ kg s}^{-1} \text{ mol}^{-1}$ at 277°K. The ^{99}Tc NMR spectrum initially showed a singlet.

Steadily a doublet, a triplet and finally a quadruplet appeared, indicating the complete exchange off all three ^{12}CO ligands by ^{13}CO . When the solution was kept under pressure for a longer time, new ^{99}Tc resonances came up, characteristic for the higher carbonyl complexes $[\text{}^{99}\text{Tc}(\text{OH}_2)_2(\text{CO})_4]^+$, $[\text{}^{99}\text{Tc}(\text{OH}_2)(\text{CO})_5]^+$ and finally $[\text{}^{99}\text{Tc}(\text{CO})_6]^+$.^[65] After CO pressure was released all complexes with more than three CO ligands lost the “excess” CO very rapidly and returned to the original complex $[\text{}^{99}\text{Tc}(\text{OH}_2)_3(\text{CO})_3]^+$. Since $[\text{}^{99}\text{Tc}(\text{CO})_6]^+$ partly precipitated from the aqueous solution as $[\text{}^{99}\text{Tc}(\text{CO})_6][\text{ClO}_4]$, it was possible to isolate this compound. The corresponding NMR spectra are depicted in Figure 3.

The availability and convenience of $[\text{M}(\text{OH}_2)_3(\text{CO})_3]^+$ -type complexes raised the question about carbonyl-aqua complexes with more or less than three CO ligands. The aforementioned NMR investigations clearly showed that Tc complexes with more than three CO ligands replaced “excess” CO very rapidly by water with the formation of the thermodynamic product $[\text{}^{99}\text{Tc}(\text{OH}_2)_3(\text{CO})_3]^+$ because of the strong *trans* effect. The situation with manganese might be

more extreme whereas rhenium is a promising candidate owing to its slower kinetics. Numerous attempts to prepare $[\text{M}(\text{OH}_2)_4(\text{CO})_2]^+$ or $[\text{M}(\text{OH}_2)_5(\text{CO})]^+$ in our and other groups have proved unsuccessful so far. Supposedly, inappropriate synthetic approaches were chosen or more likely the d^6 metal centre became strongly reducing upon release of one CO and was simply oxidized by water. Indeed, recent theoretical calculations showed *fac*- $[\text{}^{99}\text{Tc}(\text{OH}_2)_3(\text{CO})_3]^+$ to be the most stable form by far. Only the homoleptic complex $[\text{}^{99}\text{Tc}(\text{CO})_6]^+$ is more stable but this is of less interest in the context of aqueous chemistry.^[66] It is worth mentioning that the nitrosyl-carbonyl-aqua ion *fac*- $[\text{M}(\text{NO})(\text{CO})_2(\text{OH}_2)_3]^{2+}$ ($\text{M} = ^{99}\text{Tc}, \text{Re}$) has been synthesized and characterized in a number of new complexes.^[67–71] The chemistry in water starting from $[\text{MCl}_3(\text{NO})(\text{CO})_2]^-$ is more difficult since the corresponding aqua complex was very acidic and underwent rapid and essentially irreversible formation of $\mu\text{-OH-}$ or $\mu\text{-O-}$ bridged polynuclear species. Still the corresponding $^{99\text{m}}\text{Tc}$ complexes were synthesized and used for the labelling of biomolecules. Since the concentrations of $^{99\text{m}}\text{Tc}$ are in the nM to mM range, oligomerization did not occur for kinetic reasons.

The well-explored characteristics and interesting properties of $[\text{}^{99}\text{Tc}(\text{OH}_2)_3(\text{CO})_3]^+$ in water initiated endeavours of preparing the analogous $^{99\text{m}}\text{Tc}$ complex. The incentive of preparing carbonyl complexes in water was induced by potential applications in radiopharmacy. Whereas carbonyl complexes are generally prepared under high pressure, such a procedure is evidently not applicable in clinical practice. The key idea to the solution of making CO complexes in water was a very simple compound, which was described for the first time a long time ago.^[72] The boranocarbonate compound $[\text{H}_3\text{BCO}_2\text{H}]^-$ combines reductive properties with

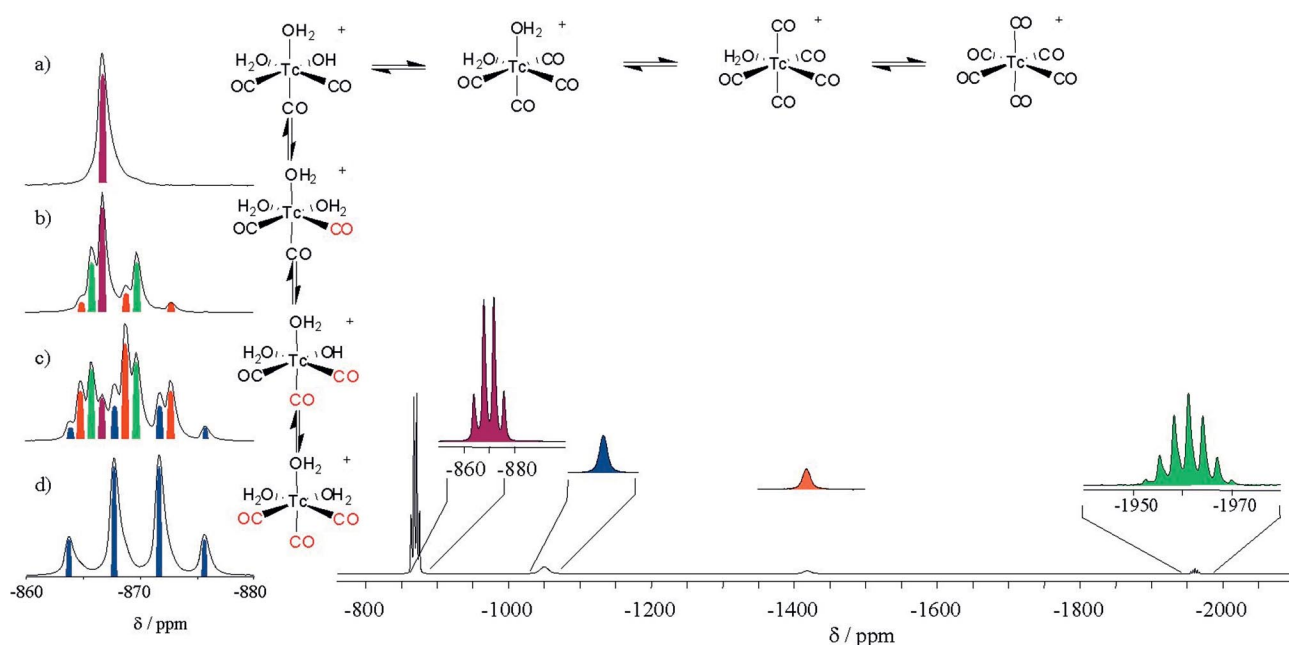


Figure 3. ^{99}Tc NMR spectra of the stepwise $^{12}\text{CO} \rightarrow ^{13}\text{CO}$ exchange (vertical) and the complete carbonylation after extended time.^[65]

the characteristics of an in situ CO source. This compound was finally the key to a synthesis that provided the $^{99m}\text{Tc}^{\text{I}}$ aqua ion in quantitative yield.^[73,74] The preparation of the ^{188}Re homologue demonstrated not only gradual but principle differences between the two elements. Technetium and rhenium are often characterized as a “matched pair”, however, the synthesis of $[\text{}^{188}\text{Re}(\text{OH}_2)_3(\text{CO})_3]^+$ did not work under the same conditions and a different approach had to be developed.^[75,76] Although the mechanisms of both approaches remain elusive, the straightforward way to tricarbonyl complexes encourages the, so far unsuccessful, search for novel aqua ions with less CO ligands, other spectator ligands or even different metal centres.

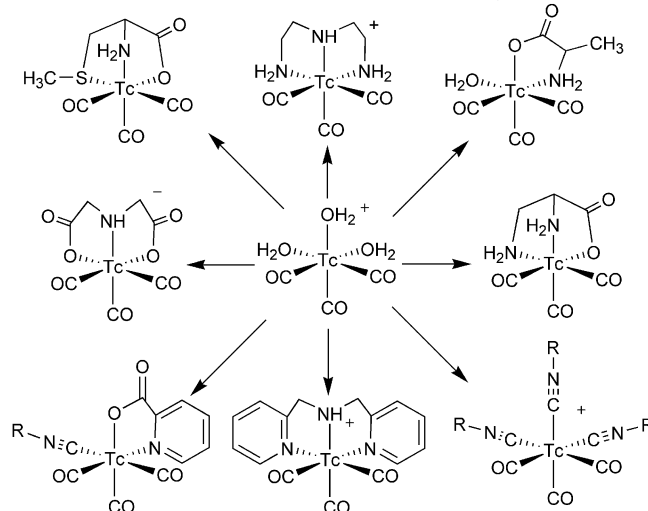
Basic Chemistry of $[\text{M}(\text{OH}_2)_3(\text{CO})_3]^+$ in Water

The beauty of aqua-ion chemistry is the principal reversibility of their coordination chemistry, even if hydroxo- or oxo-bridged oligonuclear species are formed. This was especially shown for the above mentioned M^{3+} family ($\text{M} = {}^{67}\text{Ga}$, ${}^{90}\text{Y}$, ${}^{111}\text{In}$, ${}^{177}\text{Lu}$ and others) for the labelling of targeting molecules. Labelling with aqua ions proceeded smoothly according to equilibrium in solution and without the need for performing redox chemistry or the introduction of stabilizing intermediates. The same situation was encountered with $[\text{M}(\text{OH}_2)_3(\text{CO})_3]^+$ for which fundamental aspects of coordination or organometallic chemistry became accessible and allowed the design and syntheses of appropriate bioconjugates for molecular imaging or therapy.^[77]

Coordination Chemistry with $[\text{M}(\text{OH}_2)_3(\text{CO})_3]^+$

Since the availability and aqueous properties of $[\text{ReBr}_3(\text{CO})_3]^{2-}$ and $[\text{}^{99}\text{TcCl}_3(\text{CO})_3]^{2-}$ have been elucidated, numerous coordination compounds with the *fac*- $[\text{M}(\text{CO})_3]^+$ core have been synthesized and characterized from reactions in water.^[2,78,79] Because of the strong M–C bonds and the kinetic stability of the complexes the CO ligands were generally not cleaved in these reactions. Consequently, coordination chemistry was performed with an aqua complex comprising only three replaceable water ligands and not six, as commonly encountered in aqua ions. Owing to the kinetic stability of the Tc^{I} core, complexes with monobi- and tridentate ligands are equally stable and hardly decomposed under physiological conditions. Complexes with the all classical “Werner-type ligands” have been described and utilized in labelling. A small (and arbitrary) selection is given in Scheme 5.

Besides the normal coordination compounds, some complexes exhibited very particular and uncommon features in water. Worth mentioning is the formation of $[\text{BH}_4]^-$ -based complexes with coordinating, bridging hydrides from water. Bridging hydrides are, if ever, found in typical organometallic chemistry but not in water. Aqueous solutions of



Scheme 5. A small selection of coordination compounds prepared from the organometallic aqua ion $[\text{}^{99}\text{Tc}(\text{OH}_2)_3(\text{CO})_3]^+$ directly in water.

$[\text{}^{99}\text{Tc}(\text{OH}_2)_3(\text{CO})_3]^+$ and $[\text{}^{99m}\text{Tc}(\text{OH}_2)_3(\text{CO})_3]^+$ formed these complexes very efficiently and, for ^{99m}Tc , at very low ligand concentrations.^[80,81] ORTEP diagrams of these compounds are given in Figure 4.

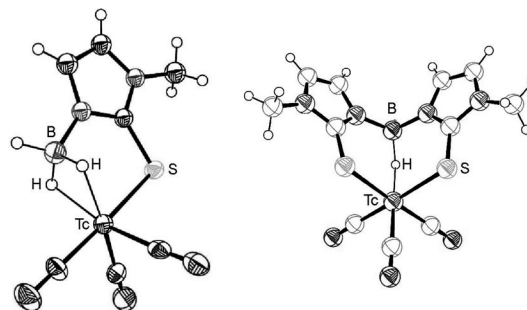
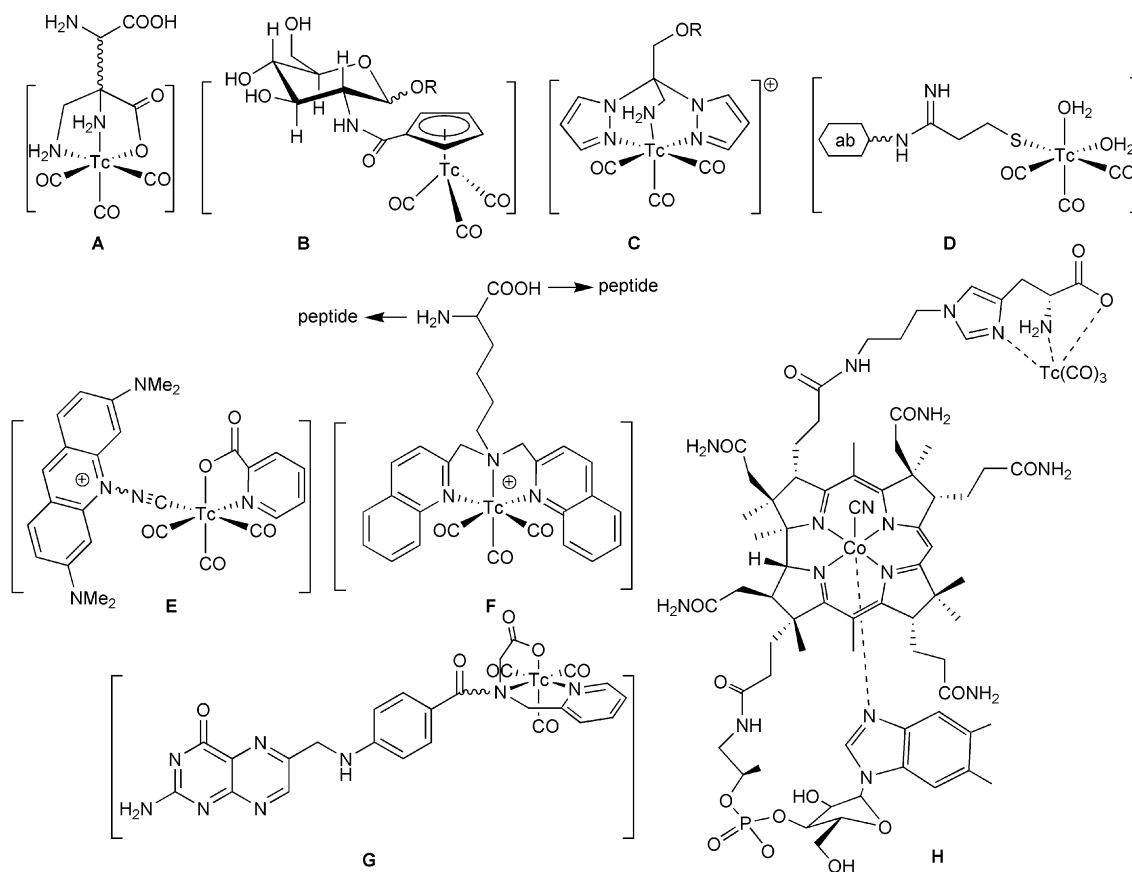


Figure 4. Unusual complexes with $(\mu\text{-H})$ and $(\mu\text{-H})_2$ motifs from the reaction of $[\text{}^{99}\text{Tc}(\text{OH}_2)_3(\text{CO})_3]^+$ with the corresponding ligands in water.^[80,81]

Because of the high ligand variability able to stably coordinate to the *fac*- $[\text{}^{99m}\text{Tc}(\text{CO})_3]^+$ and *fac*- $[\text{}^{188/186}\text{Re}(\text{CO})_3]^+$ core, the properties of a complex pendant to a targeting biomolecule could conveniently be tuned by proper ligand selection. Accordingly, practically all different kinds of biomolecules have been labelled via simple coordination chemistry with an aqua ion of technetium. The high affinity for aromatic amines for instance has been beneficial for the direct labelling of recombinant antibodies bearing a pentahistidine tag^[82] or by direct interaction with adenoviruses.^[83] Strong efforts have been undertaken to label the metabolic tracer vitamin B_{12} . One of these compounds recently entered clinical trials.^[84–86] A major focus in radiopharmaceutical research is the replacement of the ^{18}F FDG with ^{99m}Tc compounds. Since glucose is a relatively sensitive molecule, the combination of an aqua ion with a chelator conjugated to glucose would be ideal.^[87–89] Still, all ap-



Scheme 6. Selected examples of labelled biomolecules starting from the aqua ion $[^{99\text{m}}\text{Tc}(\text{OH}_2)_3(\text{CO})_3]^+$: labelled amino acid (A), $[^{99\text{m}}\text{Tc}]$ labelled glucose (B), $[^{100\text{m}}\text{Tc}]$ new type of myocardial imaging agent (C), $[^{99\text{m}}\text{Tc}]$ labelling of antibodies via iminothiolane derivatization (D), $[^{101\text{m}}\text{Tc}]$ nuclear-targeting agent (E), $[^{94\text{m}}\text{Tc}]$ peptide labelling via the SAAC approach (F), $[^{96\text{m}}\text{Tc}]$ labelled folate (G) and vitamin B₁₂ (H).^[102]

proaches have not yet led to a new, bioactive $^{99\text{m}}\text{Tc}$ -analogue of ^{18}F FDG but this is rather related to the high selectivity of the glucose transporter GLUT-1 than to an inappropriate design of the radio-bioconjugate. An inspiring review was recently introduced in carbohydrate research related to $^{99\text{m}}\text{Tc}$ radiopharmacy.^[90] Promising new cationic compounds have been synthesized for myocardial imaging, complementing the current standard Cardiolite®.^[91] A new direction in $^{99\text{m}}\text{Tc}$ radiopharmacy and chemistry was followed with attempts to target the cell nucleus. Complexes bearing a pendent nuclear-targeting agent such as acridine-orange or nuclear localizing sequence (NLS) peptides have been shown by fluorescence microscopy to accumulate in the cell nucleus. Thereby, the Auger electrons emitted from the isomeric transition may become opportune for therapeutic purposes besides classical imaging.^[92–95] In the context of combined fluorescence-radioimaging the metal-dependent luminescence of rhenium amino-heterocycle complexes has been used to detect the localization of peptides on a cellular level. So-called single amino acid chelates (SAAC) were incorporated in the targeting fMLF sequence and then used for in vitro screening.^[96–98] A selection of the discussed targeting agents are shown in Scheme 6.

Classical coordination chemistry with the $[\text{M}(\text{OH}_2)_3(\text{CO})_3]^+$ aqua ion also led to the syntheses of simple tripod ligands that have not been synthesized before. A representa-

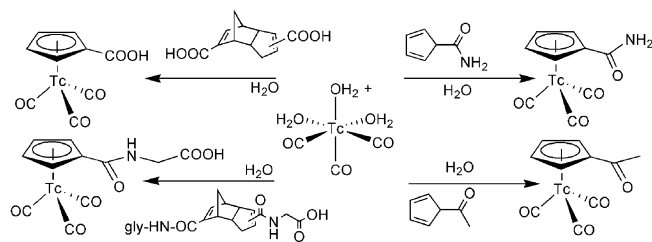
tive example is a tripod N_2O ligand that was connected via the bridgehead carbon to an amino acid functionality (Scheme 6 compound A). The objective of this approach was the labelling of amino acids with the retention of their active transportation through the transmembrane protein LAT-1, an amino acid transporter for various neutral and natural amino acids. Despite the comparatively bulky metal complex attached to one of the smallest biological functionalities, it was possible for the first time to obtain a metal-labelled small molecule that is still recognized by the transporter and actively carried into a cell.^[99] The selection given in Scheme 6 is far from being comprehensive and just intended to depict some examples that underline the biological importance of group 7 aqua ions.

We emphasize that the widespread biomedical research and development as described above was initiated by the availability of aqua ions. The highly specific introduction of complex moieties into derivatised biomolecules requires facile and smooth coordination to a ligand of choice for which the simple replacement of water ligands is the most convenient approach. If one compares the coordination chemistry of $[\text{M}(\text{OH}_2)_3(\text{CO})_3]^+$ to that of the $\text{M}^{3+}(\text{aq})$ family, the importance of kinetic stability becomes evident. Whereas the labile M^{3+} cations require multidentate (e.g. DOTA or DTPA) ligands for in vivo stabilization of the metal cations, the *fac*- $[\text{M}(\text{CO})_3]^+$ core can even be stabilized

by a monodentate ligand. Thereby a substantially higher degree of flexibility is introduced as compared to $M^{3+}(\text{aq})$.

Organometallic Chemistry with $[\text{M}(\text{OH}_2)_3(\text{CO})_3]^+$ in Water

The previous section described common coordination chemistry with an organometallic fragment in water. A consequent next step were investigations into replacing H_2O by classical organometallic ligands. For manganese and rhenium this was achieved by working in organic solvents. For technetium, however, reactions in water are essential if one aims at using such complexes in imaging or, for rhenium, in therapy (see Introduction).^[103] Until recently this constraint excluded classical organometallic ligands such as cyclopentadienyl because of incompatibility with water. Of course, text book complexes such as the piano-stool-type cymantrene analogue “cytctrene” have been known for a while but have been prepared along traditional routes. With $^{99\text{m}}\text{Tc}$ some techniques have been developed to access $[\text{C}_5\text{H}_5]^-$ complexes. Still, these applied high temperatures and organic solvents are hardly applicable on a routine level.^[104–106] Complexes of the type $[(\text{Cp-R})^{99\text{m}}\text{Tc}(\text{CO})_3]$ would be particularly interesting since it has been shown many times in bioorganometallic chemistry that piano-stool-structured compounds can topologically mimic phenyl rings in pharmaceuticals.^[107–109] Whereas cyclopentadiene is insoluble and unstable in water, we found acetylcyclopentadiene (AHCp) to have a $\text{p}K_{\text{a}}$ in water of about 8 and to decompose only very slowly. Consequently, some AHCp was soluble in water and reacted with $^{99\text{m}}\text{Tc}(\text{OH}_2)_3(\text{CO})_3]^+$ like a normal “Werner-type ligand” with the formation of $[(\text{AHCp})\text{Tc}(\text{CO})_3]$.^[110,111] Such aqueous cyclopentadienyl chemistry was unprecedented and exclusively based on the presence of an organometallic aqua ion. The reaction involves the submission of metal–aqua ions other than those of group 7 to similar reactions with the scope of preparing e.g. novel mixed Cp– H_2O complexes with other metal cations, thus far unknown or inaccessible (Scheme 7).



Scheme 7. Reaction of $^{99\text{m}}\text{Tc}(\text{OH}_2)_3(\text{CO})_3]^+$ with cyclopentadiene derivatives and some Diels–Alder dimerized compounds.^[110,112]

Extending the water chemistry of cyclopentadiene derivatives we found that the direct reaction of $^{99\text{m}}\text{Tc}(\text{OH}_2)_3(\text{CO})_3]^+$ with Diels–Alder dimerized HCp derivatives led directly to the corresponding $[(\text{Cp-R})^{99\text{m}}\text{Tc}(\text{CO})_3]$ compounds (Scheme 7). Whereas cyclopentadiene derivatives are more or less air and water sensitive the dimerized products are not. Again, this unexpected reaction introduced a great degree of flexibility in applying the cyclopentadienyl

ligand for the labelling of biomolecules. Mechanistically, we proposed that the retro Diels–Alder reaction depicted in Scheme 7 was metal mediated with concomitant coordination to the *fac*- $^{99\text{m}}\text{Tc}(\text{CO})_3]^+$ core.^[112] Along this route, the application of piano-stool complexes as mimics of phenyl rings in pharmacophores became a real option. As a kind of analogy to cyclopentadienyl chemistry in water, carboranes have been introduced as ligands in a purely aqueous environment.^[113,114] Carboranes have been coordinated to aqua ions in water, for instance to $\text{Co}^{2+}(\text{aq})$ in the well-known fly-trap approach,^[115] and the chemistry of Mn–, Re– and Tc–carbonyl complexes behaved analogously.

This section discussed a few unexpected examples of organometallic chemistry in water with aqua ions of the group 7 elements. Although the formed complexes are nothing special from a chemical point of view, the route to synthesizing them in high yield was innovative. The solution to the challenging question about how to synthesize a particular type of complex starting from aqua ions (or initially from permethylates) was the incentive, rather than the complexes as such. These novel, aqua-ion-based approaches have enabled new fields of application in molecular imaging and therapy to be tackled, an opportunity that was followed by many renowned research groups.

Conclusions

It was the objective of this microreview to introduce the chemistry of aqua ions in the manganese triad elements, particularly those complexes related to biomedical applications. Whereas the aqua ion of Mn^{2+} does exist, no binary aqua ions for the higher homologues are known. One of the decisive advantages of aqua ions is the reduction of the labelling step to purely ligand-exchange based coordination chemistry. No parallel redox reactions or the exchange of strong auxiliary ligands bound to the metal centre are required. The preparation of the organometallic aqua ions $[\text{M}(\text{OH}_2)_3(\text{CO})_3]^+$ rendered such a strategy possible. The exploration of numerous new fields in inorganic biomedical chemistry is in support of this conclusion. Since the complexes exist for all group 7 elements, basic chemical insights into physico-chemical trends along this series could also be obtained. The fact that only a minor number of compounds have found entry into clinical trials may not mirror chemical drawbacks but rather the interest and the focuses of the market. Still, the application of aqua ions is of great promise and this microreview is aimed at inspiring the search for similar organometallic aqua ions with other transition elements likely to exist.

Acknowledgments

Financial support from Tyco-Mallinckrodt Med. B.V., Petten, The Netherlands and the Bundesamt für Wissenschaft und Technik, Switzerland (COST D39) is acknowledged. Special thanks go to Dr. Hector Knight and Dr. Geert Ensing for their ongoing interest in and support of this project.

- [1] R. Alberto, *Comprehensive Coordination Chemistry II* (Eds.: J. A. McCleverty, T. J. Meyer), Elsevier Science, Amsterdam, **2003**, pp. 127–271.
- [2] S. R. Banerjee, K. P. Maresca, L. Francesconi, J. Valliant, J. W. Babich, J. Zubieta, *Nucl. Med. Biol.* **2005**, *32*, 1–20.
- [3] K. Schwachau *Technetium - Chemistry and Radiopharmaceutical Applications*, Wiley-VCH, Weinheim (Germany), **2000**, 446.
- [4] R. E. Weiner, M. L. Thakur, *Biodrugs* **2005**, *19*, 145–163.
- [5] A. Lin, M. E. Ray, *Cancer Metastasis Rev.* **2006**, *25*, 669–675.
- [6] B. J. Lewis, W. T. Thompson, F. Akbari, C. Morrison, A. Husain, *J. Nucl. Mater.* **2005**, *340*, 69–82.
- [7] D. T. Richens, *The Chemistry of Aqua Ions*, 1st ed., Wiley & Sons, Chichester, **1997**.
- [8] P. Bernhard, H. B. Burgi, J. Hauser, H. Lehmann, A. Ludi, *Inorg. Chem.* **1982**, *21*, 3936–3941.
- [9] E. F. Hills, M. Moszner, A. G. Sykes, *Inorg. Chem.* **1986**, *25*, 339–341.
- [10] P. Beutler, H. Gamsjager, *J. Chem. Soc., Chem. Commun.* **1976**, 554–555.
- [11] C. L. Rulfs, R. Pacer, A. Anderson, *J. Electroanal. Chem.* **1967**, *15*, 61–66.
- [12] C. L. Rulfs, R. A. Pacer, R. F. Hirsch, *J. Inorg. Nucl. Chem.* **1967**, *29*, 681–691.
- [13] C. D. Russell, A. G. Cash, *J. Electroanal. Chem.* **1978**, *92*, 85–99.
- [14] J. C. Bryan, F. A. Cotton, L. M. Daniels, S. C. Haefner, A. P. Sattelberger, *Inorg. Chem.* **1995**, *34*, 1875–1883.
- [15] F. A. Cotton, S. C. Haefner, A. P. Sattelberger, *J. Am. Chem. Soc.* **1996**, *118*, 5486–5487.
- [16] F. A. Cotton, S. C. Haefner, A. P. Sattelberger, *Inorg. Chim. Acta* **1997**, *266*, 55–63.
- [17] S. J. Lippard, J. M. Berg *Principles of Bioinorganic Chemistry*, University Science Books, Mill Valley, California, **1994**.
- [18] L. J. Radonovich, J. L. Hoard, *J. Phys. Chem.* **1984**, *88*, 6711–6716.
- [19] J. D. Eakins, D. G. Humphreys, C. E. Mellish, *J. Chem. Soc.* **1963**, *24/138*, 6012–6016.
- [20] R. A. Armstrong, H. Taube, *Inorg. Chem.* **1976**, *15*, 1904–1909.
- [21] J. Baldas, S. F. Colmanet, G. A. Williams, *Inorg. Chim. Acta* **1991**, *179*, 189–194.
- [22] J. Baldas, J. Bonnyman, G. A. Williams, *J. Chem. Soc., Dalton Trans.* **1984**, 833–837.
- [23] K. Dehnicke, J. Strahle, *Angew. Chem. Int. Ed. Engl.* **1981**, *20*, 413–426.
- [24] J. Baldas, J. F. Boas, Z. Ivanov, B. D. James, *Inorg. Chim. Acta* **1993**, *204*, 199–212.
- [25] J. Baldas, S. F. Colmanet, *Inorg. Chim. Acta* **1990**, *176*, 1–3.
- [26] J. Baldas, J. Bonnyman, *Int. J. Appl. Radiat. Isot.* **1985**, *36*, 133–139.
- [27] J. Baldas, J. F. Boas, S. F. Colmanet, G. A. Williams, *J. Chem. Soc., Dalton Trans.* **1992**, 2845–2853.
- [28] C. Bolzati, A. Boschi, A. Duatti, S. Prakash, L. Uccelli, *J. Am. Chem. Soc.* **2000**, *122*, 4510–4511.
- [29] C. Bolzati, L. Uccelli, A. Boschi, S. Prakash, E. Malago, A. Duatti, A. Piffanelli, F. Refosco, F. Tisato, *J. Nucl. Med.* **2000**, *41*, 248p–248p.
- [30] A. Boschi, C. Bolzati, E. Benini, E. Malago, L. Uccelli, A. Duatti, A. Piffanelli, F. Refosco, F. Tisato, *Bioconjugate Chem.* **2001**, *12*, 1035–1042.
- [31] A. Boschi, A. Duatti, L. Uccelli, *Top. Curr. Chem.* **2005**, *252*, 85–115.
- [32] R. Hübener, U. Abram, W. Hiller, *Acta Crystallogr., Sect. C* **1994**, *50*, 188–190.
- [33] A. Marchi, R. Rossi, L. Magon, A. Duatti, U. Casellato, R. Graziani, M. Vidal, F. Riche, *J. Chem. Soc., Dalton Trans.* **1990**, 1935–1940.
- [34] Y. Kani, T. Takayama, S. Inomata, T. Sekine, H. Kudo, *Chem. Lett.* **1995**, 1059–1060.
- [35] Y. Kani, T. Takayama, T. Sekine, H. Kudo, *J. Chem. Soc., Dalton Trans.* **1999**, 209–213.
- [36] C. Bolzati, A. Mahmood, E. Malago, L. Uccelli, A. Boschi, A. G. Jones, F. Refosco, A. Duatti, F. Tisato, *Bioconjugate Chem.* **2003**, *14*, 1231–1242.
- [37] C. K. Jørgensen, *Inorg. Chem.* **1964**, *3*, 1201–1202.
- [38] U. Koelle, *Coord. Chem. Rev.* **1994**, *135*, 623–650.
- [39] R. H. Fish, G. Jaouen, *Organometallics* **2003**, *22*, 2166–2177.
- [40] Y. Hung, W. J. Kung, H. Taube, *Inorg. Chem.* **1981**, *20*, 457–463.
- [41] I. Rapaport, L. Helm, A. E. Merbach, P. Bernhard, A. Ludi, *Inorg. Chem.* **1988**, *27*, 873–879.
- [42] U. Kolle, G. Flunkert, R. Gorissen, M. U. Schmidt, U. Englert, *Angew. Chem. Int. Ed. Engl.* **1992**, *31*, 440–442.
- [43] M. J. Hannon, *Pure Appl. Chem.* **2007**, *79*, 2243–2261.
- [44] W. H. Ang, P. J. Dyson, *Eur. J. Inorg. Chem.* **2006**, 4003–4018.
- [45] P. J. Dyson, G. Sava, *Dalton Trans.* **2006**, 1929–1933.
- [46] Y. K. Yan, M. Melchart, A. Habtemariam, P. J. Sadler, *Chem. Commun.* **2005**, 4764–4776.
- [47] C. Scolaro, T. J. Geldbach, S. Rochat, A. Dorcier, C. Gossens, A. Bergamo, M. Cocchietto, I. Tavernelli, G. Sava, U. Rothlisberger, P. J. Dyson, *Organometallics* **2006**, *25*, 756–765.
- [48] B. Serli, E. Zangrando, T. Gianferrara, C. Scolaro, P. J. Dyson, A. Bergamo, E. Alessio, *Eur. J. Inorg. Chem.* **2005**, 3423–3434.
- [49] A. Habtemariam, M. Melchart, R. Fernandez, S. Parsons, I. D. H. Oswald, A. Parkin, F. P. A. Fabbiani, J. E. Davidson, A. Dawson, R. E. Aird, D. I. Jodrell, P. J. Sadler, *J. Med. Chem.* **2006**, *49*, 6858–6868.
- [50] S. J. Dougan, P. J. Sadler, *Chimia* **2007**, *61*, 704–715.
- [51] S. Ogo, O. Buriez, J. B. Kerr, R. H. Fish, *J. Organomet. Chem.* **1999**, *589*, 66–74.
- [52] G. Laurenczy, L. Helm, A. Ludi, A. E. Merbach, *Helv. Chim. Acta* **1991**, *74*, 1236–1238.
- [53] R. Alberto, R. Schibli, A. Egli, P. A. Schubiger, W. A. Herrmann, G. Artus, U. Abram, T. A. Kaden, *J. Organomet. Chem.* **1995**, *493*, 119–127.
- [54] R. Alberto, R. Schibli, R. Waibel, U. Abram, A. P. Schubiger, *Coord. Chem. Rev.* **1999**, *192*, 901–919.
- [55] R. Alberto, D. Angst, U. Abram, K. Ortner, T. A. Kaden, A. P. Schubiger, *Chem. Commun.* **1999**, 1513–1514.
- [56] N. Lazarova, S. James, J. Babich, J. Zubieta, *Inorg. Chem. Commun.* **2004**, *7*, 1023–1026.
- [57] U. Prinz, U. Koelle, S. Ulrich, A. E. Merbach, O. Maas, K. Hegetschweiler, *Inorg. Chem.* **2004**, *43*, 2387–2391.
- [58] D. A. Edwards, J. Marshalsea, *J. Organomet. Chem.* **1977**, *131*, 73–91.
- [59] R. S. Herrick, C. J. Ziegler, A. Cetin, B. R. Franklin, *Eur. J. Inorg. Chem.* **2007**, 1632–1634.
- [60] A. Egli, K. Hegetschweiler, R. Alberto, U. Abram, R. Schibli, R. Hedinger, V. Gramlich, R. Kissner, P. A. Schubiger, *Organometallics* **1997**, *16*, 1833.
- [61] R. Alberto, A. Egli, U. Abram, K. Hegetschweiler, V. Gramlich, P. A. Schubiger, *J. Chem. Soc., Dalton Trans.* **1994**, 2815–2820.
- [62] P. V. Grundler, L. Helm, R. Alberto, A. E. Merbach, *Inorg. Chem.* **2006**, *45*, 10378–10390.
- [63] B. Salignac, P. V. Grundler, S. Cayemittes, U. Frey, R. Scopelliti, A. E. Merbach, R. Hedinger, K. Hegetschweiler, R. Alberto, U. Prinz, G. Raabe, U. Kolle, S. Hall, *Inorg. Chem.* **2003**, *42*, 3516–3526.
- [64] L. A. O'Connell, R. M. Pearlstein, A. Davison, J. R. Thornback, J. F. Kronauge, A. G. Jones, *Inorg. Chim. Acta* **1989**, *161*, 39–43.
- [65] N. Aebischer, R. Schibli, R. Alberto, A. E. Merbach, *Angew. Chem. Int. Ed.* **2000**, *39*, 254–256.
- [66] X. Y. Wang, Y. Wang, X. Q. Liu, T. W. Chu, S. W. Hu, X. H. Wei, B. L. Liu, *Phys. Chem. Chem. Phys.* **2003**, *5*, 456–460.
- [67] D. Rattat, A. Verbruggen, H. Berke, R. Alberto, *J. Organomet. Chem.* **2004**, *689*, 4833–4836.

- [68] D. Rattat, A. Verbruggen, H. Schmalte, H. Berke, R. Alberto, *Tetrahedron Lett.* **2004**, 45, 4089–4092.
- [69] R. Schibli, N. Marti, P. Maurer, B. Spingler, M. L. Lehaire, V. Gramlich, C. L. Barnes, *Inorg. Chem.* **2005**, 44, 683–690.
- [70] P. Kurz, D. Rattat, D. Angst, H. Schmalte, B. Spingler, R. Alberto, H. Berke, W. Beck, *Dalton Trans.* **2005**, 804–810.
- [71] N. Marti, B. Spingler, F. Breher, R. Schibli, *Inorg. Chem.* **2005**, 44, 6082–6091.
- [72] L. J. Malone, R. W. Parry, *Inorg. Chem.* **1967**, 6, 817–822.
- [73] R. Alberto, K. Ortner, N. Wheatley, R. Schibli, A. P. Schubiger, *J. Am. Chem. Soc.* **2001**, 123, 3135–3136.
- [74] R. Alberto, R. Schibli, A. Egli, A. P. Schubiger, U. Abram, T. A. Kaden, *J. Am. Chem. Soc.* **1998**, 120, 7987–7988.
- [75] R. Schibli, R. Schwarzbach, R. Alberto, K. Ortner, H. Schmalte, C. Dumas, A. Egli, P. A. Schubiger, *Bioconjugate Chem.* **2002**, 13, 750–756.
- [76] S. H. Park, S. Seifert, H. J. Pietzsch, *Bioconjugate Chem.* **2006**, 17, 223–225.
- [77] N. Metzler-Nolte, *Angew. Chem. Int. Ed.* **2001**, 40, 1040–1042.
- [78] S. Liu, *Chem. Soc. Rev.* **2004**, 33, 445–461.
- [79] R. Schibli, P. A. Schubiger, *Eur. J. Nucl. Med. Mol. Imaging* **2002**, 29, 1529–1542.
- [80] R. Garcia, A. Paulo, A. Domingos, I. Santos, K. Ortner, R. Alberto, *J. Am. Chem. Soc.* **2000**, 122, 11240–11241.
- [81] L. Maria, A. Paulo, I. C. Santos, I. Santos, P. Kurz, B. Spingler, R. Alberto, *J. Am. Chem. Soc.* **2006**, 128, 14590–14598.
- [82] R. Waibel, R. Alberto, J. Willuda, R. Finnnern, R. Schibli, A. Stichelberger, A. Egli, U. Abram, J. P. Mach, A. Plueckthun, P. A. Schubiger, *Nat. Biotechnol.* **1999**, 17, 897–901.
- [83] S. M. Verwijnen, P. A. E. S. Smitt, H. Knight, W. A. P. Bree-man, R. C. Hoeben, L. Wiebe, E. P. Krenning, M. de Jong, *Eur. J. Nucl. Med. Mol. Imaging* **2004**, 31, S210.
- [84] S. Kunze, F. Zobi, P. Kurz, B. Spingler, R. Alberto, *Angew. Chem. Int. Ed.* **2004**, 43, 5025–5029.
- [85] D. R. van Staveren, R. Waibel, S. Mundwiler, P. A. Schubiger, R. Alberto, *J. Organomet. Chem.* **2004**, 689, 4803–4810.
- [86] B. Spingler, S. Mundwiler, P. Ruiz-Sanchez, D. R. van Staveren, R. Alberto, *Eur. J. Inorg. Chem.* **2007**, 2641–2647.
- [87] J. Petrig, R. Schibli, C. Dumas, R. Alberto, P. A. Schubiger, *Chem. Eur. J.* **2001**, 7, 1868–1873.
- [88] T. Storr, C. L. Fisher, Y. Mikata, S. Yano, M. J. Adam, C. Orvig, *Dalton Trans.* **2005**, 654–655.
- [89] T. Storr, M. Obata, C. L. Fisher, S. R. Bayly, D. E. Green, I. Brudzinska, Y. Mikata, B. O. Patrick, M. J. Adam, S. Yano, C. Orvig, *Chem. Eur. J.* **2005**, 11, 195–203.
- [90] M. L. Bowen, C. Orvig, *Chem. Commun.* **2008**, asap article, DOI: 10.1039/b809365b.
- [91] L. Maria, S. Cunha, M. Videira, L. Gano, A. Paulo, I. C. Santos, I. Santos, *Dalton Trans.* **2007**, 3010–3019.
- [92] P. Haefliger, N. Agorastos, B. Spingler, O. Georgiev, G. Viola, R. Alberto, *ChemBioChem* **2005**, 6, 414–421.
- [93] P. Haefliger, N. Agorastos, A. Renard, G. Giambonini-Brugnoli, C. Marty, R. Alberto, *Bioconjugate Chem.* **2005**, 16, 582–587.
- [94] N. Agorastos, L. Borsig, A. Renard, P. Antoni, G. Viola, B. Spingler, P. Kurz, R. Alberto, *Chem. Eur. J.* **2007**, 13, 3842–3852.
- [95] R. F. Vitor, I. Correia, M. Videira, F. Marques, A. Paulo, J. C. Pessoa, G. Viola, G. G. Martins, I. Santos, *ChemBioChem* **2008**, 9, 131–142.
- [96] K. A. Stephenson, S. R. Banerjee, T. Besanger, O. O. Sogbein, M. K. Levadala, N. McFarlane, J. A. Lemon, D. R. Boreham, K. P. Maresca, J. D. Brennan, J. W. Babich, J. Zubieta, J. F. Valliant, *J. Am. Chem. Soc.* **2004**, 126, 8598–8599.
- [97] S. R. Banerjee, M. K. Levadala, N. Lazarova, L. H. Wei, J. F. Valliant, K. A. Stephenson, J. W. Babich, K. P. Maresca, J. Zubieta, *Inorg. Chem.* **2002**, 41, 6417–6425.
- [98] P. J. A. G. Schaffer, J. A. Lemon, L. C. Reid, L. K. K. Pacey, T. H. Farncombe, D. R. Boreham, J. Zubieta, J. W. Babich, L. C. Doering, J. F. Valliant, *Nucl. Med. Biol.* **2008**, 35, 159–169.
- [99] Y. Liu, J.-K. Pak, P. Schmutz, M. Bauwens, J. Mertens, H. Knight, R. Alberto, *J. Am. Chem. Soc.* **2006**, 128, 15996–15997.
- [100] C. L. Ferreira, C. B. Ewart, S. R. Bayly, B. O. Patrick, J. Steele, M. J. Adam, C. Orvig, *Inorg. Chem.* **2006**, 45, 6979–6987.
- [101] M. L. Biechlin, A. Bonmartin, F. N. Gilly, M. Fraysse, A. D. d'Hardemare, *Nucl. Med. Biol.* **2008**, 35, 679–687.
- [102] C. Muller, P. A. Schubiger, R. Schibli, *Nucl. Med. Biol.* **2007**, 34, 595–601.
- [103] R. Alberto, *J. Organomet. Chem.* **2007**, 692, 1179–1186.
- [104] T. W. Spradau, J. A. Katzenellenbogen, *Organometallics* **1998**, 17, 2009–2017.
- [105] T. W. Spradau, W. B. Edwards, C. J. Anderson, M. J. Welch, J. A. Katzenellenbogen, *Nucl. Med. Biol.* **1999**, 26, 1–7.
- [106] F. Minutolo, J. A. Katzenellenbogen, *J. Am. Chem. Soc.* **1998**, 120, 4514–4515.
- [107] S. Masi, S. Top, L. Boubekeur, G. Jaouen, S. Mundwiler, B. Spingler, R. Alberto, *Eur. J. Inorg. Chem.* **2004**, 2013–2017.
- [108] S. Top, S. Masi, G. Jaouen, *Eur. J. Inorg. Chem.* **2002**, 1848–1853.
- [109] S. Top, A. Vessieres, P. Pigeon, M. N. Rager, M. Huche, E. Salomon, C. Cabestaing, J. Vaissermann, G. Jaouen, *ChemBioChem* **2004**, 5, 1104–1113.
- [110] J. Wald, R. Alberto, K. Ortner, L. Candreaia, *Angew. Chem. Int. Ed.* **2001**, 40, 3062–3066.
- [111] J. Bernard, K. Ortner, B. Spingler, H. J. Pietzsch, R. Alberto, *Inorg. Chem.* **2003**, 42, 1014–1022.
- [112] Y. Liu, B. Spingler, P. Schmutz, R. Alberto, *J. Am. Chem. Soc.* **2008**, 130, 1554.
- [113] J. F. Valliant, P. Morel, P. Schaffer, J. H. Kaldis, *Inorg. Chem.* **2002**, 41, 628–630.
- [114] O. O. Sogbein, P. Merdy, P. Morel, J. F. Valliant, *Inorg. Chem.* **2004**, 43, 3032–3034.
- [115] M. F. Hawthorne, A. Maderna, *Chem. Rev.* **1999**, 99, 3421–3434.

Received: September 11, 2008

Published Online: November 21, 2008

Oxidovanadium Complexes for the Consumption of Alkylating Toxins

Jessica M. Fautch,^[a] Phillip E. Fanwick,^[a] and Jonathan J. Wilker*^[a]

Keywords: Bioinorganic chemistry / Vanadates / Alkylation / Hydrolysis / Substituent effects

Carcinogens found in cooked foods, tobacco smoke, and vehicle exhaust undergo metabolic activation to pernicious alkylating toxins, yield damaged DNA, and promote cancerous growth. Vanadium has been shown to decrease the occurrence of cancers, possibly by intercepting such toxins before DNA damage can occur. According to recent results, nucleophilic oxido salts of vanadium can prevent this DNA alkylation. Although effective at detoxification and preventing DNA damage, vanadate salts equilibrate in solution to multiple coexisting species and can exhibit toxicity. Ligand-enforced coordination geometries may minimize such equilibrations, thereby decreasing toxicity and providing a means to control reactivity. As part of our efforts to detoxify alkylating agents, here we are studying reactions between oxidovanadium complexes and toxins. Alkylating agents such as di-

ethyl sulfate were treated with a series of new oxidovanadium complexes of the salicylidenehydrazide ligand, $[\text{VO}_2(\text{salhyph}(\text{R})_2)]^-$. These complexes consumed a collection of alkylating agents and brought about transformation to alcohols. Changing the ligand substituents ($\text{R} = -\text{OCH}_3$, $-\text{CH}_3$, $-\text{H}$, $-\text{NO}_2$) yielded a series of compounds with varied degrees of electron density. Kinetic experiments indicated that there may be a correlation between electron density and reactivity with alkylating toxins. The design and reactivity of these compounds indicate that we may be able to exert control over interactions between carcinogens and metal complexes. Such principles may be helpful in developing new compounds for the prevention of cancer.

(© Wiley-VCH Verlag GmbH & Co. KGaA, 69451 Weinheim, Germany, 2009)

Introduction

We are constantly exposed to carcinogens resulting from the combustion of organic matter. Cooked food, tobacco smoke, and vehicle exhaust all contain alkylating carcinogens such as the polycyclic aromatic hydrocarbons (PAHs) and nitrosamines.^[1–3] Toxicity of these compounds is a result of enzymatic oxidation into electrophiles that attack nucleophilic positions on DNA. The resulting alkylated bases can mispair during replication, yield mutations, and bring about cancerous growth.^[4,5] In order to develop new approaches to cancer prevention, we are focusing attention on ways to minimize such DNA damage. Recent studies have shown that salts of vanadium^[6–10] and selenium^[11–13] prevent cancers induced by alkylating toxins. In aqueous solutions vanadium^[14,15] and selenium^[16] equilibrate to anionic metal-oxido species such as $(\text{H}_2\text{VO}_4)^-$ and $(\text{SeO}_4)^{2-}$. From a mechanistic perspective, however, few detailed insights are available to explain the anticancer properties of vanadium or selenium. We have previously proposed, and provided evidence to show, that the cancer preventing properties of vanadium may result from a “carcinogen interception” process.^[17] Nucleophilic metal-oxido species can react directly with electrophilic alkylating carcinogens, thereby

consuming the toxin prior to the onset of DNA damage.^[17,18] Although a new mechanism for preventing DNA damage is exciting, concentrating efforts on simple metal-oxido salts will not permit control over reactivity and toxicity. Problems with using simple salts include solution equilibration to multiple coexisting species, thus enhancing toxicity and complicating mechanistic studies. Introduction of chelating ligands to the metal-oxido moiety will minimize such equilibria and also facilitate the design of chemopreventative metal complexes with controllable chemistry.

A rich history surrounds complexes in which vanadium is bound by organic ligands. Perhaps the most widely known examples are those of the insulin mimetic vanadium compounds.^[19–22] Other prominent examples of oxidovanadium complexes include oxidation catalysts, photocatalysts, and model complexes for vanadium-containing enzymes.^[23–27] Use of organic ligands to bind metals can provide control over the compound charge, nuclearity, metal coordination number, nature of the ligand donor atoms, and the extent of ligand electron donation to the metal center. Occupation of multiple coordination sites about vanadium centers minimizes unwanted reactions and interconversions (e.g., monomer \leftrightarrow dimer \leftrightarrow trimer), consequently simplifying the mechanistic chemistry at hand. Greater complex stability may also reduce toxicity by preventing vanadium from mimicking phosphate [i.e., $(\text{VO}_4)^{3-}$ vs. $(\text{PO}_4)^{3-}$] and inhibiting phosphate-processing enzymes.^[28] Proper choice and design of ligands provides us with inroads to developing cancer preventing complexes with controlled reac-

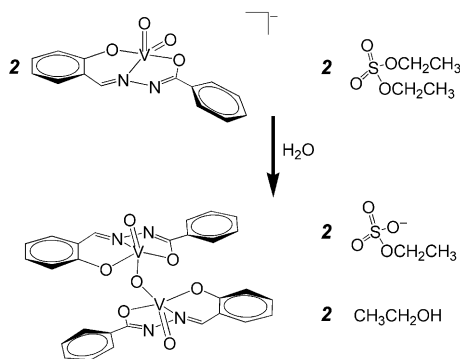
[a] Department of Chemistry, Purdue University, 560 Oval Drive, West Lafayette, IN 47907-2084, USA
Fax: +1-765-494-0239
E-mail: wilker@purdue.edu

Supporting information for this article is available on the WWW under <http://www.eurjic.org> or from the author.

tivity toward toxins. In this report we describe a series of new oxidovanadium complexes and reactions with alkylating agents.

Results and Discussion

Dioxidovanadium(V) compounds of the salicylidenehydrazide ("salhyph") ligand provide an excellent entry into alkylation studies of oxidovanadium compounds (Scheme 1). Two terminal oxido ligands are present for reactions with alkylating agents and, overall, $[\text{VO}_2(\text{salhyph})]^-$ is anionic, thereby indicating potential nucleophilicity. The starting $\text{K}[\text{VO}_2(\text{salhyph})]\cdot\text{CH}_3\text{OH}^{[29]}$ was combined 1:1 with the alkylating toxin diethyl sulfate, $(\text{CH}_3\text{CH}_2\text{O})_2\text{SO}_2$. Diethyl sulfate is a reagent used commonly in carcinogenesis studies.^[30] This reaction was carried out in distilled $[\text{D}_6]$ -DMSO and monitored by ^1H NMR spectroscopy. Figure 1 shows a ^1H NMR spectrum of this reaction in progress, focusing on the aliphatic resonances. Full spectroscopic data are provided in the Supporting Information. The starting $(\text{CH}_3\text{CH}_2\text{O})_2\text{SO}_2$ was consumed while the products $(\text{CH}_3\text{CH}_2\text{O})\text{SO}_3^-$ and $\text{CH}_3\text{CH}_2\text{OH}$ were formed. Methanol was also observed, persisting from the crystallization of the starting $\text{K}[\text{VO}_2(\text{salhyph})]\cdot\text{CH}_3\text{OH}$. Control solutions of $(\text{CH}_3\text{CH}_2\text{O})_2\text{SO}_2$ in $[\text{D}_6]$ -DMSO did not yield $\text{CH}_3\text{CH}_2\text{OH}$ on a comparable time scale.



Scheme 1. Proposed alkylation reaction of $[\text{VO}_2(\text{salhyph})]^-$.

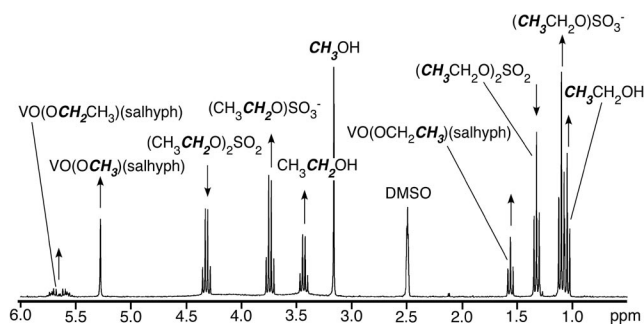


Figure 1. A ^1H NMR spectrum in $[\text{D}_6]$ -DMSO of the 1:1 reaction, in progress at approximately 8 h, between $\text{K}[\text{VO}_2(\text{salhyph})]\cdot\text{CH}_3\text{OH}$ and $(\text{CH}_3\text{CH}_2\text{O})_2\text{SO}_2$. Arrows indicate peak intensity changes during the course of the reaction.

These results indicate that this oxidovanadium compound can promote detoxification by transforming this alkylating agent into an alcohol. Such reactivity appears to be a general phenomenon for $[\text{VO}_2(\text{salhyph})]^-$. Analogous experiments showed that the alkylating agents $\text{CH}_3\text{CH}_2\text{I}$, $\text{CF}_3\text{SO}_2\text{O}-\text{CH}_2\text{CH}_3$, $\text{NH}_2\text{CON}(\text{NO})-\text{CH}_3$, and $\text{CH}_3\text{SO}_2\text{O}-\text{CH}_3$ were each consumed by $[\text{VO}_2(\text{salhyph})]^-$ and yielded the less toxic alcohols CH_3OH or $\text{CH}_2\text{CH}_3\text{OH}$. A proposed mechanism is electrophilic attack of an alkyl cation onto a nucleophilic terminal oxido of $[\text{VO}_2(\text{salhyph})]^-$. Support for this mechanism comes from observations of the $\text{VO}(\text{OCH}_2\text{CH}_3)(\text{salhyph})$ intermediate at $\delta = 1.56$ and 5.62 ppm in the ^1H NMR spectra.^[31] Subsequent protonation from residual water may then release $\text{CH}_3\text{CH}_2\text{OH}$.

In order to gain insights on the vanadium-containing product of this process, a reaction was run in acetone and then ether was diffused therein. Large, red-brown crystals resulted and were examined by single-crystal X-ray diffraction methods (see Supporting Information). The structure found was that of $\{[\text{VO}(\text{salhyph})]_2\text{O}\}$, a known compound prepared previously via an unrelated route.^[32] Scheme 1 shows a proposed reaction in which $\{[\text{VO}(\text{salhyph})]_2\text{O}\}$ is produced from $[\text{VO}_2(\text{salhyph})]^-$ and $(\text{CH}_3\text{CH}_2\text{O})_2\text{SO}_2$. This reaction product resembles a dimer of the starting $[\text{VO}_2(\text{salhyph})]^-$, however one oxygen short. This "missing" oxygen was likely extracted during formation of the ethanol product. Such results are consistent with our prior work wherein simple vanadates such as $(\text{V}_3\text{O}_9)^{3-}$ [i.e. $(\text{VO}_3^-)_3$] reacted with alkylating agents to yield alcohols and $(\text{V}_5\text{O}_{14})^{3-}$ [i.e. one oxygen "missing" from $(\text{VO}_3^-)_5$].^[17,33] Inclusion of a ligand system here preserves the nucleophilic reactivity of the oxidovanadium moiety and provides a platform for subsequent modifications.

Electron donating ($-\text{OCH}_3$, $-\text{CH}_3$) and withdrawing ($-\text{NO}_2$) substituents were placed onto the salhyph ligand framework.^[34] The resulting new $\text{K}[\text{VO}_2(\text{salhyph}(\text{R}))]^-$ compounds, where $\text{R} = \text{H}$ is the parent $[\text{VO}_2(\text{salhyph})]^-$, were prepared and are depicted in Figure 2. Substituent electron donation into the aromatic rings may then increase electron density on the O and N ligand donor atoms. The central metal ion would exhibit enhanced electron density and may then increase nucleophilicity of the terminal oxygen ligands. As a consequence, reactivity toward alkylating agents could be enhanced. Given the long distances between added substituents and the terminal oxidos, such electronic effects are expected to be subtle, but may serve to indicate that limited control over reactivity is possible.

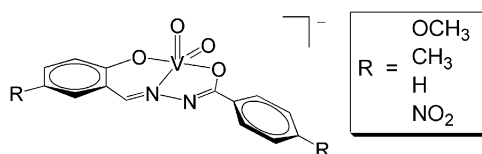


Figure 2. Electron-donating and -withdrawing substituents on $[\text{VO}_2(\text{salhyph}(\text{R}))]^-$.

Each of the substituted $[\text{VO}_2(\text{sallyph}(\text{R})_2)]^-$ compounds reacted readily with $(\text{CH}_3\text{CH}_2\text{O})_2\text{SO}_2$, as well as all of the other alkylating agents mentioned above. Product characterization by ^1H NMR spectroscopy showed formation of $\text{CH}_3\text{CH}_2\text{OH}$ from ethylating toxins or CH_3OH from methylating toxins, similar to experiments with the parent, unsubstituted $[\text{VO}_2(\text{sallyph})]^-$ compound. Next we examined kinetics of the reactions between the $[\text{VO}_2(\text{sallyph}(\text{R})_2)]^-$ compounds and $(\text{CH}_3\text{CH}_2\text{O})_2\text{SO}_2$. Pseudo-first-order conditions were employed with a 10 : 1 $[\text{VO}_2(\text{sallyph}(\text{R})_2)]^- / (\text{CH}_3\text{CH}_2\text{O})_2\text{SO}_2$ ratio and concentrations of 200 mM and 20 mM, respectively. Rate constants, each determined in triplicate, were obtained by following the reduction of resonances from $(\text{CH}_3\text{CH}_2\text{O})_2\text{SO}_2$ and plotting concentration vs. time. The methylene resonances of $(\text{CH}_3\text{CH}_2\text{O})_2\text{SO}_2$ were monitored owing to a clear baseline on either side of the peak. Two processes may be noted in the plot (see Supporting Information), one of which is background hydrolysis of $(\text{CH}_3\text{CH}_2\text{O})_2\text{SO}_2$ in distilled $[\text{D}_6]\text{DMSO}$, measured independently to be $k_{\text{obsd.}} = 1.1 \times 10^{-5} \text{ s}^{-1}$. Although reagent decomposition is significant under these conditions, use of dmsol was dictated by finding one solvent in which all derivatives of $[\text{VO}_2(\text{sallyph}(\text{R})_2)]^-$ are soluble. Kinetic data were fit to a biexponential containing a fixed component to account for the hydrolysis. Figure 3 shows typical kinetic data along with a curve fit. The rate constants presented in Table 1 indicate subtle differences in reactivity between these complexes. The degree of electron donation or withdrawal from the aryl ring substituents may correlate with alkylation reactivity.

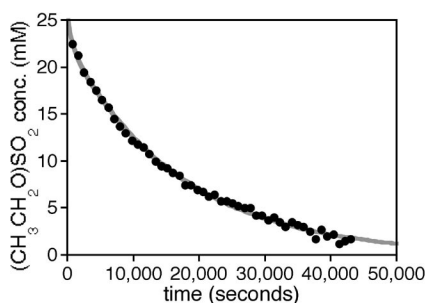


Figure 3. Plot of $(\text{CH}_3\text{CH}_2\text{O})_2\text{SO}_2$ concentrations vs. time for the 10:1 (200:20 mM) reaction of $[\text{VO}_2(\text{sallyph}(\text{H})_2)]^-$ and $(\text{CH}_3\text{CH}_2\text{O})_2\text{SO}_2$.

Table 1. Pseudo-first-order rate constants for the alkylation reactions of $[\text{VO}_2(\text{sallyph}(\text{R})_2)]^-$ compounds with $(\text{CH}_3\text{CH}_2\text{O})_2\text{SO}_2$.

| Substituent R | Hammett value σ | Rate constant ^[a] $k_{\text{obsd.}} [\text{s}^{-1}]$ |
|-------------------|------------------------|---|
| –NO ₂ | +0.78 | $(4.3 \pm 0.7) \times 10^{-5}$ |
| –H | 0 | $(5.5 \pm 1.5) \times 10^{-5}$ |
| –CH ₃ | –0.17 | $(6.3 \pm 1.1) \times 10^{-5}$ |
| –OCH ₃ | –0.27 | $(6.5 \pm 0.3) \times 10^{-5}$ |

[a] Each rate constant is an average of three runs. The error shows one standard deviation.

Conclusions

Here we have shown that a family of oxidovanadium complexes reacts with alkylating carcinogens and yields alcohols. Introduction of ligands can be a useful tool in moderating the nucleophilicity of metal oxides. Thus changes in ligand architecture may provide an avenue toward nucleophilic compounds for consuming toxins.

Experimental Section

H₂sallyph(OCH₃)₂: This compound was prepared by modifying a published procedure for the unsubstituted sallyph ligand.^[35] In a round-bottomed flask, 4-methoxybenzhydrazide (1.734 g, 10.44 mmol) was dissolved in 1-propanol (40 mL) and 2-hydroxy-5-methoxybenzaldehyde (1.30 mL, 10.43 mmol) was added with stirring. The yellow reaction mixture was heated at reflux for 17 h, cooled, and left to stand for 6 h. Light yellow crystals precipitated, were removed by gravity filtration, and dried under vacuum (2.80 g, 89.6%). ^1H NMR (200 MHz, $[\text{D}_6]\text{DMSO}$, 22 °C): δ = 3.72 (s, 3 H, –OCH₃), 3.82 (s, 1 H, –OCH₃), 6.85 (br. m, 2 H, ar), 7.05 (br. m, 3 H, ar), 7.90 (d, $^3J_{\text{H-H}}$ = 8.6 Hz, 2 H, ar), 8.58 (s, 1 H, N=C–H), 10.78 (br. s, 1 H, –OH), 11.99 (br. s, 1 H, –NH) ppm.

H₂sallyph(CH₃)₂: In 1-propanol (40 mL), *p*-toluic hydrazide (1.803 g, 12.0 mmol) was dissolved slightly and 2-hydroxy-5-methylbenzaldehyde (1.633 g, 12.0 mmol) added with stirring. The reaction mixture was heated at reflux for 21 h. The solution was cooled and left to stand for 19 h. Off-white crystals precipitated and were removed by gravity filtration and dried under vacuum (2.70 g, 83.8%). ^1H NMR (300 MHz, $[\text{D}_6]\text{DMSO}$, 22 °C): δ = 2.24 (s, 3 H, –CH₃), 2.37 (s, 1 H, –CH₃), 6.82 (d, $^3J_{\text{H-H}}$ = 8.4 Hz, 1 H, ar), 7.09 (d, $^3J_{\text{H-H}}$ = 8.1 Hz, 1 H, ar), 7.35 (m, 3 H, ar), 7.84 (d, $^3J_{\text{H-H}}$ = 8.1 Hz, 2 H, ar), 8.58 (s, 1 H, N=C–H), 11.1 (br. s, 1 H, –OH), 12.0 (br. s, 1 H, –NH) ppm.

H₂sallyph(NO₂)₂: To a solution of 4-nitrobenzhydrazide (1.812 g, 10.0 mmol) in 1-propanol (40 mL), 2-hydroxy-5-nitrosalicylaldehyde (1.672 g, 10.0 mmol) was added with stirring. The reaction mixture was heated at reflux for 5 h, cooled, and left to stand overnight. A yellow solid was removed by gravity filtration and dried under vacuum (3.48 g, 90.4%). ^1H NMR (200 MHz, $[\text{D}_6]\text{DMSO}$, 22 °C): δ = 7.09 (d, $^3J_{\text{H-H}}$ = 8.8 Hz, 1 H, ar), 8.15 (br. m, 3 H, ar), 8.36 (d, $^3J_{\text{H-H}}$ = 8.2 Hz, 2 H, ar), 8.58 (s, 1 H, ar), 8.73 (s, 1 H, N=C–H), 12.2 (br. s, 1 H, –OH), 12.43 (br. s, 1 H, –NH) ppm.

K[VO₂(sallyph(OCH₃)₂)]: This compound was prepared as described previously for the unsubstituted K[VO₂(sallyph)] compound.^[29] Potassium metavanadate, KVO₃ (0.5518 g, 4.0 mmol), was stirred in methanol (50 mL) to which H₂sallyph(OCH₃)₂ (1.202 g, 4.0 mmol) was added and the mixture was heated at reflux for 5 h. Crude yellow product was collected by gravity filtration from the hot reaction mixture and dried under vacuum (1.01 g, 60.1%). Needle-like crystals were obtained when the crude product was dissolved in *N,N*-dimethylformamide, followed by slow vapor diffusion of diethyl ether for ten days. Crystals were isolated by gravity filtration, rinsed with diethyl ether, and dried in vacuo. ^1H NMR (300 MHz, $[\text{D}_6]\text{DMSO}$, 22 °C): δ = 3.72 (s, 3 H, –OCH₃), 3.81 (s, 3 H, –OCH₃), 6.70 (d, $^3J_{\text{H-H}}$ = 9.3 Hz, 1 H, ar), 6.9–7.0 (m, 3 H, ar), 7.11 (d, $^3J_{\text{H-H}}$ = 3.0 Hz, 1 H, ar), 7.93 (d, $^3J_{\text{H-H}}$ = 8.7 Hz, 2 H, ar), 8.88 (s, 1 H, C=N–H) ppm. K[C₁₆H₁₄N₂O₆V] (420.34): calcd. C 45.72, H 3.36, N 6.66; found C 45.43, H 3.38, N 6.53.

K[VO₂(salhyph(CH₃)₂)]: This compound was prepared as described for K[VO₂(salhyph(OCH₃)₂)], using the appropriate starting ligand, H₂salhyph(CH₃)₂. After 4 h of reflux the solution was filtered while hot. Upon standing, yellow needles precipitated. After cooling to room temperature, crystals of the desired compound were filtered by gravity and dried in vacuo (1.07 g, 68.9%). ¹H NMR (300 MHz, [D₆]DMSO, 22 °C): δ = 2.24 (s, 3 H, –CH₃), 2.35 (s, 3 H, –CH₃), 6.67 (d, ³J_{H–H} = 8.1 Hz, 1 H, ar), 7.15 (d, ³J_{H–H} = 8.1 Hz, 1 H, ar), 7.24 (d, ³J_{H–H} = 7.8 Hz, 2 H, ar), 7.31 (s, 1 H, ar), 7.88 (d, ³J_{H–H} = 8.1 Hz, 2 H, ar), 8.86 (s, 1 H, C=N–H) ppm. K[C₁₆H₁₄N₂O₄V] (388.34): calcd. C 49.49, H 3.63, N 7.21; found C 49.11, H 3.62, N 7.06.

K[VO₂(salhyph(NO₂)₂)]·H₂O: This compound was prepared as described for K[VO₂(salhyph(OCH₃)₂)], using the appropriate starting ligand, H₂salhyph(NO₂)₂. The pale yellow slurry was heated at reflux for 4.5 h and cooled to room temperature. A yellow solid was filtered by gravity and dried under vacuum (1.59 g, 84.9%). The product was recrystallized from nearly boiling acetonitrile. ¹H NMR (300 MHz, [D₆]DMSO, 22 °C): δ = 6.94 (d, ³J_{H–H} = 9.3 Hz, 1 H, ar), 8.1–8.4 (m, 5 H, ar), 8.71 (s, 1 H, ar), 9.27 (s, 1 H, C=N–H) ppm. K[C₁₄H₈N₄O₈V]·H₂O (468.29): calcd. C 35.91, H 2.15, N 11.96; found C 35.91, H 1.99, N 11.80.

{[VO(salhyph)]₂O}: Under an inert argon atmosphere, K[VO₂(salhyph)]·CH₃OH (0.393 g, 1.0 mmol), was added to acetone (20 mL) and diethyl sulfate, (CH₃CH₂O)₂SO₂, (131 μL, 1.0 mmol), was added to the reaction flask. The pale yellow reaction was stirred under argon for 5 d, resulting in a dark black-brown solution. A small portion (approximately 5 mL) of the acetone reaction mixture was removed. Diethyl ether was vapor diffused into the solution for 4 d. The vapor diffusion yielded yellow solids and large (0.4 × 0.4 × 0.4 mm), dark brown-black cubes. After gravity filtration of the mixture, the cubes were separated from the yellow solids using tweezers. The cubes were then rinsed with hexanes, dichloromethane, and water to dissolve residual yellow solids. The resulting X-ray quality crystals, {[VO₂(salhyph)]₂O}, were dried in vacuo. Given that only a portion of the reaction solution was subjected to vapor diffusion, an exact yield cannot be determined. However, back calculation from the approximately 81 mg of brown-black cubes indicates that {[VO(salhyph)]₂O} can be formed and crystallized with a rough yield of 324 mg, 52%. ¹H NMR (300 MHz, [D₆]DMSO, 22 °C): δ = 6.90 (d, ³J_{H–H} = 8.7 Hz, 2 H, ar), 7.05 (t, ³J_{H–H} = 7.8 Hz, 2 H, ar), 7.3–7.6 (m, 8 H, ar), 7.79 (d, ³J_{H–H} = 7.2 Hz, 2 H, ar), 8.01 (d, ³J_{H–H} = 7.8 Hz, 4 H, ar), 9.02 (s, 2 H, C=N–H) ppm. C₂₈H₂₀N₄O₇V₂ (626.37): calcd. C 53.69, H 3.22, N 8.94; found C 53.53, H 3.24, N 8.71.

Kinetic Experiments: Each of the K[VO₂{salhyph(R)}₂] compounds was combined with diethyl sulfate (DES), (CH₃CH₂O)₂SO₂, in distilled [D₆]DMSO. Dimethylformamide (dmf) was used for an internal concentration standard. Pseudo-first-order reaction conditions were employed with a 10:1:5 ratio of V/DES/dmf. Concentrations were 200 mM, 20 mM, and 100 mM, respectively. The ¹H NMR spectra at 22 °C were acquired every 12 min. Kinetic data were examined by monitoring the reduction of the (CH₃CH₂O)₂SO₂ methylene resonances over time. This resonance was used consistently, owing to a clear baseline on both sides for each [VO₂(salhyph(R)₂)]⁺ (R = H, NO₂, OCH₃, CH₃) compound (cf., Figure 1 at approximately 4.3 ppm). We could monitor the peak changes associated with production of (CH₃CH₂O)SO₃[–] and CH₃CH₂OH, however, the concentration vs. time plots were not nearly as clean owing to peaks overlapping with other species. Control kinetic runs of (CH₃CH₂O)₂SO₂ in [D₆]DMSO alone, without a vanadium complex, yielded a *k*_{obsd.} = (1.1 ± 0.1) × 10^{–5} s^{–1}.

Supporting Information (see also the footnote on the first page of this article): Complete ¹H NMR spectra for select alkylation reactions and controls, and crystal structure data for {[VO(salhyph)]₂O}.

Acknowledgments

We thank Ian Henry and John Harwood for assistance with the kinetic ¹H NMR experiments. We also thank and Dale Margerum and Tong Ren for helpful discussions. Generous support was provided by the Prevent Cancer Foundation and Alfred P. Sloan Foundation (research fellowship).

- [1] G. S. Bailey, D. E. Williams, *Food Technol.* **1993**, 47, 105–118.
- [2] S. S. Hecht, *Chem. Res. Toxicol.* **1998**, 11, 559–603.
- [3] J. C. Ball, B. Green, W. C. Young, J. F. O. Richert, I. T. Salmeen, *Environ. Sci. Technol.* **1990**, 24, 890–894.
- [4] E. C. Friedberg, G. C. Walker, W. Siede, *DNA Repair and Mutagenesis*, ASM Press, Washington D. C., **1995**.
- [5] B. Singer, *Environ. Health Perspec.* **1985**, 62, 41–48.
- [6] A. M. Evangelou, *Crit. Rev. Oncol. Hemat.* **2002**, 42, 249–265.
- [7] H. J. Thompson, N. D. Chasteen, L. D. Meeker, *Carcinogenesis* **1984**, 5, 849–851.
- [8] A. Bishayee, R. Karmakar, A. Mandal, S. N. Kundu, M. Chatterjee, *Eur. J. Cancer Prevention* **1997**, 6, 58–70.
- [9] R. S. Ray, B. Ghosh, A. Rana, M. Chatterjee, *Int. J. Cancer* **2006**, 120, 13–23.
- [10] A. Bishayee, M. Chatterjee, *Br. J. Cancer* **1995**, 71, 1214–1220.
- [11] E. A. Klein, I. M. Thompson, S. M. Lippman, P. J. Goodman, D. Albanes, P. R. Taylor, C. Coltman, *Urol. Oncol.* **2003**, 21, 59–65.
- [12] J. W. Finley, C. Ip, D. J. Lisk, C. D. Davis, K. J. Hintze, P. D. Whanger, *J. Agric. Food Chem.* **2001**, 49, 2679–2683.
- [13] H. E. Ganther, *Carcinogenesis* **1999**, 20, 1657–1666.
- [14] D. C. Crans, C. D. Rithner, L. A. Theisen, *J. Am. Chem. Soc.* **1990**, 112, 2901–2908.
- [15] L. Pettersson, B. Hedman, I. Andersson, N. Ingri, *Chem. Scr.* **1983**, 22, 254–264.
- [16] H. Robberecht, R. V. Grieken, *Talanta* **1982**, 29, 823–844.
- [17] E. E. Hamilton, J. J. Wilker, *Angew. Chem. Int. Ed.* **2004**, 43, 3290–3292.
- [18] E. E. Hamilton, J. J. Wilker, *J. Biol. Inorg. Chem.* **2004**, 9, 894–902.
- [19] C. E. Heyliger, A. G. Tahiliani, J. H. McNeill, *Science* **1985**, 227, 1474–1477.
- [20] J. H. McNeill, V. G. Yuen, H. R. Hoveyda, C. Orvig, *J. Med. Chem.* **1992**, 35, 1489–1491.
- [21] D. C. Crans, L. Yang, T. Jakusch, T. Kiss, *Inorg. Chem.* **2000**, 39, 4409–4416.
- [22] J. Gatjens, B. Meier, Y. Adachi, H. Sakurai, D. Rehder, *Eur. J. Inorg. Chem.* **2006**, 3575–3585.
- [23] M. Tada, T. Taniike, L. M. Kantam, Y. Iwasawa, *Chem. Commun.* **2004**, 2542–2543.
- [24] J. Liu, R. Yang, S. Li, *Rare Met.* **2006**, 25, 636–642.
- [25] M. Bettinelli, V. Dallacasa, D. Falcomer, P. Fornasiero, V. Gombac, T. Montini, L. Romano, A. Speghini, *J. Hazard. Mater.* **2007**, 146, 529–534.
- [26] C. R. Cornman, G. J. Colpas, J. D. Hoeschele, J. Kampf, V. L. Pecoraro, *J. Am. Chem. Soc.* **1992**, 114, 9925–9933.
- [27] D. Rehder, *Coord. Chem. Rev.* **1999**, 182, 297–322.
- [28] D. Rehder, *Angew. Chem. Int. Ed. Engl.* **1991**, 30, 148–167.
- [29] W. Plass, A. Pohlmann, H.-P. Yozgatli, *J. Inorg. Biochem.* **2000**, 80, 181–183.
- [30] J. A. Swenberg, D. G. Hoel, P. N. Magee, *Cancer Res.* **1991**, 51, 6409–6414.

- [31] M. Sutradhar, G. Mukherjee, M. G. B. Drew, S. Ghosh, *Inorg. Chem.* **2006**, *45*, 5150–5161.
- [32] N. R. Sangeetha, S. Pal, *Bull. Chem. Soc. Jpn.* **2000**, *73*, 357–363.
- [33] E. E. Hamilton, P. E. Fanwick, J. J. Wilker, *J. Am. Chem. Soc.* **2006**, *128*, 3388–3395.
- [34] H. C. Brown, Y. Okamoto, *J. Am. Chem. Soc.* **1958**, *80*, 4979–4987.
- [35] A. Kotali, M. Papapetrou, V. Dimos, P. A. Harris, *Org. Prep. Proced. Int.* **1998**, *30*, 177–181.

Received: September 26, 2008

Published Online: November 14, 2008

Synthesis and Structure of an Unprecedented Linear Pentanuclear Bismuth(III) Zwitterionic Thiolate Complex

Jin-Xiang Chen,^[a,b] Xiao-Yan Tang,^[a] Zhi-Gang Ren,^[a] Yong Zhang,^[a] and Jian-Ping Lang^{*[a]}

Keywords: Bismuth / Zwitterions / S ligands / Structure elucidation

A unique pentanuclear bismuth(III) zwitterionic thiolate complex, $[\text{Bi}_5(\text{Tab})_{18}](\text{PF}_6)_7(\text{NO}_3)_8 \cdot 6\text{MeCN}$ (**1**; Tab = 4-(trimethylammonio)benzenethiolato), was obtained from the reaction of $\text{Bi}(\text{NO}_3)_3$ with TabHPF_6 in a 1:4 molar ratio in MeCN/MeOH in the presence of Et_3N and structurally characterized. Single-crystal X-ray diffraction revealed that **1** consists of an unprecedented linear $[\text{Bi}_5(\text{Tab})_{18}]^{15+}$ cation,

and both $[\text{PF}_6]^-$ and $[\text{NO}_3]^-$ anions in the crystal cooperatively work as anionic templates to form interesting anionic honeycomb-like cavities for encapsulating the $[\text{Bi}_5(\text{Tab})_{18}]^{15+}$ cations.

(© Wiley-VCH Verlag GmbH & Co. KGaA, 69451 Weinheim, Germany, 2009)

Introduction

In the past decades, the chemistry of bismuth thiolate complexes has received much attention because bismuth centers tend to adopt high coordination numbers^[1] and they can be used as fungicides,^[2] antitumor agents,^[3] vulcanization catalysts,^[4] analytical reagent,^[5] and models for bismuth incorporation into metallothioneins.^[6] However, the structural chemistry of bismuth zwitterionic ammonium thiolates remains less explored due to their hydrolytic instability in solution and their generally poor solubility properties.^[7]

Recently, we have been interested in the preparation of metal complexes of zwitterionic ammonium thiolate Tab [Tab = 4-(trimethylammonio)benzenethiolato], and a series of metal/Tab compounds have been synthesized and structurally determined.^[8] These metal/Tab complexes are mainly involved in group 11 and 12 metals (e.g., Ag^+ , Au^+ , Hg^{2+}) and only two are related to main-group elements. In fact, only one Bi/Tab compound $[\text{Bi}(\text{Tab})_3](\text{ClO}_4)_3$ was isolated by using an electrochemical reaction.^[9] Being aware that few examples of bismuth zwitterionic thiolate complexes have been reported,^[1j,7c,10] we attempted the reaction of $\text{Bi}(\text{NO}_3)_3$ with TabHPF_6 in the presence of Et_3N by using standard Schlenk techniques, and we successfully iso-

lated an unusual polynuclear bismuth complex with the Tab ligand, $[\text{Bi}_5(\text{Tab})_{18}](\text{PF}_6)_7(\text{NO}_3)_8 \cdot 6\text{MeCN}$ (**1**). In this paper, we report its isolation and structural characterization.

Results and Discussion

Treatment of a suspension of $\text{Bi}(\text{NO}_3)_3$ in MeOH with TabHPF_6 (4 equiv.) in MeCN in the presence of Et_3N gave rise to a dark-red solution. The resulting mixture was stirred for 1 h and filtered. Diethyl ether was layered onto the filtrate to form dark-red crystals of **1** in 72% yield. Compound **1** is air and moisture sensitive. It gradually turned black upon exposure to air. It is insoluble in MeCN, MeOH, EtOH, and CH_2Cl_2 , but somewhat soluble in DMF and DMSO. The elemental analysis was consistent with its chemical formula. The strong bands at ca. 828 and 559 cm^{-1} in its IR spectrum may be assigned to the P–F stretching vibrations of the uncoordinated PF_6^- anions, whereas the peak at 1351 cm^{-1} indicated the presence of the dissociated NO_3^- anions.^[8a] The weak peak at 2262 cm^{-1} indicated the $\text{C}\equiv\text{N}$ vibration of the crystal solvent MeCN.^[8d] The ^1H NMR spectrum of **1** in $[\text{D}_6]\text{DMSO}$ at room temperature showed a multiplet for the protons of the Ph groups in the region 7.42–7.81 ppm, a singlet related to the protons of the NMe_3 group at ca. 3.34 ppm, and a singlet for the protons of the methyl groups of the MeCN molecules at ca. 2.09 ppm.^[8d] The structure of **1** was finally confirmed by X-ray crystallography.

Compound **1** crystallizes in the trigonal space group $R\bar{3}$ and its asymmetric unit contains one-sixth of the $[\text{Bi}_5(\text{Tab})_{18}]^{15+}$ cation, one and one-sixth of the $[\text{PF}_6]^-$

[a] College of Chemistry, Chemical Engineering and Materials Science, Suzhou University, Suzhou 215123, Jiangsu, People's Republic of China
Fax: +86-512-65880089
E-mail: jplang@suda.edu.cn

[b] School of Pharmaceutical Science, Southern Medical University, Guangzhou 510515 Guangdong, People's Republic of China

anions, one and one-third of the $[\text{NO}_3]^-$ anions, and one MeCN solvent molecule. The perspective view of the $[\text{Bi}_5(\text{Tab})_{18}]^{15+}$ cation is shown in Figure 1.

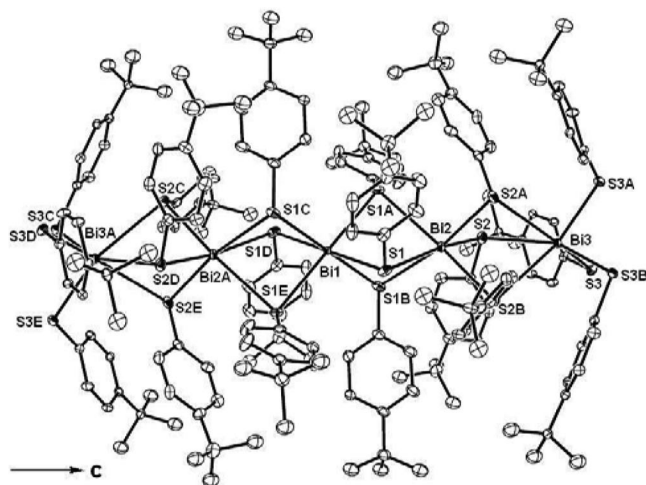


Figure 1. Perspective view of the $[\text{Bi}_5(\text{Tab})_{18}]^{15+}$ cation of **1** with 50% thermal ellipsoids. All H atoms are omitted for clarity. Selected bond lengths [Å] and angles [°]: Bi1–S1 2.831(4), Bi2–S1 3.027(4), Bi2–S2 2.721(3), Bi3–S2 3.210(3), Bi3–S3 2.626(3), S1–Bi1–S1A 80.74(11), S1–Bi1–S1E 99.26(11), S1–Bi1–S1D 179.98(1), S2–Bi2–S2A 83.87(12), S2–Bi2–S1B 107.08(11), S2–Bi2–S1A 95.08(10), S1–Bi2–S1A 74.58(11), S2–Bi2–S1 168.86(11), S3–Bi3–S3A 88.39(11), S3–Bi3–S2A 158.79(11), S3–Bi3–S2 112.81(10), S2–Bi3–S2A 69.02(10), S3–Bi3–S2B 91.51(10). Symmetry codes: A: $1 - y, x - y, z$; B: $1 - x + y, 1 - x, z$; C: $4/3 - x, 2/3 - y, 2/3 - z$; D: $1/3 + x - y, -1/3 + x, 2/3 - z$; E: $1/3 + y, 2/3 - x + y, 2/3 - z$.

The cation of **1** is composed of a linear chain of five Bi atoms, which extends along the c axis. There is a crystallographic threefold axis running through this chain. The two outer Bi atoms (Bi3 and Bi3A) are coordinated by three terminal and three bridging Tab ligands, whereas the three inner Bi atoms (Bi1, Bi2, and Bi2A) are coordinated by six bridging Tab ligands, thereby forming a unique Bi_5S_{18} core. Each Bi atom has a six-coordinate environment and each $\text{Bi}(\text{Tab})_6^{3+}$ octahedron shares six edges with the two adjacent ones. The difference is that Bi2, Bi3, Bi2A, and Bi3A have a distorted octahedral geometry, whereas Bi1 adopts a standard octahedral geometry. Alternatively, the overall geometry of the Bi_5S_{18} core may be described as five pairs of trigonal prismatic with a face-sharing octahedron on both trigonal faces. Another intriguing feature of **1** is that it holds a rare high positive charge (15+).^[8d,11]

In **1**, the six terminal Bi3–S3 bond lengths [2.626(3) Å] are significantly shorter than those of the bridging Bi–S_{br} bonds [2.831(4) Å for Bi1–S1, 3.027(4) Å for Bi2–S1, 2.721(3) Å for Bi2–S2, 3.210(3) Å for Bi3–S2], and those of the corresponding bond lengths in $[\text{Bi}(\text{SCH}_2\text{CH}_2\text{NHMe}_2)\text{Cl}_3]$ [2.798(3) Å],^[10] but close to those of the corresponding bond lengths in the bismuth thiolates $[\text{Bi}(\text{Tab})_3](\text{ClO}_4)_3$ [2.599(3) Å],^[9] $\text{Bi}[\text{SC}_6\text{H}_2(2,4,6\text{-}t\text{Bu}_3)]_3$ [2.559(8) Å],^[12] and $(\text{NH}_4)_3[\text{Bi}(2\text{-SC}_6\text{H}_4\text{COO})_3] \cdot 2\text{H}_2\text{O}$ [2.596(8) Å].^[13] The difference in the Bi–S bond lengths in **1** may be due to the

different steric hindrance of the terminal and bridging Tab ligands. In addition, the Bi···Bi contacts in **1** are 4.025 and 4.1587 Å, which are shorter than that in $[\text{Bi}(\text{Tab})_3](\text{ClO}_4)_3$ [4.244(3) Å] and still excludes any bismuth–bismuth interaction.

Interestingly, the cationic chains in the crystals of **1** are parallel to each other along the c axis and the separations between the neighboring chains are 18.54 Å. Looking down the c axis, it appears that the $[\text{P}(2)\text{F}_6]^-$ and $[\text{N}(5)\text{O}_3]^-$ anions in **1** act as two anionic templates, both with three symmetry-related quaternary ammonium ions arranged around them as shown in Figure 2a,b. It is quite rare that two different anions cooperatively work as two different anionic templates in the same structure.

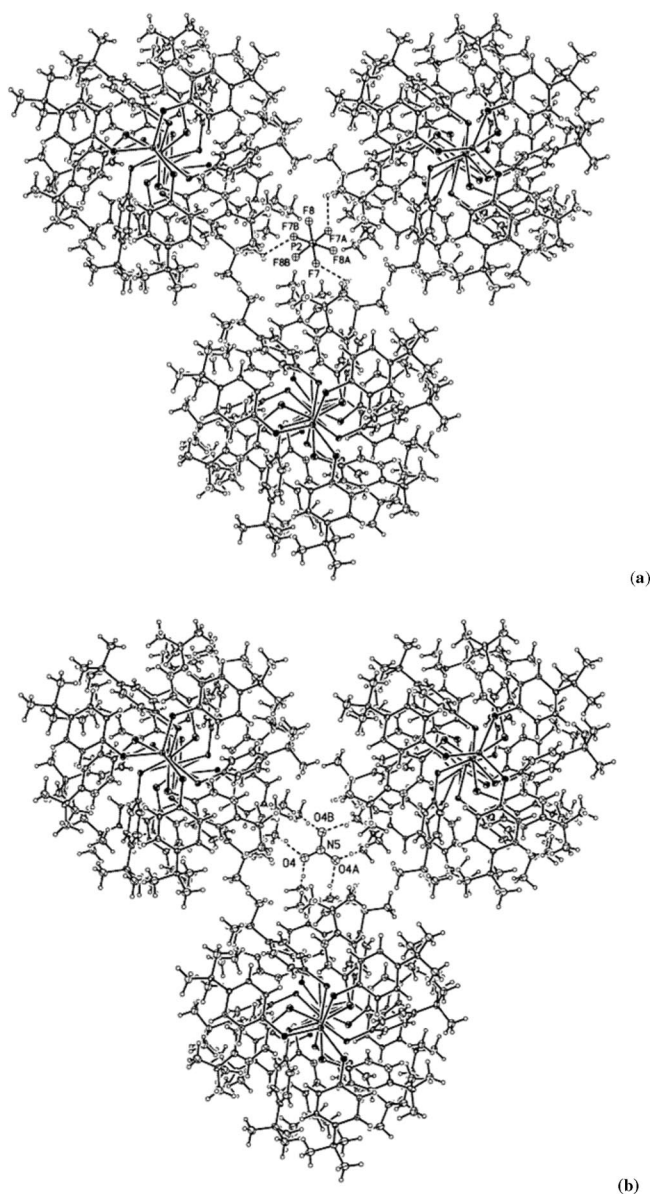


Figure 2. Stacking of **1** looking down the c axis, which highlights a $[\text{P}(2)\text{F}_6]^-$ anion (a) or a $[\text{N}(5)\text{O}_3]^-$ anion (b) acting as an anionic template.

The two anions thus form anionic honeycomb-like cavities, into which the $[\text{Bi}_5(\text{Tab})_{18}]^{15+}$ cations fit nicely. All the Bi atoms and the P2 and N5 atoms lie on the same C_3 axis. Furthermore, there are complicated intermolecular hydrogen-bonding interactions in **1**, forming a 3D hydrogen-bonded network.

Conclusions

We successfully prepared new pentanuclear bismuth/thiolate complex **1** from the reaction of $\text{Bi}(\text{NO}_3)_3$ with TabHPF_6 in the presence of Et_3N by using Schlenk techniques. Single-crystal X-ray diffraction showed that **1** has an unprecedented linear $[\text{Bi}_5\text{S}_{18}]$ core and both $[\text{PF}_6]^-$ and $[\text{NO}_3]^-$ anions act as anionic templates to form anionic honeycomb-like cavities for enveloping the $[\text{Bi}_5(\text{Tab})_{18}]^{15+}$ cations. Further investigation on the preparation of other main-group metal complexes with Tab ligands by this method is currently under way in our laboratory.

Experimental Section

Materials and Physical Measurements: All manipulation were carried out under an atmosphere of argon by using Schlenk techniques. TabHPF_6 was prepared according to a literature method.^[14] Other chemicals and reagents were obtained from commercial sources and used as received. All solvents were predried with activated molecular sieves and heated at reflux over the appropriate drying agents under an atmosphere of argon. The IR spectra were recorded with a Nicolet MagNa-IR 550 as KBr disks ($4000\text{--}400\text{ cm}^{-1}$). The elemental analyses for C, H, and N were performed with an EA1110 CHNS elemental analyzer. ^1H NMR spectra were recorded at ambient temperature with a Varian UNITY-400 spectrometer. ^1H NMR chemical shifts were referenced to the $[\text{D}_6]\text{-DMSO}$ signal.

1: To a solution of TabHPF_6 (1252 mg, 4 mmol) in MeCN (15 mL) was added Et_3N (2.5 mL). The colorless solution was then added into a 100-mL Schlenk flask containing a slurry of anhydrous $\text{Bi}(\text{NO}_3)_3$ (396 mg, 1 mmol) in MeOH (30 mL) at room temperature. The mixture was stirred for 1 h and filtered off by cannula. The dark-red filtrate was concentrated to ca. 20 mL and then Et_2O (20 mL) was layered onto the solution to form dark-red crystals of **1**. Yield: 0.421 g (72%). $\text{C}_{174}\text{H}_{252}\text{Bi}_5\text{F}_{42}\text{N}_{32}\text{O}_{24}\text{P}_7\text{S}_{18}$ (5813.03): calcd. C 35.95, H 4.37, N 7.71; found C 35.75, H 4.11, N 7.93. IR (KBr): $\tilde{\nu} = 2262$ (w), 1575 (m), 1486 (m), 1411 (s), 1351 (s), 1126 (vs), 1010 (s), 956 (s), 828 (s), 744 (s), 559 (s) cm^{-1} . ^1H NMR [400 MHz, $(\text{CD}_3)_2\text{SO}$]: $\delta = 3.34$ (s, 9 H, NMe_3), 7.42–7.81 (m, 4 H, Ph), 2.09 (s, 3 H, MeCN) ppm.

Crystal Data for 1: $\text{C}_{174}\text{H}_{252}\text{Bi}_5\text{F}_{42}\text{N}_{32}\text{O}_{24}\text{P}_7\text{S}_{18}$, $M_r = 5813.03$, trigonal, space group $R\bar{3}$, $a = 18.5443(14)\text{ \AA}$, $b = 18.5443(14)\text{ \AA}$, $c = 60.725(6)\text{ \AA}$, $\gamma = 120^\circ$, $V = 18085(3)\text{ \AA}^3$, $Z = 3$, $D_{\text{calcd.}} = 1.601\text{ g cm}^{-3}$, $F(000) = 8694$, $\mu = 3.934\text{ mm}^{-1}$, $T = 193\text{ K}$. 59818 reflections collected, 7373 unique ($R_{\text{int}} = 0.0591$). $R_1 = 0.0874$, $wR_2 = 0.2407$ and $S = 1.047$ based on 6258 observed reflections with $I > 2\sigma(I)$. Data collections were performed with a Rigaku Mercury CCD diffractometer with graphite-monochromated $\text{Mo-K}\alpha$ radiation ($\lambda = 0.71073\text{ \AA}$). The structure was solved by direct methods and refined with the full-matrix least-squares technique by using

the SHELXL-97 program.^[15] All non-hydrogen atoms except those of the PF_6^- anions were refined anisotropically, whereas all the H atoms were placed in geometrically idealized positions and constrained to ride on their parent atoms. CCDC-687345 (for **1**) contains the supplementary crystallographic data for this paper. These data can be obtained free of charge from The Cambridge Crystallographic Data Centre via www.ccdc.cam.ac.uk/data_request/cif.

Acknowledgments

This work was supported by the National Nature Science Foundation of China (20525101 and 20871088), the Soochow Scholar Program and Program for Innovative Research Team of Suzhou University, and the Nature Science Foundation of Gudong Province (No. 7300449). We are grateful to the editor and the reviewers for their helpful suggestions.

- [1] a) J. Waters, D. Crouch, J. Raftery, P. O'Brien, *Chem. Mater.* **2004**, *16*, 3289–3298; b) H. X. Li, Q. F. Xu, Q. Shen, J. P. Lang, *Chem. Lett.* **2003**, *32*, 642–643; c) J. P. H. Charmant, A. H. M. M. Jahan, N. C. Norman, A. G. Orpen, *Inorg. Chim. Acta* **2005**, *358*, 1358–1364; d) R. Cammi, M. Lanfranchi, L. Marchio, C. Mora, C. Paiola, M. A. Pellinghelli, *Inorg. Chem.* **2003**, *42*, 1769–1778; e) S. V. Larionov, T. G. Leonova, L. A. Glinskaya, R. F. Klevtsova, N. I. Batrachenko, V. E. Platonov, A. M. Maksimov, V. P. Fadeeva, *Zh. Neorg. Khim.* **2003**, *48*, 598–600; f) A. R. J. Genge, W. Levason, G. Reid, *Chem. Commun.* **1998**, 2159–2160; g) L. J. Farrugia, F. J. Lawlor, N. C. Norman, *Polyhedron* **1995**, *14*, 311–314; h) O. C. Monteiro, H. I. S. Nogueira, T. Trindade, M. Motevalli, *Chem. Mater.* **2001**, *13*, 2103–2111; i) Y. W. Koh, C. S. Lai, A. Y. Du, E. R. T. Tiekink, K. P. Loh, *Chem. Mater.* **2003**, *15*, 4544–4554; j) X. Y. Tang, H. X. Li, J. X. Chen, Z. G. Ren, J. P. Lang, *Coord. Chem. Rev.* **2008**, *252*, 2026–2049.
- [2] T. Klapötke, P. Gowik, *Z. Naturforsch., Teil B* **1987**, *42*, 940–942.
- [3] P. Köpi-Maier, T. Klapötke, *Inorg. Chim. Acta* **1988**, *152*, 49–52.
- [4] T. Lemiszka, L. Minchler, D. L. Cottle, US. Patent 2, 992, 202.
- [5] V. I. Suprunovich, S. T. Vashchenko, *Zh. Anal. Khim.* **1982**, *37*, 632–635.
- [6] A. Jadwiger, M. J. Stillman, *Biochem. Biophys. Res. Commun.* **1982**, *108*, 919–925.
- [7] a) R. Klement, A. May, *Eur. Des. Chem. Ges.* **1935**, *68A*, 1761–1766; b) T. B. Brill, N. C. Campbell, *Inorg. Chem.* **1973**, *12*, 1884–1888; c) G. G. Briand, N. Burford, T. S. Cameron, W. Kwiatkowski, *J. Am. Chem. Soc.* **1998**, *120*, 11374–11379; d) J. P. H. Charmant, A. H. M. M. Jahan, N. C. Norman, A. G. Orpen, T. J. Podesta, *CrystEngComm* **2004**, *6*, 29–33; e) M. W. DeGroot, J. F. Corrigan, *J. Chem. Soc., Dalton Trans.* **2000**, 1235–1236; f) R. Ahlrichs, A. Eichhofer, D. Fenske, K. May, H. Sommer, *Angew. Chem. Int. Ed.* **2007**, *46*, 8254–8257; g) H. Sommer, A. Eichhofer, D. Fenske, *Z. Anorg. Allg. Chem.* **2008**, *634*, 436–440.
- [8] a) J. X. Chen, W. H. Zhang, X. Y. Tang, Z. G. Ren, Y. Zhang, J. P. Lang, *Inorg. Chem.* **2006**, *45*, 2568–2580; b) J. X. Chen, Q. F. Xu, Y. Zhang, Z. N. Chen, J. P. Lang, *J. Organomet. Chem.* **2004**, *689*, 1071–1077; c) J. X. Chen, W. H. Zhang, X. Y. Tang, Z. G. Ren, H. X. Li, Y. Zhang, J. P. Lang, *Inorg. Chem.* **2006**, *45*, 7671–7680; d) J. X. Chen, Q. F. Xu, Y. Xu, Y. Zhang, Z. N. Chen, J. P. Lang, *Eur. J. Inorg. Chem.* **2004**, 4247–4252.
- [9] Z. G. Ren, X. Y. Tang, L. Li, G. F. Liu, H. X. Li, Y. Chen, Y. Zhang, J. P. Lang, *Inorg. Chem. Commun.* **2007**, *10*, 1253–1256.
- [10] G. G. Briand, N. Burford, T. S. Cameron, *Chem. Commun.* **1997**, 2365–2366.

- [11] P. González-Duarte, W. Clegg, I. Casals, J. Sola, J. Rius, *J. Am. Chem. Soc.* **1998**, *120*, 1260–1266.
- [12] D. A. Atwood, A. H. Cowley, R. D. Hernandez, R. A. Jones, L. L. Rand, S. C. Bott, J. L. Atwood, *Inorg. Chem.* **1993**, *32*, 2972–2974.
- [13] D. S. Sagatys, G. Smith, R. C. Bott, P. C. Healthy, *Aust. J. Chem.* **2003**, *56*, 941–943.
- [14] B. V. DePamphilis, B. A. Averill, T. Herskovitz, L. Que Jr, R. H. Holm, *J. Am. Chem. Soc.* **1974**, *96*, 4159–4167.
- [15] G. M. Sheldrick, *SHELXS-97 and SHELXL-97: Programs for X-ray Crystal Structure Solution and Refinement*, University of Göttingen, **1997**.

Received: October 3, 2008

Published Online: November 25, 2008

Structural Studies on (–)-Sparteine-Coordinated Lithiosilanes

Christian Däschlein^[a] and Carsten Strohmann^{*[a]}**Keywords:** Lithium / Silanes / X-ray diffraction / Arene ligands / NMR spectroscopy

A series of (–)-sparteine-coordinated lithiosilanes was synthesised and studied by X-ray structural analysis. All lithiosilanes are monomers in the solid state; yet, increasing sizes of substituents at silicon significantly influences their molecular structures. Due to the given stereochemistry of the dinitrogen (–)-sparteine ligand, all systems possess stereoinformation. NMR spectroscopic studies were used to obtain deeper insight into the structures of these compounds in solution. Observed coupling between the silicon and lithium atoms as

well as the presence of only one signal for each atom in the NMR spectra are indicative of monomeric structures of the lithiosilanes in solution. Additional quantum chemical calculations on one of the examined (–)-sparteine-coordinated systems provided very small energy differences between the diastereomers.

(© Wiley-VCH Verlag GmbH & Co. KGaA, 69451 Weinheim, Germany, 2009)

Introduction

Lithiated compounds like alkylolithiums^[1] and silyl-lithiums are important building blocks for organic, metal-organic and polymerisation chemistry.^[2–4] Besides their common usage as reagents in deprotonation reactions,^[5] they possess crucial importance for the nucleophilic introduction of alkyl and silyl groups^[6,7] to a wide number of functionalised materials.^[8] Yet, many details concerning the structure–reactivity patterns of functionalised lithiosilanes remain unclear. In general, the key to understanding their reactivity is the determination of the molecular structure and the clarification of the structural situation in solution. Contrary to the high number of oligomeric lithiumalkyls in nondonating solvents (such as tetrameric *t*BuLi in *n*-pentane or polymeric MeLi in hexane),^[2] lithiosilanes are almost exclusively accessible in donating solvents like thf or in the presence of highly disaggregating additives.^[9] Therefore, almost all known solid-state structures of lithiosilanes are deaggregated to monomeric, donor-base-stabilised, contact-ion pairs (see Figure 1) and only few higher aggregated examples are known [e.g., (Me₃SiMe₂SiLi)₄]^[10] and (Me₃SiLi)₆.^[11] However, detailed information of the structural situation of these compounds in solution is rare and extremely difficult to accomplish due to their high sensitivity and reactivity.

Over the last decades, NMR spectroscopy has served as one tool for the determination of the molecular structure for lithiated systems in solution (e.g., alkylolithiums).^[12] However, fast processes, including, solvent exchange,^[13]

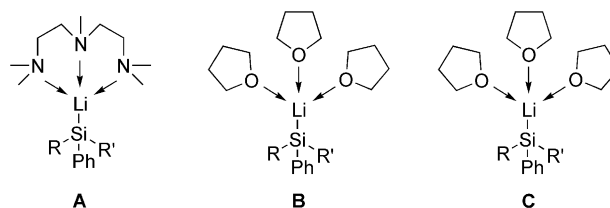


Figure 1. Selected examples of structurally characterised, monomeric silyllithiums with donating additives; in general: R, R' = alkyl, aryl, silyl; e.g.: **A**: R = Ph, R' = NEt₂;^[20] **B**: R = R' = Ph;^[21] **C**: R = Ph, R' = NEt₂.^[22]

conformational equilibria^[14] and chelate isomerisations,^[15] are often only observable on NMR spectroscopic timescales at low temperatures during the measurements. Moreover, due to the quadrupole moment of both ⁶Li and ⁷Li (spin quantum number > 1/2, ⁶Li = 1, ⁷Li = 3/2), NMR signals are often broadened and not fully resolved.^[16,17] In general, desired couplings to adjacent atoms are often more visible at lower temperatures. Thereby, especially resolved coupling patterns are of great interest for the understanding of the structural situation in solution, as the coupling between two atoms is a hint to the actual structure. In general, coupling between two atoms indicates a strong fixation on the NMR timescale and, thus, in the molecule. Nevertheless, the absence of coupling at a certain temperature does not exclude bonding of two atoms, but may be a result of relaxation processes at this temperature. Unfortunately, decreased solubility of lithiated compounds at very low temperatures in nonpolar solvents often hinders further decreases in the temperature. Changing to more polar solvents is in most cases impossible, as the lithiated compound may react with the solvent (e.g., ether cleavage),^[18,19] or in general, different structure motives like solvent-separated ion pairs (SSIP) oc-

[a] Technische Universität Dortmund, Anorganische Chemie, Otto-Hahn-Straße 6, 44227 Dortmund
E-mail: mail@carsten-strohmman.de

Supporting information for this article is available on the WWW under <http://www.eurjic.org> or from the author.

cur. In addition, selective synthesis, controllable reactivity and stability for several days, at least, are further desired features. Therefore, suitable model compounds to study the structure of lithiosilanes in solution are very rare.

Most recently we reported on the synthesis of the first chiral, monomeric, (–)-sparteine-coordinated lithiosilanes.^[22] X-ray diffraction analyses were used to clarify their molecular structures in the crystal. NMR spectroscopic studies indicated monomeric structures in solution, too. On the basis thereof, we present here detailed studies on the molecular structures of a series of chiral, (–)-sparteine-coordinated lithiosilanes. Four different systems were examined to understand the influence of the steric demand of the substituents at silicon on the molecular structures. The combination of X-ray structural analysis and NMR spectroscopic studies was used to elucidate the structural situation of the lithiosilanes, both in the solid state and in solution. The defined stereochemistry of the (–)-sparteine ligand served as a probe for determination of the molecular structure in solution. Additional DFT calculations on one of these lithiosilanes were accomplished to determine the relative energy ratios between the different diastereomers in the gas phase.

Results and Discussion

X-ray Structural Analysis of (–)-Sparteine Coordinated Lithiosilanes

To investigate the influence of the size of the substituents at silicon of lithiosilanes on the solid-state structure and the structural situation in solution, we synthesised a series of (–)-sparteine-coordinated systems for detailed investi-

gations. Figures 2 and 3 show the examined compounds. In addition to the already-synthesised lithiosilanes $\text{PhMe}_2\text{SiLi}\cdot(-)\text{-sparteine}\cdot\text{thf}$ [**1**·(–)-sparteine·thf] and $\text{Ph}_2(\text{Et}_2\text{N})\text{SiLi}\cdot(-)\text{-sparteine}$ [**2**·(–)-sparteine]^[22] (see Figure 2), we prepared the two new (–)-sparteine-coordinated systems $\text{Ph}_2\text{MeSiLi}\cdot(-)\text{-sparteine}\cdot\text{thf}$ [**3**·(–)-sparteine·thf] and $\text{Ph}(\text{Et}_2\text{N})_2\text{SiLi}\cdot(-)\text{-sparteine}\cdot\text{thf}$ [**4**·(–)-sparteine·thf] (see Figure 3).

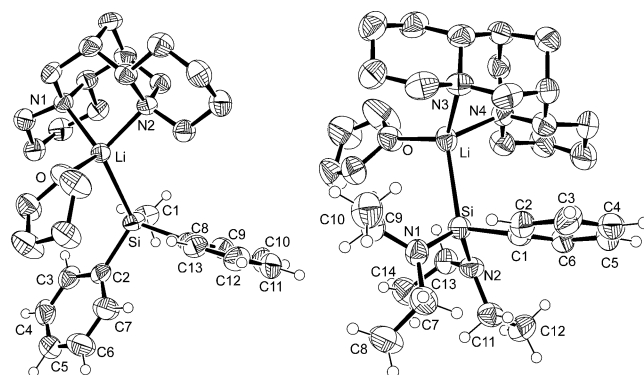


Figure 3. Molecular structure and numbering scheme of **3**·(–)-sparteine·thf (left) and **4**·(–)-sparteine·thf (right) (ORTEP plot at 50% probability level, numbering scheme and hydrogen atoms of the coordinating ligands are omitted for clarity). Selected bond lengths [Å] and angles [°]: **3**·(–)-sparteine·thf: C1–Si 1.941(4), C2–Si 1.945(3), C8–Si 1.938(3), Li–Si 2.706(5), C8–Si–C1 102.53(17), C8–Si–C2 102.14(13), C1–Si–C2 99.88(16); **4**·(–)-sparteine·thf: C1–Si 1.946(4), N1–Si 1.787(4), N2–Si 1.796(3), Li–Si 2.743(6), C9–N1–C7 116.4(4), C9–N1–Si 121.2(3), C7–N1–Si 122.3(3), C13–N2–C11 113.8(3), C13–N2–Si 117.6(3), C11–N2–Si 124.1(3), N1–Si–N2 111.52(16), N1–Si–C1 100.78(17), N2–Si–C1 98.76(17).

Compounds **1**·(–)-sparteine·thf, **2**·(–)-sparteine and **3**·(–)-sparteine·thf could be obtained with a common method by treatment of the corresponding disilane with elemental lithium in thf, whereas **4** was synthesised by starting with bis(diethylamino)phenylchlorosilane (**5**) due to the impossibility of the cleavage of the corresponding disilane (see Scheme 1).^[22] After subsequent removal of the solvent and

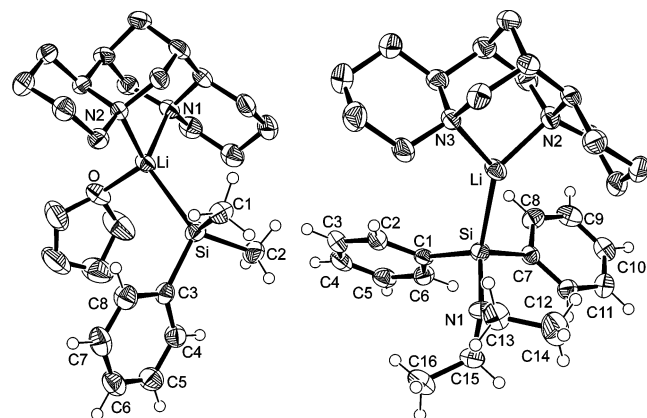
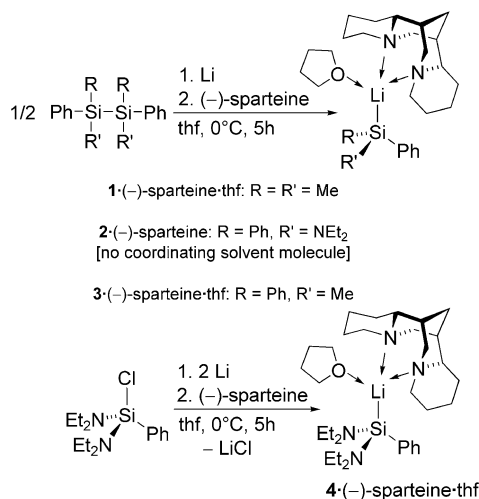


Figure 2. Molecular structure and numbering scheme of **1**·(–)-sparteine·thf (left) and **2**·(–)-sparteine (right) (ORTEP plot at 50% probability level, numbering scheme and hydrogen atoms of the coordinating ligands are omitted for clarity). Selected bond lengths [Å] and angles [°]: **1**·(–)-sparteine·thf: C1–Si 1.948(3), C2–Si 1.932(3), C3–Si 1.934(3), Li–Si 2.675(4), C2–Si–C3 101.82(11), C2–Si–C1 100.09(13), C3–Si–C1 101.09(11), C2–Si–Li 118.99(12), C3–Si–Li 119.72(11), C1–Si–Li 112.02(11); **2**·(–)-sparteine: C1–Si 1.923(4), C7–Si 1.922(4), N1–Si 1.763(3), Li–Si 2.600(5), C7–Si–C1 100.57(17), N1–Si–Li 117.00(19), C7–Si–Li 107.46(17), C1–Si–Li 120.17(19), C13–N1–Si 122.2(2), C15–N1–Si 123.3(3), C13–N1–C15 114.4(3).



Scheme 1. Synthesis of (–)-sparteine-coordinated lithiosilanes **1**·(–)-sparteine·thf, **2**·(–)-sparteine, **3**·(–)-sparteine·thf (top) and **4**·(–)-sparteine·thf (bottom).

the byproduct in the synthesis of **4** (LiCl), the oily residues were dissolved again in Et₂O and one equivalent of (–)-sparteine was added. Afterwards the brown solutions were stored at –80 °C to yield the desired compounds as crystalline solids. Compound **3**·(–)-sparteine·thf crystallised from Et₂O in the orthorhombic crystal system *P*2₁2₁2₁ as brownish blocks and **4**·(–)-sparteine·thf from Et₂O in the monoclinic crystal system *P*2₁ as brown needles (see Table 4 for additional crystal data and refinement details). In both compounds, the lithium metal has a coordination number of four. Together with the silyl unit, one molecule of thf and one molecule of the diamine coordinate to the lithium atom to form monomeric structures in the solid state. Therefore, the newly synthesised systems underline the domination of the monomeric structural motif in functionalised lithiosilanes.

Due to the given configuration of the chiral (–)-sparteine ligand, the lithium atoms also become stereogenic centres. Under usage of the CIP nomenclature we can formulate *Lis*-configuration for **3**·(–)-sparteine·thf and *Lir*-configuration for **4**·(–)-sparteine·thf [for a more detailed discussion on this topic, see the section entitled “NMR Spectroscopic Studies of the (–)-Sparteine-Coordinated Lithiosilanes in Solution”]. To justify the observed configuration of these systems, several crystals were measured for each compound, all showing the same absolute configuration at lithium.

With the presented series of differently substituted (–)-sparteine-coordinated lithiosilanes, the question arises: What impact does the different steric demand of the substituents at silicon have on the structure parameters in the solid state? The first apparent difference of the four molecules is the threefold-coordinated lithium atom in **2**·(–)-sparteine, whereas the other three lithiosilanes possess a coordination number of four at lithium. Starting with the smallest of the four systems **1**·(–)-sparteine·thf, the steric demand of the substituents at silicon increases over **3**·(–)-sparteine·thf to **4**·(–)-sparteine·thf and ends with the most bulky compound, **2**·(–)-sparteine. Therefore, the relatively flexible diethylamino substituents claim less space around the silicon atom than the more fixed arenes. This increasing steric demand from **1**·(–)-sparteine·thf over **3**·(–)-sparteine·thf and **4**·(–)-sparteine·thf to **2**·(–)-sparteine is supported by the value of the silicon–lithium distance: with a length of 2.600(5) Å, the Si–Li bond in **2**·(–)-sparteine is the shortest of the investigated molecules and significantly shorter than those in the other three lithiosilanes with a coordination number of four at lithium [**1**·(–)-sparteine·thf 2.675(4) Å, **3**·(–)-sparteine·thf 2.706(5) Å, **4**·(–)-sparteine·thf 2.743(6) Å]. Therefore, as demonstrated, the silicon–lithium distance increases with increasing steric demand of the substituents at silicon until the bulky substituents cause a change in the coordination number at lithium. This change in coordination number is accompanied with a significantly shortened bond length owing to less charge distribution in the threefold-coordinated lithiosilane.

The sum of the C–Si–C, C–Si–N and N–Si–N angles at silicon have values of 303.0 [**1**·(–)-sparteine·thf], 311.1 [**2**·(–)-sparteine], 304.1 [**3**·(–)-sparteine·thf] and 310.3°

[**4**·(–)-sparteine·thf] and thus are in the range of other functionalised lithiosilanes.^[9] However, it is noteworthy that the angles at silicon are affected by the size of the substituents at silicon: increasing the steric demand of the substituents results in an increasing sum of the angles around the silicon atom. The sum of bond angles on the nitrogen atoms in the amino-functionalised systems are 359.9 [**2**·(–)-sparteine], 355.5 and 360.0° [**4**·(–)-sparteine·thf], indicating an almost planar environment in both molecules, typical for other amino-substituted lithiosilanes.^[3n,22]

Most recently we reported on the crystal structures of PMDTA-coordinated lithiosilanes (PMDTA = pentamethyldiethylenediamine).^[20] On the basis of quantum chemical calculations, indicating Pauli repulsion of the electrons in the occupied frontier orbitals, we were able to explain the reasons for bent arenes in anionic group 14 systems (silicon to lead). The (–)-sparteine-coordinated lithiosilanes presented herein are another outstanding example for this deformation: all shown systems possess bent phenyl groups with torsional angles <<180°. Thereby, **4**·(–)-sparteine·thf possesses the most bent phenyl group in all known lithiosilanes so far (Si–C_i–C_o–C_m –168.5/+168.2). This is easy to understand, as the highly electronegative nitrogen substituents at silicon increase the *s* character of the “lone pair”. Thus, the arenes in **2**·(–)-sparteine and **4**·(–)-sparteine·thf are significantly more bent than the ones in the solely organyl-substituted systems. Moreover, due to the necessity of correct orientation of the occupied orbitals at the phenyl substituents and the “lone pair” at silicon, one of the arenes is always clearly more bent than the second in **2**·(–)-sparteine and **3**·(–)-sparteine·thf. Finally, all angles at C_i are significantly smaller than 120° (which can be explained by Bent’s Rule) and due to the σ-donating capability of silicon, the C–C bond lengths within the ring decrease with increasing distance to the silicon atom (*a* > *b* > *c*, Figure 4; detailed descriptions concerning these deformations for related systems can be found in ref.^[20]). Figure 4 and Table 1 give an overview of the described deformations of the aromatic substituents.

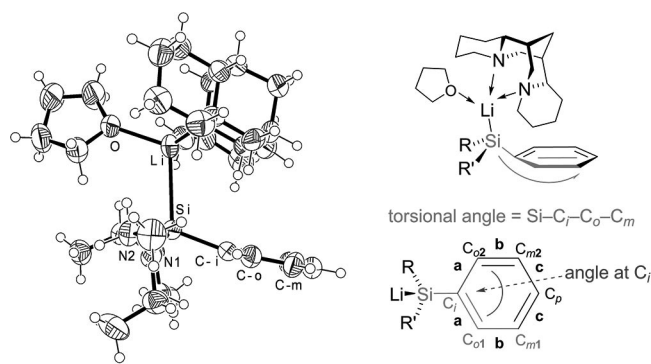


Figure 4. Molecular structure of **4**·(–)-sparteine·thf (left) as an example for the bent aromatic substituents in the lithiosilanes (ORTEP plot at 50% probability level). Scheme of the bent phenyl substituents and the deformation within the ring (right).

Table 1. Bond lengths a , b and c , angles at C_i and torsional angles $\text{Si}-C_i-C_o-C_m$ of (–)-sparteine-coordinated lithiosilanes **1**, **2**, **3** and **4** (negative values: $\text{Si}-C_i-C_{o1}-C_{m1}$; positive values: $\text{Si}-C_i-C_{o2}-C_{m2}$; for details, see Figure 4).

| Lithiosilane | a [Å] | b [Å] | c [Å] | Angle at C_i [°] | Torsional angle ($\text{Si}-C_i-C_o-C_m$) [°] |
|-----------------------------|----------|----------|----------|--------------------|---|
| 1 ·(–)-Sparteine·thf | 1.407(4) | 1.382(5) | 1.377(5) | 114.95(0.24) | –176.9(0.22), +177.1(0.24) |
| 2 ·(–)-Sparteine | 1.410(5) | 1.390(6) | 1.387(6) | 114.51(0.33) | –179.0(0.31), +179.6(0.31), –171.4(0.32), +171.6(0.30) |
| 3 ·(–)-Sparteine·thf | 1.412(5) | 1.390(6) | 1.382(6) | 114.99(0.33) | –179.1(0.30), +178.8(0.37), –176.2(0.27), +176.4(0.28) |
| 4 ·(–)-Sparteine·thf | 1.404(5) | 1.387(5) | 1.376(6) | 115.31(0.29) | –179.1(0.30), +178.8(0.37), –176.2(0.27), +176.4(0.28) |
| | 1.400(5) | 1.373(6) | 1.383(8) | 115.75(0.34) | –168.5(0.36), +168.2(0.35) |
| | 1.394(6) | 1.392(7) | 1.372(8) | 115.34(0.39) | |

NMR Spectroscopic Studies of the (–)-Sparteine-Coordinated Lithiosilanes in Solution

One of the most important questions for the determination of the reactivity patterns of the stereochemically defined lithiosilanes is their structural situation in solution. To clarify this decisive topic, we performed NMR spectroscopic studies of the former measured crystals in $[\text{D}_8]\text{toluene}$. To minimise the signal-broadening quadrupole moment of lithium and to exclude the overlay of different signals due to dynamical processes at higher temperatures, the measurements were performed at -50°C in addition to room temperature. As mentioned above, all described compounds possess stereoinformation because of the chiral (–)-sparteine ligand. For **2**·(–)-sparteine, it is possible to design one defined stereoisomer, whereas there are two possible diastereomeric forms for the compounds with a four-coordinated lithium atom [**1**·(–)-sparteine·thf, **3**·(–)-sparteine·thf and **4**·(–)-sparteine·thf]. Due to the given configuration of (–)-sparteine, one diastereomer with Lis- and one with Lir-configuration can be formulated. Figure 5 summarises the configuration of each compound observed in the crystal.

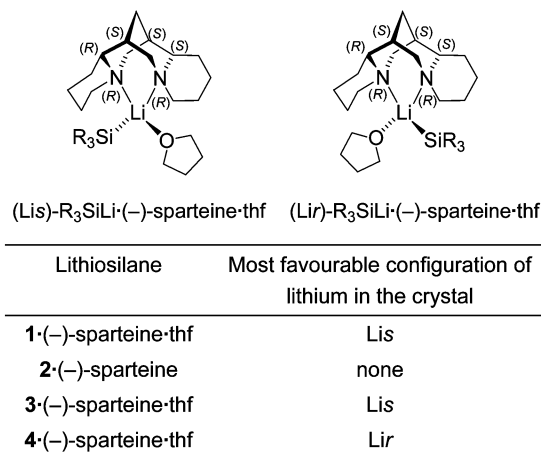


Figure 5. Possible diastereomeric forms of the lithiosilanes caused by the fourfold coordination of the lithium atom and the given configuration at the (–)-sparteine ligand; $\text{R}_3\text{Si} = \text{Ph}_2\text{MeSi}$, PhMe_2Si , $\text{Ph}(\text{Et}_2\text{N})_2\text{Si}$ (top); configuration of the lithiosilanes observed in the crystal (bottom).

On the basis of the determined solid-state structures, the central question concerning the NMR spectroscopic studies of the lithiosilanes is: what is their structural situation in solution? To answer this question, several NMR spectroscopic tools can be used. Whereas the presence of coupling between the silicon and lithium atoms indicates a strong

and fixed contact between them, the observation of only one signal for the same atom would be a clear hint to the existence of one defined diastereomer in solution. The recognition of diastereotopic signals at a certain temperature indicates a molecule containing the silane unit and the (–)-sparteine ligand.

For **2**·(–)-sparteine, there is only one stereoisomer possible. In accordance with this, we observed only one signal for each atom in the NMR spectra. At both temperatures (r.t. and -50°C), a coupling between the silicon and the lithium atoms was detected in the ^{29}Si NMR spectrum (see Figure 6). This coupling supports the strong $\text{Si}-\text{Li}$ contact of $2.600(5)$ Å, already found in the crystal.^[9,22] The coupling constants have values of $^1J_{\text{Si,Li}} = 53.3$ Hz at -50°C and $^1J_{\text{Si,Li}} = 65.3$ Hz at room temperature. The strong $\text{Si}-\text{Li}$ contact is furthermore supported by different signals for the diastereotopic phenyl groups: at room temperature, all carbon atoms of the arenes are different, whereas the *para*- and *ipso*-carbon atoms are different at -50°C (the signals for the *meta*- and *ortho*-carbon atoms fall together). The chemical shift of the lithium atom has a value of 1.61 ppm at room temperature and 1.16 ppm at -50°C .

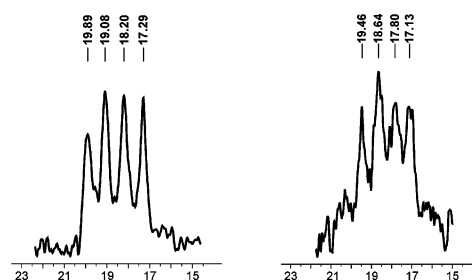


Figure 6. Section of the ^{29}Si NMR spectrum [ppm] of **2**·(–)-sparteine at -50°C (left, $^1J_{\text{Si,Li}} = 53.3$ Hz) and at room temperature (right, $^1J_{\text{Si,Li}} = 65.3$ Hz).

A quartet with four equal peaks is expected for $^{29}\text{Si}, ^7\text{Li}$ coupling; yet, the observed signal form is not symmetric. This can be caused by an overlap of the $^{29}\text{Si}, ^6\text{Li}$ coupling of the second NMR-active isotope of lithium (natural abundance $^7\text{Li}/^6\text{Li} \approx 92.5:7.5$). To rationalise the shape, a simulated $^{29}\text{Si}, \text{Li}$ coupling of **2**·(–)-sparteine was performed (see Figure 7). Spectrum **A** in Figure 7 shows the superimposed simulated spectra of the $^{29}\text{Si}, ^7\text{Li}$ - and $^{29}\text{Si}, ^6\text{Li}$ coupling, whereas **B** shows the same for the $^{29}\text{Si}, ^7\text{Li}$ coupling and **C** shows the $^{29}\text{Si}, ^6\text{Li}$ coupling. In all three cases the magenta line refers to the simulated spectrum and the black line to the experimental spectrum. Obviously, the experimental line shape of the nonsymmetric quartet is a result of the overlay

of the coupling between ^{29}Si and ^6Li (C). The addition with the symmetric line shape of the simulated ^{29}Si , ^7Li coupling (B) results in the observed experimental shape ($A = B + C$). Consequently, all information obtained by the NMR spectroscopic studies indicates that the lithium atom is still bonded to the silicon atom in solution and that only one molecule is present. Therefore, the molecular structure of $2\cdot(-)$ -sparteine in solution should be identical to the one determined in the solid state.

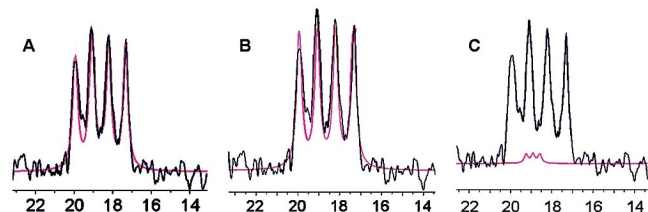


Figure 7. Section of the simulated ^{29}Si NMR spectrum [ppm] of $2\cdot(-)$ -sparteine: black line shape: experimental ^{29}Si , ^7Li coupling; magenta line shape: simulated ^{29}Si , ^7Li coupling; (A) ^{29}Si , ^7Li and ^{29}Si , ^6Li coupling added up; (B) ^{29}Si , ^7Li coupling; (C) ^{29}Si , ^6Li coupling.

For $1\cdot(-)$ -sparteine·thf, $3\cdot(-)$ -sparteine·thf and $4\cdot(-)$ -sparteine·thf, we obtained only one of the two possible diastereomers in the crystal (after measuring several crystals each). Moreover, we observed only one set of signals for each atom in the NMR spectra, both at room temperature and at $-50\text{ }^{\circ}\text{C}$. This absence of a second set of signals even at $-50\text{ }^{\circ}\text{C}$ is a clear clue for the presence of only one diastereomer in solution. Yet, a possible detachment of the thf molecules from the lithium – forming one stereoisomer – would also result in only one set of signals for each atom. Therefore, the coordination number of lithium has to be regarded in these systems. To differ between fourfold-coordinated lithium in the lithiosilanes, where one molecule of thf is still bonded to the lithium, and a threefold-coordinated system, the first possible differentiation one may think of is the chemical shifts of the lithium atoms. Several groups have reported the influence of solvents to the resonance signals of lithium in NMR spectroscopy.^[23] Hence, some systems are known for which a significant shift is observed when a polar, coordinating solvent like ethyl ether is used instead of a nonpolar solvent (e.g., cyclopentane).^[23a] However, it is also well known that factors like viscosity, temperature and concentration are often in the same order as the shift changes induced due to structural ef-

fects.^[17a,23a,24] Therefore, especially if the shift changes are only small, the information gained from the ^6Li NMR resonance signals have to be interpreted with great caution.

Table 2 shows the obtained lithium NMR chemical shifts of the four investigated (–)-sparteine-coordinated systems. For each compound, the values for the lithium signals at room temperature are significantly shifted to higher field relative to those at $-50\text{ }^{\circ}\text{C}$. Besides, the two amino-function-alised systems possess significantly higher values as the solely organyl-substituted systems. Nevertheless, the Li resonance signals of the four systems are too close to each other to make a clear statement concerning its coordination sphere. Finally, the chemical shifts of the thf molecules can be considered. Fortunately, the resonance signals of ^{13}C (see Table 2) and ^1H in these three diastereomeric compounds are comparable to thf molecules coordinated to lithium atoms in other lithiated systems^[25] and, thus, indicate the same coordination sphere of lithium in solution as in the solid state.

For all three compounds, no resolved coupling between the silicon and the lithium atoms was detected in the ^{29}Si NMR spectrum at room temperature, underlining the significantly weaker Si–Li contacts in comparison to that in $2\cdot(-)$ -sparteine. For all three compounds, the measurement at $-50\text{ }^{\circ}\text{C}$ provided the desired, resolved coupling between the silicon and lithium atoms (see Figure 8). Moreover, only one coupling in each spectrum was detected, which is an important hint for the presence of only one diastereomer in solution. The coupling constants have values of $^1J_{\text{Si,Li}} = 47.9\text{ Hz}$ [$1\cdot(-)$ -sparteine·thf], $^1J_{\text{Si,Li}} = 44.3\text{ Hz}$ [$3\cdot(-)$ -sparteine·thf] and $^1J_{\text{Si,Li}} = 58.3\text{ Hz}$ [$4\cdot(-)$ -sparteine·thf]. Again, the unsymmetrical line shape of the quartets can be explained with the overlap of the ^{29}Si , ^6Li coupling.

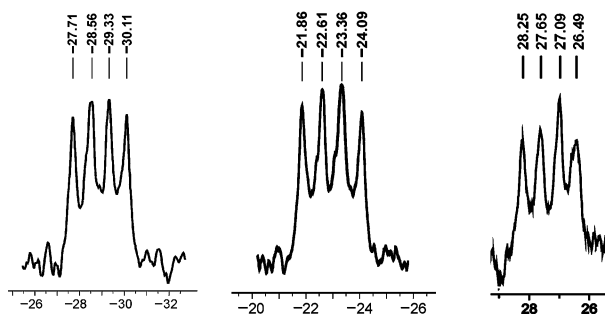


Figure 8. Section of the ^{29}Si NMR spectrum [ppm] of $1\cdot(-)$ -sparteine·thf (left, $^1J_{\text{Si,Li}} = 47.9\text{ Hz}$), $3\cdot(-)$ -sparteine·thf (middle, $^1J_{\text{Si,Li}} = 44.3\text{ Hz}$) and $4\cdot(-)$ -sparteine·thf (right, $^1J_{\text{Si,Li}} = 58.3\text{ Hz}$) at $-50\text{ }^{\circ}\text{C}$.

Table 2. Chemical shifts [ppm] of the lithium atoms at room temperature and at $-50\text{ }^{\circ}\text{C}$ for the (–)-sparteine-coordinated lithiosilanes.

| | $1\cdot(-)$ -Sparteine·thf | $2\cdot(-)$ -Sparteine | $3\cdot(-)$ -Sparteine·thf | $4\cdot(-)$ -Sparteine·thf |
|---|---|------------------------|---|--|
| Li signal at r.t. | 1.10 | 1.61 | 1.02 | 1.60 |
| Li signal at $-50\text{ }^{\circ}\text{C}$ | 0.90 | 1.16 | 0.82 | 1.13 |
| ^{13}C signals of the thf ligands at r.t. | 25.7 (2 C) (CH_2CO) 68.2 (2 C) (CH_2O) | none | 25.5 (2 C) (CH_2CO) 68.4 (2 C) (CH_2O) | 25.76 (2 C) (OCCH_2) 67.9 (2 C) (OCH_2) |
| ^{13}C signals of the thf ligands at $-50\text{ }^{\circ}\text{C}$ | 25.5 (2 C) (CH_2CO) 68.1 (2 C) (CH_2O) | none | 25.2 (2 C) (CH_2CO) 68.3 (2 C) (CH_2O) | 25.5 (2 C) (OCCH_2) 68.0 (2 C) (OCH_2) |

By comparing the values of the coupling between the silicon and lithium atoms for all compounds at -50°C one recognises that the J values for the two solely organyl-substituted systems **1**·(–)-sparteine·thf [$^1J_{\text{Si,Li}} = 47.9\text{ Hz}$] and **3**·(–)-sparteine·thf [$^1J_{\text{Si,Li}} = 44.3\text{ Hz}$] are significantly smaller than the ones for the amino-functionalised systems **2**·(–)-sparteine [$^1J_{\text{Si,Li}} = 53.3\text{ Hz}$] and **4**·(–)-sparteine·thf [$^1J_{\text{Si,Li}} = 58.3\text{ Hz}$]. Compound **4**·(–)-sparteine·thf bearing two diethylamino groups has the highest value for the $^{29}\text{Si,Li}$ coupling. Therefore, the coupling constant in these (–)-sparteine-coordinated lithiosilanes increases with increasing number of nitrogen substituents bonded to the silicon atom.

Another noteworthy observation is the value for the resonance signal of silicon: as one can see, **1**·(–)-sparteine·thf and **3**·(–)-sparteine·thf have positive values in the ^{29}Si NMR spectra, whereas **2**·(–)-sparteine and **4**·(–)-sparteine·thf have negative values. This is not in agreement with the common understanding of the chemical shifts of functionalised lithiosilanes and can be explained by the simultaneous presence of electronegative and electropositive substituents, resulting in large coupling constants between occupied and unoccupied orbitals with significant silicon character and relatively small energy differences (for a detailed discussion, see ref.^[37]).

Altogether, several clear hints show the presence of only one diastereomer in solution, and it seems that the (–)-sparteine-coordinated lithiosilanes presented herein are monomers in solution as well.

Additional DFT Calculations of **3**·(–)-Sparteine·thf

In 2006, we performed DFT calculations on **1**·(–)-sparteine·thf [B3LYP/6-31+G(d) level].^[22] Starting with six different isomers (the starting structural parameters were taken from the solid-state structure), the two diastereomeric conformations (Lis)-**1**·(–)-sparteine·thf and (Lir)-**1**·(–)-sparteine·thf proved to be the most favoured isomers after the energy optimisation in the gas-phase calculations. The final energy difference between the two isomers was only 2.9 kJ mol^{-1} , with (Lis)-**1**·(–)-sparteine·thf, the most favourable stereoisomer in the crystal, as the most stable diastereomer in the gas phase, too.

To acquire better understanding of whether the results of gas-phase calculations can be used to clearly predict the preferred molecular structure of lithiosilanes in solution and in the solid state, we performed additional DFT calculations [B3LYP/6-31+G(d)] on the newly synthesised system **3**·(–)-sparteine·thf.^[26] To answer the question, the relative energy ratios between the different diastereomers were calculated. Harmonic vibrational frequency analyses on the smaller theoretical level B3LYP/3-21+G* to establish the nature of the global minima showed no imaginary frequencies. The starting structural parameters for six different isomers were taken from the solid-state structure. A preoptimisation with the PM3 method showed that there is one conformer for each diastereomer that is energetically

strongly unfavoured. Therefore, only four conformers of **3**·(–)-sparteine·thf were considered for the following discussion. The final results of the DFT calculations are shown in Figure 9 and Table 3.

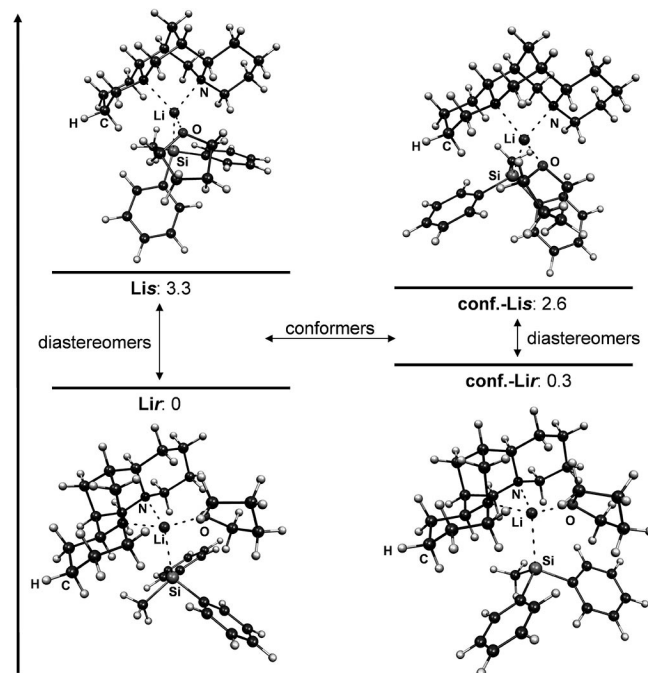


Figure 9. Profile of the relative energies E_{rel} [kJ mol^{-1}] of the four optimised isomers of **3**·(–)-sparteine·thf; molekel-plot.^[27]

Table 3. Total and zero-point energies of the calculated stereoisomers of **3**·(–)-sparteine·thf.

| | Method/basis | | |
|-----------|-----------------|---------------|---------------|
| | B3LYP/6-31+G(d) | B3LYP/3-21+G* | |
| | SCF [Hartree] | SCF [Hartree] | ZPE [Hartree] |
| Lir | –1729, 5588 | –1720, 4288 | –1719, 6851 |
| conf.-Lir | –1729, 5587 | –1720, 4300 | –1719, 6860 |
| conf.-Lis | –1729, 5578 | –1720, 4284 | –1719, 6844 |
| Lis | –1729, 5575 | –1720, 4288 | –1719, 6849 |

The two decisive conformers were (Lis)-**3**·(–)-sparteine·thf (found in the crystal) and (Lir)-**3**·(–)-sparteine·thf (its diastereomer). The most favoured energy was obtained for (Lir)-**3**·(–)-sparteine·thf, the diastereomer that was not found in the crystal. Moreover, the other two possible conformers are also slightly lower in energy; yet, the energy difference of the two diastereomers is only 3.3 kJ mol^{-1} . That means, in comparison to the DFT studies accomplished in 2006 for model compound **1**·(–)-sparteine·thf, where the diastereomer lowest in energy in the calculations was the same as that in the crystal, the stereoisomer found in the crystal for **3**·(–)-sparteine·thf is not the most favourable one in the theoretical investigations. As a conclusion, the energy difference between the different stereoisomers of (–)-sparteine-coordinated lithiosilanes is too close to each other to make a definite statement concerning their molecular structure in solution, although the experimental results provide only one defined diastereomer

in the crystal. Yet, many crucial details concerning solvent, thermodynamic (e.g., epimerisation) and packing effects remain unconsidered in the gas phase and may easily shift the small energy differences of the calculations.

Conclusions

On the basis of a series of (–)-sparteine-coordinated lithiosilanes (possessing all the stereoinformation due to the chiral diamine), we examined the influence of the steric demand of the substituents at silicon on the molecular structure in the solid state. The more bulky the situation, the longer the silicon–lithium contact until the coordination number of the lithium changes to three as in **2**·(–)-sparteine. This finally results in a significantly shortened silicon–lithium distance due to less charge distribution in the threefold-coordinated system. Moreover, increasing size of the substituents also results in increased values for the sum of the bond angles around the silicon atom. All torsional angles in the aromatic substituents are significantly below the ideal value of 180° [smallest: 168.2° in **4**·(–)-sparteine·thf]. This is a result of Pauli repulsion of the electrons in the occupied frontier orbitals, mostly pronounced in the systems with electronegative nitrogen substituents. Therefore, **4**·(–)-sparteine·thf, bearing two amino groups, has the smallest torsional angle ($\text{Si}-\text{C}_i-\text{C}_o-\text{C}_m$ –168.5/+168.2) observed in all lithiosilanes so far.

NMR spectroscopic studies were accomplished to examine the structural situation of (–)-sparteine-coordinated lithiosilanes in solution: all four systems showed only one coupling between the silicon and lithium atoms at –50 °C as well as only one signal for each atom in the ^{13}C and ^1H NMR spectra. Moreover, the coupling between the silicon and lithium atoms in each ^{29}Si NMR spectrum at –50 °C clearly indicates the intact bond of the lithium and the silicon in solution. These points are clear hints to the presence of only one stereoisomer in solution and underline the preferred monomeric structure of lithiosilanes. Unequal peaks for the quartets of the ^{29}Si ·Li couplings in these spectra can be explained by an overlap of the coupling of ^{29}Si · ^6Li with that of ^{29}Si · ^7Li and are therefore not due to the second imaginable diastereomer. The coupling constant increases with increasing number of nitrogen substituents.

Additional quantum chemical calculations on one of the examined (–)-sparteine-coordinated systems provided only small energy differences between diastereomers.

Experimental Section

Experimental Details: All experiments were carried out under a dry, oxygen-free argon atmosphere by using standard Schlenk techniques. Involved solvents were dried with sodium and distilled prior to use. ^1H , ^7Li , ^{13}C and ^{29}Si NMR spectra were recorded with DRX-300 and AMX-500 Bruker spectrometers at 22 °C. Assignment of the signals was supported by additional DEPT-135, C, H-COSY and H, H-COSY experiments and by data acquired from other authors.^[28,29] In the ^1H NMR spectra nondistinguishable signals of the (–)-sparteine ligand were grouped together (see Figure 10).

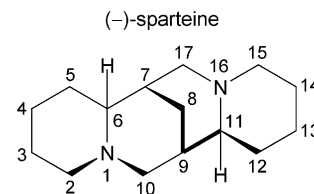


Figure 10. Lewis structure (including numbering scheme) of (–)-sparteine.

The following abbreviations are used: s = singlet, d = doublet, t = triplet, q = quartet, m = multiplet, br. = broad signal. Carbon and hydrogen atoms of the phenyl substituents are abbreviated as follows: *C-i* = carbon atom in the *ipso* position, *C-o* = carbon atom in the *ortho* position, *C-m* = carbon atom in the *meta* position, *C-p* = carbon atom in the *para* position; if an exact assignment of hydrogen atoms to these positions was possible the signals were abbreviated analogously otherwise indicated as aromatic H. Starting compounds 1,2-dimethyl-1,1,2,2-tetraphenyldisilane and (–)-sparteine were trading products of ABCR and Sigma–Aldrich; bis(diethylamino)phenylchlorosilane was synthesized according to a known method.^[30] The synthesis of **1**·(–)-sparteine·thf and **2**·(–)-sparteine as well as their characterisation was reported elsewhere.^[22]

3·(–)-Sparteine·thf: 1,2-Dimethyl-1,1,2,2-tetraphenyldisilane (750 mg, 2.77 mmol) was added at room temperature to a twofold excess of lithium (38.5 mg, 5.54 mmol) suspended in thf (5 mL). On the first occurrence of discoloration the reaction mixture was cooled to 0 °C and stirred for 5 h at this temperature. After removal of all volatile compounds under reduced pressure, the oily residue was suspended in a small amount of ethyl ether and (–)-sparteine (1.30 g, 5.54 mmol, 1 equiv.) was added. Storing the brown solution at –80 °C for 24 h resulted in the formation of **3**·(–)-sparteine·thf as a crystalline solid. ^1H NMR (300.1 MHz, $[\text{D}_8]\text{toluene}$, r.t.): δ = 0.60–0.75 (m, 1 H, H4/H13), 0.82 (s, 3 H, SiCH_3), 0.85–1.00 (m, 1 H, H5/H12), 0.90–1.05 (m, 1 H, H4/H13), 0.90–1.10 (m, 1 H, H5/H12), 1.00–1.10 (m, 2 H, H7/H9), 1.00–1.15, 1.15–1.30 (m, 1 H each, H3/H14), 1.15–1.20 (m, 4 H, CH_2CO), 1.25–1.35 (m, 1 H, H4/H13), 1.30–1.45 (m, 1 H, H4/H13), 1.40–1.55 (m, 1 H each, H5/H12, H2/H15), 1.55–1.65 (m, 2 H, H3/H14, H8), 1.55–1.70 (m, 1 H each, H6/H11, H5/H12), 1.75–1.85 (m, 1 H, H2/H15), 1.85–1.95 (m, 2 H, H3/H14, H8), 2.25–2.35, 2.50–2.60 (m, 1 H each, H10/H17), 2.65–2.75 (m, 2 H, H2/H15), 2.75–2.85, 2.85–2.95 (m, 1 H each, H10/H17), 2.85–2.95 (m, 1 H, H6/H11), 3.45–3.55 (m, 4 H, CH_2O), 7.00–7.15 (m, 2 H, *p*-H), 7.20–7.30 (m, 4 H, *m*-H), 7.75–7.85 (m, 4 H, *o*-H) ppm. $\{^1\text{H}\}^{13}\text{C}$ NMR (75.5 MHz, $[\text{D}_8]\text{toluene}$, r.t.): δ = 4.7 (1 C, SiCH_3), 18.3, 24.3, 25.0, 25.2, 25.3 (1 C each, C3, C4, C8, C13, C14), 25.5 (2 C, CH_2CO), 28.6, 29.7 (1 C each, C5, C12), 35.3, 35.5 (1 C each, C7, C9), 45.8, 53.7 (1 C each, C10, C17), 57.7 (1 C, C2/C15), 59.3 (1 C, C6/C11), 61.1 (1 C, C2/C15), 67.4 (1 C, C6/C11), 68.4 (2 C, CH_2O), 124.00, 124.05 (1 C each, *C-p*), 126.81, 126.82 (2 C each, *C-m*), 135.04, 135.06 (2 C each, *C-o*), 158.77, 158.81 (1 C each, *C-i*) ppm. $\{^1\text{H}\}^{29}\text{Si}$ NMR (59.6 MHz, $[\text{D}_8]\text{toluene}$, r.t.): δ = –22.5 (q, not resolved, 1 Si) ppm. ^7Li NMR (116.6 MHz, $[\text{D}_8]\text{toluene}$, r.t.): δ = 1.02 (1 Li) ppm. ^1H NMR (300.1 MHz, $[\text{D}_8]\text{toluene}$, –50 °C): δ = 0.55–0.70 (m, 2 H, H4/H13), 0.85–0.95 (m, 2 H, H5/H12), 0.90–1.10 (m, 2 H, H7/H9), 0.96 (s, 3 H, SiCH_3), 1.20–1.35 (m, 4 H, CH_2CO), 1.35–1.55 (m, 5 H, H4, H5, H12, H13, H2/H15), 1.45–1.55 (m, 1 H, H6/H11), 1.50–1.75 (m, 4 H, H3/H14, H8), 1.65–1.85 (m, 1 H, H2/H15), 1.90–2.05 (m, 2 H, H3/H14, H8), 2.30–2.50 (m, 2 H, H10/H17), 2.60–2.75 (m, 1 H, H2/H15), 2.70–2.90 (m, 3 H, H2/H15, H10/H17), 2.75–2.90 (m,

1 H, H6/H11), 3.30–3.55 (m, 4 H, CH₂O), 7.10–7.25 (m, 2 H, p-H), 7.25–7.40 (m, 4 H, m-H), 7.85–7.95 (m, 4 H, o-H) ppm. ¹H/¹³C NMR (75.5 MHz, [D₈]toluene, –50 °C): δ = 4.9 (1 C, SiCH₃), 23.8, 24.8 (1 C each, C4, C13), 25.0 (1 C), 25.3 (2 C, C3, C8, C14), 25.2 (2 C, CH₂CO), 28.2, 29.2 (1 C each, C5, C12), 34.8, 35.1 (1 C each, C7, C9), 45.4, 53.4 (1 C each, C10, C17), 57.5 (1 C, C2/C15), 59.1 (1 C, C6/C11), 60.8 (1 C, C2/C15), 67.2 (1 C, C6/C11), 68.3 (2 C, CH₂O), 123.7, 123.9 (1 C each, C-*p*), 126.7 (4 C, C-*m*), 134.7, 134.9 (2 C each, C-*o*), 159.0, 159.1 (1 C each, C-*i*) ppm. ¹H/²⁹Si NMR (59.6 MHz, [D₈]toluene, –50 °C): δ = –23.0 (q, ¹J_{Si,Li} = 44.3 Hz, 1 Si) ppm. ⁷Li NMR (116.6 MHz, [D₈]toluene, –50 °C): δ = 0.82 (1 Li) ppm.

4·(–)-Sparteine·thf: Bis(diethylamino)phenylchlorosilane (450 mg, 1.98 mmol) was added at –20 °C to a twofold excess of lithium (27.5 mg, 3.97 mmol) suspended in thf (5 mL), and the mixture was stirred for 5 h at this temperature. After removal of the lithium chloride and all volatile compounds under reduced pressure, the oily residue was suspended in a small amount of ethyl ether and (–)-sparteine (0.93 g, 3.97 mmol, 1 equiv.) was added. Storing the yellow/brown solution at –80 °C for 24 h resulted in the formation of 4·(–)-sparteine·thf as a crystalline solid. ¹H NMR (300.1 MHz, [D₈]toluene, r.t.): δ = 0.50–0.60 (m, 1 H, H4/H13), 0.75–0.90 (m, 1 H each, H4/H13, H5/H12), 0.85–0.90 (m, 2 H, H7/H9), 0.85–0.95 (m, 2 H, H5/H12), 0.95–1.05 (m, 1 H, H4/H13), 1.10–1.25 (m, 1 H, H4/H13), 1.15–1.25 (m, 2 H, H3/H14), 1.24 (t, ³J_{H,H} = 6.9 Hz, 12 H, NCH₂CH₃), 1.30–1.45 (m, 1 H each, H5/H12, H3/H14), 1.35–1.45 (m, 1 H, H2/H15), 1.38–1.45 (m, 4 H, OCH₂CH₂), 1.40–1.50 (m, 1 H, H6/H11), 1.45–1.55 (m, 1 H each, H3/H14, H8), 1.65–1.75 (m, 1 H, H2/H15), 1.75–1.85 (m, 1 H, H8), 1.95–2.05 (m, 1 H, H10/H17), 2.40–2.50 (m, 2 H, H10/H17), 2.55–2.70 (m, 1 H, H10/H17), 2.60–2.70 (m, 1 H, H2/H15), 2.60–2.75 (m, 1 H, H6/H11), 2.95–3.05 (m, 1 H, H2/H15) 3.39 (q, not resolved, 8 H,

SiNCH₂CH₃), 3.45–3.55 (m, 4 H, OCH₂CH₂), 7.10–7.20 (m, 1 H, H-*p*), 7.25–7.35 (m, 2 H, m-H), 7.85–7.95 (m, 2 H, o-H) ppm. ¹H/¹³C NMR (75.5 MHz, [D₈]toluene, r.t.): δ = 16.4, 16.5 (2 C each, NCH₂CH₃), 18.1, 24.0, 24.7, 24.9, 25.84 (1 C each, C3, C4, C8, C13, C14), 25.76 (2 C, OCCH₂), 28.3, 30.4 (1 C each, C5, C12), 34.9, 35.1 (1 C each, C7, C9), 43.72, 43.74 (2 C each, SiNCH₂CH₃), 45.8, 53.8, 57.4, 60.5 (1 C each, C2, C10, C15, C17), 58.8, 66.5 (1 C each, C6, C11), 67.9 (2 C, OCH₂), 124.0 (1 C, C-*p*), 127.0 (2 C, C-*m*), 135.0 (2 C, C-*o*), 157.7 (1 C, C-*i*) ppm. ¹H/²⁹Si NMR (59.6 MHz, [D₈]toluene, r.t.): δ = 26.02 (q, not resolved, 1 Si) ppm. ⁷Li NMR (116.6 MHz, [D₈]toluene, –50 °C): δ = 1.60 (1 Li) ppm. ¹H NMR (500.1 MHz, [D₈]toluene, –50 °C): δ = 0.60–0.70 (m, 1 H, H4/H13), 0.75–0.85 (m, 1 H each, H4/H13, H5/H12), 0.85–0.90 (m, 1 H, H7/H9), 0.85–0.90 (m, 2 H, H5/H12), 0.90–0.95 (m, 1 H, H4/H13), 1.00–1.05 (m, 1 H, H4/H13), 1.15–1.25 (m, 1 H, H3/H14), 1.25–1.30 (m, 1 H, H3/H14), 1.17 (t, ³J_{H,H} = 7.0 Hz, 12 H, NCH₂CH₃), 1.35–1.50 (m, 1 H each, H5/H12, H3/H14, H2/H15, H7/H9), 1.40–1.45 (m, 4 H, OCH₂CH₂), 1.55–1.65 (m, 1 H, H6/H11), 1.45–1.55 (m, 1 H each, H3/H14, H8), 1.65–1.75 (m, 1 H, H2/H15), 1.70–1.75 (m, 1 H, H8), 2.00–2.05 (m, 1 H, H10/H17), 2.40–2.45 (m, 1 H, H10/H17), 2.55–2.60 (m, 1 H, H10/H17), 2.75–2.85 (m, 1 H, H2/H15), 2.85–2.90 (m, 1 H, H10/H17), 2.95–3.05 (m, 1 H, H2/H15), 3.20–3.30 (m, 1 H, H6/H11), 3.50–3.60 (m, 4 H, OCH₂CH₂), 3.55–3.65 (q, not resolved, 8 H, SiNCH₂CH₃), 7.15–7.25 (m, 1 H, p-H), 7.45–7.50 (m, 2 H, m-H), 7.70–7.80 (m, 2 H, o-H) ppm. ¹H/¹³C NMR (125.8 MHz, [D₈]toluene, –50 °C): δ = 15.66, 15.73 (2 C each, NCH₂CH₃), 18.1, 23.7, 24.7, 25.03, 25.08 (1 C each, C3, C4, C8, C13, C14), 25.5 (2 C, OCH₂CH₂), 28.4, 39.4 (1 C each, C5, C12), 34.8, 35.2 (1 C each, C7, C9), 42.71, 42.75 (2 C each, SiNCH₂CH₃), 45.4, 52.8, 57.2, 60.2 (1 C each, C2, C10, C15, C17), 57.9, 66.0 (1 C each, C6, C11), 68.0 (2 C, OCH₂CH₃), 123.7 (1 C, C-*p*), 126.9 (2 C, C-*m*), 134.7 (2 C, C-*o*), 158.1 (1 C, C-*i*) ppm. ¹H/²⁹Si NMR (99.4 MHz, [D₈]toluene,

Table 4. Crystal data and refinement details for 3·(–)-sparteine·thf and 4·(–)-sparteine·thf.

| | 3·(–)-Sparteine·thf | 4·(–)-Sparteine·thf |
|---|---|---|
| Empirical formula | C ₃₂ H ₄₇ LiN ₂ OSi | C ₃₃ H ₅₉ LiN ₄ OSi |
| Molecular mass [g mol ^{–1}] | 510.75 | 562.87 |
| Temperature [K] | 173(2) | 193(2) |
| Wavelength [Å] | 0.71073 | 0.71073 |
| Crystal system | orthorhombic | monoclinic |
| Space group (Nr.) | P2 ₁ 2 ₁ 2 ₁ (19) | P2 ₁ (4) |
| <i>a</i> [Å] | 10.7842(16) | 11.207(4) |
| <i>b</i> [Å] | 16.849(7) | 14.742(3) |
| <i>c</i> [Å] | 16.834(3) | 11.510(8) |
| β [°] | – | 116.28(4) |
| <i>V</i> [Å ³] | 3058.7(14) | 1705.0(8) |
| <i>Z</i> | 4 | 2 |
| $\rho_{\text{calcd.}}$ [g cm ^{–3}] | 1.109 | 1.096 |
| μ [mm ^{–1}] | 0.102 | 0.098 |
| <i>F</i> (000) | 1112 | 620 |
| Crystal size [mm] | 0.30 × 0.30 × 0.20 | 0.20 × 0.20 × 0.10 |
| 2 θ range [°] | 2.24–25.00 | 2.41–25.00 |
| Index ranges | –11 ≤ <i>h</i> ≤ 12 –13 ≤ <i>k</i> ≤ 20 –16 ≤ <i>l</i> ≤ 19 | –13 ≤ <i>h</i> ≤ 13 –16 ≤ <i>k</i> ≤ 17 –13 ≤ <i>l</i> ≤ 13 |
| Reflections collected | 7628 | 9018 |
| Independent reflections | 4909 (<i>R</i> _{int} = 0.0438) | 5613 (<i>R</i> _{int} = 0.0550) |
| Refinement method | full-matrix least squares on <i>F</i> ² | full-matrix least squares on <i>F</i> ² |
| Data/restraints/parameter | 4909/0/335 | 5613/1/365 |
| Goodness-of-fit on <i>F</i> ² | 1.042 | 1.018 |
| Final <i>R</i> values [<i>I</i> > 2 σ (<i>I</i>)] | <i>R</i> ₁ = 0.0526, <i>wR</i> ₂ = 0.1350 | <i>R</i> ₁ = 0.0530, <i>wR</i> ₂ = 0.0885 |
| <i>R</i> values (all data) | <i>R</i> ₁ = 0.0676, <i>wR</i> ₂ = 0.1429 | <i>R</i> ₁ = 0.0971, <i>wR</i> ₂ = 0.0983 |
| Absolute structure parameter | –0.07(17) | –0.23(18) |
| Largest diff. peak and hole [e Å ^{–3}] | 0.212 and –0.202 | 0.192 and –0.192 |

–50 °C): $\delta = 27.37$ (q, $^1J_{\text{Si,Li}} = 58.3$ Hz, 1 Si) ppm. ^7Li NMR (194.4 MHz, $[\text{D}_8]\text{toluene}$, –50 °C): $\delta = 1.13$ (1 Li) ppm.

Crystallographic Details: The crystal structures were measured with a Stoe IPDS diffractometer; data collection: Expose in IPDS (Stoe & Cie, 1999), cell determination and refinement: Cell in IPDS (Stoe & Cie, 1999), integration: Integrate in IPDS (Stoe & Cie, 1999); numerical absorption correction: Faceit in IPDS (Stoe & Cie, 1999). The crystals were mounted at –80 °C (N_2 stream) by using the X-TEMP 2 device,^[31] the crystal structure determination was effected at –100 °C (type of radiation: Mo- K_α , $\lambda = 0.71073$ Å; Table 4). The structure was solved by applying direct and fourier methods by using SHELXS-90 (G. M. Sheldrick, University of Göttingen, 1990) and SHELXL-97 (G. M. Sheldrick, SHELXL97, University of Göttingen, 1997). CCDC-697066 [for **3**-(–)-sparteine·thf] and -697067 [for **4**-(–)-sparteine·thf] contain the supplementary crystallographic data for this paper. These data can be obtained free of charge from The Cambridge Crystallographic Data Centre via www.ccdc.cam.ac.uk/data_request/cif.

Computational Details: All calculations were performed with Gaussian 03^[26] and without symmetry restrictions. Starting coordinates were obtained from the crystal coordinates. Full density functional theory (DFT) calculations with the use of the B3LYP/6-31+G(d) functional were used. Additional harmonic vibrational frequency analyses (to establish the nature of stationary points on the potential energy surface) were performed on the same level. Harmonic vibrational frequency analyses showed no imaginary frequencies. Table 3 lists the total and zero-point energies of all isomers. Standard orientations of the calculated compounds are in the Supporting Information.

Supporting Information (see footnote on the first page of this article): Computational studies for the stereoisomers of **3**-(–)-sparteine·thf.

Acknowledgments

We are grateful to Fonds der Chemischen Industrie and the DFG for financial support. Furthermore, we acknowledge the Wacker Chemie AG for providing us with special chemicals. C. D. thanks the Studienstiftung des Deutschen Volkes for a doctoral scholarship.

- [1] For selected examples, see: a) C. Strohmman, V. H. Gessner, *Angew. Chem.* **2007**, *119*, 4650–4653; *Angew. Chem. Int. Ed.* **2007**, *46*, 4566–4569; b) C. Strohmman, V. H. Gessner, *Angew. Chem.* **2007**, *119*, 8429–8432; *Angew. Chem. Int. Ed.* **2007**, *46*, 8281–8283; c) C. Strohmman, V. H. Gessner, A. Damme, *Chem. Commun.* **2008**, 3381–3383; d) C. Strohmman, V. H. Gessner, *Z. Anorg. Allg. Chem.* **2007**, 2285–2287.
- [2] For an overview of alkylolithiums, see: T. Stey, D. Stalke in *The Chemistry of Organolithium Compounds* (Eds.: Z. Rappoport, I. Marek), Wiley, Chichester, **2004**, vol. 1, pp. 47–120.
- [3] For selected work on lithiosilanes, see: a) M. Omote, T. Tokita, Y. Shimizu, I. Imae, E. Shirakawa, Y. Kawakami, *J. Organomet. Chem.* **2000**, *611*, 20–25; b) C. Strohmman, C. Däschlein, *Organometallics* **2008**, *27*, 2499–2504; c) C. Strohmman, J. Hörnig, D. Auer, *Chem. Commun.* **2002**, 766–767; d) C. Strohmman, M. Bindl, V. C. Vraaß, J. Hörnig, *Angew. Chem.* **2004**, *116*, 1029–1032; *Angew. Chem. Int. Ed.* **2004**, *43*, 1011–1014; e) C. Strohmman, C. Däschlein, M. Kellert, D. Auer, *Angew. Chem.* **2007**, *119*, 4864–4866; *Angew. Chem. Int. Ed.* **2007**, *46*, 4780–4782; f) D. Auer, M. Kaupp, C. Strohmman, *Organometallics* **2004**, *23*, 3647–3655; g) C. Strohmman, D. Schildbach, D. Auer, *J. Am. Chem. Soc.* **2005**, *127*, 7968–7969; h) M. Nanjo, M. Masayuki, Y. Ushida, Y. Awamura, K. Mochida, *Tetrahedron Lett.* **2005**, *46*, 8945–8947; i) D. Bravo-Zhivotovskii, I. Ruderfer, S. Melamed, M. Botoshansky, B. Tumanskii, Y. Apeloig, *Angew. Chem.* **2005**, *117*, 749–753; *Angew. Chem. Int. Ed.* **2005**, *44*, 739–743; j) L. H. Sommer, R. Mason, *J. Am. Chem. Soc.* **1965**, *87*, 1619–1620; k) L. H. Sommer, J. E. Lyons, H. Fujimoto, *J. Am. Chem. Soc.* **1969**, *91*, 7051–7061; l) E. Colomer, R. Corriu, *J. Chem. Soc., Chem. Commun.* **1976**, 176–177; m) E. Colomer, R. Corriu, *J. Organomet. Chem.* **1977**, *133*, 159–168; n) C. Strohmman, O. Ulbrich, D. Auer, *Eur. J. Inorg. Chem.* **2001**, 1013–1018; o) H.-W. Lerner, S. Scholz, M. Bolte, M. Wagner, *Z. Anorg. Allg. Chem.* **2004**, *630*, 443–451; p) T. I. Kückmann, F. Dornhaus, M. Bolte, H.-W. Lerner, M. C. Holthausen, M. Wagner, *Eur. J. Inorg. Chem.* **2007**, 1989–2003; q) D. Scheschkewitz, *Angew. Chem.* **2004**, *116*, 3014–3016; *Angew. Chem. Int. Ed.* **2004**, *43*, 2965–2967.
- [4] For examples of silicon-based polymers, see: a) H.-S. Oh, L.-S. Park, Y. Kawakami, *Chirality* **2003**, *15*, 646–653; b) W. Uhlig, *J. Organomet. Chem.* **2003**, 685, 70–78.
- [5] For example, see: T. Kottke, D. Stalke, *Angew. Chem.* **1993**, *105*, 619–621; *Angew. Chem. Int. Ed. Engl.* **1993**, *32*, 580–582.
- [6] For example, see: D. Frank, J. Baumgartner, C. Marschner, *Chem. Commun.* **2002**, 1190–1191.
- [7] For studies on silyl anions, see: a) J. B. Lambert, M. Urdaneta-Perez, H.-N. Sun, *J. Chem. Soc., Chem. Commun.* **1976**, 806–807; b) J. B. Lambert, M. Urdaneta-Perez, *J. Am. Chem. Soc.* **1978**, *100*, 157–162; c) M. Flock, C. Marschner, *Chem. Eur. J.* **2002**, *8*, 1024–1030; d) M. Flock, C. Marschner, *Chem. Eur. J.* **2005**, *11*, 4635–4642.
- [8] For some examples concerning the applications of alkylolithiums in asymmetric synthesis, see: a) D. Hoppe, T. Hense, *Angew. Chem. Int. Ed. Engl.* **1997**, *36*, 2282–2316; b) P. Beak, A. Basu, D. J. Gallagher, Y. S. Park, S. Thayumanavan, *Acc. Chem. Res.* **1996**, *29*, 552–556; c) M. C. Whisler, S. MacNeil, V. Snieckus, P. Beak, *Angew. Chem. Int. Ed.* **2004**, *43*, 2206–2225.
- [9] For an overview, see: H.-W. Lerner, *Coord. Chem. Rev.* **2005**, *249*, 781–798.
- [10] A. Sekiguchi, M. Nanjo, C. Kabuto, H. Sakurai, *Organometallics* **1995**, *14*, 2630–2632.
- [11] T. F. Schaaf, W. Butler, M. D. Glick, J. P. Oliver, *J. Am. Chem. Soc.* **1974**, *96*, 7593–7594.
- [12] For some examples, see: a) J. L. Rutherford, D. B. Collum, *J. Am. Chem. Soc.* **1999**, *121*, 10198–10202; b) X. Sun, M. D. Winemiller, B. Xiang, D. B. Collum, *J. Am. Chem. Soc.* **2001**, *123*, 8039–8046; c) A. J. McNeil, G. E. S. Toombes, S. V. Chandramouli, B. J. Vanasse, T. A. Ayers, M. K. O'Brian, E. Lobkovsky, S. M. Gruner, J. A. Marohn, D. B. Collum, *J. Am. Chem. Soc.* **2004**, *126*, 5938–5939; d) R. L. Parsons Jr., J. M. Fortunak, R. L. Dorow, G. D. Harris, G. S. Kauffman, W. A. Nugent, M. D. Winemiller, T. F. Briggs, B. Xiang, D. B. Collum, *J. Am. Chem. Soc.* **2001**, *123*, 9135–9143; e) H. Günther, *J. Braz. Chem. Soc.* **1999**, *10*, 241–262.
- [13] For leading references, see: B. L. Lucht, D. B. Collum, *Acc. Chem. Res.* **1999**, *32*, 1035–1042.
- [14] G. Boche, G. Fraenkel, J. Cabral, K. Harms, N. J. R. van Eikema Hommes, M. Marsch, P. v. R. Schleyer, *J. Am. Chem. Soc.* **1992**, *114*, 1562–1565.
- [15] H. J. Reich, W. S. Goldenberg, A. W. Sanders, K. L. Jantzi, C. C. Tzschucke, *J. Am. Chem. Soc.* **2003**, *125*, 3509–3521.
- [16] G. Fraenkel, A. Chow, R. Fleischer, H. Liu, *J. Am. Chem. Soc.* **2004**, *126*, 3983–3995.
- [17] a) D. Johnels, H. Günther in *The Chemistry of Organolithium Compounds* (Eds.: Z. Rappoport, I. Marek), Wiley, Chichester, **2004**, vol. 1, pp. 137–203; b) S. Jost, M. Kühnen, H. Günther, *Magn. Reson. Chem.* **2006**, *44*, 909–916.
- [18] A. Maercker, W. Demuth, *Angew. Chem.* **1973**, *85*, 90–92.
- [19] C. Strohmman, V. H. Gessner, *J. Am. Chem. Soc.* **2007**, *129*, 8952–8953.

- [20] C. Strohmann, C. Däschlein, *Chem. Commun.* **2008**, 2791–2793.
- [21] H. V. R. Dias, M. M. Olmstead, K. Ruhland-Senge, P. P. Power, *J. Organomet. Chem.* **1993**, 462, 1–6.
- [22] C. Strohmann, C. Däschlein, D. Auer, *J. Am. Chem. Soc.* **2006**, 128, 704–705.
- [23] For example, see: a) P. A. Scherr, R. J. Hogan, J. P. Oliver, *J. Am. Chem. Soc.* **1974**, 96, 6055–6059; b) R. H. Cox, H. W. Terry Jr., *J. Magn. Reson.* **1974**, 14, 317–322.
- [24] Y. M. Cahen, P. R. Handy, E. T. Roach, A. I. Popov, *J. Phys. Chem.* **1975**, 79, 80–85.
- [25] For example, see: C. Strohmann, B. C. Abele, K. Lehmen, D. Schildbach, *Angew. Chem.* **2005**, 117, 3196–3199; *Angew. Chem. Int. Ed.* **2005**, 44, 3136–3139.
- [26] M. J. Frisch, G. W. Trucks, H. B. Schlegel, G. E. Scuseria, M. A. Robb, J. R. Cheeseman, J. A. Montgomery Jr., T. Vreven, K. N. Kudin, J. C. Burant, J. M. Millam, S. S. Iyengar, J. Tomasi, V. Barone, B. Mennucci, M. Cossi, G. Scalmani, N. Rega, G. A. Petersson, H. Nakatsuji, M. Hada, M. Ehara, K. Toyota, R. Fukuda, J. Hasegawa, M. Ishida, T. Nakajima, Y. Honda, O. Kitao, H. Nakai, M. Klene, X. Li, J. E. Knox, H. P. Hratchian, J. B. Cross, C. Adamo, J. Jaramillo, R. Gomperts, R. E. Stratmann, O. Yazyev, A. J. Austin, R. Cammi, C. Pomelli, J. W. Ochterski, P. Y. Ayala, K. Morokuma, G. A. Voth, P. Salvador, J. J. Dannenberg, V. G. Zakrzewski, S. Dapprich, A. D. Daniels, M. C. Strain, O. Farkas, D. K. Malick, A. D. Rabuck, K. Raghavachari, J. B. Foresman, J. V. Ortiz, Q. Cui, A. G. Baboul, S. Clifford, J. Cioslowski, B. B. Stefanov, G. Liu, A. Liashenko, P. Piskorz, I. Komaromi, R. L. Martin, D. J. Fox, T. Keith, M. A. Al-Laham, C. Y. Peng, A. Nanayakkara, M. Challacombe, P. M. W. Gill, B. Johnson, W. Chen, M. W. Wong, C. Gonzalez, J. A. Pople, *Gaussian 03* (Revision B.04), Gaussian, Inc., Pittsburgh, PA, **2003**.
- [27] P. Flükiger, H. P. Lüthi, S. Portmann, J. Weber, *Molekel 4.3*, Swiss Center for Scientific Computing, Manno, Switzerland, **2000–2002**.
- [28] T. Buttler, I. Fleming, S. Gonsior, B.-H. Kim, A.-Y. Sung, H.-G. Woo, *Org. Biomol. Chem.* **2005**, 3, 1557–1567.
- [29] B. Jasiewicz, W. Boczon, *J. Mol. Struct.* **2005**, 752, 115–123.
- [30] K. Trommer, U. Herzog, U. Georgi, G. Roewer, *J. Prakt. Chem./Chem.-Ztg.* **1998**, 340, 557–561.
- [31] T. Kottke, D. Stalke, *J. Appl. Crystallogr.* **1993**, 26, 615.

Received: August 17, 2008

Published Online: November 18, 2008

(Polypyridyl)ruthenium(II) Complexes Based on a *Back-to-Back* Bis(pyrazolylpyridine) Bridging Ligand

Frank Schramm,^[a] Rajadurai Chandrasekar,^{[a][‡]} Thomas A. Zevaco,^[b] Manfred Rudolph,^[c] Helmar Görls,^[c] Wolfgang Poppitz,^[c] and Mario Ruben*^[a]

Keywords: Ruthenium / Back-to-back ligands / N ligands / Bridging ligands

Two (polypyridyl)ruthenium(II) complexes, [(tpy)Ru^{II}(L)](PF₆)₂ (**1**) and [(tpy)Ru^{II}(L)Ru^{II}(tpy)](PF₆)₄ (**2**) {tpy is 2,2':6',2''-terpyridine and L is 1,4-bis[(2,6-dipyrzazol-1-yl)pyrid-4-yl]benzene}, were synthesised and studied in view of their electrochemical and photophysical properties. The structural characterisation of **1** and **2** was carried out by ¹H and ¹³C NMR spectroscopy, MALDI-TOF/ESI mass spectrometry and single-crystal X-ray analysis. The spectro- and electrochemical consequences of the introduction of 2,6-dipyrzazol-1-ylpyridine coordinating units into Ru^{II} polypyridyl complexes were investigated by UV/Vis, low-temperature emission

spectroscopy and square-wave voltammetry. It was shown that ligand L can be used as a *back-to-back* bridging ligand in the construction of multinuclear ruthenium(II) ion arrays. In comparison to the widely used 2,2':6',2''-terpyridyl system, the 2,6-dipyrzazol-1-ylpyrid-4-yl unit was found to act as a relatively strong σ -donor and weak π -acceptor ligand which allows its use as a structural and electronic alternative in multinuclear architectures.

(© Wiley-VCH Verlag GmbH & Co. KGaA, 69451 Weinheim, Germany, 2009)

Introduction

During the last decades, ruthenium(II)-based polypyridyl complexes have been the object of an active field of research.^[1,2] Light-absorbing and light-emitting properties of ruthenium complexes elevate them to the ranks of prominent candidates for applications dealing with light-driven conversion processes such as, e.g., artificial photosynthesis,^[3] photocatalytic production of hydrogen,^[4] vectorially controlled energy transfer,^[5] photoactivated reactions,^[6] dye-sensitised solar cells,^[7] photomolecular switches,^[8] as well as ion-specific sensing systems,^[9] and other related molecular devices.^[10]

Oligonuclear ruthenium complexes are frequently used to enhance photochemical and photophysical properties of photoactive systems by antenna-like light-harvesting.^[11–13]

The design of multinuclear metal complexes requires organic molecules which can act as bridging ligands, e.g. aro-

matic bis(terdentate) or bis(bidentate) *back-to-back* coupled polypyridines. In particular, ligand systems involving the bis(2,2':6',2''-terpyridin-4'-yl) {tpy} moiety have been used extensively in the construction of multimetallic molecular coordination arrays and artificial antenna systems.^[14–28]

As there are only few examples of known bis(terdentate ligand) complexes that are not based on tpy systems,^[29–33] we decided to investigate the suitability of the equally terdentate 2,6-dipyrzazol-1-ylpyridine coordination unit as a bridging ligand motif.^[34] Towards this goal, the multicoordination behaviour of the *back-to-back* ligand 1,4-bis[(2,6-dipyrzazol-1-yl)pyrid-4-yl]benzene (L) was studied exemplarily in the synthesis of mono- and binuclear Ru^{II} polypyridyl complexes involving L. Thereby, it was necessary to apply a *mixed-ligand approach* incorporating both bridging ligand L and peripheral tpy ligands.

Herein, we report on the synthesis, X-ray structure, NMR spectroscopic characterisation, optical and electrochemical properties of the mononuclear complex [(tpy)Ru(L)](PF₆)₂ (**1**) and its binuclear equivalent [(tpy)Ru(L)Ru(tpy)](PF₆)₄ (**2**), elucidating the electronic properties of ligand L.

Results and Discussion

Synthesis of Complexes [(tpy)Ru(L)](PF₆)₂ (**1**) and [(tpy)Ru(L)Ru(tpy)](PF₆)₄ (**2**)

The synthesis of complexes **1** and **2** was carried out as described in Scheme 1, whereby the bridging ligand L was

[a] Institut für Nanotechnologie, Forschungszentrum Karlsruhe GmbH,
P. O. Box 3640, 76021 Karlsruhe, Germany

E-mail: mario.ruben@int.fzk.de

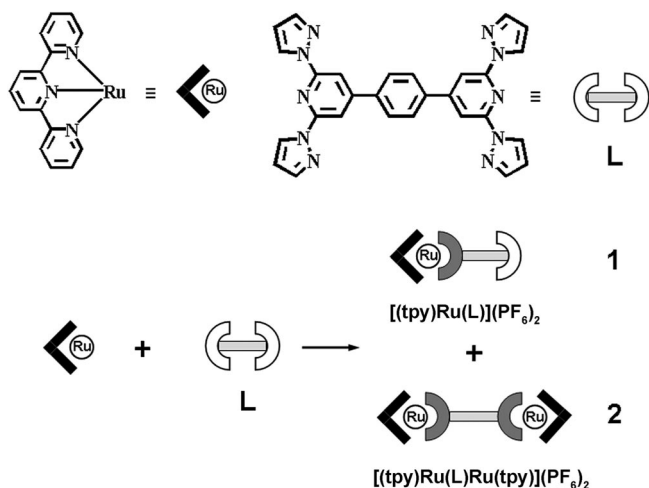
[b] Institut für Technische Chemie – Chemisch-Physikalische Verfahren, Forschungszentrum Karlsruhe GmbH,
Karlsruhe, Germany

[c] Friedrich-Schiller-Universität Jena, Institut für anorganische und analytische Chemie
August-Bebel-Str. 2, 07743 Jena, Germany

[‡] Present address: School of Chemistry, University of Hyderabad, Central University
P. O. Box, Gachhi Bowli, Hyderabad 500046, India

Supporting information for this article is available on the WWW under <http://www.eurjic.org> or from the author.

used as described recently.^[35] One equivalent of ligand L was treated with 1.5 equiv. of an in situ prepared tetrafluoroborate salt of mono(2:2',6':2''-terpyridyl)ruthenium.^[5d] After 12 h of reaction time at 120 °C in dmf, the resulting red-orange solid was purified by column chromatography on silica gel, from which the two different nitrate salts of complex **1** and **2** were obtained. Red-brown coloured prismatic single crystals of complex **1**·(NO₃)₂ were suitable for X-ray diffraction studies.



Scheme 1. Schematic presentation of the synthesis of $[(\text{tpy})\text{Ru}(\text{L})](\text{PF}_6)_2$ (**1**) and $[(\text{tpy})\text{Ru}(\text{L})\text{Ru}(\text{tpy})](\text{PF}_6)_4$ (**2**).

Anion exchange was carried out by dissolving complexes **1** or **2** in methanol/water (4:1), respectively. Adding aqueous NH₄PF₆ solution initiated immediate precipitation of the respective PF₆ salt complex material. If not otherwise noted, the PF₆ salt complexes were used in the investigations without further purification.

NMR Spectroscopic Data

Figure 1 shows the ¹H NMR spectra of ligand L and of complexes **1** and **2** in [D₆]dmsO solution. In all cases, ¹H and ¹³C NMR spectra give well-resolved signals. As ligand L is poorly soluble in deuteriated dimethyl sulfoxide, [D₆]dmsO, the spectrum was taken at 70 °C. Since L is a covalent, aprotic ligand, it is supposed that temperature dependence has only a minor influence on the chemical shifts.^[37]

Ligand L itself displays a clear *D*_{2h} symmetry in solution, giving five signals for the ¹H atoms (Figure 1a) and eight signals for the ¹³C atoms. The presence of *s-trans*, *trans* conformations of the pyrazolyl groups with respect to the central pyridine groups can be concluded from the observed chemical shifts for L in the uncoordinated form (Figure 1a).^[38,39] Due to the substitution at the N¹ atom of the pyrazole, the chemical shift of H_{pz5} is largely downfield-shifted. This shift is attributed to the interaction of the H_{pz5} proton with the electron density of the pyridine lone pair, causing local deshielding of the magnetic field.

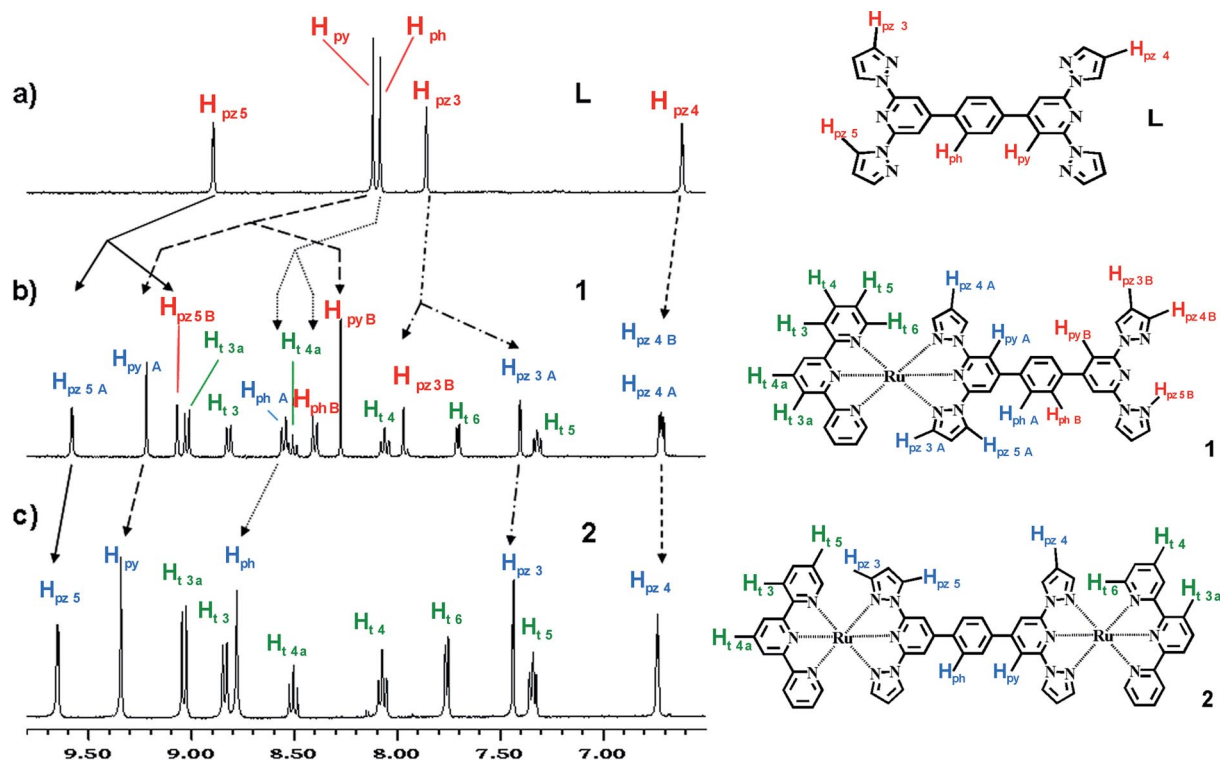


Figure 1. Representation of the aromatic region of the ¹H NMR spectra (a) of L in [D₆]dmsO together with the indication of the observed shifts of the aromatic protons upon complexation by (b) one or (c) two Ru(tpy) units, yielding complex **1** or **2**, respectively (left). The assignment codes of the protons are depicted in the structural formulae (right).

Extensive NMR spectroscopic studies such as two-dimensional techniques – ^1H , ^1H -correlation spectroscopy (H,H-gCOSY), and ^1H , ^{13}C short-range (gHSQC) and long-range correlation spectroscopic (gHMBC) techniques – were employed to achieve full assignment of all signals (see also Supporting Information).

The ^1H NMR spectrum of mononuclear complex **1** shows that the symmetry of ligand **L** in **1** is reduced to C_{2v} symmetry, which results in two sets of NMR signals belonging to two subunits of **L**. Accordingly, ten signals are observed in the ^1H NMR spectrum for **L**, in addition to the terpyridine-related signals (Figure 1b, green colour code). Since upon complexation of **L**, rotation of the pyrazole residues into the *s-cis,cis* conformation has to occur, a strong difference in the chemical shifts of the pyrazolyl protons is observed, discriminating the different coordination states of **L**. The ^1H NMR signals of **1** split into a “chelated” (blue colour code in Figure 1b) and an “unchelated” (red colour code in Figure 1b) set of signals. In particular, the signals H_{pyA} and H_{pz5A} show downfield shifts of 0.94 ppm and 0.51 ppm with respect to their unchelated “B” equivalents. This can be explained by the forced structural vicinity of these two protons, which causes deshielding of both. On the other hand, H_{pz3A} receives an upfield shift of 0.47 ppm in comparison to H_{pz3B} , which is ascribed to a redistribution of electron density at this position due to metal complexation. As expected, the ^{13}C NMR spectrum of **1** exhibits the 16 signals of the asymmetrically coordinated ligand **L**.

Upon introduction of the second (terpyridyl)ruthenium(II) moiety, binuclear complex **2** exhibits D_{2h} symmetry. This leads to simplified NMR spectra exhibiting five signals in the ^1H NMR spectrum, featuring the all-chelated situation, and eight signals in the ^{13}C NMR spectrum (Figure 1c).

MALDI-TOF and ESI Mass Spectrometric Analyses

Matrix-assisted laser desorption/ionisation-time of flight (MALDI-TOF) mass spectrometric analytical data further confirmed the structural identity of compounds **1** and **2**. The analysis of **1** exhibits a molecular peak at $m/z = 829.7$ $[(\text{tpy})\text{Ru}(\text{L}) - 2\text{H}]^+$ with 100% intensity, which is often accompanied by a peak at $m/z = 802$ with 30% intensity, corresponding to the loss of a “ CH_3N ” or “ HN_2 ” fragment. Similarly, ions like $[(\text{tpy})\text{RuOH}]^+$ at $m/z = 351$ are frequently found in the spectra.

The spectrum of binuclear complex **2** (as the nitrate salt) shows the highest mass peak at $m/z = 1161.7$ with 12% intensity, which corresponds to the singly charged mass of the binuclear complex $[(\text{tpy})\text{Ru}(\text{L})\text{Ru}(\text{tpy}) - 5\text{H}]^+$ lacking five hydrogen atoms and all anions. In fact, the isotope pattern of this peak matches the theoretical values of the natural isotope contribution. The dominating peak in the spectrum at $m/z = 829.2$ with 65% intensity can be attributed to $[(\text{tpy})\text{Ru}(\text{L}) - 2\text{H}]^+$.

Additionally, electrospray ionisation time-of-flight (ESI-TOF) measurements were applied to the PF_6 salts of both

1 and **2**. Complex **1** shows different peaks of the molecular ion as $[\text{1} \cdot \text{PF}_6]^+$ at $m/z = 976.13$, $[\text{1} \cdot (\text{PF}_6)_2 \cdot \text{PF}_5]^{2+}$ at $m/z = 623.64$ and $[\text{1}]^{2+}$ at $m/z = 415.59$. Similar results were found for complex **2** with ion peaks of $[\text{2} \cdot (\text{PF}_6)_2]^{2+}$ at $m/z = 728.05$, $[\text{2} \cdot \text{PF}_6]^{3+}$ at $m/z = 437.04$ and $[\text{2}]^{4+}$ at $m/z = 291.54$. In general, ESI-TOF leaves the molecular ions of the complexes relatively intact (see also Supporting Information).

Single-Crystal X-ray Structure of **1**

The result of the single-crystal X-ray diffraction studies on complex **1** (as its nitrate salt), at 180 K is depicted in Figure 2. The compound crystallises in the monoclinic space group $P2_1/n$. Four molecules of **1** are included in the unit cell together with four molecules of methanol and eight nitrate counteranions. The bond lengths of the coordination sphere are within the expected range for hexacoordinate ruthenium(II) complexes and vary from 1.974(4) Å (Ru–N12) to 1.992(4) Å (Ru–N3) at the central pyridine rings and from 2.049(4) Å (Ru–N1 and Ru–N11) to 2.087(4) Å (Ru–N5) for the angular nitrogen atoms of the coordinated li-

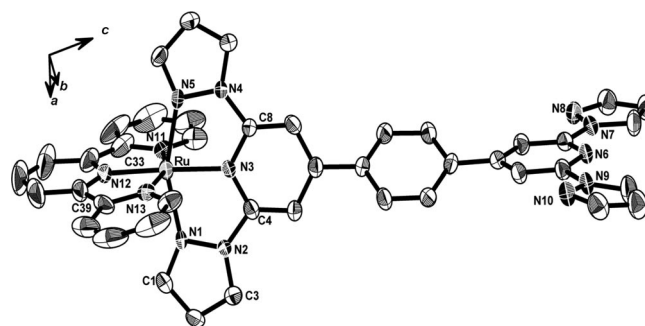


Figure 2. ORTEP plot of the $[(\text{tpy})\text{Ru}^{\text{II}}(\text{L})]^{2+}$ cation of complex **1** (thermal ellipsoids at the 50% probability level) – nitrate anions, hydrogen atoms and solvent molecules are omitted for clarity.

Table 1. Selected bond lengths and angles of the complex cation **1**.^[a]

| Selected distances / Å | | Selected angles / ° | |
|------------------------|----------|---------------------|------------|
| Ru–N1 | 2.049(4) | N1–Ru–N3 | 78.52(15) |
| Ru–N3 | 1.992(4) | N3–Ru–N5 | 77.77(15) |
| Ru–N5 | 2.087(4) | N1–Ru–N5 | 156.27(14) |
| Ru–N11 | 2.054(4) | N11–Ru–N12 | 79.42(18) |
| Ru–N12 | 1.974(4) | N12–Ru–N13 | 79.64(18) |
| Ru–N13 | 2.073(4) | N11–Ru–N13 | 159.04(17) |
| N1–N2 | 1.393(5) | N1–Ru–N11 | 95.78(16) |
| N1–C1 | 1.324(6) | N1–Ru–N12 | 98.77(16) |
| N2–C4 | 1.399(6) | N1–Ru–N13 | 86.73(15) |
| N2–C3 | 1.364(6) | N5–Ru–N11 | 88.69(16) |
| N3–C4 | 1.352(6) | N5–Ru–N12 | 104.96(16) |
| N3–C8 | 1.337(6) | N5–Ru–N13 | 97.36(16) |
| N4–C8 | 1.401(6) | N3–Ru–N12 | 176.61(17) |
| N4–N5 | 1.395(5) | N1–N2–C4 | 119.0(4) |
| N4–C9 | 1.363(6) | N2–C4–N3 | 110.8(4) |
| N5–C11 | 1.326(6) | C4–N3–C8 | 119.0(4) |
| N11–C33 | 1.371(7) | N11–C33–C34 | 114.0(5) |
| N12–C38 | 1.339(7) | C34–N12–C38 | 123.2(5) |
| N12–C34 | 1.358(7) | N12–C38–C39 | 113.0(4) |

[a] Dihedral angles: Ru–py–ph 48.66(9)°, ph–py(free) 29.65(9)°.

gands L and tpy. However, the relatively small bite angle of L [N1–Ru–N5 156.27(14)°] produces a significant constraint of the coordination sphere at the Ru^{II} centre (Table 1).

Within the ligand structure of L, the connecting benzene ring exhibits a dihedral angle towards the chelated pyridine ring of 48.66(9)° and towards the unchelated pyridine ring of 29.65(9)°.

In the case of the binuclear complex **2**, single-crystal X-ray diffraction studies could not be carried out because of the low diffraction quality of the obtained crystals.

Absorption and Emission Spectroscopy

Ruthenium(II) ions comprising chelate ligands with strong π -acceptor properties exhibit interesting photophysical properties.^[1,2,11] Table 2 and Figure 3 display the results of the photophysical measurements for complexes **1** and **2**. Both mononuclear complex **1** and binuclear complex **2** exhibit only minor differences in their absorption behaviour.

Table 2. UV/Vis data for compounds **1** and **2** as the nitrate salts in methanol solution in 1 cm cuvettes.

| Complex | IL | ¹ MLCT (L) λ /nm (ϵ /M ⁻¹ cm ⁻¹) | ¹ MLCT (tpy) λ /nm (ϵ /M ⁻¹ cm ⁻¹) | Emission λ /nm at 100 K |
|----------|-------------|---|---|------------------------------------|
| 1 | 308 (84300) | 366 (8830) | 443 (24900) | 605 |
| 2 | 309 (96400) | 371 (12750) | 453 (44880) | 619 |

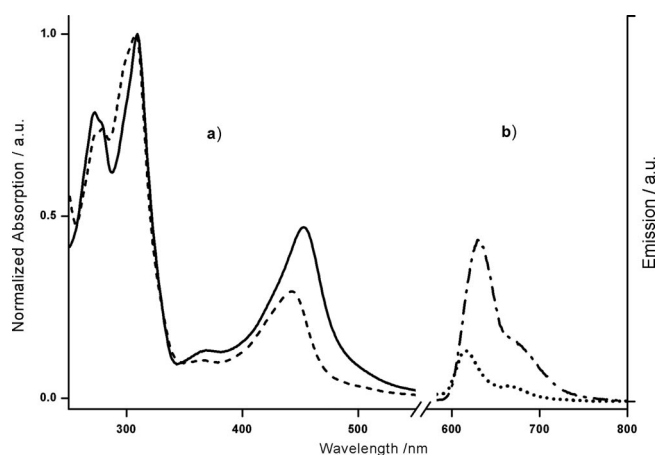


Figure 3. Absorption (room temperature) and emission (100 K) spectra of the PF₆ salts of complexes **1** and **2**. (a) Absorption spectra of complex **1** (dashed line) and complex **2** (solid line) in 10⁻⁵ M methanol/acetonitrile solution. (b) Uncorrected emission spectra at 100 K of complex **1** (dotted line) and complex **2** (dash-dotted line) in a saturated solid matrix consisting of acetonitrile/dmf, 10:1 v/v.

In both complexes, the ligand π – π^* absorptions appear as the most intense peaks of the spectra below 340 nm. Differences between **1** and **2** are observed in the “metal-based”

absorptions. There are two different “metal-to-ligand charge transfer” (MLCT) bands involving each one of the ligand types tpy and L. The intensities and maxima of these transitions can be distinguished by comparing the electronic spectra of complexes **1** and **2**.

The tpy-based ¹MLCT band of mononuclear complex **1** (λ = 443 nm) is 45% lower in intensity and displays a hypsochromic shift of 10 nm in comparison with the respective band of binuclear complex **2** (λ = 453 nm). Furthermore, the ¹MLCT band of the chelated 2,6-dipyrazol-1-ylpyridine (bpp) unit of L is located at λ = 366 nm for complex **1** and at λ = 371 nm for complex **2**. The electronic spectra are in agreement with reported values of the homoleptic complexes [Ru(tpy)₂]²⁺ (λ = 476 nm) and [Ru(bpp)₂]²⁺ (λ = 377 nm).^[14,40] In addition, a reported heteroleptic complex of [Ru(tpy)(dmpp)]²⁺ {where dmpp is 2,6-bis(3,5-dimethyl-*N*-pyrazolyl)pyridine and ttpy is 4'-tolyl-2,2':6',2''-terpyridine} exhibits two different transitions at λ = 359 nm and λ = 457 nm in a very similar way.^[15,22]

In general, the lowest energetic transitions of a Ru^{II}–N₆ coordination compound are directly referred to the promotion of an electron from the highest occupied (metal based) molecular orbital to the lowest unoccupied electronic level of the respective ligand (MLCT).^[1,36,44] In mixed-ligand compounds such as complexes **1** and **2**, different ligands involve different absorption energies from the same initial metal-based orbital. The absorption spectra of complexes **1** and **2** exhibit a higher energetic MLCT band towards L (around 370 nm) and a lower MLCT band towards tpy (around 450 nm) in accordance with literature values.^[14] Thus, it can be deduced that the coordinating bpp moiety in ligand L possesses a higher electron density, causing stronger repulsion for additional electron density in comparison with the structurally similar tpy moiety. This renders L a stronger σ -donor and a weaker π -acceptor than tpy and lowers the overall ligand-field strength of the 2,6-dipyrazol-1-ylpyridine coordination unit in L with respect to the analogous terpyridyl system.

The light-emitting behaviour of complexes **1** and **2** was investigated at reduced temperatures in a solid matrix of acetonitrile/dmf (10:1 v/v). Only at very low temperatures – below 100 K – luminescence could be detected at 605 nm for complex **1** and at 619 nm for complex **2**. In both cases, the intensity of the luminescence increased further upon cooling (see Supporting Information). At low temperature, both complexes exhibit a red-sided shoulder, as it is common for the Franck-Condon progression of most polypyridylruthenium(II) complexes.^[28] As the parent complex [Ru(tpy)₂]²⁺ emits light at an identical wavelength, the luminescence could be assigned to the radiative depopulation of terpyridine-based ³MLCT states in **1** and **2**.^[44]

The weakness at higher temperatures as well as the strong temperature-dependence of the emission may be related to the weak ligand field of the 2,6-dipyrazol-1-ylpyridine coordination unit, which renders the occupation of a stable ³MLCT state less probable and so favours a nonradiative decay through metal-centred states (³MC).^[41]

Table 3. Comparison of the cyclovoltammetric data of the complexes **1** and **2** measured in dmf with (Bu₄N)ClO₄ vs. the ferrocene/ferrocenium couple. All literature values are calculated with a respective reference electrode adaptation according to reference [22].

| Complex | $E_{1/2}(\text{ox})$ /V | $E_{1/2}(\text{red})$ /V | | | |
|--|-------------------------|--------------------------|--------|--------|--------|
| 1 | +0.765 | –1.715 | –1.865 | –2.050 | –2.235 |
| 2 ^[a] | +0.765 | –1.630 | –1.713 | –1.849 | –1.930 |
| [Ru(bpp) ₂] ²⁺ ^[b] | +0.866 | –2.044 | | | |
| [(dmpp)Ru(tpy)] ²⁺ ^[c] | +0.74 | –1.66 | | | |
| [Ru(tpy) ₂] ²⁺ ^[d] | +0.96 | –1.36 | | | |
| [(ttpy)Ru(tpy-ph-tpy)] ²⁺ ^[e] | +0.87 | –1.62 | –1.84 | | |
| [(ttpy)Ru(tpy-ph-tpy)Ru(tpy)] ⁴⁺ ^[f] | +0.89 | –1.56 | –1.83 | | |

[a] Peak separations have been determined by fitting simulated square-wave voltammograms (SWVs) to experimental ones excluding the region around the adsorption peak at –1.9 V (see Supporting Information). [b] Values taken from ref.^[14] measured vs. SSCE. [c] Values taken from ref.^[40] measured vs. SCE. [d] Values taken from ref.^[18] [e] Complex [(ttpy)Ru(tpy-ph-tpy)](PF₆)₂ values vs. SCE taken from ref.^[19c,19d] [f] Complex [(ttpy)Ru(tpy-ph-tpy)Ru(tpy)](PF₆)₄ values vs. SCE taken from ref.^[19a,19d]

Electrochemical Data

The results of the electrochemical analysis obtained by cyclic voltammetry and square-wave voltammetry of complexes **1** and **2** are summarised in Table 3. As the complexes are poorly soluble in acetonitrile, dmf solutions with tetra-*n*-butylammonium perchlorate as electrolyte were used.

In both complexes, mononuclear **1** and binuclear **2**, the first oxidation waves occur at the same half-wave potential of $E_{1/2} = +0.765$ V and are fully reversible. Integration of the peak area of the oxidation half-wave curves implies a single-electron oxidation in the case of **1** and a two-electron oxidation in the case of **2**, under the assumption that the diffusion coefficients are equal. To support this assumption, the peak current values of both the reduction (vide infra) and the oxidation of dinuclear complex **2** were compared. As a result, the oxidation wave of complex **2** exhibits a current value that is double that of the single-electron reductions, which clearly supports the above argumentation (see Supporting Information).

In comparison to the homoleptic parent complexes Ru(tpy)₂ [$E_{1/2} = +0.96$ V] and Ru(bpp)₂ [$E_{1/2} = +0.866$ V],^[14,21,40] complexes **1** and **2** are oxidised at less positive potentials. In accordance to the electronic spectra, the introduction of ligand L induces higher electron density onto the ruthenium ion, thus facilitating the oxidation of **1** and **2**. Since complex **2** is twofold oxidised at the same potential like complex **1**, it can be concluded that both ruthenium(II) ions act independently from each other. This electronic situation strongly reminds of the complex [(ttpy)Ru(tpy-ph-tpy)Ru(tpy)](PF₆)₄ [where ttpy is 4'-*p*-tolyl-2,2':6,2''-terpyridine and tpy-ph-tpy is 1,4-bis(2,2':6,2''-terpyridin-4'-yl)benzene] involving the analogous tpy bridging ligand.^[19,24]

The reduction of complex **1** reveals four well-separated and equally intense waves, which are fully reversible up to the second reduction. After the third reduction, the electrochemical reversibility is partially lost. The first reduction is found to be at a remarkably high voltage of $E_{1/2} = -1.715$ V, which is close the average value for the parent complexes [Ru(bpp)₂]²⁺ and [Ru(tpy)₂]²⁺. However, it is still more cathodically shifted as the value reported for the mixed-ligand complex [Ru(bpp)(tpy)]²⁺ (see Table 3 and Supporting Information).^[40] In accordance with the results of absorption

spectroscopy, the first reduction of complex **1** can be directly correlated with the electronic transition with lowest energy – the ¹MLCT transition onto the tpy ligand. Further reductions follow at –1.865, –2.050 and –2.235 V. These values cannot unambiguously be assigned to a specific ligand reduction, as the repulsion of an already negatively charged tpy ligand competes against the electron density of the bpp moiety. Since the absorption spectroscopy of **1** shows that the ¹MLCT onto ligand L is around 0.5 eV higher in energy than the respective ¹MLCT onto the tpy ligand, the first reduction of ligand L is found at more cathodic potentials than $E_{1/2} = -1.865$ V.

The reduction of complex **2** exhibits four fully reversible and equally intense reductions that are not well separated, and the fourth reduction is overlaid with an additional adsorption peak. The fact that all four reductions show equal values of the peak currents in comparison with the peak currents of the reductions of complex **1** allows for the interpretation that all are single-electron processes. The fitting of the reduction waves allows the separation of the respective half-wave potentials: The first reduction wave of complex **2** appears at $E_{1/2} = -1.630$ V, which corresponds to an anodic shift of $\Delta E_{1/2} = 85$ mV in comparison with the first reduction of complex **1**. Again, this first reduction can be attributed to the reduction of one tpy ligand. Further increase in the cathodic potential results in three additional reduction waves in **2** at values of $E_{1/2} = -1.713$, –1.849 and –1.930 V. The second reduction is again proven to be a one-electron process exhibiting a small cathodic shift of $\Delta E_{1/2} = 83$ mV with respect to the first reduction. Thus, this wave can be assigned to the reduction of the second tpy ligand of **2**. Apparently, on the reduction side, a weak communication via the metal ions and the bridging ligand L needs to be considered, which is in clear distinction to the parent tpy-based *back-to-back* ligand (see Supporting Information).^[42] The third and fourth reduction in complex **2** cannot be ascribed with satisfactory certainty, but a reduction of ligand L is suggested.

Conclusions

Two *mixed-ligand* ruthenium(II) complexes, [(tpy)Ru^{II}(L)](PF₆)₂ (**1**) and [(tpy)Ru(L)Ru(tpy)](PF₆)₄ (**2**), involving

the *back-to-back* ligand 1,4-bis[(2,6-dipyrzazol-1-yl)pyrid-4-yl]benzene (L) were synthesised. Both complexes were fully characterised by NMR spectroscopy, MALDI-TOF/ESI mass spectrometric analysis and UV/Vis absorption spectroscopy. Furthermore, the molecular structure of the mononuclear complex **1** was determined by single-crystal X-ray diffraction methods, and the spectro- and electrochemical behaviour of both complexes was studied. The appearance of a low-temperature luminescence of the ruthenium-tpy backbone is strongly connected with the strong σ -donor behaviour of ligand L, which causes a weak ligand field and probably inhibits the stabilisation of the tpy-based $^3\text{MLCT}$ at high temperatures. The presence of the coordinating dipyrzazol-1-ylpyridyl subunit in ligand L has a marked influence on the chemical properties of the coordination compounds in comparison with the related bis(terpyridyl)benzene systems.^[16,43,44] The substitution of the outer 2-pyridyl residues by 1-pyrazolyl residues results in major changes of the electron-donating capability of the coordinating unit, making the coordinating 2,6-dipyrzolyldipyridine units of L act electronically as relatively strong σ -donors and weak π -acceptors.^[45] The electrochemical investigation of the homobimetallic complex **2** indicates the ability of ligand L to mediate weak communication between the peripheral moieties of the complex. It was shown that the *back-to-back* ligand 1,4-bis[(2,6-dipyrzazol-1-yl)pyrid-4-yl]benzene (L) can be used as a new bridging ligand system in the construction of multinuclear metal ion coordination arrays, a property which is under current investigation in surface-confined self-assembly studies.^[46]

Experimental Section

Ligand L was synthesised by following a procedure reported previously.^[35] For the synthesis of the complexes, $\text{Ru}(\text{tpy})\text{Cl}_3$ ^[36] was treated with AgBF_4 in acetone prior to use in order to increase its reactivity towards complexation. The Ru precursor was synthesised in dmf with a $\text{Ru}(\text{tpy})/\text{ligand}$ molar ratio of 1.5:1 to support the formation of both mononuclear complex **1** and binuclear complex **2**. After 12 h the reaction was stopped, and after evaporation of the solvents in vacuo the mixture was purified by column chromatography on silica. A mixture of acetonitrile, water and an aqueous solution of potassium nitrate was used as eluent. The first red-orange fraction eluted from the column contains the mononuclear complex **1** in 29% yield. As the binuclear complex **2** shows a more polar behaviour towards silica, the nitrate content was increased in order to displace it. This procedure yielded 9% of complex **2**. After removing the eluent, the mixture was slightly heated in methanol. The small amount of potassium nitrate, which dissolved in methanol, was removed from the complex salt by washing with a small portion of water (3 mL), and the residual red to orange solids were dried. Another way to separate the complexes from the potassium nitrate is to exchange the anion. Thus a methanol solution of the complex is treated with aqueous ammonium hexafluorophosphate solution, and the fast-precipitating solid is filtered off, washed with water and dried. The PF_6 salts show a decreased solubility in organic solvents. The nitrate salts are well soluble in methanol, dimethylformamide, nitromethane, very well soluble in solvent mixtures with water, and slightly soluble in water and acetonitrile (see Supporting Information).

The NMR spectra of the ligands and of the ruthenium complexes were recorded in solutions in $[\text{D}_6]\text{dmso}$ (Chemotrade, Leipzig) with a Varian Inova 400 spectrometer (Oxford magnet; ^1H : 400 MHz, ^{13}C : 100.54 MHz) with 5 mm probe heads ($^1\text{H}/\text{X}$ inverse detection for the 2D experiments and $^1\text{H}/\text{X}$ -BB direct detection for $^{13}\text{C}/\text{DEPT135}$ experiments). TMS was used as internal standard (^{13}C , ^1H) with different deuterated solvents. The observed chemical shifts δ (in ppm) are then given relative to the residual signal of the solvent. The numbering of the atoms are according to the actual IUPAC nomenclature.^[47]

Cyclic square-wave measurements were performed by employing a 3-electrode technique with a "homebuilt" computer-controlled instrument based on the PCI 6110-E data acquisition board (National Instruments). The experiments were conducted in dimethylformamide (containing 0.25 M tetra-*n*-butylammonium perchlorate) under a blanket of solvent-saturated argon. The ohmic resistance which had to be compensated for was determined by measuring the impedance of the system at potentials where the Faraday current was negligibly small. Experimental SWVs used for data fitting were background-corrected by subtracting the current curves of the blank electrolyte containing the same concentration of supporting electrolyte. The reference electrode was an Ag/AgCl electrode in acetonitrile containing 0.25 M tetra-*n*-butylammonium chloride. As recommended by IUPAC,^[48] all data reported in the paper refer to the ferrocenium/ferrocene couple, which was measured at the end of the experiments. The working electrode was either a platinum disk electrode ($d = 1.7$ mm) or a hanging mercury drop ($m = 2.79$ mg) produced by a CGME instrument (Bioanalytical Systems, Inc., West Lafayette, USA). Theoretical SWVs were simulated by using the DigiElch simulation package available from <http://www.DigiElch.de>. The simulation algorithm used in this program has been described in several publications.^[49]

MALDI-TOF MS data were acquired with a Voyager-DE PRO Bio spectrometry work station. Micro-ESI-MS analyses were performed by Dr. W. Poppitz with a Finnigan MAT 95 XL Trap. ESI-TOF mass spectrometry was carried out by Dr. Oliver Hampe and Dr. Verena Tellström at a micrOTOF-Q II at Bruker Daltonik GmbH, Bremen (Germany). Elemental analyses were carried out by Mikroanalytisches Labor Pascher An der Pulvermühle 1, D-53424 Remagen-Bandorf (Germany). UV/Vis analyses were carried out with a Varian Cary 500 Scan UV/Vis/NIR spectrophotometer. Low-temperature luminescence spectra were recorded by Dr. Sergei Lebedkin with a Fluorolog-3 fluorescence spectrometer (Jobin Yvon).

For the crystal structure determination, the intensity data for the compounds were collected with a Nonius KappaCCD diffractometer, by using graphite-monochromated Mo-K_α radiation. Data were corrected for Lorentz and polarisation effects, but not for absorption effects.^[50,51] The structure was solved by direct methods (SHELXS)^[52] and refined by full-matrix least-squares techniques against F_o^2 (SHELXL-97)^[53]. All hydrogen atoms were included at calculated positions with fixed thermal parameters. All non-hydrogen atoms were refined anisotropically.^[53] Diamond v3.1d (Crystal Impact GbR, Bonn, Germany) was used for structure representations.

[(2,2':6',2''-Terpyridyl)ruthenium]{1,4-bis[(2,6-dipyrzazol-1-yl)pyrid-4-yl]benzene}[bis(hexafluorophosphate)] – $[(\text{tpy})\text{Ru}^{\text{II}}(\text{L})](\text{PF}_6)_2$ (**1**): ^1H NMR (400 MHz, $[\text{D}_6]\text{dmso}$, 25 °C): $\delta = 6.71$ [t_{d}], $^3J_{\text{H,H}} = 2.8$, $^4J_{\text{H,H}} = 0.8$ Hz, 2 H, pz H(4A)], 6.73 [t_{d}], $^3J_{\text{H,H}} = 2.8$, $^4J_{\text{H,H}} = 0.8$ Hz, 2 H, pz H(4B)], 7.32 [dt, $^3J_{\text{H,H}} = 6.6$, $^4J_{\text{H,H}} = 0.8$ Hz, 2 H, tpy H(5), H(5'')], 7.40 [d, $^3J_{\text{H,H}} = 2.0$ Hz, 2 H, pz H(3A)], 7.71 [dd, $^3J_{\text{H,H}} = 5.6$, $^4J_{\text{H,H}} = 0.4$ Hz, 2 H, tpy H(6), H(6'')], 7.97 [d,

$^3J_{\text{H,H}} = 0.8 \text{ Hz}$, 2 H, pz H(3B)], 8.06 [dt, $^3J_{\text{H,H}} = 8.0$, $^4J_{\text{H,H}} = 1.2 \text{ Hz}$, 2 H, tpy H(4), H(4'')], 8.28 [s, 2 H, L-py H(3B), H(5B)], 8.40 [d, $^3J_{\text{H,H}} = 8.4 \text{ Hz}$, 2 H, L-ph H(B)], 8.51 [t, $^3J_{\text{H,H}} = 8.4 \text{ Hz}$, 1 H, tpy H(4'')], 8.55 [d, $^3J_{\text{H,H}} = 8.8 \text{ Hz}$, 2 H, L-ph H(A)], 8.82 [d, $^3J_{\text{H,H}} = 8.0 \text{ Hz}$, 2 H, tpy H(3), H(3'')], 9.02 [d, $^3J_{\text{H,H}} = 8.0 \text{ Hz}$, 2 H, tpy H(3'), H(5')], 9.07 [d, $^3J_{\text{H,H}} = 2.4 \text{ Hz}$, 2 H, pz H(5B)], 9.22 [s, 2 H, L-py H(3A), H(5A)], 9.58 [d, $^3J_{\text{H,H}} = 3.2 \text{ Hz}$, 2 H, pz H(5A)] ppm. ^{13}C NMR (100 MHz, $[\text{D}_6]\text{dmsO}$, 25 °C): $\delta = 106.96$ [L-py C(3A), C(5A)], 107.22 [L-py C(3B), C(5B)], 109.38 [pz C(4B)], 111.24 [pz C(4A)], 124.04 [tpy C(3'), C(5')], 124.79 [tpy C(3), C(3'')], 128.14 [tpy C(5), C(5'')], 129.03 [L-ph CH(B)], 129.11 [L-ph CH(A)], 129.14 [pz C(5B)], 134.09 [pz-C(5A)], 136.81 [tpy C(4')], 137.98 [L-ph C(1A)], 138.88 [tpy C(4), C(4'')], 139.45 [L-ph C(1B)], 143.56 [pz C(3B)], 146.59 [pz C(3A)], 149.45 [L-py C(2A), C(6A)], 150.69 [L-py C(4A)], 151.14 [L-py C(2B), C(6B)], 153.16 [L-py C(4B)], 153.53 [tpy C(6), C(6'')], 156.89 [tpy C(2'), C(6')], 159.05 [tpy C(2), C(2'')] ppm. "A" refers to chelated side of L, and "B" to the unchelated side. UV/Vis (NO_3^- salt, MeOH): $\lambda_{\text{max}} = 280$ ($\pi \rightarrow \pi^*$ tpy), 308 ($\pi \rightarrow \pi^*$ L), 365 (w, $^1\text{MLCT}$ towards L), 442 (s, $^1\text{MLCT}$ towards tpy) nm. MALDI-TOF MS: $m/z = 829.7$ ($[\text{C}_{43}\text{H}_{29}\text{N}_{13}\text{Ru}]^+$, $[\text{M} - 2\text{PF}_6 - 2\text{H}]$). ESI-TOF MS (acetonitrile/water, 1:1): m/z (%) = 415.59 (100) $[\text{I}]^{2+}$, 437.04 (9) $[\text{I} \cdot \text{F} - \text{H}]^{2+}$, 631.62 (0.5) $[\text{I} \cdot (\text{PF}_6)_3 - \text{H}]^{2+}$, 976.13 (1) $[\text{I} \cdot \text{PF}_6]^+$. $\text{C}_{43}\text{H}_{31}\text{F}_{12}\text{N}_{13}\text{P}_2\text{Ru} \cdot 0.5\text{C}_6\text{H}_{14}$ (1163.89): calcd. C 47.47, H 3.29, N 15.65, Ru 8.68; found C 47.43, H 3.07, N 15.7, Ru 8.73. Because of the insufficient amount of pure complex $\text{I} \cdot (\text{PF}_6)_2$, the sample used for elemental analysis was precipitated with hexane from a NMR-pure $[\text{D}_6]\text{dmsO}$ solution in order to remove dmsO by extraction with water.

Crystal Data for 1: $[\text{C}_{43}\text{H}_{31}\text{N}_{13}\text{ORu}]^{2+} \cdot 2[\text{NO}_3]^- \cdot 0.75\text{CH}_4\text{O}$, $M_r = 978.93 \text{ g mol}^{-1}$, red-brown prism, size $0.06 \times 0.06 \times 0.05 \text{ mm}^3$, monoclinic, space group $P2_1/n$, $a = 12.7803(6) \text{ \AA}$, $b = 14.1300(7) \text{ \AA}$, $c = 23.5751(8) \text{ \AA}$, $\beta = 104.030(3)^\circ$, $V = 4130.3(3) \text{ \AA}^3$, $T = -90^\circ \text{C}$, $Z = 4$, $\rho_{\text{calcd.}} = 1.574 \text{ g cm}^{-3}$, μ (Mo- K_α) = 4.53 cm^{-1} , $F(000) = 1998$, 26629 reflections in $h(-16/16)$, $k(-16/18)$, $l(-29/30)$, measured in the range $2.05^\circ \leq \theta \leq 27.49^\circ$, completeness $\theta_{\text{max}} = 99.4\%$, 9417 independent reflections, $R_{\text{int}} = 0.0975$, 5582 reflections with $F_o > 4\sigma(F_o)$, 599 parameters, 1 restraints, $R_{\text{1obs}} = 0.0639$, $wR_{\text{2obs}} = 0.1265$, $R_{\text{1all}} = 0.1332$, $wR_{\text{2all}} = 0.1539$, GooF = 1.007, largest difference peak and hole: $0.747/-0.621 \text{ e \AA}^{-3}$.

CCDC-654680 (1) contains the supplementary crystallographic data for this paper. These data can be obtained free of charge from The Cambridge Crystallographic Data Centre via www.ccdc.cam.ac.uk/data_request/cif.

[{Bis(2,2':6',2''-terpyridyl)ruthenium}{1,4-bis(2,6-dipyrzyl-1-yl)pyrid-4-yl}benzene}]tetrakis(hexafluorophosphate) - [(tpy)Ru(L)Ru(tpy)](PF₆)₄ (2): ^1H NMR (400 MHz, $[\text{D}_6]\text{dmsO}$, 25 °C): $\delta = 6.74$ [t, $^3J_{\text{H,H}} = 2.8 \text{ Hz}$, 4 H, pz H(4)], 7.34 [dt, $^3J_{\text{H,H}} = 6.4$, $^4J_{\text{H,H}} = 0.8 \text{ Hz}$, 4 H, tpy H(5), H(5'')], 7.44 [d, $^3J_{\text{H,H}} = 2.0 \text{ Hz}$, 4 H, pz H(3)], 7.76 [d, $^3J_{\text{H,H}} = 4.2 \text{ Hz}$, 4 H, tpy H(6), H(6'')], 8.07 [dt, $^3J_{\text{H,H}} = 7.2$, $^4J_{\text{H,H}} = 1.2 \text{ Hz}$, 4 H, tpy H(4), H(4'')], 8.51 [t, $^3J_{\text{H,H}} = 8.0 \text{ Hz}$, 2 H, tpy H(4'')], 8.78 [s, 4 H, L-ph], 8.84 [d, $^3J_{\text{H,H}} = 8.0 \text{ Hz}$, 4 H, tpy H(3), H(3'')], 9.04 [d, $^3J_{\text{H,H}} = 8.0 \text{ Hz}$, 4 H, tpy H(3'), H(5')], 9.34 [s, 4 H, L-py H(3), H(5)], 9.65 [d, $^3J_{\text{H,H}} = 3.2 \text{ Hz}$, 4 H, pz H(5)] ppm. ^{13}C NMR (100 MHz, $[\text{D}_6]\text{dmsO}$, 25 °C): $\delta = 107.26$ [L-py C(3), C(5)], 111.53 [pz C(4)], 124.34 [tpy C(3'), C(5')], 125.09 [tpy C(3), C(3'')], 128.40 [tpy C(5), C(5'')], 129.51 [L-ph CH], 134.41 [pz C(5)], 137.19 [tpy C(4')], 138.76 [L-ph C(1)], 139.17 [tpy C(4), C(4'')], 146.89 [pz C(3)], 149.74 [L-py C(2), C(6)], 150.57 [L-py C(4)], 153.77 [tpy C(6), C(6'')], 157.10 [tpy C(2'), C(6')], 159.32 [tpy C(2), C(2'')] ppm. UV/Vis (NO_3^- salt MeOH): $\lambda_{\text{max}} = 273$ ($\pi \rightarrow \pi^*$ tpy), 309 ($\pi \rightarrow \pi^*$ L), 369 (w, $^1\text{MLCT}$ towards L), 453 (s, $^1\text{MLCT}$ towards tpy) nm. MALDI-TOF MS (grid-voltage 80%,

guide wire 0.02%, positive reflector mode): $m/z = 1161.74$ ($[\text{C}_{58}\text{H}_{37}\text{N}_{16}\text{Ru}_2]^+$, $[\text{M} - 5\text{H} - 4\text{NO}_3]$). Micro-ESI (acetonitrile/methanol): $m/z = 1600.8$ ($[\text{C}_{58}\text{H}_{42}\text{F}_{18}\text{N}_{16}\text{P}_3\text{Ru}_2]$, $[\text{M} - \text{PF}_6]$). ESI-TOF (acetonitrile/water, 1:1): m/z (%) = 291.54 (100) $[\text{2} \cdot (\text{PF}_6)_2]^{4+}$, 388.39 (6) $[\text{2}^{3+}]$, 437.04 (35) $[\text{2} \cdot \text{PF}_6]^{3+}$, 728.05, (1) $[\text{2}]^{2+}$. $\text{C}_{58}\text{H}_{42}\text{F}_{24}\text{N}_{16}\text{P}_4\text{Ru}_4(\text{CH}_3)_2\text{SO}$ (2057.6): calcd. C 38.52, H 3.23, N 10.89, Ru 9.82; found C 38.60, H 3.50, N 10.7, Ru 9.68. Because of the insufficient amount of pure complex $\text{2} \cdot (\text{PF}_6)_4$, the sample used for elemental analysis was precipitated with hexane from a NMR-pure $[\text{D}_6]\text{dmsO}$ solution in order to remove excessive dmsO by extraction with water. Residual solvent was removed at elevated temperature in vacuo.

Supporting Information (see footnote on the first page of this article): Original mass spectrometric analysis spectra, 1D and 2D NMR spectra, square-wave voltammograms and low-temperature emission spectra.

Acknowledgments

The authors thank the Deutsche Forschungsgemeinschaft (DFG) for financial support within the frame of the project "Inducing charge states in single molecule junctions" DFG-SPP 1243. Velimir Meded is acknowledged for his help in the preparation of the manuscript. Furthermore, the authors thank Oliver Hampe and Verena Tellström for the measurement of the ESI-TOF spectra and Sergei Lebedkin for the low-temperature emission spectroscopy measurements. We are grateful to the referees who gave helpful advices for this manuscript.

- a) V. Balzani, A. Juris, M. Venturi, S. Campagna, S. Serroni, *Chem. Rev.* **1996**, *96*, 759–833; b) S. Campagna, F. Puntiero, N. Nastasi, G. Baergamini, V. Balzani, *Top. Curr. Chem.* **2007**, *280*, 117–214.
- J. P. Sauvage, J. P. Collin, J. C. Chambron, S. Guillerez, C. Coaudret, V. Balzani, F. Barigelletti, L. De Cola, L. Flamigni, *Chem. Rev.* **1994**, *94*, 993–1019.
- a) H. Inoue, S. Funyu, Y. Shimada, S. Takagi, *Pure Appl. Chem.* **2005**, *77*, 1019–1033; b) K. L. Wouters, N. R. de Tacconi, R. Konduri, R. O. Lezna, F. M. MacDonnell, *Photosynth. Res.* **2006**, *87*, 41–55.
- S. Rau, B. Schäfer, D. Gleich, E. Anders, M. Rudolph, M. Friedrich, H. Görls, W. Henry, J. G. Vos, *Angew. Chem. Int. Ed.* **2006**, *45*, 6215–6218.
- a) J. A. Faiz, R. M. Williams, M. J. J. Pereira Silva, L. De Cola, Z. Pikramenou, *J. Am. Chem. Soc.* **2006**, *128*, 4520–4521; b) J. M. Haider, R. M. Williams, L. De Cola, Z. Pikramenou, *Angew. Chem. Int. Ed.* **2003**, *42*, 1830–1833; c) H. Wolpher, S. Sinha, J. X. Pan, A. Johansson, M. J. Lundqvist, P. Persson, R. Lomoth, J. Bergquist, L. C. Sun, V. Sundström, B. Åkermar, T. Polyvka, *Inorg. Chem.* **2007**, *46*, 638–651; d) M. Borgström, S. Ott, R. Lomoth, J. Bergquist, L. Hammarström, O. Johansson, *Inorg. Chem.* **2006**, *45*, 4820–4829.
- R. T. F. Jukes, B. Bozic, F. Hartl, P. Belser, L. De Cola, *Inorg. Chem.* **2006**, *45*, 8326–8341.
- a) Md. K. Nazeeruddin, S. M. Zakeeruddin, J. J. Lagref, P. Liska, P. Comte, C. Barolo, G. Viscardi, K. Schenk, M. Graetzel, *Coord. Chem. Rev.* **2004**, *248*, 1317–1328; b) Md. K. Nazeeruddin, C. Klein, P. Liska, M. Graetzel, *Coord. Chem. Rev.* **2005**, *249*, 1460–1467; c) F. T. Kong, S. Y. Dai, K. J. Wang, *Chin. J. Chem.* **2007**, *25*, 168–171.
- a) J. D. Badjic, C. M. Ronconi, J. F. Stoddart, V. Balzani, S. Silvi, A. Credi, *J. Am. Chem. Soc.* **2006**, *128*, 1489–1499; b) A. Petitjean, F. Puntiero, S. Campagna, A. Juris, J. M. Lehn, *Eur. J. Inorg. Chem.* **2006**, *19*, 3878–3892; c) V. Balzani, G. Bergamini, F. Marchioni, P. Ceroni, *Coord. Chem. Rev.* **2006**,

- 250, 1254–1266; d) S. Nitahara, N. Terasaki, T. Akiyama, S. Yamada, *Thin Solid Films* **2006**, 499, 354–358.
- [9] a) M. Ruben, S. Rau, A. Skirl, K. Krause, H. Görls, D. Walther, J. G. Vos, *Inorg. Chim. Acta* **2000**, 206–214; b) F. Schramm, H. Görls, D. Walther, *Z. Anorg. Allg. Chem.* **2006**, 632, 391–399; c) F. Schramm, D. Walther, H. Görls, C. Käßpflinger, R. Beckert, *Z. Naturforsch.* **2005**, 60b, 843–852; d) M. Schmitt, H. W. Lin, E. Thiel, A. J. Meixner, H. Ammon, *Dalton Trans.* **2006**, 4020–4028.
- [10] a) S. Bonnet, J. P. Collin, M. Koizumi, P. Mobian, J. P. Sauvage, *Adv. Mater.* **2006**, 18, 1239–1250; b) V. Balzani, A. Credi, S. Silvi, M. Venturi, *Chem. Soc. Rev.* **2006**, 35, 1135–1149.
- [11] a) W. R. Browne, N. M. O’Boyle, W. Henry, A. L. Guckian, S. Horn, T. Fett, C. M. O’Connor, M. Duati, L. De Cola, C. G. Coates, K. L. Ronayne, J. J. McGarvey, J. G. Vos, *J. Am. Chem. Soc.* **2005**, 127, 1229–1241; b) W. R. Browne, R. Hage, J. G. Vos, *Coord. Chem. Rev.* **2006**, 250, 1653–1668.
- [12] B. Dietzek, W. Kiefer, J. Blumhoff, L. Böttcher, S. Rau, D. Walther, U. Uhlemann, M. Schmitt, J. Popp, *Chem. Eur. J.* **2006**, 12, 5105–5115.
- [13] a) M. I. J. Polson, F. Loiseau, S. Campagna, G. S. Hanan, *Chem. Commun.* **2006**, 1301–1303; b) E. A. Medlycott, G. S. Hanan, *Coord. Chem. Rev.* **2006**, 250, 1763–1782; c) E. A. Medlycott, G. S. Hanan, *Chem. Soc. Rev.* **2005**, 34, 133–142.
- [14] D. L. Jameson, J. K. Blaho, K. T. Kruger, K. A. Goldsby, *Inorg. Chem.* **1989**, 28, 4312–4314.
- [15] Surprisingly, the heteroleptic complex Ru(bpp)tpy exhibits only one ¹MLCT band at 430 nm “indicating strong coupling between the π^* orbitals of the mixed ligand complex” according to ref.^[14]
- [16] F. Kröhnke, *Synthesis* **1976**, 1–24.
- [17] D. G. Kurth, F. Caruso, C. Schüler, *Chem. Commun.* **1999**, 1579–1580.
- [18] E. C. Constable, A. M. W. Cargill Thompson, *J. Chem. Soc., Dalton Trans.* **1992**, 3467–3475.
- [19] a) J. P. Collin, P. Lainé, J. P. Launay, J. P. Sauvage, A. Sour, *J. Chem. Soc., Chem. Commun.* **1993**, 434–435; b) L. Hammarström, F. Barigelletti, L. Flamigni, M. T. Indelli, N. Armadori, G. Calogero, M. Guardigli, A. Sour, J. P. Collin, J. P. Sauvage, *J. Phys. Chem. A* **1997**, 101, 9061–9069; c) M. T. Indelli, F. Scandola, J.-P. Collin, J. P. Sauvage, A. Sour, *Inorg. Chem.* **1996**, 35, 303–312; d) ttpy is 4'-p-tolyl-2,2':6,2''-terpyridine, and tpy-ph-tpy is 1,4-bis(2,2':6,2''-terpyridin-4'-yl)benzene.
- [20] F. Barigelletti, L. Flamigni, M. Guardigli, J. P. Sauvage, J. P. Collin, A. Sour, *Chem. Commun.* **1996**, 1329–1330.
- [21] a) F. Barigelletti, L. Flamigni, V. Balzani, J. P. Collin, J. P. Sauvage, A. Sour, E. C. Constable, A. M. W. Cargill Thompson, *J. Am. Chem. Soc.* **1994**, 116, 7692–7699; b) M. Abrahamsson, H. Wolpher, O. Johansson, J. Larsson, M. Kritikos, L. Eriksson, P. O. Norrby, J. Bergquist, L. Sun, B. Åkermarck, L. Hammarström, *Inorg. Chem.* **2005**, 44, 3215–3225.
- [22] V. V. Pavlishchuk, A. W. Addison, *Inorg. Chim. Acta* **2000**, 298, 97–102. The authors used a +0.38 V addition for the adaptation of SCE vs. ferrocene and a +0.384 V addition towards SSCE values.
- [23] T. E. Janini, J. L. Fattore, D. L. Mohler, *J. Organomet. Chem.* **1999**, 578, 260–263.
- [24] S. Văduvescu, P. G. Potvin, *Eur. J. Inorg. Chem.* **2004**, 1763–1769.
- [25] M. Schmitt, V. Kalsani, P. Mal, J. W. Bats, *Inorg. Chem.* **2006**, 45, 6370–6377.
- [26] M. Schmitt, V. Kalsani, R. S. K. Kishore, H. Cölfen, J. W. Bats, *J. Am. Chem. Soc.* **2005**, 127, 11544–11545.
- [27] Y. Bodenthin, U. Pietsch, H. Möhwald, D. G. Kurth, *J. Am. Chem. Soc.* **2005**, 127, 3110–3115.
- [28] H. Torieda, A. Yoshimura, K. Nozaki, S. Sakai, T. Ohno, *J. Phys. Chem. A* **2002**, 106, 11034–11044.
- [29] A. J. Downard, G. E. Honey, P. J. Steel, *Inorg. Chem.* **1991**, 30, 3733–3737.
- [30] a) M.-A. Haga, N. Kato, H. Monjushiro, K. Wang, Md. D. Hossain, *Supramol. Sci.* **1998**, 5, 337–342; b) M.-a. Haga, T. Takasugi, A. Tomie, M. Ishizuya, T. Yamada, Md. D. Hossain, M. Inoue, *Dalton Trans.* **2003**, 2069–2079; c) M.-a. Haga, M. Ohta, H. Machida, M. Chikira, N. Tonegawa, *Thin Solid Films* **2006**, 499, 201–206; d) B. Mondal, S. Chakraborty, P. Munshi, M. G. Walawalkar, G. K. Lahiri, *J. Chem. Soc., Dalton Trans.* **2000**, 2327–2335.
- [31] a) M. Duati, S. Tasca, F. C. Lynch, H. Bohlen, J. G. Vos, S. Stagni, M. D. Ward, *Inorg. Chem.* **2003**, 42, 8377–8384; b) M. Duati, S. Fanni, J. G. Vos, *Inorg. Chem. Commun.* **2000**, 3, 68–70.
- [32] a) O. Johansson, R. Lomoth, *Chem. Commun.* **2005**, 1578–1580; b) H. Wolpher, O. Johansson, M. Abrahamsson, M. Kritikos, L. C. Sun, B. Åkermarck, *Inorg. Chem. Commun.* **2004**, 7, 337–340.
- [33] a) R. P. Thummel, V. Hegde, Y. Jahn, *Inorg. Chem.* **1989**, 28, 3264–3267; b) Y. Jahng, S. W. Moon, R. P. Thummel, *Bull. Korean Chem. Soc.* **1997**, 18, 174–185; c) A. Winter, J. Hummel, N. Risch, *J. Org. Chem.* **2006**, 71, 4862–4871.
- [34] a) V. A. Money, I. Radosavljevic Evans, M. A. Halcrow, A. E. Goeta, J. A. K. Howard, *Chem. Commun.* **2003**, 158–159; b) J. M. Holland, J. A. McAllister, C. A. Kilner, M. Thornton-Pett, A. J. Bridgeman, M. A. Halcrow, *J. Chem. Soc., Dalton Trans.* **2002**, 548–554; c) C. Carbonera, J. Sánchez Costa, V. A. Money, J. Elhaik, J. A. K. Howard, M. A. Halcrow, J. F. Létard, *Dalton Trans.* **2006**, 3058–3066; d) N. K. Solanki, E. J. L. McInnes, F. E. Mabbs, S. Radojevic, M. McPartlin, N. Feeder, J. E. Davies, M. A. Halcrow, *Angew. Chem. Int. Ed.* **1998**, 37, 2221–2223; e) T. Ayers, S. Scott, J. Goins, N. Caylor, D. Hathcock, S. J. Slattery, D. L. Jameson, *Inorg. Chim. Acta* **2000**, 307, 7–12.
- [35] a) J. M. Holland, J. A. McAllister, Z. Lu, C. A. Kilner, M. Thornton-Pett, M. A. Halcrow, *Chem. Commun.* **2001**, 557–560; b) C. Rajadurai, F. Schramm, S. Brink, O. Fuhr, M. Ghafari, R. Kruk, M. Ruben, *Inorg. Chem.* **2006**, 45, 10019–10021; c) C. Rajadurai, O. Fuhr, R. Kruk, M. Ghafari, H. Hahn, M. Ruben, *Chem. Commun.* **2007**, 2636–2638.
- [36] B. P. Sullivan, J. M. Calvert, T. J. Meyer, *Inorg. Chem.* **1980**, 19, 1404–1407.
- [37] H. Friebolin, *Basic One- and Two-Dimensional NMR Spectroscopy*, Wiley-VCH Weinheim (Germany), **2005**, 4th rev. ed..
- [38] H. Elsbernd, J. K. Beattie, *J. Inorg. Nucl. Chem.* **1972**, 34, 771–774.
- [39] J. Elguero, A. Fruchier, A. De La Hoz, F. A. Jalón, B. R. Manzano, A. Otero, F. Gómez-De La Torre, *Chem. Ber.* **1996**, 129, 589–594.
- [40] A. C. Laemmel, J. P. Collin, J. P. Sauvage, *C. R. Acad. Sci. Paris, Série IIc, Chemistry* **2000**, 43–49; therein: ttpy = 4'-tolyl-2,2':6,2''-terpyridine, dmpp = 2,6-bis(3,5-dimethyl-N-pyrazolyl)pyridine.
- [41] J. P. Lecomte, A. Kirsch-De Mesmaeker, G. Orellana, *J. Phys. Chem.* **1994**, 98, 5382–5388.
- [42] D. Walther, L. Böttcher, J. Blumhoff, S. Schebesta, H. Görls, K. Schmuck, S. Rau, M. Rudolph, *Eur. J. Inorg. Chem.* **2006**, 12, 2385–2392.
- [43] R. Hage, R. Prins, J. G. Haasnot, J. Reedijk, J. G. Vos, *J. Chem. Soc., Dalton Trans.* **1987**, 1389–1395.
- [44] a) B. P. Sullivan, D. J. Salmon, T. J. Meyer, J. Peedin, *Inorg. Chem.* **1979**, 18, 3369–3374; b) M. L. Stone, G. A. Crosby, *Chem. Phys. Lett.* **1981**, 79, 169–173.
- [45] P. J. Steel, F. Lahousse, D. Lerner, C. Marzin, *Inorg. Chem.* **1983**, 22, 1488–1493.
- [46] a) M. Ruben, *Angew. Chem. Int. Ed.* **2005**, 44, 1594–1596; b) N. Lin, S. Stepanow, F. Vidal, K. Kern, M. S. Alam, S. Strömsdörfer, V. Dremov, P. Müller, A. Landa, M. Ruben, *Dalton Trans.* **2006**, 2794–2800.
- [47] G. P. Moss, P. A. S. Smith, D. Tavernier, *Pure Appl. Chem.* **1995**, 67, 1307–1375.
- [48] G. Gritzner, J. Kuta, *Pure Appl. Chem.* **1982**, 54, 1527–1532.

- [49] M. Rudolph, *J. Comput. Chem.* **2005**, 26, 1193–1204 and references cited therein.
- [50] *COLLECT*, Data Collection Software, Nonius B. V., Netherlands, **1998**.
- [51] Z. Otwinowski, W. Minor, *Methods Enzymol.* **1997**, 276, 307–326.
- [52] G. M. Sheldrick, *Acta Crystallogr., Sect. A* **1990**, 46, 467–473.
- [53] G. M. Sheldrick, *SHELXL-97* (Release 97–2), *Program for the Refinement of Crystal Structures*, University of Göttingen, Germany, **1997**.

Received: June 20, 2008
Published Online: November 28, 2008

Synthesis, Protonation and Cu^{II} Complexes of Two Novel Isomeric Pentaazacyclophane Ligands: Potentiometric, DFT, Kinetic and AMP Recognition Studies

Andrés G. Algarra,^[a] Manuel G. Basallote,^{*[a]} Raquel Belda,^[b] Salvador Blasco,^[b] C. Esther Castillo,^[a] José M. Llinares,^[c] Enrique García-España,^{*[b]} Laura Gil,^[b] M. Ángeles Máñez,^[a] Conxa Soriano,^[c] and Begoña Verdejo^[b]

Keywords: Cyclophanes / Macrocyclic ligands / Copper / Kinetics / Density functional calculations

The synthesis and coordination chemistry of two novel ligands, 2,6,9,12,16-pentaaza[17]metacyclophane (**L**¹) and 2,6,9,12,16-pentaaza[17]paracyclophane (**L**²), is described. Potentiometric studies indicate that **L**¹ and **L**² form a variety of mononuclear complexes the stability constants of which reveal a change in the denticity of the ligand when moving from **L**¹ to **L**², a behaviour that can be qualitatively explained by the inability of the paracyclophanes to simultaneously use both benzylic nitrogen atoms for coordination to a single metal centre. In contrast, the formation of dinuclear hydroxylated complexes is more favoured for the *para* **L**² ligand. DFT calculations have been carried out to compare the geometries and relative energies of isomeric forms of the [CuL]²⁺ complexes of **L**¹ and **L**² in which the cyclophane acts either as tri- or tetradentate. The results indicate that the energy cost associated with a change in the coordination mode of the cyclophane from tri- to tetradentate is moderate for both ligands so that the actual coordination mode can be determined not only by the characteristics of the first coordination sphere but also by the specific interactions with additional

nearby water molecules. The kinetics of the acid promoted decomposition of the mono- and dinuclear Cu^{II} complexes of both cyclophanes have also been studied. For both ligands, dinuclear complexes convert rapidly to mononuclear species upon addition of excess acid, the release of the first metal ion occurring within the mixing time of the stopped-flow instrument. Decomposition of the mononuclear [CuL²]²⁺ and [CuHL²]³⁺ species occurs with the same kinetics, thus showing that protonation of [CuL²]²⁺ occurs at an uncoordinated amine group. In contrast, the [CuL¹]²⁺ and [CuHL¹]³⁺ species show different decomposition kinetics indicating the existence of significant structural reorganisation upon protonation of the [CuL¹]²⁺ species. The interaction of AMP with the protonated forms of the cyclophanes and the formation of mixed complexes in the systems Cu–**L**¹–AMP, Cu–**L**²–AMP, and Cu–**L**³–AMP, where **L**³ is the related pyridinophane containing the same polyamine chain and 2,6-dimethylpyridine as a spacer, is also reported.

(© Wiley-VCH Verlag GmbH & Co. KGaA, 69451 Weinheim, Germany, 2009)

Introduction

In the last years some of us have focused on the synthesis and study of new families of cyclic ligands formed by linking together the ends of a polyamine and an aromatic spacer through methylene carbon atoms.^[1–5] Perhaps one of the most interesting aspects of the coordination chemistry

of these compounds is their ability to form metal complexes containing coordinatively unsaturated metal sites. In each case, the actual details of the coordination environments are affected by different factors such as the kind of aromatic spacer, the number of nitrogen atoms and the size and flexibility of the polyamine chain.

The role of the aromatic spacer, in particular the type of substitution (*ortho*, *meta* or *para*), becomes fundamental in the coordination chemistry of synthetic cyclophanes, especially in those with polyamine chains of small size. For example, the rigidity of the *p*-xylyl unit prevents the simultaneous participation of both benzylic nitrogen atoms in the coordination of a single metal ion which results in a higher tendency for the formation of dinuclear complexes than that exhibited by analogous ligands with *o*- or *m*-xylyl spacers.^[2,6] In contrast, small and medium-sized cyclophanes with one *o*-xylyl spacer usually form only mononuclear complexes. The larger the size of the polyamine, the less drastic these changes are so that the coordination chemistry

[a] Departamento de Ciencia de Materiales e Ingeniería Metalúrgica y Química Inorgánica, Facultad de Ciencias, Universidad de Cádiz, Apartado 40, Puerto Real, 11510 Cádiz, Spain
E-mail: manuel.basallote@uca.es

[b] Departamento de Química Inorgánica, Instituto de Ciencia Molecular, Universidad de Valencia, Apartado Correos 22085, 46071 Valencia, Spain
E-mail: enrique.garcia-es@uv.es

[c] Departamento de Química Orgánica, Facultad de Farmacia, Universidad de Valencia, Avda. Vicente Andrés Estellés s/n, 46100 Burjassot (Valencia), Spain

Supporting information for this article is available on the WWW under <http://www.eurjic.org> or from the author.

of these isomers becomes more similar. In the present work, we decided to analyse the case of the isomeric cyclophanes **L**¹ and **L**² (see Figure 1), paying special attention to their behaviour towards protonation and to their ability to form mono- and dinuclear Cu^{II} complexes. In addition, the kinetic properties of the latter complexes have been also examined in order to obtain additional information about the lability of closely related metal complexes differing only in their protonation states. In this sense, recent reports have shown that the different CuH_xL^{z+} species of a given ligand can decompose with different kinetics which reveals the existence of extensive structural reorganisation of the Cu^{II} complexes upon protonation.^[7] The paper also includes some exploratory work on the stability of the AMP species formed by the cyclophanes and their copper complexes. The nucleotide-recognition capability of protonated noncyclic and macrocyclic polyamines was discovered decades ago^[8–13] and it has been exploited for nucleotide sensing and separation.^[14–17] The interaction of the ammonium groups in the H_xL^{z+} species with the phosphate anions of adenosine-5'-monophosphate (AMP), adenosine-5'-diphosphate (ADP) and adenosine-5'-triphosphate (ATP) leads to the formation of H_xLA^{(x-z)+} (A^{z-} = nucleotide anion) species with increased stability as a consequence of π stacking interactions with aromatic rings in the polyamine. To gain insight into the stability of this kind of species, an initial approach to the nucleotide-recognition capability of the **L**¹–**L**³ cyclophanes and their Cu^{II} complexes was made by studying their interaction with AMP.

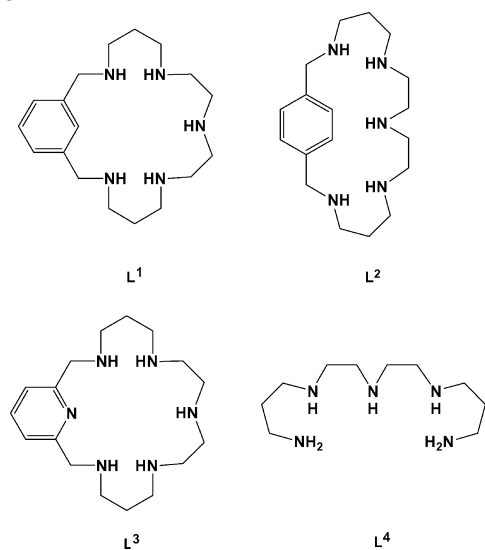


Figure 1. Ligands and abbreviations used in this work.

Results and Discussion

Equilibrium Studies on Ligand Protonation and Cu^{II} Complexation

The stepwise protonation constants for the **L**¹ and **L**² ligands are included in Table 1 and compared with those previously reported for the open-chain counterpart **L**⁴^[18]

and the corresponding pyridine derivative **L**³.^[19] In all cases the five expected protonation steps can be identified within the pH range of the study (2–11) and the trend in the values of the stepwise constants can be easily rationalised on the basis of minimisation of electrostatic repulsion between the positive charges generated at the protonated amine groups. Thus, the new **L**¹ cyclophane shows large values of the constants for the first two protonation steps whereas the third and fourth protonation steps occur with constants with intermediate values and the last step occurs with a much more reduced protonation constant as a consequence of the fact that the incoming proton is forced to bind to the central nitrogen of the polyamine chain while being surrounded by two protonated sites separated by ethylenic chains. These results are quite similar to those previously reported for the analogous pyridinophane **L**³^[19] for which the proposed protonation sequence was confirmed by ¹H and ¹³C NMR spectroscopy at variable pH values. For these two ligands (**L**¹ and **L**³), the protonation constants are always smaller than those corresponding to the open-chain **L**⁴ ligand. In contrast, although the results obtained for **L**² are quite parallel, a greater basicity is observed for all the protonation steps in this ligand, probably because the *para* substitution at the aromatic spacer facilitates the separation of the positive charges generated at the cyclophane upon protonation. As a consequence of this capability, the protonation constants for **L**² become closer to those obtained for the open-chain polyamine **L**⁴.^[18]

Table 1. Stepwise protonation constants for the **L**¹ and **L**² ligands.^[a] Literature values^[18,19] for the protonation constants of **L**³ and **L**⁴ are also included for comparison.

| Reaction ^[b] | L ¹ | L ² | L ⁴ | L ³ |
|---|-----------------------|-----------------------|-----------------------|-----------------------|
| H + L = HL | 9.70(2) | 10.69(2) | 10.55 | 9.65 |
| H + HL = H ₂ L | 9.37(2) | 9.66(1) | 9.89 | 9.32 |
| H + H ₂ L = H ₃ L | 7.81(2) | 8.32(2) | 8.69 | 7.62 |
| H + H ₃ L = H ₄ L | 6.99(2) | 7.21(2) | 7.55 | 6.62 |
| H + H ₄ L = H ₅ L | 2.80(4) | 3.03(3) | 3.55 | 2.86 |
| log β_5 | 36.67 | 38.91 | 40.23 | 36.07 |

[a] At 298.1 K in the presence of 0.15 M NaClO₄. The values in parentheses correspond to the standard deviations in the last significant figure. [b] Charges omitted for clarity.

The stability constants for the formation of Cu²⁺ complexes with the **L**¹ and **L**² cyclophanes are included in Table 2 together with those previously reported for **L**³ and **L**⁴.^[18,19] All three cyclophanes allow for the formation of both mono- and dinuclear metal complexes whereas the open-chain **L**⁴ ligand only forms mononuclear species. As usually occurs in these kinds of ligands, the nuclearity of the species formed is strongly dependent on the M/L molar ratio so that while for **L**¹ at a 1:1 ratio only mononuclear species are detected throughout the whole pH range studied, for a 2:1 ratio the dinuclear hydroxylated complex is the only species in solution above pH 6 (Figure 2). As expected from the change in the substitution at the aromatic spacer, the stability of the dinuclear species increases for the *para*-substituted **L**² cyclophane. For a 2:1 molar ratio several dinuclear species can be detected which also dominate the species distribution curves above pH 6 (Figure 3).

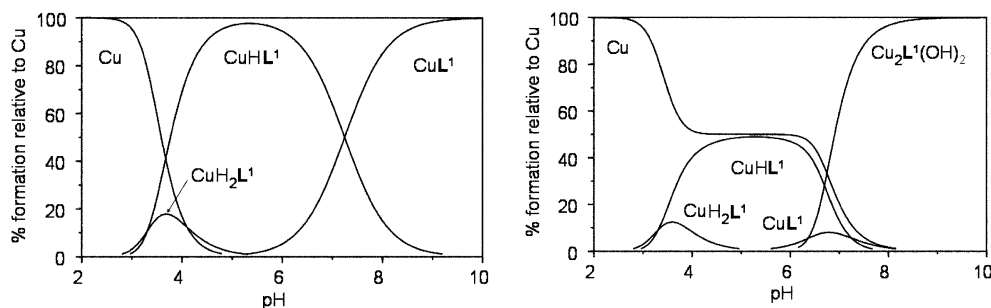


Figure 2. Distribution diagram for the system $\text{Cu}^{2+}\text{-L}^1$. (A) $[\text{Cu}^{2+}] = [\text{L}^1] = 10^{-3} \text{ mol dm}^{-3}$. (B) $[\text{Cu}^{2+}] = 2 \times 10^{-3} \text{ mol dm}^{-3}$, $[\text{L}^1] = 10^{-3} \text{ mol dm}^{-3}$.

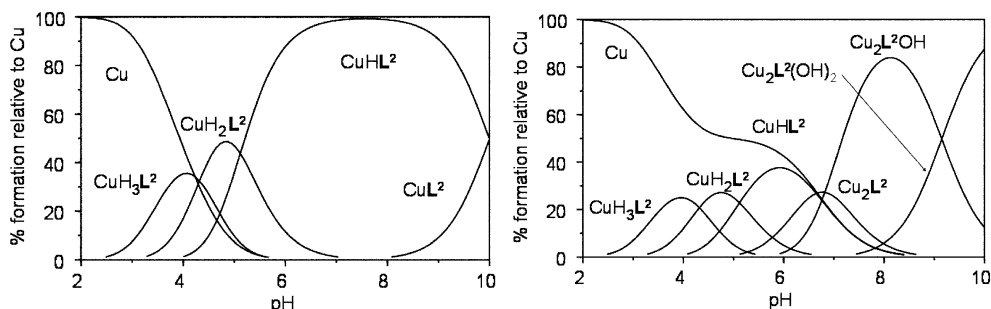


Figure 3. Distribution diagram for the system $\text{Cu}^{2+}\text{-L}^2$. (A) $[\text{Cu}^{2+}] = [\text{L}^2] = 10^{-3} \text{ mol dm}^{-3}$. (B) $[\text{Cu}^{2+}] = 2 \times 10^{-3} \text{ mol dm}^{-3}$, $[\text{L}^2] = 10^{-3} \text{ mol dm}^{-3}$.

Table 2. Stepwise stability constants for the formation of Cu^{2+} complexes with the L^1 and L^2 cyclophanes.^[a] Literature values^[18,19] for the systems $\text{Cu}^{2+}\text{-L}^3$ and $\text{Cu}^{2+}\text{-L}^4$ are also included for comparative purposes.

| Reaction ^[b] | L^1 | L^2 | L^3 | L^4 |
|--|--------------|--------------|--------------|--------------|
| $\text{Cu} + \text{L} = \text{CuL}$ | 19.05 (1) | 15.70(4) | 20.44 | 21.28 |
| $\text{CuL} + \text{H} = \text{CuHL}$ | 7.25 (3) | 10.00(4) | 6.96 | 8.86 |
| $\text{CuHL} + \text{H} = \text{CuH}_2\text{L}$ | 3.33 (2) | 5.12(2) | 2.75 | 3.39 |
| $2 \text{ Cu} + \text{L} = \text{Cu}_2\text{L}$ | — | 22.00(6) | — | — |
| $2 \text{ Cu} + \text{L} + \text{H}_2\text{O} = \text{Cu}_2\text{L}(\text{OH}) + \text{H}$ | — | 15.19(2) | 20.65 | — |
| $2 \text{ Cu} + \text{L} + 2 \text{ H}_2\text{O} = \text{Cu}_2\text{L}(\text{OH})_2 + 2 \text{ H}$ | 9.05 (1) | 6.04(3) | 10.84 | — |

[a] At 298.1 K in the presence of 0.15 M NaClO_4 . The values in parentheses correspond to the standard deviations in the last significant figure. [b] Charges omitted for clarity.

With regards to the actual values of the stability constants, the major observation made from the values in Table 2 is that the stability of the $[\text{CuL}^2]^{2+}$ species is significantly lower than that found for the same species with the other ligands suggesting a lower coordination number of the cyclophane in this case. The previously reported crystal structure of the $[\text{CuL}^3]^{2+}$ complex reveals a very distorted octahedral coordination sphere about the metal centre so that the coordination number of the ligand can be best described as being four.^[19] A coordination number of four has also been established for the Cu^{II} complex of the acyclic L^4 ligand.^[19,20] Although deriving coordination numbers by taking into account only free energy terms can be misleading, a careful consideration of the stability constants of the different protonated and nonprotonated complex species, in comparison with the protonation of the free ligands, can provide some valuable information. In this sense, Table 2

reveals that the first protonation constant for the $[\text{CuL}^1]^{2+}$, $[\text{CuL}^2]^{2+}$ and $[\text{CuL}^3]^{2+}$ complexes has values that compare well with the third protonation step of the free ligands seen in Table 1, a step in which there are the same charge changes. This comparison suggests that not all the nitrogen atoms in the ligand are involved in metal coordination, as confirmed by the crystal structure for the case of L^3 commented on above. However, the formation constant of $[\text{CuL}^2]^{2+}$ is much smaller than that obtained for the equivalent L^3 species. This fact, and the high value for the second protonation constant for $[\text{CuL}^2]^{2+}$ strongly suggests that in this case there are only three nitrogen atoms tightly bound to the metal ion which contrasts with the tetradentate coordination observed for the $\text{L}^3\text{-Cu}$ complex.^[19] Therefore, *p*-substitution at the aromatic ring of L^2 appears to prevent the simultaneous participation of both benzylic nitrogen atoms in the coordination to a single metal ion, a conclusion supported by several previous reports of crystal structures involving *para*-azacyclophanes.^[2–4]

In attempts to obtain additional information about the denticity of the L^1 and L^2 cyclophanes in their Cu^{II} complexes by using experimental techniques different from potentiometric data, were carried out instead EPR and UV/Vis spectroscopic studies. EPR spectra recorded at the pH values where the mononuclear species $[\text{CuHL}^1]^{3+}$, $[\text{CuL}^1]^{2+}$, $[\text{CuHL}^2]^{3+}$ and $[\text{CuL}^2]^{2+}$ predominate in solution (see some representative examples in the Supporting Information) are in all cases very similar to each other and they do not show any superhyperfine structure due to interaction with ^{14}N nuclei so that no direct information about the number of coordinated nitrogen atoms could be obtained. However,

since it has been reported that there is an approximate additivity of the influence of the number of nitrogen donors on the parameters in the EPR spectra of Cu-polyamine complexes,^[21] a more detailed analysis of the EPR spectra at 100 K was made. The only species with an EPR spectrum significantly different from the other species is $[\text{CuHL}^1]^{3+}$ and this shows an isotropic spectrum with a g value of 2.09 which suggests that protonation of $[\text{CuL}^2]^{2+}$ leads to a change in the geometry towards a tetrahedral structure. However, it was found that the spectra of the $[\text{CuHL}^1]^{3+}$, $[\text{CuL}^1]^{2+}$ and $[\text{CuL}^2]^{2+}$ complexes are similar in all cases with values of $g_{\perp} = 2.08$, $g = 2.21$ and $A = 190$ G. These values compare well with those reported for $\text{Cu}(\text{en})_2^{2+}$, $\text{Cu}(\text{trien})^{2+}$ and $\text{Cu}(\text{cyclam})^{2+}$ ^[21] but no conclusions about differences in the denticity of the ligand in the L^1 and L^2 complexes could be established. Nevertheless, further evidence for the change in the denticity of the L^1 and L^2 ligands in their Cu complexes is provided by the electronic spectra which show an absorption maximum centred at 570 nm in the case of $[\text{HCuL}^1]^{3+}$ ($\epsilon = 194 \text{ M}^{-1} \text{ cm}^{-1}$), 565 nm for $[\text{CuL}^1]^{2+}$ ($\epsilon = 191 \text{ M}^{-1} \text{ cm}^{-1}$), 585 nm for $[\text{HCuL}^2]^{3+}$ ($\epsilon = 85 \text{ M}^{-1} \text{ cm}^{-1}$), 585 nm for $[\text{CuL}^2]^{2+}$ ($\epsilon = 110 \text{ M}^{-1} \text{ cm}^{-1}$) and 610 nm for $[\text{Cu}_2\text{L}^2(\text{OH})]^{3+}$ ($\epsilon = 215 \text{ M}^{-1} \text{ cm}^{-1}$). A maximum at wavelengths close to 575 nm has been observed for complexes with related polyamines acting as tetradentate ligands with four coordinated nitrogen atoms disposed at the vertices of a square around the metal ion whereas complexes with tridentate polyamines show absorption bands at larger wavelengths, close to that found for $[\text{CuL}^2]^{2+}$. Thus, the $\text{Cu}(\text{dien})^{2+}$ complex shows a maximum at 605–615 nm ($\epsilon = 73\text{--}82 \text{ M}^{-1} \text{ cm}^{-1}$)^[20] and the H_3CuL complex of 4,7,10,13-tetraazahexadecane-1,16-diamine shows its maximum at 590 nm (ϵ not given in the literature).^[18] Both of these complexes contain a polyamine coordinated in a tridentate manner and coordination of an additional amine group leads to a shift of the maximum to shorter wavelengths by 15–60 nm relative to the 3 N coordinated species: $\text{Cu}(\text{dien})(\text{NH}_3)^{2+}$ has $\lambda_{\text{max}} = 576 \text{ nm}$ ($\epsilon = 84 \text{ M}^{-1} \text{ cm}^{-1}$)^[20] for the CuL^{2+} complex of 4,7,10,13-tetraazahexadecane-1,16-diamine $\lambda_{\text{max}} = 578 \text{ nm}$ ($\epsilon = 178 \text{ M}^{-1} \text{ cm}^{-1}$)^[18] and for the HCuL^{3+} and CuL^{2+} species with 4,7,10-triazatridecane-1,13-diamine the values are $\lambda_{\text{max}} = 573 \text{ nm}$ ($\epsilon = 187 \text{ M}^{-1} \text{ cm}^{-1}$) and $\lambda_{\text{max}} = 585 \text{ nm}$ ($\epsilon = 214 \text{ M}^{-1} \text{ cm}^{-1}$)^[20] respectively. Interestingly, increased molar absorptivities were also observed in the tetracoordinated species ($\epsilon = 170\text{--}200 \text{ M}^{-1} \text{ cm}^{-1}$) with respect to the corresponding tricoordinated species ($\epsilon = 70\text{--}150 \text{ M}^{-1} \text{ cm}^{-1}$), something which was attributed to distortion from an ideal square planar structure.^[20]

Another important point to consider is the formation of dinuclear hydroxy complexes. Since these ligands do not saturate the first coordination sphere of two metal ions, the metal centres must bind other ligands which should most likely be water molecules in the absence of better entering ligands. However, because of the electrostatic repulsion between the metal centres, hydrolysis of coordinated water to form μ -hydroxo species is favoured, the major species in solution being $[\text{Cu}_2\text{L}^1(\text{OH})_2]^{3+}$ above pH 7, $[\text{Cu}_2\text{L}^2(\text{OH})]^{3+}$

above pH 7 and $[\text{Cu}_2\text{L}^2(\text{OH})_2]^{2+}$ above pH 9. The low $\text{p}K_{\text{a}}$ value for the reaction of $[\text{Cu}_2\text{L}^2]^{4+}$ to give $[\text{Cu}_2\text{L}^2(\text{OH})]^{3+}$ ($\text{p}K_{\text{a}} = -6.82$) suggests that the hydroxo ligand might be bridging both metal centres. From the behaviour of related compounds, it can be anticipated that these dinuclear species can show interesting properties in the assistance of hydrolytic processes with different electrophilic substrates such as carboxylates or phosphates,^[5,22] a possibility that will be explored in future work.

DFT Calculations on the Formation of CuL^{2+} Species with the L^1 and L^2 Ligands

The most striking result in the previous section is probably the large difference in the stability constants of the $[\text{CuL}^1]^{2+}$ and $[\text{CuL}^2]^{2+}$ complexes which strongly suggests a change in the number of donor atoms used by the cyclophane in both complexes with L^1 acting as tetradentate and L^2 as tridentate. In addition, potentiometric results do not provide any evidence of coordination of these ligands through the whole set of five potential nitrogen donors in any of the species formed in solution. While the latter findings can be rationalised by invoking the steric constraints imposed by the aromatic spacer, there is no apparent reason to think that any of these cyclophanes could not behave as a tetradentate ligand in their Cu^{II} complexes and we therefore think that the reasons for the tridentate behaviour of L^2 must be related to the stability difference between species with the ligand acting as tri- and tetradentate. For this reason, we carried out DFT calculations aimed at determining the geometries and relative energies of $[\text{CuL}]^{2+}$ species containing both tridentate and tetradentate L^1 or L^2 . As expected from the equilibrium measurements, all attempts to optimise the geometries of species with the ligand acting as pentadentate were unsuccessful because the optimisation procedure leads to dissociation of at least one Cu–N bond. In addition, the calculations confirmed the expectations in the sense that the possibility of a first coordination sphere involving both benzylic nitrogen atoms is, in the case of L^2 , prevented due to geometric constraints.

The optimised geometries and relative energies of the most stable species found for the $[\text{CuL}^1]^{2+}$ and $[\text{CuL}^2]^{2+}$ complexes are shown in Figure 4 and Table 3 which include a set of structures that can be classified in all cases as distorted square pyramidal or tetragonally distorted octahedral, with Cu–N distances that fall within the 2.0–2.2 Å range. This kind of distorted geometry has been found in the crystal structures of many Cu^{II} -polyamine complexes, the experimental Cu–N distances being in all cases ca. 2.0–2.1 Å.^[23,24] Another common feature of the calculated structures in Figure 4 is the existence of relatively large Cu–O distances with the axially coordinated water molecules. This elongation of the axial bonds is also quite common in the crystal structures of Cu-polyamine complexes, although the experimental distances tend to be smaller than those calculated by the DFT procedures.^[25] However, it must be pointed out that the DFT calculations indicate that the in-

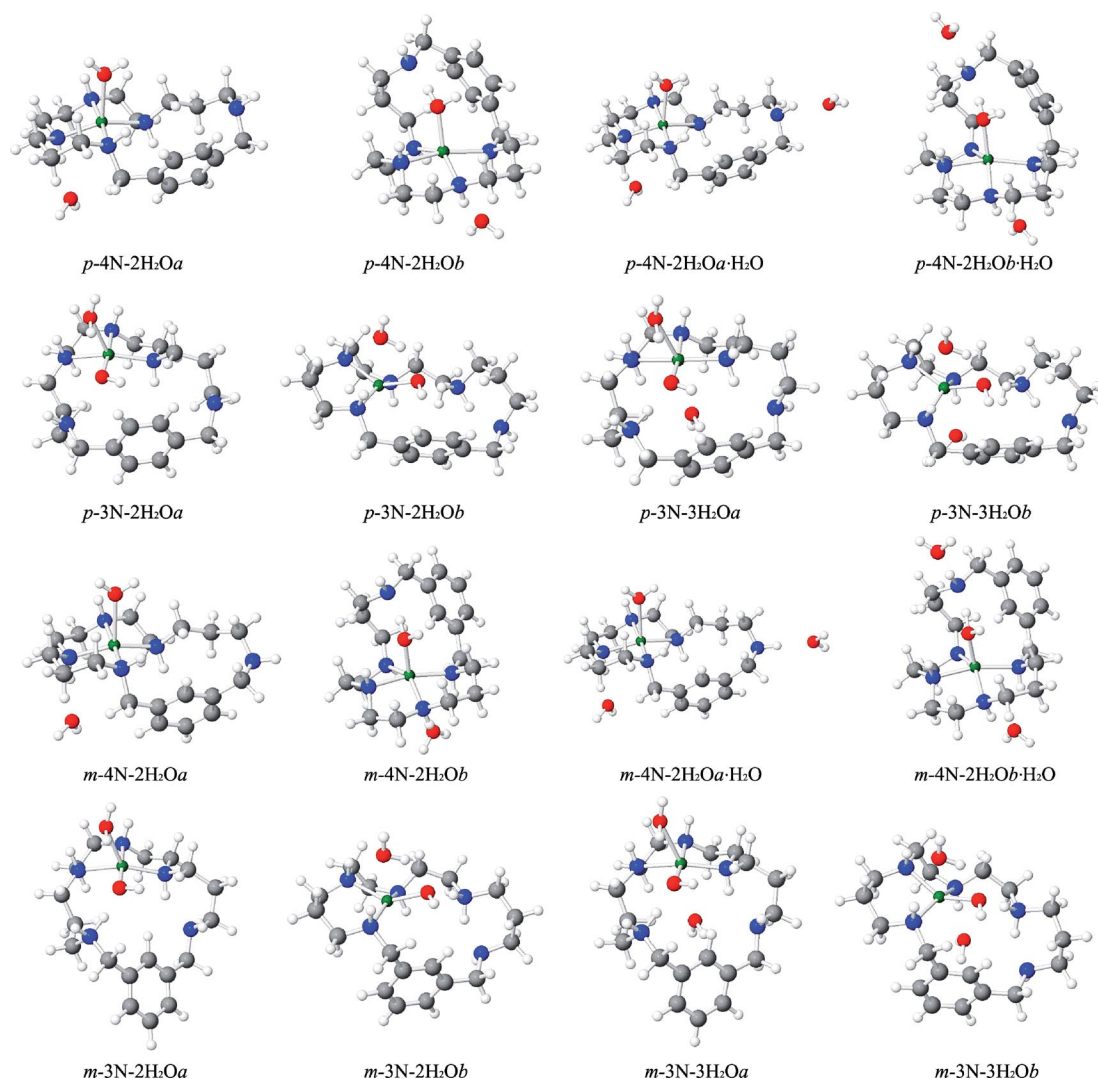


Figure 4. Optimised geometries calculated for the $[\text{CuL}^1]^{2+}$ and $[\text{CuL}^2]^{2+}$ complexes with the cyclophane acting as tri- or tetradentate. Colour code: green Cu, red O, blue N, grey C, white H.

teraction of the metal ion with the axial ligand is very weak so that relatively large changes in the bond lengths lead to small energy changes. Under these conditions, it must be expected that the actual bond lengths in solution and in the crystals will be strongly dependent on factors such as solvation, hydrogen bonding and crystal packing forces.

Optimised geometries calculated for the $[\text{CuL}^1]^{2+}$ or $[\text{CuL}^2]^{2+}$ complexes with the cyclophanes acting as tri- or tetradentate ligands are collected in Figure 4. We will first discuss the structures of the pentacoordinated complexes with three central nitrogens of the bridge and two water molecules (structures $m\text{-}3\text{N-}2\text{H}_2\text{Oa}$ and $p\text{-}3\text{N-}2\text{H}_2\text{Oa}$ in Figure 4). For both cyclophanes, the complexes display a distorted square pyramidal coordination with the three coordinated amine groups located in the basal plane and one of the coordinated waters forming a strong hydrogen bond with one of the uncoordinated benzylic nitrogen atoms. From these structures, a third water molecule was included in the calculations and located in the vacant coordination site opposed to the apical water. The calculations lead to

Table 3. Relative energy (kcal mol^{-1}) of the different species calculated for the Cu^{II} complexes with the L^1 and L^2 ligands (see optimised structures in Figure 4).

| Species | L^1 (<i>m</i>) | Aqueous solution | L^2 (<i>p</i>) | Aqueous solution |
|---|---------------------------|------------------|---------------------------|------------------|
| | Gas phase | | Gas phase | |
| $3\text{N-}2\text{H}_2\text{Oa} + \text{H}_2\text{O}$ | 0.0 | 0.0 | 0.0 | 0.0 |
| $3\text{N-}2\text{H}_2\text{Ob} + \text{H}_2\text{O}$ | 0.9 | 6.4 | −6.0 | 1.2 |
| $3\text{N-}3\text{H}_2\text{Oa}$ | −11.6 | −2.0 | −15.3 | 5.1 |
| $3\text{N-}3\text{H}_2\text{Ob}$ | −14.8 | 1.4 | −20.4 | −3.8 |
| $4\text{N-}2\text{H}_2\text{Oa} + \text{H}_2\text{O}$ | 9.6 | 6.5 | 5.9 | 5.6 |
| $4\text{N-}2\text{H}_2\text{Ob} + \text{H}_2\text{O}$ | 15.4 | 15.2 | 14.6 | 25.0 |
| $4\text{N-}2\text{H}_2\text{Oa}\cdot\text{H}_2\text{O}$ | 0.2 | 4.7 | −3.7 | 4.0 |
| $4\text{N-}2\text{H}_2\text{Ob}\cdot\text{H}_2\text{O}$ | 0.8 | 9.8 | 12.6 | 22.4 |

structures ($m\text{-}3\text{N-}3\text{H}_2\text{Oa}$ and $p\text{-}3\text{N-}3\text{H}_2\text{Oa}$) that show a very distorted octahedral geometry with one of the axial water ligands placed significantly closer to the metal ion than the other (Cu–O distances of 2.48 and 3.20 Å for $m\text{-}3\text{N-}3\text{H}_2\text{Oa}$, and 2.54 and 2.84 Å for $p\text{-}3\text{N-}3\text{H}_2\text{Oa}$). As in

the previous structures, the water in the equatorial plane forms a strong hydrogen bond with one benzylic nitrogen. As expected from its weak interaction with the metal ion, the stabilisation associated with the third water molecule is not large, so that the structures *m*-3N-3H₂O_a and *p*-3N-3H₂O_a are only 2.0 and –5.1 kcalmol^{–1} more stable in aqueous solution than a separate water molecule and *m*-3N-2H₂O_a or *p*-3N-2H₂O_a, respectively (11.6 and 15.3 kcalmol^{–1} in the gas phase). These differences are expected to be even smaller in real systems because of the possibility of hydrogen bonding between the third water and the *m*-3N-2H₂O_a or *p*-3N-2H₂O_a species.

Figure 4 also includes the optimised geometries for pentacoordinate complexes with tridentate cyclophane but with a coordination environment that includes one of the benzylic nitrogen donors. These species are named following the procedure in the previous paragraph except that they are labelled as *b* instead of *a*. Their optimised structures can be described in a parallel way to that used for the *a* family and the relative energies are also included in Table 3. It is interesting to note that the species in the *b* family are less stable than their analogues with the other coordination mode (*a* series) in the case of the **L**¹ complexes but they are more stable in the case of **L**².

Finally, Figure 4 includes the optimised geometries for species containing tetradentate **L**¹ and **L**². The only way of obtaining stable structures with this coordination was by keeping one of the benzylic nitrogen atoms uncoordinated, all attempts with all the nitrogen atoms coordinated except one of the central amine groups being unsuccessful. For this coordination, two different geometries close in energy could be optimised for each of the cyclophanes. In the structures of *m*-4N-2H₂O-*a* and *p*-4N-2H₂O-*a*, one of the water molecules is displaced from the hypothetical sixth coordination site and forms a hydrogen bond with one of the coordinated amines in the equatorial plane. The distance from this water molecule to the metal centre is so large (4.0 Å for **L**¹ and 3.9 Å for **L**²) and the H₂O–Cu–OH₂ angle deviates so much from 180° (actual values of 148.5 and 156.7° for **L**¹ and **L**², respectively) that the structures can be described as being pentacoordinate. However, these structures are not far in energy from the alternative *m*-4N-2H₂O-*b* and *p*-4N-2H₂O-*b* structures which show coordination environments with the four nitrogen atoms in the equatorial plane, one axial water located at 2.24 Å (**L**¹) or 2.16 Å (**L**²) and a weakly interacting water molecule located at 3.41 Å (**L**¹) or 3.70 Å (**L**²). The H₂O–Cu–OH₂ angle is now closer to 180° (actual values of 163.2 and 157.5° for **L**¹ and **L**², respectively). The energy difference between the *a*-*b* pairs of structures is significantly different for both ligands, those labelled as *a* being more stable by 8.7 (**L**¹) or 19.4 (**L**²) kcalmol^{–1} in solution (5.8 or 8.7 kcalmol^{–1} in the gas phase). As a whole, these results indicate that the stabilisation associated with this weak axial coordination of the second water molecule is lower than that associated with hydrogen bonding with one of the coordinated amine groups so that it is not expected to be coordinated in solution, especially in the case of **L**².

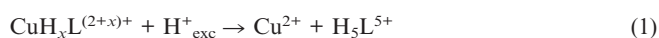
With regards to the relative energies of the optimised geometries containing tri- and tetradentate cyclophanes, the results of the DFT calculations indicate in all cases a higher stability of the structures with the tridentate cyclophane, the energy difference between the 3N-3H₂O and 4N-2H₂O structured (plus a free additional H₂O) being 8.5 (**L**¹) or 0.5 (**L**²) kcalmol^{–1} in aqueous solution (20.0 and 21.2 kcalmol^{–1} in the gas phase, respectively) if the *a* series is considered in both cases. These differences are sure to be overestimates because of the possibility of hydrogen bonding between the third water molecule and the 4N-2H₂O systems and, for this reason, the systems were optimised whilst allowing for this interaction. The resultant geometries are also included in Figure 4 and labelled as *m*- or *p*-4N-2H₂O·H₂O. The species with tridentate cyclophanes are still more stable even when this additional interaction is considered in the tetradentate systems, although the energy difference is reduced. A similar conclusion can be drawn by comparing the energies of the 3N-2H₂O and 4N-2H₂O pairs of structures which also indicates a higher stability of the tridentate form.

In any case, it must be concluded from the DFT calculations that the energy difference between the different coordination modes is small for both cyclophanes and the actual values in real systems will be strongly dependent on the extent of hydrogen bonding with additional water molecules, something not considered in the calculations. From this point of view, both coordination modes are expected to coexist in solution. Moreover, since there are no large differences between the results obtained for the **L**¹ and **L**² ligands, it must also be concluded that the experimental observation of tridentate coordination in [Cu**L**²]²⁺ and tetradentate coordination in [Cu**L**²]²⁺ cannot be attributed principally to changes in the first coordination sphere but must be better related to differences in the network of hydrogen bonds formed with uncoordinated water molecules. At this point, it is important to remember that the analysis of potentiometric results only provides direct information on the stoichiometry, Cu–L–H in the present case, and the stability of the different species but it does not allow a distinction to be made between isomeric species with the same stoichiometry, i.e. the stability constant derived for a species such as [Cu**L**]²⁺ does not discriminate between the possible relative contributions of microscopic species with the same stoichiometry but differing in the denticity of the ligand or in the number of coordinated water molecules. The results of the present DFT studies indicate that mixtures of species with different structures and even with a different denticity of the ligand can be formed in solution and that the relative amounts of each species are strongly dependent not only on the characteristics of the first coordination sphere but also on factors as difficult to quantify as the specific interactions with solvent molecules. In any case, despite the fact that calculations fail to predict the tetradentate behaviour of the cyclophane in [Cu**L**¹]²⁺, the calculations indicate that a higher stability of the tridentate form is expected to occur when changing to the *para* **L**² ligand. Inspection of the data in Table 3 reveals that changing from **L**¹ to **L**² does not

change very much the energy of the most stable tetradentate form but it leads to stabilisation of all the tridentate forms, especially those involving coordination of one benzylic nitrogen, in agreement with the tridentate coordination mode found in the crystal structure of the Hg^{II} complex with a related cyclophane.^[2b]

Kinetics of Decomposition of the Cu^{II} Complexes with the L^1 and L^2 Ligands

The species distribution curves in Figure 2 and Figure 3 show that upon addition of an excess of acid, the Cu-L^1 and Cu-L^2 complexes decompose with formation of Cu^{2+} and the fully protonated ligands, as indicated in Equation (1) for the case of a mononuclear species.



Stopped-flow experiments showed that the acid promoted decomposition of the Cu^{II} complexes with both cyclophanes occurs in all cases with a single measurable kinetic step with rate constants that change with the acid concentration according to the rate law in [Equation (2)] (Figures 5 and 6). However, whereas for the L^2 complexes the values of the observed rate constants are independent of the nature of the species in the starting solution (Figure 5) and the whole set of data can be well fitted by Equation 2 to obtain values of $a = 17.5 \pm 0.3 \text{ s}^{-1}$ and $b = 114 \pm 9 \text{ M}^{-1} \text{ s}^{-1}$, the kinetic data for the L^1 complexes change significantly for the different species studied (Figure 6). The values of the a and b parameters for each species are: $a = 24.7 \pm 0.1 \text{ s}^{-1}$ and $b = 119 \pm 2 \text{ M}^{-1} \text{ s}^{-1}$ for $[\text{CuHL}^1]^{3+}$, $a = 17.0 \pm 0.5 \text{ s}^{-1}$ and $b = 114 \pm 14 \text{ M}^{-1} \text{ s}^{-1}$ for $[\text{CuL}^1]^{2+}$, and $a = 13.3 \pm 0.3 \text{ s}^{-1}$ and $b = 23 \pm 8 \text{ M}^{-1} \text{ s}^{-1}$ for $[\text{Cu}_2\text{L}^1(\text{OH})_2]^{2+}$.

$$k_{\text{obs}} = a + b[\text{H}^+] \quad (2)$$

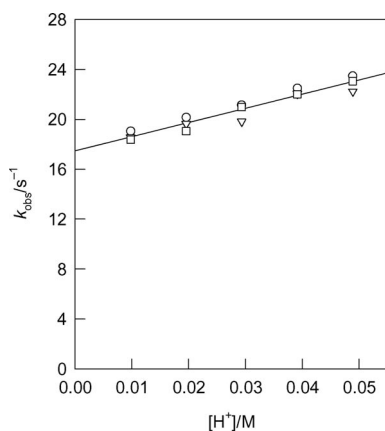


Figure 5. Plot of the observed rate constants vs. the acid concentration for the decomposition of the Cu^{II} complexes with L^2 (25.0 °C, 0.15 M NaClO_4). The solid line corresponds to the best fit of all the data in the plot.

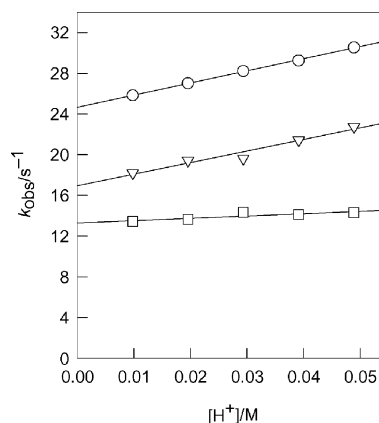


Figure 6. Plot of the observed rate constants vs. the acid concentration for the decomposition of the different Cu-L^1 complexes (25.0 °C, 0.15 M NaClO_4): $[\text{CuHL}^1]^{3+}$ (circles), $[\text{CuL}^1]^{2+}$ (triangles) and $[\text{Cu}_2\text{L}^1(\text{OH})_2]^{2+}$ (squares).

The spectra of the reaction mixture immediately after mixing in the stopped-flow instrument (ca. 2 ms) and at the end of the reaction were also recorded in all cases from the analysis of kinetic experiments using a diode-array detector and they were compared with those of the complex species before addition of the excess acid. Some representative spectra are shown in Figure 7 which includes the spectrum of the dinuclear $[\text{Cu}_2\text{L}^2(\text{OH})]^{3+}$ species in the absence of added acid (a) and the initial (b) and final (c) spectra in the kinetic experiments. These spectra clearly reveal the existence of a rapid absorbance change that occurs within the mixing time of the stopped-flow instrument. This initial fast absorbance change is only observed when the starting solution contains a dinuclear species, no rapid changes of similar characteristics being observed for the mononuclear species. Actually, the analysis of the spectroscopic changes observed during the decomposition of the mononuclear $[\text{CuHL}^2]^{3+}$ and $[\text{CuL}^2]^{2+}$ species leads to initial and final spectra similar to those in Figure 7 (b) and Figure 7 (c). It is also interesting to note that dissociation of the first metal ion from the dinuclear $[\text{Cu}_2\text{L}^2(\text{OH})]^{3+}$ species does not cause any significant change in the position of the absorption maximum despite the fact that the hydroxyl bridge must be destroyed in the process. Nevertheless this observation is in agreement with the conclusions derived from the analysis of the spectra obtained at different pH and Cu/L ratios. As the rate constants obtained for the different Cu-L^1 species are significantly different, special care was taken in this case to compare the spectra obtained for each species immediately after mixing with the acid excess. A rapid release of one Cu^{II} ion within the mixing time of the stopped-flow instrument was also observed during the decomposition of the dinuclear $[\text{Cu}_2\text{L}^1(\text{OH})_2]^{2+}$ species and in all cases an absorption maximum centred at wavelengths close to 570 nm was observed during the early stages of the stopped-flow experiment which suggests a similar coordination environment for the metal ion in all the three mononuclear Cu-L^1 species, the decomposition kinetics of which lead to the rate constants in Figure 6.

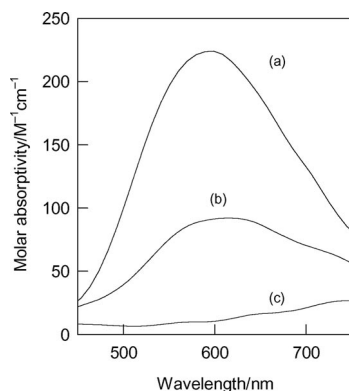


Figure 7. Comparison of the electronic spectrum of the $[\text{Cu}_2\text{-L}^2(\text{OH})]^{3+}$ species (a) with the spectra obtained from the analysis of the spectroscopic changes recorded during the acid-promoted decomposition of this species: initial spectrum (b) and final product (c).

As a summary, the kinetics results indicate that decomposition of the mononuclear Cu^{II} complexes with both cyclophanes occurs in a single step, whereas the dinuclear species decompose in two steps, the first metal ion being released much faster than the second. Unfortunately, dissociation of the first Cu^{II} occurs within the mixing time of the instrument and no kinetic data could be obtained. It is important to note that the decomposition of the dinuclear complexes formed with larger polyaza macrocycles and cryptands occurs with a lower rate and statistically controlled kinetics, i.e. both metal centres behave independently and the rate of release of the first metal ion doubles the rate corresponding to the second.^[26–29] Thus, it appears that the smaller size of the **L**¹ and **L**² cyclophanes creates important electrostatic repulsions between the metal centres in the dinuclear species and this results in the faster release of one metal ion upon treatment with acid.

The similarity of the spectroscopic changes and rate constants for the only measurable kinetic step for all the mono- and dinuclear Cu–**L**² species strongly suggests that the same process is monitored in all cases which is surely the decomposition of the most acidic mononuclear species. These results for the **L**² complexes can be easily rationalised by considering that the cyclophane does not use all the donor groups in the mononuclear complexes and the different species studied only differ by the protonation/deprotonation of some of the uncoordinated amine groups. In that case, addition of an excess of acid leads to the rapid protonation of the amine groups which remain uncoordinated and deprotonated. As a consequence, the species formed within the mixing time of the stopped-flow instrument is always the same and so the same kinetics of decomposition are observed independent of the starting species.

In contrast, the results obtained for the **L**¹ complexes cannot be explained in the same way. The three different Cu–**L**¹ mononuclear species, including that resulting from dissociation of the first ion from the dinuclear complex, decompose with different kinetics despite the fact that their spectra are also very similar in all cases. This similarity of

the electronic spectra for the different species indicates a similar coordination environment of the metal ion, i.e. the number of donor groups used by the ligand must be the same in all cases independent of the protonation state of the complex. From the position of the absorption band, a tetradentate binding mode for **L**¹ can be deduced^[20] for the three mononuclear species, the decomposition kinetics of which were monitored: $[\text{CuHL}^1]^{3+}$, $[\text{CuL}^1]^{2+}$ and the one resulting from the rapid release of one Cu^{II} ion from the dinuclear complex. Although it is evident that a species such as $[\text{CuHL}^1]^{3+}$ contains a protonated amine group that does not exist in $[\text{CuL}^1]^{2+}$, if the cyclophane is coordinated to the metal ion through the same donor groups in both complexes, the addition of the excess acid to a solution of $[\text{CuL}^1]^{2+}$ would lead to the formation of $[\text{CuHL}^1]^{3+}$ within the mixing time of the stopped-flow instrument and the same kinetics of decomposition should be observed. This reasoning leads to the conclusion that **L**¹ coordinates to the metal ion through the same number of donor atoms in both species (four according to the spectra and the equilibrium data) but the actual donor groups differ from one complex to the other. As protonation of the uncoordinated amine groups is faster than the breaking of Cu–N bonds, a species of composition $[\text{CuHL}^1]^{3+}$ is rapidly formed when an excess of acid is added to a solution of $[\text{CuL}^1]^{2+}$ but this $[\text{CuHL}^1]^{3+}$ species is an isomer of the most thermodynamically stable species with the same composition and so its kinetics of decomposition will be different. A similar reasoning can be applied to the mononuclear species formed as an intermediate during the decomposition of the dinuclear $[\text{Cu}_2\text{L}^1(\text{OH})_2]^{2+}$ complex. It appears unlikely that **L**¹ coordinates to one of the metal centres in the dinuclear species through more than three amine groups but the lability of the Cu^{II} ion again makes possible the formation of a $[\text{CuHL}^1]^{3+}$ species following the dissociation of the first metal ion. As this species decomposes with kinetics different from those observed in the study of the mononuclear species, it must be concluded that it is actually a different isomer. Thus, the different values of the *a* and *b* kinetics parameters obtained for solutions containing the $[\text{CuHL}^1]^{3+}$, $[\text{CuL}^1]^{2+}$ and $[\text{Cu}_2\text{L}^1(\text{OH})_2]^{2+}$ complexes would actually correspond to the decomposition of three isomeric forms of the $[\text{CuHL}^1]^{3+}$ species.

An attractive hypothesis is that the three species show the coordination environment depicted schematically in Figure 8. Independent of their precise structures, it can be anticipated that these isomers would have Cu–N bonds with different steric constraints that would lead to different kinetics of decomposition.^[23,30–34] We have observed recently^[7] these kinds of differences in the kinetics of decomposition for the mononuclear Cu^{II} complexes of cyclophanes with larger polyamine chains containing an additional amine group and suggested that these kinetic measurements are a useful test to detect changes in the actual coordination mode of the ligand. However, extensive DFT calculations indicated that the only way of getting a tetradentate coordination for **L**¹ in mononuclear Cu^{II} complexes is by keeping one of the benzylic nitrogen atoms uncoordinated, i.e. as

shown in the structure at the right hand side of Figure 8. Thus, the experimental observation of different kinetics of decomposition for three species with the same set of donor atoms would reveal that the complex does not reorganise rapidly to the most stable conformation of $[\text{CuHL}^1]^{3+}$ upon protonation of $[\text{CuL}^1]^{2+}$ or Cu^{II} dissociation from $[\text{Cu}_2\text{L}^1(\text{OH})_2]^{2+}$. In the latter cases, the rapid processes occurring within the mixing time of the stopped-flow instrument appear to lead to different conformations of the $[\text{CuHL}^1]^{3+}$ species. If decomposition is faster than reorganisation to the most stable conformation, these transient species will decompose with different kinetics because of the different steric constraints of the Cu–N bonds in their coordination environments.

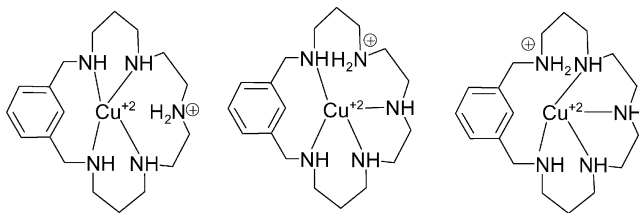
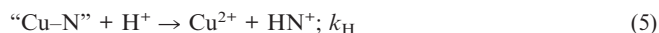
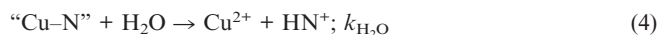


Figure 8. Schematic drawings showing three hypothetical isomeric forms of the $[\text{CuHL}^1]^{3+}$ species with the L^1 cyclophane acting as a tetradentate ligand. The actual coordination spheres can be more complex because of the presence of additional water ligands.

The comparison of the actual values of the kinetic parameters obtained in the present work with those previously reported for related complexes requires a previous consideration of the intimate mechanism of decomposition. The mechanism widely accepted in the literature^[30–32] for the decomposition of polyamine complexes of Cu^{II} assumes that the acid attack on the Cu–N bond that is broken in the rate-determining step does not occur directly because it requires the previous formation of an activated intermediate “Cu–N” with partial breaking of the Cu–N bond [Equation (3)]. The complete dissociation of the metal–ligand bond can be achieved through two parallel pathways that involve solvent or acid attacks on this intermediate [Equations (4) and (5)]. If the activated intermediate is assumed to be formed under steady-state conditions the rate law for this mechanism is given by Equation (6) which can be simplified to the form of Equation (2) with the equivalences $a = k_1 k_{\text{H}_2\text{O}} / (k_{-1} + k_{\text{H}_2\text{O}})$ and $b = k_1 k_{\text{H}} / (k_{-1} + k_{\text{H}_2\text{O}})$, assuming that $k_{\text{H}}[\text{H}^+] \ll (k_{-1} + k_{\text{H}_2\text{O}})$. Thus, the b/a quotient is equivalent to $k_{\text{H}}/k_{\text{H}_2\text{O}}$ and indicates the relative rates of attack by H^+ and H_2O on the activated intermediate.



$$k_{\text{obs}} = \frac{k_1 k_{\text{H}_2\text{O}} + k_1 k_{\text{H}} [\text{H}^+]}{k_{-1} + k_{\text{H}_2\text{O}} + k_{\text{H}} [\text{H}^+]} \quad (6)$$

For the decomposition of the Cu^{II} complexes with the open-chain polyamine L^4 ,^[19] the value of a is negligible and $b = 217 \text{ M}^{-1} \text{ s}^{-1}$. Thus, although the macrocyclic nature of the L^1 and L^2 ligands only causes small changes in the values of b , the appearance of a significant a term indicates that the contribution of the solvent-attack pathway becomes more important for the complexes with both cyclophanes. However, for the Cu^{II} complexes with the pyridinophane L^3 ,^[19] a becomes negligible again, b is somewhat larger ($520\text{--}700 \text{ M}^{-1} \text{ s}^{-1}$) and the approximation $k_{\text{H}}[\text{H}^+] \ll (k_{-1} + k_{\text{H}_2\text{O}})$ is not valid, the plots of k_{obs} vs. $[\text{H}^+]$ showing a clear curvature that allows the calculation of a new parameter $c = k_{\text{H}} / (k_{-1} + k_{\text{H}_2\text{O}}) = 27 \text{ M}^{-1}$. Thus, the cyclic nature of the polyamine is not enough to cause the appearance of a significant a term in the kinetics of decomposition of the Cu^{II} complexes. The relative importance of both parallel attacks must then be better related to differences in the nature of the activated intermediate “Cu–N” which facilitates or hinders attacks by solvent and H^+ , depending of the degree of bond dissociation. Solvent attack will be facilitated when the Cu–N bond becomes more elongated in the intermediate, whereas the assistance of H^+ is necessary when there is a small degree of bond dissociation. The extent to which the Cu–N bond is elongated in the intermediate appears to be determined by subtle changes in the steric constraints imposed by the ligand in the different species more than by the cyclic/acyclic nature of the polyamine. Thus, for the phenanthroline analogue of L^1 and L^2 , the $[\text{CuHL}]^{3+}$ species decomposes mainly through the solvent-dependent pathway ($a = 18 \text{ s}^{-1}$, $b = 1.34 \text{ M}^{-1} \text{ s}^{-1}$), whereas $[\text{CuL}]^{2+}$ decomposes exclusively through the H^+ -pathway ($a = 0$, $b = 4264 \text{ M}^{-1} \text{ s}^{-1}$, $c = 52 \text{ M}^{-1}$).^[35]

Interaction with AMP and Formation of Ternary Cu^{II} –AMP–Cyclophane Complexes

To further explore the coordination properties of these new cyclophanes, additional studies were carried out on AMP recognition. The formation of mixed $[\text{Cu}_p\text{H}_r\text{L}(\text{AMP})]^{(2p+r-2)+}$ complexes and especially their stability is of relevance in oligonucleotide binding,^[12,36–38] and the present Cu–L systems ($\text{L} = \text{L}^1, \text{L}^2, \text{L}^3$) offer an excellent opportunity for exploring the recognition capability in closely related mono- and dinuclear species.

A prerequisite for the determination of the constants of the mixed AMP– Cu^{II} complexes with L^1 , L^2 and L^3 is the knowledge of the stability constants of all the binary systems implicated. As polyammonium receptors can interact by themselves with nucleotide species, the equilibrium constants for the systems AMP– L^1 , AMP– L^2 and AMP– L^3 were determined potentiometrically and the values obtained for the global stability constants are included in Table 4. However, as both AMP and the L receptors participate in overlapping protonation processes, translating those cumulative constants into representative stepwise constants requires consideration of the basicity of AMP^[39] and the different cyclophanes. If it is assumed that the interaction be-

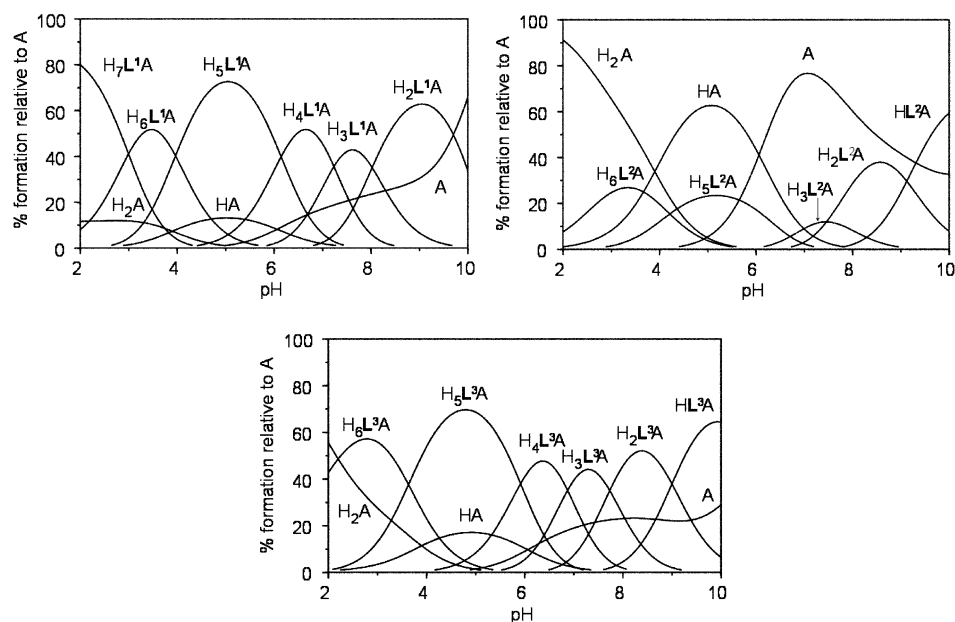


Figure 9. Species distribution curves for the L-A-H systems ($L = L^1, L^2, L^3$; $A = \text{AMP}^{2-}$; $[L]_0 = [A]_0 = 1 \times 10^{-3} \text{ M}$).

tween both species does not alter very much in the pH range in which the different protonated forms of AMP and **L** exist, the stepwise constants shown in the last part of Table 4 can be considered representative of the equilibria occurring in solution. Species distribution curves calculated from the equilibrium data in Table 4 are shown in Figure 9 which reveals that H_xL^{x+} -AMP species dominate at most pH values for the case of the L^1 and L^3 ligands, the interaction of the *para* L^2 ligand being significantly lower. This is clearly reflected in a plot of the amount of complexed AMP (**A**) by the different receptors (**A/L**, 1:1 mole ratio) shown in Figure 10.

Table 4. Logarithms of the stability constants for the L^1 -AMP, L^2 -AMP and L^3 -AMP species ($A = \text{AMP}^{2-}$) determined at $298.1 \pm 0.1 \text{ K}$ in $0.15 \text{ mol dm}^{-3} \text{ NaClO}_4$.

| Reaction ^[a] | L^1 | L^2 | L^3 |
|---|----------|-------------------------|----------|
| $A + L + H = \text{HLA}$ | – | 14.65(4) ^[b] | 14.07(5) |
| $A + L + 2 H = \text{H}_2\text{LA}$ | 22.37(1) | 23.78(4) | 23.07(5) |
| $A + L + 3 H = \text{H}_3\text{LA}$ | 30.89(1) | 31.24(9) | 30.80(4) |
| $A + L + 4 H = \text{H}_4\text{LA}$ | 38.47(1) | – | 37.67(4) |
| $A + L + 5 H = \text{H}_5\text{LA}$ | 44.84(1) | 44.65(6) | 43.59(4) |
| $A + L + 6 H = \text{H}_6\text{LA}$ | 48.89(1) | 48.87(6) | 47.22(5) |
| $A + L + 7 H = \text{H}_7\text{LA}$ | 51.46(2) | – | – |
| $A + \text{LH} = \text{HLA}$ | – | 3.96 | 4.42 |
| $A + \text{LH}_2 = \text{H}_2\text{LA}$ | 3.30 | 3.43 | 4.10 |
| $A + \text{LH}_3 = \text{H}_3\text{LA}$ | 4.01 | 2.57 | 4.21 |
| $A + \text{LH}_4 = \text{H}_4\text{LA}$ | 4.59 | – | 4.46 |
| $\text{AH} + \text{LH}_4 = \text{H}_5\text{LA}$ | 4.90 | 2.71 | 4.32 |
| $\text{AH} + \text{LH}_5 = \text{H}_6\text{LA}$ | 6.16 | 3.90 | 5.09 |
| $\text{AH}_2 + \text{LH}_4 = \text{H}_6\text{LA}$ | 5.05 | 3.03 | 4.05 |
| $\text{AH}_2 + \text{LH}_5 = \text{H}_7\text{LA}$ | 4.83 | – | – |

[a] Charges omitted for clarity. [b] Values in parentheses are standard deviations in the last significant Figure.

In general, the values of the constants in Table 4 are of the same order as those found for the interaction of AMP with the protonated forms of some other polyaza macro-

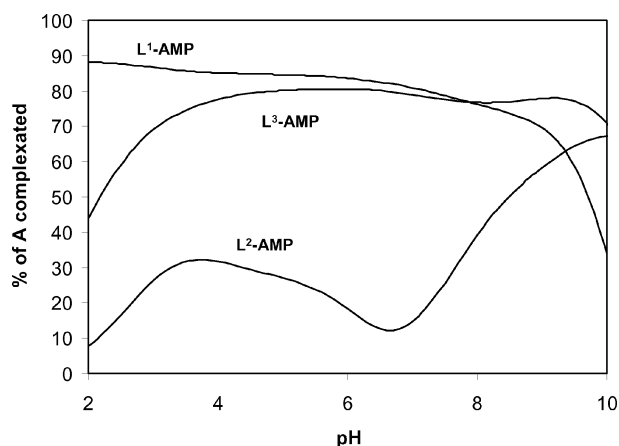


Figure 10. Plot of the percentage of complexed AMP for the three systems ($[\text{AMP}] = 10^{-3} \text{ M}$).

cycles^[36,38] and significantly higher than those found for smaller amines and for biogenic amines such as spermidine or putrescine.^[8,40] It is also interesting to note that the stability of the $\text{AMP-H}_x\text{L}$ species is also lower with polyaza macrocycles that are larger than the present cyclophanes.^[41] This appears to show that the interaction is optimised for macrocycles of intermediate size in which the phosphate group better matches the positive charges of the macrocyclic cavity. In addition, the interaction probably becomes stronger for the case of cyclophanes because of additional π stacking interactions and actually, the stability constants found in this work are larger than those found for macrocycles of a similar size but lacking aromatic spacers.^[8,36–40] Another interesting conclusion from the data in Table 4 is that the strength of the interaction between AMP^{2-} and the different H_xL^{x+} forms does not appear to be affected significantly when the positive charge on the cyclophane is in-

creased which strongly suggests that the strength of the interaction is not dominated only by charge-charge electrostatic factors. Other factors like hydrogen bonding should also significantly affect the interaction. In this sense, it must be pointed out that although the stability of H_xL^{x+} -AMP adducts usually tends to increase with the protonation state of **L** because of the increased coulombic attractions and the larger number of possible hydrogen bonds between the host and the guest,^[38,40,41] there are also literature reports showing similar stability constants for the interaction of AMP with the different protonated forms of some tripodal polyamines.^[42]

The determination of the stability constants for the Cu–L–AMP systems (**L** = **L**¹, **L**² and **L**³) through the analysis of the titration curves is much more complex because of the large number of species present in solution. The analysis was carried out by fixing the values of the protonation constants of AMP,^[39] the formation constants of the Cu²⁺–AMP complexes^[43] and the previously discussed protonation constants of the different **L** cyclophanes (Table 1), the equilibrium constants for the AMP–**L** system (Table 4) and those for the Cu–**L** complexes (Table 2). The results so obtained are included in Table 5 and representative species distribution curves are shown in Figure 10. Because of the complex nature of the equilibrium mixtures, the quality of these results was then checked by fitting together the data corresponding to titrations of binary Cu–**L** and ternary Cu–**L**–AMP systems including, as parameters to be refined, all the constants for the formation of Cu–**L** and Cu–**L**–AMP complexes. This analysis leads to results similar to those previously described, the differences being in all cases within the limits of the estimated errors.

Comparison of the data in Tables 4 and 5 indicates that the Cu^{II} complexes of the **L** cyclophanes show stability constants for the interaction with AMP quite similar to those

observed for the protonated forms of the ligand, except for the case of the mononuclear complexes of **L**³, the stability constants of which for the interaction with AMP are up to 4 log units higher than those found for the protonated ligand. However, it must be pointed out that the nature of the interaction between AMP and the receptor is presumably different in both cases because Cu–**L** complexes are coordinatively unsaturated and so they are susceptible to AMP coordination. At this point, it is interesting to note that all the log *K* values in Table 5 indicate that all the Cu–**L** complexes interact with AMP more strongly than Cu²⁺ (log *K*_{Cu–AMP} = 3.0–3.2)^[40,43–45] although the values can be considered to

Table 5. Logarithms of the stability constants for the formation of mixed Cu–**L**–AMP complexes (AMP^{2−} = A) determined at 298.1 ± 0.1 K in 0.15 mol dm^{−3} NaClO₄.

| Reaction ^[a] | L ¹ | L ² | L ³ |
|--|------------------------|-----------------------|-----------------------|
| Cu + L + A = CuLA | 23.5(1) ^[b] | – | – |
| Cu + H + L + A = CuHLA | 31.2(1) ^[b] | – | 34.08(6) |
| Cu + 2 H + L + A = CuH ₂ LA | 37.89(1) | 36.00 (3) | 40.55(6) |
| Cu + 3 H + L + A = CuH ₃ LA | 41.56(2) | 40.41(10) | 44.53(7) |
| Cu + 4 H + L + A = CuH ₄ LA | – | 45.18 (4) | 47.88(7) |
| 2 Cu + L + A = Cu ₂ LA | – | 27.78 (4) | 33.73(7) |
| 2 Cu + H + L + A = Cu ₂ HLA | – | – | 38.80(1) |
| 2 Cu + 2 H + L + A = Cu ₂ H ₂ LA | – | 39.93(4) | – |
| 2 Cu + L + A = Cu ₂ LA | 29.09(2) | – | – |
| 2 Cu + H ₂ O + L + A = Cu ₂ LA(OH) + H | 22.00(2) | 20.61(5) | 24.80(1) |
| CuH ₃ L + AH = CuH ₄ LA | – | 3.98 | – |
| CuH ₂ L + AH ₂ = CuH ₄ LA | – | 4.07 | 7.77 |
| CuH ₂ L + AH = CuH ₃ LA | 5.87 | 3.53 | 8.32 |
| CuHL + AH ₂ = CuH ₃ LA | 5.30 | 4.75 | 7.17 |
| CuHL + AH = CuH ₂ LA | 5.53 | 4.24 | 7.09 |
| CuHL + A = CuHLA | 4.90 | – | 6.68 |
| Cu ₂ L(OH) + A = Cu ₂ LA(OH) | – | 5.42 | 4.10 |

[a] Charges omitted for clarity. [b] Values in parentheses are standard deviations in the last significant Figure.

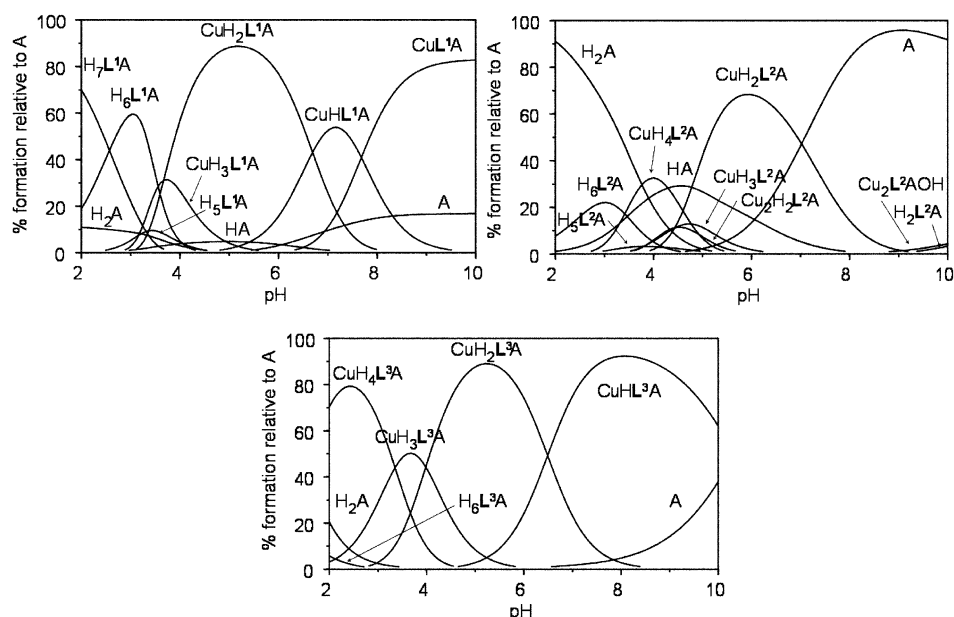


Figure 11. Species distribution diagrams for the mixed Cu–**L**–A–H systems (**L** = **L**¹, **L**², **L**³; A = AMP^{2−}; [Cu²⁺] = [**L**]₀ = [A]₀ = 1 × 10^{−3} M).

be similar to those found for other Cu–polyamine complexes.^[40,41,46] The stability of the interactions with mononuclear Cu–L³ complexes are among the most stable. These results, and especially the large stabilisation observed for the L³ complexes, strongly suggest that selectivity in recognition is probably determined more by other interactions (hydrogen bonding, π stacking) than by direct coordination to the metal centre.

However, because of the existence of multiple competitive equilibria, we have plotted the percentages of complexed AMP as a function of pH for both systems in order to better compare the affinity for AMP of the free ligands and their protonated complexes with that that displayed by the Cu^{II}–L complexes (see Figure 11 and Supporting Information). While for the systems AMP–L¹ and AMP–L³ Cu^{II} addition does not yield large increases in the amount of complexed AMP, in the case of the *para* derivative L² the amount of complexed AMP in the presence of Cu^{II} is clearly augmented over a broad pH range (Figure 12).

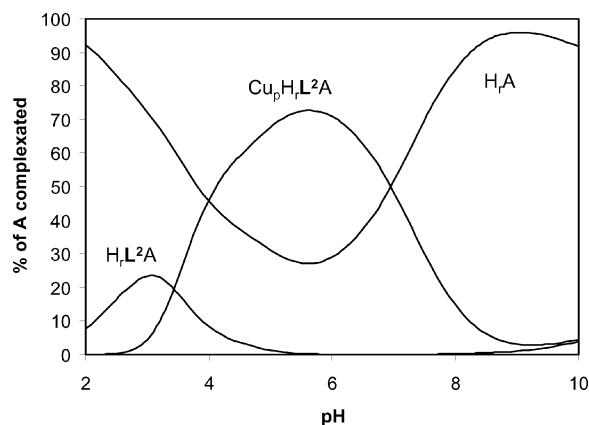


Figure 12. Percentages of complexed AMP for the system Cu^{II}–AMP–L calculated for 1:1:1 molar ratio ([AMP] = 1×10^{-3} M).

Experimental Section

Syntheses

2,6,9,12,16-Pentakis(*p*-tolylsulfonyl)-2,6,9,12,16-pentaza[17]metacyclophane (L¹·5Ts): A solution of α,α' -dibromo-*m*-xylene (2.03 g, 7.67 mmol) in a dry CH₃CN/CH₂Cl₂ (1:1 v/v, 150 mL) mixture was added dropwise to a suspension of 1,5,8,11,15-pentakis(*p*-tolylsulfonyl)-1,5,8,11,15-pentazapentadecane (7.60 g, 7.67 mmol) and K₂CO₃ (10.55 g, 76.3 mmol) in dry CH₃CN (250 mL). The suspension was heated to reflux for a further 24 h and then filtered. The resultant solution was vacuum-evaporated to dryness and the residue suspended in ethanol at reflux to give L¹·5Ts as a white solid (2.79 g, yield 37%); m.p. 108–110 °C. C₅₃H₆₃N₅O₁₀S₅ (1090.41): calcd. C 58.38, H 5.82, N 6.42; found C 58.1, H 5.9, N 6.1. ¹H NMR (CDCl₃): δ = 1.74–1.76 (m, 4 H), 2.42 (s, 6 H), 2.44 (s, 6 H), 2.46 (s, 3 H), 3.03–3.09 (m, 8 H), 3.15–3.20 (t, J = 8 Hz, 4 H), 3.26–3.29 (t, J = 8 Hz, 4 H), 4.25 (s, 4 H), 7.25–7.28 (d, J = 8 Hz, 4 H), 7.28–7.31 (d, J = 8 Hz, 4 H), 7.32–7.35 (d, J = 8 Hz, 2 H), 7.37 (s, 3 H), 7.48 (s, 1 H), 7.61–7.63 (d, J = 8 Hz, 4 H), 7.68–7.71 (d, J = 8 Hz, 4 H), 7.73–7.76 (d, J = 8 Hz, 2 H) ppm. ¹³C NMR (CDCl₃): δ = 19.1, 26.9, 45.8, 46.2, 46.4, 47.2, 51.5, 124.8, 125.1, 127.5, 127.6, 135.7, 141.2 ppm. MS (FAB): m/z = 1090 [M⁺].

2,6,9,12,16-Pentakis(*p*-tolylsulfonyl)-2,6,9,12,16-pentaza[17]paracyclophane (L²·5Ts): This compound was obtained using the procedure described for L¹·5Ts except that α,α' -dibromo-*p*-xylene was used instead of α,α' -dibromo-*m*-xylene. The product was also isolated as a white solid (5.53 g, yield 67%); m.p. 187–189 °C. C₅₃H₆₃N₅O₁₀S₅ (1090.41): calcd. C 58.38, H 5.82, N 6.42; found C 58.3, H 5.9, N 6.5. ¹H NMR (CDCl₃): δ = 1.57–1.63 (m, 4 H), 2.42 (s, 12 H), 2.46 (s, 3 H), 2.91–3.11 (m, 16 H), 4.19 (s, 4 H), 7.17 (s, 4 H), 7.29 (d, J = 8 Hz, 8 H), 7.33 (d, J = 8 Hz, 4 H), 7.63 (d, J = 8 Hz, 8 H), 7.72 (d, J = 8 Hz, 4 H) ppm. ¹³C NMR (CDCl₃): δ = 19.2, 26.8, 45.4, 46.2, 46.6, 48.0, 51.2, 124.9, 125.0, 125.8, 127.5, 127.6, 132.8, 133.6, 134.1, 138.6, 141.2, 141.7 ppm. MS (FAB): m/z = 1089 [M – H]⁺.

2,6,9,12,16-Pentaza[17]metacyclophane Pentahydrochloride (L¹·5HCl): The tosyl groups of L¹·5Ts (2.79 g, 2.56 mmol) were removed by reductive cleavage with a mixture of HBr/HAc (150 mL) and PhOH (15.20 g, 16.0 mmol) by heating at 90 °C for 24 h. The solid obtained was then filtered and washed with a mixture of EtOH/CH₂Cl₂ (1:1 v/v). The macrocycle was obtained as its hydrobromide salt and was then converted into the free amine by using an ionic exchange resin (Amberlite IRA 402). The free amine was purified by chromatography on neutral alumina using methanol as the eluent. The resultant oil was dissolved in ethanol and treated with 37% HCl until complete precipitation of a white solid which was filtered to give L¹ as its pentahydrochloride salt (0.45 g, yield 35%); m.p. 185–187 °C. C₁₈H₃₃N₅·5HCl·3H₂O (555.84): calcd. C 38.90, H 7.98, N 12.60; found C 39.0, H 8.0, N 12.6. ¹H NMR (D₂O): δ = 1.85–1.95 (m, 4 H), 2.95–2.98 (m, 8 H), 3.22 (s, 8 H), 4.04 (s, 4 H), 7.28 (s, 3 H), 7.37 (s, 1 H) ppm. ¹³C NMR (D₂O): δ = 23.2, 43.9, 44.1, 44.4, 44.9, 51.1, 130.5, 131.3, 131.6, 132.8 ppm.

2,6,9,12,16-Pentaza[17]paracyclophane Pentahydrochloride (L²·5HCl): This compound was obtained from L²·5Ts using the same procedure described above for the analogous metacyclophane (0.68 g, yield 33%); m.p. 248–250 °C. C₁₈H₃₃N₅·5HCl·3H₂O (555.84): calcd. C 38.90, H 7.98, N 12.60; found C 39.3, H 8.0, N 12.6. ¹H NMR (D₂O): δ = 1.66–1.75 (m, 4 H), 2.68–2.70 (m, 4 H), 2.75–2.85 (m, 12 H), 4.04 (s, 4 H), 7.41 (s, 4 H) ppm. ¹³C NMR (D₂O): δ = 23.2, 43.1, 44.6, 45.2, 50.6, 131.4, 131.6 ppm.

EMF Measurements: The potentiometric titrations were carried out at 298.1 ± 0.1 K using 0.15 M NaClO₄ as the supporting electrolyte. The experimental procedure (burette, potentiometer, cell, stirrer, microcomputer, etc.) has been fully described elsewhere.^[47] The acquisition of the emf data was carried out with the computer program PASAT.^[48] The reference electrode was an Ag/AgCl electrode in saturated KCl solution. The glass electrode was calibrated as a hydrogen-ion concentration probe by titration of previously standardised amounts of HCl with CO₂-free NaOH solutions and determination of the equivalent point by the Gran's method^[49] which gives the standard potential E⁰ and the ionic product of water [pK_w = 13.73(1)].

The computer program HYPERQUAD was used to calculate the protonation and stability constants from the titration curves.^[50] The protonation constants for AMP were taken from ref.^[12] The pH range investigated was 2.5–10.5 and the concentration of Cu^{II}, AMP and ligands ranged from 3×10^{-4} to a maximum value of 1.5×10^{-3} mol dm⁻³. The different titration curves for each system (at least two) were treated either as a single set or as separated curves without significant variations in the values of the stability constants. The sets of data were merged together and treated simultaneously to give the final stability constants. Moreover, in the case of the AMP–L systems several measurements were made both in

formation and in dissociation (from acid to alkaline pH and vice versa) to check the reversibility of the reactions.

DFT Calculations: All DFT calculations were performed using the Gaussian03 package^[51] and the unrestricted Becke three-parameter hybrid functional combined with the Lee–Yang–Parr correlation functional (UB3LYP).^[52,53] The Pople style 6-31G(d,p) basis set was used on the C, H, O and N atoms, and the SDD basis set^[54] and effective core potential (ECP) on Cu (as implemented in Gaussian03, SDD is D95V up to Ar and Stuttgart/Dresden ECPs for the remaining elements of the periodic Table). All geometry optimisations were performed without any symmetry constraints and efforts were made to find the lowest energy conformation by comparing the structures optimised from different starting geometries. Harmonic frequency calculations were performed to confirm that the calculated structures were minima. Aqueous solution energies were calculated using the CPCM formalism^[55,56] (water solvent, $\epsilon = 78.39$ as implemented in Gaussian03). The gas phase geometry was used for all of these calculations because it has been demonstrated in many previous studies that the change of geometry due to solvation effects is usually insignificant.^[57,58]

Kinetic Experiments: The kinetics of decomposition of the Cu^{II} complexes with the ligands **L**¹ and **L**² were studied at 298.1 ± 0.1 °C using an Applied Photophysics SX17MV stopped-flow spectrophotometer. The Cu/L ligand ratio and the pH of the starting solutions of the metal complexes were selected from the species distribution curves in order to achieve the maximum concentration for one of the complex species while maintaining a very low concentration of the others. For this reason, only those species which represent at least 80% of the total ligand under some conditions were studied. These solutions were mixed in the stopped-flow instrument with solutions containing HClO₄ at the desired concentration. The ionic strength of both solutions was adjusted to 0.15 M with NaClO₄. The decomposition of the **L**¹ and **L**² complexes was monitored at 575 nm and 610 nm, respectively, because the absorbance changes observed in preliminary experiments using a diode-array detector were at a maximum at these wavelengths. In all cases, the data for the acid-promoted decomposition of the complexes could be satisfactorily fitted by a single exponential using the software of the stopped-flow instrument. The data from the preliminary diode-array experiments were analysed with the GLINT program^[59] and yielded rate constants similar to those derived from the single-wavelength experiments in addition to the spectra of the reaction mixture immediately after mixing and at the end of the decomposition process.

Supporting Information (see footnote on the first page of this article): Additional species distribution curves, EPR spectra, Cartesian coordinates, geometries and energies of all the species optimized by DFT procedures.

Acknowledgments

We would like to acknowledge Ministerio de Ciencia y Tecnología (MCYT) and the Federación Española de Enfermedades Raras (FEDER) (Grants CTQ2006-14909-C02-01 and CTQ2006-15672-CO5-01) as well as the Junta de Andalucía (FQM-137) for financial support. Computer facilities by the Centro de Supercomputación de la Universidad de Cádiz are also acknowledged. Predoctoral grants are also acknowledged to Ayuntamiento de Valencia (to B. V.), Universidad de Cádiz (to C. E. C.), and MCYT (to S. B. and A. G. A.).

- a) A. Bencini, M. I. Burguete, E. García-España, S. V. Luis, J. F. Miravet, C. Soriano, *J. Org. Chem.* **1993**, *58*, 4749–4753; b) M. I. Burguete, B. Escuder, E. García-España, S. V. Luis, J. F. Miravet, *J. Org. Chem.* **1994**, *59*, 1067–1071; c) B. Altava, M. I. Burguete, B. Escuder, E. García-España, M. C. Muñoz, *Tetrahedron* **1997**, *53*, 2629–2640.
- a) A. Andrés, M. I. Burguete, E. García-España, S. V. Luis, J. F. Miravet, C. Soriano, *J. Chem. Soc. Perkin Trans. 2* **1993**, 749–755; b) E. García-España, J. Latorre, S. V. Luis, J. F. Miravet, P. Pozuelo, J. A. Ramírez, C. Soriano, *Inorg. Chem.* **1996**, *35*, 4591–4596; c) B. Altava, A. Bianchi, C. Bazzicalupi, M. I. Burguete, E. García-España, S. V. Luis, J. F. Miravet, *Supramol. Chem.* **1997**, *8*, 287–299; d) J. A. Aguilar, P. Díaz, A. Doménech, E. García-España, J. M. Llinares, S. V. Luis, J. A. Ramírez, C. Soriano, *J. Chem. Soc. Perkin Trans. 2* **1999**, 1159–1168; e) M. I. Burguete, P. Díaz, E. García-España, S. V. Luis, J. F. Miravet, M. Querol, J. A. Ramírez, *Chem. Commun.* **1999**, 649–650.
- A. Andrés, C. Bazzicalupi, A. Bianchi, E. García-España, S. V. Luis, J. F. Miravet, J. A. Ramírez, *J. Chem. Soc., Dalton Trans.* **1994**, 2995–3004.
- M. I. Burguete, B. Escuder, E. García-España, J. Latorre, S. V. Luis, J. A. Ramírez, *Inorg. Chim. Acta* **2000**, *300*, 970–977.
- B. Altava, M. I. Burguete, S. V. Luis, J. F. Miravet, E. García-España, V. Marcelino, C. Soriano, *Tetrahedron* **1997**, *53*, 4751–4762.
- M. I. Burguete, E. García-España, S. V. Luis, J. F. Miravet, C. Soriano, *An. Quím.* **1993**, *89*, 99–100.
- J. Aguilar, M. G. Basallote, L. Gil, J. C. Hernández, M. A. Máñez, E. García-España, C. Soriano, B. Verdejo, *Dalton Trans.* **2004**, 94–103.
- E. Kimura, M. Kodama, T. Yatsunami, *J. Am. Chem. Soc.* **1982**, *104*, 3182–3187.
- M. W. Hosseini, J. M. Lehn, M. P. Mertes, *Helv. Chim. Acta* **1983**, *66*, 2454–2466.
- B. Dietrich, M. W. Hosseini, J. M. Lehn, R. B. Sessions, *J. Am. Chem. Soc.* **1981**, *103*, 1282–1283.
- M. W. Hosseini, J. M. Lehn, *Helv. Chim. Acta* **1987**, *70*, 1312–1319.
- A. Bencini, A. Bianchi, E. García-España, E. C. Scott, L. Morales, B. Wang, T. Deffo, F. Takusagawa, M. P. Mertes, K. B. Mertes, P. Paoletti, *Bioorg. Chem.* **1992**, *20*, 8–29.
- For a recent review on ATP coordination by polyazamacrocycles see for instance: E. García-España, P. Díaz, J. M. Llinares, A. Bianchi, *Coord. Chem. Rev.* **2006**, *250*, 2952–2987.
- E. Martell, R. J. Motekaitis, Q. Lu, D. A. Nation, *Polyhedron* **1999**, *18*, 3203–3218.
- Szymanska, H. Radecka, J. Radecki, M. Pietraszkiewicz, O. Pietraszkiewicz, *Comb. Chem. High Throughput Screening* **2000**, *3*, 509–517.
- S. Y. Lin, W. H. Chen, C. Y. Liu, *Electrophoresis* **2002**, *23*, 3550–3557.
- M. T. Albelda, J. Aguilar, S. Alves, R. Aucejo, P. Díaz, C. Lodeiro, J. C. Lima, E. García-España, F. Pina, C. Soriano, *Helv. Chim. Acta* **2003**, *86*, 3118–3135.
- J. A. Aguilar, P. Díaz, F. Escartí, E. García-España, L. Gil, C. Soriano, B. Verdejo, *Inorg. Chim. Acta* **2002**, *339*, 307–316.
- P. Díaz, M. G. Basallote, M. A. Máñez, E. García-España, L. Gil, J. Latorre, C. Soriano, B. Verdejo, S. V. Luis, *Dalton Trans.* **2003**, 1186–1193.
- H. Gampp, D. Haspra, M. Maeder, A. D. Zuberbuehler, *Inorg. Chem.* **1984**, *23*, 3724–3730.
- S. Siddiqui, R. E. Shepherd, *Inorg. Chem.* **1986**, *25*, 3869–3876.
- See for instance: a) E. Kimura, I. Nakamura, T. Koike, M. Shionoya, Y. Kodama, T. Ikeda, M. Shiro, *J. Am. Chem. Soc.* **1994**, *116*, 4764–4771; b) T. Koike, S. Kajitani, I. Nakamura, E. Kimura, M. Shiro, *J. Am. Chem. Soc.* **1995**, *117*, 1210–1219; c) C. Bazzicalupi, A. Bencini, E. Berni, S. Ciattini, A. Bianchi,

- C. Giorgi, P. Paoletti, B. Valtancoli, *Inorg. Chim. Acta* **2001**, 317, 259–267.
- [23] L. H. Chen, C. S. Chung, *Inorg. Chem.* **1989**, 28, 1402–1405.
- [24] See for example: a) T. G. Fawcett, S. M. Rudich, B. H. Toby, R. A. Lalancette, J. A. Potenza, H. J. Schugar, *Inorg. Chem.* **1980**, 19, 940–945; b) Z. D. Georgousis, P. C. Christidis, D. Hadjipavlou-Litina, C. A. Bolos, *J. Mol. Struct.* **2007**, 837, 30–37; c) M. Chadim, P. Díaz, E. García-España, J. Hodacova, P. C. Junk, J. Latorre, J. M. Llinares, C. Soriano, J. Zavada, *New J. Chem.* **2003**, 27, 1132–1139; d) A. T. Chaviara, P. C. Christidis, A. Papageorgiou, E. Chrysogelou, D. J. Hadjipavlou-Litina, C. A. Bolos, *J. Inorg. Biochem.* **2005**, 99, 2102–2109; e) P. Antunes, R. Delgado, M. G. B. Drew, V. Félix, H. Maecke, *Inorg. Chem.* **2007**, 46, 3144–3153.
- [25] R. J. Deeth, *J. Chem. Soc., Dalton Trans.* **2001**, 664–669.
- [26] M. G. Basallote, J. Durán, M. J. Fernández-Trujillo, M. A. Máñez, *J. Chem. Soc., Dalton Trans.* **1999**, 3817–3823.
- [27] M. G. Basallote, J. Durán, M. J. Fernández-Trujillo, M. A. Máñez, *Polyhedron* **2001**, 20, 75–82.
- [28] M. G. Basallote, J. Durán, M. J. Fernández-Trujillo, M. A. Máñez, M. Quirós, M. A. Salas, *Polyhedron* **2001**, 20, 297–305.
- [29] M. G. Basallote, J. Durán, M. J. Fernández-Trujillo, M. A. Máñez, *J. Chem. Soc., Dalton Trans.* **2002**, 2074–2079.
- [30] R. A. Read, D. W. Margerum, *Inorg. Chem.* **1981**, 20, 3143–3149.
- [31] R. W. Hay, M. P. Pujari, R. Bembí, *Transition Met. Chem.* **1986**, 11, 261–264.
- [32] M. J. Fernández-Trujillo, B. Szpoganicz, M. A. Máñez, L. T. Kist, M. G. Basallote, *Polyhedron* **1996**, 15, 3511–3517.
- [33] S. Siddiqui, R. E. Shepherd, *Inorg. Chem.* **1983**, 22, 3726–3733.
- [34] L. H. Chen, C. S. Chung, *Inorg. Chem.* **1988**, 27, 1880–1883.
- [35] A. Mendoza, J. Aguilar, M. G. Basallote, L. Gil, J. C. Hernández, M. A. Máñez, E. García-España, L. Ruiz-Ramírez, C. Soriano, B. Verdejo, *Chem. Commun.* **2003**, 3032–3033.
- [36] a) M. W. Hosseini, J.-M. Lehn, M. P. Mertes, *Helv. Chim. Acta* **1983**, 66, 2454–2466; b) B. Dietrich, M. W. Hosseini, J.-M. Lehn, R. B. Sessions, *Helv. Chim. Acta* **1985**, 68, 289–299; c) M. W. Hosseini, J.-M. Lehn, *J. Chem. Soc., Chem. Commun.* **1985**, 1155–1157; d) M. W. Hosseini, J.-M. Lehn, L. Maggiora, K. B. Mertes, M. P. Mertes, *J. Am. Chem. Soc.* **1987**, 109, 537–544; e) P. G. Yohannes, K. E. Plute, M. P. Mertes, K. B. Mertes, *Inorg. Chem.* **1987**, 26, 1751–1755; f) M. W. Hosseini, J.-M. Lehn, *J. Am. Chem. Soc.* **1987**, 109, 7047–7058; g) H. Jahansouz, Z. Jiang, R. H. Himes, M. P. Mertes, K. B. Mertes, *J. Am. Chem. Soc.* **1985**, 107, 8288–8289; h) R. C. Bethel, G. Lowe, M. W. Hosseini, J.-M. Lehn, *Bioorg. Chem.* **1988**, 16, 418–428; i) G. M. Blackburn, G. R. J. Thatcher, M. W. Hosseini, J.-M. Lehn, *Tetrahedron Lett.* **1987**, 28, 2779–2782; j) Z. Jiang, P. Chalabi, K. B. Mertes, H. Jahansouz, R. H. Himes, M. P. Mertes, *Bioorg. Chem.* **1989**, 17, 313–329; k) M. W. Hosseini, A. J. Blacker, J.-M. Lehn, *J. Am. Chem. Soc.* **1990**, 112, 3896–3904; l) A. V. Eliseev, H.-J. Schneider, *J. Am. Chem. Soc.* **1994**, 116, 6081–6088.
- [37] a) J. Aguilar, E. García-España, J. Guerrero, S. V. Luis, J. M. Llinares, J. F. Miravet, J. A. Ramírez, C. Soriano, *J. Chem. Soc., Chem. Commun.* **1995**, 2237–2239; b) J. Aguilar, E. García-España, J. A. Guerrero, S. V. Luis, J. M. Llinares, J. A. Ramírez, C. Soriano, *Inorg. Chim. Acta* **1996**, 246, 287–294; c) J. Aguilar, B. Celda, V. Fusi, E. García-España, S. V. Luis, M. C. Martínez, J. A. Ramírez, C. Soriano, R. Tejero, *J. Chem. Soc. Perkin Trans. 2* **2000**, 7, 1323–1328; d) J. Aguilar, A. B. Descalzo, P. Díaz, V. Fusi, E. García-España, S. V. Luis, M. Micheloni, J. A. Ramírez, P. Romani, C. Soriano, *J. Chem. Soc. Perkin Trans. 2* **2000**, 6, 1187–1192.
- [38] a) R. Hettich, H. J. Schneider, *J. Am. Chem. Soc.* **1997**, 119, 5638–5647; b) S. Borah, M. S. Melvin, N. Lindquist, R. A. Manderville, *J. Am. Chem. Soc.* **1998**, 120, 4557–4562.
- [39] A. E. Martell, R. M. Smith, R. J. Motekaitis, *NIST Critically Selected Stability Constants of Metal Complexes Database*, NIST Standard Reference Database, version 4, (1997).
- [40] a) A. Gasowska, L. Lomozik, R. Jastrzab, *J. Inorg. Biochem.* **2000**, 78, 139–147; b) L. Lomozik, A. Gasowska, G. Krzysko, *J. Inorg. Biochem.* **2006**, 100, 1781–1789.
- [41] a) C. Anda, A. Llobet, V. Salvado, J. Reibenspies, R. J. Motekaitis, A. E. Martell, *Inorg. Chem.* **2000**, 39, 2986–2999; b) C. Anda, A. Llobet, V. Salvado, A. E. Martell, R. J. Motekaitis, *Inorg. Chem.* **2000**, 39, 3000–3008.
- [42] M. T. Albelda, E. García-España, H. R. Jiménez, J. M. Llinares, C. Soriano, A. Sornosa-Ten, B. Verdejo, *Dalton Trans.* **2006**, 4474–4481.
- [43] E. M. Bianchi, S. A. A. Sajadi, B. Song, H. Sigel, *Chem. Eur. J.* **2003**, 9, 881–892.
- [44] H. Sigel, S. S. Massoud, N. A. Corfú, *J. Am. Chem. Soc.* **1994**, 116, 2958–2971.
- [45] S. S. Massoud, R. Tribolet, H. Sigel, *Eur. J. Biochem.* **1990**, 187, 387–393.
- [46] A. E. Martell, R. J. Motekaitis, Q. Lu, D. A. Nation, *Polyhedron* **1999**, 18, 3203–3218.
- [47] E. García-España, M. J. Ballester, F. Lloret, J. M. Moratal, J. Faus, A. Bianchi, *J. Chem. Soc., Dalton Trans.* **1988**, 101–104.
- [48] M. Fontanelli, M. Micheloni, *Proceedings of the I Spanish-Italian Congress on Thermodynamics of metal complexes*, Diputación de Castellón, Castellón, Spain, **1990**. Program for the automatic control of the microburette and the acquisition of the electromotive force readings.
- [49] a) G. Gran, *Analyst (London)* **1952**, 77, 661–671; b) F. I. Rossotti, H. Rossotti, *J. Chem. Educ.* **1965**, 42, 375.
- [50] P. Gans, A. Sabatini, A. Vacca, *Talanta* **1996**, 43, 1739–1753.
- [51] M. J. Frisch, G. W. Trucks, H. B. Schlegel, G. E. Scuseria, M. A. Robb, J. R. Cheeseman, J. A. Montgomery, T. Vreven, K. N. Kudin, J. C. Burant, J. M. Millam, S. S. Iyengar, J. Tomasi, V. Barone, B. Mennucci, M. Cossi, G. Scalmani, N. Rega, G. H. Petersson, H. Nakatsuji, M. Hada, M. Ehara, K. Toyota, R. Fukuda, J. Hasegawa, M. Ishida, T. Nakajima, Y. Honda, O. Kitao, H. Nakai, M. Klene, X. Li, J. E. Knox, H. P. Hratchian, J. B. Cross, C. Adamo, J. Jaramillo, R. Gomperts, R. E. Stratmann, O. Yazyev, A. J. Austin, R. Cammi, C. Pomelli, J. W. Ochterski, P. Y. Ayala, K. Morokuma, G. A. Voth, P. Salvador, J. J. Dannenberg, V. G. Zakrzewski, S. Dapprich, A. D. Daniels, M. C. Strain, O. Farkas, D. K. Malick, A. D. Rabuck, K. Raghavachari, J. B. Foresman, J. V. Ortiz, Q. Cui, A. G. Baboul, S. Clifford, J. Cioslowski, B. B. Stefanov, G. Liu, A. Liashenko, P. Piskorz, I. Komaromi, R. L. Martin, D. J. Fox, T. Keith, M. A. Al-Laham, C. Y. Peng, A. Nanayakkara, M. Challacombe, P. M. W. Gill, B. Johnson, W. Chen, M. W. Wong, C. Gonzalez, J. A. Pople, *Gaussian 03, Revision E.01*, Gaussian, Inc., Pittsburgh PA, **2003**.
- [52] A. D. Becke, *J. Chem. Phys.* **1993**, 98, 5648–5652.
- [53] C. T. Lee, W. T. Yang, R. G. Parr, *Phys. Rev. B* **1988**, 37, 785–789.
- [54] D. Andrae, U. Haussermann, M. Dolg, H. Stoll, H. Preuss, *Theor. Chim. Acta* **1990**, 77, 123–141.
- [55] V. Barone, M. Cossi, *J. Phys. Chem. A* **1998**, 102, 1995–2001.
- [56] M. Cossi, N. Rega, G. Scalmani, V. Barone, *J. Comput. Chem.* **2003**, 24, 669–681.
- [57] C. J. Cramer, D. G. Truhlar, *Chem. Rev.* **1999**, 99, 2161–2200.
- [58] J. Tomasi, B. Mennucci, R. Cammi, *Chem. Rev.* **2005**, 105, 2999–3093.
- [59] GLINT Software, *Applied Photophysics Ltd.*, Leatherhead, U. K., **1997**.

Received: June 8, 2008

Published Online: November 28, 2008

Rare-Earth Metal Bis(dimethylsilyl)amide Complexes Supported by Cyclooctatetraenyl Ligands

Christian Meermann,^[a] Kouji Ohno,^[b] Karl W. Törnroos,^[a] Kazushi Mashima,^{*,[b]} and Reiner Anwander^{*,[a]}

Keywords: Cyclooctatetraenyl ligands / Silylamido ligands / Lanthanides / Iodido ligands / Agostic interactions

Monomeric cyclooctatetraenyl rare-earth metal complexes (COT)Ln(thf)₃ were examined by X-ray structure analysis for Ln = La and Sm being isostructural to the Nd and Ce congeners. Reaction of the lanthanum derivative with excess AlMe₃ led to partial thf displacement and dimerization to [(COT)La(μ-I)(thf)₂]₂. I[−]/[N(SiHMe₂)₂][−] salt metathetic ligand exchange involving (COT)LnI(thf)₃ (Ln = La, Nd, Sm) and Li[N(SiHMe₂)₂] did not give putative [(COT)Ln[N(SiHMe₂)₂](thf)_x]. Instead, depending on the metal size, the mixed iodide/amide *ate* complexes (COT)Ln(μ-I)₂[μ-N(SiHMe₂)₂]Ln-(COT)[Li(thf)₄] (Ln = Nd, Sm) and (COT)La(μ-I)[μ-

N(SiHMe₂)₂]₂La[μ-(η²:η⁸-COT)]Li(thf)₃ were obtained and identified by X-ray structure analyses. In thf solvent, these heteroleptic complexes undergo ligand redistribution to (COT)Ln[μ-(η²:η⁸-COT)]Li(thf)₃, whose solid-state structures were also analyzed by X-ray diffraction (Ln = Nd, Sm). Utilization of K[N(SiHMe₂)₂] afforded alkali-metal-free (COT)-La[N(SiHMe₂)₂](thf)₂ in good yield, whose monomeric composition was determined by X-ray structure analysis.

(© Wiley-VCH Verlag GmbH & Co. KGaA, 69451 Weinheim, Germany, 2009)

Introduction

During the past decades the cyclooctatetraenyl ligand (COT = η⁸-C₈H₈^{2−}) emerged as an important ancillary ligand in organolanthanide chemistry, launching unique and intriguing structural chemistry.^[1,2] Unfortunately, the synthesis and isolation of COT rare-earth metal precursors/complexes is often affected by side-product formation, with the Ln–COT fragment being increasingly prone to *ate* complexation and extensive ligand redistribution.^[3] Additionally, the planar 10π-e[−] system can bind a metal atom to each of the two faces of the arene in an inverse sandwich fashion.^[1,2,4] Dimeric [(COT)Ln(μ-Cl)(thf)₂]₂, which is easily accessible by reaction of anhydrous LnCl₃ with K₂[C₈H₈] in thf, is commonly used as a synthesis precursor in cyclooctatetraenyl rare-earth metal chemistry. Its utilization in salt metathesis reactions is, however, impaired by poor solubility (even in thf), formation of alkali-metal-incorporated products, and extensive complex degradation due to loss of thf.^[3]

Various motifs of *ate* complexation were detected in COT Ln^{III}–alkali metal derivatives as shown for complexes A–P in Figure 1 [on the basis of a Cambridge Structural Database (CSD) search]. For example, in situ formation of

[(COT)Ln(μ-Cl)(thf)₂]₂ followed by addition of terphenyllithium yielded complexes A and varying amounts of B;^[5] *ate* complex formation could be suppressed by use of the sterically more demanding 2,6-dimesitylphenyllithium instead.^[5] Reaction of [(COT)Ce(μ-Cl)(thf)₂]₂ with Na in the presence of *t*BuN=CH–CH=N*t*Bu did not yield the putative diazadiene complex, but also led to the formation of the heterobimetallic sandwich compound B.^[6] Alkylation of [(COT)Ln(μ-Cl)(thf)₂]₂ (Ln = Y, Sm, Lu) with LiCH(SiMe₃)₂ in thf gave inverse sandwich complexes H (Figure 1: the structurally characterized Sm derivative is shown) as main products, and compounds C were observed as side products.^[7] Contrary, the salt metathesis reaction of the chloro dimer [(COT)Ln(μ-Cl)(thf)₂]₂ (Ln = Y, Gd, Er, Lu) with Na[N(SiMe₃)₂] in toluene afforded monomeric monoamide complexes of type Q (Figure 2: the structurally characterized Lu derivative is shown).^[4] Such COT bis(trimethylsilyl)amido rare-earth metal derivatives were studied extensively for samarium, which initially produced the inverse sandwich complex U.^[4,8] Reinvestigation of the [(COT)Sm(μ-Cl)(thf)₂]₂–Na[N(SiMe₃)₂] reaction revealed that [(COT)Sm{N(SiMe₃)₂}(thf)] is readily formed in the equimolar reaction. When using 2 equiv. of Na[N(SiMe₃)₂], a mixture of the anionic pentane-soluble compound [(COT)-Sm{N(SiMe₃)₂}][−]Na⁺, monoamido species [(COT)-Sm{N(SiMe₃)₂}(thf)], and homoleptic Sm[N(SiMe₃)₂]₃ was observed. Furthermore, in [D₈]thf the additional formation of an *ate* complex [(COT)₂SmNa] was proposed (cf., B and C).^[8] As a consequence of the apparent drawbacks of complexes [(COT)Ln(μ-Cl)(thf)₂]₂, alternative and more soluble

[a] Department of Chemistry, University of Bergen, Allégaten 41, 5007 Bergen, Norway
Fax: +47-555-89490
E-mail: reiner.anwander@kj.uib.no

[b] Department of Chemistry, Graduate School of Engineering Science Osaka University, Toyonaka, Osaka 560-8531, Japan

precursors such as (COT)LnI(thf)_n (**1**, *n* = 3: Ln = La, Ce, Pr, Nd, Sm; *n* = 2: Ln = Tm) and [(COT)Ln(μ-O₃SCF₃)(thf)₂] (Ln = Ce, Pr, Nd, Sm) were developed.^[9,10] Their use as starting materials in COT chemistry is, however, still limited.^[11–14] For example, salt metathetic ex-

change of the iodido ligand in **1** with [K(thf)_n][N(PPh₂)₂] and formation of compound **R** (Figure 2) was achieved straightforwardly.^[13]

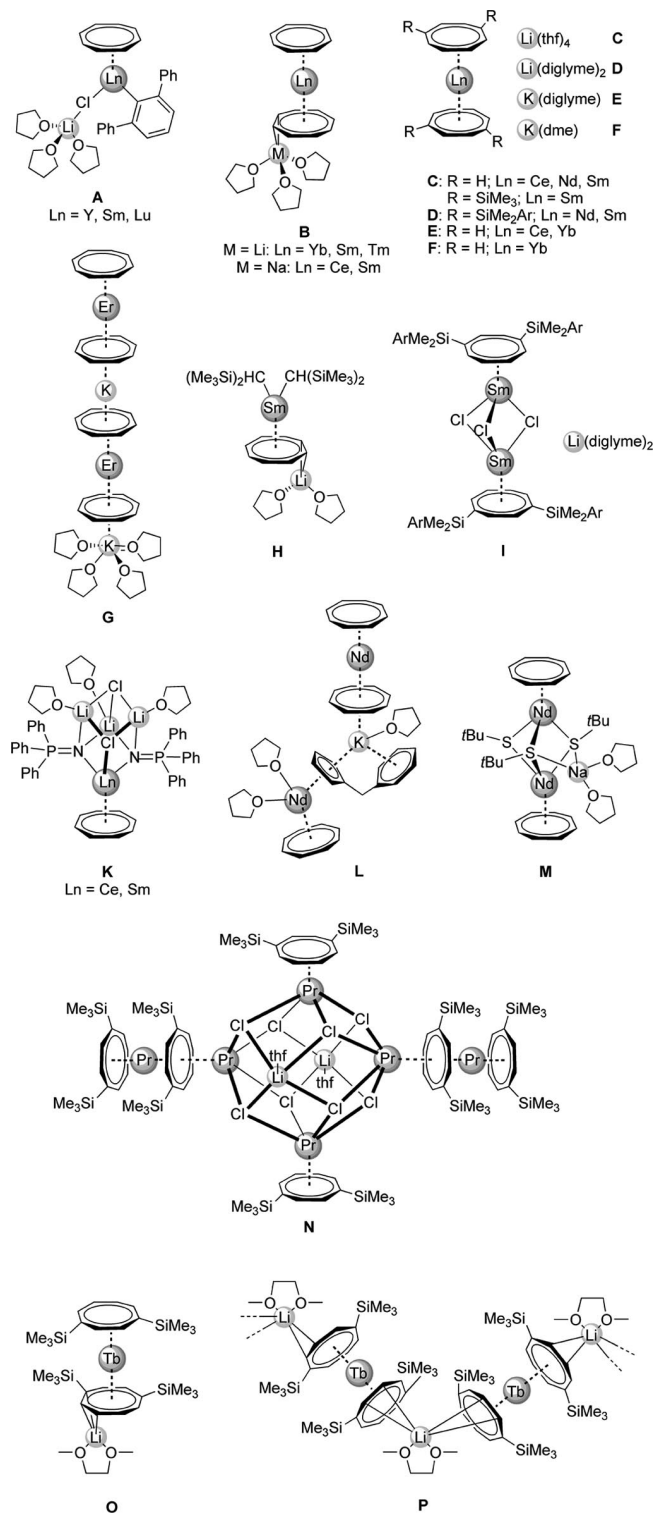


Figure 1. Structurally characterized COT lanthanide(III) alkali metal complexes **A**,^[5,15,16] **B**,^[6,11,17–19] **C**,^[6,20–22] **D**,^[23] **E**,^[24–26] **F**,^[25] **G**,^[27] **H**,^[7] **I**,^[11] **K**,^[6] **L**,^[28] **M**,^[29] **N**,^[30] **O**,^[31] **P**.^[31]

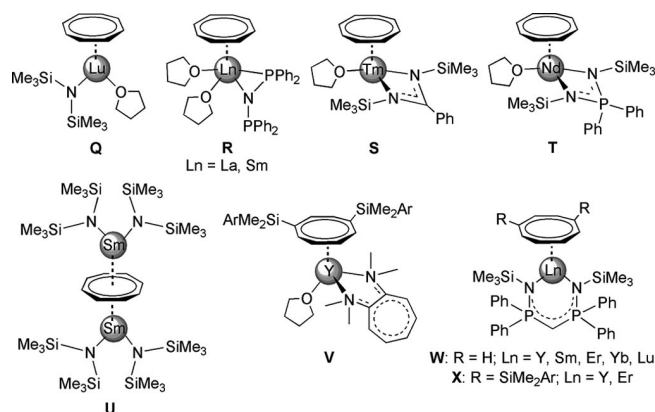


Figure 2. Structurally characterized COT Ln^{III} complexes with monoanionic *N*-donor ligands **Q**,^[4] **R**,^[13] **S**,^[32] **T**,^[32] **U**,^[4] **V**,^[12] **W**,^[14,33] **X**.^[34]

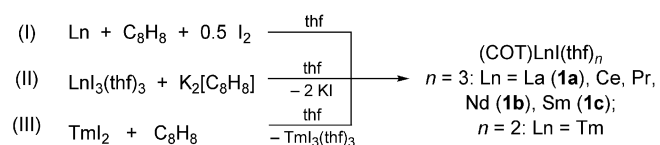
Similarly, heteroleptic COT/*N*-isopropyl-2-(isopropylamino)troponimate (**V**) (Figure 2: the structurally characterized **Y** derivative is shown) and COT/bis(phosphinimino)methanide complexes of samarium (**W**) were obtained from (COT)SmI(thf)₃ (**1c**) in thf at ambient temperature, **W** displaying hydroamination/cyclization catalysts.^[12,14] An attempt of preparing mixed-sandwich complexes from (COT)SmI(thf)₃ (**1c**) and Li₂[1,4-R₂C₈H₆] [R = *o*-(dimethylsilyl)-*N,N*-dimethylaniline], however, failed and rather resulted in the more favored and sterically less demanding rearrangement product **B**.^[11]

Given this promising reactivity of monomeric (COT)-LnI(thf)₃ toward monoanionic *N*-donor derivatives, we now examined the accessibility of respective bis(dimethylsilyl)-amide complexes. Compared to [N(SiMe₃)₂][−], its sterically less demanding counterpart [N(SiHMe₂)₂][−] might provoke new reactivity patterns and structural chemistry.^[35–40]

Results and Discussion

Synthesis and Characterization of COT/Iodide Complexes

A convenient synthesis procedure for the mononuclear cyclooctatetraenyl complexes (COT)LnI(thf)_n (**1**) of the larger rare-earth metals was developed almost 20 years ago.^[9,41] Accordingly, surface-rich rare-earth metal chips were treated with equimolar amounts of COT and iodine in thf suspension [Scheme 1, Equation (I)]. The reaction of lanthanide triiodides (Ln = Nd, Sm) with the potassium salt K₂[C₈H₈] is another approach feasible for the larger



Scheme 1. Different synthesis strategies for (COT)LnI(thf)_n.

rare-earth metal centers [Equation (II)].^[10] The third synthesis protocol was discovered more recently and seems to be limited to highly reducing rare-earth metal precursors such as rare Tm^{II}.^[42] X-ray structurally authenticated complexes (COT)LnI(thf)_n comprise the cerium (route 1, *n* = 3), the neodymium (route 2, *n* = 3), and the thulium derivative [Equation (III), *n* = 2].^[9,10,42]

In the present work we exploited the one-pot synthesis route I which avoids extensive side-product formation. Slow evaporation of the solvent from the crude reaction mixture yielded single crystals of (COT)LnI(thf)₃ [Ln = La (**1a**), Nd (**1b**), and Sm (**1c**)] suitable for X-ray structural analysis. Four-legged stool-like structures were found isostructural with the previously reported cerium and neodymium compounds (Figure 3).^[9,10] Table 1 compiles the bond lengths and angles for all structurally characterized compounds **1**. As expected, the Ln–Ct (Ct = centroid) and Ln–I distances increase with increasing metal cation size. It is noteworthy that the elemental analyses previously reported for the neodymium (**1b**) and samarium (**1c**) derivatives pointed to the coordination of two and one thf molecule, respectively.^[41]

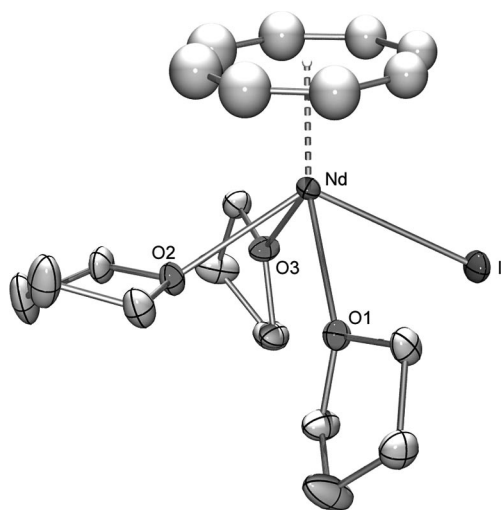
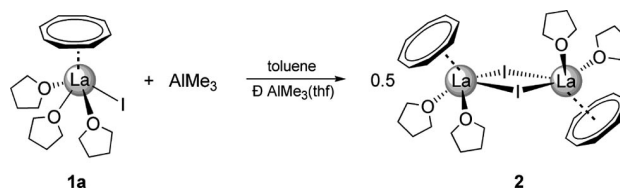


Figure 3. Molecular structure of (COT)LnI(thf)₃ (**1**) shown representatively for Nd (**1b**) with atomic displacement parameters at the 50% probability level (COT carbon atoms isotropic). Hydrogen atoms are omitted for clarity.

The present structural data suggest that the thf donor ligands might be only weakly coordinated and partially removed under reduced pressure, which would be in line with the formation of complexes [(COT)Ln(μ-Cl)(thf)₂]₂.

The latter heteroleptic chloride species were synthesized for differently sized rare-earth metal centers, including yttrium.^[43–45] Mixed COT/iodide compounds of the smaller rare-earth metal centers are still lacking, except (COT)-TmI(thf)₂ (route III, Scheme 1).^[42] Crucially, route I is not applicable for the synthesis of (COT)LnI(thf)_n of smaller rare-earth metals such as yttrium because of the reduced reactivity of such Ln metals, even under harsher conditions (high temperature/pressure tube and/or sonication).

However, by using a Lewis acid/base competition reaction with trimethylaluminum (Scheme 2),^[40,46] we were able to displace one thf ligand in **1a**, which produced the iodido-bridged dimer [(COT)La(μ-I)(thf)₂]₂ (**2**) in high yield, being structurally similar to complexes [(COT)Ln(μ-Cl)(thf)₂]₂. When crystalline **1a** was suspended in toluene and excess AlMe₃ added, the formation of a fine white precipitate was observed which readily dissolved in thf.



Scheme 2. Synthesis of dimeric iodide complex **2**.

Crystallization from thf at –35 °C gave colorless crystals of **2** (Figure 4, monoclinic space group *P2₁/n*, Tables 1 and 4). This implies that the thf abstraction/dimerization sequence is non-reversible as even in the presence of excess donor solvent the re-formation of complex **1a** is unfavored. Complex **2** did not form by simply stirring **1a** in toluene overnight, as revealed by ¹H NMR spectroscopic investigations and X-ray crystallography.

The lanthanum metal center in **2** shows a similar coordination environment as the respective structurally characterized COT/chloride complexes [(COT)Ln(μ-Cl)(thf)₂]₂ (Ln = Ce, Pr, Nd, Sm).^[47–49] The La–I distances of

Table 1. Selected bond lengths [Å], intramolecular distances [Å], and angles [°] for all structurally characterized (COT)LnI(thf)_x (**1**) and [(COT)La(μ-I)(thf)₂]₂ (**2**).

| | 1a (La) | Ce ^[9] | 1b (Nd) ^[b] | 1c (Sm) | Tm ^[42] | 2 (La) |
|----------------------|----------------|-------------------|-------------------------------|----------------|--------------------|------------------------|
| Ln–I | 3.3022(4) | 3.299(1) | 3.2626(5) | 3.2481(4) | 3.0338(11) | 3.3832(2) 3.3157(2) |
| Ln–O(1) | 2.584(3) | 2.583(7) | 2.526(4) | 2.479(3) | 2.342(8) | 2.576(2) |
| Ln–O(2) | 2.625(3) | 2.555(7) | 2.580(4) | 2.559(3) | 2.382(9) | 2.588(2) |
| Ln–O(3) | 2.560(3) | 2.640(7) | 2.509(4) | 2.501(3) | – | – |
| Ln–Ct ^[a] | 2.042 | 2.010 | 1.957 | 1.928 | 1.750 | 2.025 |
| I–Ln–Ct | 119.0 | 116.0 | 118.2 | 118.7 | 131.06 | 118.1 131.4 |
| O(1)–Ln–Ct | 131.4 | 134.2 | 130.6 | 129.0 | 126.8 | 127.4 |
| O(2)–Ln–Ct | 114.9 | 127.1 | 116.2 | 115.8 | 129.2 | 116.2 |
| O(3)–Ln–Ct | 128.9 | 116.9 | 128.9 | 129.6 | – | – |

[a] Ct = Centroid, defined by the 8 carbon atoms of COT. [b] X-ray structural data collected at ambient temperature have been presented previously by Edelmann et al.^[10]

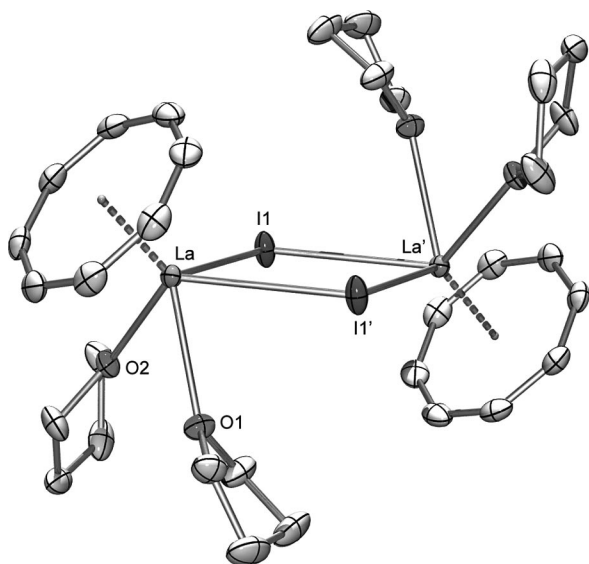


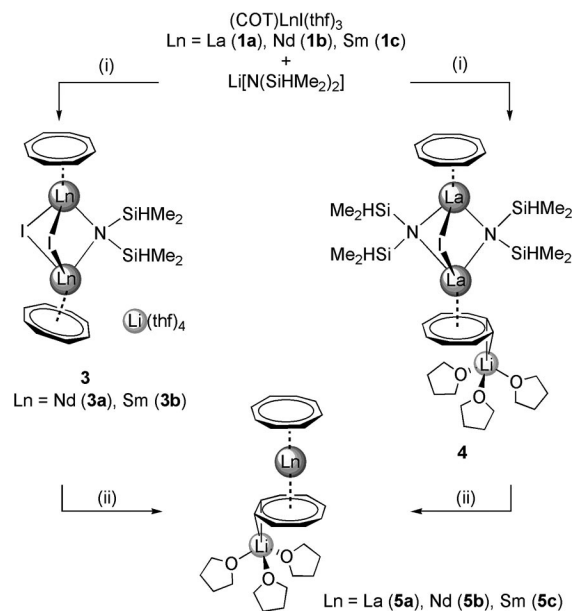
Figure 4. Molecular structure of $[(\text{COT})\text{La}(\mu\text{-I})(\text{thf})_2]_2$ (**2**) shown with atomic displacement parameters at the 50% probability level. Hydrogen atoms are omitted for clarity. Symmetry code is $-x + 1, -y + 2, -z$.

3.3157(2) Å and 3.3832(2) Å are slightly elongated compared to those in dimeric $[\text{La}(\mu\text{-I})\{\text{N}(\text{SiMe}_3)_2\}_2(\text{thf})_2]$ [av. 3.3074(11) Å] with five-coordinate metal centers.^[50] So far, few COT lanthanum complexes were structurally characterized. The approximate La–Ct distances for $(\text{COT})\text{La}(\eta^5\text{-C}_5\text{Me}_4\text{H})(\text{thf})_2$ (2.099 Å),^[51] $(\text{COT})\text{La}(\eta^5\text{-C}_4\text{H}_7\text{OCH}_2\text{C}_5\text{H}_4)(\text{thf})$ (2.067 Å),^[52] and **O** (2.047 Å)^[13] appear slightly elongated compared to compound **2** (2.025 Å).

Synthesis and Characterization of COT/Silylamide Complexes

Whereas ligand exchange reactions have been extensively studied for $[(\text{COT})\text{Ln}(\mu\text{-Cl})(\text{thf})_2]_2$, there are only a few examples for $(\text{COT})\text{LnI}(\text{thf})_n$ (**1**).^[11–14] Having in mind the structurally authenticated bis(trimethylsilyl)amide complexes **Q** and **U** (Figure 2),^[4] we examined the reactions of **1a–c** with $\text{Li}[\text{N}(\text{SiHMe}_2)_2]$ in thf (Scheme 3). The equimolar reactions produced clear solutions, which were stirred at ambient temperature overnight, filtered, and the volume reduced in vacuo until viscous liquids were obtained. To the obtained oily or waxy materials toluene was added causing instant crystallization of $(\text{COT})\text{Ln}(\mu\text{-I})_2\{\mu\text{-N}(\text{SiHMe}_2)_2\}\text{-Ln}(\text{COT})[\text{Li}(\text{thf})_4]$ ($\text{Ln} = \text{Nd}$, **3a**; Sm , **3b**) and $(\text{COT})\text{La}(\mu\text{-I})[\mu\text{-N}(\text{SiHMe}_2)_2]\text{La}[\mu\text{-}(\eta^2\text{:}\eta^8\text{-COT})]\text{Li}(\text{thf})_3$ (**4**), respectively, which were identified by X-ray structure analyses. Attempted recrystallization of **3** and **4** from thf solutions or storage of the crude thf reaction mixture at -35°C did not yield amide complexes but rather led to the scrambling products $(\text{COT})\text{Ln}[\mu\text{-}(\eta^2\text{:}\eta^8\text{-COT})]\text{Li}(\text{thf})_3$ (**5**) (Figure 1, **B**). Crystal shape and color of compounds **5** vary significantly from the starting materials **1** and from the amido-containing products **3** and **4**, allowing for easy monitoring of the reaction progress and separation of products. Such ligand

redistribution with formation of the thermodynamically favored product **5** (**B**) has been observed previously (vide supra), and the Yb, Sm, and Tm analogues were structurally characterized.^[11,17,18]



Scheme 3. Distinct reaction pathways for the salt metathesis reaction of $(\text{COT})\text{LnI}(\text{thf})_3$ (**1**) ($\text{Ln} = \text{La}$, Nd , Sm) with $\text{Li}[\text{N}(\text{SiHMe}_2)_2]$; (i) ambient temp., thf, 24 h; (ii) thf, -35°C , 2–5 d.

^1H NMR spectroscopic investigations of the thf supernatant of **5a** in C_6D_6 indicated a “complete” ligand scrambling by the absence of signals for thf-soluble **4**; however, it did not reveal the second scrambling product, which is assumed to be a mixed lanthanum amide/iodide complex in accordance with previously reported complexes $[\{\text{Nd}\{\text{N}(\text{SiHMe}_2)_2\}(\text{thf})\}_2(\text{Nd}\{\text{N}(\text{SiHMe}_2)_2\}_2)(\mu_2\text{-Cl})_2(\mu_3\text{-Cl})_2\{\mu\text{-N}(\text{SiHMe}_2)_2\}]^{[53]}$ and $[\text{La}(\mu\text{-I})\{\text{N}(\text{SiMe}_3)_2\}_2(\text{thf})_2]^{[50]}$.

The overall yields of crystallized complexes $(\text{COT})\text{Ln}[\mu\text{-}(\eta^2\text{:}\eta^8\text{-COT})]\text{Li}(\text{thf})_3$ (**5**) were low (15–30%). Ligand redistribution of the neodymium derivative **3a** to **5b** was incomplete as evidenced by unreacted **3a** in the ^1H NMR spectrum of the supernatants. In addition, minor amounts of colorless crystals formed, which were identified as $\text{LiI}(\text{thf})_3$ by X-ray structure analysis. Prolonged exposure of complexes **3** and **4** to vacuum caused either decomposition or partial loss of thf and consequently low carbon values for the elemental analyses; direct use of crystalline material gave better microanalytical data. Crystals suitable for X-ray structural investigations could be harvested for all three metals La, Nd, and Sm (Tables 2 and 4).

The neodymium and samarium complexes **3a** and **3b** (Figure 5) are isostructural (orthorhombic space group *Pbca*), crystallizing as separated anion–cation pairs. The anionic part of complexes **3** is formed by a hetero-bridged $\text{Ln}(\mu\text{-I})_2[\mu\text{-N}(\text{SiHMe}_2)_2]\text{Ln}$ moiety sandwiched by COT ligands. In the solid state, the coordination sphere of the two formally tetrahedrally coordinated metal centers is additionally saturated by $\text{La}\cdots(\text{H-Si})$ β -agostic interactions

Table 2. Selected bond lengths [Å], intramolecular distances [Å], and angles [°] for **3a**, **3b**, **4**, and **6**.

| | 3a (Nd) | 3b (Sm) | 4 (La) | | 6 (La) | |
|------------------|----------------|----------------|-------------------------------|------------|------------------|------------|
| Ln(1)–I(1) | 3.2299(3) | 3.1885(2) | La(1)–I(1) | 3.3625(5) | La(1)–N(1) | 2.410(2) |
| Ln(1)–I(2) | 3.2708(3) | 3.2366(2) | La(1)–N(1) | 2.674(4) | La(1)–O(1) | 2.573(2) |
| Ln(1)–N(1) | 2.551(3) | 2.530(2) | La(1)–N(2) | 2.629(4) | La(1)–O(2) | 2.575(3) |
| Ln(2)–I(1) | 3.2462(3) | 3.2142(2) | La(2)–I(1) | 3.3576(5) | La(1)–Ct(1) | 2.064 |
| Ln(2)–I(2) | 3.2456(3) | 3.2058(2) | La(2)–N(1) | 2.605(4) | La(1)···Si(2) | 3.3263(8) |
| Ln(2)–N(1) | 2.611(3) | 2.585(2) | La(2)–N(2) | 2.657(4) | La(1)···H(Si2) | 2.89(5) |
| Ln(1)–Ct(1) | 1.933 | 1.898 | La(1)–Ct(1) | 2.046 | | |
| Ln(2)–Ct(2) | 1.938 | 1.903 | La(2)–Ct(2) | 2.068 | | |
| Ln(1)···Si(1) | 3.2527(11) | 3.2355(8) | La(1)···Si(2) ^[a] | 3.374(2) | | |
| Ln(1)···Si(2) | 3.7707(11) | 3.7466(8) | La(1)···Si(3) ^[a] | 3.329(2) | | |
| Ln(2)···Si(1) | 3.7841(11) | 3.7623(7) | La(2)···Si(1) ^[a] | 3.313(2) | | |
| Ln(2)···Si(2) | 3.2433(11) | 3.2200(7) | La(2)···Si(4) ^[a] | 3.4226(14) | | |
| Ln(1)···H(Si1) | 2.70(5) | 2.67(3) | La(1)···H(Si2) ^[a] | 2.69(6) | | |
| Ln(2)···H(Si2) | 2.57(5) | 2.58(3) | La(1)···H(Si3) ^[a] | 2.77(6) | | |
| Ln(1)–I(2)–Ln(2) | 76.174(8) | 75.843(5) | La(1)–I(1)–La(2) | 71.066(10) | N(1)–La(1)–O(1) | 90.86(8) |
| Ln(1)–I(1)–Ln(2) | 76.734(8) | 76.397(5) | La(1)–N(1)–La(2) | 95.43(13) | N(1)–La(1)–O(2) | 95.57(8) |
| Ln(1)–N(1)–Ln(2) | 102.27(11) | 101.44(7) | La(1)–N(2)–La(2) | 95.25(13) | O(1)–La(1)–O(2) | 71.51(12) |
| Ln(1)–N(1)–Si(1) | 96.95(14) | 97.21(9) | La(1)–N(1)–Si(1) | 122.2(2) | La(1)–N(1)–Si(1) | 120.24(12) |
| Ln(1)–N(1)–Si(2) | 122.20(16) | 122.17(11) | La(1)–N(1)–Si(2) | 97.98(18) | La(1)–N(1)–Si(2) | 107.40(11) |
| Ln(2)–N(1)–Si(1) | 119.78(15) | 120.29(10) | La(2)–N(1)–Si(1) | 97.77(18) | Si(1)–N(1)–Si(2) | 130.52(14) |
| Ln(2)–N(1)–Si(2) | 94.43(14) | 94.50(9) | La(2)–N(1)–Si(2) | 123.6(2) | | |
| I(1)–Ln(1)–I(2) | 80.947(8) | 81.185(6) | N(1)–La(1)–N(2) | 77.05(13) | | |
| I(1)–Ln(1)–N(1) | 79.09(7) | 79.60(5) | I(1)–La(1)–N(2) | 77.18(9) | | |
| I(2)–Ln(1)–N(1) | 78.02(8) | 78.41(5) | I(1)–La(1)–N(1) | 76.35(9) | | |
| Si(1)–N(1)–Si(2) | 121.34(19) | 121.25(13) | Si(1)–N(1)–Si(2) | 119.3(2) | | |
| | | | Si(3)–N(2)–Si(4) | 119.7(2) | | |

[a] Shortest intramolecular La···Si/H(Si) distances in **4**.

involving the amido ligand [e.g., for **3b**: Sm1–H(Si1) 2.67 Å, Sm2–H(Si2) 2.58 Å; cf. Table 2]. For comparison, complex **I** (Figure 1) shows a similar structural motif with the two samarium atoms of the anionic part bridged by three chlorido ligands.^[11] Surprisingly, the bridging Sm–I distances in **3b** (av. 3.2113 Å) are slightly shorter than the terminal one in **1c** [3.2481(4) Å], whereas the Sm–N bonds of 2.530(2) Å (Sm1) and 2.585(2) Å (Sm2) are considerably longer than in Sm[N(SiHMe₂)₂]₃(thf)₂ (av. 2.320 Å)^[54] and **U** (av. 2.281 Å)^[4] bearing terminal silylamido ligands exclusively. As expected, for the larger neodymium metal cation in **3a** all distances are slightly elongated (Table 2). The bridging Nd–N(SiHMe₂)₂ bond lengths of 2.551(3) and 2.611(3) Å compare well to those in [{Nd{N(SiHMe₂)₂}(thf)₂}(Nd{N(SiHMe₂)₂)₂}(μ₂-Cl)₂(μ₃-Cl)₂{μ-N(SiHMe₂)₂}] [2.564(3) Å, 2.610(3) Å].^[53]

The solid-state structure of complex **4** revealed also a heterobridged Ln(μ-I)[μ-N(SiHMe₂)₂]₂Ln core; however, here the larger lanthanum metal centers accommodate two sterically demanding bis(dimethylsilyl)amido ligands (Figure 6). Moreover, the alkali metal (Li) atom in **4** is directly coordinated to one COT ring, in contrast to the separated [Li(thf)₄]⁺ cation in **3**. Such an inverse sandwich coordination La[μ-(η²:η⁸-COT)]Li(thf)₃ is well known in (COT)Ln chemistry and has been described for the alkali metals Li and Na (cf., **B** and **H**, Figure 1).^[6,7,11,17–19] The La–Ct distances of the η⁸-coordinated COT rings average 2.057 Å and are comparable to other (COT)lanthanum complexes.^[13,51,52] The La–N bond lengths lie in the range between 2.605(4) and 2.674(4) Å, matching those in dimeric {La[μ-N(SiHMe₂)₂][N(SiHMe₂)₂]₂} (av. 2.654 Å, bridging

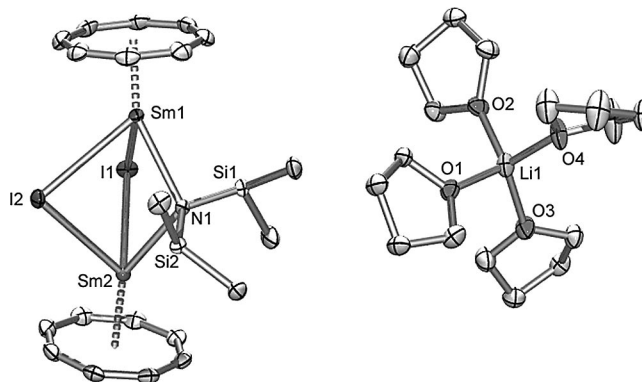


Figure 5. Molecular structure of [(COT)Ln(μ-I)₂{μ-N(SiHMe₂)₂}-Ln(COT)][Li(thf)₄] (**3**) shown exemplary for Sm (**3b**) with atomic displacement parameters at the 50% probability level. The distance between the two ions is not to scale. Hydrogen atoms are omitted for clarity.

amido groups),^[55] and [La₂(tBu₂pz)₅] (tBu₂pz = 3,5-di-*tert*-butylpyrazolato ligand) (2.689 Å, bridging pyrazolato ligand),^[56] however being elongated compared to (COT)lanthanum diphosphanylamide complex **R** [2.501(2) Å; Figure 2].^[13] La···H(Si) distances as short as 2.69 Å point to secondary interactions of the Ln metal center with the silylamido ligands.

As pointed out before, it is easy to distinguish between the different complexes under study just by crystal shape and color. In general the crystals of sandwich compounds **5** appear yellowish, whereas complexes **1b**, **3a** (green) and **1c**, **3b** (purple) are intensively colored. Both the lanthanum

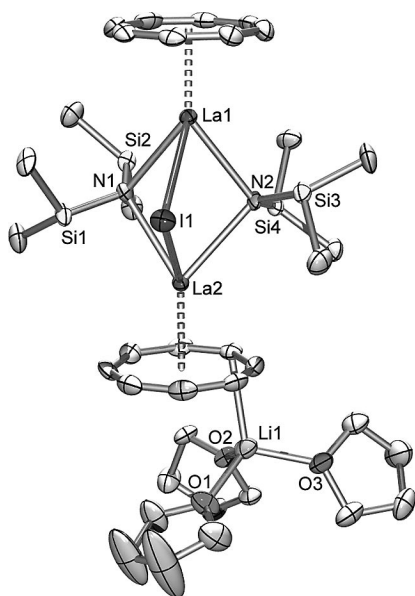


Figure 6. Molecular structure of (COT)Lan[μ-I][μ-N(SiHMe₂)₂]₂-La[μ-(η²:η⁸-COT)]Li(thf)₃ (**4**) shown with atomic displacement parameters at the 50% probability level. Hydrogen atoms are omitted for clarity.

compound **5a** and the samarium analogue **5c** have been described earlier. Wayda et al. examined the reaction of (COT)LnCl(thf)_x with alkyl lithium compounds (LiR) already in 1983.^[44] With R = CH₂SiMe₃ only one compound could be isolated and characterized that was assigned to [(COT)₂La][Li(thf)_x], however not X-ray crystallographically authenticated. The samarium complex **5c** was already X-ray structurally characterized by Roesky et al.^[11] The Tm and Yb derivatives of **5** are also X-ray structurally evidenced.^[17,18] Here, we present the solid-state structures of the lanthanum and neodymium complexes **5a** and **5b** (Figure 7). Interestingly, both compounds are isostructural but not isomorphous (**5a**: space group *P* $\bar{1}$; **5b**: *P*₂₁/*n*). The molecular structure of **5** can best be described as an anionic [Ln(COT)₂][−] sandwich flanked by an [Li(thf)₃]⁺ cation, the latter showing the same η-coordination to the COT ring as in **4**. In Table 3 bond lengths and angles are compiled for all structurally characterized compounds **5**.

As demonstrated in Figure 1 and for complexes **3**, **4**, and **5**, the formation of *ate* complexes from alkali-metal-based salt metathesis reactions is generally not surprising. In order to examine the influence of the type of alkali metal amide precursor, lanthanum species **1a** was treated with the corresponding potassium salt, instead (Scheme 4). After addition of K[N(SiHMe₂)₂] to a thf solution of the (COT)-lanthanum iodide complex instant precipitation of the less thf-soluble KI was observed. This is in contrast to afore-discussed Li amide reactions where clear solutions were obtained, independent of the metal center. To ensure quantitative conversion, the suspension was stirred for 24 h, the insoluble parts were separated and volatiles removed under vacuum. Moreover, the different reactivity behavior was ap-

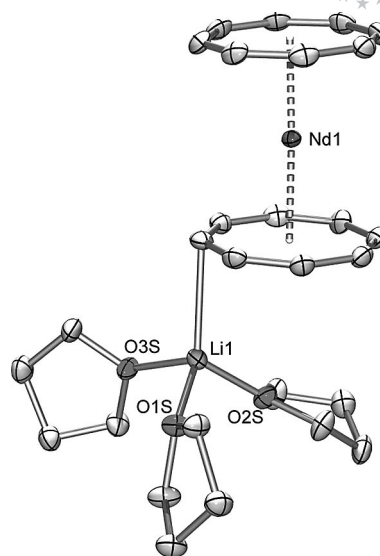


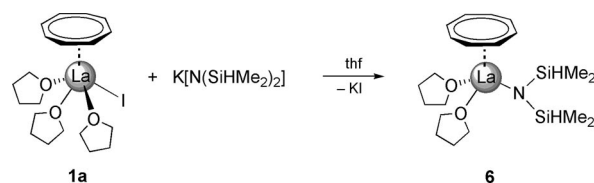
Figure 7. Molecular structure of (COT)Ln[μ-(η²:η⁸-COT)]Li(thf)₃ (**5**) shown exemplary for Nd (**5b**) with atomic displacement parameters at the 50% probability level. Hydrogen atoms are omitted for clarity.

Table 3. Selected bond lengths [Å], intramolecular distances [Å] and angles [°] for all structurally characterized (COT)Ln[μ-(η²:η⁸-COT)]Li(thf)₃ (**5**). Labels that differ for literature-known compounds are given as in **5b**.

| | La (5a) | Nd (5b) | Sm ^[11] | Tm ^[18] | Yb ^[17] |
|----------------------|--------------------|-----------------------------------|-----------------------------------|-----------------------------------|-----------------------------------|
| Space group | <i>P</i> $\bar{1}$ | <i>P</i> ₂₁ / <i>n</i> | <i>P</i> ₂₁ / <i>m</i> | <i>P</i> ₂₁ / <i>n</i> | <i>P</i> ₂₁ / <i>n</i> |
| Ln–Ct ^[a] | 2.068 | 1.981 | 1.943 | 1.830 | 1.944 |
| Ln–Ct2 | 2.106 | 2.027 | 1.984 | 1.878 | 1.987 |
| Li–C _a | 2.303(15) | 2.349(10) | 2.42(2) ^[b] | 2.346(7) | 2.338 |
| Li–C _b | 2.642(16) | 2.586(10) | 2.42(2) ^[b] | 2.606(7) | 2.589 |
| Li–O1 | 1.963(14) | 1.953(10) | 1.940(12) | 1.955(7) | 1.959(7) |
| Li–O2 | 1.880(13) | 1.874(10) | 1.90(2) | 1.893(7) | 1.895(7) |
| Li–O3 | 1.967(15) | 1.950(10) | 1.940(12) | 1.945(7) | 1.945(7) |
| Ct–Ln–Ct | 175.9 | 177.9 | 178.6 | 178.2 | 178.1 |
| O1–Li–C _a | 116.4(6) | 122.1(5) | 98.8(5) | 121.2(3) | 121.9 |
| O2–Li–C _a | 119.3(7) | 116.8(4) | 117.5(8) | 117.8(3) | 117.8 |
| O3–Li–C _a | 106.7(6) | 103.3(4) | 98.8(5) | 103.5(8) | 103.5 |

[a] Ct = Centroid, defined by the 8 carbon atoms of COT. [b] Li–C_a and Li–C_b are equal due to the mirror symmetry through the COT ring. C_a and C_b represent the Li–(η²-COT) distances.

parent as concentration to dryness was achievable, thus avoiding viscous liquids as found for the Li[N(SiHMe₂)₂] reactions.



Scheme 4. Synthesis of (COT)La[N(SiHMe₂)₂](thf)₂ (**6**).

Crystallization of the solid residue from saturated thf solution yielded colorless crystals of the composition (COT)La[N(SiHMe₂)₂](thf)₂ (**6**). As pointed out before, acquiring accurate elemental analyses is exceedingly difficult

with these systems. If the crystalline material was dried under vacuum prior to the measurement, the carbon values obtained were too low; direct usage of the crystals gave better, but still slightly off values. Nevertheless, formation of the first *ate*-free (COT)Ln bis(dimethylsilyl)amide complex was unequivocally proven by X-ray structure analysis (Figure 8, Tables 2 and 4). In **6** the lanthanum metal center is four-coordinate by one amido ligand, the COT ligand, and two thf molecules.

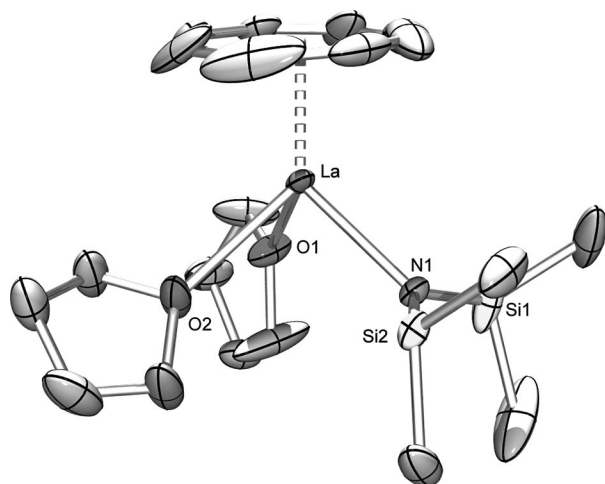


Figure 8. Molecular structure of (COT)La[N(SiHMe₂)₂](thf)₂ (**6**) shown with atomic displacement parameters at the 50% probability level. Hydrogen atoms are omitted for clarity.

The congener complex (COT)Lu[N(SiMe₃)₂](thf) (**Q**, Figure 2) shows due to the larger steric demand of the bis(trimethylsilyl)amido ligand and the significantly smaller ionic radius of lutetium coordination of only one thf molecule.^[4]

The La–N bond length of 2.410(2) Å is as expected significantly shorter than in four-coordinate bis(amido)-bridged **4** but matches those found for La[N(SiHMe₂)₂]₃(thf)₂ [2.416(5), 2.395(5), 2.407(5) Å] surprisingly well.^[40] Though, the Ln–Ct distance (2.064 Å) lies in the range of the other lanthanum complexes **1a**, **2**, **5a**, and **4** within this study. Secondary interactions of the Ln metal center with the silylamido ligand are not as pronounced as in **4**; however, La–N–Si1/2 angles of 107.4(2)° and 120.2(2)° revealed an asymmetrically bonded amido ligand, which is further expressed in one close La⋯H(Si) interaction [La⋯Si2: 3.3263(8) Å, La⋯H(Si2): 2.89(5) Å; cf., La⋯H(Si1): 3.56(6) Å].

Preliminary studies of the corresponding system (COT)-SmI(thf)₃ (**1c**)/K[N(SiHMe₂)₂] indicate the same reaction behavior.

Conclusions

Salt metathesis reactions of (COT)LnI(thf)₃ with bis(dimethylsilylamido)lithium give partially ligand-exchanged (COT)dilanthanide sandwich complexes. Depending on the Ln metal size, distinct heterobridged core moieties Ln-

(μ-I)_n[μ-N(SiHMe₂)₂]_mLn (Ln = La: *n* = 1, *m* = 2; Ln = Nd and Sm: *n* = 2, *m* = 1) are observed. Such heteroleptic complexes underlie ligand redistribution reactions producing the thermodynamically favored (COT)monolanthanide sandwich complexes (COT)Ln[μ-(η²:η⁸-COT)]Li(thf)₃, which are known for the entire Ln^{III} size range. Such *ate* complexes seem to display a random coordination of the charge-compensating alkali metal ion, either as [Li(thf)₃]⁺ interacting with the COT ring or ion-separated as [Li(thf)₄]⁺ (cf., Figure 1); *ate* complexation can be avoided by conducting potassium-based salt metathesis reactions as shown for the high-yield synthesis of complex (COT)La[N(SiHMe₂)₂](thf)₂. Moreover, complex (COT)LaI(thf)₃ could be converted into the dimer [(COT)La(μ-I)(thf)₂]₂ by a Lewis acid/base competition reaction with trimethylaluminum, which shows the same structural motif as complexes [(COT)Ln(μ-Cl)(thf)₂]₂.

Experimental Section

General: All operations were performed with rigorous exclusion of air and water by using standard Schlenk, high-vacuum, and glovebox techniques. Solvent pretreatment/purification was performed with Grubbs columns (MBraun SPS, solvent purification system) or by distillation from sodium/benzophenone ketyl. C₆D₆ was obtained from Aldrich, dried with Na for 24 h, filtered, and stored in a glovebox. Li[N(SiHMe₂)₂] was prepared from HN(SiHMe₂)₂ (Aldrich) and *n*-butyllithium (Aldrich) in hexane. K[N(SiHMe₂)₂] was prepared from KH and HN(SiHMe₂)₂ (Aldrich) according to literature procedures.^[57] COT, iodine, La ingots, Sm ingots, and Nd ingots were purchased from Aldrich. (COT)-LnI(thf)₃ (**1a–c**)^[9] were synthesized according to literature procedures. ¹H and ¹³C NMR spectra were recorded at 298 K with a Varian Mercury 300 or a Bruker BIOSPIN-AV600 (5 mm cryo probe; ¹H: 600.13 MHz; ¹³C: 150.91 MHz) spectrometer. ¹H and ¹³C shifts are referenced to internal solvent resonances and reported relative to TMS. IR spectra were recorded with a Nicolet Impact 410 FTIR spectrometer or a Jasco FT/IR-230 spectrometer as Nujol mulls sandwiched between CsI plates. Elemental analyses were performed with an Elementar Vario EL III or a Perkin–Elmer 2400II microanalyzer.

[(COT)La(μ-I)(thf)₂]₂ (**2**): **1a** (75 mg, 0.13 mmol) was suspended in toluene (4 mL), and 4 equiv. of AlMe₃ (37 mg, 0.51 mmol) was added. The milky suspension was stirred overnight, and volatiles were evaporated under reduced pressure to yield a pale yellow powder. The powder was suspended in toluene, and thf was added until most of the solid had dissolved. After filtration, the solution was stored at –35 °C. Overnight, 61 mg of colorless crystals formed (0.06 mmol, 93%). The NMR spectra were recorded in deuterated benzene, and a small amount of thf was added to increase the solubility. ¹H NMR (600 MHz, C₆D₆, 25 °C): δ = 6.59 (s, COT), 3.55 (s, thf), 1.43 (s, thf) ppm. ¹H NMR (600 MHz, [D₈]thf, 25 °C): δ = 6.26 (s, COT), 3.54 (s, thf), 1.68 (s, thf) ppm. ¹³C{¹H} NMR (150.9 MHz, [D₈]thf, 25 °C): δ = 97.9 ppm. IR: ν_{max} = 1072 (s), 1026 (s), 798 (s), 680 [vs (COT)], 628 (m), 467 (w) cm^{–1}. C₃₂H₄₈I₂·La₂O₄ (1028.35): calcd. C 37.38, H 4.70; found C 37.9, H 3.8.

Mixed Iodide/Amide Complexes 3 and 4: (COT)LnI(thf)₃ (Ln = La, Nd, Sm) was dissolved in thf (5 mL), and 1 equiv. of Li[N(SiHMe₂)₂] was added. The clear solutions were stirred at ambient temperature for 24 h, filtered, and the solvent was removed under vacuum until viscous oils were obtained. Addition of toluene

(1 mL) caused immediate formation of **3** and **4** as crystalline materials in high yields. The NMR spectra were recorded from the crystalline material, without drying under reduced pressure. For this reason, small amounts of toluene and non-coordinating thf were detected.

(COT)Nd(μ-I)₂{μ-N(SiHMe₂)₂}Nd(COT)[Li(thf)₄] (3a): Compound **1b** (101 mg, 0.19 mmol) and Li[N(SiHMe₂)₂] (27 mg, 0.19 mmol) gave dark green crystals (103 mg, 0.09 mmol, 92%). ¹H NMR (600 MHz, C₆D₆, 25 °C): δ = 6.04 (s, 12 H, SiHMe₂), 3.30 (s, 16 H, thf), 1.34 (s, 16 H, thf), −0.34 (s, 2 H, SiHMe₂) −13.07 (s, 16 H, COT) ppm. ¹³C{¹H} NMR (150.9 MHz, C₆D₆, 25 °C): δ = 161.1, 67.5 (thf), 25.6 (thf) ppm; signals assignable to the silylamido ligand could not be detected. IR: ν_{max} = 2024 {s [v(SiH)]}, 1244 (s), 1042 [vs (thf)] 985 (w), 937 (w), 884 (s), 842 (s), 758 (w), 696 (vs) cm^{−1}. C₃₆H₆₂I₂LiN₂Nd₂O₄Si₂·(C₄H₈O)₂ (1322.50): calcd. C 39.96, H 5.94, N 1.19; found C 39.1, H 5.9, N 1.2.

(COT)Sm(μ-I)₂{μ-N(SiHMe₂)₂}Sm(COT)[Li(thf)₄] (3b): Compound **1c** (100 mg, 0.17 mmol) and Li[N(SiHMe₂)₂] (23 mg, 0.17 mmol) yielded dark purple crystals (88 mg, 0.07 mmol, 87%).

¹H NMR (600 MHz, C₆D₆, 25 °C): δ = 13.31 (br. s, COT), 10.43 (s), 10.38 (s), 9.63 (s), 3.62 (s, thf), 1.33 (s, thf), 0.06, −0.67 (SiHMe₂) ppm. ¹³C{¹H} NMR (150.9 MHz, C₆D₆, 25 °C): δ = 82.2 (COT), 68.4 (thf), 30.0 (SiHMe₂), 25.3 (thf) ppm. IR: ν_{max} = 2027 {s [v(SiH)]}, 1244 (s), 1040 [vs (thf)], 934 (w), 884 (vs), 842 (w), 761 (w), 697 (vs) cm^{−1}. C₃₆H₆₂I₂LiNO₄Si₂Sm₂·(C₄H₈O)₂ (1334.74): calcd. C 39.59, H 5.89, N 1.05; found C 39.8, H 5.7, N 1.1.

(COT)La(μ-I)[μ-N(SiHMe₂)₂]La[μ-(η²:η⁸-COT)]Li(thf)₃ (4): Compound **1a** (81 mg, 0.14 mmol) and Li[N(SiHMe₂)₂] (19 mg, 0.14 mmol) gave yellow crystals (103 mg, 0.09 mmol, 92%). ¹H NMR (300 MHz, [D₈]thf, 25 °C): δ = 5.71 (s, 16 H, COT), 4.46 (s, 4 H, SiHMe₂), 3.58 (s, thf), 1.72 (s, thf), 0.11 (s, 24 H, SiHMe₂) ppm. ¹³C{¹H} NMR (75 MHz, C₆D₆, 25 °C): could not be performed; after 30 min, a precipitate formed. IR: ν_{max} = 2056 {s [v(SiH)]}, 1249 (s), 1045 [vs (thf)], 886 (s), 839 (w), 764 (w), 727 (w), 694 (vs) cm^{−1}. C₃₆H₆₈ILa₂LiN₂O₃Si₄ (1100.95): calcd. C 39.27, H 6.23, N 2.54; found C 40.9, H 7.0, N 2.1.

(COT)Ln[μ-(η²:η⁸-COT)]Li(thf)₃ (5). Route I: Crystalline **3** or **4** were dissolved in thf, filtered, and stored at −35 °C. After several

Table 4. Crystallographic data for (COT)LnI(thf)₃ (**1a,b,c**), [(COT)La(μ-I)(thf)₂]₂ (**2**), [(COT)Ln(μ-I)₂{μ-N(SiHMe₂)₂}Ln(COT)][Li(thf)₄] (**3a,b**), (COT)La(μ-I)[μ-N(SiHMe₂)₂]La[μ-(η²:η⁸-COT)]Li(thf)₃ (**4**), (COT)Ln[μ-(η²:η⁸-COT)]Li(thf)₃ (**5a,b**), and (COT)La[LiN(SiHMe₂)₂](thf)₂ (**6**).

| | 1a | 1b | 1c | 2 | 3a |
|--|---|---|--|---|--|
| Empirical formula | C ₂₀ H ₃₂ ILaO ₃ | C ₂₀ H ₃₂ INdO ₃ | C ₂₀ H ₃₂ IO ₃ Sm | C ₃₂ H ₄₈ I ₂ La ₂ O ₄ | C ₃₆ H ₆₂ I ₂ LiN ₂ Nd ₂ O ₄ Si ₂ |
| <i>M_r</i> | 586.27 | 597.71 | 597.71 | 1028.32 | 1178.27 |
| Space group | <i>Pbca</i> | <i>Pbca</i> | <i>Pbca</i> | <i>P2₁/n</i> | <i>Pbca</i> |
| <i>a</i> [Å] | 13.0432(12) | 12.963(2) | 12.9619(11) | 12.4197(4) | 20.3399(8) |
| <i>b</i> [Å] | 14.9571(14) | 14.983(2) | 14.9828(12) | 12.5340(4) | 19.1121(7) |
| <i>c</i> [Å] | 22.260(2) | 22.010(4) | 21.8118(19) | 12.6805(4) | 22.7626(8) |
| <i>α</i> [°] | 90 | 90 | 90 | 90 | 90 |
| <i>β</i> [°] | 90 | 90 | 90 | 115.895(1) | 90 |
| <i>γ</i> [°] | 90 | 90 | 90 | 90 | 90 |
| <i>V</i> [Å ³] | 4342.6(7) | 4274.9(12) | 4236.0(6) | 1775.76(10) | 8848.7(6) |
| <i>Z</i> | 8 | 8 | 8 | 2 | 8 |
| Crystal size [mm] | 0.21 × 0.21 × 0.19 | 0.50 × 0.30 × 0.05 | 0.20 × 0.20 × 0.10 | 0.43 × 0.41 × 0.18 | 0.25 × 0.17 × 0.08 |
| Color | colorless | green | purple | colorless | green |
| <i>F</i> (000) | 2288 | 2312 | 2328 | 984 | 4592 |
| <i>T</i> [K] | 120(1) | 120(2) | 120(1) | 123(2) | 100(2) |
| ρ _{calcd.} [g cm ^{−3}] | 1.793 | 1.838 | 1.874 | 1.923 | 1.769 |
| μ [mm ^{−1}] | 3.405 | 3.888 | 4.245 | 4.143 | 3.805 |
| <i>R</i> ₁ ^[a] [<i>I</i> > 2σ(<i>I</i>)], <i>wR</i> ₂ ^[b] (all) | 0.0447, 0.0682 | 0.0436, 0.1134 | 0.0304, 0.0807 | 0.0169, 0.0394 | 0.0392, 0.0673 |
| <i>S</i> ^[c] | 1.135 | 1.060 | 1.064 | 1.176 | 1.166 |

| | 3b | 4 | 5a | 5b | 6 |
|--|--|--|--|--|---|
| Empirical formula | C ₃₆ H ₆₂ I ₂ LiNO ₄ Si ₂ Sm ₂ | C ₃₆ H ₆₈ ILa ₂ LiN ₂ O ₃ Si ₄ | C ₂₈ H ₄₀ LaLiO ₃ | C ₂₈ H ₄₀ LiNdO ₃ | C ₂₀ H ₃₈ LaNO ₂ Si ₂ |
| <i>M_r</i> | 1190.49 | 1100.94 | 570.45 | 575.78 | 519.60 |
| Space group | <i>Pbca</i> | <i>P2₁/c</i> | <i>P</i> $\bar{1}$ | <i>P2₁/n</i> | <i>P</i> $\bar{1}$ |
| <i>a</i> [Å] | 20.3315(6) | 13.0810(7) | 8.9189(7) | 8.8150(4) | 8.5370(2) |
| <i>b</i> [Å] | 19.0972(6) | 19.8530(11) | 10.9399(9) | 13.8796(6) | 9.9399(3) |
| <i>c</i> [Å] | 22.6082(7) | 18.4810(11) | 14.0126(11) | 21.1407(9) | 15.3037(6) |
| <i>α</i> [°] | 90 | 90 | 85.604(1) | 90 | 88.077(1) |
| <i>β</i> [°] | 90 | 113.969(3) | 89.131(2) | 95.355(1) | 89.349(1) |
| <i>γ</i> [°] | 90 | 90 | 72.296(2) | 90 | 69.969(1) |
| <i>V</i> [Å ³] | 8778.2(5) | 4605.8(4) | 1298.6(2) | 2575.2(2) | 1219.38(7) |
| <i>Z</i> | 8 | 4 | 2 | 4 | 2 |
| Crystal size [mm] | 0.50 × 0.17 × 0.09 | 0.30 × 0.30 × 0.10 | 0.25 × 0.10 × 0.03 | 0.47 × 0.43 × 0.15 | 0.42 × 0.38 × 0.10 |
| Color | purple | yellow | pale yellow | yellow | colorless |
| <i>F</i> (000) | 4624 | 2192 | 584 | 1180 | 532 |
| <i>T</i> [K] | 123(2) | 120(2) | 123(2) | 123(2) | 103(2) |
| ρ _{calcd.} [g cm ^{−3}] | 1.802 | 1.588 | 1.459 | 1.485 | 1.415 |
| μ [mm ^{−1}] | 4.145 | 2.637 | 1.671 | 2.042 | 1.863 |
| <i>R</i> ₁ ^[a] [<i>I</i> > 2σ(<i>I</i>)], <i>wR</i> ₂ ^[b] (all) | 0.0256, 0.0493 | 0.0467, 0.1130 | 0.0668, 0.1691 | 0.0527, 0.1470 | 0.0359, 0.0904 |
| <i>S</i> ^[c] | 1.102 | 1.1043 | 1.071 | 1.153 | 1.057 |

[a] *R*₁ = Σ(|*F*_o| − |*F*_c|)/Σ|*F*_o|. [b] *wR*₂ = {Σ[*w*(*F*_o² − *F*_c²)²]/Σ[*w*(*F*_o²)²]}^{1/2}. [c] *S* = [Σ*w*(*F*_o² − *F*_c²)²/(*n*_o − *n*_p)]^{1/2}.

days, crystals formed, which were characterized as **5**. **Route II**: The crude oily reaction mixtures that were received after evaporation of the solvents in the synthesis of **3** and **4** were stored at -35°C . Addition of toluene favored crystallization, and crystalline **5** could be harvested from thf/toluene solutions in the course of one week.

(COT)La[μ -(η^2 : η^8 -COT)]Li(thf)₃ (5a**):** Previous synthesis and characterization by Wayda.^[44] In this work synthesized according to route II. **1a** (85 mg, 0.15 mmol) and Li[N(SiHMe₂)₂] (20 mg, 0.15 mmol) gave yellow crystals (first batch: 22 mg, 0.04 mmol, 27%).

(COT)Nd[μ -(η^2 : η^8 -COT)]Li(thf)₃ (5b**):** Synthesized according to route II. Compound **1b** (94 mg, 0.18 mmol) and Li[N(SiHMe₂)₂] (25 mg, 0.18 mmol) yielded yellow, slightly greenish crystals (first batch: 18 mg, 0.03 mmol, 17%). ¹H NMR (600 MHz, [D₈]thf, 25°C): δ = 12.27 (s), -9.22 (br. s) ppm. ¹³C{¹H} NMR (150.9 MHz, [D₈]thf, 25°C): δ = 127.5 ppm. IR: $\tilde{\nu}_{\text{max}}$ = 1267 (w), 1037 (m), 799 (s), 670 (s), 627 (m) cm⁻¹. Satisfactory elemental analysis could not be obtained.

(COT)Sm[μ -(η^2 : η^8 -COT)]Li(thf)₃ (5c**):** Previous synthesis and characterization by Roesky et al.^[11] In this work synthesized according to route I. Compound **3b** (79 mg, 0.67 mmol) produced yellow crystals (first batch: 32 mg, 0.05 mmol, 16%).

(COT)La[N(SiHMe₂)₂](thf)₂ (6**):** Compound **1a** (196 mg, 0.33 mmol) was dissolved in thf (4 mL), and 1 equiv. of K[N(SiHMe₂)₂] (57 mg, 0.33 mmol) was added. The suspension was stirred at ambient temperature for 24 h, filtered, and the solvent was removed under vacuum. The received crude pale yellow product (162 mg, 0.31 mmol, 94%) was dissolved in thf and stored at -35°C . Pale yellow, almost colorless crystals were obtained after 2 d (123 mg, 0.24 mmol, 72%). ¹H NMR (400 MHz, [D₈]thf, 25°C): δ = 6.24 (s, 8 H, COT), 4.25 (sept, ³J_{HH} = 3.2 Hz, 2 H, SiHMe₂), 3.54 (s, thf), 1.69 (s, thf), 0.55 (s, ³J_{HH} = 3.2 Hz, 12 H, SiHMe₂) ppm. ¹³C{¹H} NMR (75 MHz, [D₈]thf, 25°C): δ = 97.7 (COT), 68.4 (thf), 26.6 (thf), 3.6 (SiHMe₂) ppm. IR: $\tilde{\nu}_{\text{max}}$ = 2022 {br. s [v(SiH)]}, 1822 (w), 1715 (w), 1573 (w), 1340 (w), 1239 (m), 1074 (m), 1029 (m), 890 (m), 764 (m), 671 (m), 580 (w), 512 (w) cm⁻¹. C₂₀H₃₈LaNO₂Si₂ (519.61): calcd. C 46.23, H 7.37, N 2.70; found C 47.3, H 7.2, N 2.0.

Crystallography: Crystals of **1a**, **1b**, **1c**, **3a**, **3b**, and **4** were grown by standard techniques from saturated solutions using thf at ambient temperature. Crystals of **2**, **5a**, **5b**, and **6** were grown from saturated thf solutions at -35°C . Suitable single crystals of **2**, **3a**, **3b**, **5a**, **5b**, **6** were selected in a glovebox, coated with Paratone-N, fixed in a nylon loop, and measured with a Bruker SMART 2 K CCD diffractometer. Crystals of compounds **1b** and **4** were coated with mineral oil and fixed in a nylon loop, whereas **1a** and **1c** were fixed on the end of glass fibers with white Vaseline. **1a**–**c**, and **4** were measured with a Rigaku RAXIS-RAPID image plate area detector diffractometer. All data were collected by using graphite-monochromated Mo-K α radiation (λ = 0.71073 Å). Raw data were reduced and scaled with programs SAINT^[58] and R-Axis RAPID.^[59] Corrections for absorption effects were applied by using SHELXTL^[60] and ABSCOR.^[61] The structures were solved by a combination of direct methods (SHELXS^[62] and SIR92^[63]) and difference Fourier syntheses (SHELXL-97^[62]). Final model refinement was carried out by using SHELXL-97.^[62] All plots were generated by using the program ORTEP-3.^[64] Further details of the refinement and crystallographic data are listed in Table 4. CCDC-692858 (**1a**), -692859 (**1b**), -692860 (**1c**), -692861 (**2**), -692862 (**3a**), -692863 (**3b**), -692864 (**4**), -692865 (**5a**), -692866 (**5b**), -703164 (**6**) contain the supplementary crystallographic data for this paper. These data can be obtained free of charge from The Cambridge

Crystallographic Data Centre via www.ccdc.cam.ac.uk/datarequest/cif.

Acknowledgments

C. M. thanks the Japan Society for the Promotion of Science (JSPS) for a visiting stipend and A. Shima for assisting with the crystal measurements. We are also grateful to the program NANO-SCIENCE@UiB for generous support.

- [1] W. J. Evans, R. D. Clark, M. A. Ansari, J. W. Ziller, *J. Am. Chem. Soc.* **1998**, *120*, 9555–9563.
- [2] P. Poremba, F. T. Edelmann, *J. Organomet. Chem.* **1998**, *553*, 393–395.
- [3] F. T. Edelmann, *Angew. Chem. Int. Ed. Engl.* **1995**, *34*, 2466–2488.
- [4] H. Schumann, J. Winterfeld, L. Esser, G. Kociok-Köhn, *Angew. Chem. Int. Ed. Engl.* **1993**, *32*, 1208–1210.
- [5] G. W. Rabe, M. Zhang-Presse, F. A. Riederer, J. A. Golen, C. D. Incarvito, A. L. Rheingold, *Inorg. Chem.* **2003**, *42*, 7587–7592.
- [6] U. Kilimann, M. Schäfer, R. Herbst-Irmer, F. T. Edelmann, *J. Organomet. Chem.* **1994**, *469*, C15–C18.
- [7] H. Schumann, J. Winterfeld, F. H. Görlitz, J. Pickardt, *J. Chem. Soc., Chem. Commun.* **1993**, 623–625.
- [8] M. Visseaux, A. Dormond, D. Barbier-Baudry, *Eur. J. Inorg. Chem.* **1999**, 1827–1830.
- [9] K. Mashima, H. Takaya, *Tetrahedron Lett.* **1989**, *30*, 3697–3700.
- [10] U. Kilimann, M. Schäfer, R. Herbst-Irmer, F. T. Edelmann, *J. Organomet. Chem.* **1994**, *469*, C10–C14.
- [11] T. G. Wetzel, S. Dehnen, P. W. Roesky, *Organometallics* **1999**, *18*, 3835–3842.
- [12] P. W. Roesky, *J. Organomet. Chem.* **2001**, *621*, 277–283.
- [13] P. W. Roesky, M. T. Gamer, N. Marinos, *Chem. Eur. J.* **2004**, *10*, 3537–3542.
- [14] A. Zulus, T. K. Panda, M. T. Gamer, P. W. Roesky, *Chem. Commun.* **2004**, 2584–2585.
- [15] G. W. Rabe, M. Zhang-Presse, F. A. Riederer, C. D. Incarvito, J. A. Golen, A. L. Rheingold, *Acta Crystallogr., Sect. E* **2004**, *60*, m1442–m1443.
- [16] G. W. Rabe, M. Zhang-Presse, F. A. Riederer, C. D. Incarvito, J. A. Golen, A. L. Rheingold, *Acta Crystallogr., Sect. E* **2004**, *60*, m1389–m1390.
- [17] G. W. Rabe, A. L. Rheingold, private communication, **2006**, CCDC-627345.
- [18] G. W. Rabe, M. Zhang-Presse, J. A. Golen, A. L. Rheingold, *Acta Crystallogr., Sect. E* **2003**, *59*, m255–m256.
- [19] J. Jin, Z. Jin, G. Wei, W. Chen, Y. Zhang, *Chin. J. Inorg. Chem.* **1993**, *9*, 326–329.
- [20] S. Anfang, G. Seybert, K. Harms, G. Geiseler, W. Massa, K. Dehnicke, *Z. Anorg. Allg. Chem.* **1998**, *624*, 1187–1192.
- [21] G.-Z. Qi, Y.-H. Lin, S.-C. Jin, Q. Shen, *Gov. Rep. Announce. (U.S.)* **1995**, 95.
- [22] P. Poremba, U. Reissmann, M. Noltemeyer, H.-G. Schmidt, W. Bruser, F. T. Edelmann, *J. Organomet. Chem.* **1997**, *544*, 1–6.
- [23] T. G. Wetzel, P. W. Roesky, *Organometallics* **1998**, *17*, 4009–4013.
- [24] K. O. Hodgson, K. N. Raymond, *Inorg. Chem.* **1972**, *11*, 3030–3035.
- [25] S. A. Kinsley, A. Streitwieser, A. Zalkin, *Organometallics* **1985**, *4*, 52–57.
- [26] T. R. Boussie, D. C. Eisenberg, J. Rigsbee, A. Streitwieser, A. Zalkin, *Organometallics* **1991**, *10*, 1922–1928.
- [27] J. Xia, Z. Jin, W. Chen, *J. Chem. Soc., Chem. Commun.* **1991**, 1214–1215.
- [28] J. Xia, X. Zhuang, Z. Jin, W. Chen, *Polyhedron* **1996**, *15*, 3399–3403.

- [29] S. M. Cendrowski-Guillaume, G. Le Gland, M. Nierlich, M. Ephritikhine, *Organometallics* **2000**, *19*, 5654–5660.
- [30] V. Lorenz, A. Edelmann, S. Blaurock, F. Freise, F. T. Edelmann, *Organometallics* **2007**, *26*, 4708–4710.
- [31] V. Lorenz, A. Edelmann, S. Blaurock, F. Freise, F. T. Edelmann, *Organometallics* **2007**, *26*, 6681–6683.
- [32] H. Schumann, J. Winterfeld, H. Hemling, E. E. Hahn, P. Reich, K.-W. Brzezinka, F. T. Edelmann, U. Kilimann, R. Herbst-Irmer, *Chem. Ber.* **1995**, *128*, 395–404.
- [33] T. K. Panda, A. Zulys, M. T. Gamer, P. W. Roesky, *Organometallics* **2005**, *24*, 2197–2202.
- [34] T. K. Panda, P. Benndorf, P. W. Roesky, *Z. Anorg. Allg. Chem.* **2005**, *631*, 81–84.
- [35] C. Meermann, G. Gerstberger, M. Spiegler, K. W. Törnroos, R. Anwender, *Eur. J. Inorg. Chem.* **2008**, 2014–2023.
- [36] M. G. Klimpel, H. W. Görlitzer, M. Tafipolsky, M. Spiegler, W. Scherer, R. Anwender, *J. Organomet. Chem.* **2002**, *647*, 236–244.
- [37] J. Eppinger, M. Spiegler, W. Heringer, W. A. Herrmann, R. Anwender, *J. Am. Chem. Soc.* **2000**, *122*, 3080–3096.
- [38] W. A. Herrmann, J. Eppinger, M. Spiegler, O. Runte, R. Anwender, *Organometallics* **1997**, *16*, 1813–1815.
- [39] W. A. Herrmann, F. C. Munck, G. R. J. Artus, O. Runte, R. Anwender, *Organometallics* **1997**, *16*, 682–688.
- [40] R. Anwender, O. Runte, J. Eppinger, G. Gerstberger, E. Herdtweck, M. Spiegler, *J. Chem. Soc., Dalton Trans.* **1998**, 847–858.
- [41] K. Mashima, Y. Nakayama, A. Nakamura, N. Kanehisa, Y. Kai, H. Takaya, *J. Organomet. Chem.* **1994**, *473*, 85–91.
- [42] I. L. Fedushkin, M. N. Bochkarev, S. Dechert, H. Schumann, *Chem. Eur. J.* **2001**, *7*, 3558–3563.
- [43] K. O. Hodgson, F. Mares, D. F. Starks, A. Streitwieser, *J. Am. Chem. Soc.* **1973**, *95*, 8650–8658.
- [44] A. L. Wayda, *Organometallics* **1983**, *2*, 565–566.
- [45] H. Schumann, R. D. Kohn, F.-W. Reier, A. Dietrich, J. Pickardt, *Organometallics* **1989**, *8*, 1388–1392.
- [46] S. D. Stults, R. A. Andersen, A. Zalkin, *Organometallics* **1990**, *9*, 115–122.
- [47] K. O. Hodgson, K. N. Raymond, *Inorg. Chem.* **1972**, *11*, 171–175.
- [48] J.-S. Xia, Z.-S. Jin, G.-C. Wei, W.-Q. Chen, *Chin. J. Struct. Chem.* **1992**, *11*, 113–117.
- [49] M. Visseaux, F. Nief, L. Ricard, *J. Organomet. Chem.* **2002**, *647*, 139–144.
- [50] J. Collin, N. Giuseppone, N. Jaber, A. Domingos, L. Maria, I. Santos, *J. Organomet. Chem.* **2001**, *628*, 271–274.
- [51] H. Schumann, M. Glanz, J. Winterfeld, H. Hemling, *J. Organomet. Chem.* **1993**, *456*, 77–83.
- [52] Q. Liu, X. Shen, J. Huang, Y. Qian, A. S.-C. Chan, W.-T. Wong, *Polyhedron* **2000**, *19*, 453–456.
- [53] C. Meermann, K. W. Törnroos, W. Nerdal, R. Anwender, *Angew. Chem. Int. Ed.* **2007**, *46*, 6508–6513.
- [54] G. W. Rabe, G. P. A. Yap, *Z. Kristallogr. – New Cryst. Struct.* **2000**, *215*, 457–458.
- [55] H. F. Yuen, T. J. Marks, *Organometallics* **2008**, *27*, 155–158.
- [56] G. B. Deacon, A. Gitlits, P. W. Roesky, M. R. Bürgstein, K. C. Lim, B. W. Skelton, A. H. White, *Chem. Eur. J.* **2001**, *7*, 127–138.
- [57] J. Eppinger, E. Herdtweck, R. Anwender, *Polyhedron* **1998**, *17*, 1195–1201.
- [58] Bruker, *SAINT, Area detector control and data integration and reduction software*, Bruker Analytical X-ray Instruments Inc., Madison, WI, USA, **2005**.
- [59] Rigaku, *R-Axis RAPID, Diffractometer Control Software*, Rigaku Corporation, Tokyo, Japan, **2001**.
- [60] G. M. Sheldrick, *SHELXTL*, version 6.10, Bruker-AXS, Madison, WI, **2001**.
- [61] T. Higashi, *ABSCOR*, Rigaku Corporation, Tokyo, Japan, **1995**.
- [62] G. M. Sheldrick, *Acta Crystallogr., Sect. A* **2008**, *64*, 112–122.
- [63] A. Altomare, G. Casciarano, C. Giacovazzo, A. Guagliardi, *J. Appl. Crystallogr.* **1993**, *26*, 343–350.
- [64] L. J. Farrugia, *J. Appl. Crystallogr.* **1997**, *30*, 565–566.

Received: June 16, 2008

Published Online: November 13, 2008

From Molecular to Nanostructured Iron Complexes of Amphiphilic Chelators Based on 8-Hydroxyquinoline Subunits – Evidence of Self-Assembled Edifices Mimicking Siderophores from Marine Bacteria

Jérémy Brandel,^[a] Stéphane Torelli,^{*[a]} Gisèle Gellon,^[a] Guy Serratrice,^[a] Jean-Luc Putaux,^[b] and Jean-Louis Pierre^[a]

Keywords: Iron / Amphiphiles / Chelates / Nanostructures / Self-assembly

Amphiphilic iron chelators based on the 8-hydroxyquinoline moiety were synthesized in order to study their potential trend to aggregate into more complex structures. The Q^{S10} and Q^{S4} ligands only differ by the length of the lipophilic alkyl chain (C10 and C4, respectively) tethered to the chelating subunit. Physicochemical investigations in aqueous solution were performed to determine the global stability constants of the iron complexes. At physiological pH, the [Fe(Q^{S10})₃]^{3–} predominant species undergoes time-dependent reorganization, as evidenced by cryogenic transmission electron microscopy: after a few hours of equilibration, iron-

rich micelles arranged in large clustered structures were observed, whereas after several days complexes were assembled into nanospheres with typical diameters of 100 to 200 nm. This pattern is different from the previous reported amphiphilic catechol derivative and highlights the importance of the nature of the chelating subunit and the residual charge on the type of aggregates formed. These results are relevant to mimic the properties of siderophores from marine bacteria.

(© Wiley-VCH Verlag GmbH & Co. KGaA, 69451 Weinheim, Germany, 2009)

Introduction

Siderophores are low-molecular-weight, iron-chelating agents excreted by microorganisms to render iron soluble in the environment and favor its uptake.^[1] In contrast to the abundance of iron in terrestrial environments, iron concentrations in the ocean surface waters are low enough to limit the growth of marine photosynthetic microorganisms (and consequently of phytoplankton, which reduces atmospheric carbon dioxide levels). Butler and coworkers recently evidenced a noteworthy process that promotes high local iron concentrations: amphiphilic siderophores involving polar peptidic head groups and hydrophobic fatty acid tails are produced by marine bacteria. The amphiphilic surface-active nature of these siderophores leads to the formation of self-assembled structures.^[2–5] In previous papers, we described the self-assembling properties of amphiphilic iron complexes involving catechol subunits^[6,7] (Scheme 1). These ligands appeared to be good models for the physicochemical properties of siderophores from marine bacteria. Even

if almost all the natural siderophores contain a hydroxamic acid, catechol, and/or α -hydroxycarboxylic acid metal-binding group,^[8] synthetic iron chelators based on 8-hydroxyquinoline chelating subunits have been described and exhibit promising properties in iron-chelating therapy as well as in iron nutrition.^[9] In this paper, we report the preparation and characterization of new amphiphilic iron chelators based on 8-hydroxyquinoline chelating subunits (Q^{S10} and Q^{S4}, Scheme 1) and their self-assembling properties. Owing to the uncharged character of a tris(bidentate) complex with hydroxyquinolinolate chelating units, the ligands have been sulfonated to allow water solubility. They are compared to siderophores known from marine bacteria as well as to synthetic analogues involving catechol chelating moieties.

Results and Discussion

Synthesis

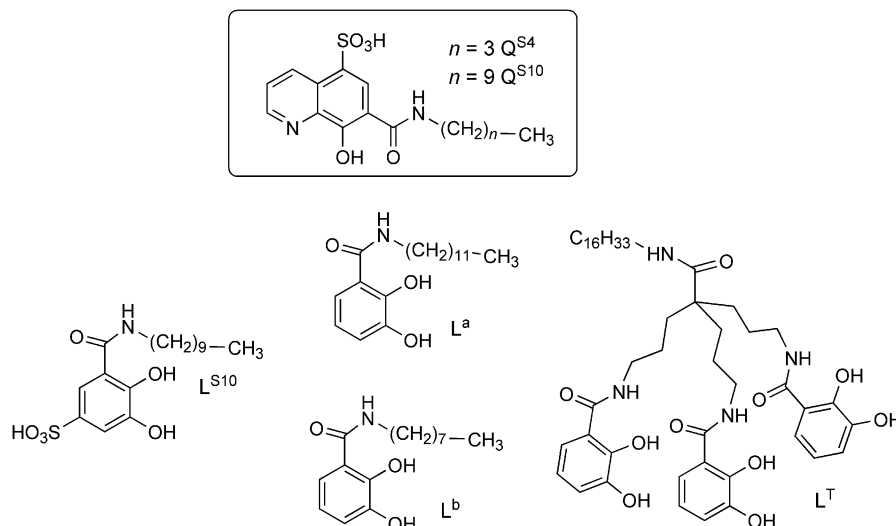
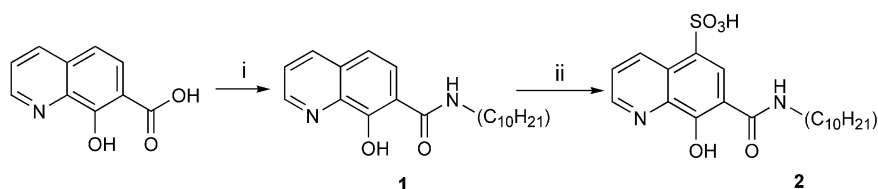
The synthetic route to Q^{S10} (Scheme 2) is relatively straightforward. The first step consists of the condensation of the CDI-activated carboxylic acid derived from 8-hydroxyquinoline with the corresponding decylamine. Then, contrarily to previous reported procedures (which employed 20 mol-% of oleum^[10–12]), the desired sulfonated derivative (Figure S1, Supporting Information) was isolated in good yield by using chlorosulfonic acid.^[13]

[a] Département de Chimie Moléculaire UMR-5250, ICMG FR-2607 CNRS, Université Joseph Fourier, B. P. 53X, 38041 Grenoble Cedex 9, France
Fax: +33-4-76514836

E-mail: Stephane.torelli@ujf-grenoble.fr

[b] Centre de Recherches sur les Macromolécules Végétales (CERMAV) CNRS, ICMG FR-2607, affiliated with Université Joseph Fourier
B. P. 53X, 38041 Grenoble Cedex 9, France

Supporting information for this article is available on the WWW under <http://www.eurjic.org> or from the author.

Scheme 1. Q^{S10} and Q^{S4} ligands (frame) used in this work and catechol derivatives previously reported (see text).Scheme 2. Reagents and conditions: (i) thf, carbonyldiimidazole, then 1-decylamine (85%); (ii) ClSO_3H (72%).

Ligand pK_a Determination

The deprotonation constants of Q^{S10} (Figure 1) were determined by spectrophotometric titration according to the observed spectral changes in the range $1.83 < \text{pH} < 9.04$.

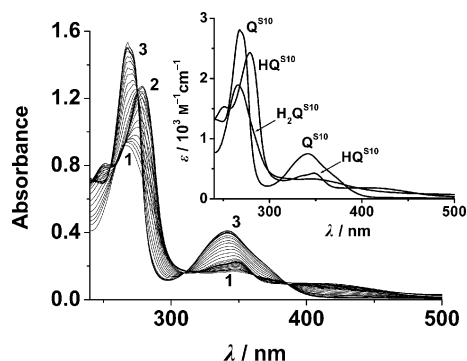
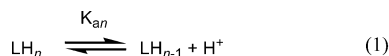


Figure 1. Spectrophotometric titration of Q^{S10} versus pH: (1) pH = 1.83; (2) pH = 4.21; (3) pH = 9.04. $[Q^{S10}]_{\text{tot}} = 5.50 \times 10^{-5} \text{ M}$. Insert: Electronic spectra of the participating species, solvent: H_2O , $T = 25.0(2)^\circ\text{C}$, $I = 0.1 \text{ M NaClO}_4$.

The sulfonate group is a moderately strong acid ($pK_a < 2$) and is considered deprotonated under our experimental conditions. Data analysis performed with the Specfit^[14] program by using Equations (1) and (2) yielded the values: $pK_{a1} = 6.77(1)$ and $pK_{a2} = 2.60(3)$. pK_a values for Q^{S4} were published elsewhere:^[15] $pK_{a1} = 6.80$ and $pK_{a2} = 2.80$.



$$K_{an} = \frac{[\text{LH}_{n-1}][\text{H}^+]}{[\text{LH}_n]} \quad (2)$$

pK_{a1} is assigned to the hydroxy proton and pK_{a2} to the pyridine nitrogen proton. These values are lower than those of other sulfonated 8-hydroxyquinoline derivatives, because of the electron-withdrawing character of the carbonyl group, which increases the mobility of the leaving protons.^[16] No noticeable differences are observed for the pK_a values determined for both molecules, indicating an insignificant effect of the alkyl chain.

Fe^{III} Complex Formation

Metal complexation equilibria were studied by UV/Vis spectrophotometry. Ferric complexes of Q^{S10} were titrated over the pH range 2.11–7.71 due to low solubility at pH < 2 (presumably related to a marked hydrophobic character) and over the pH range 0.0–4.3 for Q^{S4} . Spectral changes are depicted in Figure 2 for Q^{S10} and in Figure S2 (Supporting Information) for Q^{S4} .

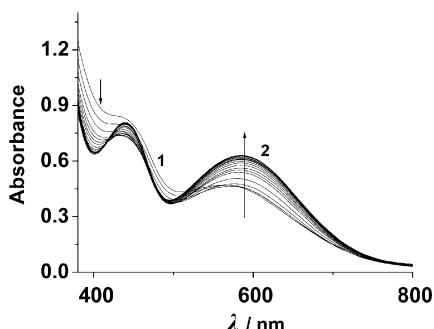


Figure 2. UV/Vis absorption spectra of a Fe^{3+} - $\text{Q}^{\text{S}10}$ mixture from (1) pH = 2.11 to (2) pH = 7.71. $[\text{Q}^{\text{S}10}]_{\text{tot}} = 5.69 \times 10^{-4}$ M, $[\text{Fe}^{3+}]_{\text{tot}} = 1.8 \times 10^{-4}$ M, solvent: H_2O , $I = 0.1$ M (NaClO_4), $T = 25.0(2)^\circ\text{C}$.

Concerning $\text{Q}^{\text{S}4}$, we observed, when raising the pH from 0 to 1, the growing of two bands at 440 and 550 nm, and then from pH = 1 to 4 a bathochromic shift of the latter band to 590 nm. Then, no spectral changes were observed until pH = 8. Analysis of the spectrophotometric data with the Specfit program^[14] by considering the $[\text{FeQ}^{\text{S}4}\text{H}]^{2+}$, $[\text{Fe}(\text{Q}^{\text{S}4})_2\text{H}]$, and $[\text{Fe}(\text{Q}^{\text{S}4})_3]^{3-}$ species gave the best fit (Table S1, Supporting Information). For $\text{Q}^{\text{S}10}$, the spectral changes are very similar to those for $\text{Q}^{\text{S}4}$ at pH > 2. The formation of the ferric complex is complete at pH 2.11 and its equilibrium constant cannot be determined. Because the spectrum is very close to that of $[\text{Fe}(\text{Q}^{\text{S}4})_2\text{H}]$ and by assuming a similar behavior for $\text{Fe}^{\text{III}}\text{-Q}^{\text{S}10}$ and $\text{Fe}^{\text{III}}\text{-Q}^{\text{S}4}$ toward complexation, data were refined by the Specfit program by considering the formation of the $[\text{Fe}(\text{Q}^{\text{S}10})_2\text{H}]$ species at pH 2.11 with the same stability constant as that for $[\text{Fe}(\text{Q}^{\text{S}4})_2\text{H}]$. This method allowed us to determine the species present over the pH range 2.11–7.71 and to estimate the formation constants. The best fit was obtained by considering the formation of $[\text{Fe}(\text{Q}^{\text{S}10})_2]^-$ and $[\text{Fe}(\text{Q}^{\text{S}10})_3]^{3-}$. The global stability constants of the $\text{Q}^{\text{S}10}$ ferric complexes β_{mlh} , which are defined by Equations (3) and (4), are reported in Table 1.



$$\beta_{\text{mlh}} = [\text{Fe}_m\text{L}_l\text{H}_h] / [\text{Fe}^{3+}]^m [\text{L}^{2-}]^l [\text{H}^+]^h \quad (4)$$

Table 1. Equilibrium constants $\log \beta_{\text{mlh}}$ and UV/Vis data determined in this work.^[a]

| <i>mlh</i> | $\log \beta_{\text{mlh}}$ | λ / nm (ϵ , $10^3 \text{ M}^{-1} \text{ cm}^{-1}$) |
|--|---------------------------|---|
| $[\text{Fe}(\text{Q}^{\text{S}10})_2\text{H}]$ | 23.1(1) ^[b] | 436 (5.15), 546 (2.84) |
| $[\text{Fe}(\text{Q}^{\text{S}10})_2]^-$ | 20.71(5) ^[b] | 452 (2.59), 583 (2.67) |
| $[\text{Fe}(\text{Q}^{\text{S}10})_3]^{3-}$ | 28.26(5) ^[b] | 441 (5.07), 585 (4.17) |
| $[\text{Fe}(\text{Q}^{\text{S}10})_2(\text{OH})_2]^{3-}$ | 5.84(5) ^[b,c] | 418 (5.24), 550 (2.49) |

[a] Solvent: H_2O , $I = 0.1$ M (NaClO_4), $T = 25.0(2)^\circ\text{C}$. [b] Data were also analyzed by the Letagrop-Spefo program and gave the same values: 23.1(1), 20.7(2), 28.2(2), and 5.75(10) for the four complexes.^[17] [c] See Supporting Information.

The spectral characteristics of $[\text{Fe}(\text{Q}^{\text{S}10})_2\text{H}]$ at pH 2.11 are in agreement with a salicylate (that involves the oxygen atoms from the carboxyl and *ortho*-hydroxy groups)/8-hydroxyquinolate (that involves the pyridine nitrogen atom and the *ortho*-hydroxy oxygen atom) coordination by com-

parison with previous studies performed on O-TRENDOX (tripodal 8-hydroxyquinoline ligand^[18]). Spectra for $[\text{Fe}(\text{Q}^{\text{S}10})_2]^-$ and $[\text{Fe}(\text{Q}^{\text{S}10})_3]^{3-}$ are in agreement with bis(8-hydroxyquinolate) and tris(8-hydroxyquinolate) coordination, respectively, by comparison with $\text{Fe}(\text{O-TRENDOX})$ and with $\text{Fe}(\text{8-hydroxy-5-sulfonated quinoline; named sulfoxine})$.^[19] As expected, the change from salicylate coordination to sulfoxinate coordination for the formation of $[\text{Fe}(\text{Q}^{\text{S}10})_2]^-$ induces a large hypochromic effect of ϵ for the band at 436 nm and a slight bathochromic shift for the band at 546 nm. It should be noted that the ϵ values are slightly lower than those reported for the complexes with the preorganized O-TRENDOX and with the sulfoxine. From pH 7.7 to 10, a decrease in absorbance of both bands at 442 and 585 nm accompanied by a hypsochromic shift of the latter was observed, together with an isosbestic point at 430 nm (Figure S3, Supporting Information). This trend is assigned to the loss of a $\text{Q}^{\text{S}10}$ ligand leading to hydroxido $[\text{Fe}(\text{Q}^{\text{S}10})_2(\text{OH})_2]^{3-}$ complexes, as confirmed by fitting of the data with Specfit and Letagrop-Spefo. The stability constants allowed the calculation of the species electronic spectra (Figure 3a; Figure S3, Supporting Information) together with the distribution diagram within our pH scale (Figure 3b) and highlighted that $[\text{Fe}(\text{Q}^{\text{S}10})_3]^{3-}$ is the predominant species at physiological pH.

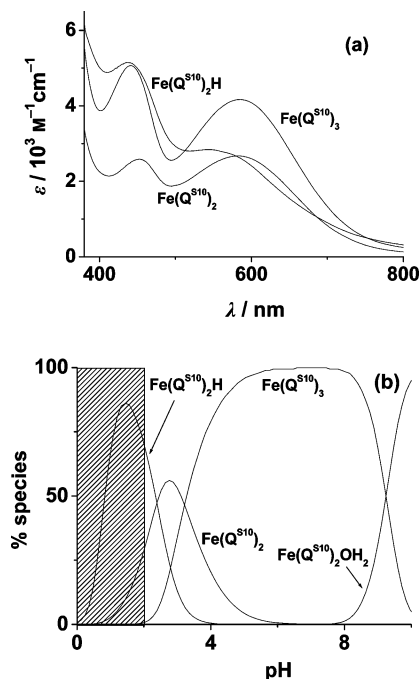


Figure 3. (a) Calculated electronic spectra of the identified complexes; (b) distribution diagram of the participating species; $[\text{Q}^{\text{S}10}]_{\text{tot}} = 5.69 \times 10^{-4}$ M, $[\text{Fe}^{3+}]_{\text{tot}} = 1.80 \times 10^{-4}$ M, solvent: H_2O , $T = 25.0(2)^\circ\text{C}$, $I = 0.1$ M (NaClO_4). The shaded region corresponds to precipitation.

The 1:3 $[\text{Fe}/\text{Q}^{\text{S}10}]$ stoichiometry of the ferric complex at pH = 7.4 was also confirmed by monitoring the charge transfer (CT) absorption band at 583 nm during the titration of $\text{Q}^{\text{S}10}$ by iron(III) in MOPS aqueous buffer (Figure S4, Supporting Information).

A $p\text{Fe}^{3+} = -\log [\text{Fe}^{3+}]$ value for $\text{Q}^{\text{S}10}$ ($[\text{Fe}^{3+}]_{\text{tot}} = 10^{-6}$ M and $[\text{L}]_{\text{tot}} = 10^{-5}$ M) of 18.6 was calculated at a pH value of 7.4. This ligand is thus a moderate iron(III) chelator, and this $p\text{Fe}$ value is comparable to the one previously obtained (i.e., 18.1) for the bidentate catechol amphiphilic $\text{L}^{\text{S}10[7]}$ and quite lower than that of the tripodal hexadentate O-TREN-SOX (29.5).^[18]

Critical Micellar Concentrations (CMC) and Dynamic Light Scattering (DLS) Measurements

In order to evaluate the ability of $\text{Q}^{\text{S}4}$, $\text{Q}^{\text{S}10}$, and their ferric derivatives $[\text{Fe}(\text{Q}^{\text{S}10})_3]^{3-}$ and $[\text{Fe}(\text{Q}^{\text{S}4})_3]^{3-}$ to aggregate, surface tension measurements were performed at pH 7.4 (Figure 4; Figure S5, Supporting Information).

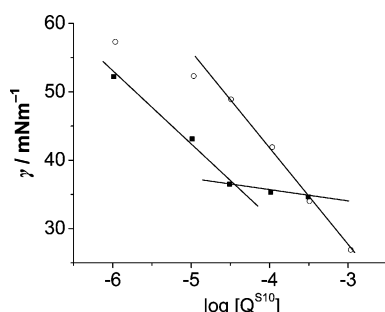


Figure 4. Dependence of the surface tension on the concentration of $\text{Q}^{\text{S}10}$ (circles, $[\text{Q}^{\text{S}10}] = 1.03 \times 10^{-6}$ to 1.03×10^{-3} M) and of a $[\text{Fe}^{3+}]/[\text{Q}^{\text{S}10}]$ mixture (squares, $[\text{Q}^{\text{S}10}] = 1.03 \times 10^{-6}$ to 3.09×10^{-4} M; $[\text{Fe}^{3+}]/[\text{Q}^{\text{S}10}] = 0.3$), solvent: MOPS 0.1 M, pH = 7.4, $T = 25.0(2)^\circ\text{C}$.

The CMC of the free $\text{Q}^{\text{S}10}$ ligand (Figure 4, circles) was not reached under our experimental conditions, as the solubility of the hydroxyquinoline moiety prevented us from preparing highly concentrated solutions (i.e., $>10^{-3}$ M). One can thus only assume a CMC value larger than 10^{-3} M. $[\text{Fe}(\text{Q}^{\text{S}10})_3]^{3-}$ behaved differently and a CMC value of 3.5×10^{-5} M was determined. This phenomenon was already observed for $\text{L}^{\text{S}10}$ and its iron complex and attributed to the higher hydrophobicity of the complex that contains three ligands and, therefore, three hydrocarbon tails.^[7] One can note that the CMC of $[\text{Fe}(\text{Q}^{\text{S}10})_3]^{3-}$ is significantly lower than the 0.45 mM value obtained for $[\text{Fe}(\text{L}^{\text{S}10})_3]^{6-}$ but close to the one determined for Marinobactin E ($\approx 75 \mu\text{M}$)^[5], which is the natural amphiphilic siderophore of *Marinobacter* sp. DS40M6. It is noticeable that the same experiments carried out on $\text{Q}^{\text{S}4}$ and its ferric complex showed no evidence of micellization. *These results highlight the importance of the length of the hydrophobic tail.*

Dynamic light scattering experiments were carried out on eight-day-old solutions (Figure 5) and allowed an estimation of the size distribution for the $[\text{Fe}(\text{Q}^{\text{S}10})_3]^{3-}$ objects formed under our conditions. It should be noted that measurement of a fresh solution provided nonexploitable and irreproducible traces with a polydispersity index (PdI) of 0.6.

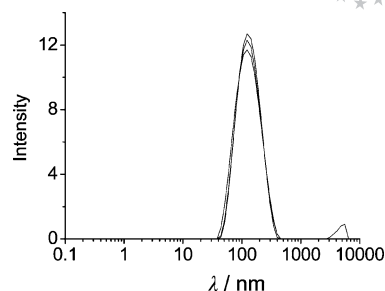


Figure 5. Size distribution of $[\text{Fe}(\text{Q}^{\text{S}10})_3]^{3-}$ at 10^{-3} M, solvent: MOPS 0.1 M, pH = 7.4, $T = 25.0(2)^\circ\text{C}$, upon filtration with a $0.45 \mu\text{m}$ PTFE membrane, 8 d.

The results for $[\text{Fe}(\text{Q}^{\text{S}10})_3]^{3-}$ at pH 7.4 in water show that the molecules self-organize in a specific monodisperse distribution of particles at $140(2)$ nm [PdI = $0.30(1)$]. These data strongly suggest the exclusive formation of a unique type of particle with an optimal size due to the shape of the $[\text{Fe}(\text{Q}^{\text{S}10})_3]^{3-}$ complex. This behavior is different from previous observations concerning $[\text{Fe}(\text{L}^{\text{S}10})_3]^{6-}$, where two size distributions were observed (around 4 and 50 nm).^[7] Moreover, these results have to be compared to data reported by Butler and coworkers on Marinobactin E showing the presence of spherical particles of 140 to 180 nm in diameter.^[2]

Cryogenic Transmission Electron Microscopy (Cryo-TEM)

Cryo-TEM experiments were performed to visualize the assemblies of $[\text{Fe}(\text{Q}^{\text{S}10})_3]^{3-}$ at pH 7.4. The time-dependent reorganization of the edifices was evaluated by performing two sets of experiments: one at 12 h (Figure 6) and one 8 d after sample preparation (Figure 7).

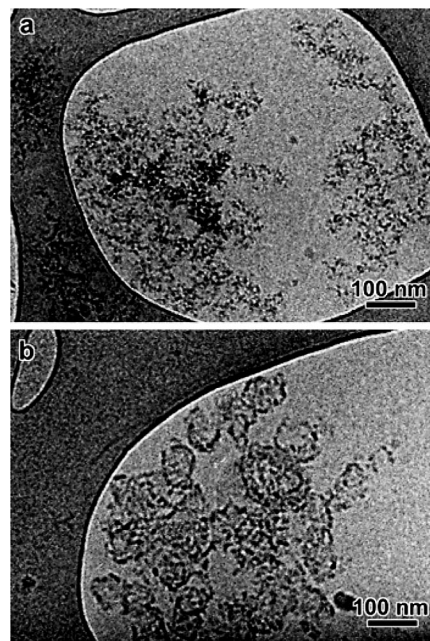


Figure 6. Cryo-TEM micrographs of a solution of $[\text{Fe}(\text{Q}^{\text{S}10})_3]^{3-}$ species observed 12 h after sample preparation. $[\text{Q}^{\text{S}10}] = 2.67 \times 10^{-3}$ M, $[\text{Fe}^{3+}] = 8.01 \times 10^{-4}$ M, solvent MOPS 0.1 M, pH = 7.4.

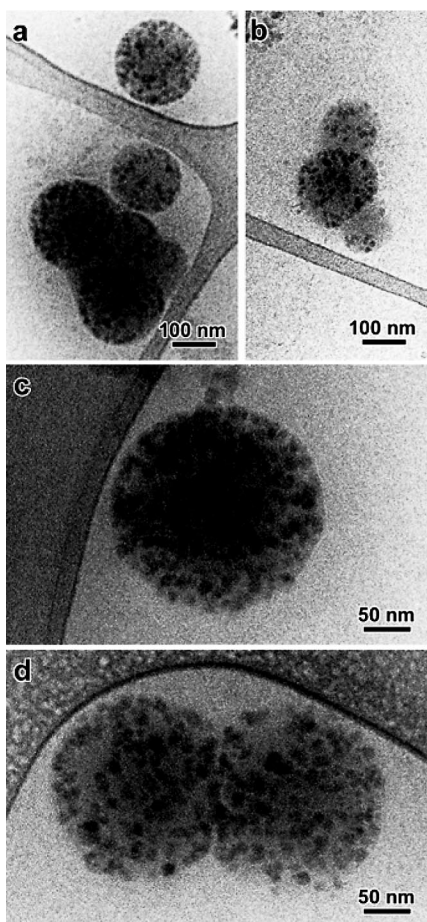


Figure 7. Cryo-TEM micrographs of a solution of $[\text{Fe}(\text{Q}^{\text{S}10})_3]^{3-}$ species observed 8 d after sample preparation. $[\text{Q}^{\text{S}10}] = 2.67 \times 10^{-3} \text{ M}$, $[\text{Fe}^{3+}] = 8.01 \times 10^{-4} \text{ M}$, solvent MOPS 0.1 M, pH = 7.4.

At 12 h, the suspension mostly contained loose networks of electron-dense nanoparticles (Figure 6a). The high contrast of the networks indicates the presence of iron(III) and suggests that, after a few hours of equilibration, the $[\text{Fe}(\text{Q}^{\text{S}10})_3]^{3-}$ complexes form iron-rich micelles that aggregate into larger clustered structures. This loose form of self-organization is in agreement with the DLS experiments, which showed a very polydisperse distribution of particles. Considering that the defocus necessary to generate a significant phase contrast in the image at this relatively low magnification creates Fresnel fringes around the micelles, it is difficult to measure their diameter with precision. An upper limit would be a diameter of 3–4 nm, which is in agreement with the average size of $[\text{Fe}(\text{Q}^{\text{S}10})_3]^{3-}$ and close to the results obtained for $[\text{Fe}(\text{L}^{\text{S}10})_3]^{6-}$.^[7] Loose networks with a different morphology were sometimes observed, such as that shown in Figure 6b. It is still composed of electron-dense nanoparticles, but they seem to be organized into irregular semicapsular aggregates. This would suggest that micelles tend to self-organize into more complex structures.

After 8 d of equilibration, we almost exclusively observed nanospheres, either individual (Figure 7a,c) or organized into aggregates of a few units (Figure 7a,b,d). Their dia-

meter typically ranges from 100 to 200 nm. They exhibit a peculiar flecked aspect with a more-or-less regular distribution of fairly well-defined 10 nm large darker “particles”, likely corresponding to regions containing higher concentrations of iron. As seen at higher magnification (Figure 7c,d), the surface of the particles appears to be relatively smooth, suggesting that they are not covered by the dark objects but contain a random distribution of iron-rich regions. In addition, although the particles clearly deform when they agglomerate, each individual particle can still be recognized without any evidence of interpenetration of dark regions. Even if it is clear that these particles belong to the starting micelles, a proposition of mechanism for this spatial reorganization/agglomeration would be presumptuous without further investigation. Moreover, the heterogeneous distribution of iron-rich regions in the $[\text{Fe}(\text{Q}^{\text{S}10})_3]^{3-}$ aggregate was unexpected in comparison to the results obtained for $[\text{Fe}(\text{L}^{\text{S}10})_3]^{6-}$, where the contrast of the resulting particles was homogeneous.^[7] This might be explained by the differences in charge and bulkiness (catechol vs. quinoline scaffolds) of the ferric complexes. However, our results are in good agreement with those obtained by Butler and co-workers on ferric complexes of Marinobactin D showing cryo-TEM pictures of spherical vesicles that are 50 to 200 nm in diameter.^[5]

Conclusions

A new type of amphiphilic iron chelator involving 8-hydroxyquinoline chelating subunits was described and compared to the catechol-based analogue. Although their iron-complexing abilities are close, the ferrated $\text{Q}^{\text{S}10}$ compound shows interesting and new self-assembling properties. Whereas a micelle-to-vesicle process occurred with the catechol derivative, we observed here the formation of nanospheres that are 100–200 nm in diameter and that contain a randomly arranged iron-rich region. This evidences that the aggregation properties are finely tuned, not only by the lipophilic moiety of the ligand, but also by the charge of the coordination sphere. Despite these differences, the natural siderophores from marine bacteria and the two types of abiotic chelators allow the formation of an “iron loft”, and so, a high local iron concentration in medium containing low Fe levels. Further studies are in progress concerning the nutrition of bacteria by using the self-assembled complexes described herein as an iron source.

Experimental Section

Solvents and Starting Materials: All solvents and chemicals were purchased from Acros Organics, Sigma–Aldrich, or Lancaster and used without further purification unless otherwise stated. The solvent, thf, was distilled from sodium/benzophenone. NMR (^1H and ^{13}C) spectra were recorded with a Bruker Avance 300 MHz spectrometer by using tetramethylsilane (TMS) or deuterated solvents as reference. Mass spectra were recorded with a Thermo Finnigan Polaris Q (EI/DCI) apparatus or a Bruker Daltonics Esquire 3000 Plus (ESI). Elemental analyses were performed by the microanaly-

sis service of the Department of Molecular Chemistry of Grenoble. 8-Hydroxyquinoline-7-carboxylic acid^[20,21] and 1-*n*-butyl-5-sulfo-8-hydroxyquinoline-7-carboxamide (Q^{S4})^[15] were prepared as described in the literature. Stock solutions of Fe^{3+} were prepared by dissolving the appropriate amount of iron perchlorate xH_2O in standardized perchloric acid or sodium perchlorate in water. The exact concentration of Fe^{3+} was determined spectrophotometrically by using a molar extinction coefficient of $4160\text{ M}^{-1}\text{ cm}^{-1}$ at 240 nm in 0.1 M aqueous $HClO_4$.^[22]

1-*n*-Decyl-8-hydroxyquinoline-7-carboxamide (1): A suspension of 8-hydroxyquinoline-7-carboxylic acid (3.0 g, 15.8 mmol) and carbonyldiimidazole (3.24 g, 20.6 mmol) in thf was heated at reflux under an atmosphere of argon for 2 h. Decylamine (5 g, 31.7 mmol) in thf (40 mL) was added dropwise, and reflux was maintained for 12 h. After evaporation of the solvent, the resulting oil was partitioned between $CHCl_3$ (100 mL) and NH_4Cl (1/2 sat.) and extracted. The organic layer was dried (Na_2SO_4) and filtered, and the solvent was evaporated. The crude thick oil was purified by column chromatography (silica gel; CH_2Cl_2 /hexane, 60:40→100:0, then CH_2Cl_2 /MeOH, 99:1) to give a white solid. Yield: 4.43 g (85%). 1H NMR (300 MHz, $CDCl_3$): δ = 0.87 (t, 3J = 6 Hz, 3 H), 1.18–1.38 (m, 14 H), 1.67 (q, 3J = 7 Hz, 2 H), 3.53 (q, 3J = 4 Hz, 2 H), 7.36 (d, 3J = 9 Hz, 1 H), 7.50 (dd, 3J = 8 Hz, 1 H), 7.82 (br., 1 H), 8.13–8.17 (m, 2 H), 8.84 (dd, 3J = 4 Hz, 4J = 2 Hz, 1 H) ppm. ^{13}C NMR (75 MHz, $CDCl_3$): δ = 14.3 ($C_{prim.}$); 22.8, 27.2, 29.4, 29.5, 29.7, 29.7, 29.8, 30.0, 40.1 ($C_{sec.}$); 117.7, 123.3, 127.4, 136.2, 148.6 ($C_{tert.}$); 114.2, 130.2, 138.8, 152.4, 166.0 ($C_{quat.}$) ppm. MS (EI): m/z = 329.1 [$M + H$] $^+$.

8-Hydroxy-7-[(decylamino)carbonyl]quinoline-5-sulfonic Acid (acidic form, Q^{S10}) (2): Chlorosulfonic acid (840 μ L, 12.6 mmol) was added to a cold (0 °C) solution of **1** (1.040 g, 3.16 mmol) in dry CH_2Cl_2 (55 mL), and the mixture was stirred for 12 h. After evaporation, the residue was dissolved in a minimum amount of MeOH, and diethyl ether was added to induce precipitation. The yellow solid was collected by filtration through paper and dried. Yield: 0.93 g (72%). 1H NMR (300 MHz, $[D_6]DMSO$): δ = 0.86 (t, 3J = 6 Hz, 3 H), 1.26–1.32 (m, 14 H), 1.63 (br., 2 H), 3.41 (m, 2 H), 6.10 (br., -OH), 8.22–8.27 (m, 1 H), 8.75 (s, 1 H), 9.17 (d, 3J = 4 Hz, 1 H), 9.72 (br., 1 H), 9.90 (d, J = 4 Hz, 1 H) ppm. ^{13}C NMR (75 MHz, $[D_6]DMSO$): δ = 12.1 ($C_{prim.}$); 20.3, 24.7, 26.7, 26.9, 27.0, 27.2, 27.2, 29.5, 37.8 ($C_{sec.}$); 122.4, 122.6, 143.0, 143.9 ($C_{tert.}$); 110.0, 126.1, 128.3, 132.4, 153.0, 167.0 ($C_{quat.}$) ppm. MS (EI): m/z = 409.0 [$M + H$] $^+$. $C_{20}H_{28}N_2O_5S \cdot 2.9H_2O$ (460.2): C 52.10, H 7.39, N 6.07; found C 52.10, H 7.04, N 5.82.

Spectrophotometry: Solutions were prepared with boiled deionized water, which was deoxygenated and flushed continuously with Ar (U grade) to exclude CO_2 and O_2 . Free-hydrogen concentrations were measured with a glass Ag/AgCl combined electrode (Metrohm filled with 0.1 M aqueous NaCl and saturated with AgCl). The electrode was calibrated in order to read the pH according to the classical method (titration of 0.01 M $HClO_4$ with 0.02 M NaOH).^[23] Spectrophotometric measurements were performed in quartz cells by using a thermostatted Perkin–Elmer Lambda 2 spectrophotometer. The spectrophotometric titrations were performed in aqueous solution with ionic strength 0.1 M ($NaClO_4$) at 25.0(2) °C in the pH range 1.83–9.04 for Q^{S10} (5.46×10^{-5} M) and 2.11–9.96 for the ferric complex ($[Q^{S10}] = 5.69 \times 10^{-4}$ M, $[Fe^{3+}] = 1.80 \times 10^{-4}$ M) and pH was adjusted with NaOH. The stoichiometry of the Fe^{III} complex at pH = 7.4 was also checked by a titration of a solution of ligand Q^{S10} (4.98×10^{-5} M) with a solution of iron(III) in buffer solution (MOPS 0.1 M). For Q^{S4} the titrations were done in two sets of measurements: in the pH range 0–2, batch solutions were prepared by

using standardized $HClO_4$ to adjust pH; in the range 2–8, pH was adjusted with NaOH and measured with a Metrohm 713 pHmeter. It should be noted that ionic strength was not maintained at 0.1 M in the pH range 0–1. Concerning Q^{S10} , 25 solutions with $2.1 < pH < 7.71$ ($380 < \lambda < 800$ nm) and 10 solutions with $7.7 < pH < 9.96$ ($380 < \lambda < 800$ nm) were analyzed by using both SPECFIT/32 Global Analysis System (Spectrum Software Associates)^[14] and Letagrop-Spefo program.^[17] These programs perform a global analysis of system equilibria. By using a nonlinear regression model, thermodynamic constants and calculated spectra of absorbing species can be determined. The range of values for the residual-squares sum $\sum (A_{exp.} - A_{calcd.})^2$ was over the range 5×10^{-2} to 5×10^{-3} .

Surface Tension Measurements: Surface tensions were measured at 25 °C by using an automatic drop tensiometer (Tracker, I.T.C Concept, Longessange, France) in rising drop mode and calculated by a mathematical analysis of the axial symmetric shape of the drop (Laplacian profile). The critical micellar concentration (cmc) was estimated from the change in surface tension due to ligand (1.08×10^{-6} M to 1.08×10^{-3} M) or complex (1.03×10^{-6} M to 3.09×10^{-4} M, $[Fe^{3+}]_{tot}/[Q^{S10}]_{tot} = 1:3$) concentrations. Starting solutions were prepared in MOPS 0.1 M at pH = 7.4.

Dynamic Light Scattering: DLS experiments were performed by using a Zetasizer Nano Series ZS apparatus from Malvern Instruments equipped with a 633 nm laser. The Non-Invasive Back-Scatter protocol was used with a detection of the scattered beam at an angle of 173°. Data were fitted with the Dispersion Technology Software (DTS) v5.00 from Malvern Instruments, which uses algorithms to extract the decay rate of the correlation function for a range of particle size. This information is then used to propose a size distribution of the hydrodynamic diameter. Experiments were performed in buffered solutions (MOPS 0.1 M, pH = 7.4) for Q^{S10} ferric complex (10^{-3} M). Starting solutions were filtered (Pall, Acrodisc CR 13 mm Syringe filter with a 0.45 μ m PTFE membrane) prior to analysis to discard dust particles.

Cryogenic Transmission Electron Microscopy: Experiments were performed for the ferric complex of Q^{S10} in buffered solutions (MOPS 0.1 M, pH = 7.4). The samples for cryo-TEM were prepared according to the procedure described elsewhere.^[24] Thin liquid films of the suspension were prepared on lacey carbon films and fast-frozen in liquid ethane. The specimens were mounted on a Gatan 626 cryoholder cooled down with liquid nitrogen and observed at low temperature (–180 °C), under low dose illumination, by using a Philips CM200 ‘Cryo’ microscope operating at 80 kV. Images were recorded with Kodak SO163 films.

Supporting Information (see footnote on the first page of this article): 1H NMR spectrum of Q^{S10} ; spectrophotometric titration of a mixture Fe^{3+}/Q^{S4} vs. pH; titration of $Fe(Q^{S10})_3$ in the range $7.71 < pH < 9.96$; titration of Q^{S10} with Fe^{3+} ; CMC measurements for Q^{S4} and its iron complex.

Acknowledgments

We gratefully acknowledge Dr. Rachel Auzely and Eric Bayma for granting access to the surface tension measurement instrument and Dr. Anabelle Varrot for access to the DLS instrument at CERMAV, Grenoble.

- [1] J. B. Neilands, *J. Biol. Chem.* **1995**, 270, 26723–26726.
- [2] J. S. Martinez, G. P. Zhang, P. D. Holt, H. T. Jung, C. J. Carano, M. G. Haygood, A. Butler, *Science* **2000**, 287, 1245–1247.
- [3] K. Barbeau, E. L. Rue, K. W. Bruland, A. Butler, *Nature* **2001**, 413, 409–412.

- [4] A. Butler, *Biometals* **2005**, *18*, 369–374.
- [5] T. Owen, R. Pynn, J. S. Martinez, A. Butler, *Langmuir* **2005**, *21*, 12109–12114.
- [6] a) M. Apostol, P. Baret, G. Serratrice, J. Desbrieres, J.-L. Putaux, M.-J. Stebe, D. Expert, J.-L. Pierre, *Angew. Chem. Int. Ed.* **2005**, *44*, 2580–2582; b) J.-L. Pierre, A. du Moulinet d'Hardemare, G. Serratrice, S. Torelli, *C. R. Chim.* **2007**, *10*, 613–621.
- [7] L. Bednarova, J. Brandel, A. du Moulinet d'Hardemare, J. Bednar, G. Serratrice, J.-L. Pierre, *Chem. Eur. J.* **2008**, *14*, 3680–3686.
- [8] A. M. Albrecht-Gary, A. L. Crumbliss, "Coordination Chemistry of Siderophores: Thermodynamics and Kinetics of Iron Chelation and Release" in *Metal Ions in Biological Systems Vol. 35: Iron Transport and Storage in Microorganisms, Plants and Animals* (Eds.: A. Sigel, H. Sigel), M. Dekker, New York, **1998**, pp. 239–327.
- [9] J. L. Pierre, P. Baret, G. Serratrice, *Curr. Med. Chem.* **2003**, *10*, 1077–1084.
- [10] N. K. Chawla, M. M. Jones, *Inorg. Chem.* **1964**, *3*, 1549–1553.
- [11] K. Matsumara, *J. Am. Chem. Soc.* **1927**, *49*, 810–818.
- [12] P. Baret, C. G. Béguin, H. Boukhalfa, C. Caris, J.-P. Laulhère, J.-L. Pierre, G. Serratrice, *J. Am. Chem. Soc.* **1995**, *117*, 9760–9761.
- [13] D. Seidel, P. Brehmer, Y. Schoof, U. Weinberg, U. Niewöhner, M. Nowakowski, *J. Labelled Compd. Radiopharm.* **2003**, *46*, 1019–1032.
- [14] a) H. Gampp, M. Maeder, C. J. Meyer, A. D. Zuberbühler, *Talanta* **1985**, *32*, 95–101; b) H. Gampp, M. Maeder, C. J. Meyer, A. D. Zuberbühler, *Talanta* **1985**, *32*, 257–264.
- [15] F. Launay, V. Alain, E. Destandau, N. Ramos, E. Bardez, P. Baret, J.-L. Pierre, *New J. Chem.* **2001**, *25*, 1269–1280.
- [16] F. C. Richard, R. L. Gustafson, A. E. Martell, *J. Am. Chem. Soc.* **1959**, *81*, 1033–1040.
- [17] L. G. Sillen, *Acta Chem. Scand.* **1964**, *18*, 1085–1098; L. G. Sillen, B. Warnqvist, *Ark. Kemi.* **1969**, *31*, 377–390.
- [18] G. Serratrice, H. Boukhalfa, C. G. Béguin, P. Baret, C. Caris, J.-L. Pierre, *Inorg. Chem.* **1997**, *36*, 3898–3910.
- [19] H. Boukhalfa, F. Thomas, G. Serratrice, C. G. Béguin, *Inorg. React. Mech.* **2002**, *3*, 153–172.
- [20] R. Schmitt, F. Engelmann, *Ber. Dtsch. Chem. Ges.* **1887**, *20*, 1217–1220.
- [21] A. S. Lindsey, H. Jeskey, *Chem. Rev.* **1957**, *57*, 583–620.
- [22] R. Bastian, R. Weberling, F. Palilla, *Anal. Chem.* **1956**, *28*, 459–462.
- [23] A. E. Martell, R. J. Motekaitis in *Determination and Use of Stability Constants*, VCH, Weinheim, **1988**, ch. 1, pp. 7–19.
- [24] J. Dubochet, M. Adrian, J. J. Chang, J. C. Homo, J. Lepault, A. W. McDowell, P. Schultz, *Rev. Biophys.* **1988**, *21*, 129–228.

Received: July 25, 2008

Published Online: November 14, 2008

Reactions of Hydrazines with $\text{AlH}_3 \cdot \text{NMe}_2\text{Et}$ – Formation of Aluminum-Nitrogen Heterocycles

Werner Uhl,^{*,[a]} and Andreas Vogelpohl^[a]

Keywords: Aluminum / Hydrazides / Heterocycles / Cage compounds

Treatment of the alane–amine adduct $\text{AlH}_3 \cdot \text{NMe}_2\text{Et}$ with 1,2-diphenylhydrazine, $\text{H}_5\text{C}_6\text{--N(H)--N(H)--C}_6\text{H}_5$, afforded a five-membered Al_2N_3 heterocycle (**1**) by the elimination of hydrogen and partial cleavage of N–N bonds. The structure of **1** comprises two aluminum atoms bridged by a dianionic diphenylhydrazinediido ($\text{H}_5\text{C}_6\text{--N--N--C}_6\text{H}_5^-$) and an imido ligand ($\text{H}_5\text{C}_6\text{--N}^{2-}$). Each aluminum atom is further attached to a terminal hydrogen atom and a (ethyl)dimethylamino group. 1-Aminopyrrole, $\text{H}_2\text{N--NC}_4\text{H}_4$ gave a singular tricyclic cage

compound (**2**) under similar conditions. The amino groups were completely deprotonated. N–N bond cleavage was not observed. Compound **2** possesses a central Al_2N_2 ring. Its nitrogen atoms are bridged by an Al_2N group, whereas an N_2Al group bridges both aluminum atoms. All nitrogen atoms are part of N–N bonds, and all metal atoms are further bonded to terminal hydrogen atoms.

(© Wiley-VCH Verlag GmbH & Co. KGaA, 69451 Weinheim, Germany, 2009)

Introduction

Organoelement hydrazides of the heavier group 13 elements found some interest in recent research for essentially two reasons: (i) They are suitable starting compounds for the generation of the corresponding element nitrides by thermolysis reactions.^[1] (ii) The particular arrangement of lone pairs of electrons at two directly connected nitrogen atoms cause the formation of a broad variety of different and unprecedented structural motifs.^[2] The reactions of organoaluminum, -gallium or -indium compounds with hydrazine derivatives gave simple adducts in the first step, which could be isolated and characterized in several cases.^[3–10] Spontaneous or thermally induced secondary reactions afforded the corresponding hydrazides by salt elimination, the release of alkanes or elemental hydrogen. These compounds were monomeric only in very few cases,^[11–13] and usually dimeric formula units were obtained containing four-, five- or six-membered heterocycles.^[5,7,9,13–23] Dianionic hydrazinediido ligands form oligomers possessing oligocyclic or cage-like structures.^[3,6,10,17,18,24–26] Several effective routes for the synthesis of these hydrazides are known in the literature and comprise the reactions of trialkylelement compounds or dialkylelement hydrides with hydrazines, the salt elimination by treatment of dialkylelement halides with lithium hydrazides and the amide replacement by treatment of aminoalanes with hydrazines. Dianionic hydrazinediido ligands were also obtained by hydroalumination of a 2,3-diazabutadiene derivative or a diazene.^[20,26]

Interestingly, dialkylaluminum hydrides or gallium hydrides did not afford hydrazides under similar conditions.^[27] Small substituents attached to the gallium or indium atom such as hydrogen atoms or methyl groups favor secondary reactions of hydrazides and the formation of oligocyclic or cage-like compounds. For the generation of similar aluminum compounds we treated $\text{AlH}_3 \cdot \text{NMe}_2\text{Et}$ with several hydrazines. However, probably caused by the high functionality of this starting compound we usually [e.g., 1-aminopiperidine or $\text{H}_2\text{N--N(H)R}$] obtained complicated mixtures of unknown products. Two successful reactions are reported here, one gave a novel cage compound having intact hydrazido groups.

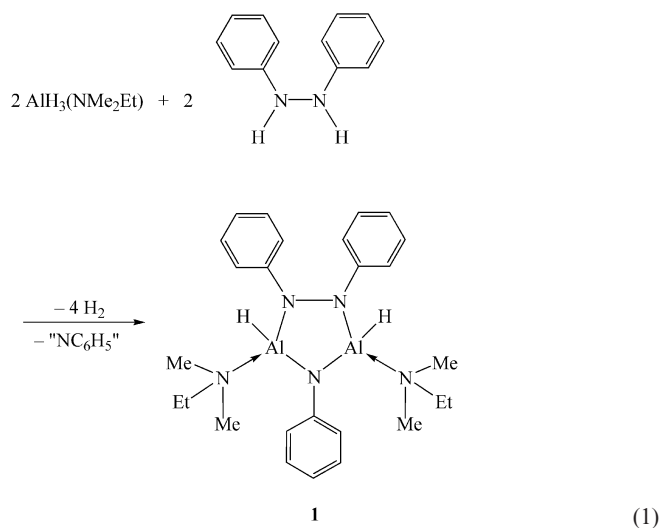
Results and Discussion

Reaction of $\text{AlH}_3 \cdot \text{NMe}_2\text{Et}$ with 1,2-Diphenylhydrazine

In an optimized reaction procedure an excess of the alane–amine adduct was added to a toluene solution of 1,2-diphenylhydrazine at room temperature. Strong gas evolution occurred for about 2 min, and the reaction mixture adopted a deep blue color. An almost colorless solution was obtained upon stirring of the reaction mixture overnight. Equation (1) gives the idealized stoichiometry of the reaction. Cooling to +3 °C afforded colorless crystals of compound **1** in 64% yield. Crystal structure determination (see below) and NMR spectroscopic data verified the formation of a heterocyclic compound with a central Al_2N_3 ring. Both aluminum atoms are bridged by a diphenylhydrazinediido and a phenylimido ligand. One hydrogen atom and an amino ligand are terminally attached to each metal atom. Thus, complete deprotonation and partial cleavage of the

[a] Institut für Anorganische und Analytische Chemie der Universität Münster, Corrensstraße 30, 48149 Münster, Germany
Fax: +49-251-8336660

starting hydrazine occurred. The deep blue color observed at the beginning of the reaction may hint at radical intermediates resulting from the homolytic cleavage of N–N bonds. We were not able to isolate or identify any by-product of the reaction. A possible mechanism may comprise the intermediate formation of $(\text{H}_2\text{Al})_2(\mu\text{-NC}_6\text{H}_5)$, which may be stabilized by amino ligands and may yield the heterocyclic product **1** by reaction with an intact hydrazine molecule. Aniline, $\text{H}_2\text{N-C}_6\text{H}_5$, may be formed, but it could not be identified by NMR spectroscopy. The ^1H NMR spectrum of **1** exhibits a broad resonance of the hydrogen atoms attached to the aluminum atom ($\delta = 4.84$ ppm). Owing to the chiral coordination sphere of the metal atoms the methyl groups and the methylene hydrogen atoms of the amino ligands are diastereotopic and give different resonances. An unambiguous assignment of resonances to the chemically different phenyl groups succeeded only in the ^{13}C NMR spectrum.



The central structural motif of compound **1** is the five-membered Al_2N_3 heterocycle (Figure 1). The Al–N distances in the heterocycle (182.6 to 186.2 pm) are relatively short compared to other hydrazides, which clearly is caused by the negative charges localized at each nitrogen atom and an increased ionic contribution to the bonding. As expected, considerably longer Al–N distances (200.9 pm on average) resulted for the bonds to the terminal amino ligands. The N–N bond length (145.5 pm) corresponds to standard values of hydrazides (see Introduction) or hydrazines.^[28] The nitrogen atom N5, which is coordinated by two aluminum atoms, has an almost ideal planar surrounding (sum of the angles 359.5°), whereas the atoms N1 and N2 of the intact hydrazinediido ligand (sum of the angles 352.3 and 355.4° , respectively) approach a pyramidal coordination sphere. The central heterocycle adopts an envelope conformation with the atom N2 35 pm above the plane of the four remaining atoms. A similar compound containing a five-membered Al_2N_3 heterocycle was obtained by Power et al. by the hydroalumination of diphenyldiazene.^[20]

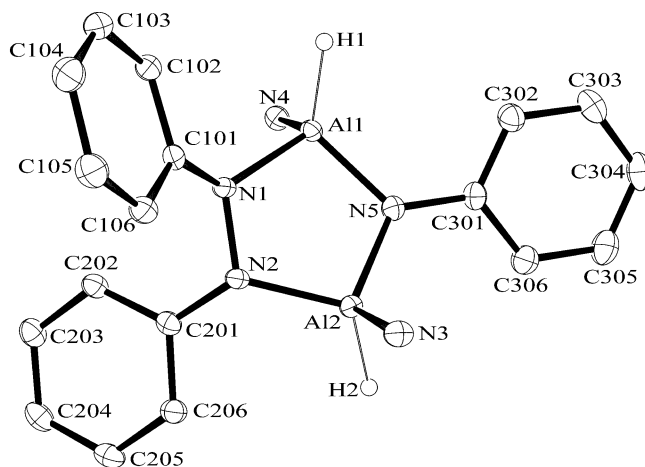
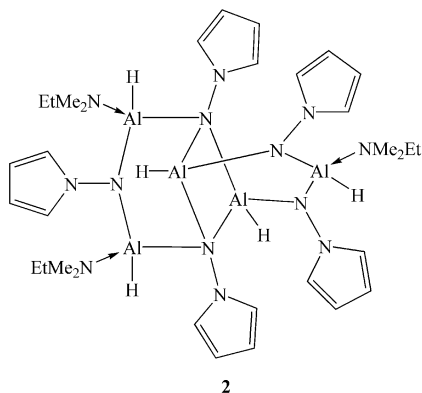
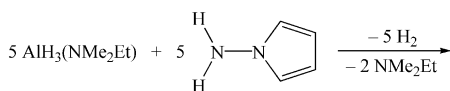


Figure 1. Molecular structure and numbering scheme of **1**; the thermal ellipsoids are drawn at the 40% probability level; hydrogen atoms with the exception of those attached to aluminum atoms and the alkyl groups of the amino ligands are omitted. Selected bond lengths [pm] and angles $^\circ$: Al1–N1 186.2(1), Al1–N4 200.5(1), Al1–N5 182.8(1), Al2–N2 186.1(1), Al2–N3 201.2(1), Al2–N5 182.6(1), N1–N2 145.5(2), Al1–N5–Al2 107.60(7), Al1–N1–N2 111.88(9), Al2–N2–N1 112.01(9), N1–Al1–N5 101.55(6), N2–Al2–N5 101.41(6).

Reaction of $\text{AlH}_3\cdot\text{NMe}_2\text{Et}$ with 1-Aminopyrrole

1-Aminopyrrole, $\text{H}_2\text{N-NC}_4\text{H}_4$, was added to a small excess of the alane–amine adduct dissolved in *n*-hexane at room temperature [Equation (2)]. Strong gas evolution occurred for 1 min, and a colorless solid of unknown composition precipitated, which was removed. Colorless crystals of the product (**2**) precipitated from the clear solution in 36% yield after cooling to $+3^\circ\text{C}$. Compound **2** gave complicated NMR spectra. Its constitution was clarified by crystal structure determination. A tricyclic, cage-like compound was formed, in which five aluminum atoms are bridged by five deprotonated aminopyrrole ligands, $\text{H}_4\text{C}_4\text{N-N}^{2-}$, containing intact N–N bonds. Each aluminum atom is further bonded to a terminal hydrogen atom. The structure comprises an inner Al_2N_2 heterocycle with alternating Al and N atoms. The Al...Al vector is bridged by an N_2Al group, and the N...N vector is bridged by an Al_2N moiety. The tricyclic structural motif of the molecular core resembles that of the corresponding hydrocarbon tricyclo[4.4.0.0^{2,7}]decane.^[29] According to the molecular symmetry in the solid state five different pyrrole rings and three different (ethyl)dimethylamino ligands were observed in the NMR spectra of solutions of **2**. The methyl groups and the CH_2 hydrogen atoms of the amine are diastereotopic and give sets of two resonances in all cases.

The molecular structure of **2** is depicted in Figure 2. The central Al_2N_2 heterocycle is strongly folded across the Al...Al axis with an angle of 48.4° between the normals of its Al_2N planes. The aluminum atoms are further bonded to a terminal hydrogen atom and a nitrogen atom of the bridging N_2Al group. The nitrogen atoms of the four-membered heterocycle are part of a hydrazido group and attached to a third aluminum atom, which belongs to the



bridging Al_2N group. The metal atoms of all bridging groups are involved in two endocyclic Al–N bonds and are further attached to a terminal hydrogen atom and an amino ligand. All nitrogen atoms in the bridges have coordination numbers of three in an almost ideally planar surrounding (sum of the angles 360.0° at N3, 359.1° at N4, 357.6° at N5). Four different ranges of Al–N distances were observed, which are clearly correlated to coordination number and charge separation: The longest ones result to the terminal amino ligands (200.8 pm) followed by those between

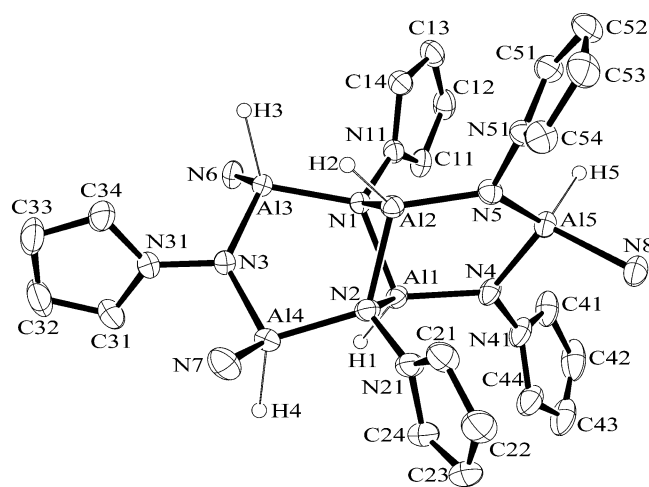


Figure 2. Molecular structure and numbering scheme of **2**; the thermal ellipsoids are drawn at the 40% probability level; hydrogen atoms with the exception of those attached to aluminum atoms and the alkyl groups of the amino ligands are omitted. Selected bond lengths [pm] and angles $[\circ]$: Al1–N1 196.0(2), Al1–N2 196.7(2), Al1–N4 180.9(2), Al2–N1 197.4(2), Al2–N2 196.1(2), Al2–N5 181.0(2), Al3–N1 190.9(2), Al3–N3 182.8(2), Al3–N6 201.6(2), Al4–N2 191.8(2), Al4–N3 182.4(2), Al4–N7 199.7(2), Al5–N4 183.9(2), Al5–N5 184.1(2), Al5–N8 201.2(2), Al1–N1–Al2 86.87(7), Al1–N2–Al2 87.00(7), N1–Al1–N2 83.01(7), N1–Al2–N2 82.81(7), N1–Al3–N3 102.51(8), Al3–N3–Al4 131.4(1), N2–Al4–N3 102.77(8), Al2–N5–Al5 124.1(1), N4–Al5–N5 102.46(8), Al1–N4–Al5 124.5(1).

the tetracoordinate atoms of the central Al_2N_2 heterocycle (196.6 pm). The shortest Al–N distances (182.5 pm) involve the tricoordinate nitrogen atoms N3, N4 and N5, whereas intermediate values (191.4 pm) were detected for the bonds Al3–N1 and Al4–N2 including the ring nitrogen atoms and metal atoms of the Al_2N bridge. The N–N distances are 144.1 pm including the tetracoordinate nitrogen atoms of the Al_2N_2 heterocycle (N1, N2) and 142.4 pm for the remaining three hydrazinediido groups (N3, N4, N5).

Experimental Section

General: All procedures were carried out under purified argon in dried solvents (*n*-hexane with LiAlH_4 , toluene with Na/benzophenone). 1,2-Diphenylhydrazine, 1-aminopyrrole and $\text{AlH}_3\cdot\text{NMe}_2\text{Et}$ were obtained according to literature procedures.^[30–32]

Reaction of $\text{AlH}_3\cdot\text{NMe}_2\text{Et}$ with 1,2-Diphenylhydrazine. Synthesis of **1:** 1,2-Diphenylhydrazine (0.300 g, 1.63 mmol) was dissolved in toluene (50 mL) and treated with $\text{AlH}_3\cdot\text{NMe}_2\text{Et}$ (0.41 mL, 0.336 g, 3.26 mmol) at room temperature. Gas evolution occurred for about 2 min, and the color changed to deep blue. Stirring at room temperature for 12 h gave an almost colorless, light-blue solution. Cooling to $+3^\circ\text{C}$ yielded colorless crystals of compound **1**. Yield: 0.271 g (64%); m.p. (argon, sealed capillary) 168°C (dec.). ^1H NMR (400 MHz, C_6D_6): δ = 0.44 (t, $^3J_{\text{H-H}} = 7.4$ Hz, 6 H, CH_2CH_3), 1.81 and 1.87 (each s, 6 H, NCH_3), 2.27 and 2.48 (each dq, $^3J_{\text{H-H}} = 7.4$, $^2J_{\text{H-H}} = 13.3$ Hz, 2 H, CH_2CH_3), 4.84 (br. s, 2 H, Al–H), 6.74, 7.02, 7.11, 7.23 and 7.47 (m, 15 H, phenyl) ppm. ^{13}C NMR (100 MHz, C_6D_6): δ = 7.1 (CH_2CH_3), 42.0 and 42.8 (NCH_3), 52.2 (CH_2CH_3) ppm; hydrazine phenyl: δ = 115.4 (*o*-phenyl-C), 123.5 (*m*-phenyl-C), 129.7 (*p*-phenyl-C), 154.2 (*i*-phenyl-C); imide phenyl: δ = 116.8 (*o*-phenyl-C), 157.8 (*i*-phenyl-C), remaining resonances covered. IR (CsBr, paraffin): $\tilde{\nu}$ = 1846 [m, $\nu(\text{AlH})$] 1589 (m), 1560 [w, phenyl] 1454 (vs), 1375 (vs, paraffin) 1302 (s), 1267 (m), 1247 (w), 1200 (w), 1169 (m), 1153 (m), 1078 (w), 1018 (vw), 966 (m), 939 (m), 887 (m), 856 [m, $\nu(\text{CN})$, $\nu(\text{NN})$, $\nu(\text{CC})$] 721 (s, paraffin) 692 (m), 646 (m, phenyl) 615 (w), 592 (vw), 501 [$\nu(\text{Al-N})$, $\nu(\text{Al-C})$] cm^{-1} . $\text{C}_{26}\text{H}_{39}\text{Al}_2\text{N}_5\cdot 1/2(\text{C}_7\text{H}_8)$ (521.7): calcd. C 67.9, H 8.3, N 13.4; found C 67.5, H 8.1, N 13.6.

Reaction of $\text{AlH}_3\cdot\text{NMe}_2\text{Et}$ with 1-Aminopyrrole. Synthesis of **2:** $\text{AlH}_3\cdot\text{NMe}_2\text{Et}$ (0.30 mL, 0.240 g, 2.33 mmol) was dissolved in *n*-hexane (25 mL) and treated with 1-aminopyrrole (0.15 mL, 0.156 g, 1.90 mmol) at room temperature. Strong gas evolution was observed for 1 min, and a colorless solid of unknown composition precipitated. It was separated. Colorless crystals of compound **2** were obtained after cooling of the clear solution to $+3^\circ\text{C}$. Yield 0.104 g (36%); m.p. (argon, sealed capillary) 195°C (dec.). In accordance with the molecular symmetry, the resonances of five different aminopyrrole rings and three different (ethyl)dimethylamine ligands were observed in the NMR spectra; they could not be assigned to particular positions in the molecule. ^1H NMR (400 MHz, C_6D_6): pyrrole I: δ = 6.04 (*pseudo*-t, 2 H, NCHCH), 6.84 and 6.87 (each *pseudo*-q, 1 H, NCHCH) ppm; pyrrole II: δ = 6.00 and 6.02 (each *pseudo*-q, 1 H, NCHCH), 7.23 and 7.43 (each *pseudo*-q, 1 H, NCHCH) ppm; pyrrole III: δ = 6.25 and 6.38 (each *pseudo*-q, 1 H, NCHCH), 7.30 and 7.34 (each *pseudo*-q, 1 H, NCHCH) ppm; pyrrole IV: δ = 6.33 and 6.35 (each *pseudo*-q, 1 H, NCHCH), 7.22 (*pseudo*-t, 2 H, NCHCH) ppm; pyrrole V: δ = 6.34 (*pseudo*-t, 2 H, NCHCH), 7.02 (*pseudo*-t, 2 H, NCHCH) ppm; amine I: δ = 0.30 (t, $^3J_{\text{H-H}} = 7.4$ Hz, 3 H, CH_2CH_3), 1.35 and 1.42 (each s, 3 H, NCH_3), 2.07 and 2.21 (each m, 1 H, N-CH_2) ppm; amine II: δ =

Table 1. Crystal data and structure refinement for compounds **1** and **2**.^[a]

| | 1 | 2 |
|--|---|---|
| Empirical formula | C ₂₆ H ₃₉ Al ₂ N ₅ ·0.5(C ₇ H ₈) | C ₃₂ H ₅₈ Al ₅ N ₁₃ |
| Temperature [K] | 153(2) | 153(2) |
| Crystal system | triclinic | triclinic |
| Space group ^[33] | <i>P</i> $\bar{1}$ (no. 2) | <i>P</i> $\bar{1}$ (no. 2) |
| <i>a</i> [pm] | 1083.72(3) | 1222.75(3) |
| <i>b</i> [pm] | 1190.00(4) | 1302.46(4) |
| <i>c</i> [pm] | 1399.07(4) | 1427.50(4) |
| α [°] | 91.719(2) | 72.257(2) |
| β [°] | 111.703(2) | 86.807(2) |
| γ [°] | 116.442(2) | 84.583(2) |
| <i>V</i> [10 ^{−30} m ³] | 1459.33(8) | 2154.7(1) |
| <i>Z</i> | 2 | 2 |
| <i>D</i> _{calcd.} [g cm ^{−3}] | 1.187 | 1.171 |
| μ [mm ^{−1}] | 1.094 | 1.510 |
| Crystal size [mm] | 0.17 × 0.13 × 0.02 | 0.30 × 0.28 × 0.27 |
| Radiation | Cu- <i>K</i> α , graphite-monochromator | |
| θ range for data collection [°] | 3.50 ≤ θ ≤ 72.55 | 3.25 ≤ θ ≤ 72.40 |
| Index ranges | −12 ≤ <i>h</i> ≤ 12 −13 ≤ <i>k</i> ≤ 14 −17 ≤ <i>l</i> ≤ 17 | −14 ≤ <i>h</i> ≤ 14 −16 ≤ <i>k</i> ≤ 14 −17 ≤ <i>l</i> ≤ 17 |
| Independent reflections | 4970 (<i>R</i> _{int} = 0.0191) | 7344 (<i>R</i> _{int} = 0.0198) |
| Parameters | 353 | 480 |
| $R = \Sigma F_o - F_c / \Sigma F_o $ [<i>I</i> > 2σ(<i>I</i>)] | 0.0381 (4648) | 0.0461 (6657) |
| $wR_2 = \{\Sigma w(F_o ^2 - F_c ^2)^2 / \Sigma F_o ^2\}^{1/2}$ (all data) | 0.1091 | 0.1317 |
| Max./min. residual electron density [10 ³⁰ e m ^{−3}] | 0.246/−0.365 | 0.980/−0.454 |

[a] Programme SHELXTL-97;^[34] solutions by direct methods, full-matrix refinement with all independent structure factors.

0.33 (t, ³*J*_{H-H} = 7.4 Hz, 3 H, CH₂CH₃), 1.46 and 1.47 (each s, 3 H, NCH₃), 2.02 and 2.14 (m, 1 H, NCH₂) ppm; amine III: δ = 0.45 (t, ³*J*_{H-H} = 7.4 Hz, 3 H, CH₂CH₃), 1.45 and 1.51 (each s, 3 H, NCH₃), 2.19 and 2.39 (each dq, ³*J*_{H-H} = 7.4 Hz, ²*J*_{H-H} = 14.0 Hz, 1 H, NCH₂) ppm. ¹³C NMR (100 MHz, C₆D₆): pyrrole I: δ = 106.1 (NCC), 121.6 and 121.7 (NCC) ppm; pyrrole II: δ = 106.0 and 106.1 (NCC), 121.5 and 121.9 (NCC) ppm; pyrrole III: δ = 106.6 and 106.8 (NCC), 121.7 and 121.9 (NCC) ppm; pyrrole IV: δ = 105.1 (NCC), 121.7 and 121.8 (NCC) ppm; pyrrole V: δ = 104.9 (NCC) and 122.5 (NCC) ppm; amine I: δ = 6.4 (CH₂CH₃), 40.5 and 40.9 (NCH₃), 50.9 (NCH₂) ppm; amine II: δ = 5.6 (CH₂CH₃), 39.5 and 39.8 (NCH₃), 49.5 (NCH₂) ppm; amine III: δ = 6.8 (CH₂CH₃), 40.5 and 41.1 (NCH₃), 51.2 (NCH₂) ppm. IR (CsBr, paraffin): $\tilde{\nu}$ = 1840 [s, ν(AlH)] 1651 [w, br. (phenyl)] 1462 (vs), 1377 (m, paraffin) 1308 (w), 1261 [w, δ(CH)] 1166 (w), 1153 (w), 1084 (w), 1057 (m), 1034 (w), 961 (s), 916 (w), 862 [s, ν(CC), ν(NN), ν(CN)] 795 (m), 773 [m, ν(NN)] 721 (s, paraffin) 671 (w), 638 (m, phenyl) 588 (w), 571 (w), 529 (vw), 473 [w, ν(AlC), ν(AlN)] cm^{−1} ppm. C₃₂H₅₈Al₅N₁₃ (759.81): calcd. C 50.6, H 7.7, N 24.0; found C 50.3, H 7.7, N 23.8.

Crystal Structure Determinations: Single crystals of compounds **1** and **2** were obtained from the reaction mixtures at + 3 °C. The crystallographic data were collected with a Bruker APEX diffractometer with graphite-monochromated Cu-*K* α radiation. The crystals were coated with a perfluoropolyether, picked up with a glass fiber and immediately mounted in the cooled nitrogen stream of the diffractometer. The crystallographic data and details of the final *R* values are provided in Table 1.^[35] All non-hydrogen atoms were refined with anisotropic displacement parameters; hydrogen atoms attached to carbon atoms were calculated in ideal positions and allowed to ride on the bonded atom with *U* = 1.2*U*_{eq}(C). The positions of the hydrogen atoms attached to aluminum atoms were taken from difference Fourier maps; they were refined with isotropic displacement parameters. The crystals of **1** include one molecule of toluene in the unit cell, which is disordered over a crystallographic center of symmetry with two positions for the methyl

group. One ethyl group of **1** (N3) showed a disorder with two positions for its methyl group (occupation factors 0.64 to 0.36).

Acknowledgments

We are grateful to the Deutsche Forschungsgemeinschaft and the Fonds der Chemischen Industrie for generous financial support.

- [1] a) B. Luo, S. Y. Lee, J. M. White, *Chem. Mater.* **2004**, *16*, 629–638; b) D. K. Gaskill, N. Bottka, M. C. Lin, *J. Cryst. Growth* **1986**, *77*, 418–423; c) R. T. Lee, G. B. Stringfellow, *J. Electron Mater.* **1999**, *28*, 963–969; d) V. Lakhota, D. A. Neumayer, A. H. Cowley, R. A. Jones, J. G. Ekerdt, *Chem. Mater.* **1995**, *7*, 546–552; e) Y. J. Hsu, L. S. Hong, K. F. Huang, J. E. Tsay, *Thin Solid Films* **2002**, *419*, 33–39; f) E. Bourret-Courchesne, Q. Ye, D. W. Peters, J. Arnold, M. Ahmed, S. J. C. Irvine, R. Kanjolia, L. M. Smith, S. A. Rushworth, *J. Cryst. Growth* **2000**, *217*, 47–54.
- [2] W. Uhl, *Structure and Bonding, Group 13 Chemistry III – Industrial Applications* (Ed.: H. W. Roesky, D. A. Atwood), Springer Verlag, Berlin–Heidelberg–New York, **2003**, p. 41–66.
- [3] D. W. Peters, E. D. Bourret, M. P. Power, J. Arnold, *J. Organomet. Chem.* **1999**, *582*, 108–115.
- [4] W. Uhl, J. Molter, W. Saak, *Z. Anorg. Allg. Chem.* **1999**, *625*, 321–328.
- [5] W. Uhl, J. Molter, B. Neumüller, W. Saak, *Z. Anorg. Allg. Chem.* **2000**, *626*, 2284–2292.
- [6] W. Uhl, J. Molter, R. Koch, *Eur. J. Inorg. Chem.* **1999**, 2021–2027.
- [7] W. Uhl, C. H. Emden, *J. Organomet. Chem.* **2005**, *690*, 1529–1539.
- [8] W. Uhl, C. H. Emden, G. Geiseler, K. Harms, *Z. Anorg. Allg. Chem.* **2003**, *629*, 2157–2167.
- [9] a) W. Uhl, A. Vogelpohl, J. Kösters, *Z. Naturforsch.* **2006**, *61b*, 854–861; b) W. Uhl, A. Vogelpohl, *Z. Naturforsch.* **2008**, *63b*, 1149–1154.

- [10] W. Uhl, T. Abel, A. Hepp, S. Grimme, M. Steinmetz, *Eur. J. Inorg. Chem.* **2008**, 543–551.
- [11] B. Luo, C. J. Cramer, W. L. Gladfelter, *Inorg. Chem.* **2003**, *42*, 3431–3437.
- [12] W. Uhl, J. Molter, B. Neumüller, *Organometallics* **2000**, *19*, 4422–4424.
- [13] H. Nöth, T. Seifert, *Eur. J. Inorg. Chem.* **1998**, 1931–1938.
- [14] W. Uhl, J. Molter, B. Neumüller, *Inorg. Chem.* **2001**, *40*, 2011–2014.
- [15] Y. Kim, J. H. Kim, J. E. Park, H. Song, J. T. Park, *J. Organomet. Chem.* **1997**, *545–546*, 99–103.
- [16] D. Cho, J. E. Park, B. J. Bae, K. Lee, B. Kim, J. T. Park, *J. Organomet. Chem.* **1999**, *592*, 162–167.
- [17] D. W. Peters, M. P. Power, E. D. Bourret, J. Arnold, *Chem. Commun.* **1998**, 753–756.
- [18] a) B. Luo, W. L. Gladfelter, *Chem. Commun.* **2000**, 825–826; b) B. Luo, W. L. Gladfelter, *J. Organomet. Chem.* **2004**, *689*, 666–671.
- [19] D. A. Neumayer, A. H. Cowley, A. Decken, R. A. Jones, V. Lakhotia, J. G. Ekerdt, *Inorg. Chem.* **1995**, *34*, 4698–4700.
- [20] R. J. Wehmschulte, P. P. Power, *Inorg. Chem.* **1996**, *35*, 2717–2718.
- [21] W. Uhl, J. Molter, R. Koch, *Eur. J. Inorg. Chem.* **2000**, 2255–2262.
- [22] W. Uhl, C. H. Emden, W. Massa, *J. Organomet. Chem.* **2006**, *691*, 1382–1388.
- [23] H. Nöth, T. Seifert, *Eur. J. Inorg. Chem.* **2002**, 602–612.
- [24] V. C. Gibson, C. Redshaw, A. J. P. White, D. J. Williams, *Angew. Chem.* **1999**, *111*, 1014–1016; *Angew. Chem. Int. Ed.* **1999**, *38*, 961–964.
- [25] J. S. Silverman, C. D. Abernethy, R. A. Jones, A. H. Cowley, *Chem. Commun.* **1999**, 1645–1646.
- [26] W. Uhl, J. Molter, B. Neumüller, *Chem. Eur. J.* **2001**, *7*, 1510–1515.
- [27] a) W. Uhl, J. Molter, B. Neumüller, F. Schmock, *Z. Anorg. Allg. Chem.* **2001**, *627*, 909–917; b) W. Uhl, J. Molter, B. Neumüller, *J. Organomet. Chem.* **2001**, *634*, 193–197.
- [28] a) K. Bode, U. Klingebiel, *Adv. Organomet. Chem.* **1996**, *40*, 1–53; b) S. Dielkus, C. Drost, R. Herbst-Irmer, U. Klingebiel, *Angew. Chem.* **1993**, *105*, 1689–1690; *Angew. Chem. Int. Ed. Engl.* **1993**, *32*, 1625–1626; c) C. Glidewell, D. W. H. Rankin, A. G. Robiette, G. M. Sheldrick, *J. Chem. Soc. A* **1970**, 318–320; d) Y. Morino, T. Iijima, Y. Murata, *Bull. Chem. Soc. Jpn.* **1960**, *33*, 46–48.
- [29] C. H. Heathcock, R. A. Badger, J. W. Patterson Jr, *J. Am. Chem. Soc.* **1967**, *89*, 4133–4145.
- [30] C.-R. Zhang, Y.-L. Wang, *Synth. Commun.* **2003**, *33*, 4205–4208.
- [31] W. Flitsch, U. Krämer, H. Zimmermann, *Chem. Ber.* **1969**, *102*, 3268–3276.
- [32] R. Dorn, M. Müller, J. Lorberth, G. Zimmermann, H. Protzmann, W. Stolz, E. O. Göbel, *Mater. Science* **1993**, *B17*, 25–28.
- [33] T. Hahn (Ed.), *International Tables for Crystallography, Space-Group Symmetry*, Kluwer Academic Publishers, Dordrecht–Boston–London, **1989**, vol. A.
- [34] *SHELXTL-Plus*, release 4.1, Siemens Analytical X-ray Instruments Inc., Madison, WI, **1990**; G. M. Sheldrick, *SHELXL-97, Program for the Refinement of Structures*, University of Göttingen, **1997**.
- [35] CCDC-700785 (for **1**) and -700786 (for **2**) contain the supplementary crystallographic data for this paper. These data can be obtained free of charge from The Cambridge Crystallographic Data Centre via www.ccdc.cam.ac.uk/data_request/cif.

Received: September 3, 2008

Published Online: November 21, 2008

Computational Results Provide a Synthetically Unprecedented Explanation for the β -Regioselectivity in the Rh-Catalyzed Hydroformylation of Vinylidene Substrates

Caterina Ghio,^[a] Raffaello Lazzaroni,^[b] and Giuliano Alagona*^[a]

Keywords: Regioselectivity / Homogeneous catalysis / Density functional calculations / Hydroformylation

The approaching path of CO to the alkyl-Rh(CO)₃ intermediate, considered for 1,1-diphenylethene as a test case to investigate the reason of its failure to produce quaternary aldehydes in hydroformylation reactions, shows a remarkable activation barrier in DFT calculations for the branched alkyl-Rh intermediate, but not for the linear one. Consideration of the free energy associated to this step strengthens this result, whereas the other steps remain fairly comparable. The path leading to the branched aldehyde is thus abandoned early, and this species then returns to the catalyst and the olefin, with subsequent reformation of the branched and linear

alkyl-Rh intermediates until consumption of the olefin. The branched backward pathway is more favourable indeed than the forward one, as can be inferred from its free energy reaction profile. The heuristic value of theoretical/computational methods in exploring experimentally inaccessible species and in rationalizing the results, together with the importance of the organic part structure in organometallic complexes, is also put forward.

(© Wiley-VCH Verlag GmbH & Co. KGaA, 69451 Weinheim, Germany, 2009)

Introduction

The hypothesis that regioselectivity in nonreversible hydroformylation reactions originates at the alkyl formation step was tested for a number of substrates^[1] and confirmed in our previous theoretical investigations on this subject^[2–5] by comparing the computed branched to linear transition state (TS) ratios (B/L) obtained by applying Equation (1) to experiments employing unmodified rhodium catalysts under mild reaction conditions.

$$B/L = \frac{\sum e^{-\Delta G_b^\ddagger/RT}}{\sum e^{-\Delta G_l^\ddagger/RT}} = \frac{\sum e^{-\Delta \Delta G^\ddagger/RT}}{\sum e^{-\Delta \Delta E^\ddagger/RT}} \quad (1)$$

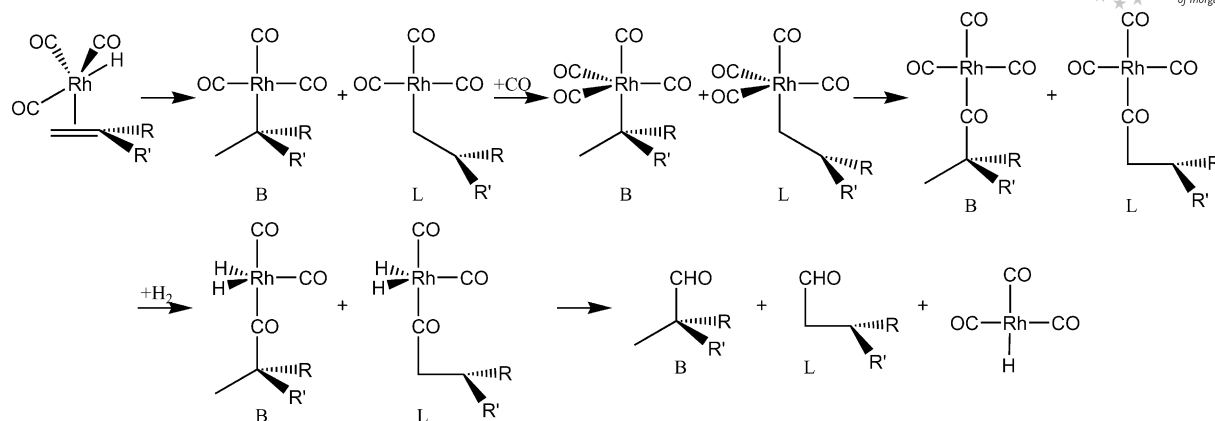
Therefore, in order to predict the reaction selectivity it was not necessary to compute the subsequent reaction steps, that is, the formation of the alkyl-Rh(CO)₃ complex, the addition of CO to give the tetracarbonyl intermediate (Int), the CO insertion into the Rh–C(alkyl) bond, the H₂ oxidative addition and the aldehyde reductive elimination

to produce aldehydes (Scheme 1). There are, however, some notable exceptions in the realm of reversible hydroformylations occurring at higher temperatures (about 100 °C) where theoretical B/L ratios remarkably differ from experimental values. Aryl or alkyl 1,1-disubstituted olefins, for instance, are known to afford the linear aldehyde as the only product.^[6–9] This result is fairly well reproduced in the case of 1,1-dimethylethene by using the TS relative stabilities.^[2] Conversely, for other substrates, the theoretical B/L ratios turn out to be about 50:50, or even 72:28 as in 1,1-diphenylethene, instead of decidedly favouring linear aldehydes.

Experimental findings, however, support that a tertiary alkyl-Rh intermediate is formed in a larger amount than the linear isomer under hydroformylation conditions of 1,1-diphenylethene in the early stage of the reaction (in agreement with our aforementioned theoretical results), but without formation of the branched aldehyde.^[10] This was attributed to the different behaviours of the Rh(CO)₄ branched species during the migratory insertion step, probably prevented by steric reasons, rather than in their formation step. Consequently the branched intermediate was considered to undergo β -elimination only.^[10] Despite the merits of deuterioformylation experiments in rationalizing mechanistic aspects, especially at partial substrate conversion, it is difficult to fully clarify the reasons for the reaction outcomes. The present computational study is devoted to a thorough investigation on 1,1-diphenylethene as a test case, in order to understand the origin and the fate of the various species.

[a] IPCF-CNR, MML,
via Moruzzi 1, 56124 Pisa, Italy
Fax: +39-050-3152442
E-mail: G.Alagona@ipcf.cnr.it

[b] Dept. of Chemistry & Industrial Chemistry (DCCI), University of Pisa,
Via Risorgimento 35, 56126 Pisa, Italy
Supporting information for this article is available on the WWW under <http://www.eurjic.org> or from the author.



Scheme 1. The Rh-catalyzed hydroformylation reaction.

Results and Discussion

The stabilities of the various forms (some of them are displayed in Figures S1–S4 and S6–S8 of the Supporting Information) along the reaction steps leading to the CO insertion intermediate have been preliminarily computed for 1,1-diphenylethene, as described in the Methods section, obtaining the energy profile reported in Figure 1.

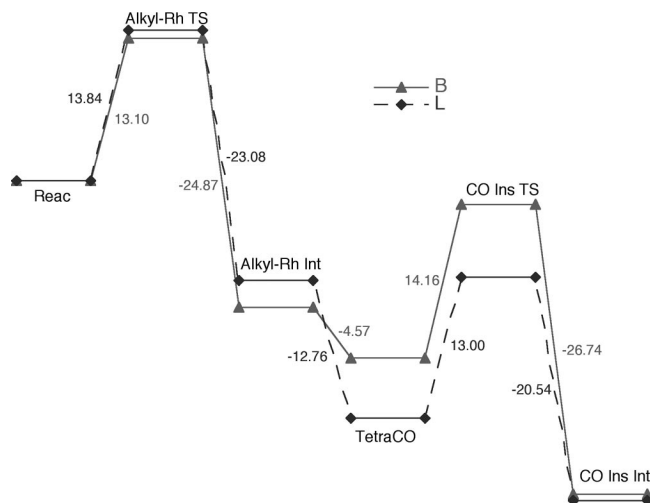


Figure 1. B3P86/6-31G*/LANL2DZ branched (B) and linear (L) reaction profiles for 1,1-diphenylethene (a CO at infinite separation is included in the first three steps for the sake of comparison).

It is worth noting, however, that this energy profile is not helpful either to shed light on the reaction experimental outcomes. Because it is generally accepted that the transformation of a tricarbonylmetal–alkyl compound into a tetracarbonylmetal–alkyl one spontaneously occurs (in Figure 1 both tetracarbonyl species turn out to be more stable than the tricarbonyl ones), the subsequent step, that is, the migratory insertion of CO into the tertiary alkyl group, has invariably been regarded as the critical step.^[9] The B path, leading to the branched aldehyde, is initially more favourable than the L one. Already, the alkyl-Rh(CO)₄ branched complex is less stable than the linear one, but the difference in barrier heights for the CO migratory insertion is not dramatic (13 vs. 14 kcal/mol). The stability of the trigonal bi-

pyramidal (TBP) compounds obtained after adding an equatorial CO group to an alkylmetal tricarbonyl intermediate was reported by other authors as well.^[11]

Due to the failure of the theoretical approach on the basis of the alkyl-Rh TS relative energies to predict the vinylidene olefin regioselectivity, in addition to the stability of alkyl-Rh(CO)₄ complexes, we decided, however, to take into account also the approaching path to Rh of the incoming CO group, because of the striking difference between linear and branched tricarbonyl intermediates (shown in Figure 2), despite that more than 30 years of experimental literature pointed to the subsequent CO migratory insertion and even though for HCo(CO)₃-catalyzed hydroformylations this step had been sometimes considered and sometimes disregarded.^[12]

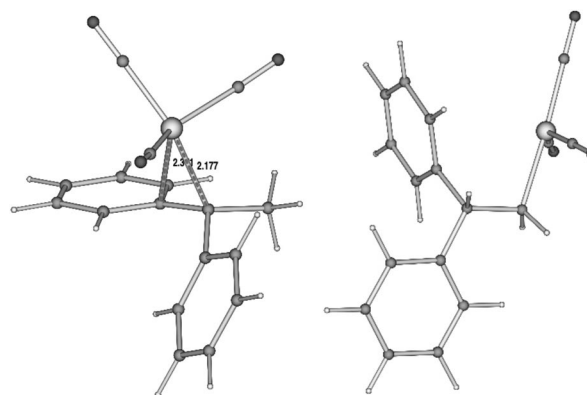
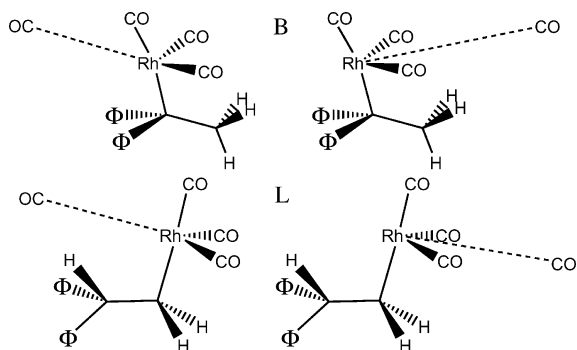


Figure 2. B3P86/6-31G*/LANL2DZ structures of the branched (left-hand side) and linear (right-hand side) tricarbonyl intermediates.

Two main approaching paths were thus examined for both B and L alkyl-Rh(CO)₃ intermediates, as shown in Scheme 2: the outer one points to Rh from behind (roughly along its supposedly vacant coordination site), whereas the inner one points along the line between the two CO groups, nearly perpendicular to the Rh–C(alkyl) bond. In the latter case, at least one of the two CO groups must span a larger displacement with respect to the CO–Rh–C(alkyl) axis to make enough room for the incoming CO.



Scheme 2. Outer (left-hand side) and inner (right-hand side) B and L approaching paths.

The four reaction profiles (Figure 3) show that an additional CO can approach Rh very easily from both directions in the case of the linear complex. In contrast, in the case of the branched one, there is a remarkable barrier (somewhat steeper along the inner approaching path, because of the need to accommodate the third CO, as described above). The barrier is due to the fact that the incoming CO has to overcome the agostic interaction (Figure 2) established in the branched tricarbonyl intermediate between Rh and one of the phenyl rings. Conversely, in the linear tricarbonyl intermediate the situation is very different, because the closest phenyl ring is farther than 3 Å from Rh. The adduct geometries are only slightly more stable than the individual partners (B or L tricarbonyl intermediates + CO) at infinite separation, although the “in” arrangement is 0.37 and 0.45 kcal/mol more favourable than the “out” one for L and B, respectively. The C...Rh equilibrium distances are 4.444 (Bout), 4.004 (Bin), 4.538 (Lout) and 3.639 Å (Lin).

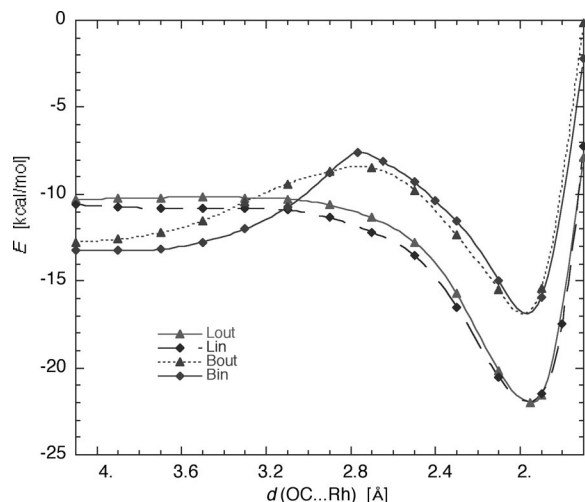


Figure 3. B3P86/6-31G*/LANL2DZ branched (B) and linear (L) inner and outer approaching paths of CO to the 1,1-diphenylethane-Rh(CO)₃ complex.

Because local minima were found for each adduct, a very accurate TS search for the CO addition was carried out even for the linear TS, and all were confirmed by frequency calculations. The intrinsic reaction coordinate (IRC) plot

along the B outer approaching path together with the relevant TS structure is displayed in Figure 4 (imaginary frequency = -68.92 cm^{-1}). The slightly less favourable inner approaching path features a TBP TS structure, with the incoming CO roughly in the methyl group direction (C–Rh–C–CH₃ -34.3°). In the alkyl-Rh(CO)₄ species the in-plane CO groups are roughly staggered with respect to the diphenyl methyl group underneath.

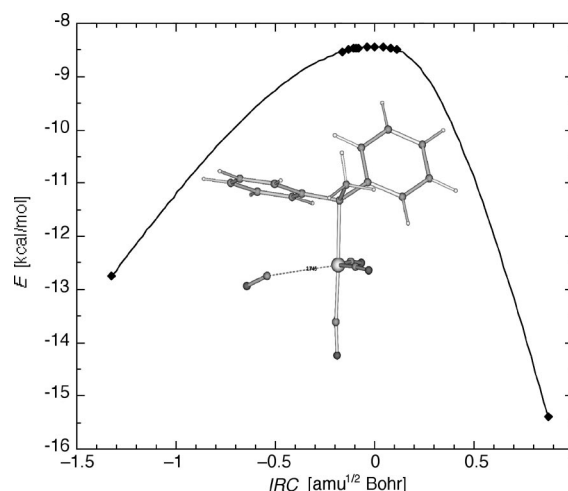


Figure 4. B3P86/6-31G*/LANL2DZ IRC along the branched outer approaching paths of CO to the 1,1-diphenylethane-Rh(CO)₃ complex and TS structure.

Interestingly, the internal energy shows shallow minima for the adducts of CO with B and L tricarbonyl intermediates (Tri...CO) at the aforementioned separations, whereas the free energy increases by about 6 kcal/mol, as can be derived from the energy levels for the most favourable B and L paths displayed in Figure 5. The subsequent linear TS (imaginary frequency = -10.16 cm^{-1}) is just 0.03/2.11 kcal/mol higher than the potential/free-energy minimum, respectively. Conversely, the branched TS is 4.38/9.94 kcal/mol, respectively, above Tri...CO. Therefore, a significant barrier is present along the branched pathway and not along the linear one, putting forward an unexpected mechanistic reason for the absence of branched aldehydes. Moreover, it is of paramount importance to take into account the free energy of the process.

All the subsequent reaction steps leading to the aldehydes have thus been investigated. Interested readers can find a number of structures in Figures S6–S12 of the Supporting Information, because all the possible conformers of each isomer (linear or branched) are to be considered not to miss the most stable ones. Again, all the stationary points have been confirmed by frequency calculations, allowing the free energies to be calculated as well. They are reported in Table 1, together with the internal energies, for the most stable species of each type (the adducts of CO and H₂, respectively, to the Tri and CO-insertion intermediates are not included). Actually, the free energies are to be taken into account in studying reaction mechanisms when the number of molecules involved in the reaction changes along the pathway.

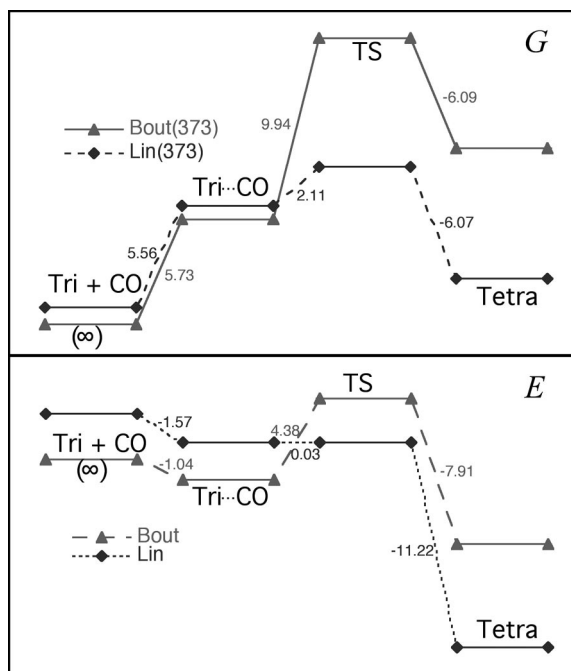


Figure 5. B3P86/6-31G*/LANL2DZ branched (B, triangles) and linear (L, diamonds) potential energy (E)/free energy (G , at 373 K) reaction profiles [kcal/mol] for 1,1-diphenylethene. The energy differences are also displayed.

Whereas the alkyl-Rh(CO)₃ TS barriers are almost insensitive to the inclusion of thermal corrections, the stabilities of the alkyl-Rh(CO)₃ intermediates are significantly reduced. Referring the Tri-Tetra TS to the Tri + CO isolated species, the picture does not change with respect to that displayed in Figure 5; a quite remarkable effect is observed on the Tri-Tetra TS for the CO addition to the branched complex, that is, for the passage from the alkyl-Rh(CO)₃ intermediate to the alkyl-Rh(CO)₄ one, whose barrier increases from 3.34 to 13.26/15.66 kcal/mol at 298/373 K, respectively. An analogous shift in the free energies is maintained for the subsequent steps, indicating that the real difference between the two pathways is due to the upward shift in the profile determined by the CO addition. This effect

can be better put forward graphically by comparing the whole reaction profiles, plotted in Figure 6 (upper part) together with the internal energy ones (lower part). The first obvious consideration is related to the overall trend of both profiles: the internal energy ones present high initial barriers for both linear and branched pathways, whereas all the other TS are in any case lower than the reactant level. In addition, the branched alkyl-Rh TS is slightly more favourable (by ca. 0.7 or 0.4 kcal/mol considering either energy or free energy, respectively) than the linear one, thus confirming the experimental results obtained at partial substrate conversion.^[9]

It is worth stressing that if the B and L profiles for the steps after the CO addition are considered and superimposed making the alkyl-Rh(CO)₄ B and L free energies coincide, they are fairly similar, as can be derived from Figure 7: the primary difference between the whole pathways indeed is the high barrier for the CO addition, obtained for the branched species, whose upward shift is maintained along the subsequent steps.

The remarkable activation free energy for the CO addition obtained for the branched alkyl-Rh intermediate provides a new key in explaining the β -regioselectivity in the hydroformylation of 1,1-diphenylethene. The earlier, usually overlooked, critical step, that is, the addition of CO to the alkyl-Rh(CO)₃ group and not the CO migratory insertion into the Rh-C(alkyl) bond, causes the free energy to raise in the branched profile by a nearly constant amount with respect to the linear pathway. The free energy reaction profile strongly suggests that the path leading to the branched aldehyde is abandoned early, because the forward barriers turn out to be higher than the backward ones. In other words, the branched alkyl-Rh intermediate should return to the reactant stage where branched and linear Rh-alkyls are formed again in the B/L proportion. This process continues until almost complete consumption of the olefin, thus yielding a product that practically consists only of the linear aldehyde. Hydro(deuterio)formylation experiments also support a β -hydride elimination mechanism,^[9,10,13] although they cannot indicate which step is responsible for that behaviour. The authors concluded that the steric hin-

Table 1. B3P86/6-31G*/LANL2DZ relative energies (ΔE) and free energies (ΔG)^[a] for branched (B) and linear (L) 1,1-diphenylethene with respect to Reac + CO + H₂.

| Species ^[b] | ΔE ^[c] | | ΔG ^[d] (298.15 K) | | ΔG ^[e] (373.15 K) | |
|------------------------|---------------------------|--------|--------------------------------------|--------|--------------------------------------|--------|
| | B | L | B | L | B | L |
| Tri TS | 13.10 | 13.84 | 13.03 | 13.41 | 13.30 | 13.67 |
| Tri Int | -11.77 | -9.23 | -7.62 | -6.35 | -7.12 | -6.22 |
| Tri-Tetra TS | -8.43 | — | 5.64 | — | 8.55 | — |
| Tetra | -16.34 | -21.99 | -0.65 | -7.36 | 2.45 | -4.62 |
| CO Ins TS | -2.18 | -8.99 | 12.63 | 5.17 | 15.68 | 7.98 |
| CO Ins Int | -28.91 | -29.52 | -12.44 | -15.18 | -9.36 | -12.68 |
| H ₂ Add TS | -13.78 | -19.78 | 11.55 | 4.14 | 16.88 | 9.02 |
| H ₂ Add Int | -23.33 | -28.48 | 4.48 | -2.59 | 9.89 | 2.29 |
| Elim TS | -13.97 | -18.69 | 13.12 | 6.64 | 18.68 | 11.67 |
| Aldehyde | -39.30 | -40.07 | -13.82 | -16.90 | -9.41 | -13.12 |

[a] Values are in kcal/mol. [b] Tri stands for alkyl-Rh(CO)₃; Tetra for alkyl-Rh(CO)₄; CO Ins for CO insertion into the Rh-C(alkyl) bond; Add for addition and Elim for aldehyde elimination. [c] Reference energy = -1108.484809 E_h. [d] Reference free energy at 298 K = -1108.305483 E_h. [e] Reference free energy at 373 K = -1108.335350 E_h.

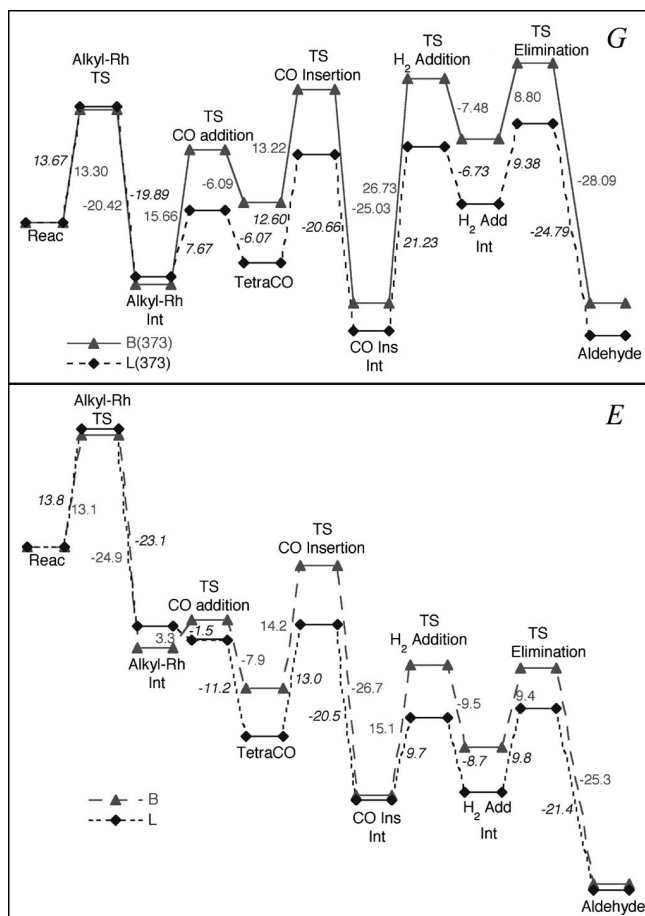


Figure 6. B3P86/6-31G*/LANL2DZ branched (B, triangles) and linear (L, diamonds) potential energy (*E*)/free energy (*G*, at 373 K) reaction profiles [kcal/mol] for 1,1-diphenylethene. Italic values are related to the linear profiles.

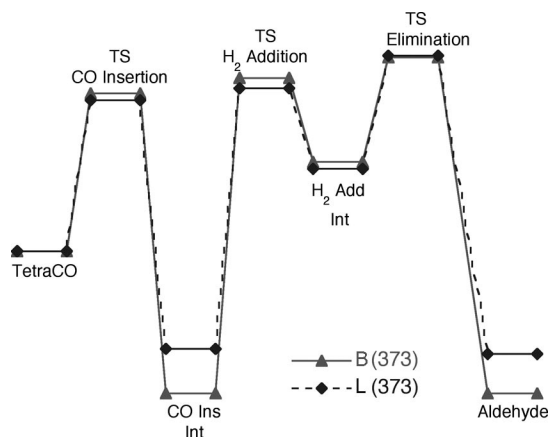


Figure 7. B3P86/6-31G*/LANL2DZ branched (B, triangles) and linear (L, diamonds) free energy (at 373 K, top) reaction profiles [kcal/mol] for 1,1-diphenylethene with TetraCO superimposed.

drance probably determines the different evolution of the tertiary alkyl with respect to the primary one when the CO migratory insertion should take place. On the basis of the

profile displayed in Figure 6, it is obvious that simple return of the branched alkyl Rh intermediate to the Reac structure is easily attainable, because a lower barrier than that for the forward reaction is to be surmounted.

Conclusions

Theoretical calculations on the hydroformylation of 1,1-diphenylethene, carried out on the approaching path of the fourth CO group, demonstrated indeed that there is an unexpected and remarkably high free energy activation barrier for the tertiary alkyl-Rh(CO)₃ intermediate, whereas the reaction pathway is practically downhill for the linear one once the linear alkyl-Rh(CO)₃...CO adduct has been formed. For the present substrate, this barrier can be ascribed to the agostic interaction with the π density of one of the aromatic rings. The formation of the alkyl-Rh(CO)₄ species, overlooked thus far because of its thermodynamic stability, instead of the subsequent steps, that is, the insertion of an alkyl group onto the coordinated CO group, previously hypothesised in the literature,^[8–10] as well as the H₂ oxidative addition and reductive elimination, whether reachable, is actually responsible for the absence of the quaternary aldehyde. This is a novel finding. Nonetheless, the barrier for the CO addition to the branched intermediate is not a peculiarity of this system: other substrates show similar behaviour. A thorough account of those results will be reported in a forthcoming article.

In summary, the importance of the organic structure in organometallic complexes is revealed from this study as is the valuable contribution of theoretical methods in exploring experimentally inaccessible species and interpreting mechanistic aspects. This study stresses that, in the case of reversible hydroformylation reactions, it is necessary to take into account any stationary points on the potential energy surface without assuming that they are negligible and unimportant according to chemical intuition and assessed concepts. The need to include zero-point energy and thermal corrections clearly emerges from the discussion.

Methods Section

Computational Details: All calculations were carried out with the Gaussian 03 system of programs^[14] in the density functional theory (DFT) framework by making use of a hybrid method, B3P86,^[15a,15b] and the 6-31G* basis set.^[16] Coupled to the B3P86/6-31G* description for C, O and H, effective core potentials were used for Rh, because they implicitly include some relativistic effects for the electrons near the nucleus, in the LANL2DZ valence basis set.^[17] We resorted to the B3P86 functionals, because they behaved well in our previous studies involving Rh-carbonyl complexes,^[2,4] where both the metal-olefin bond strength and the TS stability are sensitive to the electron correlation description.^[18] Thermal corrections for obtaining standard free energies for the various species at *T* [K] and 1 atm were calculated by using the rigid rotator-harmonic oscillator approximation.^[19]

$$G(T) = E(0) + ZPE + \Delta H(0-T) - T\Delta S(0-T)$$

Accordingly, ΔG was calculated as:

$$\Delta G(\text{species}) = G(\text{species}) - [G(\text{Reac}) + G(\text{CO}) + G(\text{H}_2)]$$

Supporting Information (see footnote on the first page of this article): Side and front view of 1,1-diphenylethene; stable Reac adducts for the rotation of the H–Rh(CO)₃ group; stable branched and linear alkyl-Rh transition states; structure of branched and linear alkyl-Rh tricarbonyl intermediates; side and upper views of the B transition state along the outer approaching path for the CO addition; structures of the B and L alkyl-Rh tetracarbonyl intermediates (Tetra); structures of the B and L transition states for the CO migratory insertion; branched and linear CO-insertion intermediates; branched and linear H₂-addition transition states; branched and linear H₂-addition intermediates; branched and linear reductive elimination transition states; branched and linear aldehyde adducts to H–Rh(CO)₃.

- [1] a) R. Lazzaroni, G. Uccello-Barretta, M. Benetti, *Organometallics* **1989**, *8*, 2323–2327; b) A. Raffaelli, S. Pucci, R. Settambolo, G. Uccello-Barretta, R. Lazzaroni, *Organometallics* **1991**, *10*, 3892–3898; c) G. Uccello-Barretta, R. Lazzaroni, R. Settambolo, P. Salvadori, *J. Organomet. Chem.* **1991**, *417*, 111–119; d) R. Lazzaroni, R. Settambolo, G. Uccello-Barretta, *Organometallics* **1995**, *14*, 4644–4650.
- [2] G. Alagona, C. Ghio, R. Lazzaroni, R. Settambolo, *Organometallics* **2001**, *20*, 5394–5404.
- [3] G. Alagona, C. Ghio, R. Lazzaroni, R. Settambolo, *Inorg. Chim. Acta* **2004**, *357*, 2980–2988.
- [4] G. Alagona, C. Ghio, *J. Organomet. Chem.* **2005**, *690*, 2339–2350.
- [5] G. Alagona, C. Ghio, S. Rocchiccioli, *J. Mol. Model.* **2007**, *13*, 823–837.
- [6] Y. Matsui, M. Orchin, *J. Organomet. Chem.* **1983**, *246*, 57–60.
- [7] I. Amer, H. Alper, *J. Am. Chem. Soc.* **1990**, *112*, 3674–3676.
- [8] C. Botteghi, L. Cazzolato, M. Marchetti, S. Paganelli, *J. Org. Chem.* **1995**, *60*, 6612–6615.
- [9] R. Lazzaroni, R. Settambolo, G. Uccello-Barretta, A. Caiazzo, S. Scamuzzi, *J. Mol. Catal. A* **1999**, *143*, 123–130.
- [10] R. Lazzaroni, G. Uccello-Barretta, S. Scamuzzi, R. Settambolo, A. Caiazzo, *Organometallics* **1996**, *15*, 4657–4659.
- [11] a) L. Versluis, T. Ziegler, E. J. Baerends, W. Ravenek, *J. Am. Chem. Soc.* **1989**, *111*, 2018–2025; b) T. Matsubara, N. Koga, Y. Ding, D. G. Musaev, K. Morokuma, *Organometallics* **1997**, *16*, 1065–1078; c) S. A. Decker, T. R. Cundari, *Organometallics* **2001**, *20*, 2827–2841; d) S. K. Goh, D. S. Marynick, *Organometallics* **2002**, *21*, 2262–2267; e) X. Luo, D. Tang, M. Li, *Int. J. Quantum Chem.* **2006**, *106*, 1844–1852; f) D. Tang, S. Qin, Z. Su, C. Hu, *Organometallics* **2007**, *26*, 33–47.
- [12] a) C.-F. Huo, Y.-W. Li, M. Beller, H. Jiao, *Organometallics* **2003**, *22*, 4665–4677; b) C.-F. Huo, Y.-W. Li, M. Beller, H. Jiao, *Chem. Eur. J.* **2005**, *11*, 889–902; c) S. Klaus, H. Neumann, H. Jiao, A. Jacobi van Wangelin, D. Gördes, D. Strübing, S. Hübner, M. Hateley, C. Weckbecker, K. Huthmacher, T. Riermeier, M. Beller, *J. Organomet. Chem.* **2004**, *689*, 3685–3700.
- [13] R. Lazzaroni, R. Settambolo, G. Prota, C. Botteghi, S. Paganelli, M. Marchetti, *Inorg. Chim. Acta* **2004**, *357*, 3079–3083.
- [14] M. J. Frisch, G. W. Trucks, H. B. Schlegel, G. E. Scuseria, M. A. Robb, J. R. Cheeseman, J. A. Montgomery Jr, T. Vreven, K. N. Kudin, J. C. Burant, J. M. Millam, S. S. Iyengar, J. Tomasi, V. Barone, B. Mennucci, M. Cossi, G. Scalmani, N. Rega, G. A. Petersson, H. Nakatsuji, M. Hada, M. Ehara, K. Toyota, R. Fukuda, J. Hasegawa, M. Ishida, T. Nakajima, Y. Honda, O. Kitao, H. Nakai, M. Klene, X. Li, J. E. Knox, H. P. Hratchian, J. B. Cross, V. Bakken, C. Adamo, J. Jaramillo, R. Gomperts, R. E. Stratmann, O. Yazyev, A. J. Austin, R. Cammi, C. Pomelli, J. W. Ochterski, P. Y. Ayala, K. Morokuma, G. A. Voth, P. Salvador, J. J. Dannenberg, V. G. Zakrzewski, S. Dapprich, A. D. Daniels, M. C. Strain, O. Farkas, D. K. Malick, A. D. Rabuck, K. Raghavachari, J. B. Foresman, J. V. Ortiz, Q. Cui, A. G. Baboul, S. Clifford, J. Cioslowski, B. B. Stefanov, G. Liu, A. Liashenko, P. Piskorz, I. Komaromi, R. L. Martin, D. J. Fox, T. Keith, M. A. Al-Laham, C. Y. Peng, A. Nanayakkara, M. Challacombe, P. M. W. Gill, B. Johnson, W. Chen, M. W. Wong, C. Gonzalez, J. A. Pople, *Gaussian 03*, Revision C.02, Gaussian Inc., Wallingford, CT, **2004**.
- [15] a) A. D. Becke, *J. Chem. Phys.* **1993**, *98*, 5648–5652; b) J. P. Perdew, *Phys. Rev. B* **1986**, *33*, 8822–8824.
- [16] W. J. Hehre, L. Radom, P. v. R. Schleyer, J. A. Pople, *Ab Initio Molecular Orbital Theory*, Wiley, New York, **1986**.
- [17] P. J. Hay, W. R. Wadt, *J. Chem. Phys.* **1985**, *82*, 270–283.
- [18] N. Koga, S. Q. Jin, K. Morokuma, *J. Am. Chem. Soc.* **1988**, *110*, 3417–3425.
- [19] D. A. McQuarrie, *Statistical Mechanics*, University Science Book, Sausalito, CA, **2000**.

Received: July 10, 2008

Published Online: November 28, 2008

Molecular Motion and Performance Enhancement of BORAZAN Fluorescent Dyes

Tyler J. Morin,^[a] Sergey V. Lindeman,^[a] and James R. Gardinier*^[a]

Keywords: Chelates / Boron / Electrochemistry / UV/Vis spectroscopy / Fluorescence / Dyes/pigments / Density functional calculations

The preparation of three 2,6-dipyrazolyl-4-X-anilines, $H(pz_2An^X)$ ($X = p\text{-CF}_3$, Cl, $t\text{Bu}$) using CuI-catalyzed amination is described. Subsequent reactions of $H(pz_2An^X)$ with triphenylboron proceeds with benzene elimination to give the corresponding $Ph_2B(pz_2An^X)$ compounds in high yields. The $Ph_2B(pz_2An^X)$ are more highly emissive in the solid state than the previously reported BORAZAN fluorophores, $Ph_2B(pzAn^X)$, their monopyrazolyl counterparts. As with the $Ph_2B(pzAn^X)$, the color of emission in $Ph_2B(pz_2An^X)$ can be tuned simply by varying the *para*-aniline substituent where the emission of $Ph_2B(pz_2An^X)$ is red-shifted relative to the corresponding $Ph_2B(pzAn^X)$ derivatives. The electronic properties were studied by cyclic voltammetry and electronic absorption/emission spectroscopy as well as by density func-

tional calculations (B3LYP/6-31G*). The di-pyrazolyl derivatives exhibit greater stability toward solvolysis and higher photoluminescent quantum yields (despite the red-shift in emission) compared to their monopyrazolyl counterparts presumably due to kinetic stabilization of the chromophore imparted by the second pyrazolyl ligand. For $Ph_2B(pz_2An^X)$, evidence for intramolecular motion of the diphenylboryl moiety traversing both pyrazolyl groups was detected by variable temperature 1H NMR spectroscopy. The rate increases with increasing electron-donor abilities of the *para*-aniline substituent.

(© Wiley-VCH Verlag GmbH & Co. KGaA, 69451 Weinheim, Germany, 2009)

Introduction

There is a longstanding interest in developing new brightly-emitting fluorophores for fundamental studies and for a variety of applications, from sensors and display technology to biomedical imaging.^[1] Boron species such as BODIPYTM^[2] and other N,N-^[3] and N,O- chelates^[4] have been particularly well-suited for such studies owing to their favourable synthetic protocol, stability, and photophysical properties. We recently reported^[5] on a series of colour tuneable fluorescent dyes based on the diphenylboron complexes of (2-pyrazolyl)-4-X-anilines, or BORAZANs (Figure 1) of the type $Ph_2B(pzAn^X)$ where pz is a pyrazolyl, An is aniline and superscript X is the *para* substituent of the aniline ring. The emission colour, intensity, and reactivity of the fluorescent dyes could be tuned in a regular way by varying the *para*-aniline substituent. For instance, the cyano derivative gave the most intense blue emission [$^{em}\lambda_{max}$ (toluene) = 452 nm, Φ_F (toluene) = 0.81] and was the most stable toward solvolysis with protonated solvents such as water or alcohols. The methoxy derivative gave much less intense yellow-green emission [$^{em}\lambda_{max}$ (toluene) = 522 nm, Φ_F (tolu-

ene) = 0.07] and readily decomposed in protic media. The quantum yields of emission were also greatly reduced in aprotic Lewis-basic solvents compared to hydrocarbon solvents. We conjectured that dynamic solution processes may be related to the low quantum yield of emission and the high reactivity of BORAZANs toward Lewis bases. That is, the integrity of the dye would be compromised if boron-pyrazolyl ring dissociation occurred; resulting in lower quantum yields and the resulting three-coordinate boron may provide a pathway for degradation. In order to test this hypothesis, we have modified the dye structure by putting an additional pyrazolyl ring at the 6-position of the aniline (Figure 2). Such a substitution was designed with the intent of kinetically stabilizing the dye by effectively doubling the rate of boron-pyrazolyl bond formation should boron-pyr-

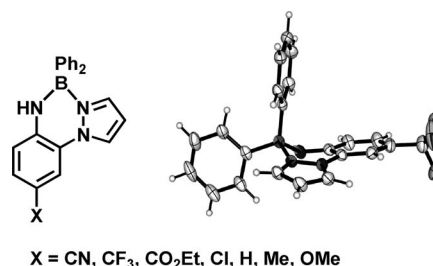


Figure 1. The BORAZAN dye framework and representative solid-state structure of $Ph_2B(pzAn^{CF_3})$ from ref.^[1]

[a] Department of Chemistry, Marquette University, Milwaukee, WI 53201-1881, USA
Fax: +1-414-288-7066
E-mail: james.gardinier@marquette.edu

Supporting information for this article is available on the WWW under <http://www.eurjic.org> or from the author.

azolyl dissociation occur in solution. Moreover, with such a substitution pattern any dynamic processes would be easily detected by NMR, as the pyrazolyl rings would be magnetically inequivalent in a static structure, such as in Figure 2, but would be equivalent if exchange occurred. We report here on the successful implementation of this structural modification for enhancing the performance of BORAZAN dyes. Moreover, the new ligand may be attractive for the future development of mono- and dimetallic transition metal systems, and the current study provides a basis for evaluating the potential photo- and electrochemical “non-innocence” of this scaffold.

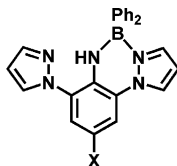
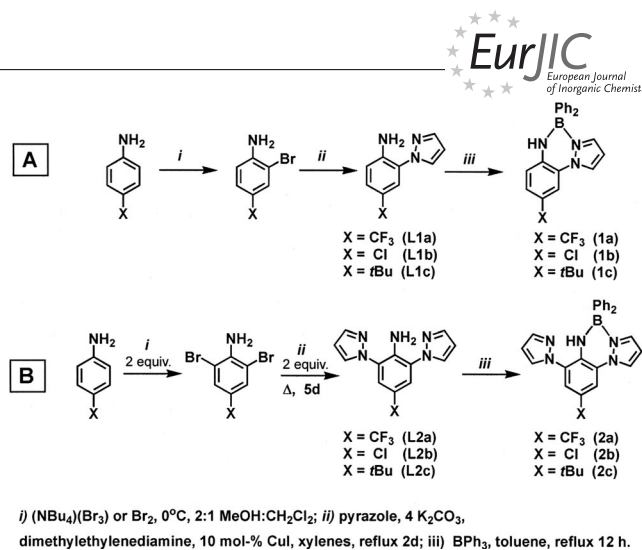


Figure 2. Representation of the 2nd-generation Ph₂B(pz₂An^X) compounds.

Results and Discussion

A summary of the preparative routes to the various ligands and BORAZAN dyes is given in Scheme 1. The syntheses of the first-generation H(pzAn^X) ligands [X = CF₃ (**L1a**), Cl (**L1b**), *t*Bu (**L1c**)] and BORAZAN dyes Ph₂B(pzAn^X) [X = CF₃ (**1a**), Cl (**1b**), *t*Bu (**1c**)] follows the literature method (Scheme 1, a),^[5] where **L1c** and **1c** represent new derivatives. The latter were prepared by monobromination of *p*-*tert*-butylaniline followed by copper-catalyzed amination by the methodology of Buchwald^[6] and Taillefer^[7] to afford **L1c** which was subsequently converted to **1c** in high yield by reaction with triphenylboron in toluene. The second-generation ligands H(pz₂An^X) [X = CF₃ (**L2a**), Cl (**L2b**), *t*Bu (**L2c**)] and BORAZAN dyes Ph₂B(pz₂An^X) [X = CF₃ (**2a**), Cl (**2b**), *t*Bu (**2c**)] were prepared by an analogous route (Scheme 1, b) after first dibrominating the appropriate aniline.^[8] The subsequent copper-catalyzed amination of the 2,6-dibromo-4-X-aniline required longer reaction times to afford the desired H(pz₂An^X) in reasonable yield. The ensuing reaction with triphenylboron proceeded smoothly to afford high yields of the desired **2a–2c** with the elimination of benzene.^[9]

The BORAZAN dyes are insoluble in hexanes, **1a–1c** are soluble in benzene whereas **2a–2c** (based on pz₂An^X) are modestly soluble, and all are soluble in toluene, halocarbons, and polar Lewis-basic solvents (THF, CH₃CN, DMF). The compound Ph₂B(pzAn^{*t*Bu}) (**1c**) rapidly decomposes (over a period of minutes) in alcohols, as found previously for Ph₂B(pzAn^X) (X = Me, MeO), but Ph₂B(pzAn^X) [X = CF₃ (**2a**), Cl (**2b**), *t*Bu (**2c**)] persist over days in this type of solvent. In addition, the second-generation BORAZAN dyes **2a–2c** appear indefinitely air stable in the solid or in solution, in stark contrast to the first generation counterparts **1a–1c** which decompose by hydrolysis



Scheme 1. Preparation of BORAZAN dyes.

over time even in the solid state. As further testament to the improved stability of the dyes, the dipyrzoly derivatives **2a–2c** can survive flash chromatography on silica gel, a procedure that immediately annihilates the monopyrazol BORAZANs **1a–1c**.

The molecular structures of the free ligand H(pz₂An^{*t*Bu}) (**L2c**) and four BORAZAN derivatives Ph₂B(pzAn^{*t*Bu}) (**1c**), and Ph₂B(pz₂An^X) (X = CF₃, Cl, *t*Bu; **2a–2c**) have been determined by single-crystal X-ray diffraction. The structures of H(pz₂An^{*t*Bu}) (**L2c**) and its BORAZAN derivative Ph₂B(pz₂An^{*t*Bu}) (**2c**) is given in Figure 3 while all other structures, a Table of metrical parameters, and full structural discussion are provided in the Supporting Information. The structure of **L1c** (Figure 3, a) reveals a pyramidal amino nitrogen (sum of angles around N1 = 341.7°) with hydrogen atoms directed below one face of the aniline ring. The pyrazolyl rings are also directed below the same face with an average dihedral of 43° with respect to the central aniline ring to give relatively long and presumably weak intramolecular hydrogen bonding interactions N1H1b...N12 (2.15 Å, 133°) and N1H1a...N22 (2.20 Å, 133°). In **2c**, the boron-bound pyrazolyl is closer to coplanarity with respect to the central aniline ring (dihedral of 14.1°) whereas the other pyrazolyl is further from coplanarity with a dihedral of 49.3° A feature in **2c** that is common to all other structurally characterized BORAZAN dyes is C_i (rather than C_s) symmetry due to puckering of the six-member chelate ring into a pseudo half-chair conformation with a distorted tetrahedral boron residing above (0.42 Å) the remaining atoms of the chelate ring As with previously reported members of the BORAZANs, the average B–N distance (1.57 Å) is 0.05 Å shorter than the average B–C distance (1.62 Å) regardless of the substitution pattern along the dye framework. Also, the B–C bond of the axial phenyl is detectably longer (1.62–1.64 Å) than that of the equatorial phenyl (1.61–1.62 Å), presumably due to the anti-bonding interaction involving the aniline moiety (see HOMO in top of Figure 5).

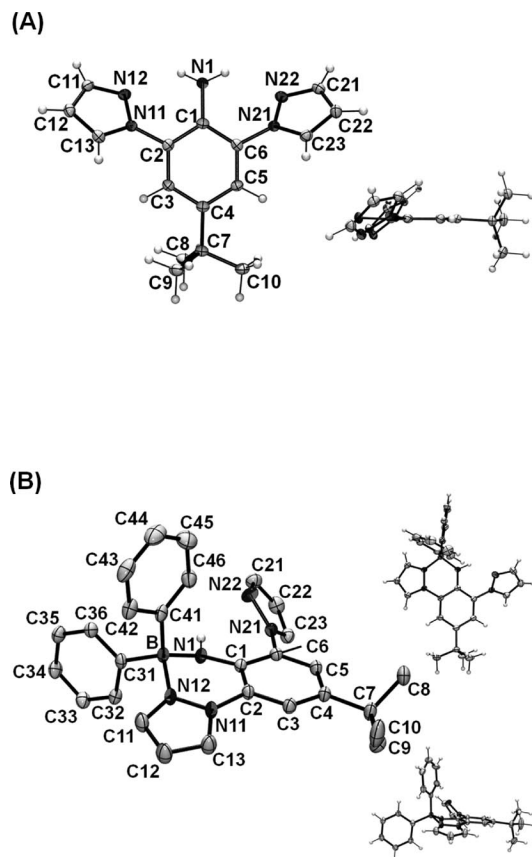


Figure 3. Molecular structure of (A) $\text{H}(\text{pz}_2\text{An}^t\text{Bu})$ (**L2c**), two views shown. (B) left: $\text{Ph}_2\text{B}(\text{pz}_2\text{An}^t\text{Bu})$ (**2c**) with atom labelling and most hydrogen atoms removed for clarity. right: alternate views with hydrogen atoms added. Ellipsoids are shown at the 50% probability level.

The solution NMR spectra of all BORAZANs [either $\text{Ph}_2\text{B}(\text{pzAn}^X)$ (**1a–1c**) or $\text{Ph}_2\text{B}(\text{pz}_2\text{An}^X)$ (**2a–2c**)] clearly show dynamic processes occur such that their solution structures appear to have higher than the C_i symmetry indicated from either solid state structural or theoretical studies (vide infra). For instance, only one set of resonances for phenyl ring hydrogen atoms is observed for all the BORAZANs even though, based on the solid-state structures, two sets are expected (one set each for “axial” and “equatorial” phenyls). We previously attributed this observation to a low energy ring-flipping process, that was fast on the NMR time-scale even at -80°C in $[\text{D}_8]\text{toluene}$, a process we still favour after considering the results of variable temperature NMR studies on the $\text{Ph}_2\text{B}(\text{pz}_2\text{An}^X)$ series of compounds which showed only one set of phenyl hydrogen resonances at -80°C . With the $\text{Ph}_2\text{B}(\text{pz}_2\text{An}^X)$ series ($X = \text{CF}_3$, Cl , $t\text{Bu}$), variable temperature studies also indicate that exchange occurs rendering the boron-bound and “free” pyrazolyl rings inequivalent at low temperatures but equivalent at higher temperatures. As a representative example, a portion of the ^1H NMR spectra of $\text{Ph}_2\text{B}(\text{pz}_2\text{An}^t\text{Bu})$ (**2c**) in the region showing the resonance(s) for the hydrogen(s) at the 4-position of the pyrazolyl at various temperatures is shown in Figure 4 ($X = t\text{Bu}$). More complete ^1H NMR

spectra for **2c** and other derivatives acquired at different temperatures are collected in the Supporting Information. At -80°C there are two resonances for 4-pyrazolyl hydrogen atoms at 5.94 and at $\delta = 5.56$ ppm. Comparisons of chemical shifts of the 4-pyrazolyl hydrogen resonances in $\text{Ph}_2\text{B}(\text{pz}_2\text{An}^t\text{Bu})$ (**2c**) with those of the related free ligands $\text{H}(\text{pzAn}^t\text{Bu})$ (**L1c**) ($\delta_{\text{H}} = 6.11$) and $\text{H}(\text{pz}_2\text{An}^t\text{Bu})$ (**L2c**) ($\delta_{\text{H}} = 6.12$) and the monopyrazolyl BORAZAN derivative $\text{Ph}_2\text{B}(\text{pzAn}^t\text{Bu})$ (**1c**) ($\delta_{\text{H}} = 5.53$) establish that the lower field resonance is due to the free pyrazolyl while the higher field resonance is for the boron-bound pyrazolyl. On warming to 0°C there is a constant downfield shift in both resonances. Above 0°C the resonances broaden and coalesce at 30°C , and above the coalescence temperature the single exchange-averaged resonance sharpens. Similar characteristics are shared in the spectra of **2a** and **2b**. The activation barriers for (in hence, the rate of) exchange varies in a regular way with the electron-donating character of the *para*-aniline substituent, as summarized in Table 1. The more electron-donating substituent gives rise to lower activation barriers and faster rates of exchange. As the activation barrier for exchange falls in line with the expected bond strength of a B–N dative interaction,^[10] the mechanism for pyrazolyl exchange, presumably involves pyrazolyl bond dissociation. In this context, electron-withdrawing *para*-aniline substituents render the aniline nitrogen electron-deficient and the nitrogen lone pair is less able to stabilize three-coordinate boron by conjugation with the empty *p*-orbital on boron. The effect is to induce more Lewis-acidic boron and, hence, more stable boron-pyrazolyl bonds.

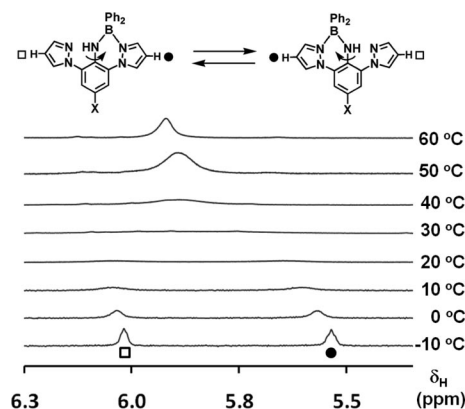


Figure 4. The 4-pyrazolyl region of the ^1H NMR spectra for a $[\text{D}_8]$ -toluene solution of $\text{Ph}_2\text{B}(\text{pz}_2\text{An}^t\text{Bu})$ acquired at various temperatures.

Density functional calculations (B3LYP/6-31G*, SPARTAN06)^[12] were performed on the free ligands $\text{H}(\text{pzAn}^t\text{Bu})$ (**L1c**), $\text{H}(\text{pz}_2\text{An}^X)$ (**L2a–L2c**), and the boron derivatives, $\text{Ph}_2\text{B}(\text{pz}_n\text{An}^X)$ ($n = 1, 2$; $X = \text{CF}_3$, Cl , $t\text{Bu}$), **1a–1c** and **2a–2c**, respectively) using ab initio (HF/321-G) energy-minimized structures in an effort to rationalize the rather unexpected electronic properties of the BORAZAN dyes. The geometry optimization showed good correlation with the solid-state structures in both bond lengths and angles, especially showing chelate ring-puckering as found

Table 1. Activation parameters for pyrazolyl exchange in $\text{Ph}_2\text{B}(\text{pz}_2\text{An}^X)$ ($X = \text{CF}_3$, Cl , $t\text{Bu}$).

| Compound | T_c [K] | $\Delta\nu$ [Hz] ^[a] | k_c [s ⁻¹] ^[b] | ΔG^\ddagger [kcal/mol] ^[c] |
|---|-----------|---------------------------------|---|---|
| $\text{Ph}_2\text{B}(\text{pz}_2\text{An}^{\text{CF}_3})$ | 343 | 132 | 586.46 | 15.8 |
| $\text{Ph}_2\text{B}(\text{pz}_2\text{An}^{\text{Cl}})$ | 318 | 152 | 675.32 | 14.5 |
| $\text{Ph}_2\text{B}(\text{pz}_2\text{An}^{t\text{Bu}})$ | 303 | 232 | 1030.75 | 13.6 |

[a] Chemical shift difference in the absence of exchange. [b] Rate constant at coalescence temperature $k_c = \pi\Delta\nu(2)^{-1/2}$. [c] $\Delta G^\ddagger = 4.57(T_c)[10.32 + \log(T_c/k_c)]$ as in reference.^[11]

in the solid state. A representative set of frontier orbitals (HOMO and LUMO) for **2a** is given in the top of Figure 5 while a comparison of energy levels of a more extensive set of frontier orbitals [LUMO(+4) to HOMO(−4)] for all the ligands, $\text{H}(\text{pz}_n\text{An}^X)$ ($n = 1, 2$; $X = \text{CF}_3$, Cl , $t\text{Bu}$) and their corresponding BORAZANs $\text{Ph}_2\text{B}(\text{pz}_n\text{An}^X)$ ($n = 1, 2$) are given in the bottom of Figure 5. Complete molecular orbital diagrams are provided in the Supporting Information. For all, the HOMO is mainly the nonbonding representation of the aniline-centred pi-system, encompassing the nitrogen-centered lone pair of the aniline.

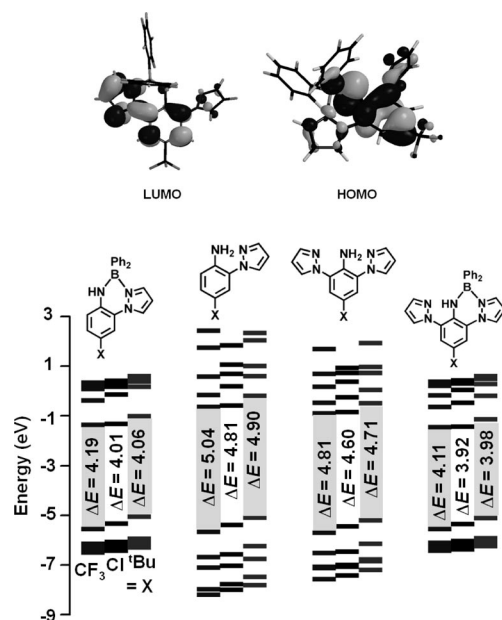


Figure 5. Top: HOMO and LUMO for representative complex **2a**. Bottom: comparison of the energy levels of frontier orbitals LUMO(+4) to HOMO(−4) for $\text{H}(\text{pz}_n\text{An}^X)$ ($n = 1, 2$) and corresponding BORAZANs $\text{Ph}_2\text{B}(\text{pz}_n\text{An}^X)$ ($n = 1, 2$) where $X = \text{CF}_3$, Cl , and $t\text{Bu}$ (left to right) for each compound type from density functional calculations (B3LYP/6-31G*). Vertical scale represents relative energy. Gas-phase HOMO–LUMO gap energy is ΔE .

There is also a significant (pi-antibonding) contribution from the orbitals of the *para*-aniline substituent to the HOMO. Following the convention established by from the seminal work of Kasha and Rawls on the photophysics of aniline derivatives,^[13] it is convenient to refer to the HOMO (and other frontier orbitals containing significant contributions from the conjugated aniline lone pair) as a π_L (pi-lone-pair) to provide a distinction from a pure π orbital. Deviations from aniline nonplanarity such as twisting of

the H_2N -aryl moiety about C–N bond (or other distortions) change the photophysics of the molecule by affording more nonbonding character to the nitrogen lone pair. The LUMO of each compound is π^* in character and spans the pi-systems of both the aniline and the pyrazolyl rings with only a small contribution from the conjugated *p*-orbital of the aniline nitrogen. For the $\text{H}(\text{pz}_n\text{An}^X)$ ($n = 1, 2$) ligands, the HOMO(−4) to HOMO(−1) orbitals are π -bonding, the virtual orbitals LUMO(+1) to LUMO(+3) are π^* antibonding, while the LUMO(+4) and higher are σ^* antibonding. In the $\text{Ph}_2\text{B}(\text{pz}_n\text{An}^X)$ ($n = 1, 2$), orbital contributions from the diphenylboron moiety distinguish the BORAZANs from the ligands. The HOMO(−1) to HOMO(−4), are essentially four linear combinations of boron-phenyl π -orbitals; the next-lowest pzAn -based π_L -orbital is HOMO(−5). The corresponding four π^* orbitals include contributions from both the pzAn and diphenylboron moieties and constitute the virtual orbitals LUMO(+1) to LUMO(+5).

The relative energies of the frontier orbitals for the twelve compounds in the bottom of Figure 5 (and Supporting Information) reveals a number of trends that correlate well with experimental data. When comparing the relative energy of the HOMO of a given $\text{H}(\text{pzAn}^X)$ ligand with that for its corresponding BORAZAN (Figure 5), the latter is destabilized owing to an antibonding pi-interaction between the boron-bound carbon atoms and the *p*-orbital of the aniline nitrogen, which is not present in the former. There is a stabilization of the HOMO with an increase in electron-withdrawing character of the *para* substituent of the aniline, rendering the aniline a poorer donor, as expected. Contrary to initial expectations based solely on inductive effects, substitution of the *ortho* hydrogen with a pyrazolyl results in a small stabilization of the HOMO that arises due to increased conjugation with the pi-system of the new pyrazolyl group. This increase in conjugation for the dipyrazolyl system causes a significant stabilization of the LUMO, which results in an overall smaller HOMO/LUMO energy gap compared to the monopyrazolyl systems. As with the monopyrazolyl systems the HOMO is destabilized to a greater extent than the LUMO is stabilized on changing *para*-aniline substituents, which provides an additional basis for tuning the electronic properties of the BORAZAN dyes.

Electrochemistry

As aniline derivatives are well known electron donors,^[14] and BORAZAN derivatives were previously found to be electroactive,^[5] the electrochemistry of CH_3CN solutions of the new ligands and BORAZANs were examined by cyclic voltammetry. The electrochemical data are collected in Table 2 while voltammograms for the ligands and complexes are found in the Supporting Information. Each of the compounds exhibited an irreversible oxidation in the range of 0.7–1.4 V (vs. Ag/AgCl), where the reported potentials are those for the anodic wave observed at a scan rate

Table 2. Electronic properties of various pyrazolylaniline ligands and diphenylboryl complexes.

| Compound | $E_{1/2}$ (V vs. Ag/AgCl) ^[a] | | Absorption ^[d] λ_{max} (ϵ , M ⁻¹ cm ⁻¹), CH ₂ Cl ₂ | Emission ^[d] | | Ref. |
|---|--|--------------------------|--|---|--|------|
| | Oxidation ^[b] | Reduction ^[c] | | $\lambda_{\text{max}}^{\text{em}}$ (nm) | Φ_{F} (C ₇ H ₈ , CH ₃ CN) | |
| H(pzAn ^{CF3}), L1a | 1.23 | – | 234 (21,000), 259 (8,600), 305 (3,700) | – | – | [2] |
| H(pzAn ^{Cl}), L1b | 1.01 | – | 233 (24,000), 255 (9,600), 317 (4,700) | – | – | [2] |
| H(pzAn ^{<i>t</i>Bu}), L1c | 0.88 | – | 234 (17,825), 251sh (7,252), 305 (3,755) | – | – | [e] |
| H(pz ₂ An ^{CF3}), L2a | 1.41 | –2.60 | 237 (24,971), 259sh (7,135), 310 (5,049) | – | – | [e] |
| H(pz ₂ An ^{Cl}), L2b | 1.24 | –2.50 | 240 (24,814), 263sh (5,109), 329 (4,369) | – | – | [e] |
| H(pz ₂ An ^{<i>t</i>Bu}), L2c | 0.99 | – | 229 (26,464), 262sh (6,935), 315 (5,433) | – | – | [e] |
| Ph ₂ B(pzAn ^{CF3}), 1a | 1.04 | –2.39 | 248 (31,000), 288 (13,000), 358 (4,700) | 468 | 0.66, 0.49 | [2] |
| Ph ₂ B(pzAn ^{Cl}), 1b | 0.84 | –2.41 | 249 (32,000), 289 (7,800), 375 (6,600) | 481 | 0.44, 0.23 | [e] |
| Ph ₂ B(pzAn ^{<i>t</i>Bu}), 1c | 0.74 | –2.64 | 245 (32,251), 371 (4,853) | 495 | 0.33, 0.03 | [e] |
| Ph ₂ B(pz ₂ An ^{CF3}), 2a | 1.13 | –2.43 | 252 (30,016), 292 (6,500), 372 (6,359) | 474 | 0.75, 0.55 | [e] |
| Ph ₂ B(pz ₂ An ^{Cl}), 2b | 1.10 | –2.58 | 251 (26,768), 289sh (3,528), 388 (5,460) | 493 | 0.53, 0.31 | [e] |
| Ph ₂ B(pz ₂ An ^{<i>t</i>Bu}), 2c | 0.86 | –2.65 | 247 (28,505), 380 (5,706) | 502 | 0.46, 0.16 | [e] |

[a] Scan rate of 100 mV/s in CH₃CN with NBu₄(PF)₆ as supporting electrolyte. [b] Anodic peak potential. [c] Cathodic peak potential. [d] 295 K, CH₂Cl₂. [e] This work.

of 0.100 V/s; the cathodic wave is either absent or noticeably less intense than expected. For each series of ligands and BORAZANs, the oxidation becomes more favourable with increasing electron donating character of the *para*-aniline substituent, in accord with previous findings and with the calculations that showed a destabilization of the HOMO for such substitution. Thus, for the BPh₂(pz₂An^X), the oxidation potentials increase along the series X = *t*Bu (E_{pa} = 0.86 V) < X = Cl (E_{pa} = 1.10 V) < X = CF₃ (E_{pa} = 1.13 V). Also in agreement with calculations and earlier results, the oxidations of the BORAZAN complexes are more favourable than those for the free ligands because there is a destabilization of the HOMO brought about by antibonding interactions with the σ -orbitals of the boron-bound carbon atoms. The dipyrzoly derivatives (both free ligands and BORAZAN complexes) are more difficult to oxidize than the monopyrazolyl analogues. Thus, the oxidation potentials for the series Ph₂B(pz₂An^X) [X = CF₃ (1.13 V), Cl (1.10 V), *t*Bu (0.86 V)] are higher than the corresponding potentials for the Ph₂B(pzAn^X) series [X = CF₃, (1.04 V), Cl (0.84 V), *t*Bu (0.74 V)]. While this result is surprising on first inspection considering the expected inductive effects of replacing hydrogen with a more electron-donating pyrazolyl, this trend was correctly predicted by the calculations, which showed that the origin is due to stabilization of the HOMO via conjugation with the pi-orbitals of the second pyrazolyl.

Electronic Spectra

The electronic (absorption/emission) spectra of the newly prepared H(pz_{*n*}An^X) ligands and Ph₂B(pz_{*n*}An^X) (*n* = 1,2; X = CF₃, Cl, *t*Bu) compounds parallel those of the previously reported monopyrazolyl (*n* = 1; X = CF₃, Cl) derivatives. A summary of the electronic properties are collected in Table 2 and complete spectra are found in the Supporting Information. The electronic absorption spectrum of each H(pz_{*n*}An^X) (*n* = 1,2) ligand consists of three bands for π - π^* transitions; one high-intensity, high-energy band at ca. 230 nm ($\epsilon \approx 20,000$), a second less intense band at ca. 250 ($\epsilon \approx 7000$) nm (in some cases this band occurs as a shoulder

to the high-energy band), and a low-energy, low-intensity band for the $\pi_{\text{L}}-\pi^*$ (HOMO–LUMO) transition above about 300 nm ($\epsilon \approx 3000$). As indicated from the calculations, the energies of all the absorption bands of the dipyrzoly derivatives are red-shifted with respect to the monopyrazolyl derivatives. With the BORAZANs, each band undergoes both hyper- and bathochromic shifts and a new high energy band (presumably for the $\pi-\pi^*$ transitions involving the boron-phenyl groups) appears as a shoulder near 200 nm.

The ligands are not emissive under irradiation with UV-light but the BORAZANs exhibit intense emission (either in the solid state or in hydrocarbon or halocarbon solution) that varies from blue for derivatives with electron-withdrawing trifluoromethyl *para*-aniline substituents to green for the *tert*-butyl derivatives (Figure 6). Previous excited-state lifetime measurements of Ph₂B(pzAn^X) (X = CN, CF₃, CO₂Et, Cl, Me, OMe) established the fluorescent nature (ns lifetimes) of emission. As with the previously reported monopyrazolyl derivatives, the emission of the di-pyrazolyl derivatives Ph₂B(pz₂An^X) (X = CF₃, Cl, *t*Bu) exhibit a regular red-shift of emission with increasing electron-donating character of the *para*-aniline substituent. Thus, the emission maximum of Ph₂B(pz₂An^X) occurs at $\lambda_{\text{max}}^{\text{em}}$ 474, 493, and 502 nm for X = CF₃ (**2a**), Cl (**2b**), and *t*Bu (**2c**), respectively. The quantum yields of emission diminish regularly along the series X = CF₃, Cl, *t*Bu (0.75, 0.53, 0.46 respectively) in accord with the energy gap law which delineates that quantum yields for emission will decrease with lower energy emission.^[15] After considering the implications of the energy gap law, there is a remarkable improvement in the quantum yields of emission of **2a–2c** vs. the corresponding monopyrazolyl derivatives **1a–1c**. That is, despite the fact that di-pyrazolyl derivatives **2a–2c** exhibit red-shifted emission compared to **1a–1c** (Supporting Information), the former enjoy a 10–20% increase in fluorescence quantum yield (Table 2) with respect to the latter. We tentatively attribute the improvement in quantum yield to the kinetic stabilization of the dye framework brought about by the additional pyrazolyl (increasing the amount of chelated boron) which is supported by the observation that the Stokes shift (6000 ± 500 cm⁻¹) in toluene is slightly smaller for the di-

pyrazolyl derivatives compared to that observed for the monopyrazolyl derivatives (Stokes shift $6400 \pm 500 \text{ cm}^{-1}$). Moreover, the fluorescent quantum yields for **2a–2c** in CH_3CN are lower than in toluene but are higher than for analogous **1a–1c** in the Lewis-base solvent. As with the previously reported derivatives, the efficacy of fluorescence quenching of **2a–2c** in acetonitrile most greatly affects derivatives with electron-rich *para*-aniline substituents [with weaker (or less inert) boron-pyrazolyl dative bonds]. Acetonitrile could be envisioned to coordinate the Lewis-acidic boron centers in the dyes, compromising the integrity of the chelate ring and destroying the chromophore. The bis(pyrazolyl)aniline ligand scaffolds appear to offer a greater resistance to such a degenerative process compared to mono-(pyrazolyl)aniline derivatives.

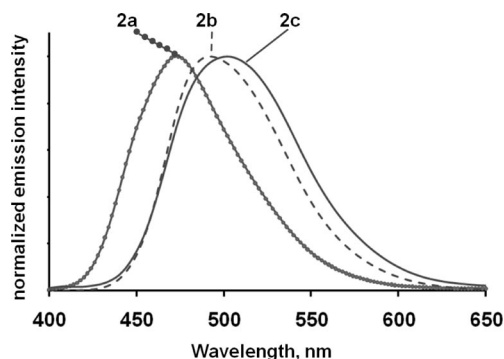


Figure 6. Overlay of normalized emission spectra of $\text{Ph}_2\text{B}(\text{pz}_2\text{An}^X)$ where ($X = \text{CF}_3$, **2a** left beaded line; $X = \text{Cl}$, **2b** centre dashed line; $X = t\text{Bu}$, **2c** right solid line).

Conclusions

Three examples of 2,6-dipyrazolylanilines $\text{H}(\text{pz}_n\text{An}^X)$ ($X = \text{CF}_3$, Cl , $t\text{Bu}$) have been prepared by exploiting copper-catalyzed amination reactions between pyrazole and 2,6-dibromoaniline. The reaction chemistry of these derivatives with triphenylboron afforded $\text{Ph}_2\text{B}(\text{pz}_2\text{An}^X)$ [$X = \text{CF}_3$ (**2a**), Cl (**2b**), $t\text{Bu}$ (**2c**)] with chelated diphenylboryl moieties, as indicated by X-ray structural studies. These new highly emissive compounds exhibit a number of adventitious properties compared to the first generation of BORAZAN fluorescent dyes, $\text{Ph}_2\text{B}(\text{pzAn}^X)$ [$X = \text{CF}_3$ (**1a**), Cl (**1b**), $t\text{Bu}$ (**1c**)], that have only one pyrazolyl group on the heterocyclic ligand scaffold. The emission of the new di-pyrazolyl BORAZANs is colour-tuneable from blue for the derivative with an electron-withdrawing $-\text{CF}_3$ *para*-aniline substituent to green for the derivative with a *tert*-butyl substituent, where the emission of the dipyrazolyl derivatives **2a–2c** are lower in energy than the corresponding monopyrazolyl derivatives **1a–1c**. Despite exhibiting lower energy emissions, the dipyrazolyl BORAZANs display higher luminescence quantum yields than monopyrazolyl analogues. Moreover, the di-pyrazolyl derivatives enjoy a significant increase in stability towards solvolysis relative to their monopyrazolyl counterparts. Both of the above properties are thought to arise from a kinetic stabilization of the dye framework

brought about by the additional pyrazolyl group that could favour an increased rate of boron-pyrazolyl bond formation should dissociation occur. In fact, such dissociation was easily detected by variable-temperature NMR spectroscopic studies of toluene solutions of C_1 -symmetric **2a–2c** since the resonances for “free” and boron-bound pyrazolyl groups undergo exchange. The rates of boron-pyrazolyl dissociation decrease (hence, the stability of the chelate ring increases) in the order $t\text{Bu} > \text{Cl} > \text{CF}_3$, an order that may be indicative of the anticipated (in)ability of the aniline to stabilize a three-coordinate boron by conjugation between the aniline lone pair and the empty *p*-orbital on boron. We are further probing the reaction chemistry of these new ligands towards transition metals and for the construction of supramolecular assemblies.

CCDC-698323 (for $\text{Ph}_2\text{B}(\text{pzAn}^{t\text{Bu}})$ **1c**), -698324 (for $\text{H}(\text{pz}_2\text{An}^{t\text{Bu}})$ **L2c**), -698325 (for $\text{Ph}_2\text{B}(\text{pz}_2\text{An}^{\text{CF}_3})$ **2a**), -698326 (for $\text{Ph}_2\text{B}(\text{pz}_2\text{An}^{\text{Cl}})$ **2b**), -698327 (for $\text{Ph}_2\text{B}(\text{pz}_2\text{An}^{t\text{Bu}})$ **2c**), and -698328 (for $(\text{Ph}_2\text{B})_2(\text{pz}_2\text{An}^{t\text{Bu}})$ **3c**) contain the supplementary crystallographic data for this paper. These data can be obtained free of charge from The Cambridge Crystallographic Data Centre via www.ccdc.cam.ac.uk/data_request/cif.

Supporting Information (see also the footnote on the first page of this article): Complete experimental details. Details of X-ray crystallographic studies, tables of X-ray data, molecular and supramolecular structural discussion, NMR spectra, cyclic voltammograms, UV/Vis and emission spectra, details of computational studies, comparison of results from different basis sets, frontier orbital diagrams.

Acknowledgments

J. R. G. thanks Marquette University, the Petroleum Research Fund (74371-G), and the National Science Foundation (NSF) (CHE-0521323) for support.

- a) B. Valeur, *Molecular Fluorescence, Principles and Applications*, Wiley-VCH, New York, **2002**; b) J.-P. Desvergne, A. W. Czarnik (Eds.), *Chemosensors of Ion and Molecule Recognition*, Kluwer, Dordrecht, The Netherlands, **1997**.
- a) A. Loudet, K. Burgess, *Chem. Rev.* **2007**, *107*, 4891–4932; b) R. P. Haugland, H. C. Kang, U. S. Patent 4, 774, 339, **1988**; c) R. P. Haugland, *Handbook of Fluorescent Probes and Research Chemicals*, 6th ed., Molecular Probes, Eugene, OR, **1996**; d) A. Treibs, F.-H. Kreuzer, *Justus Liebigs Ann. Chem.* **1968**, *718*, 208–223; e) J. H. Boyer, A. M. Haag, G. Sathyamoorthi, M. L. Soong, K. Thangaraj, T. G. Pavlopoulos, *Heteroat. Chem.* **1993**, *4*, 39–49; f) G. Beer, C. Niederaht, S. Grimme, J. Daub, *Angew. Chem. Int. Ed.* **2000**, *39*, 3252–3255; g) M. Kollmannsberger, K. Rurack, U. Resch-Genger, J. Daub, *J. Phys. Chem. A* **1998**, *102*, 10211–10220; h) M. Kollmannsberger, T. Gareis, S. Heintz, J. Breu, J. Daub, *Angew. Chem. Int. Ed. Engl.* **1997**, *36*, 1333–1335; i) L. Zeng, E. W. Miller, A. Pralle, E. Y. Isacoff, C. J. Chang, *J. Am. Chem. Soc.* **2006**, *128*, 10–11; j) S. Hattori, K. Ohkubo, Y. Urano, H. Sunahara, T. Nagano, Y. Wada, N. V. Tkachenko, H. Lemmetyinen, S. Fukuzumi, *J. Phys. Chem. B* **2005**, *109*, 15368–15375; k) H. Imahori, H. Norieda, H. Yamada, Y. Nishimura, I. Yamazaki, Y. Sakata, S. Fukuzumi, *J. Am. Chem. Soc.* **2001**, *123*, 100–110; l) R. W. Wagner, J. S. Lindsey, *Pure Appl. Chem.* **1996**, *68*, 1373–1380.
- For example: a) S. O. McDonnell, D. F. O’Shea, *Org. Lett.* **2006**, *8*, 3493–3496; b) T.-R. Chen, R.-H. Chien, M.-S. Jan, A.

- Yeh, J.-D. Chen, *J. Organomet. Chem.* **2006**, *691*, 799–804; c) Q. D. Liu, M. S. Mudadu, R. Thummel, Y. Tao, S. Wang, *Adv. Funct. Mater.* **2005**, *15*, 143–154; d) H.-Y. Chen, Y. Chi, C.-S. Liu, J.-K. Yu, Y.-M. Cheng, K.-S. Chen, P.-T. Chou, S.-M. Peng, G.-H. Lee, A. J. Carty, S.-J. Yeh, C.-T. Chen, *Adv. Funct. Mater.* **2005**, *15*, 567–574; e) N. G. Park, J. E. Lee, Y. H. Park, Y. S. Kim, *Synth. Met.* **2004**, *145*, 279–283; f) G. M. Kaplan, A. N. Frolov, N. I. Rtishchev, A. V. El'tsov, *Zhur. Org. Khim.* **1991**, *27*, 872–877; g) G. M. Kaplan, A. N. Frolov, N. I. Rtishchev, A. V. El'tsov, T. K. Ponomareva, *Zhur. Obsch. Khim.* **1991**, *61*, 1810–1814; h) Y. Cui, Q.-D. Liu, D. R. Bai, W.-L. Jia, Y. Tao, S. Wang, *Inorg. Chem.* **2005**, *44*, 601–609.
- [4] a) F. P. Macedo, C. Gwengo, S. V. Lindeman, M. D. Smith, J. R. Gardinier, *Eur. J. Inorg. Chem.* **2008**, 3200–3211; b) Y. Qin, Y. Kiburu, S. Shah, F. Jäkle, *Macromolecules* **2006**, *39*, 9041–9048; c) Y. Qin, Y. Kiburu, S. Shah, F. Jäkle, *Org. Lett.* **2006**, *8*, 5227–5230.
- [5] B. J. Liddle, R. M. Silva, T. J. Morin, F. P. Macedo, R. Shukla, S. V. Lindeman, J. R. Gardinier, *J. Org. Chem.* **2007**, *72*, 5637–5646.
- [6] J. C. Antilla, J. M. Baskin, T. E. Barder, S. L. Buchwald, *J. Org. Chem.* **2004**, *69*, 5578–5587.
- [7] a) H.-J. Cristau, P. P. Cellier, J.-F. Spindler, M. Taillefer, *Eur. J. Org. Chem.* **2004**, 695–709; b) M. Taillefer, N. Xia, A. Ouali, *Angew. Chem. Int. Ed.* **2007**, *46*, 934–936; c) H.-J. Cristau, P. P. Cellier, J.-F. Spindler, M. Taillefer, *Chem. Eur. J.* **2004**, *10*, 5607–5622; d) H.-J. Cristau, P. P. Cellier, J.-F. Spindler, M. Taillefer, *Eur. J. Org. Chem.* **2004**, 695–709; e) See also, J. M. Lindley, I. M. McRobbie, O. Meth-Cohn, H. Suschitzky, *J. Chem. Soc. Perkin Trans. 1* **1980**, *4*, 982–994.
- [8] a) M. Austin, O. J. Egan, R. Tully, A. C. Pratt, *Org. Biomol. Chem.* **2007**, *5*, 3778–3786; b) Q. Zhang, Y. Peng, W. J. Welsh, *Heterocycles* **2006**, *68*, 2635–2645; c) S. H. Lee, B.-B. Jang, Z. H. Kafafi, *J. Am. Chem. Soc.* **2005**, *127*, 9071–9078; d) T. C. Bedard, J. S. Moore, *J. Am. Chem. Soc.* **1995**, *117*, 10662–10671; e) Y. Miura, H. Oka, M. Momoki, *Synthesis* **1995**, 1419–1422; f) A. R. Hajipour, H. Imanieh, S. A. Pourmousavi, *Synth. Commun.* **2004**, *34*, 4597–4604; g) F. Toda, J. Schmeyer, *Green Chem.* **2003**, *5*, 701–703; h) C. Popeney, Z. Guan, *Organometallics* **2005**, *24*, 1145–1155; i) C. Koradin, W. Dohle, A. L. Rodriguez, B. Schmid, P. Knochel, *Tetrahedron* **2003**, *59*, 1571–1587.
- [9] It was possible to isolate a few crystals of a side product (Ph₂B)₂-(μ-pz₂An^{tBu}) **3c** (see structure in the Supporting Information).
- As of yet, the intentional synthesis of **3c** has been hampered by poor reproducibility and/or high reactivity. We are currently pursuing reliable preparations of this and other dinuclear species, which will be the subjects of a future report.
- [10] a) P. D. Livant, D. J. D. Northcott, Y. Shen, T. R. Webb, *J. Org. Chem.* **2004**, *69*, 6564–6571; b) T. M. Gilbert, *J. Phys. Chem. A* **2004**, *108*, 2550–2554.
- [11] H. Kessler, *Angew. Chem. Int. Ed. Engl.* **1970**, *9*, 219–235.
- [12] a) Y. Shao, L. F. Molnar, Y. Jung, J. Kussmann, C. Ochsenfeld, S. T. Brown, A. T. B. Gilbert, L. V. Slipchenko, S. V. Levchenko, D. P. O'Neill, R. A. DiStasio Jr., R. C. Lochan, T. Wang, G. J. O. Beran, N. A. Besley, J. M. Herbert, C. Y. Lin, T. Van Voorhis, S. H. Chien, A. Sodt, R. P. Steele, V. A. Rassolov, P. E. Maslen, P. P. Korambath, R. D. Adamson, B. Austin, J. Baker, E. F. C. Byrd, H. Dachsel, R. J. Doerksen, A. Dreuw, B. D. Dunietz, A. D. Dutoi, T. R. Furlani, S. R. Gwaltney, A. Heyden, S. Hirata, C.-P. Hsu, G. Kedziora, R. Z. Khalliulin, P. Klunzinger, A. M. Lee, M. S. Lee, W. Z. Liang, I. Lotan, N. Nair, B. Peters, E. I. Proynov, P. A. Pieniazek, Y. M. Rhee, J. Ritchie, E. Rosta, C. D. Sherrill, A. C. Simmonett, J. E. Subotnik, H. L. Woodcock III, W. Zhang, A. T. Bell, A. K. Chakraborty, D. M. Chipman, F. J. Keil, A. Warshel, W. J. Hehre, H. F. Schaefer, J. Kong, A. I. Krylov, P. M. W. Gill, M. Head-Gordon, *Phys. Chem. Chem. Phys.* **2006**, *8*, 3172–3191; b) W. J. Hehre, *A Guide to Molecular Mechanics and Quantum Chemical Calculations*, 2nd ed., Wavefunction, Inc., Irvine, CA, **2006**.
- [13] M. Kasha, R. Rawls, *Photochem. Photobiol.* **1968**, *7*, 561–569.
- [14] a) Z. Galus, R. N. Adams, *J. Phys. Chem.* **1963**, *67*, 862–866; b) J. Bacon, R. N. Adams, *J. Am. Chem. Soc.* **1968**, *90*, 6596–6599; c) R. L. Hand, R. F. Nelson, *J. Am. Chem. Soc.* **1974**, *96*, 850–860; d) A. G. MacDiarmid, A. J. Epstein, *Faraday Discuss. Chem. Soc.* **1989**, *88*, 317–332; e) A. G. MacDiarmid, *Angew. Chem. Int. Ed.* **2001**, *40*, 2581–2590; f) A. J. Heeger, *Angew. Chem. Int. Ed.* **2001**, *40*, 2591–2611; g) L. R. Sharma, A. K. Manchanda, G. Singh, R. S. Verma, *Electrochim. Acta* **1982**, *27*, 223–233; h) D. G. H. Daniels, F. T. Naylor, B. C. Saunders, *J. Chem. Soc.* **1951**, 3433–3435.
- [15] a) J. V. Caspar, B. P. Sullivan, E. M. Kober, T. J. Meyer, *Chem. Phys. Lett.* **1982**, *91*, 91–95; b) A. P. Penner, W. Siebrand, M. Z. Zgierski, *J. Chem. Phys.* **1978**, *69*, 5496–5508; c) R. Englman, J. Jortner, *Mol. Phys.* **1970**, *18*, 145–164.

Received: August 12, 2008

Published Online: November 25, 2008

Synthesis and Structural and Physicochemical Characterization of $\{[\text{Rh}_2(\mu\text{-OOCCH}_3)_2(\text{dmbpy})_2][\text{BF}_4]\}_n$ Molecular Wire

Magdalena Rak,^[a] Florian. P. Pruchnik,^{*[a]} Leszek Z. Ciunik,^[a] Frédéric Lafalet,^[b] Sylvie Chardon-Noblat,^[b] and Alain Deronzier^[b]

Keywords: Rhodium / Mixed-valent compounds / Nanostructures / Electrochemistry / Magnetic properties

Dinuclear Rh^{II} compounds $[\text{Rh}_2(\mu\text{-OOCCH}_3)_2(\text{dmbpy})_2(\text{H}_2\text{O})_2](\text{CH}_3\text{COO})_2$ (**1**) and $[\text{Rh}_2(\mu\text{-OOCCH}_3)_2(\text{dmbpy})_2(\text{H}_2\text{O})_2](\text{BF}_4)_2 \cdot 2.5\text{H}_2\text{O}$ (**2**) (dmbpy = 4,4'-dimethyl-2,2'-bipyridine) were synthesized and characterized with spectroscopic methods. The structure of complex **2** was determined by using X-ray crystallography. The rhodium atoms in compound **2** have distorted octahedral coordination with O and N atoms in equatorial positions and a Rh atom and a H_2O molecule in axial coordination sites. Reduction of compound **2** with aqueous alcohols leads to the formation of the molecular wire $\{[\text{Rh}_2(\mu\text{-OOCCH}_3)_2(\text{dmbpy})_2][\text{BF}_4]\}_n \cdot 2n\text{H}_2\text{O}$ (**3**) con-

taining a $[\text{Rh}_2]^{3+}$ core. Compound **3** shows strong antiferromagnetic properties, $J = -780 \text{ cm}^{-1}$ and $\mu = 0.128\text{--}1.349 \text{ B.M.}$ in the range 1.8–300 K. The electrochemistry of compound **2** in acetonitrile was investigated. Complex **2** is irreversibly oxidized to a Rh^{III} compound at $E_{\text{pa}} = 1.5 \text{ V}$ and reduced to a wire with a $[\text{Rh}_4]^{6+}$ core at $E_{1/2} = -0.87 \text{ V}$ showing the same properties as those of the product obtained during chemical reduction.

(© Wiley-VCH Verlag GmbH & Co. KGaA, 69451 Weinheim, Germany, 2009)

Introduction

Dinuclear (carboxylato)rhodium(II) complexes $[\text{Rh}_2\text{Cl}_2(\text{OOCR})_2(\text{N-N})_2]$ and $[\text{Rh}_2(\text{OOCR})_2(\text{N-N})_2(\text{H}_2\text{O})_2]^{2+}$ [$\text{R} = \text{H, Me, Et, Pr, Bu, Ph, PhCHOH, N-N} = 2,2'\text{-bipyridine (bpy), 1,10-phenanthroline (phen) and their derivatives}$] belong to the most intensely investigated compounds, because of their very interesting reactivity and catalytic, antibacterial and antitumour properties.^[1–6] Besides their important properties, these complexes can, by reduction, afford a unique class of molecular wires (MWs) based on infinite Rh–Rh chains. It was previously shown that the $[\text{Rh}_2(\text{OOCR})_2(\text{N-N})_2(\text{H}_2\text{O})_2]^{2+}$ complexes can be effectively reduced with ethanol and 2-propanol and other alcohols to MWs of the type $[\text{Rh}_2(\mu\text{-OOCR})_2(\text{bpy})_2]_n\text{X}_n$ and $[\text{Rh}_2(\mu\text{-OOCR})_2(\text{phen})_2]_n\text{X}_n$ ($\text{R} = \text{H, Me, X} = \text{BF}_4^-, \text{PF}_6^-, \text{RCOO}^-$).^[7,9,26] In the acetate complex with the phen ligand, the dinuclear units $[\text{Rh}_2(\mu\text{-OOCR})_2(\text{phen})_2]^+$ are associated into tetranuclear moieties, which in turn form infinite Rh–Rh wires with Rh–Rh bond lengths of 2.562, 2.739 and 2.832 Å.^[7–9] Recently, electrochemical synthesis of $\{[\text{Rh}_2(\mu\text{-OOCCH}_3)_2(\text{phen})_2][\text{BF}_4]_2\}_n$ was also performed, and its electrochemical and physicochemical properties were inves-

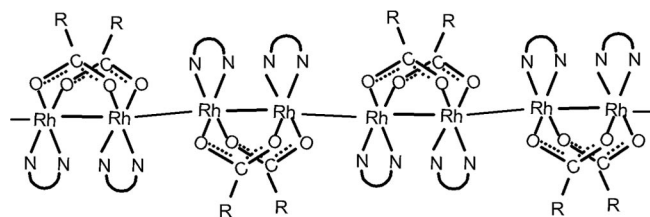
tigated.^[10] It was demonstrated that the compound obtained chemically is similar to that prepared electrochemically. A simpler $\text{Rh}^{\text{I}}\text{--Rh}^{\text{II}}$ MW $[\text{Rh}_2(\text{NCCH}_3)_8](\text{BF}_4)_{3n}$ was previously obtained in the electrochemical reduction of the dinuclear rhodium(II) complex $[\text{Rh}_2(\text{NCCH}_3)_{10}](\text{BF}_4)_2$. In this compound, the Rh–Rh distances are longer (2.8442 and 2.9277 Å),^[11,12] which suggests that rhodium MWs containing carboxylato bridging ligands are more stable. This conclusion was confirmed by formation of formate complexes $[\text{Rh}_4(\mu\text{-OOCH})_4(\text{bpy})_4][\text{PF}_6]_2$ and $\{[\text{Rh}_4(\mu\text{-OOCH})_4(\text{bpy})_4](\text{BF}_4)\}_n \cdot 0.5n\text{C}_4\text{H}_8\text{O}_2$ containing $[\text{Rh}_4]^{6+}$ and $[\text{Rh}_4]^{5+}$ cores, respectively.^[8,9]

More generally, polymetallic complexes with metal–metal bonded chains are of interest because of their unusual and valuable properties. For instance, they can be useful for electronic applications as semiconductors or conducting MWs.^[13,14] MWs with infinite M–M bonds are synthesized by chemical reduction of mononuclear or dinuclear metal complexes. The other, very convenient method is the electrochemical reduction of the appropriate coordination compounds especially developed for Ru and Os wires.^[15–17] The properties of $\{[\text{Rh}_2(\text{OOCR})_2(\text{N-N})_2]\text{X}\}_n$ molecular wires depend on the carboxylato bridging ligands and the polypyridyl ligands (Scheme 1).

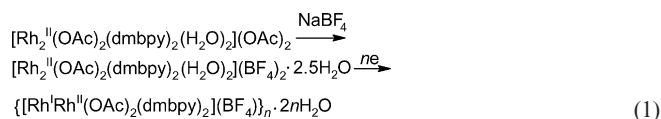
Earlier properties and spectra of the $[\text{Rh}_2(\text{OOCMe})_2(\text{dmbpy})_2(\text{MeCN})_2](\text{BF}_4)_2$ complex with 4,4'-dimethyl-2,2'-bipyridine was described;^[18] however, its X-ray structure was not determined. Until now, only (carboxylato)rhodium MWs with bpy and phen ligands were characterized. In order to have a better understanding of the influence that the

[a] Faculty of Chemistry, University of Wrocław, Joliot-Curie 14, 50-383 Wrocław, Poland

[b] Université Joseph Fourier Grenoble 1/CNRS, Département de Chimie Moléculaire, UMR-5250, Institut de Chimie Moléculaire de Grenoble FR CNRS-2607, B. P. 53, 38041 Grenoble Cedex 9, France
Fax: +48-71-3204232
E-mail: pruchnik@wchuwr.chem.uni.wroc.pl

Scheme 1. Structure of $\{[\text{Rh}_2(\text{OOCR})_2(\text{N-N})_2]^+\}_n$ wires.

substituents of the polypyridyl ligands have on the properties of the rhodium complexes and rhodium MWs, we report here the properties of $[\text{Rh}_2(\mu\text{-OOCCH}_3)_2(\text{dmbpy})_2(\text{H}_2\text{O})_2](\text{CH}_3\text{COO})_2$ (**1**) and $[\text{Rh}_2(\mu\text{-OOCCH}_3)_2(\text{dmbpy})_2(\text{H}_2\text{O})_2](\text{BF}_4)_2 \cdot 2.5\text{H}_2\text{O}$ (**2**), the X-ray structure of the latter complex and the chemical and electrochemical synthesis [Equation (1)] of $\{[\text{Rh}_2(\mu\text{-OOCCH}_3)_2(\text{dmbpy})_2][\text{BF}_4]\}_n \cdot 2n\text{H}_2\text{O}$ (**3**) molecular wire. Utilizing the dmbpy ligand renders the molecular wire more soluble in CH_3CN .

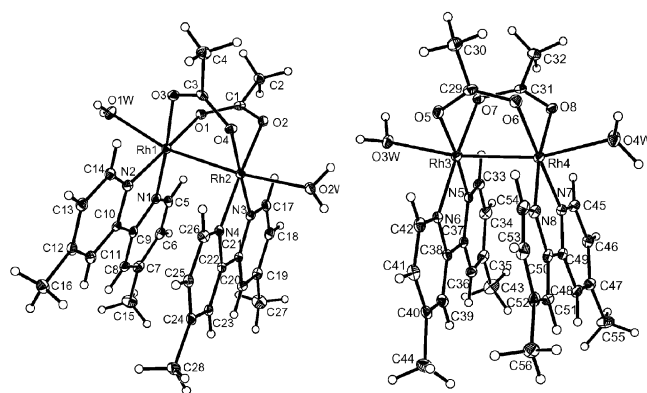


Results and Discussion

Structure and Spectroscopy of Complexes

The molecular structure of $[\text{Rh}_2(\text{OOCCH}_3)_2(\text{dmbpy})_2(\text{H}_2\text{O})_2](\text{BF}_4)_2 \cdot 2.5\text{H}_2\text{O}$ (**2**) is shown in Figure 1. Selected bond lengths and angles are given in Table 1, and the crystallographic data is presented in Table 3. There are two independent molecules of complex **2** in the crystal. Each rhodium atom has distorted octahedral coordination. The equatorial positions are occupied by two nitrogen and two oxygen atoms of the bridging acetato ligands. The remaining axial coordination sites are occupied by the oxygen atom of the water molecule and a rhodium atom (Figure 1). The Rh1–Rh2 distance [2.5190(4) Å] is the shortest one found in $[\text{Rh}_2(\text{OOCCH}_3)_2(\text{N-N})_2\text{L}_2]^{2+}$ complexes (N–N = bpy, phen and their derivatives).^[7–9] The Rh3–Rh4 bond is a little longer [2.5380(4) Å]. Both molecules have distorted eclipsed conformation. Torsion angles N2–Rh1–Rh2–N4 and O3–Rh1–Rh2–O4 are equal to 18.50(12) and 16.56(10)°, respectively. For the second molecule, the analogous angles N5–Rh3–Rh4–N7 and O5–Rh3–Rh4–O6 are –11.30 and –11.44°, respectively. The larger torsion angles in the first molecule lead to the shorter Rh–Rh bond, because repulsion between ligands is smaller. There are relatively strong O–H···O and O–H···F hydrogen bonds, and they stabilize the crystal structure of the compound. The packing diagram of the unit cell along the *b* direction of complex **2**, including the hydrogen bonds, are shown in Figure 2 and the lengths of these bonds are given in Table 2.

Compounds **1** and **2** can be readily reduced with 2-propanol or ethanol. Reduction proceeds especially well in alcohols containing 20–30% water. The reduction is com-

Figure 1. ORTEP representation of complex **2** with crystallographic numbering.Table 1. Bond lengths and angles for **2**.

| Bond lengths [Å] | | Bond angles [°] | |
|------------------|-----------|-----------------|------------|
| Rh1–N2 | 1.997(3) | N2–Rh1–N1 | 80.63(12) |
| Rh1–N1 | 2.010(3) | N2–Rh1–O3 | 95.55(11) |
| Rh1–O3 | 2.052(2) | N1–Rh1–O3 | 175.93(12) |
| Rh1–O1 | 2.055(2) | N2–Rh1–O1 | 176.47(11) |
| Rh1–O1W | 2.221(3) | N1–Rh1–O1 | 96.78(11) |
| Rh1–Rh2 | 2.5190(4) | O3–Rh1–O1 | 86.97(10) |
| Rh2–N4 | 1.994(3) | N1–Rh1–O1W | 93.49(11) |
| Rh2–N3 | 1.999(3) | O3–Rh1–O1W | 85.22(10) |
| Rh2–O4 | 2.062(2) | N2–Rh1–Rh2 | 97.14(8) |
| Rh2–O2 | 2.075(2) | N1–Rh1–Rh2 | 97.15(8) |
| Rh2–O2W | 2.285(3) | O3–Rh1–Rh2 | 84.66(7) |
| Rh3–N6 | 1.999(3) | O1W–Rh1–Rh2 | 166.99(7) |
| Rh3–N5 | 2.011(3) | N4–Rh2–N3 | 80.99(12) |
| Rh3–O5 | 2.037(3) | N4–Rh2–O4 | 97.33(11) |
| Rh3–O7 | 2.068(3) | N3–Rh2–O4 | 177.18(11) |
| Rh3–O3W | 2.258(3) | N4–Rh2–O2 | 174.92(11) |
| Rh3–Rh4 | 2.5380(4) | N3–Rh2–O2 | 93.98(11) |
| Rh4–N7 | 2.000(3) | O4–Rh2–O2 | 87.66(10) |
| Rh4–N8 | 2.004(3) | O2W–Rh2–Rh1 | 170.59(7) |
| Rh4–O8 | 2.037(2) | O1W–Rh1–Rh2 | 166.99(7) |
| Rh4–O6 | 2.052(3) | O3W–Rh3–Rh4 | 170.16(7) |
| Rh4–O4W | 2.247(3) | O4W–Rh4–Rh3 | 165.84(7) |

plete within hours at room temperature and in several minutes when the reaction mixture is heated to reflux. Compound **3** is rather sparingly soluble in alcohols and can be obtained with very high yields. It dissolves best in acetonitrile. The electronic spectra of complexes **1–3** are similar to those of $[\text{Rh}_2(\text{CH}_3\text{COO})_2(\text{N-N})_2(\text{H}_2\text{O})_2]^{2+}$ and the MWs $\{[\text{Rh}_2(\text{CH}_3\text{COO})_2(\text{N-N})_2(\text{X})]\}_n$ (N–N = bpy, phen, X = BF_4^- , BPh_4^- , PF_6^-).^[7–9] In the spectra of Rh^{II} compounds **1** and **2** in the visible region there are two characteristic bands at 568 and 412 nm, which are assigned to the $\pi^*(\text{Rh}2) \rightarrow \sigma^*(\text{Rh}2)$ and $\sigma(\text{Rh}2) \rightarrow \pi^*(\text{dmbpy})$ transitions, respectively.^[19] The electronic reflectance spectrum of complex **3** shows transitions at 750 (sh.), 702 (sh.), 596, 557 and 420 (sh.) nm and are typical of carboxylato $\{[\text{Rh}_4(\text{RCOO})_4(\text{N-N})_4](\text{X})_2\}_n$ wires.^[7–9]

The IR spectra of complexes **1** and **2** in KBr and nujol indicate that the CH_3COO^- ligands form symmetrical bridges with the rhodium atoms. This follows from small difference between $\nu^{\text{as}}(\text{COO})$ and $\nu^{\text{s}}(\text{COO})$ for this compound.

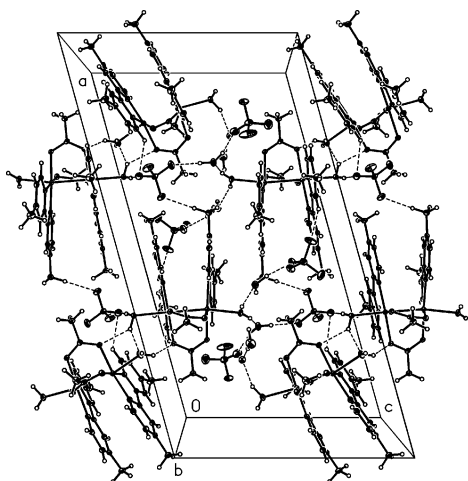


Figure 2. The packing diagram of the unit cell along the *b* direction of complex **2** and hydrogen bonds.

Table 2. Lengths and angles of the hydrogen bonds.^[a]

| D-H...A | <i>d</i> (DA) [Å] | <i>d</i> (H...A) [Å] | ∠(D-H...A) [°] |
|------------------|-------------------|----------------------|----------------|
| O1W-H1W...O8W | 2.681(4) | 1.74 | 159.3 |
| O1W-H2W...O5W#1 | 2.736(4) | 1.95 | 149.4 |
| O2W-H3W...F2#2 | 2.756(4) | 2.07 | 153.1 |
| O2W-H4W...O4W | 2.922(4) | 2.22 | 134.9 |
| O2W-H4W...O8 | 2.935(4) | 2.25 | 132.3 |
| O3W-H5W...O7W#3 | 2.756(4) | 1.85 | 157.4 |
| O3W-H6W...F12#4 | 3.017(4) | 2.14 | 153.5 |
| O3W-H6W...F11#4 | 2.910(4) | 2.26 | 124.4 |
| O4W-H7W...O2 | 2.810(4) | 1.90 | 152.3 |
| O4W-H8W...O9W#5 | 2.699(5) | 1.79 | 158.8 |
| O5W-H9W...O6W#3 | 2.842(4) | 2.02 | 151.4 |
| O5W-H10W...F5 | 2.763(4) | 1.85 | 170.3 |
| O6W-H11W...F8#1 | 2.827(4) | 2.21 | 126.2 |
| O6W-H12W...O4#6 | 2.992(4) | 2.04 | 179.8 |
| O8W-H15W...F15#2 | 2.723(4) | 1.71 | 159.7 |
| O8W-H16W...F3#7 | 2.762(4) | 1.87 | 163.4 |
| O9W-H17W...O7W | 2.969(5) | 2.05 | 179.3 |
| O9W-H18W...O6W#5 | 2.794(5) | 1.86 | 179.3 |

[a] Symmetry transformations used to generate equivalent atoms: #1: *x*, −*y* + 3/2, *z* + 1/2; #2: *x*, −*y* + 1/2, *z* − 1/2; #3: *x*, *y*, *z* − 1; #4: −*x*, −*y* + 1, −*z* − 1; #5: *x*, −*y* + 3/2, *z* − 1/2; #6: *x*, *y*, *z* + 1; #7: *x*, −*y* + 1/2, *z* + 1/2.

The bands assigned to $\nu^{\text{as}}(\text{COO})$ were observed in the range 1570–1600 cm^{−1} and the $\nu^{\text{s}}(\text{COO})$ bands at approximately 1375 and 1345 cm^{−1}.

The ¹H NMR spectrum of **3** in CD₃CN exhibits broad signals of the dmbpy protons at relatively low chemical shifts (2.55, 6.85, 7.00, 7.18, 7.47, 7.64, 7.95 and 8.11 ppm).

The increased line widths, relatively low chemical shifts and loss of resolution were observed also for other MWs and are indicative of the weak paramagnetism of compound **3**. After oxidation of the solutions in air, a high-resolution NMR spectrum identical to that of the diamagnetic rhodium(II) complexes [Rh₂(OAc)₂(N-N)₂(CH₃CN)₂]²⁺ was observed.

Compound **3** in the solid state at 78 K shows axial EPR spectrum with one signal in the region of g_{\perp} , as well as two signals in the region of g_{\parallel} $g_{\perp} = 2.2282$ and $g_{\parallel} = 2.0482$ and

1.9951. At room temperature, $g_{\perp} = 2.2324$ and $g_{\parallel} = 1.9986$. Thus, the EPR spectra are consistent with the unpaired electron being in an orbital of $\sigma(\text{Rh-Rh})$ symmetry. In this case, g_{\parallel} should be close to the free-electron value, 2.0023, because of small spin-orbit coupling, g_{\perp} should be greater than g_e owing to mixing of matrix elements in the degenerate rhodium π orbitals. If the unpaired electron were in the π^* orbital one might expect $g_{\parallel} > g_{\perp}$. The EPR spectrum of complex **3** is similar to the spectra of the chain compounds {[Rh₂(μ-OOCR)₂(N-N)₂][X]}_n^[7–9] and [Rh₂(NCMe)₈]_n-(BF₄)_{3n}^[12] but different to that of the discrete dinuclear paramagnetic complex [Rh₂(μ-OOCCH₃)₂(bpy)₂(NCCH₃)₂][BF₄]^[18]. It was suggested that in the latter compound the unpaired electron is delocalized over the bpy ligand. The presence of two signals in the region of g_{\parallel} indicates that in solid MWs, {[Rh₂(OOCCH₃)₂(dmbpy)₂][BF₄]}_n with odd *n* values are formed. However, the MW prepared electrochemically under a strictly deoxygenated atmosphere is EPR silent.^[10] This indicates that the MW obtained in the electrochemical reduction of the Rh^{II} compound [Rh₂(μ-OOCCH₃)₂(bpy)₂(NCCH₃)₂](BF₄)₂ has the formula {[Rh₄(μ-OOCCH₃)₄(bpy)₄]²⁺(BF₄)₂]_m with diamagnetic tetranuclear cores Rh₄⁶⁺. The latter MW, after short exposure to air, gives a paramagnetic compound ($g_x = 2.083$, $g_y = 2.033$ and $g_z = 2.002$) with a Rh₄⁷⁺ core.^[10] Thus, MWs prepared during reduction with alcohols have different structures than those obtained electrochemically. The former contain {Rh₂³⁺}_n cores with odd and even values of *n*, and the latter with only even values of *n*.

Magnetic Properties of Complex 3

Magnetic susceptibility measurements of complex **3** (Figure 3) were performed in the range 1.8–300 K. The electronic absorption spectra, IR and ¹H NMR spectra and elemental analysis indicate that compound {[Rh₂(μ-OOCCH₃)₂(dmbpy)₂][BF₄]}_n·2*n*H₂O (**3**) is a MW with infinite Rh–Rh chains and with a structure analogous to [Rh₂(OOCMe)₂(phen)₂]_n(PF₆)_n·0.5*n*Me₂CHOH^[7] and other similar MWs of formulae [Rh₂(μ-OOCR)₂(N-N)₂]_n·[X]_n (R = H, Me, N-N = bpy, phen). The Rh–Rh distances in dinuclear units [Rh₂(OOCMe)₂(N-N)₂]⁺ (N-N = bpy, phen) with Rh–Rh bonds supported by two acetato bridges are considerably shorter than unsupported Rh–Rh bonds. The supported bonds in the complex with the phen ligand is 2.652(1) Å and other bonds are equal to 2.739(1) and 2.832(1) Å.^[7] For the bpy complex, only two Rh–Rh distances were found: 2.666(2) and 2.833(2) Å for the supported and unsupported bonds, respectively.^[20] These data indicate that the magnetic properties of compound **3** should be discussed assuming formation of an alternating magnetic chain of dinuclear [Rh₂(OOCMe)₂(N-N)₂]⁺ units with two interaction parameters *J* and *aJ*.^[21,22] The Hamiltonian for the Heisenberg alternating linear chain is given in Equation (2).

$$H = -J \sum_{i=1}^{n/2} [S_{2i}S_{2i-1} + aS_{2i}S_{2i+1}] \quad (2)$$

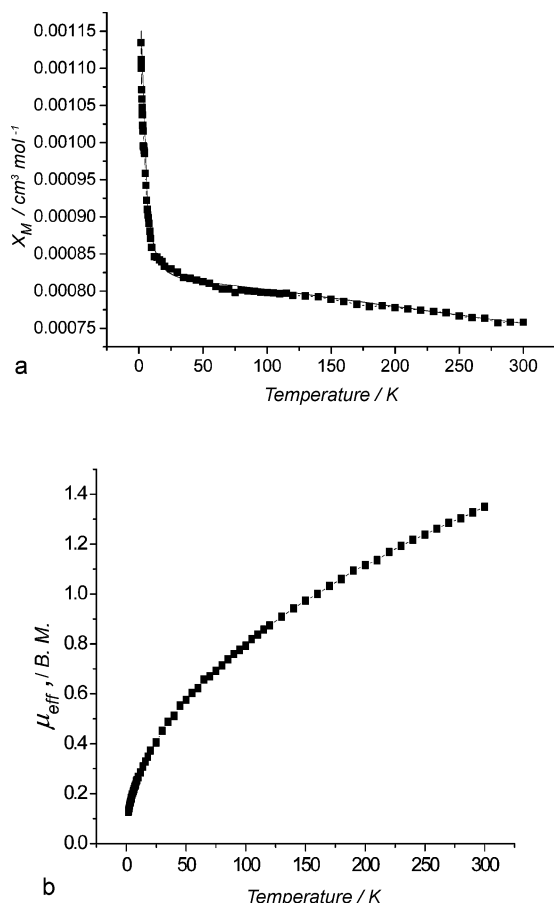


Figure 3. The dependencies of molecular susceptibility (■ experimental, — calculated) (a) and magnetic moment (b) of complex 3 on temperature.

where J is the exchange integral between a spin and its right neighbour, aJ is the exchange integral between a spin and its left neighbour and a is the alternating parameter equal to or less than one; $a = 1$ corresponds to uniform chain and $a = 0$ corresponds to isolated pairs of dinuclear units $\{[\text{Rh}_2(\text{OOCMe})_2(\text{N-N})_2]^+\}_2$, thus to the tetranuclear fragments of wire. The magnetic susceptibility for an alternating ring chain with 10 local 1/2 spins may be calculated by using Equation (3).^[22,23]

$$\chi_M = \frac{Ng^2\beta^2}{kT} \frac{A + Bx + Cx^2}{1 + Dx + Ex^2 + Fx^3} \quad (3)$$

where $x = |J|/kT$. The parameters A – F depend on the coefficient of a . Two sets of these parameters were calculated for: $0 \leq a \leq 0.4$ and $0.4 \leq a \leq 1$. The results for a 10-membered ring are good approximations for infinite systems. This was confirmed for many Cu^{II} chain compounds. Therefore, we assumed that the magnetic properties of the rhodium chain compounds may be explained by using the above formula for $a > 0.4$ by taking into account the proportion λ of non-coupled dinuclear $[\text{Rh}_2(\text{OOCMe})_2(\text{N-N})_2]^+$ units, including impurities and ends of chain,^[21,24] as well as temperature-independent paramagnetism (TIP) (constant G) [Equation (4)].

$$\chi_M^{\text{cor}} = \frac{Ng^2\beta^2}{kT} \frac{A + Bx + Cx^2}{1 + Dx + Ex^2 + Fx^3} (1 - \lambda) + \lambda Ng^2\beta^2/4kT + G \quad (4)$$

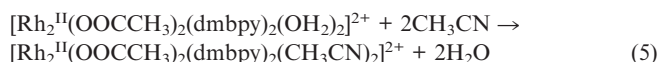
It was assumed that impurities are dinuclear compounds $[\text{Rh}_2(\text{OOCMe})_2(\text{N-N})_2][\text{BF}_4] \cdot \text{solv}$ of the same molecular weight as the basis units of the chain and that their magnetic susceptibility followed the Curie law ($Ng^2\beta^2/4kT$).

The dependencies of magnetic susceptibility and effective magnetic moment as well as calculated magnetic susceptibility on temperature are given in the Figure 3. For compound 3, the following results were obtained: $g = 2.167$, $J = -780 \text{ cm}^{-1}$, $a = 0.69$, $\lambda = 0.006$, $\text{TIP} = 440 \times 10^{-6} \text{ cm}^3 \text{ mol}^{-1}$. The average g_{av} value determined from the EPR spectra is 2.1594.

The presented magnetic properties are characteristic of chains with very strong antiferromagnetic interactions. Compound 3 shows temperature-independent paramagnetism similar to that in dinuclear Rh^{II} complexes, for example, $\text{Na}_4[\text{Rh}_2(\text{CO}_3)_4] \cdot 2.5\text{H}_2\text{O}$ ($500 \times 10^{-6} \text{ cm}^3 \text{ mol}^{-1}$) and $(\text{NH}_4)_4[\text{Rh}_2(\text{CO}_3)_4] \cdot 4.5\text{H}_2\text{O}$ ($240 \times 10^{-6} \text{ cm}^3 \text{ mol}^{-1}$).^[25] The content of the paramagnetic ends of the chain and the impurities is small: 0.6%. This indicates that the chains in complex 3 are long (n is large). The alternating parameter a is relatively small; thus, antiferromagnetic interactions between $[\text{Rh}_2(\text{OOCCH}_3)_2(\text{N-N})_2]^+$ differ considerably. Complex 3 and other molecular wires, for example, $[\text{Rh}_2(\mu\text{-OOCCH}_3)_2(\text{bpy})_2]_n[\text{BF}_4]_n \cdot n\text{H}_2\text{O}$ and $[\text{Rh}_2(\text{OOCCH}_3)_2(\text{phen})_2]_n(\text{PF}_6)_n \cdot 0.5n\text{Me}_2\text{CHOH}$, in the solid state show antiferromagnetic properties, in contrast to solutions of $[\text{Rh}_2(\text{OOCCH}_3)_2(\text{phen})_2]_n(\text{PF}_6)_n$ in CH_3CN ,^[10] which is EPR silent. This indicates that in solution, in acetonitrile, diamagnetic $[\text{Rh}_2(\text{OOCCH}_3)_2(\text{phen})_2]_n^{x+}$ cations (with even values of n) are formed.^[10] The same was found for solutions of a complex with bpy ligands, $[\text{Rh}_2(\text{OOCCH}_3)_2(\text{bpy})_2]_n(\text{OOCMe})$.^[26] Thus molecular wires in the solid state contain $[\text{Rh}_2(\text{OOCCH}_3)_2(\text{N-N})_2]_n^{x+}$ fragments with odd values of n or interaction between dinuclear $[\text{Rh}_2(\text{OOCCH}_3)_2(\text{N-N})_2]_n^+$ units in the solid state is too weak to lead to spin pairing.

Redox Properties of $[\text{Rh}^{\text{II}}_2(\text{OOCCH}_3)_2(\text{dmbpy})_2(\text{OH}_2)_2][\text{BF}_4]_2$ (2)

Dissolution of complex 2 in acetonitrile leads immediately to substitution of aqua ligands for MeCN molecules giving an orange-yellow solution showing absorption at 19000, 24400, 28200, 32800, 37200 and 38700 cm^{-1} . The energy of the first band depends strongly on the properties of the axial ligands. Its energy for rhodium(II) carboxylates with ligands coordinated through the oxygen atom is considerably lower than that for complexes with nitrogen axial ligands. In aqueous solutions, electronic spectra of 1 and 2 are essentially identical and show bands at 17600, 24200, 27900, 32400, 35600, 37100 and 38900 cm^{-1} . The exchange of aqua axial ligands for MeCN proceeds very fast, less than 1 s. [Equation (5)].



However, the electrochemical behaviour of aqua complex **2** dissolved in CH₃CN + 0.1 M TBAP electrolyte at a Pt or glassy carbon (GC) disk electrode is slightly different than the behaviour of the complex [Rh^{II}₂(OOCCH₃)₂(phen)₂(OH₂)₂](BF₄)₂ that we previously studied in great detail, especially in the reduction part.^[10] In agreement with the previously published CV measurements on [Rh^{II}₂(OOCCH₃)₂(dmbpy)₂(CH₃CN)₂](BF₄)₂,^[18] the cyclic voltammogram of [Rh^{II}₂(OOCCH₃)₂(dmbpy)₂(OH₂)₂](BF₄)₂ (**2**) in the negative potential area exhibits a closely reversible one-electron redox system at $E_{1/2} = -0.87$ V (Figure 4a; $\Delta E_p = 0.07$ V at 100 mV s⁻¹) and in the positive potential area an irreversible two-electron oxidation at $E_{\text{pa}} = 1.50$ V (Figure 4b). Similar values were found for [Rh^{II}₂(OOCCH₃)₂(bpy)₂(OH₂)₂]²⁺.^[27]

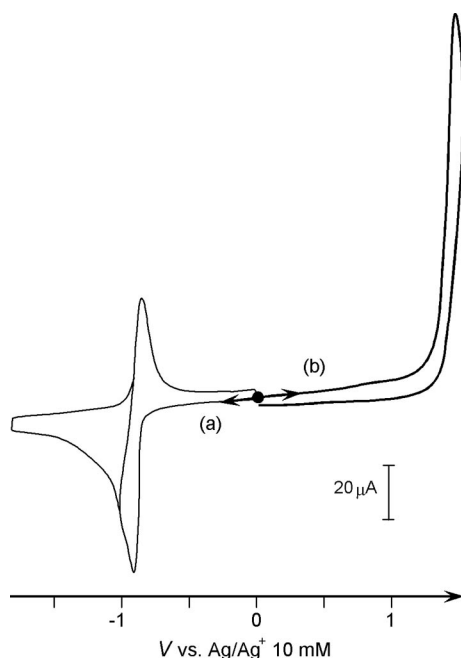


Figure 4. (a) CV of **2**, 1.2 mM in CH₃CN + 0.1 M TBAP on a Pt electrode (diam. 5 mm), from 0 to -1.8 V (a) and 1.5 V (b); $\nu = 100$ mV s⁻¹.

Iterative CVs and also microelectrolysis at applied potential (-0.90 V) did not lead to the formation of an adherent redox-active solid on the working electrode (WE) surface, as was observed under the same experimental conditions for the analogous phen complex.^[10] However, an exhaustive controlled potential electrolysis, carried out on a large Pt WE surface at -0.90 V, shows that the reduction is an irreversible process. Indeed, after one mol of electron per mol of **2** precursor has been consumed (quantitative faradic yield), a brown solution containing a fine precipitate was formed.

The UV/Vis absorption spectrum of the solution obtained after removing the precipitate by filtration shows broad absorption bands ($\lambda_{\text{max}} = 274, 356, 431, 524, 592$ nm)

close to those observed for a solid sample of **3** prepared chemically (cf. above). The CV curves of the brown solution show, in the reduction part [Figure 5A(a)], a poorly reversible system at $E_{1/2} = -0.96$ V ($\Delta E_p = 0.13$ V at 100 mV s⁻¹) very close to the reduction potential of **2** ($\Delta E_{1/2} = -0.09$ V). This system is followed by a second reduction at $E_{1/2} = -1.53$ V ($\Delta E_p = 0.11$ V at 100 mV s⁻¹). In the cathodic area, the electrochemical properties of the soluble electrogenerated species are very close to the electrochemical properties of solid polymer **3** synthesized chemically [Figure 5C(a)]. The present results are in accordance with our previous detailed electrochemical studies of Rh wires^[10] and show that the monoelectronic reduced soluble [Rh^IRh^{II}] species obtained from **2** and the polymetallic species prepared chemically are nearly identical and have the general formula {[Rh^{II}₂Rh^I₂(dmbpy)₄(OOCCH₃)₄](BF₄)₂]_n ($n \geq 1$) corresponding to species **3**; they contain different solvent molecules in the lattice. This Rh MW can be generated by following the global reaction presented in Equation (1) by reaction with a chemical electron donor or by electrolysis on a conductive electrode.

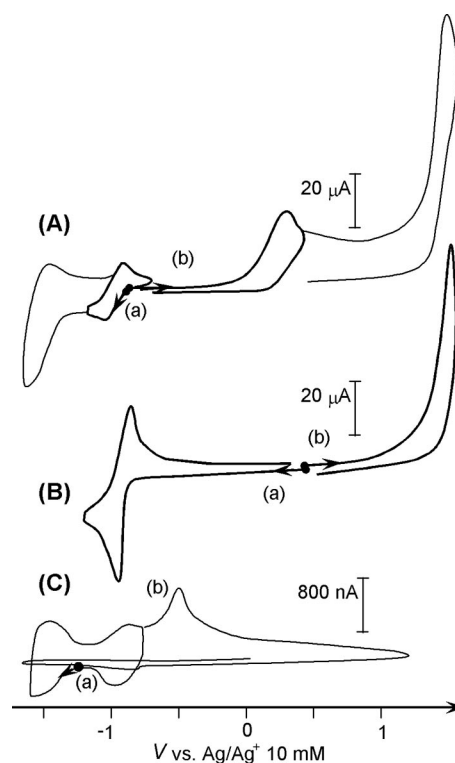
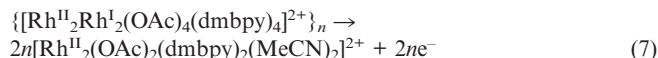
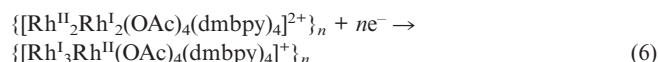


Figure 5. (A) CVs of **3** obtained by exhaustive reduction of **2** 1.2 mM in CH₃CN + 0.1 M TBAP at -0.90 V; Pt electrode (diam. 5 mm); from -0.90 to -1.82 V (a) and +1.52 V (b). (B) CVs after exhaustive oxidation of the latter solution at +0.50 V: from +0.50 to -1.80 V (a) and to +1.52 V (b); (C) CVs of chemically synthesized powdered **3** recorded by using a Pt CME (diam. 60 μm; depth 20 μm) from -0.80 to -1.60 V (a) and to 1.10 V (b), $\nu = 100$ mV s⁻¹.

Equations (6) and (7) summarize, respectively, the hypothetical electron-transfer reactions occurring during the first reduction and the first oxidation processes of the Rh-soluble product [Figure 5A(a,b)], in agreement with our previous published Rh MW redox properties.^[10]



The exhaustive oxidation of the produced mixture (solution + precipitate) on a Pt sheet at 0.50 V generated a limpid orange-yellow solution, which was characterized by its cyclic voltammograms (Figure 5B) and UV/Vis spectrum. The shape of the CV curves and UV/Vis properties show that initial dinuclear complex **2** is recovered after this exhaustive oxidation [Equation (6)] with a 60% yield.

Redox Solid-State Properties of $\{[\text{Rh}^{\text{II}}_2\text{Rh}^{\text{I}}_2(\text{OOCCH}_3)_4(\text{dmbpy})_4](\text{BF}_4)_2\}_n$ (**3**)

Cyclic voltammograms of powdered **3**, obtained by chemical synthesis from **2**, were investigated by using a cavity microelectrode (CME) as the working electrode (cavity volume $\approx 4 \times 10^{-8} \text{ cm}^3$)^[28] in $\text{CH}_3\text{CN} + 0.1 \text{ M TBAP}$. A typical voltammogram, recorded on a powdered sample of **3** at a scan rate of 100 mVs^{-1} , is presented in Figure 5C(a). The stability of the redox signal after one cycle, in the potential range of -0.70 to -1.82 V , indicates a fast equilibrium between the electrolyte and the powdered sample included in the cavity. The CV [curve (a)] presents two broad reversible systems at -0.96 V ($\Delta E_p = 0.09 \text{ V}$) and -0.51 V ($\Delta E_p = 0.05 \text{ V}$), which look like those observed on the CV of the reduced soluble species obtained from **2** [Figure 5A(a); see above in the text]. The broad shape of the redox systems [curve (a)] is the result of the use of such CME. Indeed, the outline and the features of the CVs of the powder are related to the structural parameters of the compound studied (size and shape of the grains), the configuration of the powder within the cavity (space distribution of the electroactive sites) and also to the geometry of the CME used (Pt diameter and deepness of the microcavity).^[28] A scan up to 1.10 V [Figure 5C(b)], beyond the oxidation peak at -0.69 V , leads to the formation of a soluble species that diffuses into the electrolyte solution and induces the cleaning of the cavity. The oxidation peak potential of **3** in the solid state [Figure 5A(b)] is in agreement with that observed previously for the corresponding $\{[\text{Rh}_4(\text{OOCCH}_3)_4(\text{phen})_4]_n(\text{BF}_4)_2\}_n$ polymetallic species deposited on a macroscopic Pt electrode.^[10]

Conclusions

Spectroscopic methods reveal that the $[\text{Rh}_2(\mu\text{-OOCCH}_3)_2(\text{dmbpy})_2(\text{H}_2\text{O})_2](\text{CH}_3\text{COO})_2$ (**1**) and $[\text{Rh}_2(\mu\text{-OOCCH}_3)_2(\text{dmbpy})_2(\text{H}_2\text{O})_2][\text{BF}_4]_2 \cdot 2.5\text{H}_2\text{O}$ (**2**) complexes are dinuclear compounds with water molecules coordinated along the Rh–Rh axis. X-ray crystallography of compound **2** showed that there are two independent molecules in the crystal. The Rh–Rh distances are equal to $2.5190(4)$ and $2.5380(4) \text{ \AA}$. The former is the shortest bond observed in complexes

of the type $[\text{Rh}_2(\mu\text{-OOCCH}_3)_2(\text{N-N})_2(\text{H}_2\text{O})_2]^{2+}$. Torsion angles N–Rh–Rh–N and O–Rh–Rh–O are greater for the molecule with the shorter Rh–Rh distance, because of smaller repulsion between ligands. Crystals are additionally stabilized by relatively strong O–H \cdots O and O–H \cdots F hydrogen bonds. Reduction of compound **2** with aqueous alcohols leads to the formation of the molecular wire $\{[\text{Rh}_2(\mu\text{-OOCCH}_3)_2(\text{dmbpy})_2][\text{BF}_4]\}_n \cdot 2n\text{H}_2\text{O}$ (**3**) containing a $[\text{Rh}_4]^{6+}$ core. Compound **3** shows strong antiferromagnetic properties, $J = -780 \text{ cm}^{-1}$ and $\mu_{\text{eff}} = 0.128\text{--}1.349 \text{ B.M.}$ in the range $1.8\text{--}300 \text{ K}$. The electrochemical properties of compound **2** in acetonitrile were also investigated, and **2** is irreversibly oxidized to a Rh^{III} compound at $E_{\text{pa}} = 1.5 \text{ V}$ and reduced to a wire with a $[\text{Rh}_4]^{6+}$ core at $E_{1/2} = -0.87 \text{ V}$ showing the same properties as those of the product obtained by chemical reduction.

Experimental Section

Starting Materials and Methods: The reagents 4,4'-dimethyl-2,2'-bipyridine (dmbpy) and $\text{RhCl}_3 \cdot 3\text{H}_2\text{O}$ were purchased from Aldrich. Rhodium(II) acetate $[\text{Rh}_2(\mu\text{-OOCCH}_3)_4]$ was prepared as described in the literature.^[29] ^1H NMR spectra were measured with a Bruker AMX 300 and Avance 500 spectrometers, IR spectra were measured with a Bruker IFS 113v spectrometer, EPR spectra were obtained with a Bruker ESP 300E and UV/Vis spectra were recorded with a Beckman DU-7500, Cary 5 and Cary 500 spectrometers. The reflectance spectra of the powdered samples of complex **3** were recorded by using MgO as a reference. The temperature dependence of the magnetic susceptibility was measured with a Quantum Design MPMS-XL-5 SQUID susceptometer operating at a magnetic field of 0.5 T in the temperature range $1.8\text{--}300 \text{ K}$. A sample of the compound was sealed in a quartz tube under an atmosphere of argon. The susceptibilities were corrected for the diamagnetism of the constituent atoms by using Pascal's constants.^[21]

$[\text{Rh}_2(\text{CH}_3\text{COO})_2(\text{C}_{12}\text{H}_{12}\text{N}_2)_2(\text{H}_2\text{O})_2](\text{CH}_3\text{COO})_2$ (1**):** A solution of $[\text{Rh}_2(\mu\text{-OOCCH}_3)_4]$ (0.442 g , 1 mmol) and dmbpy (0.369 g , 2 mmol) was heated at reflux in ethanol/water (5:1, 10 mL) until a deep blue-green solution of the $\text{Rh}^{\text{I}}\text{Rh}^{\text{II}}$ compound was formed. The solution was then air-oxidized and concentrated to ca. 3 mL . The product was precipitated by the addition of a large excess of diethyl ether, and the solid was then washed with diethyl ether and dried in vacuo. IR (KBr): $\tilde{\nu} = 424 (\text{w})$, $467 (\text{w})$, $520 (\text{m})$, $577 (\text{w})$, $626 (\text{w})$, $649 (\text{m})$, $703 (\text{m})$, $730 (\text{m})$, $740 (\text{w})$, $764 (\text{w})$, $822 (\text{m})$, $838 (\text{m})$, $905 (\text{v w})$, $923 (\text{w})$, $1019 (\text{w})$, $1037 (\text{w})$, $1119 (\text{w})$, $1135 (\text{w})$, $1221 (\text{w})$, $1244 (\text{w})$, $1270 (\text{w})$, $1300 (\text{w})$, $1320 (\text{m})$, $1350 (\text{m})$, $1409 (\text{vs})$, $1435 (\text{vs})$, $1482 (\text{s})$, $1558 (\text{vs})$, $1620 (\text{s})$, $2519 (\text{m})$, $2855 (\text{m})$, $2921 (\text{s})$, $2955 (\text{s})$, $3023 (\text{s})$, $3046 (\text{s})$, $3116 (\text{s})$, $3414 (\text{vs})$, $3507 (\text{vs}) \text{ cm}^{-1}$. UV/Vis (H_2O): $1/\lambda (\epsilon, \text{ dm}^3 \text{ mol}^{-1} \text{ cm}^{-1}) = 17800 (203)$, $23700 (2000)$, $28000 (4500)$, $32400 (13500)$, $36900 (33700)$, $38600 (36700) \text{ cm}^{-1}$. UV/Vis (MeCN): $1/\lambda (\epsilon, \text{ dm}^3 \text{ mol}^{-1} \text{ cm}^{-1}) = 18900 (240)$, $24300 (2600)$, $28100 (5400)$, $32500 (20800)$, $36500 (34400)$, $37200 (36000) \text{ cm}^{-1}$. ^1H NMR (300 MHz , D_2O): $\delta = 7.99 (\text{d}, {}^3J_{5,6} = 5.9 \text{ Hz}$, 4 H , $\text{H}^{6,6})$, $7.68 (\text{d}, {}^4J_{3,5} = 1.1 \text{ Hz}$, 4 H , $\text{H}^{3,3'})$, $7.18 (\text{dd}, 4 \text{ H}$, $\text{H}^{5,5'})$, $2.46 (\text{s}, 6 \text{ H}, \mu\text{-CH}_3\text{COO})$, $2.44 (\text{s}, 12 \text{ H}, \text{CH}_3)$, $1.85 (\text{s}, 6 \text{ H}, \text{CH}_3\text{COO}) \text{ ppm}$. $\text{C}_{32}\text{H}_{40}\text{N}_4\text{O}_{10}\text{Rh}_2$ (846.50): calcd. C 45.40 , H 4.76 , N 6.62 ; found C 45.18 , H 4.51 , N 6.38 .

$[\text{Rh}_2(\text{CH}_3\text{COO})_2(\text{C}_{12}\text{H}_{12}\text{N}_2)_2(\text{H}_2\text{O})_2](\text{BF}_4)_2 \cdot 2.5\text{H}_2\text{O}$ (2**):** To a solution of **1** in ethanol/water (5:1, 4 mL) was added NaBF_4 (2 mmol)

in EtOH/H₂O. The resulting solid was recrystallized from water to give red-black crystals. The product was dried in air. IR (KBr): $\tilde{\nu}$ = 422 (m), 472 (m), 522 (m), 578 (m), 627 (w), 668 (w), 707 (m), 730 (w), 765 (w), 832 (m), 924 (w), 1037 (vs), 1067 (s), 1083 (vs), 1121 (s), 1223 (w), 1244 (w), 1272 (w), 1300 (w), 1359 (w), 1384 (w), 1444 (s), 1485 (m), 1558 (s), 1622 (s), 2866 (m), 2924 (m), 2979 (m), 3021 (m), 3042 (m), 3066 (m), 3120 (m), 3253 (s), 3439 (vs) cm⁻¹. UV/Vis (H₂O): $1/\lambda$ (ϵ , dm³ mol⁻¹ cm⁻¹) = 17600 (220), 24200 (2300), 27900 (4900), 32400 (19600), 35600 (33400), 37100 (sh.), 38900 (55400) cm⁻¹. UV/Vis (MeCN): $1/\lambda$ (ϵ , dm³ mol⁻¹ cm⁻¹) = 19000 (260), 24400 (2700), 28200 (5200), 32800 (22000), 37200 (45000), 38700 (49400) cm⁻¹. ¹H NMR (500 MHz, D₂O): δ = 7.97 (d, ³J_{5,6} = 5.9 Hz, 4 H, H⁶), 7.67 (d, ⁴J_{3,5} = 1.1 Hz, 4 H, H³), 7.17 (dd, 4 H, H⁵), 2.47 (s, 6 H, μ-CH₃COO), 2.45 (s, 12 H, CH₃). C₂₈H₃₉B₂F₈N₄O_{8.5}Rh₂ (947.05): calcd. C 35.51, H 4.15, N 5.92; found C 35.32, H 4.37, N 5.71.

{[Rh₂(OOCCH₃)₂(C₁₂H₁₂N₂)₂](BF₄)}_n·2nH₂O (3): A solution of 1 (0.423 g, 0.5 mmol) in 2-propanol/water (3:1, 5 mL) under an argon atmosphere was heated at reflux until a deep blue-green solution of the Rh^IRh^{II} compound was formed. Then, a deaerated solution of [NBu₄]BF₄ (0.165 g, 0.5 mmol) in 2-propanol/H₂O was added, and the mixture was heated at reflux for 10 min. The resulting black precipitate was filtered off, washed with aqueous 2-propanol and dried in vacuo. The product was dried in vacuo and stored under an atmosphere of argon. IR (nujol): $\tilde{\nu}$ = 522 (w), 727 (w), 833 (m), 924 (m), 1037 (s), 1060 (s), 1378 (s), 1463 (s), 1558 (s), 1617 (s), 3021 (m), 3042 (m), 3066 (m), 3120 (m) cm⁻¹. UV/Vis (reflectance spectrum): $1/\lambda$ = 13300, 14200, 17400, 16800, 18000, 23800 cm⁻¹. C₂₈H₃₄BF₄N₄O₆Rh₂ (815.21): calcd. C 41.25, H 4.20, N 6.87; found C 41.30, H 3.88, N 6.70.

X-ray Crystallography Study: X-ray data were collected at low temperature by using an Oxford Cryosystem device with a Kuma KM4CCD κ -axis diffractometer with graphite-monochromated Mo- K_{α} radiation (λ = 0.71073 Å). Accurate cell parameters were

determined and refined by least-squares fit of 7350 of the strongest reflections. The data were corrected for Lorentz and polarization effects as well as for analytical absorption correction. Data reduction and analysis were carried out with the Oxford Diffraction (Poland) Sp. z o.o. programs. The structure was solved by direct methods (program SHELXS-97^[30]) and refined by the full-matrix least-squares method on all F^2 data by using the SHELXL-97^[31] programs. Non-hydrogen atoms were refined with anisotropic displacement parameters; hydrogen atoms were included from geometry of molecules and $\Delta\rho$ maps. They were fixed or treated as riding groups during refinement of the structure. Crystal data are given in Table 3, together with refinement details. CCDC-698582 contains the supplementary crystallographic data for this paper. These data can be obtained free of charge from The Cambridge Crystallographic Data Centre via www.ccdc.cam.ac.uk/data_request/cif.

Electrochemistry: Tetra-*n*-butylammonium perchlorate Bu₄NClO₄ (TBAP) was purchased from Fluka and used without purification. HPLC-grade acetonitrile (Rathburn) was used as received. Cyclic voltammetric (CV) measurements and bulk electrolyses were performed under an atmosphere of argon in a dry box (Jaram) by using a PAR Model 173 potentiostat equipped with a digital coulometer. All cyclic voltammograms were recorded with a conventional single-compartment three-electrode cell. All electrode potentials reported in this work are given relative to Ag/Ag⁺ (0.01 M in CH₃CN containing 0.1 M TBAP electrolyte). Conversion into the ferrocene-ferrocenium reference system can be done by adding −0.087 V. The working electrodes for CV measurements were platinum or GC discs (active surface areas of 0.19 and 0.07 cm², respectively) polished with a 2 μm diamond paste (Mecaprex Presi). Exhaustive electrolyses were carried out on a platinum sheet (2 cm²). The auxiliary electrode was a Pt wire in acetonitrile + 0.1 M TBAP electrolyte. Electrochemistry of solid powder polymer 3 was performed by using a Pt cavity microelectrode CMEs (diam. 60 μm). The cavity ($\approx 6 \times 10^{-8}$ cm³) was filled up with material grains by using the electrode as a pestle. The Pt CMEs were obtained from the Cavity Microelectrode Users Network, CNRS-France, <http://www.icmpe.cnrs.fr/spip.php?rubrique104>.

Table 3. Crystal data and structure refinement for [Rh₂(CH₃COO)₂-(C₁₂H₁₂N₂)₂(H₂O)₂](BF₄)₂·2.5H₂O (2).

| | |
|---|--|
| Empirical formula | (C ₂₈ H ₃₄ N ₄ O ₆ Rh ₂)(BF ₄) ₂ ·2.5H ₂ O |
| Formula weight | 947.05 |
| T / K | 100(2) |
| $\lambda / \text{\AA}$ | 0.71073 |
| Crystal system | monoclinic |
| Space group | $P2_1/c$ |
| $a / \text{\AA}$ | 25.9495 (7) |
| $b / \text{\AA}$ | 20.2529(6) |
| $c / \text{\AA}$ | 14.1376(5) |
| $\alpha / ^\circ$ | 90 |
| $\beta / ^\circ$ | 105.448(3) |
| $\gamma / ^\circ$ | 90 |
| $V / \text{\AA}^3$ | 7161.6(4) |
| Z | 8 |
| $D_{\text{calcd.}} / \text{Mg m}^{-3}$ | 1.757 |
| μ / mm^{-1} | 1.017 |
| $F(000)$ | 3800 |
| Crystal size / mm | 0.15 × 0.14 × 0.12 |
| θ range for data collection / ° | 3.05–27.00 |
| Ranges of h, k, l | −32→33, −20→25, −18→18 |
| Reflections collected | 55087 |
| Independent reflections (R_{int}) | 15573 (0.0608) |
| Data/parameters | 15573/958 |
| Absorption coefficients min./max. | 0.862/0.888 |
| GOF(F_2) | 1.049 |
| Final R_1, wR_2 indices ($I > 2\sigma_I$) | 0.0421, 0.0881 |
| Largest diff. peak, hole / e Å ⁻³ | 1.551, −0.696 |

Acknowledgments

This work was supported by the Ministry of Science and Higher Education of Poland (grant PBZ-KBN-118/T09/09) and by a PAI POLONIUM program (Minister of Foreign Affairs of France). F. L. acknowledges support from a CNRS postdoctoral fellowship.

- [1] F. P. Pruchnik, *Pure Appl. Chem.* **1989**, 61, 795–804.
- [2] H. T. Chifotides, K. R. Dunbar, “Rhodium Compounds” in *Multiple Bonds Between Metal Atoms* (Eds.: F. A. Cotton, C. A. Murillo, R. A. Walton), Springer, New York, **2005**.
- [3] M. Bieñ, T. M. Lachowicz, A. Rybka, F. P. Pruchnik, L. Trynda, *Met.-Based Drugs* **1997**, 4, 81–88.
- [4] F. P. Pruchnik, D. Duś, *J. Inorg. Biochem.* **1996**, 61, 55–61.
- [5] M. Bieñ, F. P. Pruchnik, A. Seniuk, T. M. Lachowicz, P. Jakimowicz, *J. Inorg. Biochem.* **1999**, 73, 49–55.
- [6] H. T. Chifotides, K. R. Dunbar, *Acc. Chem. Res.* **2005**, 38, 146–156.
- [7] F. P. Pruchnik, P. Jakimowicz, Z. Ciunik, *Inorg. Chem. Commun.* **2001**, 4, 726–729.
- [8] F. P. Pruchnik, A. Jutarska, Z. Ciunik, M. Pruchnik, *Inorg. Chim. Acta* **2003**, 350, 609–616.
- [9] F. P. Pruchnik, A. Jutarska, Z. Ciunik, M. Pruchnik, *Inorg. Chim. Acta* **2004**, 357, 3019–3026.
- [10] F. Lafolet, S. Chardon-Noblat, C. Duboc, A. Deronzier, F. P. Pruchnik, M. Rak, *Dalton Trans.* **2008**, 2149–2156.

- [11] J. K. Bera, K. R. Dunbar, *Angew. Chem. Int. Ed.* **2002**, *41*, 4453–4457.
- [12] M. E. Prater, L. E. Pence, R. Clerac, G. M. Finnis, C. Campana, P. Auban-Senzier, D. Jerome, E. Canadell, K. R. Dunbar, *J. Am. Chem. Soc.* **1999**, *121*, 8005–8016.
- [13] D. R. Tyler, *Frontiers in Transition Metal-Containing Polymers* (Eds.: A. S. Abd-El-Aziz, I. Manners), Wiley-Interscience, Weinheim, **2007**, p. 287.
- [14] J. F. Berry, F. A. Cotton, P. Lei, T. Lu, C. A. Murillo, *Inorg. Chem.* **2003**, *42*, 3534–3539.
- [15] a) M.-N. Collomb-Dunand-Sauthier, A. Deronzier, R. Ziessel, *Inorg. Chem.* **1994**, *33*, 2961–2967; b) S. Chardon-Noblat, M.-N. Collomb-Dunand-Sauthier, A. Deronzier, R. Ziessel, D. Zsoldos, *Inorg. Chem.* **1994**, *33*, 4410–4412; c) S. Chardon-Noblat, A. Deronzier, R. Ziessel, D. Zsoldos, *Inorg. Chem.* **1997**, *36*, 5384–5389.
- [16] F. Hartl, T. Mahabiersing, S. Chardon-Noblat, P. Da Costa, A. Deronzier, *Inorg. Chem.* **2004**, *43*, 7250–7258.
- [17] S. Myllynen, M. Wasberg, M. Haukka, *J. Electroanal. Chem.* **2006**, *586*, 217–224.
- [18] C. A. Crawford, J. H. Matonic, J. C. Huffman, K. Folting, K. R. Dunbar, G. Christou, *Inorg. Chem.* **1997**, *36*, 2361–2371.
- [19] L. Natkaniec, F. P. Pruchnik, *J. Chem. Soc., Dalton Trans.* **1994**, 3261–3266.
- [20] F. P. Pruchnik, P. Jakimowicz, Z. Ciunik, K. Stanislawek, L. A. Oro, C. Tejel, M. A. Ciriano, *Inorg. Chem. Commun.* **2001**, *4*, 19–22.
- [21] O. Kahn, *Molecular Magnetism*, VCH, New York **1993**.
- [22] J. W. Hall, W. E. Marsch, R. R. Weller, W. E. Hatfield, *Inorg. Chem.* **1981**, *20*, 1033–1037.
- [23] M. M. Olmstead, W. K. Musker, L. W. Ter Haar, W. E. Hatfield, *J. Am. Chem. Soc.* **1982**, *104*, 6627–6631.
- [24] J. J. Girerd, O. Kahn, M. Verdaguer, *Inorg. Chem.* **1980**, *19*, 274–276.
- [25] C. R. Wilson, H. Taube, *Inorg. Chem.* **1975**, *14*, 405–409.
- [26] E. Gałdecka, Z. Gałdecki, F. P. Pruchnik, P. Jakimowicz, *Transition Met. Chem.* **2000**, *25*, 315–319.
- [27] A. Szymaszek, F. P. Pruchnik, *Pol. J. Chem.* **1992**, *66*, 1859–1865.
- [28] V. Vivier, C. Cachet-Vivier, D. Michel, J.-Y. Nedelec, L. T. Yu, *Synt. Met.* **2002**, *126*, 253–262.
- [29] G. L. Rempel, P. Legzdins, H. Smith, G. Wilkinson, *Inorg. Synth.* **1972**, *13*, 90–91.
- [30] G. M. Sheldrick, *SHELXS-97: Program for Solution of Crystal Structures*, University of Göttingen, Göttingen, Germany, **1997**.
- [31] G. M. Sheldrick, *SHELXL-97: Program for Crystal Structure Refinement*, University of Göttingen, Göttingen, Germany, **1997**.

Received: August 18, 2008

Published Online: November 27, 2008

Lanthanide(III) Complexes of Phosphorus Acid Analogues of H₄DOTA as Model Compounds for the Evaluation of the Second-Sphere Hydration

Zuzana Kotková,^[a] Giovannia A. Pereira,^[b] Kristina Djanashvili,^[c] Jan Kotecký,^[a] Jakub Rudovský,^[a] Petr Hermann,^[a] Luce Vander Elst,^[d] Robert N. Muller,^[d] Carlos F. G. C. Geraldes,^[b] Ivan Lukeš,^{*[a]} and Joop A. Peters^{*[c]}

Keywords: Contrast agents / Lanthanides / NMR spectroscopy / Phosphinate complexes / Phosphonate complexes

Five DOTA-like ligands lacking a water molecule in the first coordination sphere of their Gd^{III} complexes, namely the phosphinates H₄DOTP^H, H₄DOTP^{hm} and H₄DOTP^{Et}, and the phosphonate monoesters H₄DOTP^{OEt} and H₄DOTP^{OBu}, were synthesized with the aim of exploring the influence of the second hydration sphere on the relaxivity of Gd^{III} complexes. The H₄DOTP^H, H₄DOTP^{hm} and H₄DOTP^{OEt} ligands and their Ln^{III} complexes were characterized by potentiometry and time-resolved luminescence; the Gd^{III} complexes are thermodynamically much less stable than that of H₄DOTA, and no water is coordinated in the inner sphere. The crystal structures of the free ligand H₄DOTP^{OEt} and of the Gd^{III} complexes of H₄DOTP^H and H₄DOTP^{OEt} were determined by X-ray diffraction. The complexes have the expected octadentate coordination mode with an N₄O₄ arrangement; no water molecule is bound to the Gd^{III} ion. Information on the structures of the Ln^{III} complexes of all five ligands in aqueous solution were obtained from ¹H and ³¹P NMR spectra. The NMR spectra of the [Ln(DOTP^{hm})]⁺ and [Ln(DOTP^{Et})]⁺ com-

plexes show that these compounds have a clear preference for a specific arrangement of phosphorus atoms which gives rise to the symmetrical RRRR (or SSSS) isomer. However, many diastereoisomers were observed for all other complexes. Ln^{III}-induced ¹⁷O NMR shift data reveal that the spatial location of the second-sphere water molecules for the two groups of complexes differs. The parameters governing the effect of the second hydration sphere on the relaxivity of the Gd^{III} complexes of all ligands were evaluated by EPR, variable-temperature ¹⁷O NMR spectroscopy and ¹H NMRD relaxometry. The presence of second-sphere water molecules is clearly confirmed, depending on the character of the pendant arms. As the relaxivity does not depend significantly on the nature of the phosphorus substituents and/or on the isomerism present in solution, the second-sphere water molecules should be located close to the phosphorus-oxygen atoms.

(© Wiley-VCH Verlag GmbH & Co. KGaA, 69451 Weinheim, Germany, 2009)

Introduction

Magnetic resonance imaging (MRI) is one of the most widely used medical diagnostic techniques. Gadolinium(III)-based contrast agents (CAs) have significantly extended the applicability of this imaging method, and optimizing the efficacy of CAs has been an important goal for

more than a decade.^[1–5] The research undertaken has led to a much better understanding of the parameters governing the effectiveness of these CAs, which is usually expressed by the relaxivity (the enhancement of the water proton relaxation rate in a 1 mM solution of CA).^[1–6] The structure of the ligand can be tuned to optimize some of the parameters for optimal contrast efficiency, including the rotational correlation time (τ_R), the number of water molecules directly bound to the central metal ion (q) and their residence time in the first coordination sphere (τ_M). These parameters mainly influence the so-called inner-sphere contribution to the overall relaxivity. Other parameters, such as the electronic relaxation rates ($T_{1e,2e}$) of the Gd^{III} ion^[1,2,7,8] or the contribution of water molecule(s) in the second hydration sphere,^[9] are less well understood.

The second-sphere contribution to the relaxivity originates from water molecules held in the close proximity to the Gd^{III} ion by hydrogen bonds to the organic ligand of the complex.^[9] This contribution can enhance the overall relaxivity by 5–15% depending on the structure of the complex. Some years ago, it was demonstrated that complexes

[a] Department of Inorganic Chemistry, Univerzita Karlova (Charles University), Hlavova 2030, 12840 Prague, Czech Republic
Fax: +420-22195-1253
E-mail: lukes@natur.cuni.cz

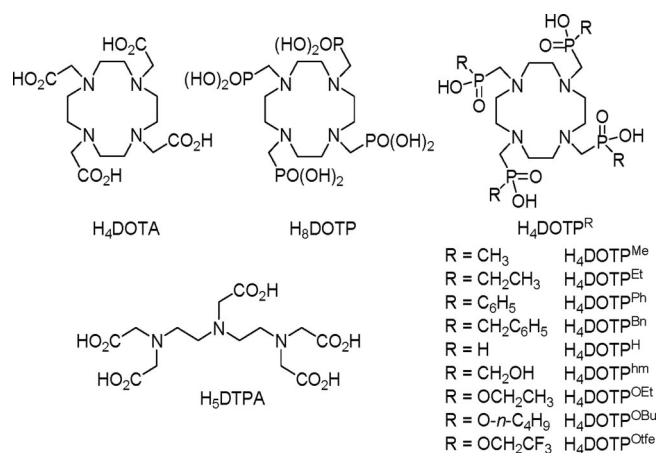
[b] Departamento de Bioquímica, Faculdade de Ciências e Tecnologia, e Centro de Neurociências, Universidade de Coimbra, 3049 Coimbra, Portugal

[c] Laboratory for Biocatalysis and Organic Chemistry, Department of Biotechnology, Delft University of Technology, Julianalaan 136, 2628 BL Delft, The Netherlands
Fax: +31-152-784-289
E-mail: j.a.peters@tudelft.nl

[d] NMR Laboratory, Department of Organic Chemistry, University of Mons-Hainaut, 7000 Mons, Belgium

Supporting information for this article is available on the WWW under <http://www.eurjic.org> or from the author.

of phosphorus-containing ligands exhibit a higher hydration (i.e. more extended second hydration sphere) than complexes of carboxylate ligands. This is particularly true for lanthanide(III) complexes of H_8DOTP [$H_8DOTP = 1,4,7,10$ -tetraazacyclododecane-1,4,7,10-tetrakis(methylphosphonic acid), Scheme 1], whose Gd^{III} complex does not contain any directly coordinated water molecule^[10] but has a relaxivity (r_1) comparable to that of the clinically used $[Gd(H_2O)(DOTA)]^-$ complex ($H_4DOTA = 1,4,7,10$ -tetraazacyclododecane-1,4,7,10-tetraacetic acid, Scheme 1), which has one water molecule in the first coordination sphere.^[11] The water relaxation enhancement by the DOTP complex results exclusively from the second-sphere contribution after conjugation to a macromolecule.^[12] A previous relaxometric study concerning Gd^{III} complexes of the related ethylphosphinate ligand (H_4DOTP^{Et}), and of the ethyl- and butylphosphonate monoesters (H_4DOTP^{OEt} and H_4DOTP^{OBu} , respectively), indicated only poor hydration (coordination number lower than one).^[13] The absence of directly coordinated water molecules and the presence of second-sphere water molecule(s) has been demonstrated for Gd^{III} complexes of phosphinic acid analogues of H_4DOTA having methyl (H_4DOTP^{Me}),^[14] phenyl (H_4DOTP^{Ph})^[15] or benzyl (H_4DOTP^{Bn})^[16] substituents on the phosphorus atom (Scheme 1).



Scheme 1. Formulas of ligands mentioned in the text.

The structures of complexes of these tetraphosphorus acid derivatives are analogous to those of complexes of the parent ligand H_4DOTA , where the lanthanide(III) ion is sandwiched between N_4 - and O_4 -planes. The H_4DOTA complexes are present in solution in two diastereoisomeric forms that differ in the mutual rotation of N_4 - and O_4 -planes to give a square-antiprismatic (SA) arrangement [torsion angle $>35^\circ$, with opposite signs of rotation of the pendant arms (Δ/Δ) and the conformation of the ethylene bridges in the macrocycle ring (δ/λ), represented as the Δ - $\lambda\lambda\lambda\lambda/\Delta$ - $\delta\delta\delta\delta$ isomeric pair, traditionally termed “M”] and a twisted-square-antiprismatic (TSA) arrangement (torsion angle $<30^\circ$, with the same sign of rotation leading to Δ - $\lambda\lambda\lambda\lambda/\Delta$ - $\delta\delta\delta\delta$ antipodes, traditionally termed “m”).^[17] Complexes of H_4DOTP^R ligands, on the other hand, occur exclusively in a TSA arrangement as their pendant arms con-

tain more bulky phosphorus atoms.^[10,15,16,18,19] The presence of just one phosphorus-based pendant arm causes an increased population of the TSA isomer.^[20–24] As stated above, the Gd^{III} complexes of all the tetraphosphorus ligands under study have no coordinated water molecules. In fact, direct coordination of a water molecule was observed, in the solid state, only for the La^{III} and Ce^{III} complexes.^[15,16b]

A rich, second-sphere hydration has also been observed in Gd^{III} complexes of pyridine-containing macrocycles containing phosphonic acid pendant arms.^[25] It has been shown recently that the second-sphere contribution to the overall relaxivity is significant even in complexes of H_5DTPA ($H_5DTPA = 1,4,7$ -triazasheptane-1,1,4,7,7-pentaacetic acid, Scheme 1)^[26] or H_4DOTA derivatives containing only one phosphonic/phosphinic acid group.^[20–22] This contribution was found to be more pronounced when complexes of these monophosphorus acid ligands were bound to macromolecules.^[27,28] Theoretical approaches to treat the second-sphere hydration have confirmed that phosphonic acid groups enhance the hydration of complexes of DOTA-like ligands^[29] as well as of open-chain ligands.^[30] In this paper, we evaluate the second-sphere contribution to the overall relaxivity in a series of Ln^{III} complexes of tetraphosphorus acid analogues of H_4DOTA with phosphinic (H_4DOTP^H), hydroxymethylphosphinic (H_4DOTP^{hm}), ethylphosphinic (H_4DOTP^{Et}) and phosphonate ethyl monoester (H_4DOTP^{OEt}) and butyl monoester (H_4DOTP^{OBu}) pendant arms (Scheme 1) by means of a combination of relaxometric and other spectroscopic methods. In addition, the influence of the substituent on the phosphorus atom to this contribution is investigated.

Results and Discussion

Syntheses

H_4DOTP^H was prepared by a Mannich reaction between cyclen, paraformaldehyde and hypophosphorous acid according to a slightly modified literature procedure;^[31] milder conditions were applied, for this reaction and during the workup, to reduce the amount of by-products, including derivatives with various numbers of pendant arms with hydroxymethyl and hydrogen substituents (e.g. intermediates in H_4DOTP^{hm} formation) and partially *N*-methylated derivatives of cyclen having a smaller number of phosphinate pendants. Despite the optimized reaction conditions, the amount of by-products was still high, and the yield of isolated product was only 20%. H_4DOTP^{hm} was obtained as a by-product during the synthesis of H_4DOTP^H , but could also be prepared more conveniently from pure H_4DOTP^H upon treatment with an excess of paraformaldehyde. In this way, less by-products were present in the final reaction mixture and the isolated yield of H_4DOTP^{hm} was 50%. H_4DOTP^{OEt} was prepared by treating cyclen with paraformaldehyde and triethyl phosphite (without solvent) at $40^\circ C$.^[32] The octaethyl ester Et_8DOTP obtained was hydrolyzed in aqueous NaOH to give the desired product in

an overall yield of 90%. H₄DOTP^{Et} and H₄DOTP^{OBu} were synthesized according to literature procedures.^[13,33] All ligands were purified, as mentioned in the Experimental Section, to a purity of at least 99%. The lanthanide(III) complexes were formed at a pH around 7 and at room temperature in 1 h (confirmed by ³¹P NMR spectroscopy), which demonstrates that the complexation rates are rapid.

Crystal Structures

Crystal Structure of H₄DOTP^{OEt}·H₂O

The structurally independent unit in the crystal structure of H₄DOTP^{OEt}·H₂O contains two ligand molecules, with similar conformations, and two solvate water molecules (see Figure 1 and Figure S1 in the Supporting Information). The free ligand H₄DOTP^{OEt} crystallizes as a zwitterion, with two (mutually “trans”) macrocycle nitrogen atoms protonated. The two remaining protons are bound to the pendant phosphonate groups attached to the unprotonated amino groups in opposite positions. The macrocyclic part adopts a conformation typical for doubly protonated substituted cyclens, with intramolecular hydrogen bonds between protonated and unprotonated amino groups and all substituents pointing in the same direction with respect to the macrocyclic plane.^[34] Both protonated pendant arms are turned above the macrocycle (and participate in hydrogen bonding with protonated amino groups), and the remaining two pendants are turned outwards from the macrocycle cavity. The quality of the crystal data was rather poor – some ethyl ester groups and the solvate water molecules were found to be disordered. A similar orientation of the pendant arms is also found in the structures of the parent H₈DOTP^[35] and H₄DOTA.^[36]

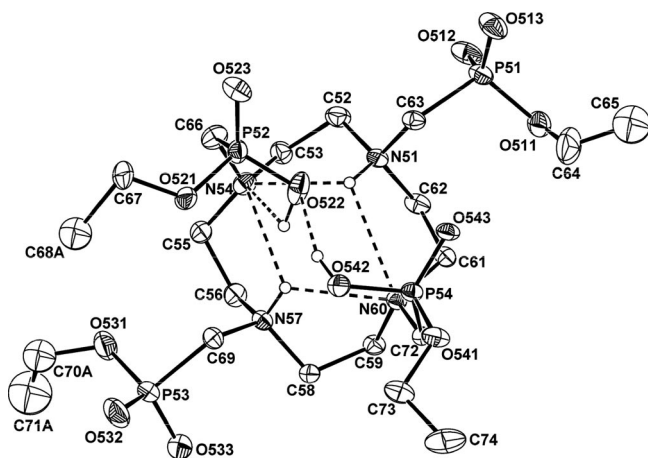


Figure 1. Molecular structure of one independent ligand molecule found in the crystal structure of H₄DOTP^{OEt}·H₂O, showing the intramolecular hydrogen bonds (dashed). Hydrogen atoms attached to carbon atoms have been omitted for clarity. Only one position of the disordered parts of molecule (phosphonate ester groups) is shown.

Crystal Structure of Li[Gd(DOTP^H)]·6H₂O

The central Gd^{III} ion in the crystal structure of Li[Gd(DOTP^H)]·6H₂O (Figure 2) is coordinated to four ni-

trogen atoms of the macrocycle and four oxygen atoms of the pendant arms to form two parallel N₄- and O₄-planes. As the complex possesses the symmetry of a crystallographic twofold axis, only half of the molecule forms the independent unit. The sign of rotation of the pendant arms (Λ/Δ) is the same as that of the conformation of the ethylene bridges in the macrocycle ring (δ/λ). This leads to a TSA (Λ - $\lambda\lambda\lambda\lambda/\Delta$ - $\delta\delta\delta\delta$) environment and confirms the results found by NMR spectroscopy (see below). The torsion angle between the N₄- and O₄-planes is about 30°, which is typical for a TSA coordination sphere [an SA isomer (Δ - $\lambda\lambda\lambda\lambda/\Lambda$ - $\delta\delta\delta\delta$) would typically have a torsion angle of more than 35°].^[23,24] The O22 oxygen atom of one pendant arm was best fitted as disordered in two positions with relative occupancies 60(A):40(B), with the phosphinate hydrogen atom placed in the theoretical position. This leads to two diastereoisomers (each of which is present in both enantiomeric forms as the space group is centrosymmetric), namely *SSSS*- Δ - $\delta\delta\delta\delta$ (+*RRRR*- Λ - $\lambda\lambda\lambda\lambda$) and *SRSR*- Δ - $\delta\delta\delta\delta$ (+*SRSR*- Λ - $\lambda\lambda\lambda\lambda$). The opening angles O–Gd–O are around 125°, which is too small for the coordination of a water molecule.^[37]

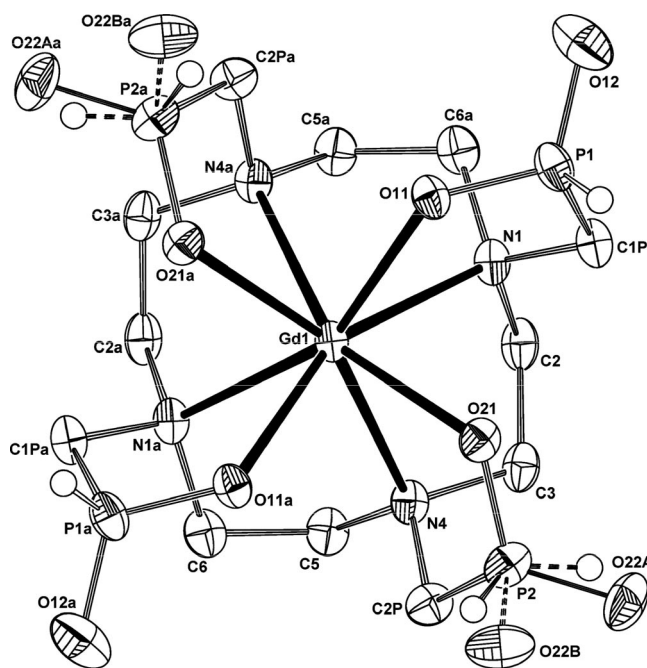


Figure 2. Molecular structure of the [Gd(DOTP^H)][−] species found in the crystal structure of Li[Gd(DOTP^H)]·6H₂O. Hydrogen atoms attached to carbon atoms have been omitted for clarity. Both positions of the disordered phosphinate pendant arm, with *SSSS*- Δ - $\delta\delta\delta\delta$ (60%, O22A) and *SRSR*- Δ - $\delta\delta\delta\delta$ (40%, O22B) configurations, are shown.

The molecules in this complex are packed in a polymeric chain due to coordination through the lithium counterion. This ion was also refined as being disordered over two positions as it is coordinated by the disordered oxygen atom O22. The coordination sphere of the lithium ion is completed by two water molecules, which are located far from the metal centre and the pseudo-*C*₄ axis (the closest Gd...Ow distance is 5.67 Å and the QN–QO–Ow angle is

Table 1. Selected geometrical parameters found in the crystal structures of $\text{Li}[\text{Gd}(\text{DOTP}^{\text{H}})] \cdot 6\text{H}_2\text{O}$ and $\text{Li}[\text{Gd}(\text{DOTP}^{\text{OEt}})] \cdot 0.5\text{Me}_2\text{CO} \cdot 8\text{H}_2\text{O}$.

| | $\text{Li}[\text{Gd}(\text{DOTP}^{\text{H}})] \cdot 6\text{H}_2\text{O}$ | $\text{Li}[\text{Gd}(\text{DOTP}^{\text{OEt}})] \cdot 0.5\text{Me}_2\text{CO} \cdot 8\text{H}_2\text{O}$ | |
|---|--|--|------------|
| | | Molecule 1 | Molecule 2 |
| Distances [Å] | | | |
| Gd1–N1 | 2.636(2) | 2.663(4) | 2.693(5) |
| Gd1–N4 | 2.635(2) | 2.667(4) | 2.670(5) |
| Gd1–N7 | – | 2.662(5) | 2.649(5) |
| Gd1–N10 | – | 2.665(4) | 2.670(5) |
| Gd1–O11 | 2.311(2) | 2.315(4) | 2.320(3) |
| Gd1–O21 | 2.319(2) | 2.332(4) | 2.308(3) |
| Gd1–O31 | – | 2.323(4) | 2.315(3) |
| Gd1–O41 | – | 2.307(4) | 2.307(4) |
| Gd1–QN ^[a] | 1.6053(2) | 1.6390(2) | 1.6520(2) |
| Gd1–QO ^[a] | 1.0503(2) | 1.0495(2) | 1.0491(2) |
| Angles [°] | | | |
| O11–Gd1–O31 | 124.6(1) ^[b] | 124.7(1) | 127.2(1) |
| O21–Gd1–O41 | 127.4(1) ^[b] | 127.6(1) | 124.9(1) |
| N1–QN–QO–O11 ^[a] | 29.21(8) | 26.7(2) | 27.7(2) |
| N4–QN–QO–O11 ^[a] | 30.50(8) | 27.4(2) | 26.1(2) |
| N7–QN–QO–O11 ^[a] | – | 27.0(2) | 28.2(2) |
| N10–QN–QO–O11 ^[a] | – | 28.6(2) | 26.3(2) |
| N ₄ -plane–O ₄ -plane | 0 | 1.09(2) | 0.86(3) |

[a] QN is the centroid (centre of gravity) of the N₄-plane and QO the centroid of the O₄-plane. [b] O31/O11[#] and O41/O21[#] are related by a twofold symmetry axis; [#]: $-x, y, -z + 1/2$.

around 98°, where QN is the centroid of the N₄-plane and QO the centroid of the O₄-plane). Selected geometrical parameters are listed in Table 1.

Crystal Structure of $\text{Li}[\text{Gd}(\text{DOTP}^{\text{OEt}})] \cdot 0.5\text{Me}_2\text{CO} \cdot 8\text{H}_2\text{O}$

The independent part of the crystal structure of $\text{Li}[\text{Gd}(\text{DOTP}^{\text{OEt}})] \cdot 0.5\text{Me}_2\text{CO} \cdot 8\text{H}_2\text{O}$ (Figure 3) consists of two complex molecules. Similarly to the previous case, the central Gd^{III} ions in both molecules are coordinated by four nitrogen atoms of the macrocycle and four oxygen atoms of the pendant arms to form two parallel N₄- and O₄-planes. The stereochemistry of the complex molecules is also TSA ($\Delta\text{-}\lambda\lambda\lambda\lambda/\Delta\text{-}\delta\delta\delta\delta$), with torsion angles between the N₄- and O₄-planes of about 28°. The absolute configuration of the

phosphonate monoesters is alternating, leading to *SRSR*- $\Delta\text{-}\delta\delta\delta\delta$ and *SRSR*- $\Delta\text{-}\lambda\lambda\lambda\lambda$ species, as was observed in the case of $\text{H}_4\text{DOTP}^{\text{Ph}}$ complexes.^[15] One of the lithium counterions is coordinated by O23X and by three water molecules in an approximately tetrahedral arrangement. The other lithium ion is tetrahedrally coordinated by four water molecules. Similarly to the previous structure, the water molecules are located away from the metal centre and the pseudo-C₄ axis of the complexes (the distances of the closest water molecules from metal centre are in the range 5.37–5.60 Å, with corresponding QN–QO–Ow angles of 97–102°). Selected geometrical parameters are listed in Table 1.

Potentiometry

Protonation Constants of the Ligands

The protonation constants of the free ligands are given in Table 2. These ligands adopt the general protonation scheme of DOTA-like compounds. The first two protonations occur on macrocyclic nitrogen atoms (with pK_a values of about 10–11 and 7–8, respectively). The overall basicity of the macrocyclic nitrogen atoms [$\text{pK}(\text{HL}) + \text{pK}(\text{H}_2\text{L}) = \log\beta(\text{H}_2\text{L})$] is rather low and corresponds well to the generally observed order phosphinates \approx phosphonate monoesters < carboxylates < phosphonates (Table 2).^[37] The proton dissociation constants of the H_2L^{2-} species of the ligands studied, as well as those of $\text{H}_4\text{DOTP}^{\text{Ph}}$ (ref.^[38]) and $\text{H}_4\text{DOTP}^{\text{OEt}}$ (ref.^[39]), depend on the electronic properties of the substituent on the phosphorus atoms, in agreement with previous observations on simple aminomethylphosphonic acids – more electronegative substituents result in lower pK_a values.^[40] The protonations in the acidic region

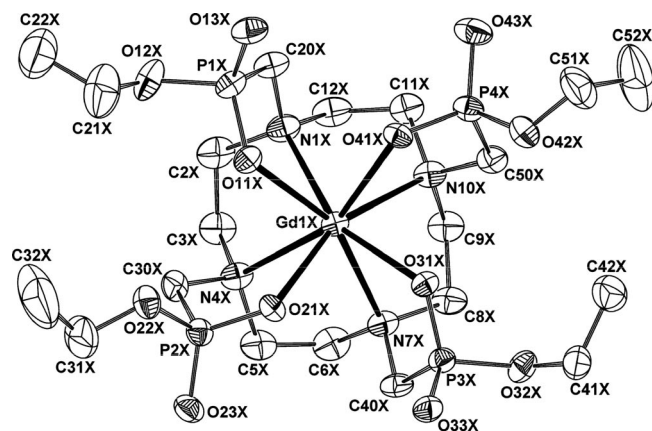


Figure 3. Molecular structure of one (the independent molecule labelled X) of the $[\text{Gd}(\text{DOTP}^{\text{OEt}})]$ species found in the crystal structure of $\text{Li}[\text{Gd}(\text{DOTP}^{\text{OEt}})] \cdot 0.5\text{Me}_2\text{CO} \cdot 8\text{H}_2\text{O}$. Hydrogen atoms have been omitted for the sake of clarity. The picture shows the species with *SRSR*- $\Delta\text{-}\delta\delta\delta\delta$ configuration.

Table 2. Protonation constants^[a] and corresponding pK_a values^[b] of the studied ligands.

| <i>h</i> | Species ^[c] | H ₄ DOTP ^{H[d]} | | H ₄ DOTP ^{hm[d]} | | H ₄ DOTP ^{Et[c]} | H ₄ DOTP ^{OEt[f]} | H ₄ DOTP ^{OBu[g]} | H ₈ DOTP ^[h] | H ₄ DOTA ^[i] |
|----------|------------------------|-------------------------------------|-----------------|--------------------------------------|-----------------|--------------------------------------|---------------------------------------|---------------------------------------|------------------------------------|------------------------------------|
| | | log β _h | pK _a | log β _h | pK _a | pK _a | pK _a | pK _a | pK _a | pK _a |
| 1 | HL | 10.58(2) | 10.58 | 10.60(2) | 10.60 | 10.94 | 11.57 | 10.34 | >13 | 11.9 |
| 2 | H ₂ L | 17.51(3) | 6.93 | 18.46(2) | 7.86 | 8.24 | 7.94 | 7.72 | 12.45 | 9.72 |
| 3 | H ₃ L | 19.41(3) | 1.90 | 20.21(3) | 1.75 | 3.71 | 1.80 | 2.42 | 9.18 | 4.60 |
| 4 | H ₄ L | — | — | 21.13(5) | 0.92 | — | — | — | 7.95 | 4.13 |
| 5 | H ₅ L | — | — | — | — | — | 2.3 [j] | — | 6.08 | 2.36 |
| 6 | H ₆ L | — | — | — | — | — | — | — | 5.20 | — |
| 7 | H ₇ L | — | — | — | — | — | — | — | 1.85 | — |

[a] β_h = [H_hL^(h-4)]/([H⁺]^h × [L⁴⁻]). [b] pK_a = β_h - β_{h-1}. [c] Charges have been omitted for clarity. [d] This work. [e] Ref.^[41] [f] Ref.^[32] [g] Ref.^[33] [h] Ref.^[42] [i] Ref.^[43] [j] Simultaneous deprotonations over two steps.

(pK_a < 2–3) can be assigned to those of the phosphinate/phosphonate monoester moieties and/or the remaining macrocyclic amino groups.

Stability of the Gadolinium(III) Complexes

The stability constants of complexes with phosphinate and phosphonate monoester ligands (Table 3) are much lower than those of the parent ligands H₈DOTP and H₄DOTA, which can be ascribed to the lower overall basicity of the ligands. Consequently, the complexes are formed at higher pH – the Gd^{III} ion, for example, is only fully complexed above a pH of about 5. The distribution diagram for Gd^{III}-containing species in the Gd^{III}-H₄DOTP^{OEt} system under equilibrium conditions is shown in Figure 4 as an example. The proton dissociation constants of the

[Gd(HDOTP^{R,OR})] species (formally the [hlm] = [111] species) are relatively high at around 4. This suggests that the proton in these species is probably bound to a nitrogen atom in the macrocycle under the equilibrium conditions, in other words the macrocycle is not fully coordinated, and the Gd^{III} ion is bound mainly by the oxygen atoms of the pendant arms. Proton removal from the protonated species leads to full coordination of the ligand in the normal N₄O₄ mode. The potentials do not change after prolonged standing of the samples – the same values were observed after six weeks as after three weeks, which confirms that thermodynamic equilibrium was reached in the solutions used. Although these Ln^{III} complexes have a relatively low thermodynamic stability, they have a high kinetic stability both in vitro and in vivo.^[32]

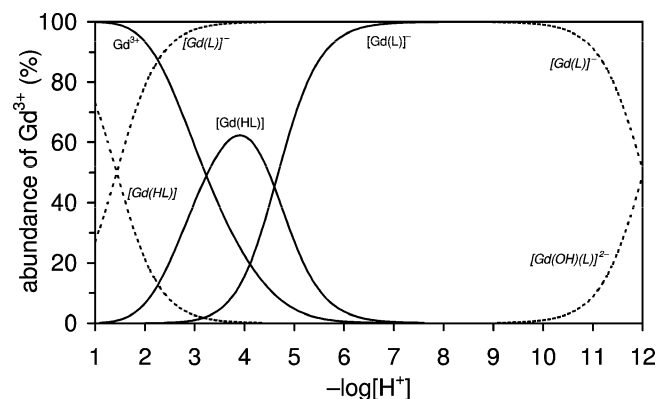


Figure 4. Distribution of Gd^{III}-containing species in the Gd^{III}/H₄DOTP^{OEt} (H₄DOTP^{OEt} = H₄L) system under equilibrium conditions [*c*(Gd^{III}) = *c*(H₄L) = 0.004 M; full lines]. Distribution of Gd^{III}-containing species during titration of the pre-formed [Gd(L)]⁻ complex (*c*{[Gd(L)]⁻} = 0.004 M; dashed lines, formulae in italics). The protonated [Gd(HL)] species probably bind the proton at a nitrogen atom under equilibrium conditions and an oxygen atom in the pre-formed complex.

Protonation of the Gadolinium(III) Complexes

The relaxivity of [Gd(DOTP^{hm})]⁻ appears to be dependent on the pH (see below), whereas the relaxivity of the other complexes is pH-independent. To gain more insight into the observed behaviour, we performed a potentiometric study of pre-formed Gd^{III} complexes of H₄DOTP^{hm} and, for comparison, of H₄DOTP^{OEt}. During these measurements, we explored the kinetically controlled pseudo-equilibrium associated with the complex protonation as the complexes are kinetically stable under these conditions. Solutions of the Gd^{III} complexes of H₄DOTP^{hm} and H₄DOTP^{OEt} were prepared in sealed ampoules (see Experimental Section) and used for the determination of their protonation/dissociation constants. The obtained constants are given in Table 4, and the corresponding distribution diagram is shown in Figure 4. The [Gd(HDOTP^{R,OR})] complexes behave as monovalent strong acids with a pK_a of about 1.4. Such dissociation constants correspond well with those of the pendant arms in the free ligands, although the pK_a values are somewhat lower in the complexes due to the

Table 3. Stability constants^[a] of gadolinium(III) complexes of the studied ligands.

| <i>h</i> | <i>l</i> | <i>m</i> | H ₄ DOTP ^{H[b]} | H ₄ DOTP ^{hm[b]} | H ₄ DOTP ^{Et[c]} | H ₄ DOTP ^{OEt[b]} | H ₄ DOTP ^{OBu[d]} | H ₈ DOTP ^[e] | H ₄ DOTA ^[f] |
|----------|----------|----------|-------------------------------------|--------------------------------------|--------------------------------------|---------------------------------------|---------------------------------------|------------------------------------|------------------------------------|
| | | | log β _{hlm} | log β _{hlm} | log β _{hlm} | log β _{hlm} | log β _{hlm} | log β _{hlm} | log β _{hlm} |
| 0 | 1 | 1 | 14.0(1) | 16.09(4) | 16.50 | 14.4(2) | 12.19 | 28.8 | 24.67 |
| 1 | 1 | 1 | 18.11(5) ^[g] | 19.25(5) ^[g] | — | 19.0(1) ^[g] | — | 36.4 ^[g] | — |
| | | | 4.1 | 3.2 | — | 4.6 | — | 7.6 | — |

[a] β_{hlm} = [H_hL_lM_m^{(h-4)l+3m}]/([H⁺]^h × [L⁴⁻]^l × [M³⁺]^m). [b] This work. [c] Ref.^[41] [d] Ref.^[33] [e] Ref.^[44]; the other pK_a values are: 6.3, 5.4 and 4.0. [f] Ref.^[45] [g] The corresponding pK_a values are given in italics.

coordination of the pendant arms. Thus, the low pK_a value points to the kinetic inertness of the complex species, at least on the time scale of the potentiometric measurements, and that the complexes are protonated at an oxygen atom of the pendant arms. As no other protonations occur in the pH range 3–10, the relaxivity change observed for the $[Gd(DOTPh^{hm})]^-$ complex in this region (see below) cannot be associated with the presence of any protonation/deprotonation event (e.g. dissociation of a proton from the PCH_2OH groups); therefore, the relaxivity change must be associated with the H^+/OH^- catalysis of the prototropic exchange.^[36,46]

Table 4. Equilibrium constants (pK_a) of the pre-formed Gd^{III} complexes with H_4DOTPh^{hm} and H_4DOTPh^{OEt} .

| Equilibrium | $[Gd(DOTPh^{hm})]^-$ | $[Gd(DOTPh^{OEt})]^-$ |
|--|----------------------|-----------------------|
| $[HML] \rightleftharpoons H^+ + [ML]^-$ | 1.39(3) | 1.43(3) |
| $[ML]^- \rightleftharpoons H^+ + [H_1ML]^{2-}$ | 11.29(1) | 12.01(2) |

Interestingly, the fits of the potentiometric data improved dramatically after inclusion of deprotonated species (pK_a of around 12) in the chemical model. Since deprotonated species were observed for the complexes of both H_4DOTPh^{hm} and H_4DOTPh^{OEt} , this improvement cannot be explained by dissociation of a hydroxymethyl moiety of the former complex. As no water is coordinated in the inner sphere of the complexes (see below), the deprotonation can only be explained by coordination of a hydroxide anion after decoordination of one of the pendant arms. Such behaviour points to a relatively weak coordination of the phosphinic acid or phosphonic monoester functions, probably due to the low nucleophilicity of their oxygen atoms^[37] and the high affinity of lanthanide(III) ions for the hydroxide anion.

From the distribution diagram (Figure 4) and published data on other lanthanide(III) complexes,^[32] it is clear that the pre-formed $[Gd(DOTPh^{R,OR})]^-$ complexes are kinetically relatively inert on the potentiometry time scale (ca. 20 min). Above a pH of about 4, the concentration of the $[Gd(HDOTPh^{R,OR})]$ species is negligible. Since the most likely mechanism of dissociation of the complex involves protonation of the pendant arm followed by proton transfer to the nitrogen atoms and subsequent dissociation of the complex, it may be concluded that the complexes are stable under the experimental conditions applied for the investigation of the pH dependence of the 1H NMRD profiles (see below).

Luminescence and UV/Vis Measurements of Eu^{III} Complexes

To confirm the absence of a directly coordinated water molecule in the Gd^{III} complexes studied, we measured luminescence lifetimes of the excited states of selected Eu^{III} complexes in H_2O and D_2O (see Table S1 in the Supporting Information).

The luminescence lifetimes obtained for the $[Eu(DOTPh^{OEt})]^-$ and $[Eu(H_{1.5}DOTPh)]^{3.5-}$ ($pH \approx 7$) complexes in H_2O solution are relatively long compared to those for

complexes with one coordinated water molecule {e.g. $[Eu(H_2O)(DOTA)]^-$, where the lifetimes observed in H_2O are about 650 μs }, but still significantly shorter than the lifetimes measured in D_2O solution. For $[Eu(DOTPh^H)]^-$ and $[Eu(DOTPh^{hm})]^-$ complexes, the lifetimes observed in H_2O are even closer to the values of $[Eu(H_2O)(DOTA)]^-$ itself. However, using the relevant equations published in the literature,^[47,48] the hydration number, q , was estimated to be 0.3–0.7 (Table S1 in the Supporting Information). This fact is usually attributed to a partial hydration of the complexes (i.e. equilibrium between complex species with $q = 0$ and 1, respectively). Alternatively, a high second-sphere hydration also gives such an effect.^[48] As the published equations used to calculate q were derived mostly for amide derivatives, which have a lower second-sphere hydration, the correction for second-sphere contribution can be underestimated. In our case, the richer hydration sphere of the phosphorus acid complexes contributes more to the decay rates. All in all, however, the luminescence data do not allow an unambiguous conclusion regarding the value of q for the Eu^{III} complexes of the tetraphosphorus acid derivatives; therefore, we recorded absorption spectra for the $^5D_0 \leftarrow ^7F_0$ transition. Only a single symmetrical absorption peak was observed in the spectra (Figure S2 in the Supporting Information). Since the $^5D_0 \leftarrow ^7F_0$ transition is extremely sensitive to the local coordination environment of the central Eu^{III} ion, a change in hydration [i.e. change in coordination number (CN) between 8 and 9] would have resulted in a substantial difference in the corresponding two spectral bands with a separation of the peaks typically larger than 0.5 nm.^[30,49] We can therefore conclude that only non-hydrated complex species (i.e. having CN = 8) are present in the solutions; the luminescence lifetimes given above (i.e. slight shortening of τ_{H_2O} in comparison with τ_{D_2O}) should be significantly shorter for any hydrated complex. The non-zero hydration numbers ($q = 0.4$ – 0.6) calculated from the luminescence lifetimes are therefore due to the effect of the second-sphere water molecules and/or of neighbouring OH oscillators in the case of the $[Eu(DOTPh^{hm})]^-$ complex.^[48]

NMR Studies of the Complexes

^{31}P and 1H NMR Spectra

1H and ^{31}P NMR spectra of the complexes with Nd^{III} , Eu^{III} and Yb^{III} were recorded in order to obtain information about the solution structure of the complexes. It is well known that all lanthanide(III) complexes of tetraphosphonate/phosphinate analogues of H_4DOTA selectively adopt TSA-type (Λ - $\lambda\lambda\lambda\lambda/\Delta$ - $\delta\delta\delta\delta$) structures.^[10,15,16,18,19] However, since the presently studied ligands have a substituent on the phosphorus atoms, four additional chirality centres are created upon coordination of the prochiral phosphorus atoms, which leads to R/S isomerism centred on the phosphorus atoms. Six diastereoisomers ($RRRR$, $RRRS$, $RRSS$, $RSRS$, $SSSR$ and $SSSS$) with a relative statistical abundance of 1:4:4:2:4:1 are therefore possible for the TSA arrangement. This, in principle, gives rise to a

quite complicated isomeric mixture. The isomerism of the lanthanide(III) complexes with analogous ligands such as DOTP^{OEt} (ref.^[39]) and DOTP^{Ph} (ref.^[15]) has been discussed in detail previously.

The ³¹P NMR spectra of the [Eu(DOTP^H)][−], [Eu(DOTP^{OEt})][−] and [Eu(DOTP^{OBu})][−] complexes show the full set of possible isomers (sixteen ³¹P NMR signals for the six isomers) with no predominant isomer, as observed previously for other complexes.^[15,39] The ³¹P NMR spectra of the Yb^{III} and Nd^{III} complexes of H₄DOTP^H, H₄DOTP^{OEt}, and DOTP^{OBu} show a similar pattern (Figures S3, S6 and S7 in the Supporting Information). The ³¹P NMR spectra of the [Eu(DOTP^{hm})][−] and [Eu(DOTP^{Et})][−] complexes, on the other hand, are quite simple, with one major signal (integral intensity ca. 70%) and four minor ones (integral ratio 1:1:1:1, total integral intensity ca. 25%) being present in the spectra of the [Eu(DOTP^{hm})][−] complex (Figure S4 in the Supporting Information). The major resonance can be assigned to the totally symmetric *RRRR* (or *SSSS*) and the four minor resonances to the *RRRS* (or *SSSR*) isomers, respectively. Signals for other possible diastereomers are negligible (total integral intensity <5%). The Yb^{III} and Nd^{III} complexes of H₄DOTP^{hm} and H₄DOTP^{Et} also have ³¹P NMR spectra very similar to those of the corresponding Eu^{III} complexes (Figures S4 and S5 in the Supporting Information). This points to a strong preference for a single arrangement around all the phosphorus atoms in complexes of these two phosphinate ligands, in other words the formation of only one of the possible diastereomeric pairs – *RRRR*- Λ - $\lambda\lambda\lambda\lambda$ (+*SSSS*- Δ - $\delta\delta\delta\delta$) or *SSSS*- Λ - $\lambda\lambda\lambda\lambda$ (+*RRRR*- Δ - $\delta\delta\delta\delta$). A similar preference for these isomers was observed previously for complexes of H₄DOTP^{Bn} (ref.^[16a]) as well as for complexes of tris(phosphinate) monoacetamide cyclen derivatives.^[50] Unfortunately, it was not possible to unambiguously determine the absolute configuration of these complexes. The chemical exchange between the major (*RRRR*/*SSSS*) and minor isomers (*RRRS*/*SSSR*) could be demonstrated by the presence of exchange cross-peaks in the two-dimensional exchange (EXSY) NMR spectrum of the [Yb(DOTP^H)][−] derivative (Figure S8 in the Supporting Information). In addition, the dynamic behaviour of the isomer mixture (by variable-temperature ³¹P NMR spectra) was also observed in the cases of other ligands (Figure S9 in the Supporting Information).

The ¹H NMR spectra of the Eu^{III} complexes of all ligands (see example in Figure S10 in the Supporting Information) have resonances for the axial protons at δ = 22–32 ppm, which confirms the exclusive presence of the TSA isomer as no signal was observed at the characteristic chemical shifts for axial protons of the SA isomer (above δ = 35 ppm)^[17,20,21a,22] The [Eu(DOTP^{OEt})][−], [Eu(DOTP^H)][−] and [Eu(DOTP^{OBu})][−] complexes have very complex ¹H NMR spectra, thus indicating the presence of many diastereoisomers (a set of resonances was observed for each proton). In contrast, the ¹H NMR spectrum of the [Eu(DOTP^{hm})][−] complex contains a set of eight dominant peaks, which corresponds to the non-equivalent protons of a dominant isomeric species with C₄ symmetry (*RRRR* or

SSSS), and very weak signals (four for each of the eight types of protons), which correspond to a very minor asymmetric isomer (*RRRS* or *SSSR*, Figure S10, ¹H NMR). A similar situation occurs for the [Eu(DOTP^{Et})][−] complex.

In summary, the ³¹P and ¹H NMR spectra show the presence of complex diastereomeric mixtures for [Ln(DOTP^{OEt})][−], [Ln(DOTP^H)][−] and [Ln(DOTP^{OBu})][−] complexes, whereas the [Ln(DOTP^{hm})][−] and [Ln(DOTP^{Et})][−] complexes have a preference for a single configuration.

The solution structures of the H₄DOTP^{OEt}, H₄DOTP^H and DOTP^{OBu} complexes can be explained in a similar manner to the complexes of the trifluoroethyl phosphonate monoester derivative.^[39] There, the ¹⁹F NMR spectra show the presence of all six possible isomers, with the abundances of the *RRRR*/*SSSS* pair slightly higher than, and that of the *RSRS* isomers slightly lower than, the statistical values by a factor of 1.4–1.5. These deviations were interpreted by using a neighbouring interaction model whereby the population differences between the various isomers depend only on the energy difference of the interactions of the substituent groups on neighbouring phosphorus atoms in the *RR* (or *SS*) (*E_{RR}* \approx *E_{SS}*) and *RS* (or *SR*) (*E_{RS}* \approx *E_{SR}*) orientations; *E_{RS}* is smaller than *E_{RR}* in these compounds by 0.47 kJ mol^{−1}. This small difference should result from a higher steric hindrance between the ester groups and electronic repulsions between the partially charged oxygen atoms in the *RS* orientation. Such a small energy difference could also be present in the complexes of the phosphonate monoester derivatives. The absence of the ester groups should decrease the energy difference between those two interactions, with isomer abundances closer to the statistical distribution.

The preference for a single configuration observed for H₄DOTP^{hm} could be rationalized by hydrogen-bonding interactions between the hydroxy moieties on one phosphorus acid side-chain and the oxygen atoms of the neighbour phosphinate groups. However, such hydrogen bonds are not possible for [Ln(DOTP^{Et})][−] complexes, which also show a strong preference for a single configuration. We can speculate that this isomerism may be a consequence of the electronic properties rather than the steric demands of the substituents on the phosphorus atoms. Thus, ligands in complexes of H₄DOTP^{OEt}, H₄DOTP^H and H₄DOTP^{OBu} (and also H₄DOTP^{Ph} and H₄DOTP^{OEt}),^[23,39] which form a mixture of isomers, contain electron-withdrawing substituents and those of H₄DOTP^{Et} and H₄DOTP^{hm} (and also H₄DOTP^{Bn}),^[16a] which show a preferential isomerism, have electron-donating alkyl substituents on the phosphorus atoms. The electronic properties could alter the electron distribution inside the PO₂[−] moiety and therefore the different preferences for the isomers.

¹⁷O and ³¹P Lanthanide-Induced Shifts

The ¹⁷O lanthanide-induced shifts (LISs) were measured for selected complexes, namely the [Ln(DOTP^{hm})][−] complexes as representatives of the group of compounds with a dominant diastereoisomer (*RRRR*/*SSSS*) and the

$[\text{Ln}(\text{DOTP}^{\text{OEt}})]^-$ and $[\text{Ln}(\text{DOTP}^{\text{H}})]^-$ complexes as representatives of the other group which shows no preference for either of the possible isomeric forms.

The LIS (Δ , the lanthanide-induced shift for a concentration of 1 M of Ln^{III} ion)^[51] consists of diamagnetic (Δ_{d}), contact (Δ_{c}) and pseudocontact (Δ_{p}) contributions [Equation (1)].

$$\Delta = \Delta_{\text{d}} + \Delta_{\text{c}} + \Delta_{\text{p}} \quad (1)$$

The paramagnetic contribution to the LIS, Δ' , obtained after subtraction of the diamagnetic term, Δ_{d} , can be expressed as Equation (2), which contains terms that are characteristic of each lanthanide(III) ion but independent of the ligand ($\langle S_z \rangle$ and C^{D} for Δ_{c} and Δ_{p} , respectively) and characteristic of the nucleus under study but independent of the lanthanide(III) cation (F and G for Δ_{c} and Δ_{p} , respectively).

$$\Delta' = q(\langle S_z \rangle \times F + C^{\text{D}} \times G) \quad (2)$$

Equation (2) can be linearized to obtain either qF in the contact contribution from the slope of the plot obtained from Equation (3) or the geometric term qG in the pseudocontact contribution from the slope of the plot corresponding to Equation (4).

$$\Delta'/C^{\text{D}} = (\langle S_z \rangle / C^{\text{D}}) \times qF + qG \quad (3)$$

$$\Delta' / \langle S_z \rangle = qF + (C^{\text{D}} / \langle S_z \rangle) \times G \quad (4)$$

Equation (3) is best used to study nuclei with a dominant contact contribution, such as the ^{17}O nucleus of the water oxygen atom directly bound to the central lanthanide(III) ion in the complexes with inner-sphere water, whereas Equation (4) is preferably used to study nuclei where the pseudocontact contribution dominates, usually those nuclei lacking any direct bonding to the central lanthanide(III) ion, which in the present case is the phosphorus atoms. When the series of lanthanide(III) complexes with a particular ligand are isostructural, the plots obtained from Equations (3) and (4) are straight lines.

Analysis of the ^{17}O LIS data for the Ln^{III} complexes of $\text{H}_4\text{DOTP}^{\text{H}}$, $\text{H}_4\text{DOTP}^{\text{hm}}$ and $\text{H}_4\text{DOTP}^{\text{OEt}}$ according to Equations (3) and (4) is shown in Figure 5. Data for the complexes of H_8DOTP are also given for comparison. The data for the complexes of $\text{H}_4\text{DOTP}^{\text{hm}}$ show a linear trend across the lanthanide series, which indicates that these complexes are isostructural. The slope (qF) of the plot according to Equation (3) is -30 , and since the value of F is around -90 under the conditions applied,^[51] this gives q value of around 0.3 . A comparable value was obtained by luminescence lifetime measurements on Eu^{III} complexes. However, combining these results with the UV/Vis study, which clearly showed the presence of a single coordination structure, suggests that q is actually 0 . The relatively small negative slope is probably due to the presence of water in the second coordination sphere.

The plots for the lanthanide complexes of the other ligands deviate from linearity towards more negative values for one or more of the lighter lanthanides (Ce^{III} for $\text{H}_4\text{DOTP}^{\text{H}}$ and $\text{H}_4\text{DOTP}^{\text{OEt}}$; Ce^{III} , Pr^{III} , and Nd^{III} for H_8DOTP).^[51] The line through the data according to Equation (3) for Ce^{III} , Pr^{III} and Nd^{III} complexes of H_8DOTP has a slope (qF) of -80 , which indicates that these light lanthanides form complexes of H_8DOTP with one water molecule in the first coordination sphere of the lanthanide(III) ions. The large negative values of Δ'/C^{D} for the Ce^{III} complexes of $\text{H}_4\text{DOTP}^{\text{H}}$ and $\text{H}_4\text{DOTP}^{\text{OEt}}$ suggest that these complexes contain the water molecule in the first coordination sphere as well. The plots obtained from Equation (4) (Figure 5), where the points corresponding to the Ce^{III} complexes of $\text{H}_4\text{DOTP}^{\text{H}}$ and $\text{H}_4\text{DOTP}^{\text{OEt}}$ and those for the Ce^{III} , Pr^{III} and Nd^{III} complexes of H_8DOTP lie significantly far from the linear fits, support this conclusion.

The negative sign of the slope of the plots obtained from Equation (4) for the lanthanide(III) complexes of $\text{H}_4\text{DOTP}^{\text{hm}}$ is rather surprising when compared with those observed for the other ligands (Figure 5). As such slopes are proportional to the geometric term G of the ^{17}O nuclei of the water molecules, a change in the sign of the slope could be a consequence of a different spatial orientation of the second-sphere hydration shell around the lanthanide(III) complexes of $\text{H}_4\text{DOTP}^{\text{hm}}$ in comparison with the complexes of the other ligands. As all the ligands are symmetrical, the main magnetic axis of their lanthanide(III) complexes should have the same direction as their pseudo- C_4 axis. Thus, the sign of the ^{17}O G value is given by the spatial location of the second-sphere water molecules relative to the dipolar cone defined by the “magic” angle $\theta = 54.7^\circ$ which cancels out the geometric term $G = (3 \times \cos^2\theta - 1)/r^3$, where θ is the angle between the main magnetic axis of the complex and the line connecting the ion with the ^{17}O nucleus at distance r . When these water molecules pass from the inside to the outside part of the cone, the sign of G and of the corresponding pseudocontact shift is reversed. The value of G is positive inside the cone, whereas it is negative outside. The second-sphere water molecules are therefore located outside of the dipolar cone in the $\text{H}_4\text{DOTP}^{\text{hm}}$ complexes, whereas for $\text{H}_4\text{DOTP}^{\text{H}}$, $\text{H}_4\text{DOTP}^{\text{OEt}}$ and H_8DOTP they are inside this cone (Figure S11 in the Supporting Information).

These findings suggest that all alkyl groups in the complexes of $\text{H}_4\text{DOTP}^{\text{hm}}$ and $\text{H}_4\text{DOTP}^{\text{Et}}$ are oriented above the O_4 -plane, thus avoiding an approach of the water molecule inside the cone. This is supported by the crystal structures of several lanthanide(III) complexes with $\text{H}_4\text{DOTP}^{\text{Bn}}$, in which all benzylic groups are directed above the O_4 -plane to form a hydrophobic cavity. This arrangement leads exclusively to $RRRR$ - Λ - $\lambda\lambda\lambda\lambda$ + $SSSS$ - Δ - $\delta\delta\delta\delta$ enantiomeric pairs in the solid state, and these complexes are also present in the solution as the single isomer.^[16] It is also supported by the high stability of the symmetric arrangement, as evidenced by the relatively high interconversion energy between isomers of $[\text{Yb}(\text{DOTP}^{\text{hm}})]^-$ compared to more labile

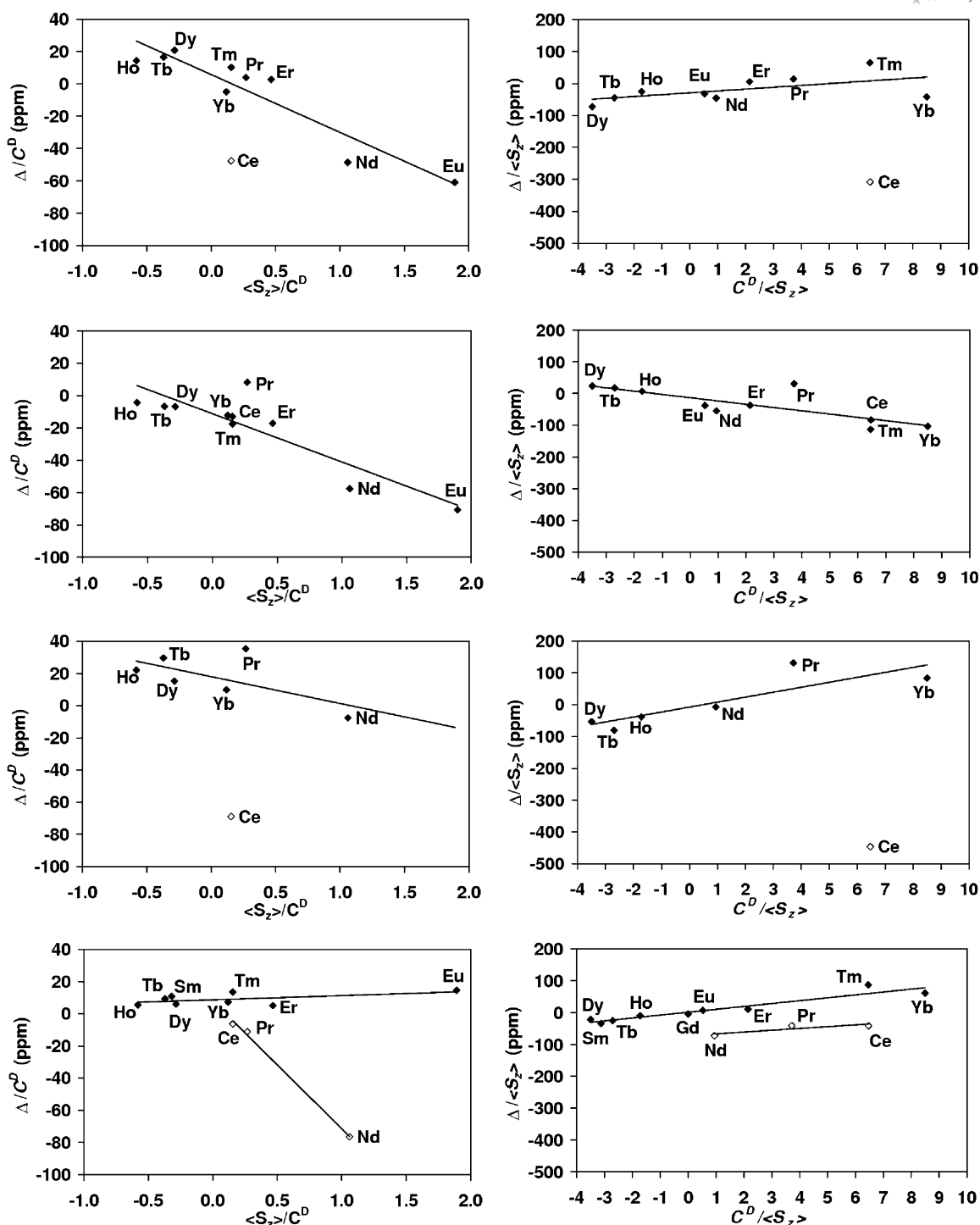


Figure 5. Linearization of the ^{17}O LIS data for the lanthanide(III) complexes of $\text{H}_4\text{DOTP}^{\text{H}}$ (top), $\text{H}_4\text{DOTP}^{\text{hm}}$ (center top), $\text{H}_4\text{DOTP}^{\text{OEt}}$ (center bottom) and H_8DOTP (bottom) according to Equations (3) (slope = contact shift, left) and (4) (slope = pseudocontact shift, right); $T = 301\text{ K}$, $\text{pH } 7$.

$[\text{Yb}(\text{DOTP}^{\text{OEt}})]^-$ (see the variable-temperature ^{31}P NMR spectra in Figure S9 of the Supporting Information).

Similar equations can be derived for the ^{31}P NMR LIS values [q in Equations (3) and (4) should be replaced by 1]. In the case of $[\text{Ln}(\text{DOTP}^{\text{hm}})]^-$ and $[\text{Ln}(\text{DOTP}^{\text{Et}})]^-$ complexes, the ^{31}P LIS values for $[\text{Ln}(\text{DOTP}^{\text{hm}})]^-$ and

$[\text{Ln}(\text{DOTP}^{\text{Et}})]^-$ were determined for the major *RRRR* (SSSS) isomer as its signal can easily be assigned in the spectra (Figure 6). The plots obtained from Equations (3) and (4) clearly show a break between the first and second half of the Ln series, thus indicating a non-isostructurality of these complexes across the lanthanide series. The com-

plex isomeric mixtures present for the $[\text{Ln}(\text{DOTP}^{\text{H}})]^-$, $[\text{Ln}(\text{DOTP}^{\text{OEt}})]^-$ and $[\text{Ln}(\text{DOTP}^{\text{OBu}})]^-$ complexes do not allow a reliable assignment of the resonances, therefore the weighted average of the chemical shifts for all isomers (i.e. the chemical shift corresponding to half of the total intensity of all signals in the ^{31}P NMR spectra) was used. The corresponding plots are very similar to the previous case

{the data for $[\text{Ln}(\text{DOTP}^{\text{H}})]^-$ are included in Figure 6}. Analogous ^{31}P LIS phenomena have also been observed previously for Ln^{III} complexes of $\text{H}_4\text{DOTP}^{\text{Ph}}$ and $\text{H}_4\text{DOTP}^{\text{Bn}}$ [15,16]

The positions of the breaks observed in the plots of the ^{31}P NMR spectroscopic data do not fully correspond with those observed in the ^{17}O NMR spectroscopic data, poss-

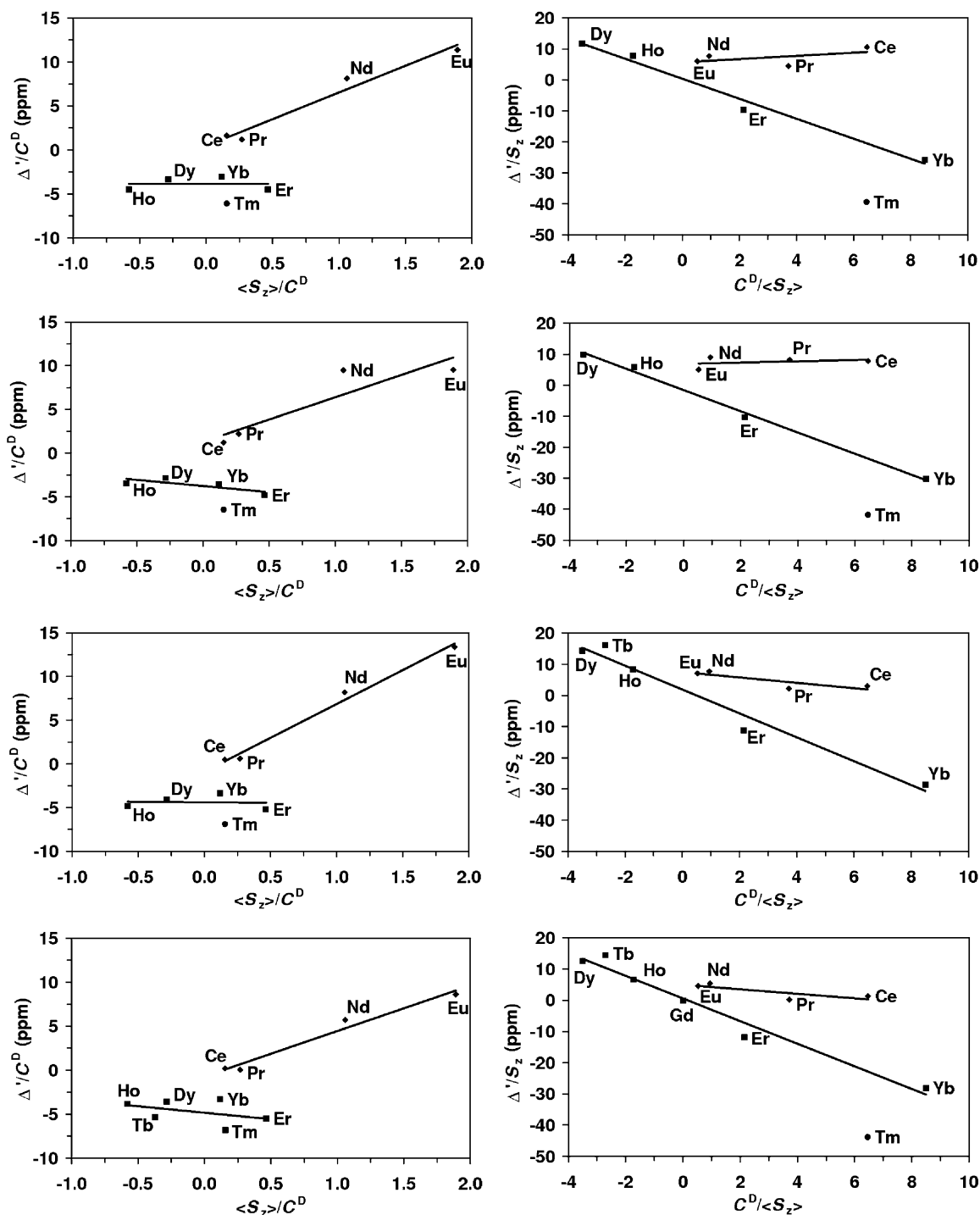


Figure 6. Separation of the contact [Equation (3), left] and pseudocontact [Equation (4), right] contributions to the ^{31}P LIS for the weighted chemical shift for the $[\text{Ln}(\text{DOTP}^{\text{H}})]^-$ complexes (top), the *RRRR* (*SSSS*) isomers of the $[\text{Ln}(\text{DOTP}^{\text{Bm}})]^-$ (center top) and $[\text{Ln}(\text{DOTP}^{\text{Et}})]^-$ (center bottom) complexes, and $[\text{Ln}(\text{H}_{1.5}\text{DOTP})]^{3.5-}$ (bottom); $T = 301\text{ K}$, $\text{pH } 7$.

ibly due to a change in the water coordination of the lanthanide ions. Since the breaks in Figure 6 indicate a change of both F and G for the ^{31}P nuclei of these complexes across the lanthanide series, it is highly likely that some geometric change in the TSA coordination sphere is occurring. The ions along the lanthanide(III) series gradually move inside the ligand cavity (closer to the N_4 -plane) in the TSA isomers – the Ln-QN distance (QN is the centre of gravity of the N_4 -plane) drops steeply from around 1.85 Å for La^{III} to around 1.65 Å for Eu^{III} , and remains in the range 1.65–1.55 Å for the rest of the series.^[23,37] This leads to a change

of geometry of the donor atom environment between large ($\text{La}^{\text{III}}\text{--Eu}^{\text{III}}$) and small ($\text{Eu}^{\text{III}}\text{--Lu}^{\text{III}}$) ions, which is apparently reflected in changes of both F and G for the ^{31}P nuclei.

Relaxometric and EPR Measurements

Variable-temperature ^{17}O NMR spectroscopic data [T_1 and T_2 relaxation times and ^{17}O angular frequencies (ω_{O})] were collected for the Gd^{III} complexes of $\text{H}_4\text{DOTP}^{\text{hm}}$, $\text{H}_4\text{DOTP}^{\text{H}}$ and $\text{H}_4\text{DOTP}^{\text{OEt}}$. For comparative purposes,

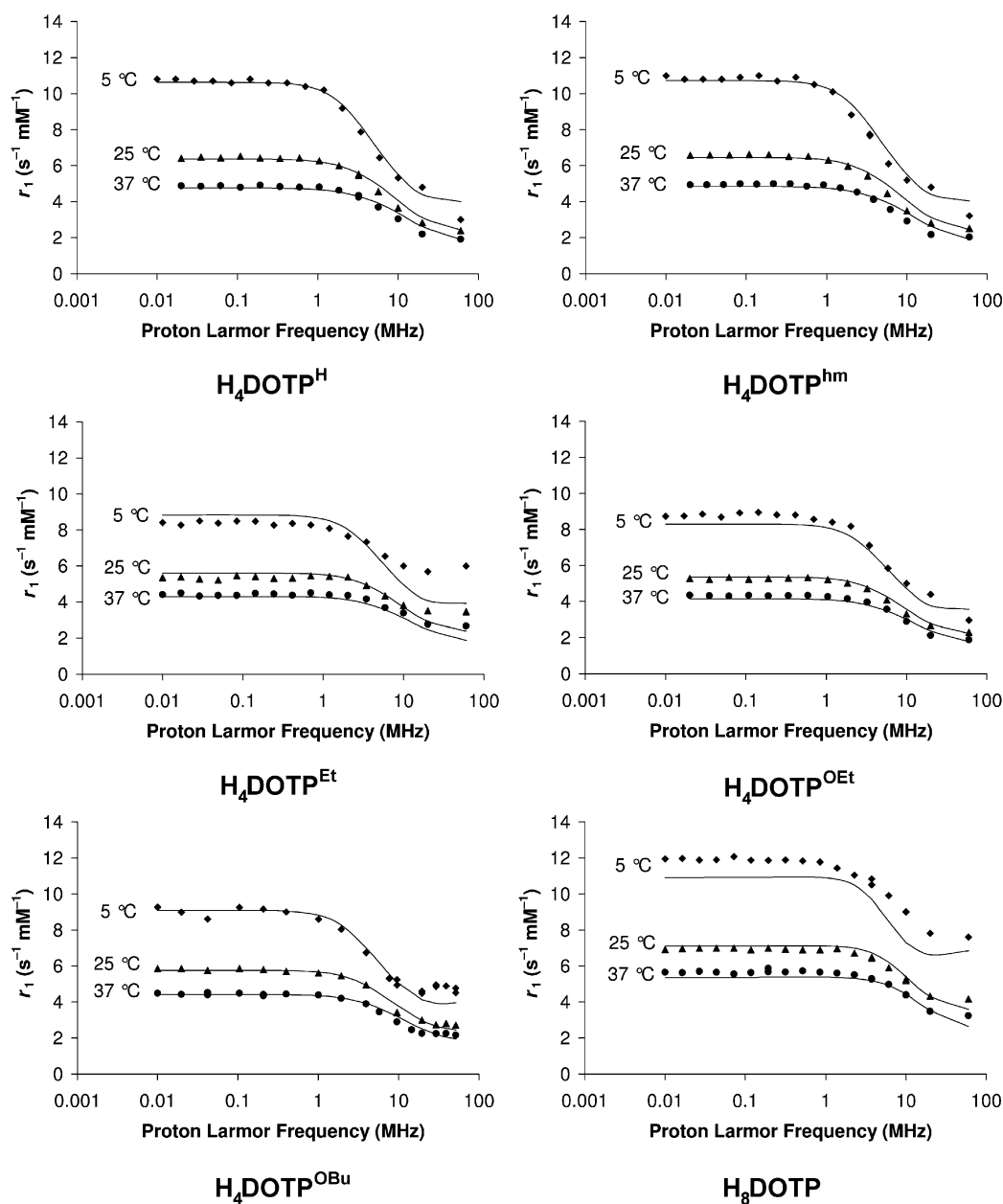


Figure 7. The ^1H NMRD profiles for the Gd^{III} complexes of $\text{H}_4\text{DOTP}^{\text{H}}$, $\text{H}_4\text{DOTP}^{\text{hm}}$, $\text{H}_4\text{DOTP}^{\text{Et}}$, $\text{H}_4\text{DOTP}^{\text{OEt}}$, $\text{H}_4\text{DOTP}^{\text{OBu}}$ and H_8DOTP . Profiles were measured at pH 7 (except for H_8DOTP) and 10 (H_8DOTP). The full lines represent the results of the best simultaneous fits of ^1H NMRD and EPR data.

the data for the $[\text{Gd}(\text{DOTP})]^{5-}$ complex were also measured at a pH of around 10 (where all pendant arms are fully deprotonated) and a pH of about 7 {where approximately 1.5 protons are bound to the ligand, i.e. $[\text{Gd}(\text{H}_{1.5-}\text{DOTP})]^{3.5-44}$ }. In this case, no significant influence of the pH on the data obtained was observed. The ^{17}O NMR spectroscopic data are shown in Figure S12 (see the Supporting Information). Since $q = 0$ for these systems, the paramagnetic effects on the ^{17}O NMR parameters are so small that a fitting to theoretical models is not feasible.

The ^1H NMRD profiles of the Gd^{III} complexes of $\text{H}_4\text{DOTP}^{\text{H}}$, $\text{H}_4\text{DOTP}^{\text{hm}}$, $\text{H}_4\text{DOTP}^{\text{Et}}$, $\text{H}_4\text{DOTP}^{\text{OEt}}$, $\text{H}_4\text{DOTP}^{\text{OBu}}$ and H_8DOTP at 5, 25 and 37 °C are shown in Figure 7. The Gd^{III} complexes of $\text{H}_4\text{DOTP}^{\text{Et}}$, $\text{H}_4\text{DOTP}^{\text{OEt}}$ and H_8DOTP were re-measured, and the published ^1H NMRD profile for the $\text{H}_4\text{DOTP}^{\text{OBu}}$ complex^[13] was used. These profiles were re-analysed as the second-sphere hydration was not considered in previous relaxometric studies.^[13] The values of the r_1 relaxivities of phosphinates and phosphonate monoesters are about half those measured for $[\text{Gd}(\text{H}_2\text{O})(\text{DOTA})]^-$; for example, the relaxivity at 20 MHz and 310 K is about $2.1 \text{ s}^{-1} \text{ mm}^{-1}$ for all these complexes (Table 6). The ^1H NMRD profiles of the $[\text{Gd}(\text{DOTP}^{\text{H}})]^-$ and $[\text{Gd}(\text{DOTP}^{\text{hm}})]^-$ complexes are similar to each other, in contrast to those of the $[\text{Gd}(\text{DOTP}^{\text{Et}})]^-$, $[\text{Gd}(\text{DOTP}^{\text{OEt}})]^-$ and $[\text{Gd}(\text{DOTP}^{\text{OBu}})]^-$ complexes, which have significantly lower relaxivities at low fields. As all these complexes have approximately the same molecular size, these differences can be attributed to a slower electronic spin relaxation and/or to a somewhat higher polarity of the $\text{H}_4\text{DOTP}^{\text{H}}$ and $\text{H}_4\text{DOTP}^{\text{hm}}$ complexes in comparison to the other complexes, which can lead to a richer second hydration sphere in the former complexes.

To obtain more information about electronic parameters, transverse electronic spin relaxation times ($T_{2e,\text{exp}}$) were calculated from the peak-to-peak EPR line widths (ΔH_{pp}) according to Equation (5), where g_L is the Landé g factor (Table 5).^[52] The ^1H NMRD data were then fitted simultaneously with the X-band EPR data by using a set of equations suitable for complexes with an extended second hydration sphere.^[22,27b]

$$T_{2e,\text{exp}} = \frac{h}{\pi \times g_L \times \beta \times \Delta H_{\text{pp}} \times \sqrt{3}} \quad (5)$$

Since the number of parameters in these equations is rather large, and some of them correlate strongly, we fixed many of them. The diffusion coefficients of the various complexes were fixed at values obtained by a semi-empirical

method from their molecular weights, and the corresponding activation energy was fixed at 18.2 kJ mol^{-1} .^[53] The shortest distance of a water proton to the Gd^{III} nucleus (the closest approach, a_{GdH}) was fixed at 3.50 \AA , the same value as in most previous studies. The water molecules in the second coordination sphere are assumed to be hydrogen-bonded to the Gd^{III} -coordinated O-atoms of the ligands. Accordingly, the effective distance between Gd^{III} and these protons (R_{GdH}) was fixed at 3.6 \AA . The residence time of the second-sphere water molecules ($\tau_{\text{M,ss}}$) was taken as 56 ps, the value calculated by Borel et al. for $[\text{Gd}(\text{DOTP})]^{5-}$ by molecular dynamics, and the corresponding activation energy was fixed at 35 kJ mol^{-1} .^[29] The rotational correlation times (τ_R) were estimated from the previously evaluated correlation time for $[\text{Gd}(\text{H}_2\text{O})(\text{DOTA})]^-$ after application of a correction for the molecular volume by means of the Stokes–Debye–Einstein equation, and the activation energy for this correlation time was fixed at 25.4 kJ mol^{-1} for all complexes. Only q_{ss} , the mean-square zero-field splitting energy (Δ^2) and the correlation time for the modulation of the zero-field splitting interaction (τ_v) remained as adjustable parameters in the fitting procedure. The activation energy of the latter parameter was fixed to a reasonable value of 1 kJ mol^{-1} because fittings with this as a variable parameter led to negative values. Inclusion of the ^1H NMRD profiles measured at 5 °C resulted in very unreasonable values of Δ^2 and τ_v , therefore these profiles were given zero weight in the fittings.

The best values of the adjustable parameters for the Gd^{III} complexes of these ligands are given in Table 6. The values of $T_{2e,\text{exp}}$ (from EPR data) and $T_{2e,\text{calc}}$, calculated by using the best-fit parameters τ_v and Δ^2 , are in good agreement (Table 5). The calculated ^1H NMRD profiles are represented by the curves in Figure 7.

The values of the electronic parameters τ_v and Δ^2 could not be determined accurately from the ^1H NMRD profiles, although the profiles appeared to be very sensitive to the value of q_{ss} . The best-fit parameters obtained (Table 6) also support the preliminary conclusion made above, namely that the $[\text{Gd}(\text{DOTP}^{\text{H}})]^-$ and $[\text{Gd}(\text{DOTP}^{\text{hm}})]^-$ complexes have a slower electronic spin relaxation and a somewhat richer second hydration sphere than the $[\text{Gd}(\text{DOTP}^{\text{Et}})]^-$, $[\text{Gd}(\text{DOTP}^{\text{OEt}})]^-$ and $[\text{Gd}(\text{DOTP}^{\text{OBu}})]^-$ complexes (see also the luminescence measurements). As expected, the highest second-sphere hydration was found in the case of $[\text{Gd}(\text{DOTP})]^{5-}$. The values for Δ^2 are an order of magnitude larger than that for $[\text{Gd}(\text{H}_2\text{O})(\text{DOTA})]^-$, which may attributed to the lower rigidity of the complexes of $\text{H}_4\text{DOTP}^{\text{R}}$

Table 5. Experimental ($1/T_{2e,\text{exp}}$, calculated from EPR ΔH_{pp}) and calculated ($1/T_{2e,\text{fit}}$, simultaneous fitting of ^1H NMRD and EPR data) $1/T_{2e}$ values for the Gd^{III} complexes.

| Parameter | $[\text{Gd}(\text{DOTP}^{\text{H}})]^-$ | $[\text{Gd}(\text{DOTP}^{\text{hm}})]^-$ | $[\text{Gd}(\text{DOTP}^{\text{Et}})]^-$ | $[\text{Gd}(\text{DOTP}^{\text{OEt}})]^-$ | $[\text{Gd}(\text{DOTP}^{\text{OBu}})]^-$ | $[\text{Gd}(\text{DOTP})]^{5-}$ | $[\text{Gd}(\text{H}_2\text{O})(\text{DOTA})]^-$ |
|--|---|--|--|---|---|---------------------------------|--|
| ΔH_{pp} [Gauss] | 275 ± 5 | 280 ± 5 | 415 ± 2 | 425 ± 5 | 362 ± 16 | 605 ± 10 | $91^{\text{[a]}}$ |
| $1/T_{2e,\text{exp}}$ [10^9 s^{-1}] ^[b] | 4.19 | 4.27 | 6.33 | 6.40 | 5.49 | 9.22 | 1.40 |
| $1/T_{2e,\text{fit}}$ [10^9 s^{-1}] | 4.19 | 4.27 | 6.33 | 6.40 | 5.49 | 9.25 | – |

[a] Ref.^[3] [b] Values calculated according to Equation (5).

Table 6. Results of multi-parameter simultaneous fitting of ¹H NMRD and EPR data for Gd^{III} complexes of the H₄DOTP^R derivatives (at pH 7) and H₈DOTP (at pH 10). The values in italics were fixed during the fitting.

| Parameter | [Gd(DOTP ^H)] [−] | [Gd(DOTP ^{hm})] [−] | [Gd(DOTP ^{OE})] [−] | [Gd(DOTP ^{OBu})] [−] | [Gd(DOTP ^{Et})] [−] | [Gd(DOTP)] ^{5−} | [Gd(H ₂ O)(DOTA)] [−] |
|--|---------------------------------------|--|--|---|--|--------------------------|---|
| ³¹⁰ <i>r</i> _{1,exp} [s ^{−1} mm ^{−1}] | 2.2 ^[a] | 2.2 ^[a] | 2.1 ^[a] | 2.3 ^[a] | 2.8 ^[a] | 3.5 ^[a] | 3.8 ^[b] |
| ³¹⁰ <i>r</i> _{1,calc} [s ^{−1} mm ^{−1}] | 2.6 ^[c] | 2.6 ^[c] | 2.4 ^[c] | 2.5 ^[c] | 2.5 ^[c] | 3.5 ^[c] | 4.4 ^[d] |
| ³¹⁰ <i>r</i> _{1os,calc} [s ^{−1} mm ^{−1}] | 2.1 ^[e] | 2.1 ^[e] | 2.1 ^[e] | 2.2 ^[e] | 2.1 ^[e] | 2.1 ^[e] | 2.4 ^[f] |
| ³¹⁰ <i>r</i> _{1ss,calc} [s ^{−1} mm ^{−1}] | 0.5 ^[g] | 0.5 ^[g] | 0.3 ^[g] | 0.4 ^[g] | 0.3 ^[g] | 1.4 ^[g] | 0 ^[h] |
| <i>q</i> _{ss} | 1.32 ± 0.05 | 1.22 ± 0.06 | 0.68 ± 0.04 | 0.80 ± 0.04 | 0.79 ± 0.06 | 3.3 ± 0.1 | 0 |
| ²⁹⁸ τ _R [ps] | 86.6 ^[i] | 106.0 ^[i] | 127.7 ^[i] | 162.0 ^[i] | 117.3 ^[i] | 90.7 ^[i] | 77 ^[i] |
| ²⁹⁸ τ _v [ps] | 2.7 ± 1.7 | 2.6 ± 2.0 | 3.8 ± 1.3 | 4.8 ± 1.1 | 5.0 ± 4.6 | 12.7 ± 0.2 | 11 ^[i] |
| Δ ² [10 ²⁰ s ^{−2}] | 1.4 ± 0.8 | 1.5 ± 1.0 | 1.6 ± 0.5 | 1.1 ± 0.2 | 1.0 ± 0.8 | 0.9 ± 0.1 | 0.16 ^[i] |
| ²⁹⁸ τ _{SO} [ps] ^[k] | 220 | 214 | 137 | 158 | 157 | 73 | 473 |
| ²⁹⁸ <i>D</i> _{GdH} [10 ^{−9} m ² s ^{−1}] ^[l] | 2.48 | 2.40 | 2.37 | 2.33 | 2.38 | 2.43 | – |

[a] Experimental relaxivity values as measured at 310 K and 20 MHz. [b] Ref.^[54], 312 K. [c] Relaxivity at 310 K and 20 MHz as calculated with the best-fit parameters reported in this paper. [d] Relaxivity at 310 K and 20 MHz as calculated with the best-fit parameters reported in ref.^[54] [e] Outer-sphere contribution to relaxivity at 310 K and 20 MHz as calculated with the best-fit parameters reported in this paper. [f] Outer-sphere contribution to relaxivity at 310 K and 20 MHz as calculated with the best-fit parameters reported in ref.^[54] [g] Second-sphere contribution to relaxivity at 310 K and 20 MHz as calculated with the best-fit parameters reported in this paper. [h] Second-sphere contribution to relaxivity at 310 K and 20 MHz as calculated with the best-fit parameters reported in ref.^[54] [i] Calculated using a molecular volume as evaluated with HyperChem[®] and the Stokes–Debye–Einstein equation. [j] Ref.^[54] [k] Low field limiting value of the electronic relaxation correlation time as calculated with τ_{SO} = (12 Δ² τ_v)^{−1}. [l] Calculated from the molecular weight using a previously reported equation.^[52]

and H₈DOTP due to the lack of an inner-sphere water molecule, which leads to larger deformation of the complexes upon collision with solvent molecules. As a result, the electronic relaxation rates of the presently studied complexes are lower than that of [Gd(H₂O)(DOTA)][−] (ref.^[54]), which means that the outer-sphere contribution to the relaxivity of these complexes is somewhat lower. The second-sphere water molecules {except for [Gd(DOTP)]^{5−} complex} have a contribution of 10–20% to the total relaxivity (Table 6).

The pH-dependence of the relaxivity of the Gd^{III} complexes in solution was also examined. No protonation of the pendant arms is expected above a pH of around 3 for phosphinic acid or phosphonic monoester groups as they are highly acidic (see above),^[37] therefore no pH dependence was expected. Surprisingly, the relaxivity of the [Gd(DOTP^{hm})][−] complex was found to be highly dependent on the pH, in sharp contrast to the relaxivities of other complexes, which were found to be independent of the pH (tested at pH 4, 7 and 10). The relaxivity of the [Gd(DOTP^{hm})][−] complex increases by more than 50% upon going from neutral to both acidic and alkaline pH regions (Figure S13 in the Supporting Information). This observation can be explained by a prototropic exchange similar to that observed for the Gd^{III} complexes of H₄DOTA amides.^[46] In the strongly acid region (pH < 2), a partial decomplexation probably takes place leading to a further relaxivity increase.

Conclusions

We have synthesized and studied a series of tetraphosphorus acid ligands and, in particular, their complexes with Ln^{III} ions. These ligands and their complexes were characterized by several methods in order to gain insight into their stabilities and structures. The ligands are less basic than the

parent system H₄DOTA and, consequently, the Gd^{III} complexes are thermodynamically much less stable. Titrations have shown that there is no (de)protonation of the pre-formed complexes in the pH range 3–10. Luminescence data do not allow an unambiguous conclusion regarding the value of *q* for the Eu^{III} complexes of the tetraphosphorus acid derivatives as the measured lifetimes suggest *q* values of around 0.5. However, UV/Vis measurements on the Eu^{III} complexes confirm that heavier lanthanide(III) complexes lack an inner-sphere water molecule.

This finding was confirmed by the X-ray structures of the Gd^{III} complexes. Exclusive formation of the TSA isomer was observed by both multinuclear NMR spectroscopy and by X-ray diffraction. The presence of inner-sphere coordinated water was found only for the [Ce(H₂O)(DOTP^H)][−], [Ce(H₂O)(DOTP^{OE})][−] and [Ln(H₂O)(DOTP)]^{5−} (Ln = Ce, Pr, Nd) complexes through the measurements of ¹⁷O lanthanide-induced shifts. The ³¹P NMR study revealed striking differences in isomerism between the [Ln(DOTP^{hm})][−] and [Ln(DOTP^{Et})][−] complexes on the one hand and the [Ln(DOTP^H)][−], [Ln(DOTP^{OE})][−] and [Ln(DOTP^{OBu})][−] complexes on the other. Thus, whereas rich isomeric mixtures were found in the latter cases, the [Ln(DOTP^{hm})][−] and [Ln(DOTP^{Et})][−] complexes show a clear preference for the *RRRR/SSSS* arrangement on the phosphorus atoms, although they probably form *RRRR-Δ-λλλλ* + *SSSS-Δ-δδδδ* enantiomeric pairs similar to those found previously in the case of [Ln(DOTP^{Bn})][−] complexes.^[16] This is probably caused by a strong interaction of the side-chains in the preferential arrangement.

To explore the second-hydration sphere in more detail, a relaxometric study on all the Gd^{III} complexes was also performed. The ¹H NMRD and EPR data were fitted simultaneously, and the best-fit parameters suggest that about three second-sphere water molecules are present in the case of [Gd(DOTP)]^{5−} and about one second-sphere

water molecule is present in the other complexes. The electronic spin relaxation parameters τ_v and Δ^2 obtained suggest that the more hydrophilic $[\text{Gd}(\text{DOTP}^{\text{H}})]^-$ and $[\text{Gd}(\text{DOTP}^{\text{hm}})]^-$ complexes have a slower electronic spin relaxation and a somewhat richer second hydration sphere than the $[\text{Gd}(\text{DOTP}^{\text{Et}})]^-$, $[\text{Gd}(\text{DOTP}^{\text{OEt}})]^-$ and $[\text{Gd}(\text{DOTP}^{\text{OBu}})]^-$ complexes. The pH-dependence of the relaxivity observed for the $[\text{Gd}(\text{DOTP}^{\text{hm}})]^-$ complex reflects the proton/hydroxide catalysis of the prototropic exchange mechanism, similar to that observed for the Gd^{III} complexes of H_4DOTA amides.^[46]

The observed relaxivities of all $[\text{Gd}(\text{DOTP}^{\text{R}})]^-$ complexes fall into the narrow region $2.1\text{--}2.8\text{ s}^{-1}\text{ mm}^{-1}$ (20 MHz, 37 °C). The relaxivity of Gd^{III} complexes with DOTA-like ligands having one inner-sphere water molecule is higher (≈ 4),^[22,54] although in these cases the inner-sphere contributions are about 50% of the final value, whereas the second-sphere water molecules of the presently studied complexes have a contribution of only 10–15% to the total relaxivity. The ligands studied differ in the size and hydrophilic/hydrophobic character of the substituents on the phosphorus atoms and in the isomeric distributions of their complexes in solution. However, this has only a marginal influence on the relaxivity. This indicates that the second-sphere water molecules contributing to the relaxivity (i.e. residing close to the central Gd^{III} ion) are mainly connected with the oxygen atoms of electronegative PO_2^- moiety through hydrogen bonds, independently on the orientation of the side chains and, consequently, on the local arrangement of the second-sphere water molecules.

Experimental Section

General: Cyclen (1,4,7,10-tetraazacyclododecane, Strem or CheMatech), hypophosphorous acid (Fluka), triethyl phosphite (Fluka), LnCl_3 hydrates (Strem or Aldrich), D_2O (99.95% D , Chemtrade) and Dowex 50 ($\times 4$, 100–200 mesh, Fluka) were used without further purification. Paraformaldehyde was filtered from an old formaldehyde solution and dried over P_2O_5 in vacuo. Anhydrous EtOH was obtained from Lachema (Czech Republic). $\text{H}_4\text{DOTP}^{\text{Et}}$ and $\text{H}_4\text{DOTP}^{\text{OBu}}$ were synthesized according to literature procedures.^[13,33] ^1H (400 MHz), ^{13}C (101 MHz) and ^{31}P (162 MHz) NMR spectra were recorded with a Varian INOVA 400 spectrometer in CDCl_3 , D_2O or H_2O solutions at 25 °C, or with a Varian Unity 500 spectrometer (^1H : 499.82 MHz; ^{31}P : 202.33 MHz). For measurements in D_2O , the internal standard was $t\text{BuOH}$; in CDCl_3 , the internal standard was TMS; for ^{31}P , 85% H_3PO_4 was used as an external standard. The elemental analyses were carried out at the Institute of Macromolecular Chemistry (Academy of Sciences of the Czech Republic, Prague). Luminescence measurements were performed with an Aminco Bowman® Series 2 spectrometer by using the excitation at the $^5\text{L}_6 \leftarrow ^7\text{F}_0$ band (396 nm). Emission lifetimes were measured for the $^7\text{F}_2 \leftarrow ^5\text{D}_0$ transition (615 and 621 nm). In general, the samples prepared for NMR measurements were also used for luminescence measurements. UV/Vis spectra of the $^5\text{D}_0 \leftarrow ^7\text{F}_0$ transition were acquired with a Perkin–Elmer Lambda 19 spectrometer, in data steps of 0.01 nm. The concentration of the samples was around 0.02 M.

1,4,7,10-Tetraazacyclododecane-1,4,7,10-tetrakis(methylphosphinic acid) ($\text{H}_4\text{DOTP}^{\text{H}}$): Cyclen (1.00 g, 5.80 mmol) and 50% aqueous

hypophosphorous acid (7.2 mL, 66 mmol) were mixed in water (20 mL). The mixture was heated to 40 °C whilst being stirred, and solid paraformaldehyde (0.78 g, 26 mmol) was added in small portions over 60 min. The mixture was further heated at this temperature for 1 d. Excess paraformaldehyde was then filtered off. After concentration to a small volume under reduced pressure, the reaction mixture was purified on a cation exchange resin (Dowex 50, H^+ -form, 300 mL, elution with water). Phosphinic acid and other acidic impurities were eluted first followed by the product. Fractions containing the pure ligand (checked by ^{31}P NMR) were combined and concentrated in vacuo. Microcrystalline $\text{H}_4\text{DOTP}^{\text{H}} \cdot 0.5\text{H}_2\text{O}$ (0.66 g, 23%) was obtained after slow evaporation of the solvent from an aqueous ligand solution. ^1H NMR (D_2O): δ = 2.53–2.55 (m, $^2J_{\text{P,H}}$ = 8.8 Hz, 24 H, CH_2P , $\text{NCH}_2\text{CH}_2\text{N}$), 7.04 (d, $^1J_{\text{P,H}}$ = 504.0 Hz, 4 H, PH) ppm. ^{31}P NMR (D_2O): δ = 22.5 (dt, $^1J_{\text{P,H}}$ = 504, $^2J_{\text{P,H}}$ = 9.2 Hz) ppm. $^{31}\text{P}\{^1\text{H}\}$ NMR (D_2O): δ = 22.5 (s) ppm. $\text{C}_{12}\text{H}_{32}\text{N}_4\text{O}_8\text{P}_4 \cdot 0.5\text{H}_2\text{O}$ (493.31): calcd. C 29.22, H 6.74, N 11.36; found C 29.29, H 6.62, N 11.38.

1,4,7,10-Tetraazacyclododecane-1,4,7,10-tetrakis(hydroxymethyl(methyl)phosphinic acid) ($\text{H}_4\text{DOTP}^{\text{hm}}$): Paraformaldehyde (0.93 g, 31 mmol) was added to an aqueous solution of $\text{H}_4\text{DOTP}^{\text{H}}$ hydrate (1.00 g, 2.03 mmol), and the mixture was stirred and heated under reflux for 1 d. The mixture was then concentrated to dryness under reduced pressure and redissolved in a small amount of water. The solution was purified on a cation exchange column (Dowex 50, H^+ -form, 300 mL, elution with water). The first fractions containing the product were combined, and the solvent was evaporated. The residue was dissolved in a small amount of water, and the product was precipitated by addition of acetone. The solid was filtered off and dried with P_2O_5 . A white microcrystalline solid was isolated in 51% yield (0.65 g). ^1H NMR (D_2O): δ = 2.70–2.60 (m, 24 H, CH_2OH , $\text{NCH}_2\text{CH}_2\text{N}$), 3.46 (d, $^2J_{\text{P,H}}$ = 5.6 Hz, 8 H, NCH_2P) ppm. $^{31}\text{P}\{^1\text{H}\}$ NMR (D_2O): δ = 38.2 (s) ppm. $\text{C}_{16}\text{H}_{40}\text{N}_4\text{O}_{12}\text{P}_4 \cdot 1.5\text{H}_2\text{O}$ (631.43): calcd. C 30.44, H 6.86, N 8.87; found C 30.50, H 6.68, N 8.66.

Monoethyl 1,4,7,10-Tetraazacyclododecane-1,4,7,10-tetrakis(methylphosphonate) ($\text{H}_4\text{DOTP}^{\text{OEt}}$):^[32] Cyclen (1.00 g, 5.80 mmol) was treated with paraformaldehyde (0.87 g, 29 mmol) and triethyl phosphite (9.8 g, 59 mmol, as solvent) to produce the octaethyl ester Et_8DOTP . The mixture was stirred at 40 °C for 3 d and then loaded onto a cation exchange column (Dowex 50, H^+ -form, 300 mL). Di- and triethyl phosphite were eluted with EtOH, and Et_8DOTP was washed out with a 1:3 (v:v) mixture of 25% aq. NH_3/EtOH . The fractions containing the desired ester were concentrated in vacuo, after which the purity and the identity of this compound was verified by NMR spectroscopy [^1H NMR (CDCl_3): δ = 1.27 (t, $^3J_{\text{H,H}}$ = 7.2 Hz, 24 H, CH_3), 2.82 (s, 16 H, $\text{NCH}_2\text{CH}_2\text{N}$), 2.94 (d, $^2J_{\text{P,H}}$ = 9.2 Hz, 8 H, NCH_2P), 4.03–4.11 (m, 16 H, OCH_2) ppm. ^{13}C NMR (CDCl_3): δ = 16.5 s (CH_3), 50.6 (d, $^1J_{\text{C,P}}$ = 151.5 Hz, NCH_2P), 53.4 (s, $\text{NCH}_2\text{CH}_2\text{N}$), 61.5 (s, OCH_2) ppm. $^{31}\text{P}\{^1\text{H}\}$ NMR (CDCl_3): δ = 26.7 (s) ppm. The target ligand was obtained after hydrolysis (1 d, 50 °C) of this ester in aq. NaOH (10%, 25 mL). The sodium ions were completely removed by passing the reaction mixture through a cation exchange resin (Dowex 50, H^+ -form, 300 mL, elution with water). Evaporation of the water from the eluate resulted in a colourless oil. The ligand was obtained as a white microcrystalline solid after precipitation from its aqueous solution by slow addition of acetone, filtering and drying over P_2O_5 (3.91 g, 92% based on cyclen). ^1H NMR (D_2O): δ = 1.18 (t, $^3J_{\text{H,H}}$ = 6.8 Hz, 12 H, CH_3), 3.20–3.27 (m, 24 H, NCH_2P , $\text{NCH}_2\text{CH}_2\text{N}$), 3.89–3.96 (m, 8 H, OCH_2) ppm. $^{31}\text{P}\{^1\text{H}\}$ NMR (D_2O): δ = 19.4 (s) ppm. $\text{C}_{20}\text{H}_{48}\text{N}_4\text{O}_{12}\text{P}_4 \cdot 4\text{H}_2\text{O}$ (732.57): calcd. C 32.79, H 7.70, N 7.65; found C 32.65, H 6.94, N 7.63.

1,4,7,10-Tetraazacyclododecane-1,4,7,10-tetrakis(methylphosphonic acid) (H₄DOTP): The target ligand was obtained after acid hydrolysis (aq. HCl 1:1, 2 d, reflux) of the ester obtained as above. The reaction mixture was concentrated, and the residue was recrystallized from boiling water. The ligand, in the form of a white microcrystalline solid, was collected by filtration and dried in air (95% based on cyclen). Spectroscopic data were identical with those reported in the literature.^[35] C₁₂H₃₂N₄O₁₂P₄·1.5H₂O (575.33): calcd. C 25.05, H 6.13, N 9.74; found C 25.01, H 6.04, N 9.78.

Lanthanide(III) Complexes of the Ligands: Samples of the Ln^{III} complexes for NMR measurements were prepared by dissolving LnCl₃·6H₂O and a 10% molar excess of the ligand in water, increasing the pH to about 7 with an aq. KOH solution and leaving the mixture for 1 h; ¹⁷O-enriched water was added to the samples for ¹⁷O variable-temperature and LIS NMR measurements to a concentration of about 0.5% ¹⁷O. The samples for structural studies were prepared analogously, but in D₂O, to yield 0.1 M solutions of the complexes in all cases. The samples for ³¹P NMR LIS were prepared in 20% D₂O. The pH of all resulting solutions was adjusted to 7 with either dilute HCl (DCl) or KOH (KOD). The absence of free Ln^{III} ions was verified by using xylenol orange as indicator in acetate buffer at a pH of about 5.5. Samples of the Eu^{III} complexes for UV/Vis spectroscopy were prepared analogously, and the samples originally prepared for NMR studies were used for luminescence experiments. The samples for measurements of ¹H NMRD profiles were prepared by exact dilution of the samples for ¹⁷O NMR measurements to the final concentration of 5 mM.

X-ray Studies: Single crystals of all studied compounds were obtained by slow vapour diffusion of acetone into aqueous solutions of the compounds. For the complexes, dilute aq. LiOH was used for pH adjustment. The diffraction data were collected by using a Nonius Kappa CCD diffractometer (Enraf–Nonius) at 150(1) K with Mo-K α radiation (λ = 0.71073 Å) and analysed by using the HKL program package.^[55] The structures were solved by direct methods and refined by full-matrix least-squares techniques (SIR92^[56] and SHELXL97^[57]). Scattering factors for neutral atoms were included in the SHELXL97 program. Experimental data are given in Table 7. All non-hydrogen atoms in the structure of

H₄DOTP^{OEt}·H₂O were refined anisotropically except for some disordered ethyl groups of the pendant arms. The hydrogen atoms belonging to the carbon atoms were fixed in the theoretical positions by using the riding model with $U_{eq}(H) = 1.2 U_{eq}(C)$. Some hydrogen atoms attached to amino groups or oxygen atoms were located in the electron density difference map. In the case of the amino groups, the protons were fixed in the theoretical positions, and the protons of the oxygen atoms were refined in the original positions with thermal parameters $U_{eq}(H) = 1.2 U_{eq}(X)$. All non-hydrogen atoms in the structure of Li[Gd(DOTP^H)]·6H₂O were refined anisotropically, and all hydrogen atoms were fixed in their theoretical (C–H and P–H) or original (O–H) positions by using $U_{eq}(H) = 1.2 U_{eq}(X)$. One pendant arm was best refined when turned into two positions (with *R* and *S* configuration on the phosphorus atom, respectively), and the lithium counterion was fitted in two positions as well (as it is coordinated by an oxygen atom of a partially occupied oxygen atom of a disordered phosphinate). All non-hydrogen atoms in the structure of Li[Gd(DOTP^{OEt})]·0.5Me₂CO·8H₂O were refined anisotropically except for one disordered ethyl group of the pendant arms and one disordered water solvate molecule. The hydrogen atoms belonging to carbon atoms were fixed in their theoretical positions by using the riding model with $U_{eq}(H) = 1.2 U_{eq}(C)$. Some of the hydrogen atoms attached to the solvate molecules were localized in the difference Fourier map and were treated in their original positions with $U_{eq}(H) = 1.2 U_{eq}(O)$. CCDC-704357 (H₄DOTP^{OEt}·H₂O), -704358 {Li[Gd(DOTP^{OEt})]·0.5Me₂CO·8H₂O}, and -704359 {Li[Gd(DOTP^H)]·6H₂O} contain the supplementary crystallographic data for this paper. These data can be obtained free of charge from The Cambridge Crystallographic Data Centre via www.ccdc.cam.ac.uk/data_request/cif.

Potentiometric Measurements: Potentiometric titrations were run, and the data obtained were treated according to a previously published procedure.^[58] Protonation/dissociation and stability constants of H₄DOTP^H or H₄DOTP^{bm} and their complexes were determined in 0.1 M Me₄NCl at 25 °C. The stability constants of Gd^{III} complexes were obtained by the out-of-cell method with a waiting time for equilibrium of three weeks (some solutions were checked after six weeks and found to give the same data). Titrations were performed in the pH range 1.8–6.0 with around 30 data points per

Table 7. Crystallographic parameters of the studied compounds.

| Compound | H ₄ DOTP ^{OEt} ·H ₂ O | Li[Gd(DOTP ^H)]·6H ₂ O | Li[Gd(DOTP ^{OEt})]·0.5Me ₂ CO·8H ₂ O |
|--|---|---|---|
| Empirical formula | C ₂₀ H ₅₀ N ₄ O ₁₃ P ₄ | C ₁₂ H ₄₀ GdLiN ₄ O ₁₄ P ₄ | C _{21.5} H ₆₃ GdLiN ₄ O _{20.5} P ₄ |
| <i>M_r</i> | 678.52 | 752.55 | 993.83 |
| Colour, | colourless | colourless | colourless |
| Habit | rod | rod | prism |
| Crystal system | rhombic | monoclinic | rhombic |
| Space group | <i>Pca</i> 2 ₁ | <i>C</i> 2/ <i>c</i> | <i>P</i> 2 ₁ 2 ₁ |
| <i>a</i> [Å] | 19.4095(2) | 17.5713(3) | 14.2862(1) |
| <i>b</i> [Å] | 13.4920(2) | 6.9336(1) | 24.2628(2) |
| <i>c</i> [Å] | 24.5857(3) | 22.3551(4) | 25.0544(2) |
| β [°] | 90 | 101.177(1) | 90 |
| <i>V</i> [Å ³] | 6438.3(1) | 2671.92(8) | 8684.4(1) |
| <i>Z</i> | 8 | 4 | 8 |
| <i>D</i> _{calcd.} [g cm ^{−3}] | 1.400 | 1.871 | 1.520 |
| μ [mm ^{−1}] | 0.298 | 2.790 | 1.748 |
| Total refl. | 12198 | 3055 | 19853 |
| Obsd. refl. [<i>I</i> > 2σ(<i>I</i>)] | 10090 | 2965 | 17491 |
| <i>R</i> | 0.0535 | 0.0235 | 0.0395 |
| <i>R'</i> [<i>I</i> > 2σ(<i>I</i>)] | 0.0697 | 0.0246 | 0.0503 |
| <i>wR</i> | 0.1348 | 0.0581 | 0.0926 |
| <i>wR'</i> [<i>I</i> > 2σ(<i>I</i>)] | 0.1468 | 0.0589 | 0.0987 |

titration and three titrations per system. The pre-formed gadolinium(III) complexes in solution were obtained by mixing a known amount of ligand (5% molar excess) with GdCl_3 (as a defined stock solution) in a glass ampoule. A standard Me_4NOH solution (just to neutralize the ligand amount) was slowly added, and the ampoule was sealed and left at 80 °C overnight to fully complex the metal ion. The ampoules were opened, and aliquots of the solutions of the gadolinium(III) complexes were transferred to a titration vessel. Excess of HCl and Me_4NCl solutions were added (to reach a pH of about 2 and 0.1 M Me_4NCl in the final solution) and the solution was immediately titrated with a standard Me_4NOH solution up to a pH of about 12 at 25 °C, acquiring around 45 data points for each of three titrations.

EPR Measurements: X-band EPR spectra of aqueous solutions of the Gd^{III} chelates (1 mM, pH of about 7.0) were obtained at 25 °C by using a Bruker ESP-300E spectrometer operating at 9.43 GHz (0.34 T) with a quartz flat cell. Spectral acquisition parameters: sweep width: 40 mT; microwave power: 0.632 mW; modulation amplitude: 0.32 mT; time constant: 20.48 ms.

NMR and Relaxation Studies of the Lanthanide(III) Complexes: ^1H (300.0 MHz), ^{17}O (40.7 MHz) and ^{31}P (121.5 MHz) NMR spectra were acquired with a Varian VNMRs 300 spectrometer by using a 5 mm broadband probe. ^1H (400.0 MHz), ^{17}O (54.2 MHz) and ^{31}P (161.9 MHz) NMR spectra were also acquired with a Varian Unity INOVA 400 spectrometer and ^1H (500.0 MHz) and ^{31}P (202.3 MHz) NMR spectra with a Varian Unity 500 spectrometer using the same type of probe. BMS effects were corrected by using the internal D_2O lock signals. Water was used as solvent for the variable-temperature ^{17}O NMR shifts and LIS measurements, therefore no frequency lock could be applied. In this case, the correction for the BMS shifts was performed with the ^1H resonance of the internal standard $t\text{BuOH}$. H_3PO_4 (85%) was used as an external chemical shift reference for ^{31}P spectra. COSY spectra of some of the diamagnetic complexes were obtained by using 2048×2048 data points in F_1 and F_2 . Pure absorption mode EXSY spectra were recorded by using the conventional NOESY $90^\circ - t_1 - 90^\circ - \tau_{\text{mix}} - 90^\circ$ -acq. phase-sensitive pulse sequence in D_2O as solvent. The ^{31}P EXSY data were acquired with a variable mixing time between 2 and 150 ms and processed with the program Messtec EXSY CALC v. 1.0.^[59] Longitudinal relaxation rates ($1/T_1$) were obtained by the inversion-recovery method, and transverse relaxation rates ($1/T_2$) were measured by the Carr–Purcell–Meiboom–Gill spin-echo technique. At each temperature, the spectral parameters were measured for both the sample with gadolinium(III) complex and the sample of acidified water (pH 6) under exactly the same conditions. No frequency lock was applied. The $1/T_1$ nuclear magnetic relaxation dispersion (^1H NMRD) profiles of water protons at several temperatures (5, 25 and 37 °C) were obtained with a Stellar Master FFC-2000 relaxometer by using the field-cycling method and covering a continuum of magnetic fields from 2.35×10^{-4} to 0.35 T (corresponding to a proton Larmor frequency range from 0.01 MHz to 15 MHz). The spin-lattice proton relaxation rates at 0.47 (20) and 1.41 T (60 MHz) were measured with a Bruker Minispec mq-20 and a Bruker Minispec mq-60 spin analyzer, respectively. Relaxivity at different pH values (2–12) was measured with a Bruker Minispec mq-20 at 37 °C. The Ln^{III} contents in all samples were estimated from the bulk magnetic susceptibility (BMS) shift.^[60]

Data Evaluation: Potentiometric data were evaluated with the program package OPIUM.^[61] Relaxometric data were evaluated with Origin™, Version 6.0. All calculations using relaxometric data were carried out with least-squares fitting by the program SCIEN-

TIST® for WINDOWS™ by Micromath® (ref.^[62]) using a set of equations published previously.^[27a] Molecular sizes of the complexes were estimated by constructing molecular models with HyperChem®, Version 7.5.^[63]

Supporting Information (see footnote on the first page of this article): Molecular structures of two independent units found in the structure of $\text{H}_4\text{DOTP}^{\text{OEt}} \cdot \text{H}_2\text{O}$; UV/Vis spectra for the $^5\text{D}_0 \leftarrow ^7\text{F}_0$ transition of $[\text{Eu}(\text{DOTP}^{\text{H}})]^-$ and $[\text{Eu}(\text{DOTP}^{\text{OEt}})]^-$ complexes; $^{31}\text{P}\{^1\text{H}\}$ NMR spectra of Nd^{III} , Eu^{III} and Yb^{III} complexes of $\text{H}_4\text{DOTP}^{\text{H}}$, $\text{H}_4\text{DOTP}^{\text{hm}}$, $\text{H}_4\text{DOTP}^{\text{Et}}$, $\text{H}_4\text{DOTP}^{\text{OEt}}$ and $\text{H}_4\text{DOTP}^{\text{OBu}}$; an example of a ^{31}P EXSY NMR spectrum for the $[\text{Yb}(\text{DOTP}^{\text{H}})]^-$ complex; temperature dependence of the ^{31}P NMR spectra of the $[\text{Yb}(\text{DOTP}^{\text{OEt}})]^-$, $[\text{Eu}(\text{DOTP}^{\text{OEt}})]^-$ and $[\text{Yb}(\text{DOTP}^{\text{hm}})]^-$ complexes; ^1H NMR spectra of the $[\text{Eu}(\text{DOTP}^{\text{hm}})]^-$ and $[\text{Eu}(\text{DOTP}^{\text{OEt}})]^-$ complexes; schematic representation of the McConnell cone in the complexes; variable-temperature ^{17}O reduced relaxation rates and reduced angular frequencies of Gd^{III} complexes of $\text{H}_4\text{DOTP}^{\text{H}}$, $\text{H}_4\text{DOTP}^{\text{hm}}$, $\text{H}_4\text{DOTP}^{\text{OEt}}$ and H_8DOTP ; dependence of the relaxivity of the $[\text{Gd}(\text{DOTP}^{\text{hm}})]^-$ complex on pH; luminescence lifetimes (τ_{ex}) and the corresponding hydration numbers of selected Eu^{III} complexes.

Acknowledgments

We thank Prof. É. Tóth (CNRS, Orléans, France) for allowing us to measure UV/Vis spectra. This work was supported by the Grant Agency of the Czech Republic (grant no. 203/06/0467), the Czech Academy of Sciences (grant no. KAN201110651) and the Ministry of Education, Youth and Sport of the Czech Republic (grant no. MSM0021620857) and by the Foundation of Science and Technology (F.C.T.), Portugal (project PTDC/QUI/70063/2006 and grant SFRH/BD/9685/2002 to G. A. P.) and FEDER. This work was carried out in the framework of the COST D38 Action D38 “Metal-Based systems for Molecular Imaging Applications” and EU-FP6 “Network of Excellence” EMIL (grant no. LSHC-2004-503569) and DiMI (grant no. LSHB-2005-512146) projects.

- [1] *The Chemistry of Contrast Agents in Medical Magnetic Resonance Imaging* (Eds.: A. E. Merbach, É. Tóth), Wiley, Chichester, England, 2001.
- [2] *Topics in Current Chemistry*, Springer Verlag, Heidelberg, 2002, vol. 221.
- [3] P. Caravan, J. J. Ellison, T. J. McMurry, R. B. Laufer, *Chem. Rev.* **1999**, 99, 2293–2352.
- [4] S. Aime, M. Botta, E. Terreno, *Adv. Inorg. Chem.* **2005**, 57, 173–237.
- [5] P. Hermann, J. Kotek, V. Kubiček, I. Lukeš, *Dalton Trans.* **2008**, 3027–3047.
- [6] P. Caravan, *Chem. Soc. Rev.* **2006**, 35, 512–523.
- [7] A. Nonat, C. Gateau, P. H. Fries, M. Mazzanti, *Chem. Eur. J.* **2006**, 12, 7133–7150.
- [8] A. Borel, J. F. Bean, R. B. Clarkson, L. Helm, L. Moriggi, A. D. Sherry, M. Woods, *Chem. Eur. J.* **2008**, 14, 2658–2667.
- [9] M. Botta, *Eur. J. Inorg. Chem.* **2000**, 399–407.
- [10] F. Avecilla, J. A. Peters, C. F. G. C. Geraldes, *Eur. J. Inorg. Chem.* **2003**, 4179–4186.
- [11] S. Aime, M. Botta, E. Terreno, P. L. Anelli, F. Uggeri, *Magn. Reson. Med.* **1993**, 30, 583–591.
- [12] P. Caravan, M. T. Greenfield, X. Li, A. D. Sherry, *Inorg. Chem.* **2001**, 40, 6580–6587.
- [13] C. F. G. C. Geraldes, A. D. Sherry, I. Lázár, A. Miseta, P. Bogner, E. Berenyi, B. Sumegi, G. E. Kiefer, K. McMillan, F. Maton, R. N. Muller, *Magn. Reson. Med.* **1993**, 30, 696–703.
- [14] M. Murru, D. Parker, G. Williams, A. Beeby, *J. Chem. Soc., Chem. Commun.* **1993**, 1116–1118.

- [15] J. Rohovec, P. Vojtišek, P. Hermann, J. Mosinger, Z. Žák, I. Lukeš, *J. Chem. Soc., Dalton Trans.* **1999**, 3585–3592.
- [16] a) S. Aime, A. S. Batsanov, M. Botta, J. A. K. Howard, D. Parker, K. Senanayake, G. Williams, *Inorg. Chem.* **1994**, *33*, 4696–4706; b) S. Aime, A. S. Batsanov, M. Botta, R. S. Dickinson, S. Faulkner, C. E. Foster, A. Harrison, J. A. K. Howard, J. M. Moloney, T. J. Norman, D. Parker, L. Royle, J. A. G. Williams, *J. Chem. Soc., Dalton Trans.* **1997**, 3623–3636; R. L. Luck, C. L. Maupin, D. Parker, J. P. Riehl, J. A. G. Williams, *Inorg. Chim. Acta* **2001**, *317*, 331–337.
- [17] S. Aime, M. Botta, M. Fasano, M. P. M. Marques, C. F. G. C. Geraldes, D. Pubanz, A. E. Merbach, *Inorg. Chem.* **1997**, *36*, 2059–2068.
- [18] R. L. Luck, C. L. Maupin, D. Parker, J. P. Riehl, J. A. G. Williams, *Inorg. Chim. Acta* **2001**, *317*, 331–337.
- [19] C. F. G. C. Geraldes, A. D. Sherry, G. E. Kiefer, *J. Magn. Reson.* **1992**, *97*, 290–304.
- [20] J. Rudovský, P. Cígler, J. Kotek, P. Hermann, P. Vojtišek, I. Lukeš, J. A. Peters, L. Vander Elst, R. N. Muller, *Chem. Eur. J.* **2005**, *11*, 2373–2384.
- [21] a) J. Rudovský, J. Kotek, P. Hermann, I. Lukeš, V. Mainero, S. Aime, *Org. Biomol. Chem.* **2005**, *3*, 112–117; b) J. Rudovský, M. Botta, P. Hermann, A. Koridze, S. Aime, *Dalton Trans.* **2006**, 2323–2333.
- [22] P. Lebdušková, P. Hermann, L. Helm, É. Tóth, J. Kotek, K. Binnemans, J. Rudovský, I. Lukeš, A. E. Merbach, *Dalton Trans.* **2007**, 493–501.
- [23] P. Vojtišek, P. Cígler, J. Kotek, J. Rudovský, P. Hermann, I. Lukeš, *Inorg. Chem.* **2005**, *44*, 5591–5599.
- [24] J. Kotek, J. Rudovský, P. Hermann, I. Lukeš, *Inorg. Chem.* **2006**, *45*, 3097–3102.
- [25] a) S. Aime, E. Gianolio, D. Corpillo, C. Cavallotti, G. Palmisano, M. Sisti, G. B. Giovenzana, R. Pagliarin, *Helv. Chim. Acta* **2003**, *86*, 615–631; b) S. Aime, M. Botta, L. Frullano, S. Geninatti Crich, G. Giovenzana, R. Pagliarin, G. Palmisano, F. R. Sirtori, M. Sisti, *J. Med. Chem.* **2000**, *43*, 4017–4024; c) S. Aime, M. Botta, S. Geninatti Crich, G. Giovenzana, R. Pagliarin, M. Sisti, E. Terreno, *Magn. Reson. Chem.* **1998**, *36*, S200–S208.
- [26] a) J. Kotek, P. Lebdušková, P. Hermann, L. Vander Elst, R. N. Muller, T. Maschmeyer, I. Lukeš, J. A. Peters, *Chem. Eur. J.* **2003**, *9*, 5899–5915; b) S. Aime, Z. Baranyai, E. Gianolio, K. Ramalingam, R. Swenson, R. Ranganathan, E. Brücher, S. Aime, *Contrast Media Mol. Imaging* **2007**, *2*, 94–102.
- [27] a) P. Lebdušková, J. Kotek, P. Hermann, L. Vander Elst, R. N. Muller, I. Lukeš, J. A. Peters, *Bioconjugate Chem.* **2004**, *15*, 881–889; b) P. Lebdušková, A. Sour, L. Helm, É. Tóth, J. Kotek, I. Lukeš, A. E. Merbach, *Dalton Trans.* **2006**, 3399–3406.
- [28] a) J. Rudovský, M. Botta, P. Hermann, K. I. Hardcastle, I. Lukeš, S. Aime, *Bioconjugate Chem.* **2006**, *17*, 975–987; b) J. Rudovský, P. Hermann, M. Botta, S. Aime, I. Lukeš, *Chem. Commun.* **2005**, 2390–2392.
- [29] A. Borel, L. Helm, A. E. Merbach, *Chem. Eur. J.* **2001**, *7*, 600–610.
- [30] a) E. Balogh, M. Mato-Iglesias, C. Platas-Iglesias, E. Tóth, K. Djanashvili, J. A. Peters, A. de Blas, T. Rodríguez-Blas, *Inorg. Chem.* **2006**, *45*, 8719–8728; b) M. Mato-Iglesias, E. Balogh, C. Platas-Iglesias, É. Tóth, A. de Blas, T. Rodríguez-Blas, *Dalton Trans.* **2006**, 5404–5415.
- [31] K. Bazakas, I. Lukeš, *J. Chem. Soc., Dalton Trans.* **1995**, 1133–1137.
- [32] M. Försterová, Z. Jandurová, F. Marques, L. Gano, P. Lubal, J. Vaněk, P. Hermann, I. Santos, *J. Inorg. Biochem.* **2008**, *102*, 1531–1540.
- [33] L. Burai, R. Király, I. Lázár, E. Brücher, *Eur. J. Inorg. Chem.* **2001**, 813–820.
- [34] M. Meyer, V. Dahanoui-Ginderey, C. Lecomte, R. Guillard, *Coord. Chem. Rev.* **1998**, *178–180*, 1313–1405.
- [35] I. Lázár, D. C. Hrnčir, W.-D. Kim, C. E. Kiefer, A. D. Sherry, *Inorg. Chem.* **1992**, *31*, 4422–4424.
- [36] S. Aime, A. Barge, J. I. Bruce, M. Botta, J. A. K. Howard, J. M. Moloney, D. Parker, A. S. de Sousa, M. Woods, *J. Am. Chem. Soc.* **1999**, *121*, 5762–5771.
- [37] I. Lukeš, J. Kotek, P. Vojtišek, P. Hermann, *Coord. Chem. Rev.* **2001**, *216–217*, 287–312.
- [38] J. Rohovec, M. Kývala, P. Vojtišek, P. Hermann, I. Lukeš, *Eur. J. Inorg. Chem.* **2000**, 195–203.
- [39] W. D. Kim, G. E. Kiefer, J. Huskens, A. D. Sherry, *Inorg. Chem.* **1997**, *36*, 4128–4134.
- [40] J. Rohovec, I. Lukeš, P. Vojtišek, I. Cisařová, P. Hermann, *J. Chem. Soc., Dalton Trans.* **1996**, 2685–2691.
- [41] I. Lázár, A. D. Sherry, R. Ramasamy, E. Brücher, R. Király, *Inorg. Chem.* **1991**, *30*, 5016–5019.
- [42] R. Delgado, J. Costa, K. P. Guerra, L. M. P. Lima, *Pure Appl. Chem.* **2005**, *77*, 569–579.
- [43] G. Anderegg, F. Arnaud-Neu, R. Delgado, J. Felcman, K. Popov, *Pure Appl. Chem.* **2005**, *77*, 1445–1495.
- [44] A. D. Sherry, J. Ren, J. Huskens, E. Brücher, É. Tóth, C. F. G. C. Geraldes, M. M. Castro, W. P. Cacheris, *Inorg. Chem.* **1996**, *35*, 4604–4612.
- [45] A. Bianchi, L. Calabi, C. Giorgi, P. Losi, M. Palma, P. Paoli, P. Rossi, B. Valtancoli, M. Virtuani, *J. Chem. Soc., Dalton Trans.* **2000**, 697–705.
- [46] a) S. Aime, M. Botta, M. Fasano, E. Terreno, *Acc. Chem. Res.* **1999**, *32*, 941–949; b) S. Aime, E. Gianolio, A. Barge, D. Kostakis, I. C. Plakatouras, N. Hadjiljadjis, *Eur. J. Inorg. Chem.* **2003**, 2045–2048; c) F. K. Kálmán, M. Woods, P. Caravan, P. Jurek, M. Spiller, G. Tircsó, R. Király, E. Brücher, A. D. Sherry, *Inorg. Chem.* **2007**, *46*, 5260–5270.
- [47] W. W. De Horrocks Jr, D. R. Sudnick, *J. Am. Chem. Soc.* **1979**, *101*, 334–340.
- [48] A. Beeby, I. M. Clarkson, R. S. Dickinson, S. Faulkner, D. Parker, L. Royle, A. S. de Sousa, J. A. G. Williams, M. Woods, *J. Chem. Soc. Perkin Trans. 2* **1999**, 493–503.
- [49] a) N. Graeppe, D. H. Powell, G. Laurenczy, L. Zékány, A. E. Merbach, *Inorg. Chim. Acta* **1995**, *235*, 311–326; b) É. Tóth, O. M. Ni Dhubhghaill, G. Besson, L. Helm, A. E. Merbach, *Magn. Reson. Chem.* **1999**, *37*, 701–708; c) F. Yerly, F. A. Dunand, É. Tóth, A. Figueirinha, Z. Kovács, A. D. Sherry, C. F. G. C. Geraldes, A. E. Merbach, *Eur. J. Inorg. Chem.* **2000**, 1001–1006; d) F. A. Dunand, S. Aime, S. G. Crich, G. B. Giovenzana, A. E. Merbach, *Magn. Reson. Chem.* **2002**, *40*, 87–92; e) M. Mato-Iglesias, C. Platas-Iglesias, K. Djanashvili, J. A. Peters, É. Tóth, E. Balogh, R. N. Muller, L. Vander Elst, A. de Blas, T. Rodríguez-Blas, *Chem. Commun.* **2005**, 4729–4731.
- [50] a) S. Aime, M. Botta, D. Parker, J. A. G. Williams, *J. Chem. Soc., Dalton Trans.* **1995**, 2259–2266; b) S. Aime, M. Botta, R. C. Dickinson, C. L. Maupin, D. Parker, J. P. Riehl, J. A. G. Williams, *J. Chem. Soc., Dalton Trans.* **1998**, 881–892.
- [51] a) J. A. Peters, J. Huskens, D. J. Raber, *Prog. NMR Spectrosc.* **1996**, *28*, 283–350; b) K. Djanashvili, J. A. Peters, *Contrast Media Mol. Imaging* **2007**, *2*, 67–71.
- [52] E. Zitha-Bovens, R. N. Muller, S. Laurent, L. Vander Elst, C. F. G. C. Geraldes, H. van Bekkum, J. A. Peters, *Helv. Chim. Acta* **2005**, *88*, 618–632.
- [53] L. Vander Elst, A. Sessoye, S. Laurent, R. N. Muller, *Helv. Chim. Acta* **2005**, *88*, 574–587.
- [54] D. H. Powell, O. M. N. Dhubhghaill, D. Pubanz, L. Helm, Y. S. Lebedev, W. Schlaepfer, A. E. Merbach, *J. Am. Chem. Soc.* **1996**, *118*, 9333–9346.
- [55] Z. Otwinowski, W. Minor, *HKL Denzo and Scalepack Program Package by Nonius BV*, Delft, **1997**; Z. Otwinowski, W. Minor, *Methods Enzymol.* **1997**, *276*, 307–326.
- [56] *SIR92, Program for Automatic Solution of Crystal Structures by Direct Methods*: A. Altomare, G. Cascarano, C. Giacovazzo, A. Guagliardi, M. C. Burla, G. Polidori, M. Camalli, *J. Appl. Crystallogr.* **1994**, *27*, 435–435.
- [57] G. M. Sheldrick, *SHELXL97, Program for Crystal Structure Refinement from Diffraction Data*, University of Göttingen, Göttingen **1997**.

- [58] a) P. Táboršký, P. Lubal, J. Havel, J. Kotek, P. Hermann, I. Lukeš, *Collect. Czech. Chem. Commun.* **2005**, *70*, 1909–1942;
b) M. Försterová, I. Svobodová, P. Lubal, P. Táboršký, J. Kotek, P. Hermann, I. Lukeš, *Dalton Trans.* **2007**, 535–549.
- [59] J. C. Cobas, M. Martín-Pastor, Universidade de Santiago de Compostella, **2004**.
- [60] D. M. Corsi, C. Platas-Iglesias, H. van Bekkum, J. A. Peters, *Magn. Reson. Chem.* **2001**, *39*, 723–726.
- [61] M. Kývala, I. Lukeš, *Chemometrics '95*, Abstract book, Pardubice, Czech Republic, **1995**, p. 63; full version of OPIUM program package is available (free of charge) on <http://www.natur-cuni.cz/~kyvala/opium.html>.
- [62] *Scientist for Windows version 2.01*, Micromath Inc., Salt Lake City, UT, **1995**.
- [63] *HyperChem. Release 7.5 for Windows*, Molecular Modeling System, Hypercube Inc., Ontario, Canada, **2002**.

Received: August 25, 2008

Published Online: November 7, 2008

Bis(1,2,3-thiadiazole)s as Precursors in the Synthesis of Bis(alkynethiolate)gold(I) Derivatives

Elena Cerrada,^[a] Mariano Laguna,^{*[a]} and Nora Lardies^[a]

Keywords: S ligands / Gold / Phosphanes / Structure elucidation

The cleavage of bis(1,2,3-thiadiazole)s in the presence of strong bases in situ gives bis(alkynethiolate)s, which provide bis(alkynethiolate)gold(I) derivatives with the general formula $[\text{Au}_2(\text{S}-\text{C}\equiv\text{C}-\text{spacer}-\text{C}\equiv\text{C}-\text{S})\text{L}_2]$ (L = monophosphanes; spacer = none, 1,4- C_6H_4 , 1,3- C_6H_4 , 2,7- $\text{C}_{15}\text{H}_{12}$ and 3,5- $\text{C}_7\text{H}_7\text{N}$). The dinuclear structure was confirmed by X-ray diffraction studies of the complexes $(\text{PPN})_2[\text{Au}_2(\text{S}-\text{C}\equiv\text{C}-$

$\text{C}\equiv\text{C}-\text{S})(\text{C}_6\text{F}_5)_2]$ and $[\text{Au}_2\{3,5-(\text{S}-\text{C}\equiv\text{C})_2-\text{C}_7\text{H}_7\text{N}\}(\text{PPh}_3)_2]$ {PPN = bis(triphenylphosphane)iminium}. The use of diphosphanes gives complexes with higher nuclearity and cyclic structures.

(© Wiley-VCH Verlag GmbH & Co. KGaA, 69451 Weinheim, Germany, 2009)

Introduction

1,2,3-Thiadiazoles are heterocycles of great practical and theoretical interest.^[1] In particular, they are an important class of biologically active compounds,^[2–7] such as pharmacophores,^[8] as well as useful intermediates in organic synthesis.^[9] For example, 4,5-bis(substituted)-1,2,3-thiadiazoles were found to be active inhibitors of collagen-induced platelet aggregation in vitro^[10] and tested as potent anticancer reagents,^[11] some of the cephalosporin derivatives exhibit antimicrobial activity,^[12] biphenyl-substituted 1,2,3-thiadiazole show selective antibacterial activity against Gram-positive and Gram-negative bacteria^[13] and compounds with a terminal 1,2,3-thiadiazole moiety are antipsychotic agents.^[14] The ring cleavage of 1,2,3-thiadiazoles unsubstituted at the 5-position in the presence of strong bases (organolithium reagents, sodamide, sodium hydride and potassium *tert*-butoxide^[15,16]) gives rise to alkynethiolates. These species ($\text{R}-\text{C}\equiv\text{C}-\text{S}^-$) are known as important intermediates and can be used in further synthesis, for example, to prepare dendrimers^[17,18] or tetrathiafulvalenes^[19,20] and dithiole derivatives,^[21,22] which are excellent starting materials to build more complicated coordination solids. These basic building blocks have interesting optoelectronic properties (conductivity, magnetism or porous solid behaviour^[23]) that can be transmitted to the coordination solid to generate attractive materials from a biological, industrial or environmental point of view.^[24–27] Many methods have been developed for the synthesis of 1,2,3-thiadiazoles,^[28–30] of which the Hurd–Mori cyclisation of α -methylene ketones, firstly described in 1955,^[30] is the most convenient methodology.^[31–34]

Alkynethiolate metal complexes, such as the corresponding alkali metal salts of alkynethiolate and selenolate, have been known for some time. However, there are only a few examples of their transition-metal compounds, which, in particular, display quite versatile coordination behaviour. For example, several mononuclear alkynethiolate derivatives with these ligands acting as $\eta^1-(\text{S})$ bonded ligands have been described,^[35–42] some dinuclear complexes containing a sulfur alkynethiolate bridging group $\mu-(\text{S},\text{S})$ ^[43–49] and scarce examples with $\eta^1-(\text{C})$ ^[50] or $\eta^2-(\text{C},\text{C})$ ^[51–53] coordination, including the recent example of $\mu-\eta^2-(\text{C},\text{C})-\eta^2-(\text{S},\text{S})$ ^[54] binding of acetylenedithiolate. The presence of two alkynethiolate ends in the same ligand molecule and the coordination to two metallic centres is not represented in the literature. The synthesis of such bis(alkynethiolate) ligands can be afforded, as stated above, by the ring cleavage of 4-monosubstituted bis(1,2,3-thiadiazole)s with a base. Thus, in this paper, we report the preparation of bis(1,2,3-thiadiazole)s with the general formula 1,2,3-thiadiazole-spacer-1,2,3-thiadiazole (spacer = none, 1,4-benzene, 1,3-benzene, 9,9-dimethylfluorene and 2,6-dimethylpyridine) and the corresponding dinuclear bis(alkynethiolate)gold(I) derivatives with a $\eta^1-(\text{S})$ coordination. Higher nuclearities are also reported by using bis(diphenylphosphane)s as co-ligands, in particular, bis(diphenylphosphine)methane (dppm) or bis(diphenylphosphine)ethane (dppe), which gives rise to tetranuclear derivatives. Most of the synthesised derivatives display low crystallinity, which makes the isolation of suitable crystals for X-ray analysis difficult. However, in the case of $(\text{PPN})_2[\text{Au}_2(\text{S}-\text{C}\equiv\text{C}-\text{C}\equiv\text{C}-\text{S})(\text{C}_6\text{F}_5)_2]$ (**7**; PPN^+ = bis(triphenylphosphane)iminium) and $[\text{Au}_2\{3,5-(\text{S}-\text{C}\equiv\text{C})_2-\text{C}_7\text{H}_7\text{N}\}(\text{PPh}_3)_2]$ (**11a**), it was possible to determine the crystal structure, probably because of special features: the presence of unusual short $\pi-\pi$ stacking in the pentafluorophenyl rings in gold complexes in the latter

[a] Departamento de Química Inorgánica, Instituto de Ciencia de Materiales de Aragón, Universidad de Zaragoza – C. S. I. C., 50009 Zaragoza, Spain
E-mail: mlaguna@unizar.es

complex and short gold–gold contacts in the former. Although some organometallic compounds with $M-C_6F_5$ or $M-XC_6F_5$ ($X = N, S$) bonds that exhibit perfluoroaryl–perfluoroaryl $\pi-\pi$ stacking have been described, including with $M = Ni$,^[55] Pt ,^[56] Zn ,^[57–59] Ti ,^[60,61] Al and Ga ,^[62] no pentafluorophenyl gold derivatives have displayed this behaviour.

Results and Discussion

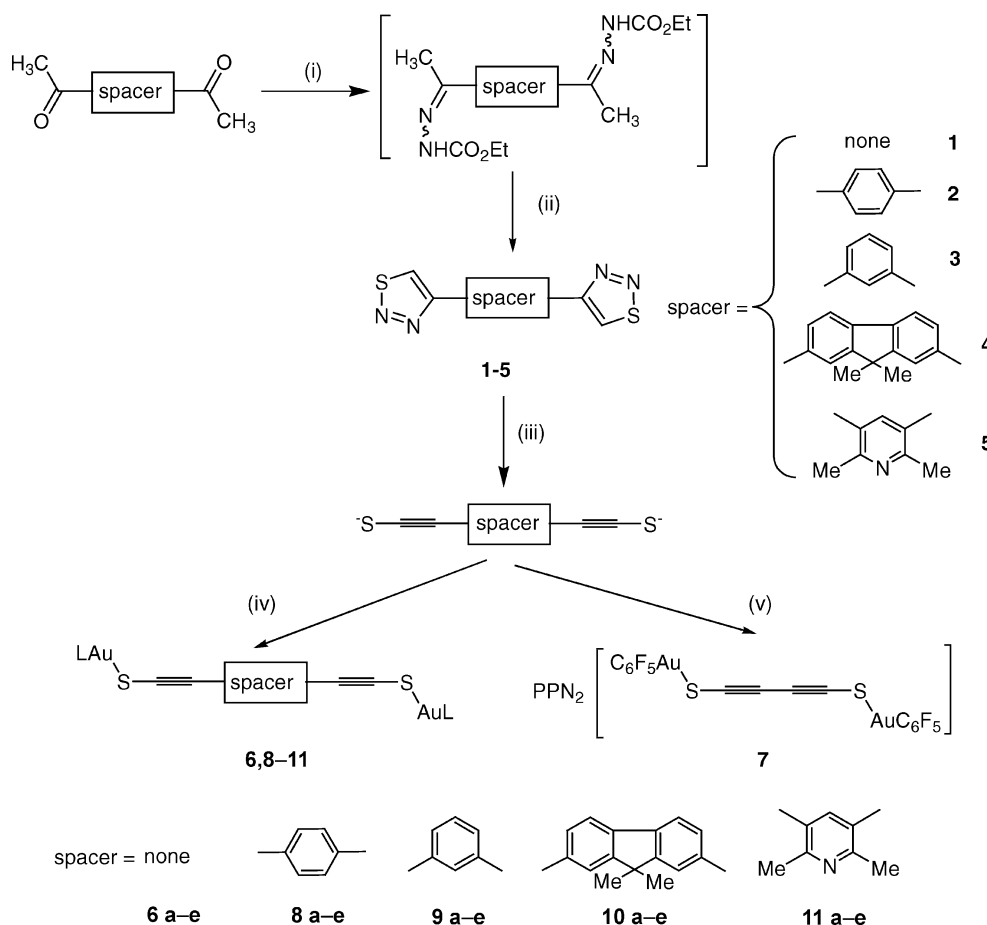
We synthesised five bis(1,2,3-thiadiazole)s derivatives (**1–5**) with two 1,2,3-thiadiazole rings in their skeleton separated by different spacers. The thiadiazoles **1–3** have been already reported by Meier et al.,^[63] their preparation involving the Hurd and Mori method with slight differences in the experimental workup. This method includes the cyclisation of α -methylene diketones in a two-step reaction. The diketones are first transformed into the corresponding *N*-acylhydrazones (which contain ethoxycarbonyl groups as good leaving groups) by using ethyl carbazate and a catalytic amount of *p*-toluenesulfonic acid in toluene. The second step involves the oxidative cyclisation of *N*-acylhydrazones with thionyl chloride, although no detailed mechanistic studies have been reported^[30] (Scheme 1). In

the case of 4,4'-bis(1,2,3-thiadiazolyl) (**1**), a few drops of concentrated hydrochloric acid and chloroform were used instead of *p*-toluenesulfonic acid and toluene to improve the yield.

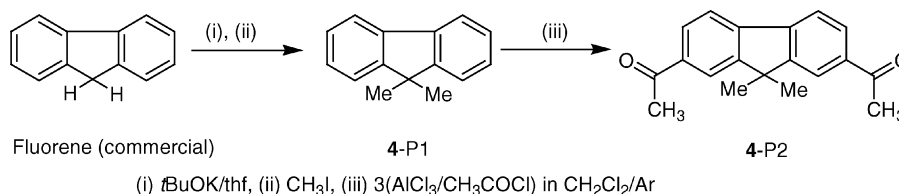
The spacers were chosen according to the commercial availability of the starting diketones and the properties of the final alkynylthiolate complexes such as solubility and ability to crystallise. Only the diketone starting material for the thiadiazole **4** was synthesised, as is shown in Scheme 2.

The mass spectra of the bis(1,2,3-thiadiazole)s show characteristic $[M-28]^+$ and $[M-56]^+$ ions arising from the loss of one or two nitrogen molecules, which shows the easy thiadiazole ring opening to give the corresponding alkynethiolates. The most noticeable feature in the 1H NMR spectra is the low-field signal observed for the proton in the thiadiazole ring (H_x) (Table 1).

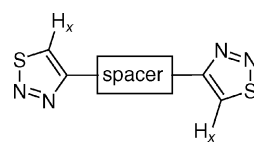
The decomposition of the bis(1,2,3-thiadiazole)s unsubstituted at the 5-position with 2 equiv. of a strong base, such as an organolithium reagent or *t*BuOK, causes cleavage of both the thiadiazole rings and the “in situ” formation of the bis(alkynethiolate) dianion. This anion is coordinated to two gold(I) metallic centres by addition of mononuclear complexes with the formula $[AuCIL]$ ($L = PPh_3, PPh_2Me$,



Scheme 1. General synthesis of bis(1,2,3-thiadiazole)s and bis(alkynethiolate)gold(I) complexes. (i) 2 $NH_2NHCOOEt$; (ii) $SOCl_2$; (iii) *t*BuOK in thf, 0 °C/Ar; (iv) $AuCIL$, $L = PPh_3$ (a), PPh_2Me (b), $PPhMe_2$ (c), PMe_3 (d), $AsPh_3$ (e); (v) $PPN[AuCl(C_6F_5)]$.



Scheme 2. Synthesis of 2,7-diacyetyl-9,9-dimethylfluorene (4-P2).

Table 1. ¹H NMR (H_x) data of bis(1,2,3-thiadiazole)s.


| Product | 1 | 2 | 3 | 4 | 5 |
|--------------------------|----------|----------|----------|----------|----------|
| δ(H _x) / ppm | 9.35 (s) | 8.74 (s) | 8.78 (s) | 8.73 (s) | 9.73 (s) |

PPhMe₂, PMe₃ and AsPh₃). PPN[AuCl(C₆F₅)] has been used because of the tendency of the C₆F₅ derivatives to crystallise readily (Scheme 1).

The presence of S–Au coordination in all the dinuclear alkynethiolate gold(I) complexes is shown by strong IR bands in the region 2025–2140 cm^{−1}, assignable to the C≡C stretching vibrational mode. The choice of the spacer fragment and the L ligand of the coordinated alkynethiolates does not affect ν_{C≡C} strongly; interestingly, the ν_{C≡C} values of the alkynethiolates without spacer shows a displacement to lower frequency by approximately 100 cm^{−1}. The ³¹P{¹H} NMR spectra exhibit a single resonance due to the equivalence of both phosphane molecules. The ¹H NMR spectroscopic data are consistent with their formulations, showing the corresponding signals for the phosphane and the spacer, which in the case of the 1,4-bis(alkynethiolate)-benzene (**8a–e**) appears as an A₂B₂ system. The poor solubility of all complexes did not allow us to measure ¹³C NMR spectra.

The use of PPN[AuCl(C₆F₅)] as starting material provides the bis(pentafluorophenyl)-bis(alkynethiolate)digold(I) derivative **7** without any spacer bridging both alkynethiolate groups. The ¹⁹F{¹H} NMR spectrum displays the three resonances characteristic of the C₆F₅ group for the *ortho*-, *meta*- and *para*-fluorine atoms. The structure of this dinuclear derivative was confirmed by an X-ray diffraction study, as was the crystalline structure of the bis(alkynethiolate) with 2,6-dimethylpyridine as the spacer group: [Au₂{μ-3,5-(S–C≡C)₂–C₇H₇N}(PPh₃)₂] (**11a**). The molecular structures of **7** and **11a** are depicted in Figures 1 and 3, respectively, and selected bond lengths and angles are summarised in Table 2. Crystallographic data are collected in Table 3.

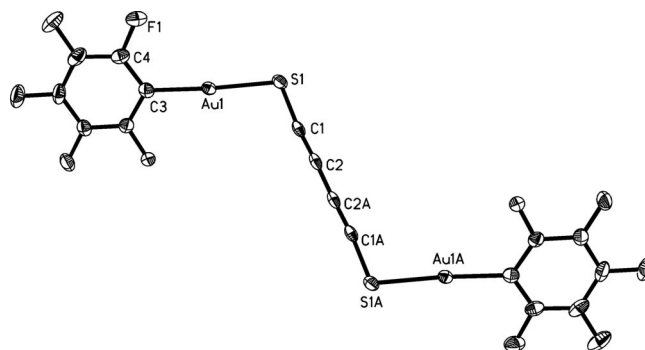


Figure 1. Molecular structure of the anion in **7**. Thermal ellipsoids are drawn at the 50% probability level. Selected bond lengths [Å] and angles [°]: Au(1)–C(3) 2.030(5), Au(1)–S(1) 2.3055(14), C(1)–C(2) 1.209(7), S(1)–C(1) 1.688(5), C(2)–C(2)#1 1.385(10), C(3)–Au(1)–S(1) 176.42(14), C(1)–S(1)–Au(1) 106.71(16), C(4)–C(3)–Au(1) 122.5(4), C(8)–C(3)–Au(1) 123.0(4), C(4)–C(3)–C(8) 114.4(5), C(2)–C(1)–S(1) 174.6(4), C(1)–C(2)–C(2)#1 177.4(6). Symmetry relations #1 = −*x* + 2, −*y*, −*z* + 1.

Complex **7** crystallises in the triclinic space group *P* $\bar{1}$ with half an anion in the asymmetric unit exhibiting a crystallographic centre of symmetry (Figure 1). Two Au–C₆F₅ fragments are bridged by the bis(alkynethiolate) unit. The most interesting feature in the structure is the presence of a close linear chain of six atoms, two sulfur and four carbon atoms, with angles of 174.6(4)° (S1–C1–C2) and 177.4(6)° (C1–C2–C2A). To date, there are only examples of cyclic structures {cyclic bis(1,3-butadiyne)s},^[64,65] determined by X-ray diffraction, with the same linear chain, and there are no examples of such a linear chain coordinated to a metal centre. The carbon chain shows an alternating short/long/short arrangement of C–C separations of 1.209(7) and 1.385(10) Å, corresponding to the conjugated 1,3-diyne (–C≡C–C≡C–) with no delocalisation of the π-electron density. These values may be compared with those found in the butadiyne molecule [1.217(1), 1.383(1) Å; strictly linear] and in bis(acetylide)gold complexes [Au(C≡C–C≡CH)(PPh₃)₂] [1.204(7), 1.379(7), 1.190(8) Å]^[66] and [Au₂–(C≡C–C≡C)(PR₃)₂] {PR₃ = PCy₃ [1.199(8), 1.37(1) Å],^[67] P(tol)₃ [1.18(2), 1.38(2) Å]}.^[68] The coordination around the metallic centre is nearly linear [S1–Au1–C3, 176.36(14)°], and the Au–C and Au–S distances [2.030(5) and 2.3055(14) Å, respectively] are in the same range as those observed in pentafluorophenyl and thiolate gold(I)

Table 2. Bond lengths [\AA] and angles [$^\circ$] for $[\text{Au}_2\{\mu\text{-}3,5\text{-(S-C}\equiv\text{C)}_2\text{-C}_7\text{H}_7\text{N}\}(\text{PPh}_3)_2]$ (**11a**).^[a]

| | |
|--------------------|------------|
| Au(1)–P(1) | 2.234(7) |
| Au(1)–S(1) | 2.316(6) |
| Au(1)–Au(2)#1 | 3.0577(15) |
| Au(2)–P(2) | 2.238(7) |
| Au(2)–S(2) | 2.313(7) |
| Au(2)–Au(1)#2 | 3.0577(15) |
| S(2)–C(11) | 1.72(3) |
| S(1)–C(1) | 1.75(3) |
| C(1)–C(2) | 1.20(3) |
| C(10)–C(11) | 1.19(3) |
| P(1)–Au(1)–S(1) | 171.8(2) |
| P(1)–Au(1)–Au(2)#1 | 102.64(17) |
| S(1)–Au(1)–Au(2)#1 | 84.44(17) |
| P(2)–Au(2)–S(2) | 170.9(2) |
| P(2)–Au(2)–Au(1)#2 | 104.44(17) |
| S(2)–Au(2)–Au(1)#2 | 84.11(17) |
| C(11)–S(2)–Au(2) | 95.4(9) |
| C(1)–S(1)–Au(1) | 94.6(8) |
| C(12)–P(1)–Au(1) | 113.7(9) |
| C(18)–P(1)–Au(1) | 113.5(8) |
| C(24)–P(1)–Au(1) | 110.3(8) |
| C(36)–P(2)–Au(2) | 113.7(9) |
| C(30)–P(2)–Au(2) | 114.6(8) |
| C(42)–P(2)–Au(2) | 109.2(9) |
| C(2)–C(1)–S(1) | 180(3) |
| C(10)–C(11)–S(2) | 174(2) |
| Au(1)–P(1) | 2.234(7) |
| Au(1)–S(1) | 2.316(6) |
| Au(1)–Au(2)#1 | 3.0577(15) |
| Au(2)–P(2) | 2.238(7) |
| Au(2)–S(2) | 2.313(7) |
| Au(2)–Au(1)#2 | 3.0577(15) |
| S(2)–C(11) | 1.72(3) |
| S(1)–C(1) | 1.75(3) |
| C(1)–C(2) | 1.20(3) |
| C(10)–C(11) | 1.19(3) |
| P(1)–Au(1)–S(1) | 171.8(2) |
| P(1)–Au(1)–Au(2)#1 | 102.64(17) |
| S(1)–Au(1)–Au(2)#1 | 84.44(17) |
| P(2)–Au(2)–S(2) | 170.9(2) |
| P(2)–Au(2)–Au(1)#2 | 104.44(17) |
| S(2)–Au(2)–Au(1)#2 | 84.11(17) |
| C(11)–S(2)–Au(2) | 95.4(9) |
| C(1)–S(1)–Au(1) | 94.6(8) |
| C(12)–P(1)–Au(1) | 113.7(9) |
| C(18)–P(1)–Au(1) | 113.5(8) |
| C(24)–P(1)–Au(1) | 110.3(8) |
| C(36)–P(2)–Au(2) | 113.7(9) |
| C(30)–P(2)–Au(2) | 114.6(8) |
| C(42)–P(2)–Au(2) | 109.2(9) |
| C(2)–C(1)–S(1) | 180(3) |
| C(10)–C(11)–S(2) | 174(2) |

[a] Symmetry relations #1 = $-x + 2/3, y - 1/2, -z + 1/2$; #2 = $-x + 3/2, y + 1/2, -z + 1/2$.

complexes.^[69–71] Additionally, the unit cell (Figure 2) shows that packing of individual anions is influenced by very long pentafluorophenyl rings interactions (closest centroid...centroid distances of 4.122 \AA , interplanar angle of 0°, perpendicular distances of 3.304 \AA with slippage of 2.464 \AA). Although we cannot consider strictly the presence of π – π interactions, these distances are the closest ones, to best of our knowledge, reported in pentafluorophenyl gold chemistry.^[72]

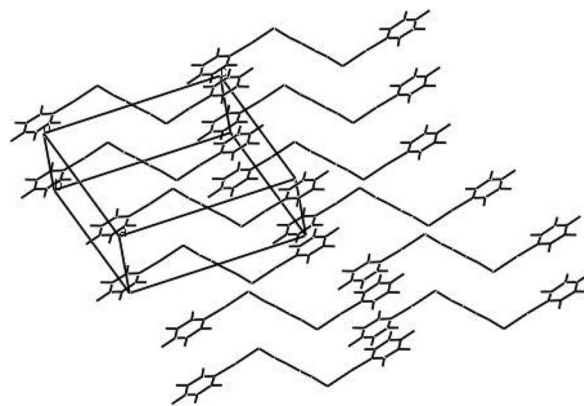


Figure 2. View of the packing in the unit cell of **7**. The cation has been omitted for clarity.

Compound **11a** crystallises with two dichloromethane solvent molecules, one of them disordered. The molecule consists on two AuPPh_3 units coordinated to the bis(alkynethiolate) unit. The C–S–Au angles are oddly smaller than those of complex **7** [C1–S1–Au1 94.6(8)° and C11–S2–Au2 95.4(9)°], probably because of the up and down disposition of both fragments with respect to the dimethylpyridine ring. Such a disposition permits short intermolecular Au...Au interactions of 3.0577(15) \AA , which is shorter than the sum of the van der Waals radii (3.60 \AA) (Figures 3 and 4). The Au–P and Au–S bond lengths [Au1–P1 2.234(7), Au2–P2 2.238(7) \AA and Au1–S1 2.316(6), Au2–S2, 2.313(7) \AA] are characteristic for gold(I) complexes with thiolate and phosphane ligands.^[73–78]

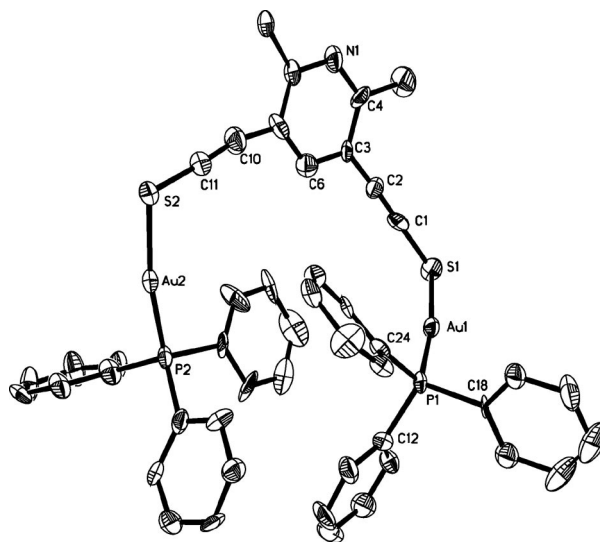


Figure 3. The structure of complex **11a**. Thermal ellipsoids are drawn at the 50% probability level, and H atoms have been omitted for clarity.

The geometric parameters of the alkynethiolate ligands in **11a** are normal. Thus, the C≡C distances of 1.19(3) and 1.20(3) \AA fall in the range for carbon–carbon triple bonds and both the S–C–C and C–C–C angles are practically linear [S1–C1–C2 180(3)°, S2–C10–C11 174(2)°, C1–C2–C3

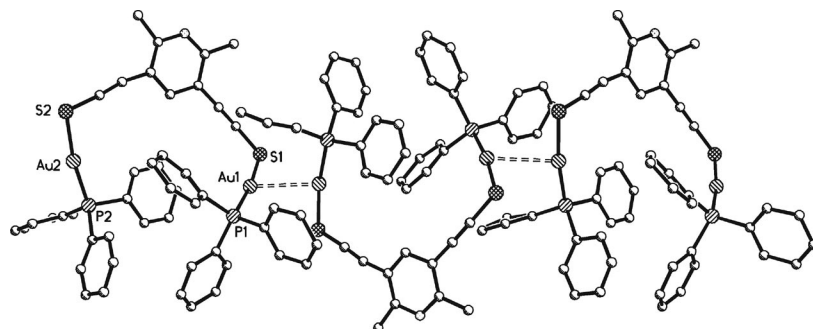
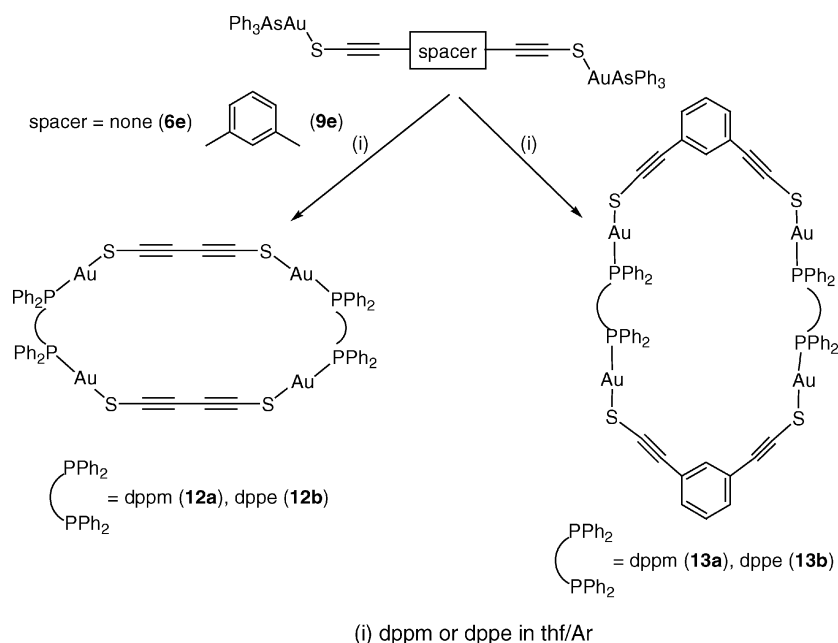


Figure 4. View of the intermolecular gold-gold interactions in **11a**.

175(3)°, C9–C10–C11 166(3)°]. These distances are quite similar to those found in other alkynethiolate derivatives: [CpRu(PPh₃)₂(SC≡CR)] (1.209 Å on average),^[36] [Pt(PPh₃)₂(SC≡CCR)₂] (R = Me, *t*Bu; 1.17 Å on average),^[40,79] [Fe₂(CO)₆(μ-C≡CPh)(μ-SC≡CPh)],^[48] [Ti(η⁵-C₅H₄SiMe₃)₂(SC≡C*t*Bu)₂] [1.144(14) Å],^[80] [TiCp₂(XC≡CPh)] (Cp = C₅H₅, MeC₅H₄; X = S, Se) [1.188(8) Å],^[81] [Au(XC≡C–S)–PPh₃]^[42] [X = *p*-CH₃–C₆H₄ 1.205(6); X = 3-C₄H₃S 1.174(13) and 1.223(13) Å], PPN[Au(*p*-CH₃–C₆H₄–C≡C–S)(C₆F₅)] [1.173(7) Å].^[42]

Attempts to obtain tetranuclear complexes with dppe and dppm ligands were unsuccessful with the corresponding dinuclear gold(I) derivative [Au₂Cl₂(PP)] (PP = dppe or dppm) as starting material. Therefore, we used as an alternative route the addition of the free diphosphane dppe or dppe to the corresponding alkynethiolate complex with the facile leaving group triphenylarsine. This method affords complexes **12a**, **12b**, **13a** and **13b** (Scheme 3). The complex [Au₂(S–C≡C–C≡C–S)(AsPPh₃)₂] (**6e**) needs to be prepared freshly to be used as a starting material because of fast decomposition even at low temperature; however, the prod-

ucts of the corresponding reaction, **12a** and **12b**, are stable even at room temperature. The shift to low frequencies of the ν_{C≡C} bands in the IR spectra of the bis(alkynethiolate) complexes with the monodentate phosphanes is now more noticeable, especially for complex **12a**, which has the lowest frequency value in the series. The ³¹P{¹H} NMR spectra display single peaks assigned to the diphosphane, and the ¹H NMR spectra show signals for the methylene group at δ = 3–4 ppm for the dppe complexes and at δ ≈ 2 ppm for the dppm derivatives. Only in the case of complex **13a** does the LSIMS⁺ mass spectrum display a molecular peak at *m/z* = 1935, and peaks arising from fragmentation products are observed in other cases. Unfortunately, crystals suitable for an X-ray analysis have not yet been obtained, but according to the spectroscopic data we suggest a tetranuclear cyclic structure (Scheme 3) closely related to that of *cyclo*-[Au₂(μ-C≡CC≡C)(μ-dppm)₂]₂, proposed previously by Bruce et al.,^[66] however, there is a difference in the angle around the metallic centre, since, in our case, there are additional S atoms, which provide typical C–S–Au angles of approximately 106°.



Scheme 3. Synthesis of tetra(alkynethiolate)gold(I) complexes **12a,b** and **13a,b**.

In summary, a family of bis(alkynethiolate) dinuclear gold(I) derivatives has been synthesised by the “in situ” preparation of the bis(alkynethiolate) dianions by ring cleavage of bis(1,2,3-thiadiazole)s in the presence of strong bases. The general structure of such derivatives consists of a spacer molecule, which bridges the two alkynethiolate units that in the cases of $(\text{PPN})_2[\text{Au}_2(\text{S}-\text{C}\equiv\text{C}-\text{C}\equiv\text{C}-\text{S})-(\text{C}_6\text{F}_5)_2]$ (**7**) and $[\text{Au}_2\{3,5-(\text{S}-\text{C}\equiv\text{C})_2-\text{C}_7\text{H}_7\text{N}\}(\text{PPh}_3)_2]$ (**11a**) was confirmed by X-ray crystal analysis. Higher nuclearities have been obtained by using the bis(diphenylphosphane)s dppm and dppe, which permits the isolation of tetranuclear derivatives.

Experimental Section

General Comments: All reactions and product manipulations were performed under an atmosphere of argon by using standard Schlenk techniques. Tetrahydrofuran was dried with and distilled from Na. NMR spectra were recorded on a Varian Gemini 300 MHz or a Bruker ARX 400 MHz spectrometer. IR spectra were measured with a Perkin–Elmer 883 or a Perkin–Elmer FT-IR Spectrum One spectrometer with samples as KBr pellets. Mass spectra were obtained with a VG Autospec mass spectrometer operating in electron impact (EI) mode and liquid secondary-ion mass spectrometry (LSIMS) mode. Elemental compositions were analysed with a Perkin–Elmer 2400B instrument. $[\text{AuClL}]$ ($\text{L} = \text{PPh}_3$, PPh_2Me , PPhMe_2 , PMe_3) complexes were prepared by replacement of tht in $[\text{AuCl}(\text{tht})]^{[82]}$ (tht = tetrahydrothiophene) by equimolecular addition of the ligand. $[\text{AuCl}(\text{AsPh}_3)]^{[83]}$ and $[\text{AuCl}(\text{C}_6\text{F}_5)]$ -PPN $^{[84]}$ were synthesised by literature procedures.

Synthesis of 4,4'-bi(1,2,3-thiadiazolyl) (1): 2,3-Butanedione (2.15 g, 25 mmol) and ethylcarbazate (6.51 g, 62.5 mmol) were dissolved in chloroform (150 mL), with some drops of concentrated hydrochloric acid, in a Dean–Stark apparatus. The solution was heated at reflux until no more water condensed (ca. 10 h). The reaction mixture was cooled to room temperature, and a white precipitate formed, was collected and washed with diethyl ether. The precipitate was cooled on a water–ice bath, and SOCl_2 (22 mL) was added dropwise. The water–ice bath was removed, with precaution because of the HCl gas evolved, and the solution was allowed to warm to room temperature and left to stand overnight. Residual SOCl_2 was evaporated in vacuo. The residue was collected by filtration and washed with diethyl ether and toluene to afford the product as a brown solid (4.17 g, 98%). ^1H NMR (CDCl_3): $\delta = 9.35$ (s), MS (EI): m/z (%) = 170 (9) $[\text{M}]^+$, 114 (17) $[\text{M} - 4\text{N}]^+$, 69 (100) $[\text{M} - 4\text{N} - \text{S} - \text{C}]^+$. $\text{C}_4\text{H}_2\text{N}_4\text{S}_2$ (170.24): calcd. C 28.28, H 1.22, N 32.90, S 37.70; found C 28.65, H 1.24, N 32.90, S 37.28.

Synthesis of 1,4-Bis(1,2,3-thiadiazol-4-yl)benzene (2): 1,4-diacetylbenzene (8.11 g, 50 mmol) and ethylcarbazate (10.41 g, 100 mmol) were dissolved in toluene (200 mL), with a catalytic amount of *p*-toluenesulfonic acid, in a Dean Stark apparatus. The solution was heated at reflux (ca. 8 h). The solvent was evaporated under vacuum and after cooling on a water–ice bath, SOCl_2 (50 mL) was added dropwise. The water–ice bath was removed, and the solution was allowed to warm to room temperature and was kept overnight. Residual SOCl_2 was evaporated in vacuo. The residue was collected and washed with diethyl ether and toluene. Recrystallisation from dimethylsulfoxide gave a brown solid (11.09 g, 90%). ^1H NMR (CDCl_3): $\delta = 8.74$ (s, 2 H), 8.21 (s, 4 H) ppm. MS (EI): m/z (%) = 216 (33) $[\text{M} - 2\text{N}]^+$, 193 (100) $[\text{M} - 4\text{N}]^+$, 147 (46) $[\text{M} - 4\text{N} - \text{S} - \text{C}]^+$. $\text{C}_{10}\text{H}_6\text{N}_4\text{S}_2$ (246.34): calcd. C

48.77, H 2.46, N 22.75, S 26.04; found C 49.00, H 2.42, N 22.65, S 26.03.

Synthesis of 1,3-Bis(1,2,3-thiadiazol-4-yl)benzene (3): This compound was prepared by a procedure similar to that of **2** but by using 1,3-diacetylbenzene (8.11 g, 50 mmol). After SOCl_2 was evaporated, the residue was dissolved in thf and filtered through silica and active carbon. The resulting solution was washed with aqueous Na_2CO_3 and dried with anhydrous MgSO_4 . The solvent was evaporated in vacuo, and diethyl ether was added to precipitate the compound as a yellow solid, which was collected by filtration. Recrystallisation was achieved from dimethyl sulfoxide or a mixture of CH_2Cl_2 and diethyl ether (9.85 g, 80%). ^1H NMR (CDCl_3): $\delta = 8.78$ (s, 2 H), 8.75 (t, $J = 1.5$ Hz, 1 H), 8.13 (dd, $J = 7.8$, 1.8 Hz, 2 H), 7.66 (t, $J = 7.8$ Hz, 1 H) ppm. MS (EI): m/z (%) = 246 (9) $[\text{M}]^+$, 218 (46) $[\text{M} - 2\text{N}]^+$, 190 (100) $[\text{M} - 4\text{N}]^+$. $\text{C}_{10}\text{H}_6\text{N}_4\text{S}_2$ (246.34): calcd. C 48.77, H 2.46, N 22.75, S 26.04; found C 48.89, H 2.36, N 22.80, S 25.95.

Synthesis of 9,9-Dimethylfluorene (4-P1): To an ice-cooled solution of fluorene (5.0 g, 30 mmol) in dry thf (30 mL) under an argon atmosphere was added *t*BuOK (7.43 g, 66 mmol), and the solution was stirred at room temperature for 1.5 h. CH_3I (3.74 mL, 60 mmol) was added, and a white precipitate of KI formed. The reaction mixture was stirred for a further 2 h. KI was then removed by filtration, and evaporation of thf afforded the product as a yellow solid (5.60 g, 96%). ^1H NMR (CDCl_3): $\delta = 7.73$ –7.70 (m, 2 H), 7.40–7.41 (m, 2 H), 7.36–7.30 (m, 4 H), 1.48 (s, 6 H) ppm. MS (LSIMS $^+$): m/z (%) = 194 (100) $[\text{M}]^+$, 179 (98) $[\text{M} - \text{CH}_3]^+$. $\text{C}_{15}\text{H}_{14}$ (194.29): calcd. C 92.78, H 6.70; found C 92.42, H 6.80.

Synthesis of 2,7-Diacetyl-9,9-dimethylfluorene (4-P2): To an ice-cooled solution of 9,9-dimethylfluorene 4-P1 (2.0 g, 10.3 mmol) in dry dichloromethane (15 mL) under an argon atmosphere was added dropwise a solution of AlCl_3 (4.12 g, 31 mmol) and acetyl chloride (2.2 mL, 31 mmol) in dry dichloromethane (20 mL) (Friedel–Crafts conditions). The reaction mixture was stirred overnight at room temperature, washed with water and dried with MgSO_4 . The solvent was removed in vacuo to afford the product as a yellow solid (2.29 g, 80%). ^1H NMR (CDCl_3): $\delta = 8.37$ –7.86 (m, 6 H), 2.68 (s, 6 H), 1.54 (s, 6 H) ppm. IR (KBr): $\tilde{\nu} = 1166$ [$\nu(\text{CO})$] cm^{-1} . MS (EI): m/z (%) = 278 (52) $[\text{M}]^+$, 263 (100) $[\text{M} - \text{CH}_3]^+$, 176 (33). $\text{C}_{19}\text{H}_{18}\text{O}_2$ (278.33): calcd. C 81.98, H 6.47; found C 81.51, H 5.99.

Synthesis of 2,7-Bis(1,2,3-thiadiazol-4-yl)-9,9-dimethylfluorene (4): This complex was prepared by a procedure similar to that of **2** but by using 2,7-diacetyl-9,9-dimethylfluorene 4-P2 (13.8 g, 50 mmol). After SOCl_2 was evaporated, the residue was dissolved in dichloromethane, filtered through silica and active carbon, washed with water and dried (MgSO_4). The solvent was eliminated in vacuo, and diethyl ether was added to precipitate the compound as a brown solid (10.87 g, 60%). ^1H NMR (CDCl_3): $\delta = 8.73$ (s, 2 H), 8.30 (s, 2 H), 8.05 (d, $J_{\text{AB}} = 7.8$ Hz, 2 H), 7.95 (d, $J_{\text{AB}} = 7.8$ Hz, 2 H), 1.63 (s, 6 H) ppm. MS (EI): m/z (%) = 362 (17) $[\text{M}]^+$, 334 (27) $[\text{M} - 2\text{N}]^+$, 306 (62) $[\text{M} - 4\text{N}]^+$, 291 (100) $[\text{M} - 4\text{N} - \text{CH}_3]^+$, 277 (53) $[\text{M} - 4\text{N} - 2\text{CH}_3]^+$. $\text{C}_{19}\text{H}_{14}\text{N}_4\text{S}_2$ (362.44): calcd. C 62.98, H 3.87, N 15.47, S 17.68; found C 62.62, H 3.93, N 15.81, S 17.59.

Synthesis of 3,5-Bis(1,2,3-thiadiazol-4-yl)-2,6-dimethylpyridine (5): This complex was prepared by a procedure similar to that of **2** but by using 3,5-diacetyl-2,6-dimethylpyridine (9.61 g, 50 mmol). After SOCl_2 was evaporated, the residue was washed with water and diethyl ether, dried with MgSO_4 and then filtered to afford the product as a pale brown solid (13.63 g, 99%). ^1H NMR (CDCl_3): $\delta = 9.73$ (s, 2 H), 8.81 (s, 1 H), 2.86 (s, 6 H) ppm. MS (EI): m/z (%) = 275 (9) $[\text{M}]^+$, 247 (57) $[\text{M} - 2\text{N}]^+$, 218 (100) $[\text{M} - 4\text{N}]^+$, 204 (7) $[\text{M} - 4\text{N} - \text{CH}_3]^+$, 186 (31) $[\text{M} - 4\text{N} - 2\text{CH}_3]^+$. $\text{C}_{11}\text{H}_9\text{N}_5\text{S}_2$ (275.37):

calcd. C 48.00, H 3.27, N 20.36, S 23.32; found C 47.65, H 2.99, N 20.02, S 22.89.

Synthesis of $[\text{Au}_2(\text{S}-\text{C}\equiv\text{C}-\text{C}\equiv\text{C}-\text{S})\text{L}_2]$ $\{\text{L} = \text{PPh}_3$ (6a**), PPh_2Me (**6b**), PPhMe_2 (**6c**), PMe_3 (**6d**), AsPh_3 (**6e**):** To an ice-cooled solution of 4,4'-bis(1,2,3-thiadiazolyl) **1** (85 mg, 0.5 mmol) in dry thf (25 mL) was added *t*BuOK (123 mg, 1.1 mmol). The mixture was stirred under an argon atmosphere for 1 h, and then $[\text{AuCl}(\text{PPh}_3)]$ (396 mg, 0.8 mmol), $[\text{AuCl}(\text{AsPh}_3)]$ (431 mg, 0.8 mmol), $[\text{AuCl}(\text{PPh}_2\text{Me})]$ (346 mg, 0.8 mmol), $[\text{AuCl}(\text{PPhMe}_2)]$ (296 mg, 0.8 mmol) or $[\text{AuCl}(\text{PMe}_3)]$ (247 mg, 0.8 mmol) was added. The mixture was stirred for a further 6 h. The resulting solution was then filtered through Celite to eliminate KCl. The solvent was evaporated under vacuum to a volume of 5 mL, and hexane (30 mL) was added to precipitate the corresponding product, which was filtered off. **6a**: grey solid (268 mg, 52%). ^1H NMR: $\delta = 7.55\text{--}7.49$ (m) ppm. $^{31}\text{P}\{^1\text{H}\}$ NMR (CDCl_3): $\delta = 37.6$ (s) ppm. IR (KBr): $\tilde{\nu} = 2059$ [$\nu(\text{C}\equiv\text{C})$] cm^{-1} . MS (LSIMS $^+$): m/z (%) = 1227 (67) [$\text{M} + \text{Au}$] $^+$, 459 (17), $[\text{AuPPh}_3]^+$, 393 (100). $\text{C}_{40}\text{H}_{30}\text{Au}_2\text{P}_2\text{S}_2$ (1030.76): calcd. C 46.65, H 2.95, S 6.20; found C 46.81, H 3.35, S 5.99. **6b**: yellow solid (199 mg, 44%). ^1H NMR (CDCl_3): $\delta = 7.71\text{--}7.65$ (m, 8 H), 7.43–7.40 (m, 12 H), 2.07 (d, $J = 7.2$ Hz, 6 H) ppm. $^{31}\text{P}\{^1\text{H}\}$ NMR (CDCl_3): $\delta = 21.7$ (s) ppm. IR (KBr): $\tilde{\nu} = 2051$ [$\nu(\text{C}\equiv\text{C})$] cm^{-1} . MS (LSIMS $^+$): m/z (%) = 1222 (19), 906 (5) [M^+], 597 (73), 397 (100) $[\text{AuPPh}_2\text{Me}]^+$. $\text{C}_{30}\text{H}_{26}\text{Au}_2\text{P}_2\text{S}_2$ (906.62): calcd. C 39.75, H 2.95, S 7.15; found C 40.06, H 2.86, S 7.46. **6c**: yellow solid (90 mg, 23%). ^1H NMR (CDCl_3): $\delta = 7.76\text{--}7.69$ (m, 5 H), 7.53–7.50 (m, 5 H), 1.86 (d, $J = 10.7$ Hz, 12 H) ppm. $^{31}\text{P}\{^1\text{H}\}$ NMR (CDCl_3): $\delta = 3.9$ (s) ppm. IR (KBr): $\tilde{\nu} = 2050$ [$\nu(\text{C}\equiv\text{C})$] cm^{-1} . MS (LSIMS $^+$): m/z (%) = 1037 (59), 782 (40) [M^+], 473 (100) $[\text{Au}(\text{PPhMe}_2)_2]^+$. $\text{C}_{20}\text{H}_{22}\text{Au}_2\text{P}_2\text{S}_2$ (782.48): calcd. C 30.70, H 2.84, S 8.20; found C 30.31, H 2.86, S 7.76. **6d**: grey solid (306 mg, 93%). ^1H NMR (CDCl_3): $\delta = 1.60$ (d, $J = 11.8$ Hz) ppm. $^{31}\text{P}\{^1\text{H}\}$ NMR (CDCl_3): $\delta = -0.8$ (s) ppm. IR (KBr): $\tilde{\nu} = 2049$ [$\nu(\text{C}\equiv\text{C})$] cm^{-1} . MS (LSIMS $^+$): m/z (%) = 851 (100) $[\text{S}(\text{AuPMe}_3)_3]^+$, 775 (41), 658 (18) [M^+]. $\text{C}_{10}\text{H}_{18}\text{Au}_2\text{P}_2\text{S}_2$ (658.32): calcd. C 18.24, H 2.74, S 9.73; found C 17.89, H 2.38, S 10.17. **6e**: yellow solid (296 mg, 53%). ^1H NMR (CDCl_3): $\delta = 7.36\text{--}7.24$ (m) ppm. IR (KBr): $\tilde{\nu} = 2053$ [$\nu(\text{C}\equiv\text{C})$] cm^{-1} . MS (LSIMS $^+$): m/z (%) = 1541 (36), 1118 (15) [M^+], 809 (100) $[\text{Au}(\text{AsPh}_3)_2]^+$, 503 (61). $\text{C}_{40}\text{H}_{30}\text{As}_2\text{Au}_2\text{S}_2$ (1118.66): calcd. C 43.00, H 2.70, S 5.72; found C 42.61, H 2.30, S 5.43.

Synthesis of $(\text{PPN})_2[\text{Au}_2(\text{S}-\text{C}\equiv\text{C}-\text{C}\equiv\text{C}-\text{S})(\text{C}_6\text{F}_5)_2]$ (7**):** This complex was prepared by a procedure similar to that of **6** but by using $\text{PPN}[\text{AuCl}(\text{C}_6\text{F}_5)]$ (750 mg, 0.8 mmol). Brown solid (671 mg, 70%). ^1H NMR (CDCl_3): $\delta = 7.64\text{--}7.47$ (m) ppm. $^{19}\text{F}\{^1\text{H}\}$ NMR (CDCl_3): $\delta = -116.8$ (s, F_o), -164.9 (s, F_p), -166.1 (s, F_m) ppm. IR (KBr): $\tilde{\nu} = 2045$ [$\nu(\text{C}\equiv\text{C})$] cm^{-1} . $\text{C}_{88}\text{H}_{60}\text{Au}_2\text{F}_{10}\text{N}_2\text{P}_4\text{S}_2$ (1917.17): calcd. C 55.08, H 3.13, N 1.46, S 3.34; found C 54.89, H 2.75, N 1.80, S 2.86.

Synthesis of $[\text{Au}_2(1,4)\text{-(S}-\text{C}\equiv\text{C}-\text{C}_6\text{H}_4-\text{C}\equiv\text{C}-\text{S})\text{L}_2]$ $\{\text{L} = \text{PPh}_3$ (8a**), PPh_2Me (**8b**), AsPh_3 (**8e**):** A solution of 1,4-bis(1,2,3-thiadiazol-4-yl)benzene **2** (123 mg, 0.5 mmol) in dry thf (20 mL) under an argon atmosphere was cooled to -78°C , and *n*BuLi (2 mL) in hexane (0.55 mL, 1.1 mmol) was added. The mixture was allowed to reach room temperature over 0.5 h. $[\text{AuCl}(\text{PPh}_3)]$ (495 mg, 1 mmol), $[\text{AuCl}(\text{AsPh}_3)]$ (538 mg, 1 mmol) or $[\text{AuCl}(\text{PPh}_2\text{Me})]$ (433 mg, 1 mmol) was then added. The mixture was stirred for a further 8 h, and the solvent was then evaporated in vacuo. The residue was dissolved in dichloromethane, and some drops of water were added to eliminate LiCl. Thereafter, anhydrous MgSO_4 was added, and the solution was then filtered through Celite. The solvent was evaporated under vacuum to 6 mL, and hexane (25 mL) was added to precipitate the

corresponding compound. **8a**: yellow solid (343 mg, 62%). ^1H NMR (CDCl_3): $\delta = 7.55\text{--}7.43$ (m, 30 H), 7.19 (4 H, A_2B_2) ppm. $^{31}\text{P}\{^1\text{H}\}$ NMR (CDCl_3): $\delta = 37.1$ (s) ppm. IR (KBr): $\tilde{\nu} = 2144$ [$\nu(\text{C}\equiv\text{C})$] cm^{-1} . MS (LSIMS $^+$): m/z (%) = 1409 (81), 1147 (16), 1107 (2) [M^+], 721 (46), 567 (55), 459 (100) $[\text{AuPPh}_3]^+$. $\text{C}_{46}\text{H}_{34}\text{Au}_2\text{P}_2\text{S}_2$ (1106.86): calcd. C 49.92, H 3.10, S 5.79; found C 50.30, H 3.22, S 5.81. **8b**: orange solid (368 mg, 75%). ^1H NMR (CDCl_3): $\delta = 7.62\text{--}7.32$ (m, 20 H), 7.21 (4 H, A_2B_2), 2.09 (d, $J = 9.3$ Hz, 6 H) ppm. $^{31}\text{P}\{^1\text{H}\}$ NMR (CDCl_3): $\delta = 22.5$ (s) ppm. IR (KBr): $\tilde{\nu} = 2141$ [$\nu(\text{C}\equiv\text{C})$] cm^{-1} . MS (LSIMS $^+$): m/z (%) = 1023 (28), 984 (22) [$\text{M} + \text{H}$] $^+$, 620 (38), 598 (21), 398 (84), 374 (100). $\text{C}_{36}\text{H}_{30}\text{Au}_2\text{P}_2\text{S}_2$ (982.45): calcd. C 43.97, H 3.05, S 6.51; found C 43.99, H 3.08, S 6.50. **8e**: yellow solid (430 mg, 72%). ^1H NMR (CDCl_3): $\delta = 7.44\text{--}7.23$ (m, 30 H), 7.21 (4 H, A_2B_2) ppm. IR (KBr): $\tilde{\nu} = 2143$ [$\nu(\text{C}\equiv\text{C})$] cm^{-1} . MS (LSIMS $^+$): m/z (%) = 1187 (17), 809 (64), 785 (31), 653 (18), 503 (18), 381 (100) $[\text{As}_2\text{Ph}_3]^+$. $\text{C}_{46}\text{H}_{34}\text{As}_2\text{Au}_2\text{S}_2$ (1194.76): calcd. C 46.24, H 2.87, S 5.38; found C 45.91, H 2.97, S 4.98.

Synthesis of $[\text{Au}_2(1,4)\text{-(S}-\text{C}\equiv\text{C}-\text{C}_6\text{H}_4-\text{C}\equiv\text{C}-\text{S})\text{L}_2]$ $\{\text{L} = \text{PPhMe}_2$ (8c**), PMe_3 (**8d**):** To an ice-cooled solution of 1,4-bis(1,2,3-thiadiazol-4-yl)benzene **2** (123 mg, 0.5 mmol) in dry thf (20 mL) was added *t*BuOK (123 mg, 1.1 mmol). The mixture was stirred under an argon atmosphere for 1 h, and then $[\text{AuCl}(\text{PPhMe}_2)]$ (296 mg, 0.8 mmol) or $[\text{AuCl}(\text{PMe}_3)]$ (247 mg, 0.8 mmol) was added. The mixture was stirred for a further 6 h. The resulting solution was then filtered through Celite to eliminate KCl. The solvent was evaporated under vacuum to a volume of 5 mL, and diethyl ether (30 mL) was added to precipitate the corresponding product, which was filtered off. **8c**: yellow solid (386 mg, 90%). ^1H NMR (CDCl_3): $\delta = 7.91\text{--}7.60$ (m, 10 H), 7.17 (s, 4 H), 1.97 (d, $J = 11.4$ Hz, 12 H) ppm. $^{31}\text{P}\{^1\text{H}\}$ NMR (CDCl_3): $\delta = 7.6$ (s) ppm. IR (KBr): $\tilde{\nu} = 2136$ [$\nu(\text{C}\equiv\text{C})$] cm^{-1} . MS (LSIMS $^+$): m/z (%) = 1037 (18), 858 (2) [M^+], 473 (32), 335 (100) $[\text{AuPPhMe}_2]^+$. $\text{C}_{26}\text{H}_{26}\text{Au}_2\text{P}_2\text{S}_2$ (858.26): calcd. C 36.35, H 3.03, S 7.46; found C 35.99, H 2.60, S 7.66. **8d**: yellow solid (334 mg, 91%). ^1H NMR (CDCl_3): $\delta = 7.70$ (4 H, A_2B_2), 1.59 (d, $J = 10.5$ Hz, 18 H) ppm. $^{31}\text{P}\{^1\text{H}\}$ NMR (CDCl_3): $\delta = -3.0$ (s) ppm. IR (KBr): $\tilde{\nu} = 2140$ [$\nu(\text{C}\equiv\text{C})$] cm^{-1} . MS (LSIMS $^+$): m/z (%) = 851 (50), 734 (27) [M^+], 426 (23), 345 (100). $\text{C}_{16}\text{H}_{22}\text{Au}_2\text{P}_2\text{S}_2$ (734.42): calcd. C 26.14, H 3.00, S 8.71; found C 25.84, H 2.76, S 8.49.

Synthesis of $[\text{Au}_2\{1,3\text{-(S}-\text{C}\equiv\text{C})_2-\text{C}_6\text{H}_4\}_2\text{L}_2]$ $\{\text{L} = \text{PPh}_3$ (9a**), PPh_2Me (**9b**):** Complexes **9a** and **9b** can be prepared by a procedure similar to that of **8a** and **8b** but by using 1,3-bis(1,2,3-thiadiazol-4-yl)benzene (**3**) (123 mg, 0.5 mmol). **9a**: orange solid (310 mg, 56%). ^1H NMR (CDCl_3): $\delta = 7.48\text{--}7.03$ (m) ppm. $^{31}\text{P}\{^1\text{H}\}$ NMR (CDCl_3): $\delta = 37.7$ (s) ppm. IR (KBr): $\tilde{\nu} = 2136$ [$\nu(\text{C}\equiv\text{C})$] cm^{-1} . MS (LSIMS $^+$): m/z (%) = 1147 (100) $[\text{AuS}(\text{PPh}_3)_2]^+$, 1107 (15) [M^+]. $\text{C}_{46}\text{H}_{34}\text{Au}_2\text{P}_2\text{S}_2$ (1106.86): calcd. C 49.92, H 3.10, S 5.79; found C 50.21, H 3.47, S 5.30. **9b**: yellow solid (196 mg, 40%). ^1H NMR (CDCl_3): $\delta = 7.61\text{--}7.12$ (m, 24 H), 2.08 (d, $J = 9.3$ Hz, 6 H) ppm. $^{31}\text{P}\{^1\text{H}\}$ NMR (CDCl_3): $\delta = 21.9$ (s) ppm. IR (KBr): $\tilde{\nu} = 2135$ [$\nu(\text{C}\equiv\text{C})$] cm^{-1} . MS (LSIMS $^+$): m/z (%) = 1619 (20), 1223 (100), 1023 (19), 793 (9), 597 (41), 397 (100) $[\text{AuPPh}_2\text{Me}]^+$. $\text{C}_{36}\text{H}_{30}\text{Au}_2\text{P}_2\text{S}_2$ (982.45): calcd. C 43.97, H 3.05, S 6.51; found C 44.37, H 3.34, S 6.50.

Synthesis of $[\text{Au}_2\{1,3\text{-(S}-\text{C}\equiv\text{C})_2-\text{C}_6\text{H}_4\}_2\text{L}_2]$ $\{\text{L} = \text{PPhMe}_2$ (9c**), PMe_3 (**9d**), AsPh_3 (**9e**):** To an ice-cooled solution of 1,3-bis(1,2,3-thiadiazol-4-yl)benzene (**3**) (123 mg, 0.5 mmol) in dry thf (20 mL) was added *t*BuOK (123 mg, 1.1 mmol) for $\text{L} = \text{PPhMe}_2$ and PMe_3 , and $\text{LiN}(\text{SiMe}_3)_2$ (1 mL, 1 mmol, 1 M in hexane) for $\text{L} = \text{AsPh}_3$. The mixture was stirred under an argon atmosphere for 1 h and then $[\text{AuCl}(\text{PPhMe}_2)]$ (296 mg, 0.8 mmol), $[\text{AuCl}(\text{PMe}_3)]$ (247 mg, 0.8 mmol) or $[\text{AuCl}(\text{AsPh}_3)]$ (538 mg, 1 mmol) was added. The

mixture was stirred for a further 6 h. The solvent was evaporated under vacuum to 5 mL, and hexane (30 mL) was added to precipitate the corresponding product, which was filtered off and washed with water. **9c**: yellow solid (356 mg, 83%). ^1H NMR ($[\text{D}_6]\text{dmsO}$): δ = 7.82–7.09 (m, 14 H), 1.92 (d, J = 11.3 Hz, 12 H) ppm. $^{31}\text{P}\{^1\text{H}\}$ NMR ($[\text{D}_6]\text{dmsO}$): δ = 6.2 (s) ppm. IR (KBr): $\tilde{\nu}$ = 2126 $[\nu(\text{C}\equiv\text{C})]$ cm^{-1} . MS (LSIMS $^+$): m/z (%) = 1037 (10), 899 (6), 705 (9), 473 (33) $[\text{Au}(\text{PPhMe}_2)_2]^+$. $\text{C}_{26}\text{H}_{26}\text{Au}_2\text{P}_2\text{S}_2$ (858.26): calcd. C 36.35, H 3.03, S 7.46; found C 35.75, H 2.71, S 7.59. **9d**: yellow solid (279 mg, 76%). ^1H NMR ($[\text{D}_6]\text{dmsO}$): δ = 7.11 (s, 4 H), 1.63 (d, J = 11.4 Hz, 18 H) ppm. $^{31}\text{P}\{^1\text{H}\}$ NMR ($[\text{D}_6]\text{dmsO}$): δ = 4.0 (s) ppm. IR (KBr): $\tilde{\nu}$ = 2132 $[\nu(\text{C}\equiv\text{C})]$ cm^{-1} . MS (LSIMS $^+$): m/z (%) = 851 (100) $[\text{S}(\text{AuPMe}_3)_3]^+$, 775 (36), 734 (18) $[\text{M}]^+$. $\text{C}_{16}\text{H}_{22}\text{Au}_2\text{P}_2\text{S}_2$ (734.42): calcd. C 26.14, H 3.00, S 8.71; found C 26.50, H 2.82, S 8.73. **9e**: pale brown solid (430 mg, 72%). ^1H NMR (CDCl_3): δ = 7.49–7.18 (m) ppm. IR (KBr): $\tilde{\nu}$ = 2134 $[\nu(\text{C}\equiv\text{C})]$ cm^{-1} . MS (LSIMS $^+$): m/z (%) = 1540 (10), 1194 (7) $[\text{M}]^+$, 809 (100) $[\text{Au}(\text{AsPh}_3)_2]^+$, 503 (70). $\text{C}_{46}\text{H}_{34}\text{As}_2\text{Au}_2\text{S}_2$ (1194.76): calcd. C 46.24, H 2.87, S 5.38; found C 45.96, H 2.90, S 5.30.

Synthesis of $[\text{Au}_2\text{-(2,7)-(S-C}\equiv\text{C-C}_6\text{H}_4\text{-C}\equiv\text{C-S)}\text{L}_2]$ $\{\text{L} = \text{PPh}_3$ (10a), PPh_2Me (10b), AsPh_3 (10e)): To an ice-cooled solution of 2,7-bis(1,2,3-thiadiazol-4-yl)-9,9-dimethylfluorene (**4**) (90 mg, 0.25 mmol) in dry thf (15 mL) was added *t*BuOK (62 mg, 0.55 mmol). The mixture was stirred under an argon atmosphere for 1 h, and then $[\text{AuCl}(\text{PPh}_3)]$ (212 mg, 0.43 mmol), $[\text{AuCl}(\text{PPh}_2\text{Me})]$ (186 mg, 0.43 mmol) or $[\text{AuCl}(\text{AsPh}_3)]$ (232 mg, 0.43 mmol) was added. The mixture was stirred for a further 6 h. The solvent was evaporated under vacuum to a volume of 5 mL, and hexane (30 mL) was added to precipitate the corresponding product, which was filtered off and washed with water. **10a**: yellow solid (238 mg, 78%). ^1H NMR ($[\text{D}_6]\text{dmsO}$): δ = 7.51–7.33 (m, 36 H), 1.39 (s, 6 H) ppm. $^{31}\text{P}\{^1\text{H}\}$ NMR ($[\text{D}_6]\text{dmsO}$): δ = 38.1 (s) ppm. IR (KBr): $\tilde{\nu}$ = 2136 $[\nu(\text{C}\equiv\text{C})]$ cm^{-1} . MS (LSIMS $^+$): m/z (%) = 1409 (71), 1223 (12) $[\text{M}]^+$, 721 (51), 459 (100) $[\text{AuPPh}_3]^+$. $\text{C}_{55}\text{H}_{42}\text{Au}_2\text{P}_2\text{S}_2$ (1222.64): calcd. C 53.99, H 3.44, S 5.23; found C 53.60, H 3.15, S 4.77. **10b**: orange solid (212 mg, 77%). ^1H NMR (CDCl_3): δ = 7.67–7.23 (m, 26 H), 2.17 (d, J = 9.6 Hz, 6 H), 1.39 (s, 6 H) ppm. $^{31}\text{P}\{^1\text{H}\}$ NMR (CDCl_3): δ = 22.0 (s) ppm. IR (KBr): $\tilde{\nu}$ = 2134 $[\nu(\text{C}\equiv\text{C})]$ cm^{-1} . MS (LSIMS $^+$): m/z (%) = 1223 (44), 1099 (7) $[\text{M} + \text{H}]^+$, 1023 (11), 613 (35), 460 (100) $[\text{AuS}(\text{PPh}_2\text{Me})]^+$. $\text{C}_{45}\text{H}_{38}\text{Au}_2\text{P}_2\text{S}_2$ (1098.83): calcd. C 49.18, H 3.46, S 5.83; found C 48.79, H 3.09, S 5.51. **10e**: orange solid (229 mg, 70%). ^1H NMR (CDCl_3): δ = 7.69–7.33 (m, 36 H), 1.39 (s, 6 H) ppm. IR (KBr): $\tilde{\nu}$ = 2130 $[\nu(\text{C}\equiv\text{C})]$ cm^{-1} . MS (LSIMS $^+$): m/z (%) = 1235 (8), 809 (16), 503 (28), 460 (100). Anal. $\text{C}_{55}\text{H}_{42}\text{Au}_2\text{As}_2\text{S}_2$ (1310.48): C, 50.36; H, 3.20; S, 4.88. Found: C, 49.96; H, 2.95; S, 5.30.

Synthesis of $[\text{Au}_2\{3,5\text{-(S-C}\equiv\text{C-C}_7\text{H}_7\text{N)}\text{L}_2]$ $\{\text{L} = \text{PPh}_3$ (11a), PPh_2Me (11b), AsPh_3 (11e)): To an ice-cooled solution of 3,5-bis(1,2,3-thiadiazol-4-yl)-2,6-dimethylpyridine (**5**) (82 mg, 0.3 mmol) in dry thf (15 mL) was added *t*BuOK (74 mg, 0.66 mmol). The mixture was stirred under an argon atmosphere for 1 h, and then $[\text{AuCl}(\text{PPh}_3)]$ (267 mg, 0.52 mmol), $[\text{AuCl}(\text{AsPh}_3)]$ (280 mg, 0.52 mmol) or $[\text{AuCl}(\text{PPh}_2\text{Me})]$ (225 mg, 0.52 mmol) was added. The mixture was stirred for a further 6 h. The solvent was evaporated under vacuum to a volume of 5 mL, and diethyl ether (30 mL) was added to precipitate the corresponding product, which was filtered off and washed with water. **11a**: yellow solid (150 mg, 44%). ^1H NMR (CDCl_3): δ = 7.53–7.47 (m, 31 H), 2.54 (s, 6 H) ppm. $^{31}\text{P}\{^1\text{H}\}$ NMR (CDCl_3): δ = 37.5 (s) ppm. IR (KBr): $\tilde{\nu}$ = 2133 $[\nu(\text{C}\equiv\text{C})]$ cm^{-1} . MS (LSIMS $^+$): m/z (%) = 1409 (58), 1147 (14), 721 (27), 460 (100) $[\text{AuPPh}_3]^+$. $\text{C}_{47}\text{H}_{37}\text{Au}_2\text{NP}_2\text{S}_2$ (1135.63): calcd. C 49.67, H 3.26, N 1.23, S 5.64; found C 49.58, H 2.89, N 1.60, S 6.10. **11b**: yellow solid (152 mg, 50%). ^1H NMR (CDCl_3):

δ = 7.68–7.47 (m, 20 H), 2.55 (s, 6 H), 2.14 (d, J = 9.9 Hz, 6 H) ppm. $^{31}\text{P}\{^1\text{H}\}$ NMR (CDCl_3): δ = 21.9 (s) ppm. IR (KBr): $\tilde{\nu}$ = 2131 $[\nu(\text{C}\equiv\text{C})]$ cm^{-1} . MS (LSIMS $^+$): m/z (%) = 1223 (32), 1023 (16), 1012 (7) $[\text{M} + \text{H}]^+$, 597 (38), 397 (100) $[\text{AuPPh}_2\text{Me}]^+$. $\text{C}_{37}\text{H}_{33}\text{Au}_2\text{NP}_2\text{S}_2$ (1011.40): calcd. C 43.90, H 3.26, N 1.38, S 6.33; found C 43.53, H 2.93, N 1.75, S 6.36. **11e**: brown solid (158 mg, 43%). ^1H NMR (CDCl_3): δ = 7.49 (m, 31 H), 2.56 (s, 6 H) ppm. IR (KBr): $\tilde{\nu}$ = 2132 $[\nu(\text{C}\equiv\text{C})]$ cm^{-1} . MS (LSIMS $^+$): m/z (%) = 1541 (50), 1224 (30) $[\text{M} + \text{H}]^+$, 809 (100) $[\text{Au}(\text{AsPh}_3)_2]^+$. $\text{C}_{47}\text{H}_{37}\text{As}_2\text{Au}_2\text{NS}_2$ (1223.48): calcd. C 46.10, H 3.02, N 1.14, S 5.23; found C 45.81, H 2.63, N 1.50, S 5.69.

Synthesis of $[\text{Au}_4\text{-(S-C}\equiv\text{C-C}\equiv\text{C-S)}_2\text{L}_2]$ $\{\text{L} = \text{dppm}$ (12a), dppe (12b)): To a solution of compound **6e** (333 mg, 0.15 mmol) in dry thf (15 mL) was added dppm (57 mg, 0.15 mmol) or dppe (60 mg, 0.15 mmol). The reaction mixture was stirred under an argon atmosphere for 12 h. The solvent was removed under vacuum to a volume of 5 mL, and diethyl ether was added to precipitate the corresponding product. **12a**: red solid (119 mg, 89%). ^1H NMR (CDCl_3): δ = 7.88–7.26 (m, 40 H), 4.72 (s, 4 H) ppm. $^{31}\text{P}\{^1\text{H}\}$ NMR (CDCl_3): δ = 33.0 (s) ppm. IR (KBr): $\tilde{\nu}$ = 2109 (w), 2025 (m) $[\nu(\text{C}\equiv\text{C})]$ cm^{-1} . MS (LSIMS $^+$): m/z (%) = 1818 (8), 1289 (22), 1162 (100) $[\text{Au}_2(\text{dppm})_2]^+$, 963 (43), 579 (45), 383 (35). $\text{C}_{58}\text{H}_{44}\text{Au}_4\text{P}_4\text{S}_4$ (1781.15): calcd. C 39.11, H 2.49, S 7.20; found C 38.92, H 2.21, S 7.62. **12b**: green solid (129 mg, 95%). ^1H NMR (CDCl_3): δ = 7.69–7.18 (m, 40 H), 2.46 (s, 8 H) ppm. $^{31}\text{P}\{^1\text{H}\}$ NMR (CDCl_3): δ = 21.5 (s) ppm. IR (KBr): $\tilde{\nu}$ = 2035 $[\nu(\text{C}\equiv\text{C})]$ cm^{-1} . MS (LSIMS $^+$): m/z (%) = 994 (100) $[\text{Au}(\text{dppe})_2]^+$, 567 (29). $\text{C}_{60}\text{H}_{48}\text{Au}_4\text{P}_4\text{S}_4$ (1809.20): calcd. C 39.83, H 2.67, S 6.85; found C 39.43, H 2.95, S 6.36.

Synthesis of $[\text{Au}_4\{1,3\text{-(S-C}\equiv\text{C-C}_6\text{H}_4)_2\text{L}_2]$ $\{\text{L} = \text{dppm}$ (13a), dppe (13b)): To a solution of compound **9e** (597 mg, 0.42 mmol) in dry thf (30 mL) was added dppm (161 mg, 0.42 mmol) or dppe (167 mg, 0.42 mmol). The reaction mixture was stirred under an argon atmosphere for 12 h. The precipitate was filtered off and washed with diethyl ether to afford the corresponding compound. **13a**: yellow solid (227 mg, 56%). ^1H NMR (dmsO): δ = 7.50–7.15 (m, 48 H), 3.72 (m, 4 H) ppm. IR (KBr): $\tilde{\nu}$ = 2131 $[\nu(\text{C}\equiv\text{C})]$ cm^{-1} . MS (LSIMS $^+$): m/z (%) = 1935 (7) $[\text{M}]^+$, 1738 (7) $[\text{M} - \text{Au}]^+$, 1161 (100) $[\text{Au}_2(\text{dppm})_2]^+$. $\text{C}_{70}\text{H}_{52}\text{Au}_4\text{P}_4\text{S}_4$ (1933.35): calcd. C 43.45, H 2.59, S 6.62; found C 43.09, H 3.01, S 6.18. **13b**: yellow solid (239 mg, 58%). ^1H NMR (CDCl_3): δ = 7.36–7.31 (m, 20 H), 7.24–7.14 (m, 28 H), 2.44 (s, 8 H) ppm. $^{31}\text{P}\{^1\text{H}\}$ NMR (CDCl_3): δ = 21.4 (s) ppm. IR (KBr): $\tilde{\nu}$ = 2133 $[\nu(\text{C}\equiv\text{C})]$ cm^{-1} . MS (LSIMS $^+$): m/z (%) = 1845 (11), 1225 (69), 977 (100), 827 (90). $\text{C}_{72}\text{H}_{56}\text{Au}_4\text{P}_4\text{S}_4$ (1961.17): calcd. C 44.06, H 2.86, S 6.53; found C 43.69, H 2.56, S 6.05.

Crystallographic Studies: Crystals suitable for X-ray diffraction were obtained by slow diffusion of diethyl ether or hexane into solutions in dichloromethane. A summary of the fundamental crystal and refinement data of compounds **7** and **11a** are given in Table 3. The crystals were mounted on glass fibre with inert oil and centred on a Bruker-Siemens Smart CCD diffractometer. The diffraction frames were integrated by using the SAINT^[85] package and corrected for absorption with SADABS.^[86] The structures were solved by direct methods with SHELXS.^[87] Full-matrix least-squares refinement was carried out by using SHELXTL^[88] minimizing $\omega(F_o^2 - F_c^2)^2$. Hydrogen atoms were included by using a riding model. Weighted R factors (R_w) and all goodness-of-fit S values are based on F^2 ; conventional R factors (R) are based on F . In the case of complex **11a** the diffraction data were weak, with mean $I/\sigma(I)$ = 2.95 in the data set before averaging of equivalents, and a R_{int} value of 10.05%. All non-hydrogen atoms were refined

anisotropically, but it was necessary to apply both rigid-bond restraints and restraints to isotropic behaviour to the anisotropic displacement parameters of the carbon atoms to avoid having a non-positive definite. The heavier atoms were refined freely. Crystallographic data and refinement details are given in Table 3. These data can be obtained free of charge from The Cambridge Crystallographic Data Centre via www.ccdc.cam.ac.uk/data_request/cif (CCDC-699224 and -699225).

Table 3. Crystal data and data collection and refinement for complexes **7** and **11a**.

| | 7 | 11a |
|---|--|--|
| Empirical formula | C ₈₈ H ₆₀ Au ₂ F ₁₀ N ₂ P ₄ S ₂ | C ₄₉ H ₄₁ Au ₂ Cl ₄ NP ₂ S ₂ |
| <i>M_w</i> | 1917.32 | 1305.62 |
| Colour, habit | light brown, block | yellow, prism |
| Space group | triclinic, <i>P</i> $\bar{1}$ | monoclinic, <i>P</i> ₂ /n |
| <i>a</i> [Å] | 10.848(5) | 15.309(5) |
| <i>b</i> [Å] | 10.991(5) | 20.540(5) |
| <i>c</i> [Å] | 15.976(5) | 16.203(5) |
| α [°] | 76.422(5) | 90 |
| β [°] | 78.796(5) | 105.124(5) |
| γ [°] | 83.898(5) | 90 |
| <i>V</i> [Å ³] | 1812.6(13) | 4919(3) |
| <i>Z</i> | 1 | 4 |
| <i>D</i> (calcd.) [g cm ⁻³] | 1.756 | 1.763 |
| Crystal size [mm] | 0.22 × 0.17 × 0.26 | 0.29 × 0.087 × 0.057 |
| μ [mm ⁻¹] | 4.265 | 6.360 |
| <i>T</i> [K] | 100(2) | 100(2) |
| θ Range [°] | 1.33 ≤ θ ≤ 28.30 | 1.63 ≤ θ ≤ 23.00 |
| No. of data collected | 11898 | 21778 |
| No. of unique data | 7946 [<i>R</i> (int) = 0.0264] | 6838 [<i>R</i> (int) = 0.1182] |
| <i>R</i> ₁ ^[a] [<i>F</i> ² > 2σ(<i>F</i> ²)] | 0.0377 | 0.0809 |
| <i>wR</i> ₂ ^[b] (all data) | 0.1007 | 0.2121 |
| <i>S</i> ^[c] (all data) | 1.020 | 1.068 |

[a] $R_1(F) = \sum ||F_o| - |F_c|| / \sum |F_o|$. [b] $wR_2(F^2) = \sum [w(F_o^2 - F_c^2)^2] / \sum [w(F_o^2)^2]^{1/2}$, $w = 1 / [\sigma^2(F_o^2) + (aP)^2 + bP]$, where $P = [\max(F_o^2, 0) + 2F_c^2] / 3$. [c] $S = \sum [w(F_o^2 - F_c^2)^2(n - p)]^{1/2}$, where *n* is the number of reflections and *p* is the number of refined parameters.

Acknowledgment

We wish to thank the Spanish Ministry for Education and Science and FEDER for financial support (grant number BQU2005-0899-CO3-01).

- [1] V. A. Vakulev, W. Dehaen, *The Chemistry of Heterocyclic Compounds*, Vol. 62, Wiley, New York, **2004**.
- [2] P. Stanetty, M. Kremslehner, *Heterocycles* **1998**, 48, 259.
- [3] T. C. Britton, T. J. Lobl, C. G. Chidester, *J. Org. Chem.* **1984**, 49, 4773.
- [4] P. Stanetty, M. Kremslehner, M. Müllner, *J. Heterocycl. Chem.* **1996**, 33, 1759.
- [5] D. BhaskarReddy, A. Somasekhar, T. Chandra, V. Padmavathi, *J. Ecotoxicol. Environ. Monit.* **1999**, 9, 225.
- [6] G. S. Lewis, P. H. Nelson, *J. Med. Chem.* **1979**, 22, 1214.
- [7] T. C. Britton, T. J. Chidester, *J. Org. Chem.* **1984**, 49, 4773.
- [8] A. R. Katritzky, D. O. Tymoshenko, G. N. Nikonov, *J. Org. Chem.* **2001**, 66, 4045.
- [9] C. Rovira, J. Veciana, N. Santalo, J. Tarres, J. Cirujeda, E. Molins, J. Llorca, E. Espinosa, *J. Org. Chem.* **1994**, 59, 3307.
- [10] E. W. Thomas, E. E. Nishizawa, D. C. Zimmermann, J. Williams, *J. Med. Chem.* **1985**, 28, 442.
- [11] M. J. Wu, Q. M. Sun, C. H. Yang, D. D. Chen, J. Ding, Y. Chen, L. P. Lin, Y. Y. Xie, *Bioorg. Med. Chem. Lett.* **2007**, 17, 869.
- [12] MDDR 3D Database: MDL Inc., Japan Patent 87099380, **1987**.
- [13] T. Balasankar, M. Gopalakrishnan, S. Nagarajan, *J. Med. Chem.* **2005**, 40, 728.
- [14] J. A. Lowe, III, Patent EP 279598, **1988**; *Chem. Abstr.* **1989**, 110, 8234q.
- [15] R. Raap, R. Micetich, *Can. J. Chem.* **1968**, 46, 1057.
- [16] G. L'aabé, B. Haelterman, W. Dehaen, *J. Chem. Soc. Perkin Trans. 1* **1994**, 2203.
- [17] G. L'aabé, B. Haelterman, W. Dehaen, *Bull. Soc. Chim. Belg.* **1996**, 105, 419.
- [18] A.-S. Mousa, *Asian J. Chem.* **2007**, 19, 1783.
- [19] R. Andreu, J. Garin, J. Orduna, M. Saviron, J. Cousseau, A. Gorgues, V. Morisson, T. Nozdryn, J. Becher, R. P. Clausen, M. R. Bryce, P. J. Skabara, W. Dehaen, *Tetrahedron Lett.* **1994**, 35, 9243.
- [20] L. Field, *Synthesis* **1972**, 101.
- [21] R. P. Clausen, J. Becher, *Tetrahedron* **1996**, 52, 3171 and references cited therein.
- [22] A. Shafiee, I. Lalezari, *J. Heterocyclic Chem.* **1973**, 10, 11.
- [23] C. Bariain, I. R. Matias, I. Romeo, M. Laguna, J. Garrido, *Appl. Phys. Lett.* **2000**, 77, 2274.
- [24] R. E. Cammack, "Iron Sulfur Clusters in Enzymes" in *Advances in Inorganic Chemistry*, Elsevier, Amsterdam, **1992**, vol. 38, p. 281.
- [25] R. A. Sanchez-Delgado, *J. Mol. Catal.* **1994**, 86, 287.
- [26] T. B. Rauchfuss, *Prog. Inorg. Chem.* **1991**, 39, 259.
- [27] C. D. Stont, T. G. Spiro, *Iron Sulfur Proteins*, Wiley, New York, **1982**.
- [28] E. W. Thomas in *Comprehensive Heterocyclic Chemistry* (Eds.: K. T. Potts, A. R. Katritzky, C. W. Rees), Pergamon Press, London **1984**, part 4B, p. 4476.
- [29] M. Fujita, T. Kobari, T. Hiyama, K. Konda, *Heterocycles* **1993**, 36, 33.
- [30] C. D. Hurd, R. I. Mori, *J. Am. Chem. Soc.* **1955**, 77, 5359.
- [31] P. Stanetty, M. Kremslehner, M. Mullner, *J. Heterocycl. Chem.* **1996**, 33, 1759.
- [32] S. Smeets, W. Dehaen, *Tetrahedron Lett.* **1998**, 39, 9841.
- [33] S. Tumkevicius, L. Labanauskas, V. Bucinskaite, A. Brukstus, G. Urbelis, *Tetrahedron Lett.* **2003**, 44, 6635.
- [34] D. J. Byron, G. W. Gray, R. C. J. Wilson, *J. Chem. Soc. (C) Org.* **1966**, 13, 840.
- [35] E. Delgado, B. Donnadieu, S. Garcia, F. Zamora, *J. Organomet. Chem.* **2002**, 649, 21.
- [36] Y. Sunada, Y. Hayashi, H. Kawaguchi, K. Tatsumi, *Inorg. Chem.* **2001**, 40, 7072.
- [37] H. Sugiyama, Y. Hayashi, H. Kawaguchi, K. Tatsumi, *Inorg. Chem.* **1998**, 37, 6773.
- [38] I. Ara, E. Delgado, J. Fornies, E. Hernandez, E. Lalinde, N. Mansilla, M. T. Moreno, *J. Chem. Soc., Dalton Trans.* **1998**, 3199.
- [39] W. Weigand, M. Weishäupl, *Z. Naturforsch., Teil B* **1996**, 51, 501.
- [40] W. Weigand, C. Robl, *Chem. Ber.* **1993**, 126, 1807.
- [41] W. W. Seidel, M. J. Meel, T. Lugger, *Z. Naturforsch., Teil B* **2007**, 62, 669.
- [42] N. Lardies, I. Romeo, E. Cerrada, M. Laguna, P. J. Skabara, *Dalton Trans.* **2007**, 5329.
- [43] E. Delgado, E. Hernandez, A. Martin, M. Menacho, *Organometallics* **2006**, 25, 2960.
- [44] A. Cabrera, E. Delgado, C. Pastor, M. A. Maestro, F. Zamora, *Inorg. Chim. Acta* **2005**, 358, 1521.
- [45] B. Alonso, C. Castejon, E. Delgado, B. Donnadieu, E. Hernandez, *Organometallics* **2004**, 23, 5115.
- [46] M. I. Alcalde, E. Delgado, B. Donnadieu, E. Hernandez, M. P. Martin, F. Zamora, *J. Organomet. Chem.* **2004**, 689, 552.
- [47] M. I. Alcalde, A. J. Carty, Y. Chi, E. Delgado, B. Donnadieu, E. Hernandez, K. Dallmann, J. Sanchez-Nieves, *J. Chem. Soc., Dalton Trans.* **2001**, 2502.

- [48] C. Rosenberg, N. Steunou, S. Jeannin, Y. Jeannin, *J. Organomet. Chem.* **1995**, 494, 17.
- [49] D. Seyferth, G. B. Womack, *Organometallics* **1986**, 5, 2360.
- [50] W. Weigand, *Z. Naturforsch., Teil B* **1991**, 46, 1333.
- [51] W. W. Seidel, M. D. I. Arias, M. Schaffrath, M. C. Jahnke, A. Hepp, T. Pape, *Inorg. Chem.* **2006**, 45, 4791.
- [52] A. F. Hill, J. M. Malget, *Chem. Commun.* **1996**, 1177.
- [53] T. Y. Lee, A. Mayr, *J. Am. Chem. Soc.* **1994**, 116, 10300.
- [54] W. Seidel, M. Schaffrath, T. Pape, *Angew. Chem. Int. Ed.* **2005**, 44, 7798.
- [55] M. A. Uson, J. M. Llanos, *J. Organomet. Chem.* **2002**, 663, 98.
- [56] J. M. Casas, B. E. Diosdado, L. R. Falvello, J. Fornies, A. Martin, A. J. Rueda, *Dalton Trans.* **2004**, 2733.
- [57] E. Martin, C. Spendley, A. J. Mountford, S. J. Coles, P. N. Horton, D. L. Hughes, M. B. Hursthouse, S. J. Lancaster, *Organometallics* **2008**, 27, 1436.
- [58] A. J. Mountford, S. J. Lancaster, S. J. Coles, P. N. Horton, D. L. Hughes, M. B. Hursthouse, M. E. Light, *Organometallics* **2006**, 25, 3837.
- [59] Y. M. Sun, W. E. Piers, M. Parvez, *Can. J. Chem.* **1998**, 76, 513.
- [60] N. Adams, H. R. Bigmore, T. L. Blundell, C. L. Boyd, S. R. Dubberley, A. J. Sealey, A. R. Cowley, M. E. G. Skinner, P. Mountford, *Inorg. Chem.* **2005**, 44, 2882.
- [61] N. Adams, A. R. Cowley, S. R. Dubberley, A. J. Sealey, M. E. G. Skinner, P. Mountford, *Chem. Commun.* **2001**, 2738.
- [62] G. S. Hair, A. H. Cowley, J. D. Gorden, J. N. Jones, R. A. Jones, C. L. B. Macdonald, *Chem. Commun.* **2003**, 424.
- [63] M. Al-Smadi, N. Hanold, H. Meier, *J. Heterocyclic Chem.* **1997**, 34, 605.
- [64] D. B. Werz, R. Gleiter, F. Rominger, *J. Org. Chem.* **2004**, 69, 2945.
- [65] D. B. Werz, R. Gleiter, F. Rominger, *J. Am. Chem. Soc.* **2002**, 124, 10638.
- [66] M. I. Bruce, B. C. Hall, B. W. Skelton, M. E. Smith, A. H. White, *J. Chem. Soc., Dalton Trans.* **2002**, 995.
- [67] C. M. Che, H. Y. Chao, V. M. Miskowski, Y. Q. Li, K. K. Cheung, *J. Am. Chem. Soc.* **2001**, 123, 4985.
- [68] M. I. Bruce, M. Jevric, B. W. Skelton, M. E. Smith, A. H. White, N. N. Zaitseva, *J. Organomet. Chem.* **2006**, 691, 361.
- [69] S. Cronje, H. G. Raubenheimer, H. S. C. Spies, C. Esterhuysen, H. Schmidbaur, A. Schier, G. J. Kruger, *Dalton Trans.* **2003**, 2859.
- [70] R. Usón, A. Laguna, M. Laguna, M. N. Fraile, I. Lazaro, M. C. Gimeno, P. G. Jones, C. Reihs, G. M. Sheldrick, *J. Chem. Soc., Dalton Trans.* **1990**, 333.
- [71] O. Crespo, E. J. Fernandez, P. G. Jones, A. Laguna, J. M. Lopez-de-Luzuriaga, M. Monge, M. E. Olmos, J. Perez, *Dalton Trans.* **2003**, 1076.
- [72] M. Laguna, E. Cerrada, M. A. Luquin in *Gold Chemistry: Current Trends and Future Directions* (Ed.: F. Mohr), Wiley-VCH, to be published.
- [73] K. Nomiya, S. Yamamoto, R. Noguchi, N. Yokoyama, C. Kasuga, K. Ohyama, C. Kato, *J. Inorg. Biochem.* **2003**, 95, 208.
- [74] S. Watase, T. Kitamura, N. Kanehisa, M. Shizuma, M. Nakamoto, Y. Kai, S. Yanagida, *Chem. Lett.* **2003**, 32, 1070.
- [75] M. Preisenberger, A. Schier, H. Schmidbaur, *J. Chem. Soc., Dalton Trans.* **1999**, 1645.
- [76] E. Cerrada, P. G. Jones, A. Laguna, M. Laguna, R. Terroba, M. D. Villacampa, *J. Organomet. Chem.* **1995**, 492, 105.
- [77] E. Cerrada, A. Laguna, M. Laguna, P. G. Jones, *J. Chem. Soc., Dalton Trans.* **1994**, 1325.
- [78] J. M. Forward, D. Bohmann, J. P. F. R. J. Staples Jr, *Inorg. Chem.* **1995**, 34, 6330.
- [79] W. Weigand, C. Robl, *Z. Naturforsch., Teil B* **1996**, 51, 501.
- [80] I. Ara, E. Delgado, J. Fornies, E. Hernandez, E. Lalinde, N. Mansilla, M. T. Moreno, *J. Chem. Soc., Dalton Trans.* **1998**, 3199.
- [81] H. Sugiyama, Y. Hayashi, H. Kawaguchi, K. Tatsumi, *Inorg. Chem.* **1998**, 37, 6773.
- [82] R. Usón, A. Laguna, M. Laguna, *Inorg. Synth.* **1989**, 26, 85.
- [83] A. D. Westland, *Can. J. Chem.* **1969**, 47, 4135.
- [84] R. Usón, A. Laguna, J. Garcia, M. Laguna, *Inorg. Chim. Acta* **1979**, 37, 201.
- [85] *SAINT*, version 5.0, Bruker Analytical X-ray Systems.
- [86] G. M. Sheldrick, *SADABS, Empirical Absorption Program*, University of Göttingen, Göttingen, Germany, **1996**.
- [87] G. M. Sheldrick, *SHELXS, Program for Crystal Structure Solution*, University of Göttingen, Göttingen, Germany, **1990**.
- [88] G. M. Sheldrick, *SHELXTL-NT 6.1*, University of Göttingen, **1998**.

Received: August 27, 2008

Published Online: November 28, 2008

Topological Diversification in Metal-Organic Frameworks: Secondary Ligand and Metal Effects

Jian-Qiang Liu,^[a] Yao-Yu Wang,^{*[a]} Ya-Nan Zhang,^[a] Ping Liu,^[a] Qi-Zhen Shi,^[a] and Stuart R. Batten^{*[b]}

Keywords: Coordination polymers / Coordination modes / Ligand effects / Crystal engineering

A series of interesting coordination polymers have been prepared by the combination of a V-shaped 4,4'-oxybis(benzoic acid) (H₂oba) and neutral organonitrogen ligands with different metal ions, namely, {[M(oba)(bpe)]·H₂O}_n [M = Mn (**1**), Co (**2**)], [M(oba)(N3)]_n [N3 = dipyridin-2-ylamine; M = Cd (**3**), Cu (**4**)] and {[Zn(oba)(N5)]·2H₂O}_n (**5**) [bpe = 1,2-bis(4-pyridyl)ethene, N5 = bis(pyridin-2-yl)pyridine-2,6-diamine]. The framework structures of these neutral polymeric complexes have been determined by single-crystal X-ray diffraction studies. Compound **1** has a threefold pcu-type network structure. Although **2** has the same ligands and coordination modes as **1**, it consists of corrugated 2D layers formed of a series of squares, which allows the sheets to interpenetrate in an unusual 2D → 3D parallel fashion. Polymers **3** and **4** ex-

hibit double-helical chains formed by π - π stacking interactions from the phenyl rings of the N3 ligands. Compound **5** forms a 2D supramolecular architecture directed by hydrogen bonding between the NH groups of the N5 ligand, the uncoordinated carboxylate oxygens, and the intercalated water molecules. This work markedly indicates that the effect of auxiliary ligands is significant in the construction of these network structures, which are also well regulated by the metal centers. Thermogravimetric analysis (TGA) and XRPD results for compound **1** as well as luminescent properties for compounds **3** and **5** are discussed.

(© Wiley-VCH Verlag GmbH & Co. KGaA, 69451 Weinheim, Germany, 2009)

Introduction

The crystal engineering of metal-organic frameworks (MOFs) is of great current interest not only because of their significant potential functions in gas storage, chemical separations, microelectronics, nonlinear optics, and heterogeneous catalysis, but also because of their intriguing architectures and intricate entangled motifs.^[1–3] The mutual entanglement of structural motifs is a commonly encountered feature in coordination polymer chemistry.^[1a–1d,2a,3–5] However, the formation of extended coordination framework solids with desired structural features and/or physicochemical properties greatly depends on the sophisticated selection and utilization of multitopic building blocks as well as tectonic interactions.^[1a,6] Conformationally nonrigid ligands are usually building elements for the assembly of interesting entangled networks, thanks to their varied geometries.^[7,8] 4,4'-Oxybis(benzoic acid) (H₂oba) is a typical example of a long, V-shaped, flexible ligand which has been used to promote the formation of polycatenated and self-penetrating

coordination polymers. For instance, {[Cu(oba)(H₂O)]₂·0.5H₂O} exhibited a unique fivefold 4-connected 4²8⁴ (lvt)^[9a,9b] interpenetrating structure with nine interwoven helices.^[9c,9d]

On the other hand, in the two-ligand MOF assembly systems, both organic and inorganic secondary ligands can manipulate the structural topologies through coordination in either terminal or bridging fashions.^[10] For example, Cao and his coworkers used the secondary ligands as terminal and bridging ligands to tune the formation of helical structures.^[11] As for the dipyridyl ligands, some analogous linkers derived from the proper modification of the classic 4,4'-bipyridine molecule have been employed,^[10] which present unrivaled backbone flexibility and thus impose profound steric effects on the direction of the unexpected coordination frameworks. Recently, we have reported a 4-crossing [2]-catenane motif based on oba and 1,3-bis(4-pyridyl)propane (bpp).^[12] However, the systematic investigation of the role of auxiliary ligands in the construction of coordination nets is not well documented to date. Therefore, the development of a comprehensive research program is required, and the rational design of new frameworks would be a long-range challenge.

With this background in mind, we continued our investigation and chose H₂oba as a bridging ligand to react with d-block metal ions. The neutral bpe, N3, and N5 ligands were introduced into the M^{II}/oba system, and a series of

[a] Key Laboratory of Synthetic and Natural Functional Molecule Chemistry of Ministry of Education, Department of Chemistry, Shaanxi Key Laboratory of Physico-Inorganic Chemistry, Northwest University, Xi'an 710069, P. R. China

[b] School of Chemistry, Monash University, Victoria 3800, Australia

Supporting information for this article is available on the WWW under <http://www.eurjic.org> or from the author.

polymers with unusual topologies were obtained, namely, $\{[M(\text{oba})(\text{bpe})]\cdot\text{H}_2\text{O}\}_n$ [$M = \text{Mn}$ (**1**), Co (**2**)], $[M(\text{oba})(\text{N}3)]_n$ [$M = \text{Cd}$ (**3**), Cu (**4**)] and $\{[\text{Zn}(\text{oba})(\text{N}5)]\cdot 2\text{H}_2\text{O}\}_n$ (**5**). To the best of our knowledge, compound **2** represents the first example in the M/oba system that possesses an interpenetrating $2\text{D} \rightarrow 3\text{D}$ structural feature. The crystal structures and topological analysis of these compounds, along with a systematic investigation of the effect of the coordination modes of the oba anions, metal ions, and neutral ligands on their ultimate frameworks, will be discussed.

Results and Discussion

$\{[\text{Mn}(\text{oba})(\text{bpe})]\cdot\text{H}_2\text{O}\}_n$ (**1**)

The structure of **1** contains one unique Mn atom, one oba ligand, one bpe ligand, and intercalated water molecules (all of which are related by symmetry). The $\{\text{MnO}_4\text{N}_2\}$ coordination spheres are each defined by two oxygen atoms from one chelating oba carboxylate, two oxygen atoms from two different bidentate-bridging carboxylate groups, and two *cis*-oriented bpe nitrogen donors. Bond lengths and angles about the metal centers in **1** are consistent with a distorted octahedral geometry caused by the presence of chelating/bidentate-bridging ligands and are given in Table 1. The Mn–O bond lengths span a range of 2.091(4) to 2.300(4) Å. The Mn atoms are bridged into pairs by carboxylate groups, and the Mn–Mn distance is 4.276 Å (Figure 1). These Mn dimers are then connected to other dimers by the oba ligand bridges. Each oba bridge bonds to two Mn atoms through one carboxylate group to form a dimer, and then to a third Mn atom, which is part of another dimer, through the other chelating carboxylate group. The bridging mode of the oba ligand is very similar to that in the $[\text{Co}(\text{oba})(\text{bpa})]_n$ [$\text{bpa} = 1,2\text{-bis}(4\text{-pyridyl})\text{ethane}$] complex,^[13] which may be responsible for their analo-

Table 1. Selected bond lengths [Å] and angles [°].

| Complex 1 | | | |
|---|------------|-------------------|------------|
| Mn(1)–O(1) | 2.304(4) | Mn(1)–O(2) | 2.262(4) |
| Mn(1)–N(1) | 2.254(4) | Mn(1)–N(2)#1 | 2.281(4) |
| Mn(1)–O(4)#2 | 2.097(4) | Mn(1)–O(5)#3 | 2.099(4) |
| O(1)–Mn(1)–O(2) | 57.76(14) | O(1)–Mn(1)–N(2) | 101.16(14) |
| O(1)–Mn(1)–N(2)#1 | 81.11(14) | O(1)–Mn(1)–O(4)#2 | 151.86(14) |
| O(2)–Mn(1)–N(2)#1 | 90.39(14) | O(2)–Mn(1)–O(4)#2 | 97.20(14) |
| O(2)–Mn(1)–O(5)#3 | 146.64(14) | N(1)–Mn(1)–N(2)#1 | 174.50(15) |
| Symmetry codes: #1: $1 + x, y, 1 + z$; #2: $2 - x, -1/2 + y, 1/2 - z$; #3: $1 + x, 1/2 - y, -1/2 + z$ | | | |
| Complex 2 | | | |
| Co(1)–O(1) | 2.011(3) | Co(1)–O(2) | 2.277(3) |
| Co(1)–N(1) | 2.052(4) | Co(1)–N(2) | 2.054(3) |
| Co(1)–O(3)#1 | 2.166(3) | Co(1)–O(4)#1 | 2.083(3) |
| O(1)–Co(1)–O(3)#1 | 97.34(10) | O(1)–Co(1)–O(4)#1 | 157.87(11) |
| O(2)–Co(1)–N(1) | 156.00(12) | O(2)–Co(1)–O(3)#1 | 87.02(9) |
| O(2)–Co(1)–O(4)#1 | 105.66(9) | N(1)–Co(1)–N(2) | 96.89(13) |
| O(3)#1–Co(1)–N(2) | 150.68(12) | O(4)#1–Co(1)–N(2) | 89.92(13) |
| Symmetry codes: #1: $x, -1 + y, 1 + z$ | | | |
| Complex 3 | | | |
| Cd(1)–O(1) | 2.380(13) | Cd(1)–O(2) | 2.348(12) |
| Cd(1)–N(1) | 2.302(13) | Cd(1)–N(3) | 2.288(13) |
| Cd(1)–O(4)#1 | 2.404(11) | Cd(1)–O(5)#1 | 2.342(11) |
| O(1)–Cd(1)–N(3) | 162.9(4) | O(1)–Cd(1)–O(4)#1 | 104.7(4) |
| O(1)–Cd(1)–O(5)#1 | 96.9(4) | O(2)–Cd(1)–N(1) | 103.7(4) |
| O(2)–Cd(1)–N(3) | 107.6(5) | O(2)–Cd(1)–O(4)#1 | 153.7(4) |
| O(2)–Cd(1)–O(5)#1 | 105.0(4) | N(1)–Cd(1)–N(3) | 84.4(4) |
| O(4)#1–Cd(1)–N(1) | 94.9(4) | O(5)#1–Cd(1)–N(1) | 150.7(4) |
| Symmetry codes: #1: $1 + x, 1/2 - y, 1/2 + z$ | | | |
| Complex 4 | | | |
| Cu(1)–O(1) | 2.414(2) | Cu(1)–O(2) | 1.984(2) |
| Cu(1)–N(1) | 1.970(2) | Cu(1)–N(3) | 1.988(2) |
| Cu(1)–O(3)#1 | 2.4524(19) | Cu(1)–O(4)#1 | 2.0137(18) |
| O(1)–Cu(1)–O(2) | 57.96(8) | O(1)–Cu(1)–N(1) | 100.71(8) |
| O(1)–Cu(1)–N(3) | 104.09(8) | O(1)–Cu(1)–O(3)#1 | 155.62(7) |
| O(1)–Cu(1)–O(4)#1 | 102.35(7) | O(2)–Cu(1)–N(1) | 158.51(9) |
| O(2)–Cu(1)–N(3) | 95.04(9) | O(2)–Cu(1)–O(3)#1 | 104.82(7) |
| O(3)#1–Cu(1)–N(3) | 93.96(8) | O(4)#1–Cu(1)–N(3) | 152.01(9) |
| Symmetry codes: #1: $1 + x, 1/2 - y, 1/2 + z$ | | | |
| Complex 5 | | | |
| Zn(1)–O(1) | 2.093(3) | Zn(1)–N(1) | 2.065(4) |
| Zn(1)–N(3) | 2.107(4) | Zn(1)–N(5) | 2.088(4) |
| Zn(1)–O(4)#1 | 2.063(3) | | |
| O(1)–Zn(1)–N(1) | 89.15(15) | O(1)–Zn(1)–N(3) | 134.46(15) |
| N(1)–Zn(1)–N(3) | 91.73(16) | N(1)–Zn(1)–N(5) | 176.37(16) |
| O(4)#1–Zn(1)–N(3) | 125.47(16) | O(4)#1–Zn(1)–N(5) | 84.22(16) |
| Symmetry codes: #1: $-1 + x, y, z$ | | | |

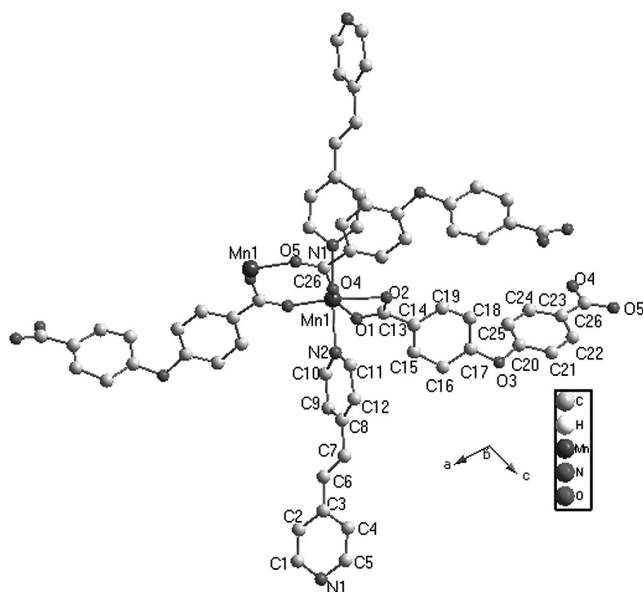


Figure 1. The coordination environment of the Mn^{II} atom in **1**.

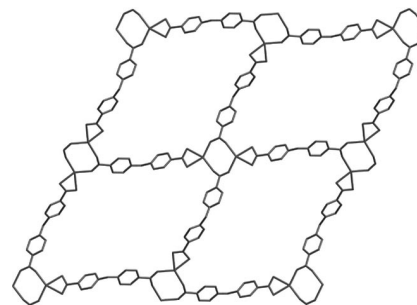


Figure 2. A view of a layer of squares in the structure of **1**.

gous structures. The dimers are thus bonded to four oba ligands, two of which bridge the Mn atoms to form the dimer, and two others which each chelate to a different Mn atom in the dimer. The dimers thus act as a 4-connecting node to generate a layer formed of a series of squares (Figure 2). These sheets are then bridged by the bpe ligands to generate a 3D network. Each Mn dimer is bridged to a dimer in the sheet above and below by pairs of bpe ligands (Figure 3). If each pair is treated as a single link, the dimers become 6-connecting nodes, and the overall topology is that

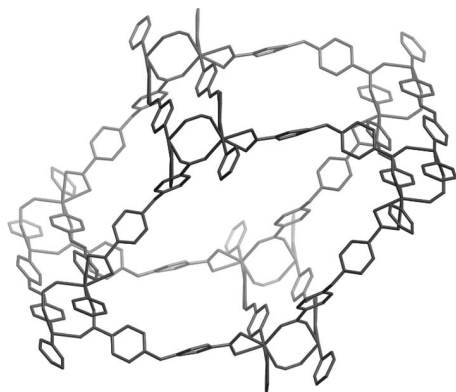


Figure 3. A single box-like cavity in **1** formed by the bridging of the layers in Figure 2 by the oba ligands.

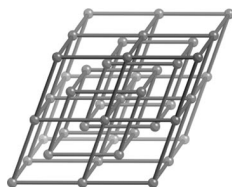


Figure 4. The three interpenetrating pcu networks in **1**. Nodes represent the centers of the Mn dimer nodes, and the links represent either oba ligand bridges or pairs of oba ligand bridges.

of a pcu-related net. Figure 4 shows a single box-like cavity of the net; the openness of the single net leads to three interpenetrating networks.

$\{[\text{Co}(\text{oba})(\text{bpe})]\cdot\text{H}_2\text{O}\}_n$ (**2**)

The asymmetric units of **2** crystallize in the triclinic $P\bar{1}$ space group (Table 2). Both contain one divalent metal atom, one oba ligand, one bpe ligand, and one lattice water molecule. The structure consists of a corrugated 2D layer formed of a series of squares in which the metal ions are bridged in one direction by the oba ligand and in the other by the bpe ligand. The open, corrugated nature of the sheets allows them to interpenetrate in an unusual 2D \rightarrow 3D parallel fashion,^[14] as shown in Figure 5. Each sheet is penetrated by two others (one above and one below), which have parallel but not coincident mean planes. This leads to an overall 3D entanglement, which is a very uncommon motif. This structure is isomorphous with the $\{[\text{Cu}(\text{oba})(\text{bpe})]\cdot\text{H}_2\text{O}\}_n$ compound, which was investigated in detail in our previous communication.^[14]

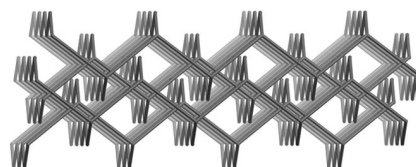


Figure 5. The unusual 2D \rightarrow 3D parallel interpenetration of the sheets in **2**.

$[\text{M}(\text{oba})(\text{N}3)]_n$ [$\text{M} = \text{Cd}$ (**3**), Cu (**4**)]

It has been noted that aromatic chelate ligands (such as 2,2'-bipyridine and 1,10-phenanthroline) often lead to 1D polymers and may provide potential supramolecular recognition sites for π - π aromatic stacking interactions to

Table 2. Crystal data and structure refinement information for compounds **1–5**.

| Compounds | 1 | 2 | 3 | 4 | 5 |
|----------------------------------|--|--|--|--|--|
| Formula | $\text{C}_{26}\text{H}_{20}\text{MnN}_2\text{O}_6$ | $\text{C}_{26}\text{H}_{20}\text{CoN}_2\text{O}_6$ | $\text{C}_{24}\text{H}_{17}\text{CdN}_3\text{O}_5$ | $\text{C}_{24}\text{H}_{17}\text{CuN}_3\text{O}_5$ | $\text{C}_{29}\text{H}_{25}\text{ZnN}_5\text{O}_7$ |
| FW | 511.38 | 515.37 | 539.82 | 490.96 | 620.93 |
| Temp. / K | 298(2) | 298(2) | 298(2) | 298(2) | 298(2) |
| Crystal system | monoclinic | triclinic | monoclinic | monoclinic | monoclinic |
| Space group | $P2_1/c$ | $P\bar{1}$ | $P2_1/c$ | $P2_1/c$ | $P2_1/c$ |
| a / Å | 10.697(3) | 9.314(5) | 12.732(10) | 12.327(2) | 14.8933(11) |
| b / Å | 18.619(5) | 11.334(7) | 15.832(13) | 15.540(3) | 8.1547(6) |
| c / Å | 12.600(3) | 12.472(7) | 11.304(9) | 11.252(2) | 23.1093(17) |
| α / ° | 90 | 69.658(9) | 90 | 90 | 90 |
| β / ° | 107.418(5) | 80.316(9) | 94.529(10) | 96.093(3) | 90.1890(10) |
| γ / ° | 90 | 87.866(9) | 90 | 90 | 90 |
| V / Å ³ | 2394.4(11) | 1216.6(12) | 2272(3) | 2143.3(7) | 2806.6(4) |
| Z | 4 | 2 | 4 | 4 | 4 |
| $F(000)$ | 1052 | 530 | 1080 | 1004 | 1280 |
| D_c / g cm ⁻³ | 1.419 | 1.407 | 1.578 | 1.521 | 1.469 |
| GOF | 0.784 | 0.638 | 1.033 | 0.513 | 1.085 |
| $R_1^{[a]}$ [$I > 2\sigma(I)$] | 0.0562 | 0.0379 | 0.1205 | 0.0294 | 0.0574 |
| $wR_2^{[a]}$ (all data) | 0.1831 | 0.0616 | 0.3499 | 0.0382 | 0.1910 |

[a] $R_1 = \sum ||F_o| - |F_c|| / \sum |F_o|$, $wR_2 = \{\sum [w(F_o^2 - F_c^2)^2] / \sum (F_o^2)^2\}^{1/2}$.

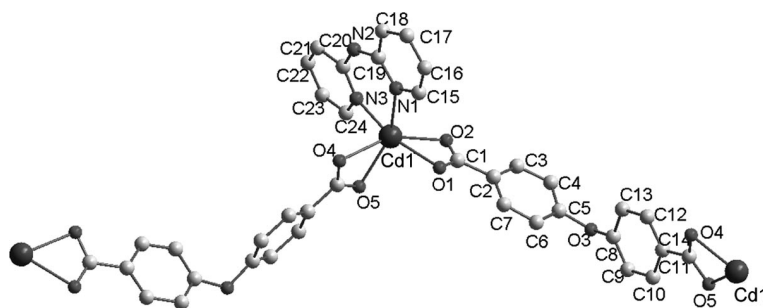


Figure 6. The coordination environment of the Cd center in **3**.

form multistranded helices.^[7g] Therefore, the heterocyclic aromatic chelate ligands, N3 (dipyridin-2-ylamine) and N5 [bis(pyridin-2-yl)pyridine-2,6-diamine], were introduced with the aim of synthesizing noninterpenetrating 1D nets. In contrast to other aromatic chelate ligands (2,2'-bipyridine), the tailored diimine contains an active amine (–NH) hydrogen, and the aromatic rings in N3 and N5 may induce intermolecular hydrogen bonding and π – π stacking interactions to lead to stable supramolecular networks.

Compounds **3** and **4** are isostructural, and thus only **3** is described here in detail. In the crystal structure of **3**, there is one Cd^{II} atom, one bis(bidentate) oba ligand, and one N3 ligand in each independent crystallographic unit (Figure 6). Each Cd^{II} atom in **3** is primarily coordinated by four oxygen atoms from two bis(bidentate) oba ligands and two nitrogen atoms from a chelating N3 to establish a distorted octahedral geometry. The average Cd–O bond length is 2.36 Å, and the largest O–Cd–O angle is 153.7(4)°, which indicates a distorted octahedral coordination sphere. Each pair of adjacent Cd^{II} atoms is bridged together by an oba ligand to form a chiral chain running along a crystallographic 2₁ axis in the *b* direction with a long pitch of 15.1 Å. These chains are decorated with N3 ligands alternating on two sides and are further extended into 2D networks through interdigitation of the lateral N3 ligands from adjacent chains in a zipper-like, offset fashion with a face-to-face distance of ca. 3.72 Å, which indicates aromatic π –

π stacking interactions (Figure 7).^[7g] To the best of our knowledge, such zipper-like double-stranded helical chains have been documented for only one previous example.^[15] The double-stranded helical chains are stabilized by hydrogen bonds between the carboxylate oxygen atom (O4) and the nitrogen atom of the –NH group of the N3 ligand.

$\{[\text{Zn}(\text{oba})(\text{N5})]\cdot 2\text{H}_2\text{O}\}_n$ (**5**)

When N5, a chelating aromatic ligand of a larger size, was used instead of N3 under similar reaction condition, an analogous neutral single-stranded chain is formed (**5**). As illustrated in Figure 8, the oba ligand adopts a bis(monodentate) mode and links neighboring Zn1 atoms to form a single-stranded chain. Zn1 is coordinated by two oxygen atoms from two different oba ligands [Zn1–O4 2.062(3), Zn1–O1 2.095(3) Å] and three nitrogen atoms from a tridentate N5 ligand [Zn–N1 2.063(4), Zn1–N5 2.087(4), Zn1–N3 2.106(4) Å]. The two oxygen atoms of the carboxylate are located in two apical positions and establish a trigonal bipyramidal N₃O₂ geometry for the Zn atom. Unlike those in **3**, the N5 ligands are attached to only one side of the single-stranded helical chain, and are oriented perpendicularly to the chain. The approximately perpendicular orientation of the N5 ligands allows for pairing of two centrosymmetrically related single-stranded helical chains directed by hydrogen bonds between an uncoordinated oxygen atom of a carboxylate group and the nitrogen atom of one of the –NH groups. These pairs are then further interconnected into 2D layers by hydrogen bonding between the other –NH groups, the intercalated water molecules, and the other uncoordinated carboxylate groups. Notably, the lateral N5 ligands from adjacent chains are not paired to

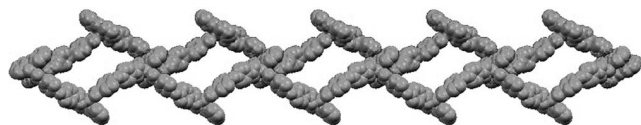


Figure 7. View of a zipper-like double-chain in the structure of **3**.

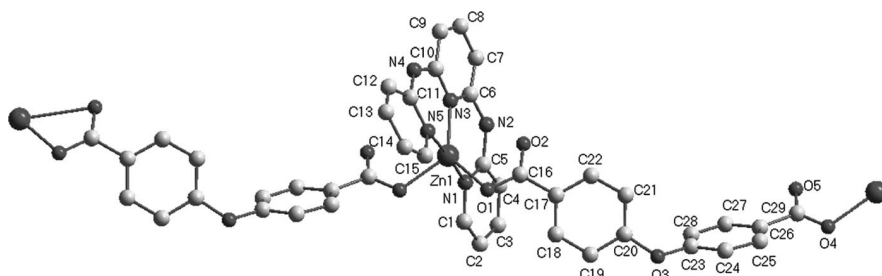


Figure 8. The coordination environment of the Zn^{II} ion in compound **5**. All hydrogen atoms have been omitted for clarity.

afford π - π stacking interactions, which may be attributed to the improper orientation between N5 molecules. The lattice water molecules intercalate into the spaces between the chains and form small water clusters, as shown in Figure 9. The lattice water molecules further bind to the uncoordinated oxygen atom (O5) to generate a chair-like formation.

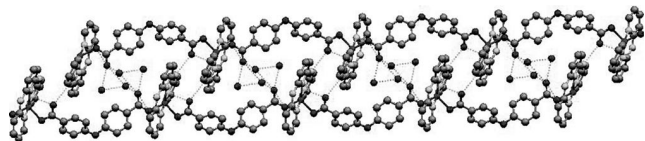


Figure 9. View of a pair of hydrogen-bonded chains in **5**.

Comparison of the Structures of Coordination Polymers

The simultaneous use of the flexible, rigid, and aromatic chelating ligands and the aromatic V-shaped dicarboxylate ligands affords diverse entangled networks, as shown in Scheme 1. Although we are unable to propose definitive reasons as to why the compounds exhibit different topologies with our present state of knowledge, some of the general trends observed are discussed below.

Effect of the Secondary Ligand

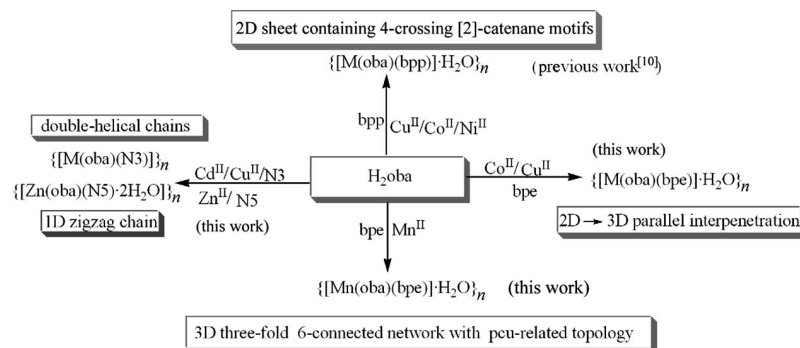
The connectivities of the polymers are strongly related to the secondary ligand. The following discussion provides a qualitative explanation for this conclusion. Although the bpp and bpe ligands are both neutral N-containing linkers, they are quite different. For example, the bpp ligand can assume different conformations (TT, TG, GG, and GG') that display quite different N-to-N distances,^[16] and it is more flexible than bpe. When the bpp ligand was introduced into the $\text{Cu}^{\text{II}}/\text{Co}^{\text{II}}/\text{Ni}^{\text{II}}/\text{H}_2\text{oba}$ system, we obtained three 2D isostructural polymers displaying 4-crossing [2]-catenane motifs (Figure S1).^[12] Another two isostructural polymers (**2** and $\{[\text{Cu}(\text{oba})(\text{bpe})]\cdot\text{H}_2\text{O}\}_n$ ^[14]) with 2D layers made up of a series of squares were prepared by the combination of bpe, oba, and $\text{Cu}^{\text{II}}/\text{Co}^{\text{II}}$. In these structures, however, each sheet is penetrated by two others (one above and one below), which have parallel but not coincident mean planes, to lead to an unusual 3D entanglement. Jin and his coworkers obtained a 3D threefold architecture for the $[\text{Co}-$

$(\text{oba})(\text{bpa})]_n$ complex.^[13] The presence of flexible bpa ligands may play an important role in the generation of further interpenetration in the $[\text{Co}(\text{oba})(\text{bpa})]_n$ complex. Furthermore, the coordination modes of the oba ligands in the $[\text{Co}(\text{oba})(\text{bpa})]_n$ and $[\text{Co}(\text{oba})(\text{bpe})]_n$ complexes are different. To further examine the influence of the secondary ligand on the self-assembly of supramolecular entities, two aromatic chelate ligands were used instead of bpp and bpe. Consequently, **3** and **4**, featuring helical chain structures, were obtained. The neighboring chains make zipper-like double-stranded chains through supramolecular recognition. In contrast, the presence of the larger aromatic N5 ligands weakens the π - π stacking interactions in **5** and results in the formation of 2D grid-like nets in the presence of hydrogen bonds. Thus the ancillary ligand has a significant effect on the formation and structure of the coordination polymers. In order to construct polymers of peculiar topologies, an effective method can be to introduce ancillary ligands.

Effect of the Metal Nature

It is interesting that, although **1** and **2** bind to the same ligands and have similar molecular compositions, the Co^{II} (**2**) and Mn^{II} (**1**) complexes give completely different products. From the structural descriptions above, the Mn^{II} compound **1** contains three interpenetrating 3D pcu-type nets, while the $\text{Cu}^{\text{II}}/\text{Co}^{\text{II}}$ complexes **2** have 2D undulated layers formed of a series of squares. Furthermore, the Co^{II} and Mn^{II} ions are all hexacoordinate and have distorted octahedral geometries, but their coordination environments are different. In compound **2** there are two chelating oba and two bpe ligands around the metal ions, whereas in complex **1**, which contains dimeric Mn units, there is one terminal chelating and two terminal bridging oba ligands and two bpe ligands around each metal ion. More ligands surround each Mn^{II} ion than the $\text{Cu}^{\text{II}}/\text{Co}^{\text{II}}$ ions. Moreover, the oba ligand adopts chelating-bidentate and bridging-bidentate coordination modes in **1**, which promotes interpenetration and higher dimensionality. Similar results are found for the other complexes with oba ligands in the presence of flexible ligands.^[13] A rational assembly of metal ions is critical for the formation of novel and higher dimensional networks.

As discussed above, a variety of framework structures can be achieved on the basis of the choice of the different



Scheme 1. Reactions of the oba ligand.

secondary ligands. Their network arrays vary from 2D open layers (4-crossing [2]-catenane motifs^[12] and unusual 2D→3D parallel interpenetration) and 3D porous structures (3D threefold interpenetration) to zipper-like double-stranded helical chains. On the other hand, the choice of metal center may also tune the resultant extended networks of the MOFs. However, all the variable factors cannot be accurately forecasted at this stage.

Thermogravimetric Analyses

To study the stability of the polymers, thermogravimetric analysis (TGA) of complex **1** was performed. The TGA diagram of **1** indicates two weight loss steps. The first weight loss began at 20 °C and was complete at 125 °C. The observed weight loss of 4.3% corresponds to the loss of the lattice water molecule (calcd. 3.6%). The second weight loss occurs in the 330–541 °C range, which can be attributed to the elimination of bpe and oba ligands (Figure S2). Additionally, to confirm the phase purity and stability of compound **1**, the original sample and the dehydrated sample were both characterized by X-ray powder diffraction (XRPD) at room temperature. The pattern that was simulated from the single-crystal X-ray data of compound **1** was in good agreement with those that were observed (Figure 10), which indicates that compound **1** was obtained as a single phase. After heating of compound **1** at 150 °C for 4 h, the guest water molecule was removed (the evacuated framework is defined as **1'**). The XRPD pattern of **1'** is similar to that of compound **1**, although minor differences can be seen in the positions, intensities, and widths of some peaks, which indicates that the framework of compound **1** is retained after the removal of the guest molecule. Immersion of the desolvated phase in H₂O regenerated a sharper XRPD pattern. Therefore the dehydration and rehydration process is reversible for the material, and it belongs to

Kitagawa's third generation of MOFs, showing a dynamic nature.^[17]

Photoluminescent Properties

The emission spectra of complexes **3** and **5** in the solid state at room temperature were investigated. It was observed that an emission occurs at 386 nm (Figure S3, λ_{ex} = 260 nm) for **3**, which is larger than that of the free N3 ligand and is probably due to the H bonding, π – π stacking, and the enhanced rigidity of **3**.^[18] It was also observed that an intense emission occurred at 400 nm (Figure S3, λ_{ex} = 260 nm) for **5**. Interestingly, a clear blueshift of the emission occurs in **5**. By comparison to the spectrum of the free N5 ligand,^[18] the emission spectrum of **5** is tentatively assigned to the intraligand (π – π^*) fluorescence. The blue fluorescent emission occurring in **3** and **5** suggests that they may be used as new blue-light-emitting materials.

Conclusions

In conclusion, the simultaneous reaction of secondary ligands and V-shaped dicarboxylate ligands with d-block metals affords a new type of interesting polymeric entangled compounds. Notably, the first example of the 2D→3D interpenetrating structural feature observed in **2** illustrates again the aesthetic diversity of coordinative network chemistry. Topological analysis of a series of related complexes indicates that longer and flexible secondary ligands are liable to form previously unobserved topologies. Also, the metal ion plays an important role in modulating the resulting dimensionality and topology of the frameworks. It is believed that more metal complexes containing N-donor ligands and aromatic V-shaped polycarboxylate with interesting structures as well as physical properties will be synthesized.

Experimental Section

Abbreviations: bpa = 1,2-bis(4-pyridyl)ethane, bpe: 1,2-bis(4-pyridyl)ethene, bpp: 1,3-bis(4-pyridyl)propane, dde = H₂oba: 4,4'-oxybis(benzoic acid), pcu: α -polonium.

Materials and Instruments: All reagents were purchased from commercial sources and used as received. IR spectra were recorded with a Perkin–Elmer Spectrum One spectrometer in the 4000–400 cm^{−1} range using KBr pellets. The luminescent spectra of the solid samples were acquired at ambient temperature with a JOBIN YVON/HORIBA SPEX Fluorolog t3 system (slit: 0.2 nm). TGA was carried out with a Mettler–Toledo TA 50 in dry dinitrogen (60 mL min^{−1}) at a heating rate of 5 °C min^{−1}. XRPD data were recorded with a Rigaku RU200 diffractometer at 60 kV, 300 mA for Cu- K_{α} radiation (λ = 1.5406 Å), a scan speed of 2 °C min^{−1}, and a step size of 0.02° in 2θ .

Synthesis of the Complexes

[M(oba)(bpe)]·H₂O}_n [M = Mn (1**); Co (**2**):** A mixture of MnSO₄·6H₂O (0.021 g, 0.11 mmol), dde (0.029 g, 0.1 mmol), bpe (0.025 g, 0.1 mmol), NaOH (0.5 M, 0.4 mL), and deionized water

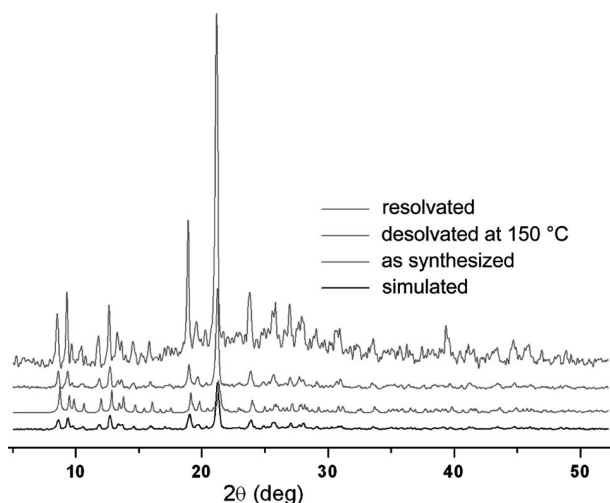


Figure 10. Comparison of XRPD patterns of the simulated pattern from the single-crystal structure determination, the as-synthesized product, and the desolvated and resolved phases in compound **1**.

(10 mL) was stirred for 20 min in air, then transferred and sealed in a 23-mL Teflon reactor, which was heated at 150 °C for 48 h. The solution was then cooled to room temperature at a rate of 5 °C h⁻¹ to yield a very fine pale yellow crystalline product (**1**) in 50% yield based on Mn. C₂₆H₂₀MnN₂O₆ (511.38): calcd. C 61.29, H 3.56, N 5.50; found C 61.52, H 3.28, N 5.62. IR (KBr): $\tilde{\nu}$ = 3469 (m), 3063 (w), 2298 (w), 1618 (m), 1597 (s), 1405 (vs), 1273 (m), 1064 (m), 882 (vs), 608 (m), 517 (w) cm⁻¹. The synthesis of **2** was performed using the same procedure as for complex **1** except that MnSO₄·6H₂O was replaced by CoSO₄·7H₂O (0.027 g, 0.1 mmol). Yield: 58% based on Co. C₂₆H₂₀CoN₂O₆ (515.37): calcd. C 60.59, H 3.91, N 5.44; found C 59.88, H 4.11, N 5.23. IR (KBr): $\tilde{\nu}$ = 3461 (m), 3058 (w), 2297 (w), 1607 (m), 1589 (s), 1410 (vs), 1275 (m), 1058 (m), 881 (vs), 605 (m), 508 (w) cm⁻¹.

[M(oba)(N3)]_n [M = Cd (**3**), Cu (**4**): Synthetic procedures similar to that for **1** were used. Yield: 52% based on Cd. C₂₄H₁₇CdN₃O₅ (539.81): calcd. C 53.39, H 3.17, N 7.78; found C 53.88, H 3.41, N 7.70. IR (KBr): $\tilde{\nu}$ = 1608 (vs), 1552 (s), 1443 (s), 1224 (m), 858 (s) cm⁻¹. C₂₄H₁₇CuN₃O₅ (490.95): calcd. C 58.83, H 3.29, N 8.58; found C 53.88, H 3.34, N 7.75. Yield: ca. 55% based on Cu. IR (KBr): $\tilde{\nu}$ = 1605 (vs), 1558 (s), 1446 (s), 1218 (m), 879 (s) cm⁻¹.

{[Zn(oba)(N5)]·2H₂O}_n (**5**): A synthetic procedure similar to that for **1** was used. Yield: 49% based on Zn. C₂₉H₂₅N₅O₇·Zn (620.91): calcd. C 56.10, H 4.06, N 11.28; found C 56.87, H 3.68, N 11.40. IR (KBr): $\tilde{\nu}$ = 13443 (v), 3303 (s), 1621 (vs), 1558 (s), 1448 (s), 1217 (m), 871 (s) cm⁻¹.

X-ray Crystallography: Single-crystal X-ray diffraction studies of **1–5** were performed with a Bruker SMART APEX II CCD diffractometer equipped with graphite-monochromated Mo-*K*_α radiation (λ = 0.71073 Å) by using an ω -2 θ scan technique at room temperature. The structures were solved by direct methods and successive Fourier difference synthesis (SHELXS-97),^[19] and refined using the full-matrix least-squares method on *F*² with anisotropic thermal parameters for all non-hydrogen atoms (SHELXL-97).^[20] The positions of the H atoms for pyridyl rings, benzene rings and –NH groups were generated by a riding model on idealized geometries, while the H atoms of water molecules were located in difference Fourier maps. In the case of **2**, the final value is not ideal, which may be attributed to the quality of the crystal. Notably, the goodness-of-fit for compound **4** was only 0.513, which was also attributed to the quality of the crystal. The crystallographic data and other pertinent information for **1–5** are summarized in Table 2. Selected bond lengths and bond angles are listed in Table 1.

Crystallographic data for the structural analysis have been deposited with the Cambridge Crystallographic Data Centre: CCDC-692071 (for **1**), -692072 (for **2**), -692072 (for **3**), and -692074 (for **4**) -692075 (for **5**). These data can be obtained free of charge from The Cambridge Crystallographic Data Centre via www.ccdc.cam.ac.uk/data_request/cif.

Supporting Information (see also the footnote on the first page of this article): Description of the 4-crossing [2]-catenane motif, TG curve for **1**, and luminescence spectra for **3** and **5**.

Acknowledgments

We gratefully acknowledge financial support of this work by the National Natural Science Foundation of China (20471048 and 20771090), Teaching and Research Award Program for Outstanding Young Teachers in Higher Education Institutes (TRAPOYT), and Specialized Research Fund for the Doctoral Program of Higher Education (SRFDP) (20050697005).

- [1] a) S. R. Batten, R. Robson, *Angew. Chem. Int. Ed.* **1998**, *37*, 1460–1494; b) V. A. Blatov, L. Carlucci, D. M. Proserpio, *CrysrEngComm* **2004**, *6*, 377–395; c) I. A. Baburin, V. A. Blatov, L. Carlucci, G. Ciani, D. M. Proserpio, *J. Solid State Chem.* **2005**, *178*, 2471–2493; d) L. Carlucci, G. Ciani, D. M. Proserpio, *Coord. Chem. Rev.* **2003**, *246*, 247–289; e) X.-H. Bu, M.-L. Tong, H. C. Chang, S. Kitagawa, S. R. Batten, *Angew. Chem. Int. Ed.* **2004**, *43*, 192–196; f) M.-L. Tong, X.-L. Chen, S. R. Batten, *J. Am. Chem. Soc.* **2003**, *125*, 16170–16171; g) A. N. Khlobystov, A. J. Blake, N. R. Champness, D. A. Lemenovskii, A. G. Majouga, N. V. Zyk, M. Schröder, *Coord. Chem. Rev.* **2001**, *222*, 155–192; h) B. Moulton, M. J. Zaworotko, *Chem. Rev.* **2001**, *101*, 1629–1658.
- [2] a) S. R. Batten, *CrysrEngComm* **2001**, *3*, 67–73; b) B. F. Abrahams, S. R. Batten, M. J. Grannas, H. Hamit, B. F. Hoskins, R. Robson, *Angew. Chem. Int. Ed.* **1999**, *38*, 1475–1477; c) O. R. Evans, W. Lin, *Acc. Chem. Res.* **2002**, *35*, 511–512; d) O. M. Yaghi, M. O’Keeffe, N. W. Ockwig, H. K. Chae, M. Edaoudi, J. Kim, *Nature* **2003**, *423*, 705–714; e) S. R. Batten, *J. Solid State Chem.* **2005**, *178*, 2475–2479; f) P. D. Akrivos, *Coord. Chem. Rev.* **2001**, *213*, 181–210; g) H. Fleischer, *Coord. Chem. Rev.* **2005**, *249*, 799–827.
- [3] <http://www.chem.monash.edu.au/staff/sbatten/interpen/> (accessed 21/12/07).
- [4] D. P. Martin, R. M. Supkowski, R. L. LaDuca, *Inorg. Chem.* **2007**, *46*, 7917–7922.
- [5] S. R. Batten, R. Robson, in *Molecular Catenanes, Rotaxanes and Knots, A Journey Through the World of Molecular Topology* (Eds.: J.-P. Sauvage, C. Dietrich-Buchecker), Wiley-VCH, Weinheim, **1999**, 77–105.
- [6] a) J.-K. Lu, M.-A. Lawandy, J. Li, *Inorg. Chem.* **1999**, *38*, 2695–2704; b) C.-D. Wu, C.-Z. Lu, W.-B. Yang, S.-F. Lu, H.-H. Zhuang, J.-S. Huang, *Eur. J. Inorg. Chem.* **2002**, *41*, 797–800; c) R. Cao, D.-F. Sun, Y.-C. Liang, M.-C. Hong, K. Tatsumi, Q. Shi, *Inorg. Chem.* **2002**, *41*, 2087–2094; d) S. Konar, P. S. Mukherjee, E. Zangrando, F. Lloret, N. R. Chaudhuri, *Angew. Chem. Int. Ed.* **2002**, *41*, 1561–1563.
- [7] a) Z. Y. Fu, X. T. Wu, J. C. Dai, L. M. Wu, C. P. Cui, S. M. Hu, *Chem. Commun.* **2001**, 1856–1857; b) L. Carlucci, G. Ciani, D. M. Proserpio, S. Rizzato, *Chem. Eur. J.* **2002**, *8*, 1520–1526; c) P. Ayyappan, O. R. Evans, W. Lin, *Inorg. Chem.* **2002**, *41*, 3328–3330; d) K. Biradha, M. Fujita, *Chem. Commun.* **2002**, 1866–1867; e) Y. H. Li, C. Y. Su, A. M. Goforth, K. D. Shimizu, K. D. Gray, M. D. Smith, H. C. zur Loye, *Chem. Commun.* **2003**, 1630–1631; f) L. Carlucci, G. Ciani, D. M. Proserpio, *Chem. Commun.* **2004**, 380–381; g) X. M. Chen, G. F. Liu, *Chem. Eur. J.* **2002**, *8*, 4811–4817; h) M. Kondo, Y. Irie, M. Miyazawa, H. Kawaguchi, S. Yasuc, K. Maeda, F. Uchida, *J. Organomet. Chem.* **2007**, *692*, 136–141.
- [8] a) M. Fujita, O. Sasaki, K. Watanabe, K. Ogura, K. Yamaguchi, *New J. Chem.* **1998**, *22*, 189–191; b) L. Carlucci, G. Ciani, M. Moret, D. M. Proserpio, S. Rizzato, *Angew. Chem. Int. Ed.* **2000**, *39*, 1506–1510; c) X. L. Wang, Q. Chao, E. B. Wang, Z. M. Su, *Chem. Eur. J.* **2006**, *12*, 2680–2691.
- [9] a) O. D. Friedrichs, M. O’Keeffe, O. M. Yaghi, *Acta Crystallogr., Sect. A* **2003**, *59*, 22; b) <http://rcsr.anu.edu.au/>; c) X. L. Wang, C. Qin, E.-B. Wang, Y.-G. Li, Z.-M. Su, *Chem. Commun.* **2005**, 5450–5452; d) H. K. Lee, D. W. Min, B. Y. Cho, S. W. Lee, *Bull. Korean Chem. Soc.* **2004**, *25*, 1959–1962.
- [10] a) S. Leininger, B. Olenyuk, P. J. Stang, *Chem. Rev.* **2000**, *100*, 853–908; b) B. Moulton, M. J. Zaworotko, *Chem. Rev.* **2001**, *101*, 1629–1658; c) J. Heo, Y. Jeon, C. A. Mirkin, *J. Am. Chem. Soc.* **2007**, *129*, 7712–7713; d) Y. G. Li, N. Hao, E. B. Wang, Y. Lu, C. W. Hu, L. Xu, *Eur. J. Inorg. Chem.* **2003**, 2567–2571; e) Q. Chu, G. X. Liu, Y. Q. Huang, X. F. Wang, W. Y. Sun, *Dalton Trans.* **2007**, 4302–4311; f) C. Y. Niu, B. L. Wu, X. F. Zheng, H. Y. Zhang, H. W. Hou, Y. Y. Niu, Z. J. Li, *Crysr. Growth Des.* **2008**, *8*, 1566–1574; g) M. Du, X. J. Jiang, X. J. Zhao, *Inorg. Chem.* **2007**, *46*, 3984–3995; h) J. Zhang, E. Chew,

- S. M. Chen, J. T. H. Pham, X. H. Bu, *Inorg. Chem.* **2008**, *47*, 3459–3497.
- [11] F. Li, Z. Ma, Y. L. Wang, R. Cao, W. H. Bi, X. Li, *CrystEngComm* **2005**, *7*, 569–574.
- [12] J. Q. Liu, Y. Y. Wang, L. F. Ma, G. L. Wen, Q. Z. Shi, S. R. Batten, D. M. Proserpio, *CrystEngComm* **2008**, *10*, 1123–1125.
- [13] C. Y. Sun, X. J. Zheng, S. Gao, L. C. Li, L. P. Jin, *Eur. J. Inorg. Chem.* **2005**, 4150–4159.
- [14] J. Q. Liu, Y. Y. Wang, L. F. Ma, F. Zhong, X. R. Zeng, W. P. Wu, Q. Z. Shi, *Inorg. Chem. Commun.* **2007**, *10*, 979–982.
- [15] P. Liu, Y. Y. Wang, D. S. Li, H. R. Ma, Q. Z. Shi, G. H. Lee, S. M. Peng, *Inorg. Chim. Acta* **2005**, *358*, 3807–3814.
- [16] L. Carlucci, G. Ciani, D. M. Proserpio, S. Rizzato, *CrystEngComm* **2002**, *4*, 121–129.
- [17] a) S. Kitagawa, R. Kitaura, S. Noro, *Angew. Chem. Int. Ed.* **2004**, *43*, 2334–2375; b) S. Kitagawa, K. Uemura, *Chem. Soc. Rev.* **2005**, *34*, 109–119.
- [18] M. A. Braverman, R. M. Supkouski, R. L. LaDuca, *J. Solid State Chem.* **2007**, *180*, 1852–1862.
- [19] G. M. Sheldrick, *Acta Crystallogr., Sect. A* **1990**, *46*, 467.
- [20] G. M. Sheldrick, *SHELXL-97*, Program for Structure Determination and Refinement, University of Göttingen, Göttingen, **1997**.

Received: September 8, 2008

Published Online: November 27, 2008

The Role of Functionalisation, Asymmetry and Shape of a New Macrocyclic Compartmental Ligand in the Formation of Mononuclear, Homo- and Heterodinuclear Lanthanide(III) Complexes

Sergio Tamburini,^{*,[a]} Sergio Sitran,^[a] Valentina Peruzzo,^[a] and Pietro Alessandro Vigato^[a]

Keywords: Compartmental macrocycles / Heterodinuclear complexes / Lanthanide(III) Schiff base / NMR of paramagnetic systems / Lanthanide oxides

The compartmental [1+1] macrocycle H_3L , obtained by self-condensation of the formyl precursor 3,3'-(3,6-dioxaoctane-1,8-diylidioxy)bis(2-hydroxybenzaldehyde) with the amine precursor *N,N*-bis(2-aminoethyl)-2-hydroxybenzylamine, contains one inner ON_3O_2 Schiff base and one outer O_2O_4 crown-like chamber. According to the experimental conditions it forms, by a template process, the stable mononuclear complexes $Ln(H_3L)(Cl)_2(CH_3COO) \cdot nS \cdot mHCl$ or $[Ln(L)] \cdot nS$ ($Ln = La, Lu, Y, Yb, Er, Dy, Tb, Gd, Eu, Ce$) with the lanthanide(III) ion encapsulated in the crown-ether-like and in the Schiff base site. The mononuclear complexes $Ln(H_3L)(Cl)_2(CH_3COO) \cdot nS \cdot mHCl$, by further complexation with a different lanthanide(III) ion, give rise to the related heterodinuclear complexes $[LnLn'(L)(Cl)_2(CH_3COO)] \cdot nS$ while the homodinuclear and the heterodinuclear complexes $[Ln_2(L)](Cl)_3 \cdot nH_2O$ and $[LnLn'(L)](Cl)_3 \cdot nS$ could be prepared by a template reaction using the appropriate molar ratio of reactants. Their properties have been studied by using SEM-

EDS microscopy, IR and NMR spectroscopy and their compositions confirmed by thermal and ESI-Mass spectrometric analyses. In the heterodinuclear complexes, the site occupancy of the different lanthanide(III) ions was determined by 1H and ^{13}C NMR spectroscopy in CD_3OD or $(CD_3)_2SO$ – it was found that heterodinuclear complexation occurs in methanol with the smaller lanthanide(III) ion mainly coordinating to the Schiff base site and the larger lanthanide(III) ion to the crown site whereas, in dimethyl sulfoxide, demetalation of the weaker coordinated lanthanide(III) ion into the crown ether chamber occurs with the subsequent formation of mononuclear species in solution. The thermal decomposition of the heterodinuclear complexes forms the related mixed oxides, the stoichiometries and properties of which were determined by SEM-EDS microscopy and X-ray powder diffraction studies (XRD).

(© Wiley-VCH Verlag GmbH & Co. KGaA, 69451 Weinheim, Germany, 2009)

Introduction

The role of macrocyclic ligands and related complexes is continuously growing both in basic and applied chemistry, biochemistry, material science and hydrometallurgy etc. Different shaped macrocyclic ligands have been synthesised to correctly ascertain the role of the different donor atoms, their relative positions, the number and the hole size of the chelating rings formed, the flexibility and the shape of the coordinating moiety on the selective binding of charged or neutral species and on the properties arising from these aggregations. The progressive enlargement of the coordinating moiety enabled studies aimed at a deep understanding of the physico-chemical properties arising from the simultaneous presence of two or more metal ions in close proximity within the same coordinating moiety.^[1–9]

Furthermore, suitable functionalisation of the cyclen-type macrocyclic moieties was successfully observed during

the formation of heteronuclear lanthanide complexes.^[10,11] Also, the synthesis of polynuclear complexes by self assembly of macrocyclic systems was recently reported as a useful means for the stabilisation of otherwise inaccessible supramolecular architectures.^[12]

These systems are mainly Schiff bases, derived from the condensation of appropriate formyl and amine precursors, quite often in the presence of a suitable templating metal ion. Also, the self-condensation of the same formyl- and amine-precursors has been successfully applied, although quite often this affords a mixture of cyclic, oligomeric and polymeric compounds which are difficult to completely separate from each other.^[13–17]

Depending on the shape of the formyl and amine precursors and/or the templating metal ion, different ring sizes can be formed during the cyclisation reaction. If one dicarbonyl moiety reacts with one diamine moiety a [1+1] macrocycle results. When two dicarbonyl precursors react with two diamines then a [2+2] macrocycle results while if three dicarbonyl precursors react with two tripodal triamine functions, a [3+2] macrobicycle is formed and so on. This synthetic procedure may form [3+3] or [4+4] superior macrocyclic

[a] Istituto di Chimica Inorganica e delle Superfici, C.N.R.,
Corso Stati Uniti 4, 35127 Padova, Italy
Fax: +39-049-8702911
E-mail: sergio.tamburini@icis.cnr.it

homologues or [1+1] polymeric species. Similarly, one tricarbonyl precursor reacts with a tripodal triamine to form a [1+1] macrobicyclic compound while two tricarbonyl precursors react with three diamines to form [2+3] macrobicyclic compounds.^[1,2]

The macrocyclic systems can be functionalised by inserting appropriate groups in the aliphatic and/or aromatic chains of the formyl or keto and amine precursors. Furthermore, the Schiff bases can be reduced to the related polyamine derivatives by treatment with an appropriate reducing agent. Similarly, the related complexes can give rise to reductive decomplexation reactions when treated with appropriate reductants with consequent formation of the corresponding polyamine derivatives. These polyamine compounds are less sensitive to hydrolysis and more flexible. Furthermore, they contain –NH groups which may be further functionalised using appropriate synthetic procedures.^[1,2]

Compartmental macrocycles are relevant because they can coordinate two or more metal ions, connected in close proximity by appropriate bridging groups which, if paramagnetic, can interact with each other through the bridging donor atoms of the ligands in a ferromagnetic or antiferromagnetic way. By changing the type of ligand, the distance between the two chambers and/or the paramagnetic centres, it is possible to tune the magnetic interaction. Thus, the complexes, in which ferromagnetic interactions occur, may be good building blocks for the preparation of molecular magnets.

When suitable asymmetry in the two compartments is introduced, heteronuclear complexation is more easily achieved since the two adjacent chambers can give rise to subsequent metal ion recognitions and, furthermore, it is well known that such a metal array is of paramount relevance in obtaining a peculiar optical or magnetic property or in favouring specific molecular or catalytic processes.^[1,2,14]

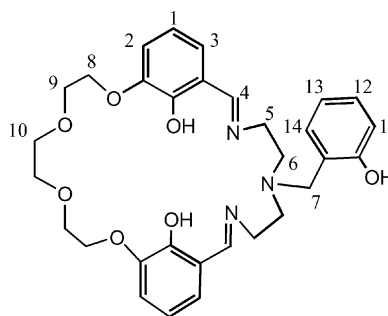
In addition, the asymmetry of these ligands allows a relatively easy formation of mononuclear complexes. The accessibility of the free adjacent site can favour a reversible site migration of the coordinated metal ion, a process which can be influenced by external stimuli such as pH, change of the oxidation state of the metal ions, the solvent involved etc., giving rise to movements which have been considered in the design of appropriate molecular machines.^[18]

It was verified that in the heteronuclear complexation, however, transmetalation can take place which causes failure in the synthesis of the designed systems. This is especially relevant when quite similar metal ions, i.e. two different lanthanide(III) ions, are employed. It was recently verified that the lanthanide(III) ions, when treated in methanol with the [1+1] asymmetric compartmental ligands H_2L_A , H_2L_B or H_2L_C , derived from the condensation of 3,3'-(3-oxapentane-1,5-diylldioxy)bis(2-hydroxybenzaldehyde) or 3,3'-(3,6-dioxaoctane-1,8-diylldioxy)bis(2-hydroxybenzaldehyde) with 1,5-diamino-3-azamethylpentane or 1,7-diamino-3-azamethylheptane and containing the inner Schiff base N_3O_2 and an outer crown ether-like O_2O_3 or

O_2O_4 chamber, form the mononuclear complexes $[Ln(H_2L_{A,B,C})(H_2O)_n](Cl)_3$ where the metal ion invariably resides into the crown ether-like site. These complexes can be dissolved in and recrystallised from methanol without chemical modification while in strongly coordinating solvents (i.e., dimethyl sulfoxide) a severe decomplexation reaction occurs with a partial migration of the metal(III) ion from the crown ether to the Schiff base chamber.^[18–21]

With these ligands, the preparation of homo- or heterodinuclear complexes was successfully achieved in a one pot or in a stepwise synthetic procedure, respectively. However, they are no longer stable in methanol or dimethyl sulfoxide since their stability does depend on the macrocycle coordination moiety and the solvent. For the heterodinuclear complexes, transmetalation and/or site migration reactions represent a further severe problem affecting the synthetic pathway, often frustrating the recovery of the designed complexes once prepared. These complexes evolve, in methanol or dimethyl sulfoxide, into a series of species which include the mononuclear and heterodinuclear complexes with a site occupancy of the metal ion which is different from that of the starting mononuclear precursor

Due to these results we focused our attention on the similar [1+1] macrocycle H_3L (Scheme 1) where the crown-ether like chamber was enlarged in order to better accommodate the second incoming metal ion and the Schiff base site had been functionalised at the central amine atom with a phenol group capable of firmly securing the metal ion into the resultant ON_3O_2 donor set. Thus, this macrocycle can really give rise to mononuclear complexes and especially to stable homo- and heterodinuclear complexes, the properties of which can be studied in the solid-state and in solution, without the occurrence of the above mentioned reactions. This paper deals with the synthesis and properties of these lanthanide(III) complexes, particularly with reference to the role of H_3L , i.e. its functionalisation, asymmetry and shape, in the formation and stabilisation of heterodinuclear lanthanide complexes in the solid-state and in different coordinating solvents.



Scheme 1.

In particular, this compartmental ligand has primarily been designed and synthesised with the aim of defining: i) the site occupancy preference of the lanthanide(III) ions in the solid-state and in methanol or dimethyl sulfoxide and, in particular, the role of the different adjacent cavities on the formation of the positional pure mononuclear com-

plexes as a consequence of the different experimental conditions; ii) the possibility of simultaneously filling both the coordination chambers, giving rise to homodinuclear complexes and to test their stability in the solid-state and especially in solution; iii) the formation of heterodinuclear positional isomers, starting from different mononuclear precursors, the site preference of the different metal ions verifying the occurrence of site migration, transmetalation and/or demetalation, and their relevance in the formation of heteronuclear complexation.

Results and Discussion

The [1+1] asymmetric compartmental macrocycle H_3L , prepared by self-condensation of equimolar amounts of the formyl precursor 3,3'-(3,6-dioxaoctane-1,8-diylidioxy)bis(2-hydroxybenzaldehyde) (H_2L') with the amine precursor *N,N*-bis(2-aminoethyl)-2-hydroxybenzylamine·3HCl (HA' ·3HCl), neutralised with appropriate amount of $N(C_2H_5)_3$ in a diethyl ether/chloroform solution under high dilution, contains one Schiff base site with a ON_3O_2 donor set, functionalised at the central amine nitrogen atom by a $-CH_2C_6H_4OH$ group, and one crown-ether like site with a O_2O_4 donor set. Its [1+1] cyclic nature was deduced from the presence of the parent peak $[M - (-CH_2PhOH) + Na]^+$ at $m/z = 480.54$ in the ESI mass spectrum and by the presence, in the IR spectrum, of a strong $\nu(C=N)$ band at 1640 cm^{-1} whereas the bands attributable to $\nu(C=O)$ or $\nu(NH_2)$ completely disappeared. Moreover, the 1H NMR spectrum in $CDCl_3$ shows a singlet at $\delta = 8.26$ ppm for the

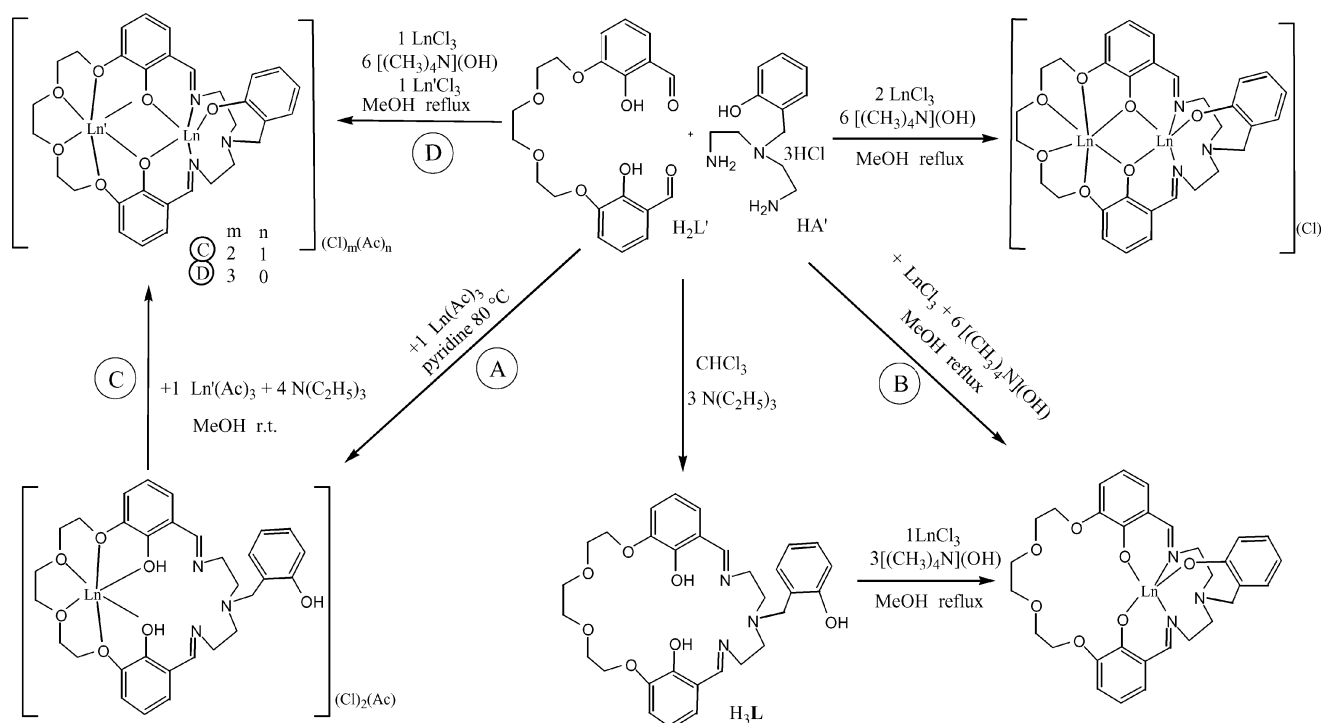
imino protons, multiplets at 7.19–6.74 ppm for the aromatic protons, at $\delta = 3.96$ ppm assigned to the methylenic protons of the phenolic pendant arm, at $\delta = 4.15$, 3.89 and 3.75 ppm assigned to the 12 protons of the crown ether chain and at $\delta = 3.70$ and 3.08 ppm due to the 8 methylenic protons of the imino chain.

The resultant mononuclear homo- and heterodinuclear complexes were prepared according to Scheme 2 and characterised by elemental analysis, SEM-EDS, mass spectrometry, IR and NMR spectroscopic measurements.

Mononuclear and Homodinuclear Complexes

Two different synthetic approaches have been followed for the preparation of the mononuclear complexes: **A**) the template condensation of the diformyl precursor with the functionalised amine (HA' ·3HCl) in the presence of $Ln(CH_3COO)_3 \cdot xH_2O$ in hot pyridine which, after work up, gives rise to $Ln(H_3L)(Cl)_2(CH_3COO)_n \cdot mHCl$ [$Ln(m,nS) = La(0, 2H_2O \cdot 2.5Py)$, $Y(1, 2.5H_2O \cdot Py)$, $Yb(1, 2H_2O \cdot 0.5Py)$, $Er(1, 2H_2O \cdot 0.7Py)$, $Tb(1, 2H_2O \cdot 0.6Py)$, $Eu(1, H_2O \cdot 0.5Py)$, $Ce(1)$]; **B**) the same condensation reaction in methanol in the presence of $[N(CH_3)_4](OH)$, using $LnCl_3 \cdot xH_2O$ as a templating agent, which after work up, gives rise to $[Ln(L)] \cdot nS$ [$Ln(nS) = Y(2.5H_2O)$, $La(3H_2O)$, $Ce(2C_2H_5OH)$, Eu , $Tb(2C_2H_5OH)$, $Dy(5H_2O)$, $Er(2.5H_2O)$, $Lu(4H_2O)$].

The two types of mononuclear complexes show different solubilities in organic solvents (high in methanol for the first and very low for the second ones) and hence different capacities to be used as starting precursors for carrying on



Scheme 2.

the synthesis of the heterodinuclear complexes. All the complexes are very soluble in dimethyl sulfoxide where, unfortunately, it is not possible to generate the heterodinuclear complexes since the strong coordination ability of this solvent toward the lanthanide(III) ions not only prevents the encapsulation of a second lanthanide(III) ion into the free chamber but can cause site migration, transmetalation and scrambling reactions, making the resultant system quite difficult to identify. Alternatively, the same mononuclear complexes could be prepared by the reaction of H_3L with $\text{LnCl}_3 \cdot x\text{H}_2\text{O}$ and $[\text{N}(\text{CH}_3)_4](\text{OH})$ in methanol in a 1:1:3 molar ratio, as verified for the yttrium derivative $[\text{Y}(\text{L})] \cdot 2.5\text{H}_2\text{O}$. For the preparation of the mononuclear complexes, synthetic route **B**) was generally followed, owing to the higher yield and the faster reaction.

The IR spectra of $[\text{Ln}(\text{H}_3\text{L})(\text{Cl})_2(\text{CH}_3\text{COO}) \cdot n\text{S} \cdot m\text{HCl}]$, the homogeneity and $\text{Ln}/\text{Cl} = 1:3$ ratio (1:2 for La) of which were established by SEM-EDS, show a strong band at $1636\text{--}1650\text{ cm}^{-1}$ at approximately the same or at higher wavelengths than that of the free ligand, indicating that the imine groups are not involved in the lanthanide(III) coordination. The presence of the acetate group was ascertained by the strong $\nu(\text{C}=\text{O})$ band at ca. 1500 cm^{-1} and a band of lower intensity at 1345 cm^{-1} due to the $\nu(\text{C}-\text{O})$ of the COO group acting as monodentate function. Furthermore, the stretching of the ether groups at $1224\text{--}1218\text{ cm}^{-1}$, $25\text{--}30\text{ cm}^{-1}$ lower than that in the free ligand, and the skeletal C–C stretching of the aliphatic groups at $1095\text{--}1098\text{ cm}^{-1}$ suggest the lanthanide(III) ion occupancy of the crown-ether chamber in the solid state. This implies that the pendant phenolic group is not involved in the lanthanide(III) coordination and remains protonated as a consequence of the employed synthetic procedure which does not imply use of basic conditions capable of deprotonating the phenolic group. For the same reason, the amine precursor ($\text{HA}'3\text{HCl}$) is not completely neutralised by pyridine and one HCl molecule is present in all lanthanide complexes except that with the lanthanum(III) ion.

^1H NMR spectra in CD_3OD of $[\text{Ln}(\text{H}_3\text{L})(\text{Cl})_2(\text{CH}_3\text{COO}) \cdot n\text{S} \cdot m\text{HCl}]$ ($\text{Ln} = \text{La}, \text{Y}$) corroborate this proposal – the imine peak at $8.46\text{--}8.42\text{ ppm}$ is comparable with that of the free ligand H_3L while the peak complexity of the signal for the aliphatic protons **9** (Scheme 1) is due to the occurrence of geminal protons. In addition, the two triplets of the aliphatic protons **5** and **6** of the Schiff base site indicate that the imine groups are not engaged in the coordination processes. In $(\text{CD}_3)_2\text{SO}$, a clear decomplexation process occurs with the consequent appearance of the signals of the free ligand.

This parallels the previous X-ray structural investigations of $[\text{Ln}(\text{H}_2\text{L}_A)(\text{H}_2\text{O})_4](\text{Cl})_3$ ($\text{Ln} = \text{Ce}, \text{Gd}, \text{Dy}, \text{Lu}$),^[22] which indicate that the lanthanide(III) ion invariably occupies the O_2O_3 crown-ether chamber in a nine-coordinate environment, the remaining coordination positions being filled by the oxygen atoms of four water molecules.

For the mononuclear complexes $[\text{Ln}(\text{L})] \cdot n\text{S}$, the absence of chloride anions was demonstrated by SEM-EDS investigations while the IR spectra, remarkably different from

those obtained for $[\text{Ln}(\text{H}_3\text{L})(\text{Cl})_2(\text{CH}_3\text{COO}) \cdot n\text{S} \cdot m\text{HCl}]$, show a significant lowering of the $\nu(\text{C}=\text{N})$ band at $1624\text{--}1630\text{ cm}^{-1}$ which is consistent with the involvement of the imine groups in the lanthanide complexation.

The great stability of these complexes can also be demonstrated by ESI-MS analysis in methanol. As an example, $[\text{La}(\text{L})] \cdot 3\text{H}_2\text{O}$ shows the parent/molecular peak of the species $[\text{La}(\text{L}) + \text{Na}]^+$ at $m/z = 722.31$. Furthermore, ^1H NMR spectra in $(\text{CD}_3)_2\text{SO}$ are drastically different from that of the free ligand indicating that these mononuclear complexes are also stable in strongly coordinating solvents. The complexity of these NMR spectra, however, does not allow an univocal assignment owing to the concomitant presence of different stereoisomers. On increasing the temperature [up to 80°C for the lanthanum(III) complex] a simpler spectrum occurs. The ^{13}C NMR spectrum of $[\text{La}(\text{L})] \cdot 3\text{H}_2\text{O}$ at 80°C in $(\text{CD}_3)_2\text{SO}$ consists of 19 resonances, 6 in the aliphatic region in the chemical shift range of $60\text{--}74\text{ ppm}$, 12 in the aromatic region in the range of $110\text{--}153\text{ ppm}$ and 1 attributable to the imine carbon at $\delta = 170\text{ ppm}$. The 2D NMR experiments, such as ^1H -NOESY and ^{13}C -HMQC, have been useful for the correct interpretation of ^1H NMR spectra and for understanding the exact coordination site of the lanthanum(III) ion. The imine peak lies at $\delta = 8.07\text{ ppm}$ [$\delta = 0.4\text{ ppm}$ upfield than the free H_3L in $(\text{CD}_3)_2\text{SO}$]. The aromatic pattern consists of one multiplet centred at $\delta = 6.74\text{ ppm}$ (protons **14**, **12** and **3**), two doublets ($6.75, 6.07\text{ ppm}$; **2**, **11**) and one triplet ($\delta = 6.21\text{ ppm}$, **11**). The aliphatic region, well ascertained by dipolar long range NOESY correlations, consists of two triplets ($4.11, 2.85\text{ ppm}$, **8**, **6**), two singlets ($3.74, 3.59\text{ ppm}$, **10**, **7**) and three multiplets ($3.83, 3.87, 3.50\text{ ppm}$, **5a**, **9**, **5b**). Only the methylenic group **5** shows a geminal pattern confirming the strong coordination of the lanthanum(III) ion in the ON_3O_2 site.

All the homodinuclear complexes $[\text{Ln}_2(\text{L})](\text{Cl})_3 \cdot n\text{H}_2\text{O}$ have been prepared by condensation of the diformyl and amine precursor in the presence of the appropriate lanthanide salt $\text{LnCl}_3 \cdot x\text{H}_2\text{O}$ as a templating agent and $[\text{N}(\text{CH}_3)_4](\text{OH})$ as the base. They are almost insoluble in alcoholic media and only moderately soluble in dimethyl sulfoxide. It was impossible to grow single crystals suitable for X-ray structural determinations: the obtained micro crystals are homogeneous and show an $\text{Ln}/\text{Cl} = 2:3$ ratio, determined by SEM-EDS. Elemental and thermogravimetric analyses suggest they can be generally formulated with a variable amount of coordinated water molecules depending on the synthetic pathway followed (vide post). The IR spectra are similar each other and show a strong $\nu(\text{C}=\text{N})$ band at $1629\text{--}1639\text{ cm}^{-1}$ which is about 10 cm^{-1} higher than those bands found in the related mononuclear complexes $[\text{Ln}(\text{L})] \cdot n\text{S}$ but lower than those found for the mononuclear complexes $[\text{Ln}(\text{H}_3\text{L})(\text{Cl})_2(\text{CH}_3\text{COO}) \cdot n\text{S} \cdot m\text{HCl}]$ in which the lanthanide(III) ion lies in the crown-ether like site. This indicates that the homodinuclear complexation gives rise to a coordination involvement of the imine groups between the two extreme situations found in the two positional mononuclear isomers.

ESI-MS spectra of the homodinuclear complex $[\text{Er}_2(\text{L})(\text{H}_2\text{O})_3](\text{H}_2\text{O})(\text{Cl})_3$ in methanol show the parent peak (with a correct Er_2Cl_2 isotopic pattern) of the species $[\text{Er}_2(\text{L})(\text{Cl})_2(\text{H}_2\text{O})_3(\text{CH}_3\text{OH})]^+$ at $m/z = 1051.37$ and the molecular peak of the mononuclear complex fragment $[\text{Er}(\text{L}) + \text{Na}]^+$ at $m/z = 749.33$, indicating that the three water solvent molecules are coordinated to the metal ions and that the mononuclear residual complex is very stable in methanol, as above reported, owing to the strong contribution of the phenolate pendant arm to the coordination.

The purity and structural conformations of the homodinuclear complexes were ascertained from their ^{13}C and ^1H NMR spectra. For the diamagnetic complexes, $[\text{Ln}_2(\text{L})](\text{Cl})_3 \cdot n\text{H}_2\text{O}$ ($\text{Ln} = \text{La}, \text{Lu}, \text{Y}$), the signals were assigned on the basis of shift values, integrations and line splitting patterns. In particular, the ^{13}C NMR spectrum of $[\text{Y}_2(\text{L})](\text{Cl})_3 \cdot 3\text{H}_2\text{O}$ at room temp. in CD_3OD consist of 19 resonances, 6 in the aliphatic region and 13 in the chemical shift range of 116–169 ppm. Clearly, this spectroscopic degeneracy indicates that a dynamic process is occurring in solution on the NMR time scale which averages the signals of pairs of atoms. More information can be gained from the proton spectra, while 2D experiments enabled us to produce a complete assignment of the peaks (see experimental section). The spectra parallel those of the heterodinuclear species (vide post) and HMQC data show that the methylenic groups **6**, **5**, **8** and **9** are split in eight geminal groups (**10** is uncertain as geminal) proving the rigidity of these coordination moieties on the NMR time scale and confirming the fact that each of the two yttrium(III) ions occupies a different site.

The rationalization of the more complex NMR spectra of the paramagnetic systems deriving from a variety of experiments and investigations, will be discussed in detail in a subsequent paragraph.

Heterodinuclear Complexes

The following different synthetic methodologies have been employed for the preparation of the heterodinuclear complexes (Scheme 2): C) the addition of a stoichiometric amount of the appropriate $\text{Ln}'(\text{CH}_3\text{COO})_3 \cdot x\text{H}_2\text{O}$ to the desired mononuclear complex $\text{Ln}(\text{H}_3\text{L})(\text{Cl})_2(\text{CH}_3\text{COO}) \cdot n\text{S} \cdot m\text{HCl}$ in the presence of $\text{N}(\text{C}_2\text{H}_5)_3$ in methanol, followed by workup of the crude products with CHCl_3 , $\text{C}_2\text{H}_5\text{OH}$ and $(\text{C}_2\text{H}_5)_2\text{O}$ to produce crystalline powders formulated as $[\text{LnLn}'(\text{L})(\text{Cl})_2(\text{CH}_3\text{COO})] \cdot n\text{S}$, the latter being quite soluble in alcoholic solution; D) the addition of equimolar amounts of the appropriate salts, LnCl_3 and $\text{Ln}'\text{Cl}_3$, in succession to the diformyl and amine precursors in methanol containing $[\text{N}(\text{CH}_3)_4](\text{OH})$. In particular, after the addition of the first lanthanide salt, the resultant solution was heated to reflux. Subsequent addition of the second lanthanide salt, after workup, led to separation of microcrystals formulated as $[\text{LnLn}'(\text{L})](\text{Cl})_3 \cdot n\text{S}$. Again, attempts to grow crystals suitable for X-ray structural determination were unsuccessful. The homogeneity and correct $\text{Ln}/\text{Ln}'/\text{Cl}$ ratio

(1:1:2 and 1:1:3 for the complexes derived from synthetic methodologies C and D, respectively) were ascertained from SEM-EDS studies.

The IR spectra of the heterodinuclear complexes, prepared by both procedures C and D parallel each other apart the additional IR bands at 1543–1575 cm^{-1} due to the $\nu(\text{C}=\text{O})$ stretching of the carboxylate groups occurring in $[\text{LnLn}'(\text{L})(\text{Cl})_2(\text{CH}_3\text{COO})] \cdot n\text{S}$. Furthermore, a strong $\nu(\text{C}=\text{N})$ peak at 1632–1638 cm^{-1} , shifted toward lower wavelengths when compared with the free macrocycle (1642 cm^{-1}) and toward higher wavelength when compared with the mononuclear complexes derived from the method B (ca. 1627 cm^{-1}) suggests that the imine group is involved in the coordination of the lanthanide ion but has a lower double bond character. This is in agreement with the behaviour observed for the homodinuclear complexes.

In the recent past^[18] during the synthesis of the heterodinuclear lanthanide(III) complexes with the above mentioned asymmetric compartmental ligands $\text{H}_2\text{L}_\text{A}$, $\text{H}_2\text{L}_\text{B}$ or $\text{H}_2\text{L}_\text{C}$, transmetalation, decomplexation and/or migration strongly dependent on the employed solvents, have been observed. The final event was the occurrence of a mixture of dinuclear and mononuclear complexes. These unwanted reactions represent a significant problem affecting the synthetic pathway, often frustrating the obtainment of the designed complexes. Thus, although pure positional heterodinuclear complexes $\text{LnLn}'(\text{L}_{\text{A,B,C}})(\text{Cl})_4(\text{H}_2\text{O})_n$ and $\text{Ln}'\text{Ln}(\text{L}_{\text{A,B,C}})(\text{Cl})_4(\text{H}_2\text{O})_n$, could be prepared and characterised thanks to the availability of the appropriate O_2O_n mononuclear complexes $[\text{Ln}(\text{H}_2\text{L}_{\text{A,B,C}})(\text{H}_2\text{O})_4](\text{Cl})_3$ and $[\text{Ln}'(\text{H}_2\text{L}_{\text{A,B,C}})(\text{H}_2\text{O})_4](\text{Cl})_3$, they easily evolve in methanol or dimethyl sulfoxide into a series of species which includes the free ligand as well as mononuclear and heterodinuclear complexes with a metal ion site occupancy which is the reverse from that of the starting complexes (scrambling reactions). This means that the two chambers, owing to their different bite and donor atom set, can act as selective receptors of a specific lanthanide ion but are not able to sufficiently stabilise such coordination in the presence of another different lanthanide.

On the contrary, in the present complexes, the same positional heterodinuclear isomers were obtained independently of the adopted synthetic procedure. Thus, the same LuEu isomeric complex, with the lutetium(III) ion in the ON_3O_2 Schiff base and the europium(III) ion in the O_2O_4 crown ether-like chamber, was obtained by the synthetic procedure D, i.e. by the addition of LuCl_3 and then EuCl_3 or vice versa. Otherwise, the synthetic pathway C is strongly affected by the ionic radius of the lanthanide of the starting mononuclear complex. For example, in the preparation of the EuLa complex, the subsequent addition of the second lanthanide(III) acetate affords the desired complex only when $\text{La}(\text{H}_3\text{L})(\text{Cl})_2(\text{CH}_3\text{COO}) \cdot \text{H}_2\text{O} \cdot 2.5\text{Py}$ is the starting complex, while the reverse sequence gives rise to products which are not completely pure.

This behaviour can be explained because of the ability of the first coordinating lanthanide(III) ion to choose the site on the basis of the best-fit metal ion coordinating size. Both

the heterodinuclear synthetic procedures, in fact, produce complexes where the site occupancy of both lanthanide ions depend on their ionic radii. Thus, the Schiff base site ON_3O_2 , having a smaller coordination dimension, will be preferentially filled by the lanthanide(III) ion with the smaller radius [i.e. the heavier lanthanide(III) ion] while the larger O_2O_4 site will preferentially accommodate the larger lanthanide(III) ion [i.e. the lighter lanthanide(III) ion]. This site occupancy preference gives rise to well defined positional isomers and not to mixtures of heterodinuclear isomers or homodinuclear complexes. The synthetic procedure **C**, starting from a preformed mononuclear complex with the O_2O_4 site filled, produces the heterodinuclear complex only when the second incoming lanthanide is heavier than the already coordinated one. In the synthetic route **D**, the two lanthanide ions are in competition for the most suitable coordination site owing to the almost simultaneous addition of the metal ions in methanol solution and, hence, they can be preferentially accommodated according to the above mentioned best-fit rule. This was substantiated by ESI-MS, SEM-EDS (see Figure 1) and NMR spectroscopic measurements.

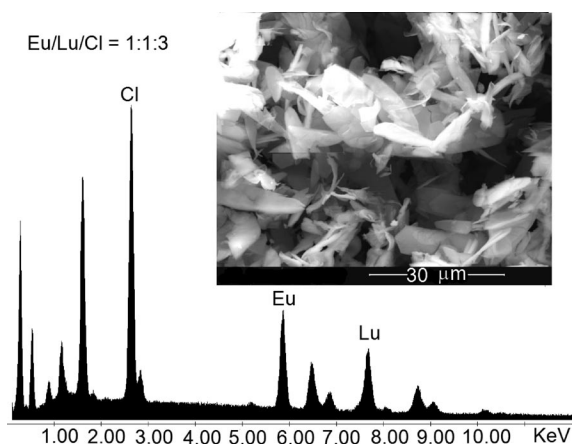
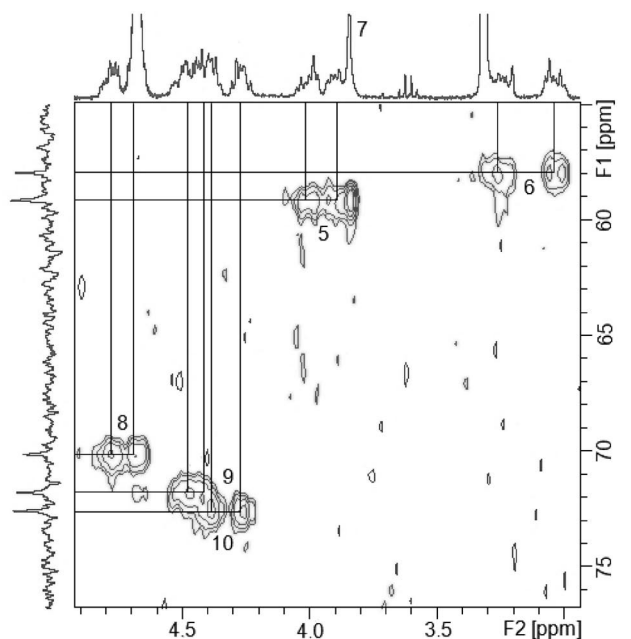


Figure 1. SEM and EDX analyses of the complex $[\text{LuEu}(\text{L})](\text{Cl})_3 \cdot 2\text{H}_2\text{O}$.

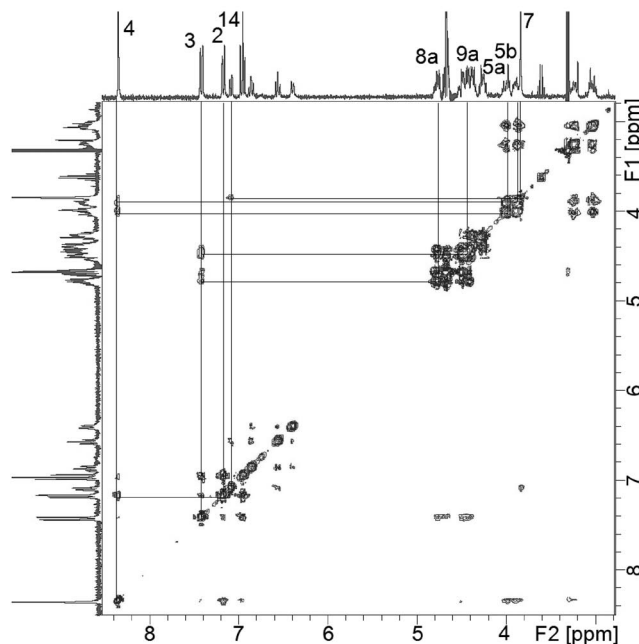
As an example, ESI-MS spectra of the heterodinuclear $[\text{LuEu}(\text{L})](\text{Cl})_3 \cdot 2\text{H}_2\text{O}$ complex in methanol shows characteristics which parallel those of the homodinuclear species with the parent peak (with correct LuEuCl_3 isotopic pattern) of the heterodinuclear species $[\text{LuEu}(\text{L})(\text{Cl})_3(\text{H}_2\text{O})_2 + \text{H}]^+$ at $m/z = 1030.33$ and the molecular peak of the mononuclear fragment $[\text{Lu}(\text{L}) + \text{Na}]^+$ at $m/z = 758.40$ confirming that the water molecules are firmly coordinated to the metal ions.

The ^{13}C NMR spectra of the diamagnetic complex $[\text{LuLa}(\text{L})](\text{Cl})_3 \cdot 2\text{H}_2\text{O}$, recorded at 298 K and 75.4 MHz in CD_3OD , show 19 resonances: 6 in the aliphatic region due to the ethylenic and the methylenic groups, and 13 between $\delta = 117$ and 171 ppm, assigned to the aromatic and iminic carbon atoms. The resonances of the aliphatic carbons can be assigned to the methylenic pendant arm group ($\delta = 59.00$ ppm), to the methylenic carbons of the oxoethylenic bridges (70.14, 75.75 and 72.63 ppm) and to the methylenic

carbons of the ON_3O_2 coordination site (57.95 and 59.12 ppm). The occurrence of this simple spectroscopic pattern is indicative of the presence, in solution, of a symmetry plane perpendicular to the molecule and passing through the LuLa axis. The corresponding ^1H NMR spectrum at 298 K shows a very complex pattern with 19 groups of resonances: a singlet at $\delta = 8.35$ ppm due to **4**, two doublets of doublets at $\delta = 7.17$ and 7.41 ppm attributed to **2**



a)



b)

Figure 2. $[\text{LuLa}(\text{L})](\text{Cl})_3 \cdot 2\text{H}_2\text{O}$ in $(\text{CD}_3)_2\text{OD}$ at 298 K. (a) 2D HETCOR ^1H (^{13}C) HMQC: geminal correlations in the aliphatic region. (b) 2D ROESY ^1H NMR (spin lock time of 200 ms): long range connections.

and **3**, a triplet at $\delta = 6.95$ ppm due to **1**, two doublets at 6.39, 7.08 ppm due to **11**, **14** and two triplets at $\delta = 6.56$ and 6.86 ppm due to protons **13**, **12**; ten multiplets in the region 3.00–4.80 ppm and a singlet at $\delta = 3.84$ ppm which can be easily assigned to **7**. The presence of multiplets for the methylenic protons reveals a much higher stereochemical rigidity for the heterodinuclear complexes when compared with the corresponding mononuclear ones (obtained by the synthetic route **B**) in which a time-averaged planar structure occurs in methanol. This additional rigidity is provided by the coordination of the lanthanum ion into the crown ether site. An HMQC experiment (298 K) (Figure 2, a): indicated the correlation of the multiplets at $\delta = 3.03$ and 3.24 ppm with the ^{13}C resonance at $\delta = 57.95$ ppm, the multiplets at $\delta = 3.88$ and 3.98 ppm with the ^{13}C resonance at $\delta = 59.12$ ppm, the multiplets at $\delta = 4.26$ and 4.37 ppm with the ^{13}C resonance at $\delta = 72.63$ ppm, the multiplets at 4.41 and 4.47 ppm with the ^{13}C resonance at $\delta = 75.75$ ppm and, finally, the multiplets at $\delta = 4.67$ and 4.77 ppm with the carbon peak at $\delta = 70.14$ ppm. Lastly, a 2 D ROESY ^1H experiment (Figure 2, b) allowed the complete assignment of the proton and carbon spectra. At 298 K and by using a spin lock time of 200 ms, cross-peaks were observed between the imino protons ($\delta = 8.35$ ppm) and the resonances at 7.17 and 3.88/3.98 ppm which were then assigned to the protons **2** and **5(a,b)**, respectively, between the methylenic resonance of the pendant arm **7** and the multiplet at 3.03 **6(a)**, and between the proton **3** and the multiplet resonances at $\delta = 4.77$ and 4.41 ppm (**8a** and **9a**). The protons of the five ethylenic groups (**5,6** and **8,9**) are in a staggered conformation and show a pattern of two triplets of doublets (axial protons) and two doublets of doublets (equatorial). Interestingly, both the ON_3O_2 and the O_4O_2 sites show a very similar multiplicity pattern, confirming that two lanthanide(III) ions are rigidly coordinated into the two chambers. Finally, in both the ^1H and ^{13}C NMR spectra, only a single solvent peak can be observed. This

implies that in solution the chloride anions are displaced by solvent molecules that are in rapid exchange (on the NMR timescale) with the bulk.

NMR Solution Study of the Heterodinuclear Paramagnetic Complexes

The spectra of the diamagnetic complexes do not provide a clear and conclusive indication of the coordination site occupancy by the two lanthanide(III) ions and do not allow the assessment of structural changes in solution across the lanthanide(III) series, as often observed in related compartmental lanthanide complexes.^[23] These points can be conveniently elucidated from the spectra of the corresponding paramagnetic derivatives. The NMR experiments of the heterodinuclear paramagnetic complexes in different coordinating solvents [i.e. CD_3OD and $(\text{CD}_3)_2\text{SO}$], in fact, turned out to be of paramount relevance in understanding the site occupancy of the different lanthanide(III) ions. As reported above, in these recognition processes the shape of the coordination cavities is quite relevant in directing the incoming ions toward a specific site. When two lanthanide ions with significantly different ionic radii are used, the smaller one invariably fills the ON_3O_2 Schiff base site of H_3L , leaving the O_2O_4 site accessible to the other larger lanthanide(III) ion. As an example, the ^1H NMR spectra of the LaEu and EuLu complexes in CD_3OD are quite complex with a very large number of resonances (showing a stereochemical behaviour similar to that found for the LuLa complex above discussed) but significantly different from each other, owing to the different site occupancy of the two lanthanide ions according to their different ionic radii (Figure 3).

The same behaviour was observed when Eu is substituted by Er. The pattern of the spectrum related to the EuLa complex spreads over -30 to $+40$ ppm with a mean band-

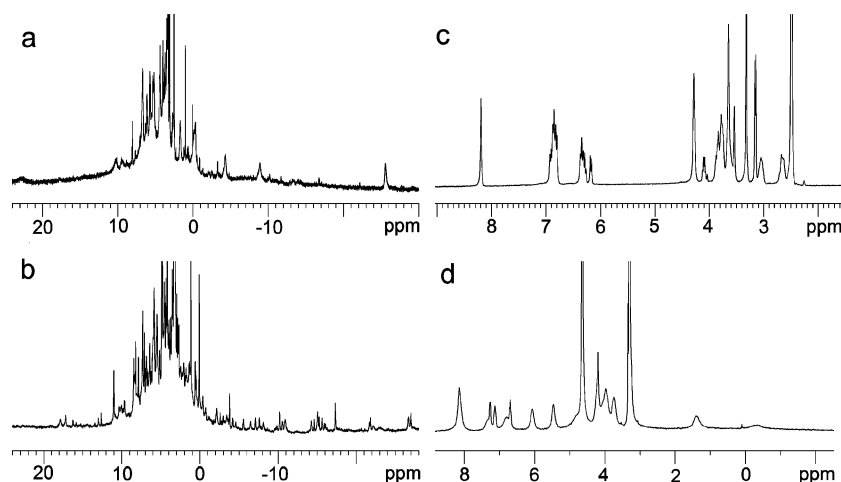


Figure 3. 300 MHz ^1H NMR spectra of the paramagnetic complexes at 298 K in $(\text{CD}_3)_2\text{SO}$: $[\text{EuLa}(\text{L})]^{3+}$ (a), $[\text{LuEu}(\text{L})]^{3+}$ (c); in CD_3OD : $[\text{EuLa}(\text{L})]^{3+}$ (b), $[\text{LuEu}(\text{L})]^{3+}$ (d).

Table 1. Site occupancy of the two lanthanide(III) ions in CD₃OD and (CD₃)₂SO for the prepared heterodinuclear complexes.^[a]

| [Ln ^S Ln ^E (L)](Cl) ₃ · <i>n</i> S | | | | | | | | | | | | | |
|---|--------------------------------|---------------------------------|---------------------------------|--|---------------------------------|---------------------------------|---------------------------------|---------------------------------|---------------------------------|---------------------------------|--------------------------------|---------------------------------|--|
| CD ₃ OD | Eu ^E Y ^S | Eu ^E Lu ^S | La ^E Eu ^S | Er ^E /Y ^S /Er ^E | Er ^E Lu ^S | La ^E Er ^S | La ^E Tb ^S | Tb ^E Lu ^S | Tb ^E Er ^S | Tb ^E Eu ^S | Ce ^E Y ^S | La ^E Yb ^S | |
| (CD ₃) ₂ SO | Y ^S | Lu ^S | Eu ^S | Y ^S Er ^S | Lu ^S | Er ^S | Tb ^S | Lu ^S | Er ^S | Eu ^S | Y ^S | Yb ^S | |

[a] Ln^E: metal ion in O₂O₄. Ln^S: metal ion in ON₃O₂.

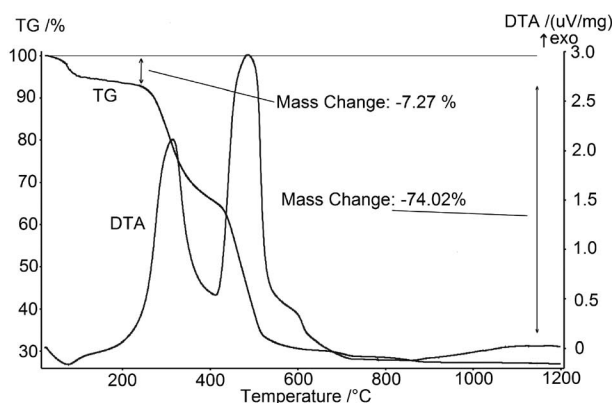
width at half-height ($\Delta\nu_{1/2}$) of 30 Hz while for the ErLa complex a -30 to $+25$ ppm range with a mean $\Delta\nu_{1/2}$ peak of 70 Hz was observed. For the related LuEu complex the range is considerably reduced ($-2/+11$ ppm) with a mean $\Delta\nu_{1/2}$ of 150 Hz while for the LuEr with a range of $-10/+17$ ppm a mean $\Delta\nu_{1/2}$ band of 100 Hz occurs. These data strongly support the site preference of paramagnetic lanthanide(III) ions as a consequence of their ionic radii. They strongly influence, in fact, the neighbouring protons, hence offering a clear picture of the coordination environment. Further evidences comes from the YEu complex. Its ¹H NMR spectrum in (CD₃)₂SO is quite similar to that of the LuEu compound since the ionic radius of the yttrium(III) ion is smaller of that of the europium(III) ion. When a strongly coordinating solvent as (CD₃)₂SO is employed, other properties of the two coordination sites of the macrocycle [L]³⁻ can be observed. They clearly indicate, for instance, that the ON₃O₂ Schiff base site, owing to the availability of a pendant phenolic group, is a better coordinating system in comparison with the O₂O₄ crown-ether like site. A strongly coordinating solvent i.e. dimethyl sulfoxide can remove the metal ion from the O₂O₄ site and this demetalation process does not cause drastic variations in the NMR signals of the diamagnetic complexes where only a reduced rigidity can be observed, whereas drastic variations occur when a paramagnetic centre is released from the coordination sphere. It was observed that when a paramagnetic lanthanide(III) ion resides in the O₂O₄ chamber, it can be easily released with (CD₃)₂SO whereas it remains firmly coordinated when encapsulated into the ON₃O₂ Schiff base site. Thus, the NMR spectra in dimethyl sulfoxide become very diagnostic of the site occupancy of a paramagnetic lanthanide(III) ion. By comparison with the spectrum of the same complex in CD₃OD, where this demetalation process does not occur, it is possible to obtain, in addition, quite convincing evidence for correctly determining the coordination preference of the different lanthanide(III) ions (Table 1).

In the homodinuclear complexes, the same behaviour occurs. The spectra in (CD₃)₂SO are, in fact, superimposable on that obtained from the heterodinuclear complexes with the same lanthanide ion in the ON₃O₂ chamber. In CD₃OD, the spectra show, as expected, a greater complexity due to the second lanthanide ion bound in the O₂O₄ crown-ether like site.

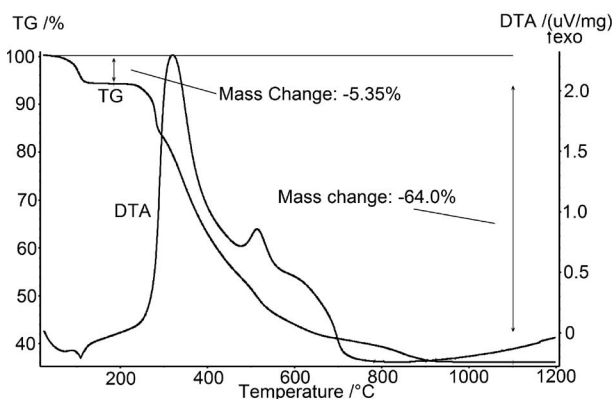
Thermal Behaviour

All the complexes have been investigated by thermogravimetric measurements in the reported conditions up to 1200 °C, the related oxides being the final product at this

temperature. The mononuclear complexes Ln(H₃L)(Cl)₂·(CH₃COO)·*n*S·*m*HCl undergo a weight loss in line with the proposed formulation, although it is not possible to define correctly their thermal behaviour. Better results were obtained with the mononuclear complexes [Ln(L)]·*n*S the weight losses of which agree well with the proposed formulation. For some of these complexes, i.e. for [Y(L)]·2.5H₂O, it is possible to verify the loss of the neutral coordinated molecules at relatively low temperature followed by a thermal stability plateau. All these mononuclear complexes give rise to the related Ln₂O₃ oxide as the final product except the lanthanum(III) complex which, according to XRD measurements and the La/Cl = 1:1 ratio determined by SEM-EDS, produces LaOCl. The thermogram of [La(L)]·3H₂O (Figure 4, a) in fact indicates the loss of water molecules in the 30–100 °C temperature range (weight loss, 7.27% against a calculated value 7.16%; endothermic peak at about 100 °C). The final weight loss of 74.02% at about



a)



b)

Figure 4. TG-DTA thermograms of [La(L)]·3H₂O (a) and [LuE-u(L)](Cl)₃·2H₂O (b).

1100 °C is consistent with the calculated value (74.74%) for LaOCl as the final product.

Satisfactory results have also been obtained for the homodinuclear complexes, in several cases the loss of neutral molecules is clearly detectable. For instance, the Eu₂ or Lu₂ complexes show the expected weight loss of the neutral coordinated molecules at relatively low temperature (60–120 °C) followed by a thermal stability plateau extending up to 190 °C and 212 °C, respectively. The final fate of the thermal decomposition is again the formation of the related Ln₂O₃ oxides as indicated by their XRD patterns which are consistent with the literature data, except for that the La₂ complex which gives rise to LaOCl as for the mononuclear lanthanum(III) complex.

Analogous to the related mononuclear complexes, the heterodinuclear [LnLn'(L)(Cl)₂(CH₃COO)]_nS species also exhibits thermal behaviour which is quite difficult to rationalise: a series of weight losses occur without any detectable certain chemical event. In contrast, the thermal behaviour of [LnLn'(L)](Cl)₃·*n*S complexes agrees perfectly with the proposed formulation: the weight loss of the neutral coordinated molecules, in the low temperature range (120–150 °C), correctly matches with the corresponding DTA endothermic peak. This event is followed by a long thermal stability plateau up to ca. 300 °C which indicates the remarkable stability of these complexes. The subsequent thermal degradation occurs in the 300–800 °C temperature range. All these heterodinuclear complexes decompose giving rise to species where a 1:1 = Ln:Ln' ratio always occurs. Again, also considering the XRD spectra of the parent Ln₂O₃ and Ln'₂O₃ compounds, the occurrence of the LnLn'O₃ oxides has been proposed except for the lanthanum containing compounds. As an example, the thermal curves of [LaYb(L)](Cl)₃·CH₃OH show the loss of MeOH (–3.10%, against a calculated value 3.16%; endothermic peak at 136 °C), a stability plateau up to 320 °C and the subsequent decomposition in the 320–800 °C temperature range. The final weight loss at this temperature (61.8%) agrees with a mixture formulated as LaOCl + ½Yb₂O₃ (63.0%) and this was clearly confirmed by the La/Yb/Cl = 1:1:1 ratio found from the SEM-EDS measurements and XRD spectra which match perfectly with an analogous mixture of the two oxides.

The thermal curve of the heterodinuclear complex [LuEu(L)](Cl)₃·2H₂O (Figure 4, b) shows an initial weight loss due to water release (–5.35% against a calculated value of 5.13%; DTA endothermic peak at 109.5 °C) followed by the thermal stability plateau ending at 230 °C. The subsequent decomposition occurs in the 230–900 °C temperature range and the final weight loss at this temperature (64.0%) agrees with the formulation of EuLuO₃ as the final product. This is clearly confirmed by the Eu/Lu = 1:1 ratio found from the SEM-EDS measurements and XRD spectra.

Conclusions

The heavy difficulties experienced in the recent past in obtaining stable heterodinuclear complexes, using dif-

ferently shaped compartmental ligands, were successfully overcome through the design and synthesis of the [1+1] functionalised ligand H₃L.

This macrocycle, thanks to the insertion of a phenolic pendant group at the central amine nitrogen of the Schiff base chamber, can adequately direct the lanthanide ions towards a specific chamber according to the metal-ion-coordinating size best fit. This, in turn, allows the formation of isomeric pure heterodinuclear complexes. Substantial structural information was obtained by ¹H and ¹³C NMR experiments with complexes containing paramagnetic lanthanide(III) ions in different coordinating solvents (i.e. methanol, dimethyl sulfoxide). Different magnetic interactions between the lanthanide(III) ion and the organic moiety produce dramatic variations in the chemical shifts useful to identify the site involved in the coordination. Thus, it was possible to verify that when two lanthanide(III) ions are simultaneously introduced into a solution containing the deprotonated [L]^{3–} macrocycle, the heavier lanthanide(III) ion almost exclusively resides in the smaller ON₃O₂ Schiff base site and the lighter lanthanide(III) ion in the O₂O₄ crown ether like site, avoiding site migration and transmetalation, etc.

Remarkably these complexes give rise, by thermal decomposition, to the related LnLn'O₃ oxides. Only the lanthanum(III) containing complexes invariably afford LnOCl when mononuclear or homodinuclear complexes are the starting sources or LnOCl + ½Ln₂O₃ when the starting materials are the heterodinuclear complexes.

The possibility of synthesising well defined heterodinuclear complexes avoiding the side transmetalation, migration and demetalation reactions opens new, quite interesting possibilities for a correct and exhaustive elucidation of the physico-chemical properties arising from this aggregation, and studies on their optical and magnetic properties are currently under severe scrutiny.

Experimental Section

Materials: Solvents, inorganic and organic compounds and the hydrated lanthanide chlorides were commercial products (Aldrich, Riedel-de Haën, Carlo-Erba or Fluka) and used as received without further purification.

Physico-Chemical Measurements: Elemental analyses were carried out using a Fison 1108 analyser. IR spectra were recorded using KBr pellets on a Mattson FTIR spectrometer. All NMR spectra (¹H, ¹³C) were recorded using a Bruker AMX300 spectrometer equipped with direct and inverse broadband multinuclear probes and a variable-temperature unit, with lanthanide(III) complexes dissolved in CD₃OD or (CD₃)₂SO, used also as the internal reference. The T1 longitudinal relaxation times and the mixing times of NOESY experiments were measured using the standard inversion recovery pulse sequence. All ESI-MS mass spectrometric measurements were performed using an LCQ mass spectrometer (Finnigan) and methanolic solutions of the samples (10^{–5} M). The thermogravimetric (TG) and differential thermo analyses (DTA) curves were obtained using a Netzsch STA449 thermoanalyser equipped with Soft Proteus Netzsch software. The measurements were carried out in the range 35–1200 °C in alumina crucibles under air (flux

rate 50 cm³ min⁻¹) and a heating rate of 5 °C min⁻¹, using neutral alumina as a reference material.

X-ray diffraction measurements were carried out on sample powders with a Philips X'Pert PW3710 diffractometer using Cu-K_α radiation (40 kV, 30 mA), a high resolution graphite monochromator, rotating sample holder and proportional detector. Measurements were carried out in the range 5° < 2θ < 90° with a step of 0.02°.

The morphology, homogeneity and the Ln/Cl or Ln/Ln'/Cl ratio of the complexes were investigated using a Fei-Esem FEI Quanta 200 FEG instrument equipped with a field emission gun, operating in high vacuum conditions at an accelerating voltage variable from 0 to 30 keV, depending on the observation needs. EDX analyses and X-ray mapping (elemental mapping) were obtained by using an EDAX Genesis energy-dispersive X-ray spectrometer at an accelerating voltage of 25 keV

Diformyl and Amine Precursors: The diformyl precursor 3,3'-(3,6-dioxaoctane-1,8-diylidioxo)bis(2-hydroxybenzaldehyde) (H₂L') was prepared according to the literature^[2] and purified by chromatography on silica gel using CHCl₃ as the eluent. The amine precursor *N,N*-bis(2-aminoethyl)-2-hydroxybenzylamine·3HCl (HA'·3HCl) was also prepared according to the literature.^[24] The proposed formulation of both the precursors was checked by elemental analysis, ESI-MS, IR and NMR spectroscopic measurements.

Macrocyclic Ligand H₃L: H₂L' (0.5 mmol, 195 mg) in CHCl₃ (30 mL) was added to the warm (40 °C) CHCl₃ (200 mL) solution of HA'·3HCl (0.5 mmol, 159.3 mg) and N(C₂H₅)₃ (1.5 mmol, 210 μL). The resultant yellow solution was then heated to reflux for 1 h then partially reduced in volume under N₂. Diethyl ether was added (30 mL) and the solution stirred overnight producing a yellow precipitate which was filtered, washed with diethyl ether and dried in vacuo (yield 10%). IR: $\tilde{\nu}$ = 1640 (C=N) cm⁻¹. ESI-MS: *m/z* (%) = 480.54 for [M - (-CH₂PhOH) + Na]⁺ {480.2 calcd. for [M - (-CH₂PhOH) + Na]⁺}. ¹H NMR [(CD₃)₂SO]: δ = 8.43 (s, 2 H, 4), 7.20 (m, 1 H, 12), 7.07 (d, 1 H, 14), 6.96 (d, 2 H, 3), 6.90 (d, 2 H, 2), 6.79–6.66 (m, 4 H, 1, 11, 13), 4.05 (br. s, 4 H, 8), 3.85 (s, 2 H, 7), 3.71 (m, 8 H, 9, 5), 3.61 (s, 4 H, 10), 2.91 (t, 4 H, 6) ppm. ¹H NMR (CDCl₃): δ = 8.26 (s, 2 H, 4), 7.19 (t, 1 H, 12), 7.05 (d, 1 H, 14), 6.93 (d, 2 H, 3), 6.89–6.77 (m, 4 H, 2, 11, 13), 6.74 (d, 2 H, 1), 4.15 (br. s, 4 H, 8), 3.96 (s, 2 H, 7), 3.89 (s, 4 H, 9), 3.75 (m, 8 H, 10, 5), 3.08 (t, 4 H, 6) ppm.

Complexes: The formulations of the complexes do not take into account coordinated and noncoordinated solvent molecules owing to the lack of crystal structures. More information about the coordination involvement is reported in the results and discussion section. The yield range reported for each synthetic route depends on the procedure adopted for the recovery of additional products from the mother liquor.

Synthetic Route A. Preparation of Ln(H₃L)(Cl)₂(CH₃COO)·*n*S·*m*HCl: H₂L' (0.3 mmol) and Ln(CH₃COO)₃·*x*H₂O (0.3 mmol) were mixed in pyridine (30 mL) at room temperature. The solution was heated at 80 °C for 2 h. HA'·3HCl (0.3 mmol) was added to this hot solution and the heating continued for 1 h. The solvent was partially evaporated and addition of diethyl ether to the solution resulted in a yellow precipitate which was filtered, washed with diethyl ether and dried in vacuo (yield 53–67%).

La(H₃L)(Cl)₂(CH₃COO)·H₂O·2.5Py: IR: $\tilde{\nu}$ = 1650 (C=N) cm⁻¹. C_{45.5}H_{54.5}Cl₂LaN_{5.5}O₁₀ (1048.24): calcd. C 45.62, H 4.76, N 4.84; found C 45.70, H 4.08, N 5.25. ¹H NMR (CD₃OD): δ = 8.46 (s, 2 H, 4), 7.30 (dd, 2 H, 3), 6.99 (dd, 2 H, 2), 6.93 (d, 1 H, 14), 6.77 (d, 1 H, 11), 6.68 (t, 2 H, 1), 6.40 (dd, 1 H, 12), 6.31 (dd, 1 H, 13), 4.56 (t, 4 H, 8), 4.46 (t, 4 H, 9), 4.16 (s, 4 H, 10), 3.73 (t, 4 H, 5),

3.56 (s, 2 H, 7), 2.96 (t, 4 H, 6) ppm. T.G. weight loss to final oxide: found 78% (calcd. 74%).

Eu(H₃L)(Cl)₂(CH₃COO)·H₂O·0.5Py·HCl: IR: $\tilde{\nu}$ = 1647 (C=N) cm⁻¹. C_{35.5}H_{45.5}Cl₃EuN_{3.5}O₁₀ (939.55): calcd. C 44.53, H 5.00, N 5.12; found C 44.70, H 5.22, N 5.49. T.G. weight loss to final oxide: found 81.62% (calcd. 79.84%).

Y(H₃L)(Cl)₂(CH₃COO)·2.5H₂O·Py·HCl: IR: $\tilde{\nu}$ = 1630 (C=N) cm⁻¹. C₃₈H₅₁Cl₃N₄O_{11.5}Y (943.06): calcd. C 48.40, H 5.45, N 5.94; found C 47.65, H 5.71, N 6.46. ¹H NMR (CD₃OD): δ = 8.44 (s, 2 H, 4), 7.38 (dd, 2 H, 3), 7.01 (dd, 2 H, 2), 6.85 (d, 1 H, 14), 6.77–6.65 (m, 3 H, 11, 1), 6.40 (m, 1 H, 12), 6.25 (m, 1 H, 13), 4.60 (t, 4 H, 8), 4.45–4.20 (m, 4 H, 9), 4.08 (s, 4 H, 10), 3.80–3.70 (m, 4 H, 5), 3.56 (s, 2 H, 7), 2.92–2.85 (m, 4 H, 6) ppm. T.G. weight loss to final oxide: found 88.01% (calcd. 88.16%).

Ce(H₃L)(Cl)₂(CH₃COO)·HCl: IR: $\tilde{\nu}$ = 1647 (C=N) cm⁻¹. C₃₃H₄₁CeCl₃N₃O₉ (870.15): calcd. C 45.55, H 4.75, N 4.83; found C 43.65, H 4.70, N 4.83. ¹H NMR (CD₃OD): δ = 8.42 (s, 2 H, 4), 7.39–7.08 (m, 4 H, 3, 2), 7.00 (d, 1 H, 14), 6.96–6.91 (m, 4 H, 11, 1, 12), 6.76 (t, 1 H, 13), 4.16 (t, 4 H, 8), 3.88 (m, 4 H, 9), 3.77 (s, 2 H, 7), 3.764.16 (s, 4 H, 10), 3.25–3.06 (m, 4 H, 5), 3.03–2.81 (m, 4 H, 6) ppm.

Yb(H₃L)(Cl)₂(CH₃COO)·2H₂O·0.5Py·HCl: IR: $\tilde{\nu}$ = 1638 (C=N) cm⁻¹. C_{35.5}H_{47.5}Cl₃N_{3.5}O₁₁Yb (978.64): calcd. C 43.57, H 4.89, N 5.01; found C 42.58, H 4.80, N 5.19. T.G. weight loss to final oxide: found 77% (calcd. 79%).

Er(H₃L)(Cl)₂(CH₃COO)·2H₂O·0.7Py·HCl: IR: $\tilde{\nu}$ = 1639.39 (C=N) cm⁻¹. C_{36.5}H_{48.5}Cl₃ErN_{3.7}O₁₁ (988.68): calcd. C 44.34, H 4.94, N 5.24; found C 44.22, H 5.13, N 5.56. T.G. weight loss to final oxide: found 79.06% (calcd. 80.64%).

Tb(H₃L)(Cl)₂(CH₃COO)·2H₂O·0.6Py·HCl: IR: $\tilde{\nu}$ = 1648.90 (C=N) cm⁻¹. C₃₆H₄₈Cl₃N_{3.6}O₁₁Tb (972.44): calcd. C 44.47, H 4.98, N 5.19; found C 44.11, H 5.21, N 5.26. T.G. weight loss to final oxide: found 80.58% (calcd. 81.20%).

Synthetic Route B. Preparation of [Ln(L)]·*n*S: The addition of HA'·3HCl (0.3 mmol) to H₂L' (0.3 mmol) and LnCl₃·*x*H₂O (0.3 mmol) in hot freshly distilled methanol (60 mL) gave rise to a brilliant yellow solution. [N(CH₃)₄](OH) (1.8 mmol) was added and the solution was heated to reflux for 3 h and then allowed to stand overnight. A precipitate separated which was filtered, washed with methanol and dried in vacuo. When no precipitation occurred, the solvent was evaporated to dryness and the residue was treated with the appropriate alcohol (ethanol or 2-propanol as indicated) to afford a solid which was filtered, washed with the appropriate alcohol and dried in vacuo (yield 35–50%).

[La(L)]·3H₂O: 2-Propanol was used as the precipitating solvent. IR: $\tilde{\nu}$ = 1630 (C=N) cm⁻¹. ESI-MS: *m/z* = 722.31 for [La(L) + Na]⁺ {722.50 calcd. for [M - (-CH₂PhOH) + Na]⁺}. C₃₁H₄₀LaN₃O₁₀ (753.55): calcd. C 49.41, H 5.35, N 5.58; found C 49.09, H 5.01, N 5.15. ¹H NMR [(CD₃)₂SO]: δ = 8.07 (s, 2 H, 4), 6.90–6.78 (m, 4 H, 14, 12, 3), 6.75 (d, 2 H, 2), 6.30 (t, 2 H, 1), 6.21 (t, 1 H, 13), 6.07 (d, 1 H, 11), 4.11 (t, 4 H, 8), 4.05–3.61 (m, 2 H, 5a), 3.91–3.83 (m, 4 H, 9), 3.74 (s, 4 H, 10), 3.59 (s, 2 H, 7), 3.56–3.44 (m, 2 H, 5b), 2.85 (t, 4 H, 6) ppm. T.G. weight loss to final oxide: found 74.02% (calcd. 74.74%).

[Eu(L)]·H₂O: IR: $\tilde{\nu}$ = 1628 (C=N) cm⁻¹. C₃₁H₃₆EuN₃O₈ (730.57): calcd. C 50.97, H 4.97, N 5.75; found C 52.39, H 5.01, N 5.45.

[Y(L)]·2.5H₂O: Ethanol was used as the precipitating solvent. IR: $\tilde{\nu}$ = 1629 (C=N) cm⁻¹. C₃₁H₃₉N₃O_{9.5}Y (694.54): calcd. C 53.61, H 5.66, N 6.05; found C 53.50, H 5.50, N 5.90. ¹H NMR [(CD₃)₂SO] 80 °C: δ = 8.14 (s, 2 H, 4), 6.91–6.71 (m, 6 H, 14, 12, 3, 2), 6.37–

6.09 (m, 4 H, 13, 1, 11), 4.19 (t, 4 H, 8), 3.80–3.40 (m, 14 H, 5, 9, 10, 7), 2.66 (t, 4 H, 6) ppm. T.G. weight loss to final oxide: found 82.28% (calcd. 83.5%).

[Er(L)]·5H₂O: Ethanol was used as precipitating solvent. IR: $\tilde{\nu}$ = 1628 (C=N) cm⁻¹. C₃₁H₄₄ErN₃O₁₂ (817.93): calcd. C 45.52, H 5.42, N 5.14; found C 46.60, H 5.40, N 4.75.

[Tb(L)]·2C₂H₅OH: Ethanol was used as precipitating solvent. IR: $\tilde{\nu}$ = 1628 (C=N) cm⁻¹. C₃₅H₄₆N₃O₉Tb (811.65): calcd. C 51.79, H 5.71, N 5.18; found C 51.28, H 5.24, N 4.71. T.G. weight loss to final oxide: found 76.22% (calcd. 77.5%).

[Ce(L)]·C₂H₅OH: Ethanol was used as precipitating solvent. IR: $\tilde{\nu}$ = 1624 (C=N) cm⁻¹. C₃₃H₄₀CeN₃O₈ (746.78): calcd. C 53.08, H 5.40, N 5.63; found C 54.54, H 5.64, N 5.85.

[Lu(L)]·4H₂O: IR: $\tilde{\nu}$ = 1628 (C=N) cm⁻¹. C₃₁H₄₂LuN₃O₁₁ (807.62): calcd. C 46.10, H 5.24, N 5.20; found C 45.44, H 4.80, N 5.46. ¹H NMR [(CD₃)₂SO] 80 °C: δ = 8.18 (s, 2 H, 4), 6.99–6.61 (m, 6 H, 14, 12, 3, 2), 6.48–6.07 (m, 4 H, 1, 13, 11), 4.30 (t, 4 H, 8), 3.98–3.36 (m, 16 H, 9, 5, 10, 7), 3.12–2.95 (m, 2 H, 6a), 2.78–2.55 (m, 2 H, 6b) ppm.

[Dy(L)]·5H₂O: Ethanol was used as precipitating solvent. IR: $\tilde{\nu}$ = 1626.40 (C=N) cm⁻¹. C₃₁H₄₄DyN₃O₁₂ (813.17): calcd. C 45.79, H 5.45, N 5.17; found C 46.57, H 5.33, N 4.59.

Synthetic Route C. Preparation of [LnLn'(L)(Cl)₂(CH₃COO)]·nS: Ln'(CH₃COO)₃·xH₂O (0.06 mmol) and N(C₂H₅)₃ (0.24 mmol) were added to an anhydrous methanol solution of the mononuclear complex Ln(H₃L)(Cl)₂(CH₃COO)·nS·mHCl (0.06 mmol) and the resultant solution maintained at room temp. for 3 h. The solvent was evaporated to dryness and the residue dissolved in CHCl₃ and the resultant solution cleared by filtration. The methanol solution was then evaporated to dryness and the residue dissolved in ethanol and precipitated with diethyl ether. The solid was collected by filtration, washed with diethyl ether and dried in vacuo (yield 35–45%).

[LaLu(L)(Cl)₂(CH₃COO)]·2.5H₂O: IR: $\tilde{\nu}$ = 1638 (C=N) cm⁻¹. C₃₃H₄₂Cl₂LaLuN₃O_{11.5} (1049.45): calcd. C 37.77, H 4.03, N 4.00; found C 38.15, H 4.13, N 3.81. ¹H NMR (CD₃OD): δ = 8.22 (s, 2 H, 4), 7.33 (d, 2 H, 3), 7.02 (d, 2 H, 2), 6.91 (d, 1 H, 14), 6.82 (t, 2 H, 1), 6.69 (t, 1 H, 12), 6.37 (t, 2 H, 13, 11), 4.70–4.49 (m, 4 H, 8), 4.42 (br. s, 2 H, 9a), 4.26–4.11 (m, 4 H, 9b, 10), 4.11–3.96 (m, 4 H, 6), 3.7 (br. s, 4 H, 5), 2.96 (s, 2 H, 7) ppm. T.G. weight loss to final oxide: found 67.32% (calcd. 67.6%).

[LaYb(L)(Cl)₂(CH₃COO)]·2.5H₂O·C₂H₅OH: IR: $\tilde{\nu}$ = 1635 (C=N) cm⁻¹. C₃₅H₄₈Cl₂LaN₃O_{12.5}Yb (1093.59): calcd. C 38.44, H 4.42, N 3.84; found C 37.46, H 4.54, N 3.58.

[EuY(L)(Cl)₂(CH₃COO)]·4H₂O: IR: $\tilde{\nu}$ = 1634 (C=N) cm⁻¹. C₃₃H₄₅Cl₂EuN₃O₁₃Y (1003.46): calcd. C 39.50, H 4.52, N 4.19; found C 39.83, H 4.92, N 3.87.

[LaEu(L)(Cl)₂(CH₃COO)]·2CH₃OH·0.3Py: IR: $\tilde{\nu}$ = 1634 (C=N) cm⁻¹. C_{36.5}H_{46.5}Cl₂EuLaN_{3.3}O₁₁ (1069.22): calcd. C 40.42, H 4.32, N 4.26; found C 40.15, H 4.70, N 4.49. T.G. weight loss to final oxide: found 69.15% (calcd. 67.34%).

[TbEr(L)(Cl)₂(CH₃COO)]·3C₂H₅OH·1.5Py: IR: $\tilde{\nu}$ = 1632 (C=N) cm⁻¹. C_{46.5}H_{62.5}Cl₂ErN_{4.5}O₁₂Tb (1273.57): calcd. C 43.85, H 4.95, N 4.95; found C 41.68, H 5.00, N 4.60. T.G. weight loss to final oxide: found 72.02% (calcd. 70.6%).

Synthetic Route D. Preparation of [LnLn'(L)](Cl)₃·nS: To a hot methanol (60 mL) solution of H₂L' (0.3 mmol) were added LnCl₃·xH₂O (0.3 mmol), HA'·3HCl (0.3 mmol) and [N(CH₃)₄]OH (1.8 mmol). After few minutes, Ln'Cl₃ (0.3 mmol) was added. The

resultant solution was heated to reflux for 3 h and then allowed to stand overnight. A precipitate separated which was filtered, washed with methanol and dried in vacuo. When no precipitate occurred, the solvent was evaporated to dryness and the residue treated with the appropriate alcohol (ethanol or 2-propanol as indicated) to afford a solid which was filtered, washed with the appropriate alcohol and dried in vacuo (yield 30–35%).

[LuEu(L)](Cl)₃·2H₂O: IR: $\tilde{\nu}$ = 1637.98 (C=N) cm⁻¹. ESI-MS: *m/z* = 1030.33 for [LuEu(L)(Cl)₃(H₂O)₂ + H]⁺ (1030.03 calcd. for [LuEu(L)(Cl)₃(H₂O)₂ + H]⁺). C₃₁H₃₈Cl₃EuLuN₃O₉ (1029.92): calcd. C 36.15, H 3.72, N 4.08; found C 35.51, H 3.81, N 3.90. ¹H NMR (CD₃OD) (paramagnetic compound). T.G. weight loss to final oxide: found 64.0% (calcd. 63.5%).

[TbEu(L)](Cl)₃·H₂O·iPrOH: 2-Propanol was used as precipitating solvent. IR: $\tilde{\nu}$ = 1630.64 (C=N) cm⁻¹. C₃₄H₄₄Cl₃EuN₃O₉Tb (1055.95): calcd. C 38.67, H 4.20, N 3.98; found C 36.40, H 4.43, N 4.50. ¹H NMR (CD₃OD) (paramagnetic compound). T.G. weight loss to final oxide: found 66.46% (calcd. 66.1%).

[LuLa(L)](Cl)₃·2.5H₂O: IR: $\tilde{\nu}$ = 1639.34 (C=N) cm⁻¹. C₃₁H₃₉Cl₃LaLuN₃O_{9.5} (1025.87): calcd. C 36.30, H 3.83, N 4.10; found C 35.25, H 3.32, N 3.71. ¹H NMR (CD₃OD): δ = 8.35 (s, 2 H, 4), 7.42 (dd, 2 H, 3), 7.17 (dd, 2 H, 2), 7.08 (dd, 1 H, 14), 6.95 (t, 2 H, 1), 6.86 (t, 1 H, 12), 6.56 (t, 1 H, 13), 6.39 (d, 1 H, 11), 4.84–4.73 (m, 2 H, 8a), 4.72–4.63 (m, 2 H, 8b), 4.58–4.33 (m, 6 H, 9a, 9b, 10a), 4.32–4.21 (m, 2 H, 10b), 4.08–3.94 (m, 2 H, 5a), 3.94–3.86 (m, 2 H, 5b), 3.84 (s, 2 H, 7), 3.29–3.17 (m, 2 H, 6b), 3.11–2.96 (m, 2 H, 6a) ppm. T.G. weight loss to final oxide: found 61.05% (calcd. 63.3%).

[YEu(L)](Cl)₃·3H₂O: IR: $\tilde{\nu}$ = 1632.70 (C=N) cm⁻¹. C₃₁H₄₀Cl₃EuN₃O₁₀Y (961.86): calcd. C 38.71, H 4.19, N 4.37; found C 38.78, H 4.11, N 4.17. ¹H NMR (CD₃OD) (paramagnetic compound). T.G. weight loss to final oxide: found 71.04% (calcd. 69.9%).

[LaYb(L)](Cl)₃·CH₃OH: IR: $\tilde{\nu}$ = 1637.66 (C=N) cm⁻¹. C₃₂H₃₈Cl₃LaN₃O₈Yb (1010.95): calcd. C 38.02, H 3.79, N 4.16; found C 38.44, H 3.39, N 3.98. ¹H NMR (CD₃OD) (paramagnetic compound). T.G. weight loss to final oxide: found 61.8% (calcd. 63%).

[LaEr(L)](Cl)₃·2H₂O: IR: $\tilde{\nu}$ = 1638.04 (C=N) cm⁻¹. C₃₁H₃₈Cl₃ErLaN₃O₉ (1009.16): calcd. C 36.90, H 3.80, N 4.16; found C 35.61, H 3.50, N 3.91. ¹H NMR (CD₃OD) (paramagnetic compound). T.G. weight loss to final oxide: found 62.61% (calcd. 65.9%).

[CeY(L)](Cl)₃·2CH₃OH: IR: $\tilde{\nu}$ = 1636.18 (C=N) cm⁻¹. C₃₃H₄₂CeCl₃N₃O₉Y (960.06): calcd. C 41.29, H 4.41, N 4.38; found C 41.39, H 4.75, N 4.57. ¹H NMR (CD₃OD) (paramagnetic compound). T.G. weight loss to final oxide: found 70.29% (calcd. 71.1%).

[TbEr(L)](Cl)₃·2H₂O·C₂H₅OH: Ethanol was used as precipitating solvent. IR: $\tilde{\nu}$ = 1636.19 (C=N) cm⁻¹. C₃₃H₄₄Cl₃ErN₃O₁₀Tb (1075.23): calcd. C 36.86, H 4.12, N 3.91; found C 36.55, H 4.33, N 3.74. ¹H NMR (CD₃OD) (paramagnetic compound). T.G. weight loss to final oxide: found 65.34% (calcd. 65.2%).

[LaEu(L)](Cl)₃·3H₂O: 2-Propanol was used as precipitating solvent. IR: $\tilde{\nu}$ = 1630.43 (C=N) cm⁻¹. C₃₁H₄₀Cl₃EuLaN₃O₁₀ (1011.87): calcd. C 36.80, H 3.98, N 4.15; found C 36.77, H 4.64, N 4.42. ¹H NMR (CD₃OD) (paramagnetic compound). T.G. weight loss to final oxide: found 62.07% (calcd. 63.7%).

[LaTb(L)](Cl)₃·5H₂O: 2-Propanol was used as precipitating solvent. IR: $\tilde{\nu}$ = 1630.28 (C=N) cm⁻¹. C₃₁H₄₄Cl₃LaN₃O₁₂Tb (1054.86): calcd. C 35.30, H 4.20, N 3.98; found C 33.39, H 4.06,

N 3.72. ^1H NMR (CD_3OD) (paramagnetic compound). T.G. weight loss to final oxide: found 60.06% (calcd. 64.6%).

[LuEr(L)](Cl) $_3$ ·3H $_2$ O: Ethanol was used as precipitating solvent. IR: $\tilde{\nu}$ = 1638.57 (C=N) cm^{-1} . $\text{C}_{31}\text{H}_{40}\text{Cl}_3\text{ErLuN}_3\text{O}_{10}$ (1063.23): calcd. C 35.02, H 3.79, N 3.95; found C 35.30, H 3.18, N 3.62. ^1H NMR (CD_3OD) (paramagnetic compound). T.G. weight loss to final oxide: found 64.10% (calcd. 65.2%).

[LuTb(L)](Cl) $_3$ ·3H $_2$ O·0.5C $_2$ H $_5$ OH: Ethanol was used as precipitating solvent. IR: $\tilde{\nu}$ = 1638.18 (C=N) cm^{-1} . $\text{C}_{32}\text{H}_{43}\text{Cl}_3\text{LuN}_3\text{O}_{10.5}\text{Tb}$ (1077.93): calcd. C 35.66, H 4.02, N 3.90; found C 35.70, H 3.68, N 3.79. ^1H NMR (CD_3OD) (paramagnetic compound). T.G. weight loss to final oxide: found 64.56% (calcd. 64.6%).

[LuDy(L)](Cl) $_3$ ·4H $_2$ O·C $_2$ H $_5$ OH: Ethanol was used as precipitating solvent. IR: $\tilde{\nu}$ = 1634.56 (C=N) cm^{-1} . $\text{C}_{33}\text{H}_{48}\text{Cl}_3\text{DyLuN}_3\text{O}_{12}$ (1122.55): calcd. C 35.31, H 4.31, N 3.74; found C 34.07, H 4.42, N 3.95. ^1H NMR (CD_3OD) (paramagnetic compound)

[LaDy(L)](Cl) $_3$ ·3H $_2$ O·C $_2$ H $_5$ OH: 2-Propanol was used as precipitating solvent. IR: $\tilde{\nu}$ = 1637.86 (C=N) cm^{-1} . $\text{C}_{33}\text{H}_{46}\text{Cl}_3\text{DyLaN}_3\text{O}_{11}$ (1068.47): calcd. C 36.42, H 3.94, N 4.11; found C 35.50, H 3.96, N 3.71. ^1H NMR (CD_3OD) (paramagnetic compound). T.G. weight loss to final oxide: found 62.78% (calcd. 63.16%).

Preparation of Homodinuclear Complexes: **[Ln $_2$ (L)](Cl) $_3$ · n H $_2$ O:** HA'·3HCl (0.3 mmol) and $[\text{N}(\text{CH}_3)_4]\text{OH}$ (1.8 mmol) were added to H $_2$ L' (0.3 mmol), and LnCl_3 (0.6 mmol) dissolved in hot methanol (60 mL) was added. The solution was heated to reflux for 3 h then allowed to stand at room temperature. The solvent was evaporated to dryness and the residue, treated with the appropriate alcohol, gave rise to a yellow solid which was filtered, washed with the appropriate alcohol (ethanol or 2-propanol as indicated) and dried in vacuo (yield 30–70%).

[Y $_2$ (L)](Cl) $_3$ ·3H $_2$ O: Ethanol was used as precipitating solvent. IR: $\tilde{\nu}$ = 1636.48 (C=N) cm^{-1} . $\text{C}_{31}\text{H}_{40}\text{Cl}_3\text{N}_3\text{O}_{10}\text{Y}_2$ (898.81): calcd. C 41.43, H 4.49, N 4.68; found C 41.33, H 4.29, N 4.37. ^1H NMR (CD_3OD): δ = 8.34 (s, 2 H, 4), 7.44 (d, 2 H, 3), 7.23 (d, 2 H, 2), 7.14 (d, 1 H, 14), 7.06–6.86 (m, 3 H, 1, 12), 6.60 (t, 1 H, 13), 6.33 (br. s, 1 H, 11), 4.86–4.71 (m, 2 H, 8b), 4.64–4.55 (m, 2 H, 8a), 4.55–4.23 (m, 8 H, 9a, 9b, 10), 4.09–3.92 (m, 2 H, 5a), 3.92–3.73 (m, 4 H, 5b, 7), 3.49–3.35 (m, 2 H, 6a), 3.17–3.02 (m, 2 H, 6b) ppm. T.G. weight loss to final oxide: found 76.88% (calcd. 75.28%).

[Eu $_2$ (L)](Cl) $_3$ ·4H $_2$ O: 2-Propanol was used as precipitating solvent. IR: $\tilde{\nu}$ = 1632.07 (C=N) cm^{-1} . $\text{C}_{31}\text{H}_{42}\text{Cl}_3\text{Eu}_2\text{N}_3\text{O}_{11}$ (1042.93): calcd. C 35.70, H 4.06, N 4.03; found C 36.32, H 4.60, N 4.42.

[La $_2$ (L)](Cl) $_3$ ·6H $_2$ O: 2-Propanol was used as precipitating solvent. IR: $\tilde{\nu}$ = 1637.16 (C=N) cm^{-1} . $\text{C}_{31}\text{H}_{46}\text{Cl}_3\text{La}_2\text{N}_3\text{O}_{13}$ (1052.86): calcd. C 35.37, H 4.40, N 3.99; found C 33.43, H 4.20, N 3.41. ^1H NMR (CD_3OD): δ = 40 °C: δ = 8.43 (s, 2 H, 4), 7.28 (d, 2 H, 3), 6.97 (d, 2 H, 2), 6.88 (d, 1 H, 14), 6.82 (d, 1 H, 11), 6.67 (t, 2 H, 1), 6.40 (t, 1 H, 13), 6.33 (t, 1 H, 12), 4.56 (t, 4 H, 8), 4.46 (m, 4 H, 9), 4.42–4.30 (m, 6 H, 10), 4.28 (s, 2 H, 7), 3.79–3.68 (m, 4 H, 5), 3.01–2.91 (m, 4 H, 6) ppm. T.G. weight loss to final oxide: found 62.99% (calcd. 66.46%).

[Lu $_2$ (L)](Cl) $_3$ ·6H $_2$ O: Ethanol was used as precipitating solvent. IR: $\tilde{\nu}$ = 1637.10 (C=N) cm^{-1} . $\text{C}_{31}\text{H}_{46}\text{Cl}_3\text{Lu}_2\text{N}_3\text{O}_{13}$ (1124.98): calcd. C 33.10, H 4.12, N 3.74; found C 32.45, H 4.08, N 3.71. ^1H NMR (CD_3OD): δ = 8.36 (s, 2 H, 4), 7.45 (d, 2 H, 3), 7.24 (d, 2 H, 2), 7.18 (d, 1 H, 14), 7.10–6.89 (m, 3 H, 1, 12), 6.63 (t, 1 H, 13), 6.51 (d, 1 H, 11), 4.80–4.69 (m, 2 H, 8b), 4.63–4.45 (m, 4 H, 8a, 9a), 4.44–4.28 (m, 6 H, 9b, 10a, 10b), 3.98–3.73 (m, 6 H, 5a, 5b, 7), 3.56–3.37 (m, 2 H, 6a), 3.11–2.99 (m, 2 H, 6b) ppm. T.G. weight loss to final oxide: found 64.73% (calcd. 64.62%).

[Tb $_2$ (L)](Cl) $_3$ ·4H $_2$ O: 2-Propanol was used as precipitating solvent. IR: $\tilde{\nu}$ = 1629.83 (C=N) cm^{-1} . $\text{C}_{31}\text{H}_{42}\text{Cl}_3\text{N}_3\text{O}_{11}\text{Tb}_2$ (1056.86): calcd. C 35.23, H 4.01, N 3.98; found C 35.92, H 4.31, N 4.39. ^1H NMR (CD_3OD) (paramagnetic compound). T.G. weight loss to final oxide: found 65.66% (calcd. 65.18%).

[Er $_2$ (L)](Cl) $_3$ ·4H $_2$ O: Ethanol was used as precipitating solvent. IR: $\tilde{\nu}$ = 1639.99 (C=N) cm^{-1} . ESI-MS: m/z = 1051.37 for $[\text{Er}_2(\text{L})(\text{Cl})_2(\text{H}_2\text{O})_3(\text{CH}_3\text{OH})]^+$ {1052.10 calcd. for $[\text{Er}_2(\text{L})(\text{Cl})_2(\text{H}_2\text{O})_3(\text{CH}_3\text{OH})]^+$. $\text{C}_{31}\text{H}_{42}\text{Cl}_3\text{Er}_2\text{N}_3\text{O}_{11}$ (1073.53): calcd. C 34.68, H 3.94, N 3.91; found C 34.78, H 4.05, N 3.79. ^1H NMR (CD_3OD) (paramagnetic compound). T.G. weight loss to final oxide: found 64.27% (calcd. 63.8%).

[Dy $_2$ (L)](Cl) $_3$ ·2H $_2$ O: 2-Propanol was used as precipitating solvent. IR: $\tilde{\nu}$ = 1630.04 (C=N) cm^{-1} . $\text{C}_{31}\text{H}_{38}\text{Cl}_3\text{Dy}_2\text{N}_3\text{O}_9$ (1027.99): calcd. C 36.22, H 3.73, N 4.09; found C 36.16, H 3.80, N 4.20. ^1H NMR (CD_3OD) (paramagnetic compound). T.G. weight loss to final oxide: found 65.50% (calcd. 63.7%).

[Gd $_2$ (L)](Cl) $_3$ ·2H $_2$ O: Ethanol was used as precipitating solvent. IR: $\tilde{\nu}$ = 1629.94 (C=N) cm^{-1} . $\text{C}_{31}\text{H}_{38}\text{Cl}_3\text{Gd}_2\text{N}_3\text{O}_9$ (1017.49): calcd. C 36.59, H 3.76, N 4.13; found C 36.67, H 3.84, N 4.18. ^1H NMR (CD_3OD) (paramagnetic compound). T.G. weight loss to final oxide: found 65.64% (calcd. 64.5%).

Acknowledgments

We thank Mr. A. Aguiari, and Mrs A. Moresco for technical assistance. We thank Ministero dell'Università e della Ricerca (MIUR) project FIRB-RBNE019H9K for financial support. The authors are indebted to FILA INDUSTRIA CHIMICA SPA, San Martino di Lupari, Padova, Italy, owner of the Fei-ESem FEI Quanta 200 FEG instrument, for allowing its use for the research work described in this article.

- [1] P. A. Vigato, S. Tamburini, L. Bertolo, *Coord. Chem. Rev.* **2007**, 251, 1311–1492.
- [2] W. Huang, H.-B. Zhu, S.-H. Gou, *Coord. Chem. Rev.* **2006**, 250, 414–423.
- [3] A. L. Gavrilova, B. Bosnich, *Chem. Rev.* **2004**, 104, 349–383.
- [4] D. Brooker, *Eur. J. Inorg. Chem.* **2002**, 2535–2547.
- [5] P. A. Gale, *Coord. Chem. Rev.* **2003**, 240, 191–221.
- [6] P. D. Beer, E. J. Hayes, *Coord. Chem. Rev.* **2003**, 240, 167–189.
- [7] V. McKee, J. Nelson, R. M. Town, *Chem. Soc. Rev.* **2003**, 32, 309–325.
- [8] C. Suksai, T. Tuntulani, *Chem. Soc. Rev.* **2003**, 32, 192–202.
- [9] R. Ziessel, *Coord. Chem. Rev.* **2001**, 216–217, 195–223.
- [10] T. Koullourou, L. S. Natrajan, H. Bhavsar, S. J. A. Pope, J. Feng, J. Narvainen, R. Shaw, E. Scales, R. Kauppinen, A. M. Kenwright, S. Faulkner, *J. Am. Chem. Soc.* **2008**, 130, 2178–2179.
- [11] S. Faulkner, S. J. A. Pope, *J. Am. Chem. Soc.* **2003**, 125, 10526–10527.
- [12] M. Ohashi, M. Konkol, I. Del Rosal, R. Poteau, L. Maron, J. Okuda, *J. Am. Chem. Soc.* **2008**, 130, 6920–6921.
- [13] V. Alexander, *Chem. Rev.* **1995**, 95, 273.
- [14] a) D. E. Fenton, H. Okawa, *Chem. Ber./Recueil* **1997**, 130, 433; b) S. R. Collinson, D. E. Fenton, *Coord. Chem. Rev.* **1996**, 148, 19; c) D. E. Fenton, *Pure Appl. Chem.* **1986**, 58, 1437.
- [15] A. Martell, J. Penitka, D. Kong, *Coord. Chem. Rev.* **2001**, 216, 55.
- [16] a) S. Brooker, *Coord. Chem. Rev.* **2001**, 222, 33; b) S. Brooker, *Eur. J. Inorg. Chem.* **2002**, 2535.
- [17] a) P. Guerriero, P. A. Vigato, D. E. Fenton, P. C. Hallier, *Acta Chem. Scand.* **1992**, 46, 1025; b) P. Zanello, S. Tamburini, P. A. Vigato, G. A. Mazzochin, *Coord. Chem. Rev.* **1987**, 77165; c)

- P. A. Vigato, S. Tamburini, D. E. Fenton, *Coord. Chem. Rev.* **1990**, *106*, 25; d) D. E. Fenton, P. A. Vigato, *Coord. Chem. Rev.* **1988**, *17*, 89; e) P. Guerriero, S. Tamburini, P. A. Vigato, *Coord. Chem. Rev.* **1995**, *134*, 17; f) S. Tamburini, P. A. Vigato, *Coord. Chem. Rev.* **2004**, *248*, 1718.
- [18] S. Tamburini, P. A. Vigato, M. Gatos, L. Bertolo, U. Casellato, *Inorg. Chim. Acta* **2006**, *359*, 183–196.
- [19] S. Tamburini, U. Casellato, L. Bertolo, P. A. Vigato, *Eur. J. Inorg. Chem.* **2005**, 2409–2422.
- [20] A. Barge, M. Botta, U. Casellato, S. Tamburini, P. A. Vigato, *Eur. J. Inorg. Chem.* **2005**, 1492–1499.
- [21] M. Botta, U. Casellato, C. Scalco, S. Tamburini, P. Tomasin, P. A. Vigato, S. Aime, A. Barge, *Chem. Eur. J.* **2002**, *8*, 3917–3926.
- [22] U. Casellato, S. Tamburini, P. Tomasin, P. A. Vigato, S. Aime, M. Botta, *Inorg. Chem.* **1999**, *38*, 2906–2916.
- [23] N. Brianese, U. Casellato, S. Tamburini, P. Tomasin, P. A. Vigato, *Inorg. Chim. Acta* **1999**, *293*, 178–194.
- [24] Q. Zeng, M. Quian, S. Gou, H.-K. Fun, C. Duan, X. You, *Inorg. Chim. Acta* **1999**, *294*, 1–7.

Received: April 17, 2008

Published Online: November 28, 2008

Hydrothermal Synthesis of Three-Dimensional Hierarchical CuO Butterfly-Like Architectures

Yajing Zhang,^[a,b] Siu Wing Or,^{*[b]} Xiaolei Wang,^[a] Tieyu Cui,^[a] Weibin Cui,^[a] Ying Zhang,^[a] and Zhidong Zhang^[a]

Keywords: Hydrothermal synthesis / Copper oxide / Nanostructures / Self-assembly

Uniform 3D hierarchical CuO butterfly-like architectures were fabricated by a surfactant-assisted hydrothermal oriented attachment route. This route included the formation of CuO butterfly-like architectures in a solution of cupric chloride ($\text{CuCl}_2 \cdot 2\text{H}_2\text{O}$) and sodium hydroxide (NaOH) at 100 °C for 15 h by using sodium dodecyl benzenesulfonate (SDBS) as surfactant. The as-prepared CuO architecture was characterized by X-ray diffraction, scanning electron microscopy and transmission electron microscopy. The CuO butterfly-like architectures, with lengths of about 6 μm and widths of 2–4 μm , were assembled from several tens of oriented attach-

ment rhombic nanosheets with a thickness of about 60 nm. A growth mechanism for the formation of the CuO butterfly-like architectures was proposed on the basis of time-dependent experiments. The synthetic parameters such as reaction temperature, the concentration of sodium hydroxide and reaction time all affected the morphology of the CuO architectures. The synthetic strategy could be extended to assemble 3D architectures of other materials.

(© Wiley-VCH Verlag GmbH & Co. KGaA, 69451 Weinheim, Germany, 2009)

Introduction

Synthesis of hierarchical micro- and/or nanomaterials, self-assembled by ordered alignment of nanobuilding blocks, has attracted much attention due to their novel properties and potential application in optics, electronics, magnetism and biology.^[1] As a result, a number of micro- and/or nanomaterials with hierarchical structures, including metals, metal oxide, hydrate, sulfide, copolymers and other materials,^[2–6] have been fabricated by different driving mechanisms, including surface tension, electric and magnetic forces, and hydrophobic interactions.^[7–9] However, synthesis of novel hierarchical structured micro- and/or nanomaterials is still an interesting topic, because they can exhibit new physicochemical behaviours and provide much promise for the fabrication of materials with advanced functionalities.

Cupric oxide, as an important *p*-type semiconductor with a narrow bandgap ($E_g = 1.2 \text{ eV}$), has been extensively investigated for its application in solar energy conversion, lithium-ion batteries, gas sensors, field emission and catalysis.^[10–13] Because there is a close relationship between the

bandgap energies of CuO nanostructures and their shapes and sizes, different synthetic routes including vapour–solid, vapour–liquid–solid and solid–liquid routes were developed for the synthesis of CuO.^[14] Various CuO micro- and/or nanomaterials, such as nanoparticles,^[15] one-dimensional (1D) nanotubes, nanorods, nanobelts and nanoneedles,^[16,17] two-dimensional (2D) nanoribbons, nanosheets, nanoleaves and nanowiskers,^[18] three-dimensional (3D) microflowers and microbranches formed through the self-assembly of nanometre-sized building blocks,^[19] have been synthesized by these routes. For example, CuO nanowires supported on various substrates were obtained by the thermal oxidation of these substrates in air.^[20] CuO nanotubes and nanorods were synthesized by controlling the concentration of the precursor.^[21] The formation of CuO rod-like, flake-like and branch-like nanostructures was achieved by adjusting the molar ratio of sodium citrate to cupric salts.^[22] CuO nanoribbons and nanorings were synthesized by a surfactant-assisted hydrothermal route for different reaction times.^[23] CuO nanoleaves were fabricated by hierarchical oriented attachment of $\text{Cu}(\text{OH})_2$ nanowires.^[24] For 3D hierarchical CuO micromaterials with two or more levels of structure, their nanometre-sized building blocks provide a high surface area, whereas their whole micrometre-sized structure provides sufficient mechanical properties, so the combination of these features will improve their electrochemical performance and adsorption ability (removal of heavy metal ions)^[25,26] However, 3D hierarchical CuO micromaterials have seldom been reported. Zeng et al. assembled hollow dandelion-like CuO microspheres com-

[a] Shenyang National Laboratory for Materials Science, Institute of Metal Research and International Centre for Materials Physics, Chinese Academy of Sciences, Shenyang 110016, P. R. China

[b] Department of Electrical Engineering, The Hong Kong Polytechnic University, Hung Hom, Kowloon, Hong Kong
E-mail: eeswor@polyu.edu.hk

Supporting information for this article is available on the WWW under <http://www.eurjic.org> or from the author.

posed of rhombic nanobuilding blocks through the oriented aggregation of smaller nanoribbons by a two-step procedure with the use of ethanol as solvent.^[27] Xu et al. fabricated CuO microflowers composed of nanosheets in ammonia solution.^[28] Nevertheless, to the best of our knowledge, 3D hierarchical CuO butterfly-like architectures have not been reported.

Here we report the controlled synthesis of 3D hierarchical butterfly-like CuO architectures by a surfactant-assisted hydrothermal oriented attachment route. The effects of the reaction parameters, such as the reaction temperature, reaction time and the concentration of NaOH, on the morphologies of CuO are investigated. The growth mechanism of the 3D hierarchical CuO butterfly-like architectures is proposed on the basis of the results of systematic time-dependent experiments. The CuO butterfly-like architectures provide a supplement of available 3D CuO architectures, and it can be expected to extend for assembling new electronic and optoelectronic micro- and/or nanodevices.

Results and Discussion

Synthesis and Characterization of Hierarchical CuO Butterfly-Like Architectures

The X-ray diffraction (XRD) patterns of the precursor, the intermediate and the final products are shown in Figure 1. Figure 1a is the XRD pattern of the precursor, in which all the peaks can be indexed to orthorhombic $\text{Cu}(\text{OH})_2$ (JCPDS No. 13-0420). Figure 1d shows the XRD pattern of the final product obtained at 100 °C after 15 h hydrothermal treatment, in which all the XRD peaks can be indexed to monoclinic CuO, which is consistent with the standard card JCPDS No.48-1548 (space group $C2/c$; $a = 4.688 \text{ \AA}$, $b = 3.423 \text{ \AA}$, $c = 5.132 \text{ \AA}$). Impurities were obviously not found in the final product, indicating it is pure CuO. Figure 1b [the mixture of $\text{Cu}(\text{OH})_2$ and CuO] and Figure 1c (CuO) are the XRD patterns of the products as-prepared at 100 °C after 1 and 5 h, respectively. The XRD

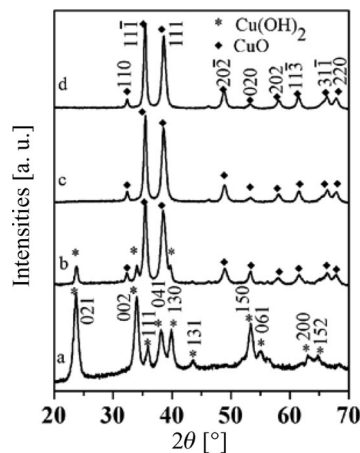


Figure 1. XRD patterns of (a) the precursor of $\text{Cu}(\text{OH})_2$ and the products collected at 100 °C for (b) 1 h, (c) 5 h and (d) 15 h.

results confirm that the final product of CuO is transformed from the initial precursor of $\text{Cu}(\text{OH})_2$. The energy-dispersive spectrum (EDS) result reveals that only the Cu and O elements are contained in the final product, and the atomic ratio of Cu to O in the product is about 1:1 (49:51), as shown in Figure 2. The EDS result further confirms that the final product is only CuO (Au element originates from the thin Au layer sputtering on the sample in the test).

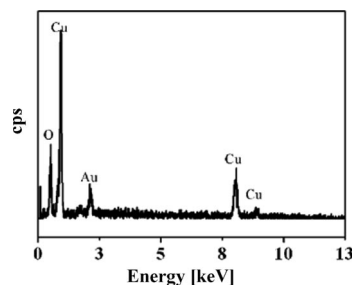


Figure 2. EDS pattern of the as-prepared CuO butterfly-like architectures at 100 °C for 15 h.

Figure 3 shows the typical morphology of the final CuO product with different magnifications. The low-magnification scanning electron microscopy (SEM) (Figure 3a) image implies that the final CuO product is highly uniform butterfly-like architectures, with a length of about 6 μm and width of 2–4 μm . The magnified SEM image (Figure 3b) shows that the CuO butterfly-like architectures are composed of several tens of order-attached rhombic nanosheets, which can be classified as a hierarchical structure. The nanosheets are about 60 nm thick, as estimated from the side view of the architecture (Figure 3c). It is also observed that the CuO nanosheets attach together in the middle part of an

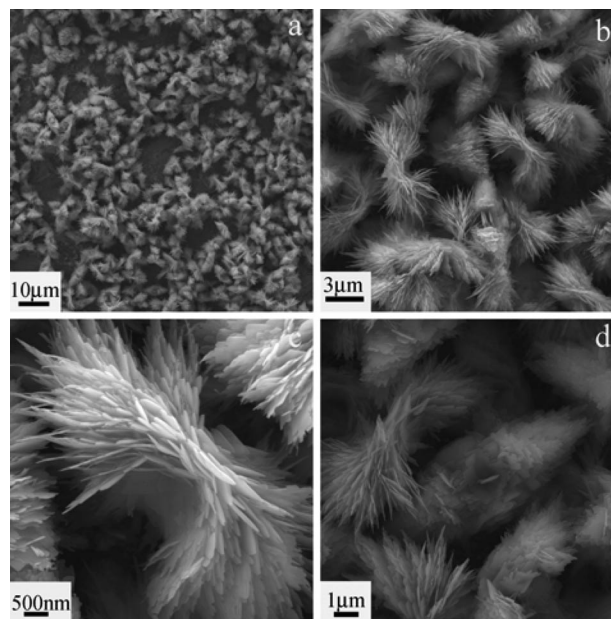


Figure 3. (a) Low-magnification and (b) high-magnification SEM images of the CuO butterfly-like architectures prepared at 100 °C for 15 h; (c) side view and (d) top view of an individual CuO butterfly-like architecture.

individual butterfly-like architecture, and they become curly and separate at the two ends. Furthermore, the two ends exhibit a symmetrical character, as displayed in the top-view image (Figure 3d). The BET surface area for the CuO butterfly-like architectures is about $17 \text{ m}^2 \text{ g}^{-1}$, which is smaller than that of the hollow dandelion-like CuO.^[27] This is attributed to the fact that the middle part of the butterfly-like architectures attach densely together. It is worth mentioning that the hierarchical CuO butterfly-like architectures are very stable and still maintain the morphology after ultrasonication for 30 min.

Growth Mechanism for the Formation of the CuO Butterfly-Like Architectures

To understand the growth mechanism of the CuO butterfly-like architectures, systematic time-dependent experiments were carried out at 100°C . The SEM and TEM images (Figure 4) of the products obtained after 1, 5 and 10 h in the hydrothermal process illustrate the evolution of the morphology of the butterfly-like CuO architectures. When the reaction time is 1 h, 1D nanoribbons, with widths of 50–60 nm and lengths of 1–2 μm , are observed as the dominant product, although several 2D rhombic nanosheets are also detected (shown by white arrow in Figure 4a). An individual nanosheet is about 500 nm in width and 1–2 μm in length. It can be obviously observed that the nanosheet is assembled by the ordered attachment of several nanoribbons. TEM results (Figure 4b) further confirm the morphologies of the nanoribbons and rhombic nanosheets, and those monodispersive nanoribbons are very flexible and tend to curve. The corresponding select area electron diffraction (SAED) of the nanosheet (the top square part shown in Figure 4b) is shown in Figure 4c. The diffraction pattern can be indexed to (020), (11 $\bar{1}$) and (20 $\bar{2}$) planes of CuO, and the obvious symmetry arc-like diffraction spots illustrate that the nanosheet is assembled by oriented building blocks.^[3b] Figure 4d is the SAED result of an individual nanoribbon (the bottom square part shown in Figure 4b), revealing the single-crystal nature of the nanoribbon, and the SAED spots can also be determined to be (020), (11 $\bar{1}$) and (20 $\bar{2}$) planes of CuO. The results further indicate that the nanosheets are formed by oriented attachment of CuO nanoribbons. This is in agreement with the earlier reports.^[23,24,27] No nanoribbons are found in the product obtained after 5 h (Figure 4e), but 2D rhombic nanosheets (shown by arrows) and 3D undeveloped butterfly-like architectures are observed. When the reaction is prolonged for 10 h, more 3D perfect butterfly-like architectures are yielded, whereas the number of 2D nanosheets becomes less, as shown in Figure 4f. It is found that 15 h is sufficient for generating well-developed CuO butterfly-like architectures, and nearly no individual 2D nanoleaves can be observed (Figure 2).

On the basis of above experimental results and the literature,^[21,23,24] a growth mechanism for the formation of the CuO butterfly-like architectures is proposed, as schemed in

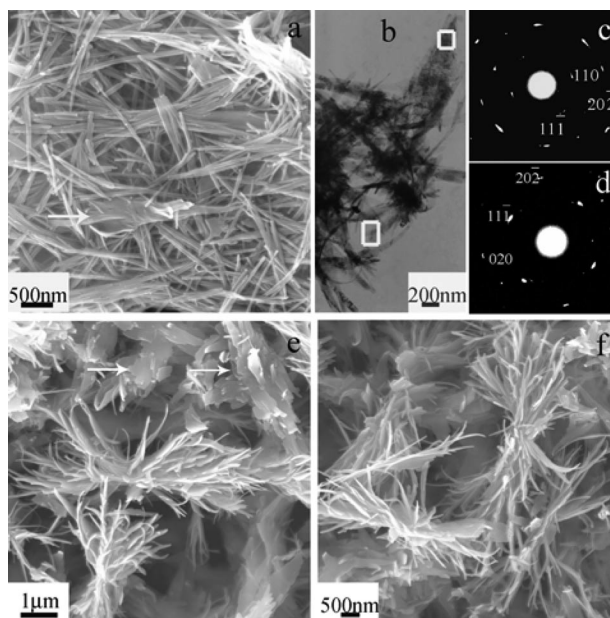


Figure 4. (a) SEM and (b) TEM images of the products prepared at 100°C for 1 h; (c) the corresponding SAED pattern of the top part of the rhombic nanosheet (shown by top square in Figure 4b); (d) the corresponding SAED pattern of the top part of the nanowire (shown by bottom square in Figure 4b); (e) SEM images of the products prepared at 100°C for 5 h and (f) 10 h.

Figure 5. The formation of the architectures possibly consists of four main steps: (1) Formation of $\text{Cu}(\text{OH})_2$ crystal nuclei (step a). (2) CuO nuclei form by the decomposition of $\text{Cu}(\text{OH})_2$ and grow into CuO nanoribbons (step b). (3) The CuO nanoribbons self-assemble into CuO rhombic nanosheets through an oriented attachment mechanism (step c). (4) CuO nanosheets attach orderly and assemble into hierarchical butterfly-like architectures (step d). The oriented attachment in both steps c and d are driven by eliminating higher surface energies.

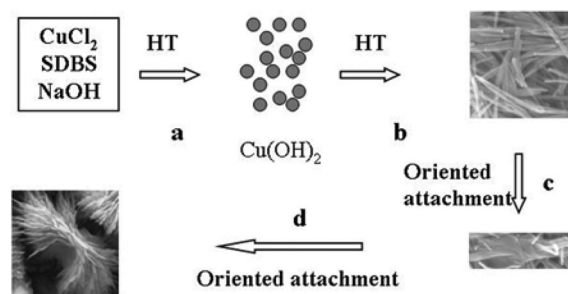
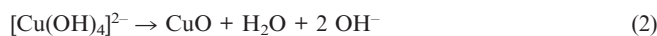
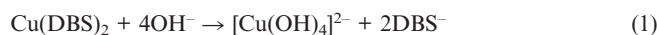


Figure 5. Schematic illustration of the formation procedure of the 3D CuO butterfly-like architectures.

To determine the role of SDBS in the formation process of CuO butterfly-like architectures, time-dependent experiments were also carried out at 100°C in the absence of SDBS, while keeping other reaction parameters unchanged. The results show that: (1) CuO nanoribbons did not form during the reaction process (Figure S1, Supporting Information). (2) The final CuO product consisted of a majority of 3D shuttle-like architectures and a minority of 2D flat

nanosheets. The results indicate that the SDBS surfactant plays a critical role in the formation of CuO nanoribbons. The nanoribbons tend to curve, because they are flexible and thin, and hence, they are prerequisite building blocks for assembling intermediate curved CuO nanosheets and then final butterfly-like architectures. The group of Qian proposed a crystal-splitting mechanism for forming CuO nanoribbons, wherein SDBS directly interacts with the surfaces of CuO flakes and subsequently its intense Brownian movement leading to CuO flakes split into CuO nanoribbons.^[23] It is understood on the basis of our experimental results that SDBS in our reaction system plays the same role. In the presence of SDBS, the Cu²⁺ cations could directly attach to the DBS[−] anions and produce Cu(DBS)₂, then Cu(DBS)₂ reacts with NaOH to form CuO. The whole reaction process can be described by Equations (1) and (2).^[23]



SDBS was also substituted with other surfactants such as sodium dodecyl sulfate (SDS), cetyltrimethylammonium bromide (CTAB) and poly(vinylpyrrolidone) (PVP). When SDS was used as surfactant, the butterfly-like architectures were also obtained (Figure 6a). In the case of CTAB and PVP, the products were poorly defined butterfly-like architectures with densely attached nanosheets and flat nanosheets, as shown in Figure 6b and c, respectively. The results demonstrate that the anionic surfactants are more favourable for achieving well-defined butterfly-like architectures in comparison to cationic and neutral surfactants. This may be ascribed to the direct interaction of anionic surfactants, such as SDBS and SDS, with cupric ions or to anion-selective adsorption on the CuO surface in solution. Cationic and nonionic surfactants, such as CTAB and PVP, cannot produce butterfly-like architectures possibly because of their weak interaction with cupric ions.^[29]

In addition, the effect of the concentration of NaOH on the morphology of the final CuO product was examined. In the controlled experiments, when the concentration of NaOH was 2 M, it did not form any butterfly-like structures; rather, shuttle-like architectures were formed by compact attached nanosheets (Figure 7a). A further increase in the concentration of NaOH to 5 M, resulted in the formation of spherical architectures composed of a number of nanosheets (Figure 7b). It can be concluded that a low concentration of NaOH is critical for the formation of CuO butterfly-like architectures. This can also be explained by the formation model proposed in Figure 5. When the concentration of NaOH in the solution is increased, the reaction rate is accelerated according to Equations (1) and (2), which leads to the formation of much thicker and less flexible nanoribbons in a short time; subsequently, they self-assemble in an oriented manner into flat and thick nanosheets instead of curved nanosheets. Finally, the flat nanosheets self-assemble in an oriented manner into CuO shuttle-like architectures. The concentration of NaOH is

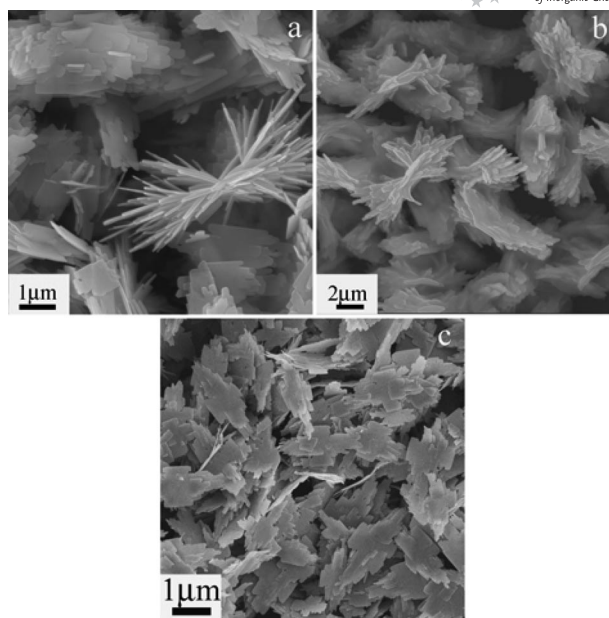


Figure 6. SEM images of the products prepared in the presence of (a) SDS, (b) CTAB and (c) PVP.

high enough (e.g., 5 M) in solution, and hence, the reaction rate is excessively fast, but the flat nanosheets cannot perform oriented self-assembly at such a fast reaction rate, so instead they attach randomly and form CuO flower-like architectures.

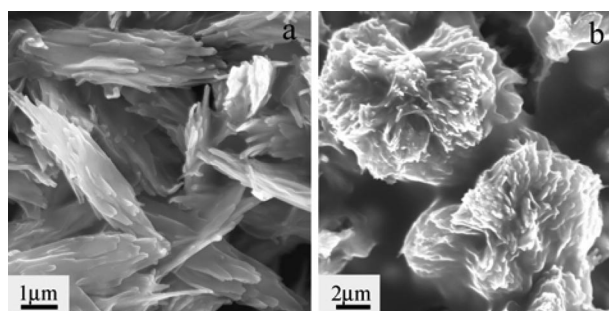


Figure 7. SEM images of the products prepared at 100 °C with different concentrations of NaOH: (a) 2 M and (b) 5 M.

Apart from the concentration of NaOH, the reaction temperature affects the morphology of the final CuO product. The controlled experiments demonstrated that a high reaction temperature is not favourable for the self-assembly of CuO butterfly-like architectures, but favours the formation of other 3D architectures. For instance, when the reaction is carried out at 120 and 140 °C, irregular structures form by random aggregation of nanoribbons, instead of oriented attachment of nanosheets (Figure 8a and b). A further increase in the reaction temperature (160 and 180 °C) leads to the formation of isotropic flower-like architectures, which are created through the self-assembly of many nanoribbons (Figure 8c and d). At a relatively low temperature, such as 80 °C (Figure S2, Supporting Information), CuO butterfly-like architectures can also be obtained, but need a relatively long reaction time. According to our proposed

formation model in Figure 5, it is understandable that isotropic spherical (or near-spherical) architectures are achieved at higher reaction temperatures, because the reaction rate rises with increasing temperature, and accordingly, more intermediate building blocks of nanoribbons are produced in a shorter reaction time, and together with the intense Brownian movement, this results in random aggregation instead of oriented attachment.^[30] This is consistent with previous reports.^[2f,27] The results reveal that the morphology of the product is strongly determined by the reaction temperature.

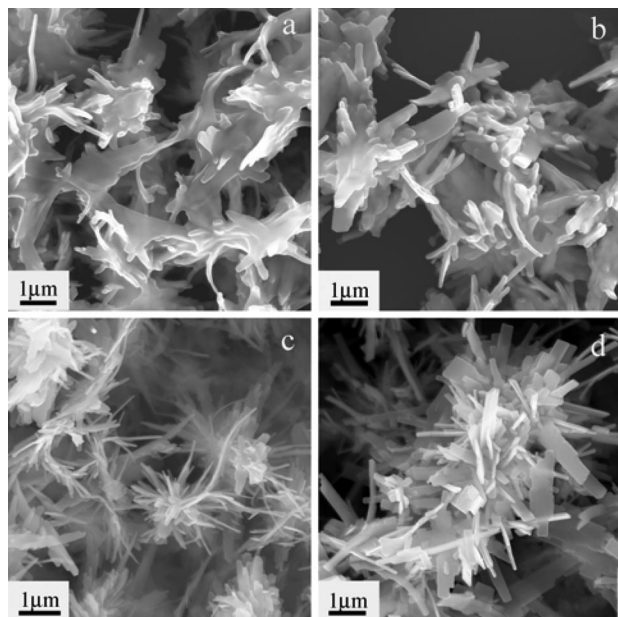


Figure 8. SEM images of the products prepared at different reaction temperatures: (a) 120 °C, (b) 140 °C, (c) 160 °C and (d) 180 °C for 15 h.

Conclusions

3D hierarchical CuO butterfly-like architectures composed of several tens of rhombic nanosheets were fabricated by a hydrothermal oriented attachment route. Experimental results suggest that the reaction temperature, the concentration of NaOH and the reaction time all influence the morphology of CuO, and the SDBS surfactant plays a key role in the formation of the CuO architectures. In addition, the CuO butterfly-like architectures were found to self-assemble through an oriented attachment mechanism. Our synthetic approach can be employed to fabricate 3D hierarchical architectures of other materials under appropriate conditions.

Experimental Section

General: All reagents were commercially available in analytical purity and used without further purification. In a typical procedure, $\text{CuCl}_2 \cdot 2\text{H}_2\text{O}$ (0.34 g, 2 mmol), SDBS (0.232 g, 1 mmol) and NaOH (1.6 g, 40 mmol) were first dissolved in distilled water (40 mL) un-

der constant stirring, and the precursor blue suspension was obtained. For obtaining the precursor, the initial blue suspension was placed static for several hours in air and then the blue precipitate was separated, washed and dried for characterization. For preparing the 3D hierarchical butterfly-like CuO architectures, the initial blue suspension was transferred into a 50-mL Teflon-lined stainless steel autoclave. The autoclave was sealed and heated at 100 °C for 15 h and then cooled to room temperature naturally. The products obtained after hydrothermal treatment were centrifuged, washed with distilled water and ethanol several times and finally dried in vacuo at 60 °C for 4 h. Control experiments were carried out by adjusting the reaction temperature (80–180 °C) and the amount of NaOH (1–5 M), while other reaction parameters were left unchanged.

The phases of all the products were identified with a Rigaku D/max 2500 pc X-ray diffractometer (XRD) with $\text{Cu-K}\alpha$ radiation ($\lambda = 1.54156 \text{ \AA}$) at a scan rate of 0.04°s^{-1} . The morphology was investigated with a Supra 35 field-emission scanning electron microscope (FESEM) equipped with energy-dispersive spectrum (EDS) operated at an acceleration voltage of 20 kV. The Brunauer-Emmett-Teller (BET) surface area was measured by the nitrogen adsorption-desorption method by using a Micromeritics (ASAP2010M) analyzer. Transmission electron microscopy (TEM) observation was carried out with a TECNAI 20 with an emission voltage of 200 kV. For sample preparation for FESEM and TEM observations, at first, a small amount of the as-prepared products was dispersed in ethanol by ultrasonic treatment for 10 min, and then one drop of the colloidal solution was deposited onto Si wafer and Cu grids coated with a carbon layer, respectively.

Supporting Information (see footnote on the first page of this article): SEM images of the products prepared at 100 °C without SDBS for different reaction time; SEM image of the products prepared at 80 °C for different reaction time.

Acknowledgments

This work was supported by the National Nature Science Foundation of China (Projects No. 50331030 and No.50703046), the Research Grants Council of the HKSAR Government (PolyU 5257/06E) and the Central Research Grant of The Hong Kong Polytechnic University (A-PA3C).

- [1] a) H. G. Yang, H. C. Zeng, *Angew. Chem. Int. Ed.* **2004**, *43*, 5930–5933; b) A. D. Dinsmore, M. F. Hsu, M. G. Nikolaides, M. Marquez, A. R. Bausch, D. A. Weitz, *Science* **2002**, *298*, 1006–1009.
- [2] a) Y. C. Zhu, Q. Yang, H. G. Zheng, W. C. Yu, Y. T. Qian, *Mater. Chem. Phys.* **2005**, *91*, 293–297; b) Y. L. Hou, H. Kondoh, T. Ohta, *Chem. Mater.* **2005**, *17*, 3994–3996; c) L. Guo, F. Liang, X. G. Wen, S. H. Yang, L. He, W. Z. Zheng, C. P. Chen, Q. P. Zhong, *Adv. Funct. Mater.* **2007**, *17*, 425–430; d) L. P. Zhu, H. M. Xiao, W. D. Zhang, Y. Yang, S. Y. Fu, *Cryst. Growth Des.* **2008**, *8*, 1113–1118; e) Y. J. Zhang, S. Ma, D. Li, Z. H. Wang, Z. D. Zhang, *Mater. Res. Bull.* **2008**, *43*, 1957–1965; f) Y. J. Zhang, Y. Zhang, Z. H. Wang, D. Li, T. Y. Cui, W. Liu, Z. D. Zhang, *Eur. J. Inorg. Chem.* **2008**, *17*, 2733–2738.
- [3] a) Z. Fang, K. B. Tang, J. M. Shen, G. Z. Shen, Q. Yang, *Cryst. Growth Des.* **2007**, *7*, 2254–2257; b) Y. Y. Li, J. P. Liu, X. T. Huang, G. Y. Li, *Cryst. Growth Des.* **2007**, *7*, 1350–1355; c) Z. Y. Yuan, A. Vantomme, A. Leonard, B. L. Su, *Chem. Commun.* **2003**, 1558–1559; d) J. Y. Lao, J. Y. Huang, D. Z. Wang, Z. F. Ren, *J. Mat. Chem.* **2004**, *14*, 770–773; e) R. S. Yuan, X. Z. Fu, X. C. Wang, P. Liu, L. Wu, Y. M. Xu, X. X. Wang, Z. Y. Wang, *Chem. Mater.* **2006**, *18*, 4700–4705; f) D. Yan, P. X.

- Yan, G. H. Yue, J. Z. Liu, J. B. Chang, Q. Yang, D. M. Qu, Z. R. Geng, J. T. Chen, G. A. Zhang, R. F. Zhuo, *Chem. Phys. Lett.* **2007**, *440*, 134–138.
- [4] a) L. X. Yang, Y. J. Zhu, L. Li, L. Zhang, H. Tong, W. W. Wang, G. F. Cheng, J. F. Zhu, *Eur. J. Inorg. Chem.* **2006**, 4787–4792; b) D. B. Wang, C. X. Song, Z. S. Hu, X. Fu, *J. Phys. Chem. B* **2005**, *109*, 1125–1129; c) J. P. Huang, X. T. Huang, Y. Y. Li, K. M. Sulieman, X. He, F. L. Sun, *J. Phys. Chem. B* **2006**, *110*, 21865–21872.
- [5] a) G. Z. Shen, Y. Bando, J. Q. Hu, D. Golberg, *Appl. Phys. Lett.* **2007**, *90*, 123101; b) X. L. Li, J. P. Ge, Y. D. Li, *Chem. Eur. J.* **2004**, *10*, 6163–6167; c) Y. R. Ma, L. M. Qi, J. M. Ma, H. M. Chen, *Cryst. Growth Des.* **2004**, *4*, 351–354; d) D. Moore, Y. Ding, Z. L. Wang, *Angew. Chem. Int. Ed.* **2006**, *45*, 5150–5154; e) Y. Cheng, Y. S. Wang, C. Jia, F. Bao, *J. Phys. Chem. B* **2006**, *110*, 24399–24402; f) Q. Z. Yao, G. Jin, G. T. Zhou, *Mater. Chem. Phys.* **2008**, *109*, 164–168.
- [6] a) H. Kang, F. A. Detcheverry, A. N. Mangham, M. P. Stoykovich, K. C. Daoulas, R. J. Hamers, M. Muller, J. J. D. Pablo, P. F. Nealey, *Phys. Rev. Lett.* **2008**, *100*, 148303; b) W. A. Lopes, H. M. Jaeger, *Nature* **2001**, *414*, 735–738; c) D. Sundrani, S. B. Darling, S. J. Sibener, *Langmuir* **2004**, *20*, 5091–5099.
- [7] a) X. W. Teng, H. Yang, *Nano Lett.* **2005**, *5*, 885–891; b) X. S. Fang, C. H. Ye, L. D. Zhang, J. X. Zhang, J. W. Zhao, P. Yan, *Small* **2005**, *1*, 422–428.
- [8] a) L. Manna, D. J. Milliron, A. Meisel, E. C. Scher, A. P. Alivisatos, *Nat. Mater.* **2003**, *2*, 382–385; b) H. Q. Yan, R. R. He, J. Johnson, M. Law, R. J. Saykally, P. D. Yang, *J. Am. Chem. Soc.* **2003**, *125*, 4728–4729; c) F. Gao, Q. Y. Lu, S. H. Xie, D. Y. Zhao, *Adv. Mater.* **2002**, *14*, 1537–1540.
- [9] a) C. B. Murray, C. R. Kagan, M. G. Bawendi, *Science* **1995**, *270*, 1335–1338; b) J. Liu, Q. Wu, Y. Ding, *Cryst. Growth Des.* **2005**, *5*, 445–449.
- [10] a) S. Anandan, X. G. Wen, S. H. Yang, *Mater. Chem. Phys.* **2005**, *93*, 35–40; b) M. Serra, D. Sainz, *Sol Energy Mater.* **1986**, *13*, 463–468.
- [11] a) X. P. Gao, J. L. Bao, G. L. Pan, H. Y. Zhu, P. X. Huang, F. Wu, D. Y. Song, *J. Phys. Chem. B* **2004**, *108*, 5547–5551; b) A. Debart, L. Dupont, P. Poizot, J. B. Leriche, J. M. Tarascon, *J. Electrochem. Soc.* **2001**, *148*, A1266–A1274; c) S. Q. Wang, J. Y. Zhang, C. H. Chen, *Scrip. Mater.* **2007**, *57*, 337–340; d) D. W. Zhang, T. H. Yi, C. H. Chen, *Nanotechnology* **2005**, *16*, 2338–2341.
- [12] a) J. T. Zhang, J. F. Liu, Q. Peng, X. Wang, Y. D. Li, *Chem. Mater.* **2006**, *18*, 867–871; b) C. T. Hsieh, J. M. Chen, H. H. Lin, H. C. Shih, *Appl. Phys. Lett.* **2003**, *83*, 3383–3387; c) Y. W. Zhu, T. Yu, F. C. Cheong, X. J. Xui, C. T. Lim, V. B. C. Tan, J. T. L. Thong, C. H. Sow, *Nanotechnology* **2005**, *16*, 88–92; d) R. B. Vasiliev, M. N. Rumyantseva, N. V. Yakovlev, A. M. Gaskov, *Sens. Actuators B* **1998**, *50*, 186–193; e) X. H. Kong, Y. D. Li, *Sens. Actuators B* **2005**, *105*, 449–453; f) V. R. Katti, A. K. Debnath, K. P. Muthe, M. Kaur, A. K. Dua, S. C. Gadkari, S. K. Gupta, V. C. Sahni, *Sens. Actuators B* **2003**, *96*, 245–252.
- [13] a) K. B. Zhou, R. P. Wang, B. Q. Xu, Y. D. Li, *Nanotechnology* **2006**, *17*, 3939–3943; b) A. Santos, P. Yustos, A. Quintanilla, G. Ruiz, F. Garcia-Ochoa, *Appl. Catal. B: Environ.* **2005**, *61*, 323–333; c) H. G. El-Shobaky, M. Mokhtar, G. A. El-Shobaky, *Appl. Catal. A: Gen.* **1999**, *61*, 335–344; d) W. H. Shen, X. P. Dong, Y. F. Zhu, H. R. Chen, J. L. Shi, *Microporous Mesoporous Mater.* **2005**, *85*, 157–162.
- [14] S. Anandan, S. H. Yang, *J. Experi. Nanosci.* **2007**, *2*, 23–56.
- [15] a) J. Q. Qi, H. Y. Tian, L. T. Li, H. L. W. Chan, *Nanoscale Res. Lett.* **2007**, *2*, 107–111; b) J. F. Xu, W. Ji, Z. X. Shen, S. H. Tang, X. R. Ye, D. Z. Jia, X. Q. Xin, *J. Solid State Chem.* **1999**, *147*, 516–519.
- [16] a) Y. Zhou, S. Kamiya, H. Minamikawa, T. Shimizu, *Adv. Mater.* **2007**, *19*, 4194–4197; b) A. A. Umar, M. Oyama, *Cryst. Growth Des.* **2007**, *7*, 2404–2409; c) G. H. Du, G. Van Tendeloo, *Chem. Phys. Lett.* **2004**, *393*, 64–69; d) W. Z. Wang, O. K. Varghese, C. M. Ruan, M. Paulose, C. A. Grimes, *J. Mater. Res.* **2003**, *18*, 2756–2759; e) X. Y. Song, H. Y. Yu, S. X. Sun, *J. Colloid Inter. Sci.* **2005**, *289*, 588–591; f) T. Yu, F. C. Cheong, C. H. Sow, *Nanotechnology* **2004**, *15*, 1732–1736.
- [17] a) M. H. Cao, Y. H. Wang, C. X. Guo, Y. J. Qi, C. W. Hu, E. B. Wang, *J. Nanosci. Nanotech.* **2004**, *4*, 824–828; b) T. Yu, X. Zhao, Z. X. Shen, Y. H. Wu, W. H. Su, *J. Cryst. Growth* **2004**, *268*, 590–595; c) M. H. Cao, C. W. Hu, Y. H. Wang, C. Xu, C. Zheng, G. Wang, *Chem. Commun.* **2003**, 1884–1885; d) C. K. Xu, Y. K. Liu, G. D. Xu, G. H. Wang, *Mater. Res. Bull.* **2002**, *37*, 2365–2372.
- [18] a) W. X. Zhang, X. G. Wen, S. H. Yang, *Inorg. Chem.* **2003**, *42*, 5005–5014; b) R. Yang, L. Gao, *Solid State Commun.* **2005**, *134*, 729–733.
- [19] a) D. Chen, G. Z. Shen, K. B. Tang, Y. T. Qian, *J. Cryst. Growth* **2003**, *254*, 225–228; b) M. Vaseem, A. Umar, S. H. Kim, Y. B. Hahn, *J. Phys. Chem. C* **2008**, *112*, 5729–5735; c) J. W. Zhu, H. P. Bi, Y. P. Wang, X. Wang, X. J. Yang, L. D. Lu, *Mater. Lett.* **2007**, *61*, 5236–5238.
- [20] X. C. Jiang, T. Herricks, Y. N. Xia, *Nano Lett.* **2002**, *2*, 1333–1338.
- [21] Y. Chang, H. C. Zeng, *Cryst. Growth Des.* **2004**, *4*, 397–402.
- [22] H. M. Xiao, S. Y. Fu, L. P. Zhu, Y. Q. Li, G. Yang, *Eur. J. Inorg. Chem.* **2007**, 1966–1971.
- [23] X. Q. Wang, G. C. Xi, S. L. Xiong, Y. K. Liu, B. J. Xi, W. C. Yu, Y. T. Qian, *Cryst. Growth Des.* **2007**, *7*, 930–934.
- [24] H. L. Xu, W. Z. Wang, W. Zhu, L. Zhou, M. L. Ruan, *Cryst. Growth Des.* **2007**, *7*, 2720–2724.
- [25] S. Q. Wang, J. Y. Zhang, C. H. Chen, *Scripta Mater.* **2007**, *57*, 337–340.
- [26] A. M. Cao, J. D. Monnel, C. Matranaga, J. M. Wu, L. L. Cao, *J. Phys. Chem. C* **2007**, *111*, 18624–18628.
- [27] B. Liu, H. C. Zeng, *J. Am. Chem. Soc.* **2004**, *126*, 8124–8125.
- [28] Y. Y. Xu, D. R. Chen, M. L. Jiao, K. Y. Xue, *Mater. Res. Bull.* **2007**, *42*, 1723–1731.
- [29] R. Xu, T. Xie, Y. G. Zhao, Y. D. Li, *Cryst. Growth Des.* **2007**, *7*, 1904–1911.
- [30] Z. P. Zhang, X. Q. Shao, H. D. Yu, Y. B. Wang, M. Y. Han, *Chem. Mater.* **2005**, *17*, 332–336.

Received: September 11, 2008

Published Online: November 25, 2008